

Loughborough University  
Institutional Repository

---

*Reconstructing the Holocene  
coastal development of the  
Laurentine Shore*

This item was submitted to Loughborough University's Institutional Repository by the/an author.

**Additional Information:**

- A Doctoral Thesis. Submitted in partial fulfillment of the requirements for the award of Doctor of Philosophy of Loughborough University.

**Metadata Record:** <https://dspace.lboro.ac.uk/2134/6109>

**Publisher:** © Andrew Robert Bicket

Please cite the published version.

This item was submitted to Loughborough's Institutional Repository (<https://dspace.lboro.ac.uk/>) by the author and is made available under the following Creative Commons Licence conditions.



CC creative commons  
COMMONS DEED

**Attribution-NonCommercial-NoDerivs 2.5**

**You are free:**

- to copy, distribute, display, and perform the work

**Under the following conditions:**

 **Attribution.** You must attribute the work in the manner specified by the author or licensor.

 **Noncommercial.** You may not use this work for commercial purposes.

 **No Derivative Works.** You may not alter, transform, or build upon this work.

- For any reuse or distribution, you must make clear to others the license terms of this work.
- Any of these conditions can be waived if you get permission from the copyright holder.

**Your fair use and other rights are in no way affected by the above.**

This is a human-readable summary of the [Legal Code \(the full license\)](#).

[Disclaimer](#) 

For the full text of this licence, please go to:  
<http://creativecommons.org/licenses/by-nc-nd/2.5/>

## Thesis Access Form

Copy No. E-THESIS Location INSTITUTIONAL REPOSITORY


Author BICKET ANDREW ROBERT

Title RECONSTRUCTING THE HOLOCENE QUATERNARY DEVELOPMENT OF THE LAURENTINE SHORE

Status of access OPEN / RESTRICTED / CONFIDENTIAL:

Moratorium Period: ..... years, ending ..... / ..... 200.....

Conditions of access approved by (CAPITALS): .....

Supervisor (Signature) 

Department of GEOGRAPHY

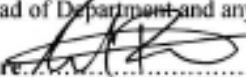
**Author's Declaration:** *I agree the following conditions:*

Open access work shall be made available (in the University and externally) and reproduced as necessary at the discretion of the University Librarian or Head of Department. It may also be digitised by the British Library and made freely available on the Internet to registered users of the EThOS service subject to the EThOS supply agreements.

*The statement itself shall apply to ALL copies including electronic copies:*

**This copy has been supplied on the understanding that it is copyright material and that no quotation from the thesis may be published without proper acknowledgement.**

**Restricted/confidential work:** All access and any photocopying shall be strictly subject to written permission from the University Head of Department and any external sponsor, if any.

Author's signature  Date 16 MARCH 2010

users declaration: for signature during any Moratorium period (Not Open work): <i>I undertake to uphold the above conditions:</i>			
Date	Name (CAPITALS)	Signature	Address

# Reconstructing the Holocene coastal development of the Laurentine Shore

by

Andrew Robert Bicket

A Doctoral Thesis

Submitted in partial fulfilment of the requirements

for the award of

D. Phil of Loughborough University

October 2009

© by Andrew Robert Bicket 2009

CERTIFICATE OF ORIGINALITY

This is to certify that I am responsible for the work submitted in this thesis, that the original work is my own except as specified in acknowledgments or in footnotes, and that neither the thesis nor the original work contained therein has been submitted to this or any other institution for a degree.

..... ( Signed )

16/03/2010..... ( Date)

## Abstract

The Laurentine Shore is the Imperial Roman palaeo-shoreline preserved up to 1km inland of the southern, distal edge of the Tiber Delta coastline of Lazio, western Central Italy. The progradation of the delta is recorded on the site as a series of shore-parallel relict dune ridges. High-status villas developed along the roman period coastline, with a service village (*Vicus Augustanus*), and other infrastructure such as roads, aqueduct, *piscinae* and several baths (*thermae*), these structures have been examined using a multi-scale geoarchaeological approach.

A sea level reconstruction based on multi-proxy palaeo-environmental analysis of a silt/peat sedimentary transition from the base of a Roman *piscina* suggests that the sea level at ca. 2400 ± 40 BP was around 1.25 ± 0.2 m below modern sea level. This analysis provides further context for assessing the development of the site during the late Holocene in relation to the progradation of the Tiber delta and for the important Imperial Roman period occupation of the Laurentine Shore and other important sites such as *Portus* and *Ostia Antica* in the central part of the Tiber delta.

At several key periods in the late Holocene, the palaeo-shoreline has been reconstructed using a geochronological framework of optical luminescence dates and geomorphological survey of the Tiber Delta dune ridge record. In particular, during the Imperial Roman period, ca. 2000 BP) it has been shown that the Laurentine Shore was settled during a period of significant Tiber delta shoreline progradation. Two-major building phases at the *Vicus Augustanus* occur within this progradation phase. By the abandonment of the site in the 5<sup>th</sup> century AD, the shoreline was around 70 m seaward of the shoreline during the 1<sup>st</sup> building phase of the *Vicus*. This rate of shoreline change could be noticeable by the population over decadal timescales and may have driven the alteration of coastal building and property plots during the 500 year lifetime of the settlement.

A combined methodology incorporating sedimentology, geochemistry and petrological analysis of diagenetically altered sediments found that early vadose diagenesis may have a deleterious effect upon luminescence dating dosimetry, inducing age underestimation, especially of reddened dune sands. Petrological analysis has also shown that a lack of anomalous fading in luminescence behaviour observed in K-feldspars may be due to a lack of complex microstructure in the mineral grains driven by the metamorphic, Alpine origin of these minerals.

An assessment of the geoarchaeological approach used in this thesis shows that a scale-driven context provides a useful structure for examining the various processes and factors affecting the geomorphological and sedimentological records improving confidence in the examination of the archaeological record.

## Keywords

Geoarchaeology, geochronology, petrology, provenance, diagenesis, Tiber Delta, coastal dune ridges, Holocene, Castelporziano, Laurentine Shore

## Acknowledgments

Technical support from Mark Szegner (Lboro Geography), David Twigg (Lboro Civil Eng.), Al Daley (Lboro Chemistry), David Townrow (Wolverhampton), and David Alderton and Inga Sevastjanova (Geology RHUL) made various aspects of this thesis possible. Dave Ryves, Jon Lewis, Keely Mills and Kaarina Weckström are thanked for valuable ideas and discussion regarding all things diatom.

Grateful acknowledgment is made to Chris, Tim, Peter, James, Ginny, Michele and Liz for invaluable fieldwork assistance and for making the long hours of excavation and surveying a pleasure rather than a chore.

Professors Amanda Claridge and Helen Rendell are thanked for their support, encouragement and insight for instigating the project, providing me with an opportunity. Helen Rendell and Joanna Bullard are also thanked for their supervision and expertise.

Many thanks are due to the excellent cohort of post-grads at Loughborough University, Dept of Geography and international colleagues I've come to know. Their good humour and support manifested as beer, curry (and occasionally hiking) will continue to be greatly appreciated.

The support and encouragement of my parents, who are unlikely to recoup their long-term financial investment in my never-ending education, is gratefully acknowledged. They are thanked for never asking when I'm getting a 'proper job'.

Emma is humbly thanked for her support, for persevering and for keeping me laughing; cheers, hon.

*"The particle. Very difficult to measure the particle. To measure it you must shine light upon it, but by doing so you distort the image of the particle making it impossible to take an accurate reading. I used smaller and smaller amounts of light, but still to no avail. Eventually I used the smallest amount of light known to man – the glove box light of a 1974 Austin Maxi."*

(Bailey, B., 2004)

## Table of Contents

Abstract .....	iii
Keywords .....	iv
Acknowledgments .....	v
List of Figures .....	xv
List of Tables .....	xviii
List of Plates .....	xx
1. Introduction .....	1
1.1. La Tenuta di Castelporziano .....	1
1.2. Research at Castelporziano .....	3
1.2.1. The Laurentine Shore Project .....	4
1.3. Aim .....	5
1.4. Objectives .....	5
1.4.1. To examine the processes affecting the coastal development of the site during the Holocene .....	5
1.4.2. To examine the chronological development of the landscape, principally by dating coastal dune ridges, sand sheets and archaeological sites .....	6
1.4.3. To examine how the geoarchaeology of the Laurentine Shore is driven by macro-, and meso-scale processes of relative sea level change, delta progradation and key anthropogenic factors .....	6
1.5. Research Questions .....	6
1.5.1. How has the coastline of the Laurentine Shore developed during the Holocene? .....	6
1.5.2. What are the processes of coastal development acting on the Laurentine Shore? .....	6
1.5.3. What is the chronology of these coastal changes? .....	6
1.5.4. What are the key interactions between anthropogenic and geomorphological processes? .....	6
1.5.5. What are the benefits of a multi-scale geoarchaeological approach and the implications for future research? .....	6
1.6. Theoretical models .....	6
1.6.1. Geomorphological model .....	7
1.6.1.1. The study of sand dunes .....	7
1.6.1.2. Holistic models: beach & foredune sediment budgets .....	7
1.6.1.3. Notes on coastal dunes at Castelporziano .....	10
1.6.2. A Geoarchaeological approach for Castelporziano .....	11
1.6.2.1. A question of scale .....	12
1.6.2.2. A multi-scale approach .....	12
1.6.2.3. Asking geoarchaeological questions .....	13



1.7.	Thesis outline.....	13
2.	Setting.....	14
2.1.	A Geoarchaeological Approach .....	14
2.1.1.	Geoarchaeology: 1976.....	14
2.1.2.	Geoarchaeology: an archaeological viewpoint.....	15
2.1.3.	Geoarchaeology: the state of the art .....	16
2.1.4.	Reassessing Geoarchaeology.....	18
2.2.	Multi-scale context .....	19
2.3.	Macro-scale context ( $10^{4-5}$ ) .....	21
2.3.1.	Sea level.....	21
2.3.2.	Weather systems .....	22
2.3.2.1.	Exterior systems.....	22
2.3.2.2.	Interior systems .....	22
2.3.3.	Cyclones & local winds .....	22
2.3.4.	The Tiber River.....	23
2.3.5.	Geomorphology of the Tiber basin.....	23
2.3.5.1.	Neotectonics.....	24
2.3.5.2.	Sediment supply .....	24
2.3.6.	Tiber Delta sequence stratigraphy .....	25
2.3.6.1.	Expression of delta progradation at the distal ends of the delta .....	27
2.3.6.2.	Marine transgression & delta progradation: a complex relationship with Holocene eustatic sea level rise	28
2.4.	Unraveling the climate of Castelporziano .....	29
2.5.	Meso-scale context ( $10^{2-3}$ ).....	29
2.5.1.	Geoarchaeological scale .....	29
2.5.2.	Interaction of key processes in the coastal zone.....	30
2.6.	Micro-scale context ( $10^{0-1}$ ) .....	31
2.6.1.	The effect of tides, waves and winds on the Castelporziano shoreline .....	31
2.6.2.	Coastal Dunes .....	33
2.6.3.	Incipient foredune formation .....	33
2.6.4.	Foredune development .....	34
2.6.5.	Foredune flora .....	34
2.6.6.	Dune soils.....	35

2.6.7.	Foredune erosion.....	38
2.6.7.1.	Wave truncation .....	38
2.6.7.2.	Blowouts .....	38
2.6.7.3.	Parabolic dunes .....	39
2.6.8.	Features behind the active foredune .....	39
2.6.8.1.	Dune ridges.....	39
2.6.8.2.	Deflation hollows.....	40
2.6.8.3.	Erosional processes acting on relict dunes.....	40
2.6.9.	Hydrogeology of the Castelporziano Estate .....	41
2.6.10.	Vegetation at Castelporziano .....	44
2.6.11.	Coastal geochemical sediments at Castelporziano .....	47
2.7.	Aeolianite.....	47
2.7.1.	Sources of cement .....	48
2.7.2.	Geochemical exchanges and carbonate species .....	49
2.7.3.	Carbonate hydrolysis & kinetic fractionation of carbonate .....	50
2.8.	Early vadose ferricrete: dune reddening geochemistry .....	50
2.8.1.	Mineralogy of rubefaction.....	51
2.8.2.	Goethite ( $\alpha$ -FeO.OH) and lepidocrocite ( $\gamma$ -FeO.OH).....	51
2.8.3.	Hematite ( $\text{Fe}_2\text{O}_3$ ).....	52
2.8.4.	Sources of Iron.....	52
2.8.5.	Mechanisms of formation .....	53
2.8.5.1.	Ferrihydrite .....	53
2.8.5.2.	Ferrihydrite to goethite or hematite transformation.....	53
2.8.5.3.	Goethite to hematite transformation .....	54
2.8.5.4.	Preservation of hematite.....	55
2.9.	Implications for Castelporziano .....	55
3.	Methodology .....	56
3.1.	The overall approach .....	56
3.2.	Site mapping.....	57
3.2.1.	Geomorphic survey.....	57
3.2.2.	Dune ridge transects.....	58
3.2.3.	Aerial photography .....	58
3.3.	Site georeferencing: Differential-GPS survey .....	58

3.3.1.	EGM '96 as a modern sea level proxy.....	59
3.3.2.	Biostratigraphic sea level reconstruction: diatom analysis .....	59
3.4.	Site Transects.....	59
3.4.1.	Sampling transects.....	60
3.4.2.	Inland transects .....	61
3.4.3.	Sampling .....	62
3.4.4.	Sampled sections .....	65
3.5.	Summary of analytical methods .....	68
3.5.1.	Grain-size analysis of sand-sized sediment and grain-coatings.....	68
3.5.2.	Loss-On-Ignition (Organic content, Carbonate equivalent content) .....	69
3.5.3.	EDX-SEM chemical analysis of diagenetic grain-coatings.....	70
3.6.	Provenance & diagenesis analysis .....	70
3.6.1.	Petrological provenance analysis .....	70
3.6.2.	Petrological diagenesis analysis.....	71
3.6.3.	Diagenesis analysis methodology .....	73
3.6.4.	Point counting.....	73
3.6.5.	X-ray Diffraction (XRD) analysis .....	74
3.7.	Optically Stimulated Luminescence (OSL) chronology from K-feldspar .....	75
3.7.1.	IRSL dating of sedimentary sample framework.....	76
3.7.1.1.	Fading experiment.....	77
3.7.1.2.	Age control .....	78
3.7.1.3.	Luminescence dosimetry .....	78
3.7.1.4.	Alpha dosimetry protocol .....	78
3.7.1.5.	Beta dosimetry protocol.....	78
3.8.	Application of methods .....	79
4.	Results & Analysis .....	80
4.1.	Topographic Survey .....	80
4.1.1.	Aerial photography .....	80
4.1.2.	Digital Elevation Models (DEM).....	82
4.1.3.	Dune ridge transects – wavelength, frequency and amplitude .....	83
4.2.	D-GPS georeferencing.....	87
4.2.1.	Summary of system & method .....	87
4.2.2.	GCP locations & GIS construction.....	89

4.2.2.1.	Mapping hydrology.....	93
4.2.2.2.	Mapping dune ridges.....	94
4.3.	Sea-level Reconstructions.....	94
4.3.1.	Core 14 sedimentary transition – <i>piscinae</i> D6.....	95
4.3.2.	Sea wall notch.....	95
4.4.	Sedimentology.....	95
4.4.1.	Grain-size analysis.....	95
4.4.2.	Loss-on-ignition (LOI).....	101
4.5.	Preliminary study: C & O stable isotope analysis of diagenetic carbonate grain coatings.....	104
4.5.1.	Iron oxide contamination for stable isotope analysis .....	104
4.6.	Petrology.....	107
4.6.1.	Preliminary results.....	107
4.6.1.1.	Light silicate suite .....	107
4.6.1.2.	Carbonates and lithics .....	109
4.6.1.3.	Heavy ferromagnesian silicates suite .....	109
4.6.1.4.	Metamorphism in heavy ferromagnesian silicates suite.....	109
4.6.2.	Provenance training set.....	111
4.6.3.	Results.....	111
4.6.3.1.	LM provenance indicators .....	112
4.6.3.2.	HM provenance indicators .....	113
4.6.3.3.	Problems of provenance.....	113
4.6.4.	Diagenesis analysis .....	116
4.6.5.	Problems of identification .....	116
4.6.5.1.	Metamorphic alteration of framework silicates.....	116
4.6.5.2.	Obtaining problematic interference figures.....	117
4.6.6.	Results.....	118
4.6.7.	X-Ray Diffraction analysis (XRD) .....	122
4.6.8.	Diagenetic decalcification.....	125
4.6.9.	Principal components analysis (PCA).....	125
4.7.	Summary of sedimentology and diagenesis.....	130
4.8.	Chronology.....	130
4.8.1.	Sampling .....	130
4.8.2.	SAAD-IRSL protocol.....	130

4.8.3.	DE determination.....	131
4.8.3.1.	Curve-fitting.....	131
4.8.3.2.	Radial plots .....	131
4.8.4.	Environmental dosimetry .....	132
4.8.4.1.	Water content .....	133
4.8.5.	Age calculation.....	133
4.8.6.	Fading experiment.....	135
4.8.7.	Mineralogical control on stored signal loss .....	135
4.8.8.	Archaeological age control .....	138
4.8.9.	IRSL ages .....	138
4.8.9.1.	Dose-rate trends.....	138
4.8.9.2.	Intra-dune age estimate variability .....	145
4.8.10.	Multivariate analysis of DE and environmental variables .....	147
4.8.11.	Dose-rate correction.....	156
4.8.12.	Age correction .....	157
4.8.13.	Geomorphological consideration of corrected age estimates .....	159
4.9.	Early vadose diagenesis: development of geochemical sediments & geochronological influences.....	160
4.9.1.	Aeolianite.....	161
4.9.2.	Early vadose laterised ferricrete.....	163
4.10.	Geochronological framework .....	164
4.10.1.	Transect 1 .....	164
4.10.1.1.	Shoreline progradation rates.....	164
4.10.1.2.	Pre-Roman development.....	165
4.10.1.3.	Roman settlement .....	166
4.10.1.4.	Post-Roman Abandonment .....	167
4.10.2.	Transect 2 .....	168
4.10.2.1.	Late Pleistocene and early Holocene aeolian features.....	169
4.10.2.2.	Mid-Holocene aeolian remobilisation .....	169
4.10.2.3.	<i>Piscinae</i> construction.....	170
4.10.3.	Transect 3 .....	171
4.10.3.1.	Early Holocene aeolian development.....	172
4.10.3.2.	Late Holocene and Historic development .....	172
4.11.	Holocene timeline of geomorphological activity.....	172

4.12.	<i>Piscinae</i> D6 Palaeoenvironmental Reconstruction.....	173
4.12.1.	Diatom analysis.....	174
4.12.2.	Sedimentology.....	174
4.12.3.	Geochemical analysis.....	174
4.12.4.	Magnetic Susceptibility.....	175
4.12.5.	Chronology.....	175
4.12.6.	Zone Interpretation .....	176
4.13.	D6 <i>Piscinae</i> Discussion of Results .....	177
4.13.1.	LOI Geochemistry .....	177
4.13.2.	Grain-size analysis.....	178
4.13.3.	Core interpretation.....	178
4.13.4.	Sediment Properties .....	178
4.13.5.	Diatom assemblage interpretation.....	180
4.13.5.1.	Zone 1 .....	181
4.13.5.2.	Zone 2 .....	181
4.13.5.3.	Zone 3 .....	182
4.13.5.4.	Zone 4 .....	183
4.13.6.	Assessment of sea level marker .....	183
4.14.	Summary of results & analysis.....	185
5.	Holocene Reconstruction .....	186
5.1.	Scale-process sensitivity & Holocene context .....	186
5.1.1.	Dune ridge scale-sensitivity .....	186
5.1.2.	Progradation and foredune-building sediment budgets.....	186
5.1.3.	Sediment supply: the Tiber flood record at Rome .....	187
5.1.4.	Foredune development .....	188
5.1.5.	Holocene chronostratigraphy.....	192
5.1.6.	Summary.....	194
5.2.	Holocene cross-section of Castelporziano.....	195
5.3.	Late Pleistocene – Mid Holocene coastal sandsheets and dune ridge formation .....	195
5.4.	Mid-Holocene progradation of Italian & western Mediterranean deltas .....	197
5.4.1.	Delta Progradation at Castelporziano .....	199
5.4.2.	Regional climate and mid-Holocene delta progradation .....	200
5.4.3.	The changing course of the Tiber .....	201

5.4.4.	Mid-Holocene aeolian sand remobilisation.....	203
5.5.	Mid-Late Holocene .....	205
5.6.	The Laurentine Shore .....	207
5.6.1.	Macro-scale context of the Laurentine Shore .....	207
5.6.2.	Local geomorphological context.....	208
5.6.3.	Sea level context.....	209
5.6.4.	A question of Roman dune management.....	209
5.6.5.	<i>Piscinae</i> (2100 – 1900 BP).....	210
5.6.6.	<i>Vicus Augustanus</i> (2010 – 1580 BP) .....	212
5.6.7.	The Severian-period sea wall and storms.....	215
5.6.8.	<i>Villae</i> & coastal infrastructure .....	220
5.6.9.	Possible inlets and harbour .....	220
5.6.10.	Roman-period hydrology and water supply .....	222
5.6.11.	Connections to the wider Roman Empire.....	223
5.7.	The decline and fall of the Laurentine Shore .....	226
5.7.1.	Aeolian inundation of archaeological buildings .....	227
5.7.2.	Regional climate and aeolian remobilisation .....	227
5.8.	Post-Roman Development.....	228
5.8.1.	Secondary dune formation (aeolian remobilisation).....	228
5.8.2.	Post-Roman flooding .....	228
5.9.	Modern shoreline management.....	229
5.9.1.	Dune ridge seeding .....	229
5.9.2.	Beach nourishment.....	229
5.10.	Summary of micro-scale themes .....	229
5.10.1.	Dune stability & remobilisation .....	230
5.10.2.	Storminess & climate instability: multi-scale effects.....	230
5.11.	Assessment of a Geoarchaeological approach and conclusions .....	231
6.	Conclusions & future work .....	232
6.1.	Addressing the aim & objectives .....	232
6.2.	Research questions.....	232
6.2.1.	What are the processes of coastal development acting on the Laurentine Shore? .....	232
6.2.2.	What is the chronology of these coastal changes? .....	233
6.2.3.	How has the coastline of the Laurentine Shore developed during the Holocene?.....	235

6.2.3.1.	Macro-scale context ( $10^3+$ ).....	235
6.2.3.2.	Meso-scale context ( $10^2$ ).....	236
6.2.3.3.	Micro-scale context ( $10^{0-1}$ ).....	237
6.2.4.	What are the key interactions between the anthropogenic and geomorphological records?.....	237
6.2.5.	What are the implications for multi-scale geoarchaeological research?.....	238
6.2.6.	The Geoarchaeological approach on the Laurentine Shore.....	239
6.3.	Future work.....	241
6.3.1.	Luminescence chronology.....	241
6.3.2.	Geoarchaeology.....	242
6.3.3.	Castelporziano and a wider Geoarchaeological context.....	243
Appendix A1 – Sediment descriptions.....		244
Appendix A2 – Petrology counts.....		248
References.....		253



## List of Figures

Figure 1.1: Location of the Castelporziano Estate.....	1
Figure 1.2: Topographic variation of the Castelporziano Estate (adapted from Busuoli et al., 2001). .....	2
Figure 1.3: Distribution of 'Laurentine Shore' villa sites within Castelporziano Estate (A. Claridge, 2000).....	3
Figure 1.4: Sediment budget model (redrawn from Psuty, 1992).....	8
Figure 1.6: Long-term morphology developments of coastal foredunes (Hesp, 2002).. .....	9
Figure 2.1: Subject areas of 143 Geoarchaeology (topic) meetings, books and articles citations featured in ISI Web of Knowledge (Thomson Reuters) within the last 5 years (7/09/2009). ( <a href="http://wok.mimas.ac.uk/">http://wok.mimas.ac.uk/</a> ). .....	16
Figure 2.2: Sea level curve from central Tiber Delta (Bellotti et al., 2007). .....	21
Figure 2.3: Geological context of the Tiber Delta (Bellotti et al., 1995).....	24
Figure 2.4: Central Tiber Delta Holocene parasequence stratigraphy (Amorosi and Milli, 2001). .....	26
Figure 2.5: Detail of Carta Geologica D'Italia Foglio 149 (Cerveteri).....	28
Figure 2.6: Wave magnitude and direction at Fiumicino (Colzani et al., 2004). .....	31
Figure 2.7: (a) Average wind direction at Fiumicino (b) Diurnal wind regime at Castelporziano during early summer. ....	32
Figure 2.8: Dune soil zone schematic (adapted from Jungerius 1990). .....	35
Figure 2.9: Distribution of planosols and luvisols in Lazio and Latium (Arnoldus-Huyzendveld et al., in press).. .....	37
Figure 2.10: Schematic sequential development of coastal dune forms .....	39
Figure 2.11: (a) Lower Tiber River catchment ca. 20 k BP and, (b) ca. 4 k BP (Bellotti et al., 2007). .....	42
Figure 2.12: Hydrogeological analysis of the Castelporziano Estate (adapted from Busuoli et al., 2001).....	43
Figure 2.13: Geochemical analysis of 22 wells across the Castelporziano Estate.....	43
Figure 2.14: Vegetation map of the Castelporziano Estate (adapted from Fares et al., 2009). .....	46
Figure 3.1: Location of transect sampling strategy.. .....	60
Figure 3.2: Detail of sampling locations described in Figure 3.1.....	61
Figure 3.3: Schematic diagrams of sampled sections, primarily from dune ridge crests and sand sheets.....	65
Figure 3.4: Core 14A, extracted from the base of <i>Piscinae</i> (D6).. .....	67
Figure 4.1: Key archaeological sites mentioned in the text .....	81
Figure 4.2: Location of archaeological DEM within the Castelporziano Estate.....	82
Figure 4.3: DEM of <i>Vicus Augustanus</i> and environs (RHUL, Dept of Classics).....	83
Figure 4.4: Extent of dune ridge transects overlain onto 1983 series aerial photograph #279.....	84
Figure 4.5: Dune ridge transects labelled in figure 4.4.....	85
Figure 4.6: <i>Piscinae</i> DEM and transect D-D' alignment (adapted from original by J. Andrews, 2009). .....	87
Figure 4.7: Georeferenced aerial photographs taken in 1983 (Istituto Geografico Militare). .....	90
Figure 4.8: Georeferenced 1954 aerial photographs (Istituto Geografico Militare).. .....	91
Figure 4.9: GIS integration of selected geological and topographic mapping, aerial photography and archaeological mapping datasets .....	92
Figure 4.10: Digitisation of hydrological features and dune ridge topography. ....	93
Figure 4.11: Crop-marks preserving 'tide-marks' of relict delta lagoon adjacent to <i>Ostia Antica</i> abutting the NW boundary of the Castelporziano Estate. ....	94
Figure 4.12: Grain-size ternary plot (Gradistat v.5) (Blott and Pye, 2001).....	96
Figure 4.13: Modern delta beach samples, modal grain-size.....	96
Figure 4.14: Modern Tiber beach samples; additional grain-size parameters, sorting ( $\sigma$ ), skewness and kurtosis. ....	97
Figure 4.15: Inland transects modal grain-size.....	97

Figure 4.16: Sub 1.4 mm grain-size distributions of transect 2 samples (left). Sub 63 $\mu\text{m}$ measurements are shown on the right highlighting the silt-sized particle-size distribution.....	99
Figure 4.17: SEM micrograph of CP07/14. ....	100
Figure 4.18: Micritic carbonate cements and amorphous platy coatings on sand grain surface (CP07/14).. ....	100
Figure 4.19: Transect 1 organic carbon and carbonate equivalent content loss-on-ignition (% dry weight).....	101
Figure 4.20: Transect 2 organic carbon and carbonate equivalent content loss-on-ignition (% dry weight).....	101
Figure 4.21: Transect 3 organic carbon and carbonate equivalent content loss-on-ignition (% dry weight).....	102
Figure 4.22: Transect 3 modal grain size LOI.....	102
Figure 4.23: Fine-grained sediments derived primarily from diagenetic grain coatings.....	103
Figure 4.24: SEM micrograph of CP07/14. Element maps are presented for this view in Figure 4.25. ....	104
Figure 4.25: Element map of selected elements from CP07/14 (Al, Si, K & Ca).....	105
Figure 4.26: CP07/14. Clay coating spectra, note the Ca, Al, Si peak.....	106
Figure 4.27: CP07/20. This spectrum is representative of the general surface of the whole sample.. ....	106
Figure 4.28: QFL ternary plot of Tyrrhenian basin provenance.....	114
Figure 4.29: HM ternary plot of Tyrrhenian Basin provenance.....	115
Figure 4.30: Stress-induced biaxial interference figures in Quartz (Starkey, 2000).....	117
Figure 4.31: Diagenesis ternary plot sorted by dominant mineralogy (i.e. metamorphic content).....	119
Figure 4.32: Key metamorphic provenance indices used by Garzanti et al (2002).....	120
Figure 4.33: Key volcanic provenance indices used by Garzanti et al (2002).....	120
Figure 4.34: HM:LM ratios organised by transect moving inland (exponential trend lines shown). ....	122
Figure 4.35: PCA bi-plot of diagenetic petrology data.. ....	128
Figure 4.36: Distribution of environmental dose-rate with inland distance relative to dune ridges along transect 1.....	139
Figure 4.37: Principal dose-rate components. ....	141
Figure 4.38: Trend in U and Th (ppm), following sorting by increasing K % (figure 4.37).....	142
Figure 4.39: U/Th ratio with standard deviation bars.....	142
Figure 4.40: DE vs dose-rate.....	144
Figure 4.41: Multiple regression bi-plot plus environmental data.....	152
Figure 4.42: Dose-rate plateau of selected carbonate EVD environment samples .....	156
Figure 4.43; Preliminary diagenesis model of Castelporziano geochemical sediments.....	162
Figure 4.44: Transect 1 age model.. ....	164
Figure 4.45: Progradation phases and rates derived from age ranges of transect 1 age model. ....	165
Figure 4.46: Boundary wall dune ridge transect relative to Roman period sea level (-1 m RSL).....	166
Figure 4.47: Dated dune ridge transect from <i>Vicus Augustanus</i> inland to the <i>Canale del Pantanello</i> . ....	167
Figure 4.48: Dated Grotte di Piastra early Imperial Roman villa dune ridge transect. ....	168
Figure 4.49: Transect 2 age model with remobilised, secondary dune form ages.....	168
Figure 4.50: Dated <i>Piscinae</i> transect relative to Roman period sea level.....	170
Figure 4.51: Transect 3 age model with remobilised, secondary formations.....	171
Figure 4.52: Timeline of primary aeolian formations, remobilised features and Roman period occupation of Castelporziano. ....	172
Figure 4.53: Timeline of primary dune ridge formation at Castelporziano.....	173
Figure 4.54: Age/depth model for core 14 diatom record.....	175
Figure 4.55: Diatom analysis of core 14a sedimentary sea level couplet.. ....	180
Figure 4.56: Georeferencing of sediment couplet recovered from <i>Piscina</i> D6.....	184

Figure 4.57: <i>Piscinae</i> -derived sea level comparison. ....	183
Figure 5.1: Late Holocene timeline of major Tiber floods (data from Bersani and Bencivenga, 2001). ....	187
Figure 5.2: Historical record of Tiber flooding frequency at Rome (Bersani and Bencivenga, 2001). ....	188
Figure 5.3: Dune phases at Castelporziano based on table 5.1.....	191
Figure 5.4: Holocene chronostratigraphy of major climatic events, in order of scale. ....	193
Figure 5.5: Schematic cross-section of the Tiber delta dune ridge sequence and "Old dunes" ferricretes.....	195
Figure 5.6: Reconstruction of mid-Holocene ferricrete dune-ridges and sandsheets, ca. 5000 BP.....	196
Figure 5.7: Timeline of pre-settlement dune ridge formation. ....	196
Figure 5.8: Holocene development of the Ebro Delta (Somoza et al., 1998). ....	198
Figure 5.9: Reconstruction of the central Tiber Delta area at ca. 7000 and 4000 BP (Bellotti et al., 2007).. ....	199
Figure 5.10: Geoarchaeological reconstruction of the relict course of the Tiber River at <i>Portus</i> .....	201
Figure 5.11: Late Holocene chronostratigraphy. ....	203
Figure 5.12: Late Holocene timeline of human occupation (pers. comm. A. Claridge 2009) and dune ridge formation..	205
Figure 5.13: Reconstruction of Tiber Delta shoreline at Castelporziano based on transect age models.. ....	206
Figure 5.14: Reconstruction of the wider Laurentine Shore, Tiber Delta context.. ....	207
Figure 5.15: Timeline of dune ridge formation and Roman period of occupation of the Laurentine Shore archaeological record. ....	208
Figure 5.16: Geomorphological map of the Laurentine Shore.. ....	209
Figure 5.17: Plan of the <i>Vicus Augustanus</i> (adapted from Rendell et al., 2007).....	213
Figure 5.18: Post-abandonment reconstruction of the <i>Vicus Augustanus</i> ca. 1600 BP.....	215
Figure 5.19: Georeferenced detail of 1903 archaeological map by Pietro Rosa.....	216
Figure 5.20: Plan of investigated area of sea wall (F2), northwest portion, the sea is to the base of the image.....	217
Figure 5.21: Western portion of sea wall, elevation looking NE.. ....	218
Figure 5.22: Holocene sea level markers from global and Italian records (Lambeck et al., 2004a).....	219
Figure 5.23: The spatial structure of a Libeccio storm wind during the 30 <sup>th</sup> December 1994.....	219
Figure 5.24: Wave data from the Ponza buoy tethered offshore to the SW of Gaeta (Speranza et al 2004).....	220
Figure 5.25: Detail of key Roman period hydrological features.....	221
Figure 5.26: Reconstruction of the Laurentine Shore by Rodolfo Lanciani (1903) focusing on Tor Paterno.....	224
Figure 5.27: Detail of Laurentine Shore between Tor Paterno and Castel Fusano (Lanciani, 1903).....	224
Figure 5.28: Preliminary reconstruction of major road network from available sources around 2000 BP. ....	226

## List of Tables

Table 2.1: Temporal scale framework of Tzedakis (2009).....	20
Table 2.2: Tiber River sediment load measured at Rome between 1934 and 1993 (Iadanza and Napolitano, 2006) .....	25
Table 2.3: Vegetation cover in the coastal plain (Fares et al., 2009). .....	44
Table 3.1: Techniques applied to answer research questions. ....	57
Table 3.2: Summary of samples and techniques undertaken in this thesis. ....	62
Table 3.3: Light and heavy mineral indices used in petrology analysis.....	71
Table 3.4: Indices employed by Garzanti et al., 2002 (supplementary data).....	72
Table 3.5: SAAD-IRSL protocol used for all samples. ....	76
Table 4.1: Ground control points, positions and point quality.....	88
Table 4.2: Aerial photo georeferencing. GCPs used for each photo and numbers of tie-points .....	89
Table 4.3: Sample data for EDX-SEM analysis of diagenetic grain coatings.....	104
Table 4.4: LM indices of modern Tiber beaches sampled in 2007 and between 1975-1984.....	111
Table 4.5: HM indices of modern Tiber beaches sampled in 2007 and between 1975-1984.....	112
Table 4.6: Modern beach samples comparison with mixed provenance of Tiber catchment.....	113
Table 4.7: HM provenance indices of 2007 sampling with Garzanti et al., 2002 data.....	114
Table 4.8: HM:LM ratios from modern Tiber beaches and inland transect samples. ....	121
Table 4.9: XRD samples organised by transect.....	124
Table 4.10: Mineral indices highlighted in diffractograms.....	124
Table 4.11: Diagenesis petrology counts implemented in PCA analysis. ....	126
Table 4.12: Supplementary sedimentology parameters used in PCA analysis.....	127
Table 4.13: Percent overdispersion (OD) of Estimated Dose (DE) estimates for all SAAD-IRSL samples.....	132
Table 4.14: SAAD-IRSL age estimates, OD, dosimetry for 10 % water content for all samples .....	134
Table 4.15: Signal storage ratio after 14 weeks .....	135
Table 4.16: Proportion (%) of detrital K- feldspar exhibiting complex microstructures .....	137
Table 4.17: Age estimate, LOI and grain-size data for samples from similar dune-ridge formations.....	145
Table 4.18: Luminescence, dosimetry and environmental variables used in dosimetry multivariate analysis. ....	148
Table 4.19: DCA summary data for luminescence dosimetry and environmental variables shown in table 4.18.....	149
Table 4.20: Multiple regression (RDA) summary output, all samples.....	149
Table 4.21: Multiple-regression summary data, model effectiveness. ....	149
Table 4.22: Forward selection for Monte Carlo tests.....	150
Table 4.23: Rationale for additional environmental variables. ....	150
Table 4.24: Multiple regression summary data, all samples using expanded environmental factors. ....	151
Table 4.25: Forward selection summary data, all samples using expanded environmental variables. ....	151
Table 4.26: Forward selection summary data, aeolianite EVD samples only.....	153
Table 4.27: Multiple-regression summary data, aeolianite EVD samples only.....	153
Table 4.28: Forward selection summary data, ferricrete EVD samples only. ....	154
Table 4.29: Multiple-regression summary data, ferricrete EVD samples only.....	154
Table 4.30: Samples displaying a homogenous dose-rate (Gy/ka).....	156
Table 4.31: Transected IRSL dosimetry data, moving inland.....	158
Table 4.32: Carbonate EVD samples exhibiting potential post-deposition weathering enrichment of K % content .....	159
Table 4.33: Potential age under-estimation based on raw 'uncorrected' and mean 'corrected' age estimates for ferricrete samples.....	160

Table 4.34: Progradation rates derived age ranges from transect 1 dune ridge age model. ....	165
Table 4.35: Modelled dune ridge ages for unsampled primary dune ridges .....	173
Table 4.36: Calibrated radiocarbon dates used in <i>Piscinae</i> core 14 age/depth model.....	175
Table 4.37: Zone interpretation and dating of diatom record. ....	176
Table 5.1: Comparison of dune ridge phases between Giraudi et al (2009) and at Castelporziano (this study).....	190

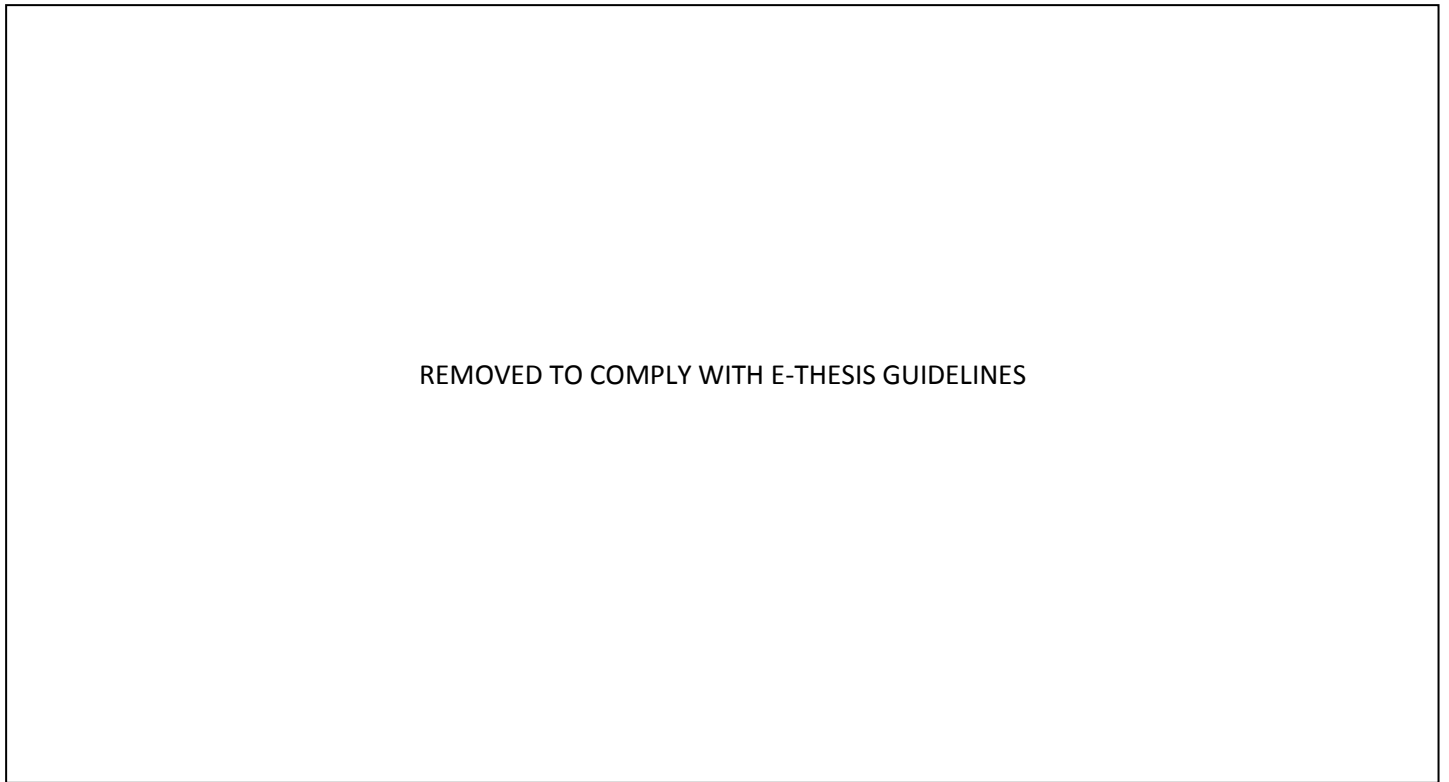
## List of Plates

Plate 1(1a): Looking NE, view of current foredune and strandline. (1b) Cleaned foredune section, aeolian sorting of light and heavy sand grains is recorded by dark bands of volcanic minerals. (1c) Looking NW, small nebkhas (20-30 cm across) aligned to onshore westerly wind (April 2008, A Bicket). .....	10
Plate 2.1: Section through mature forest soil; sampling location for CP07/22.....	36
Plate 2.2 (a) Eutric Planosol section; (b) Albic Luvisol section (Arnoldus-Huyzendveld et al., in press). .....	38
Plate 4.1: CP04/7 light mineral suite in PP (left) and XP (right) light (x200) .....	108
Plate 4.2: CP foredune sample (x40) PP (left) XP (right). Light silicates, carbonates, volcanic and metamorphic .....	110
Plate 4.3.: K-feldspar (stained yellow) exhibiting a lack of twinning and complex small-scale microstructure .....	136
Plate 5.1: Sea wall looking north. ....	217

## 1. Introduction

The research presented in this thesis is primarily derived from fieldwork undertaken between 2006 and 2009 within the Castelporziano Estate (Figure 1.1). A multi-disciplinary team specialising in Classical archaeology, geomorphology and geoarchaeology with the support of several volunteers conducted field and topographic surveys, minor but focused archaeological excavations and a geomorphological survey of key landforms in and around the Estate. The work presented here is primarily the author's but incorporates invaluable contributions from the wider research group. The background of the overall research project - the *Laurentine Shore Project* - is discussed below. The particular focus of this thesis is then developed, research questions are declared and the overall *Geoarchaeological* approach is briefly outlined.

### 1.1. La Tenuta di Castelporziano



**Figure 1.1:** Location of the Castelporziano Estate.

REMOVED TO COMPLY WITH E-THESIS GUIDELINES

**Figure 1.2:** Topographic variation of the Castelporziano Estate (adapted from Busuoli et al., 2001). The position of the Imperial Roman period archaeological remains, on the 'Laurentine Shore' is highlighted around 1 km inland from the modern coastline. Figure 1.3 highlights the distribution of the key villa sites along this alignment.

The Castelporziano Estate is an official Residence of the Italian President. Situated 20 km from Rome, the Estate is currently run as a nature reserve protecting what is regarded as a typical Mediterranean ecosystem<sup>1</sup> (Figure 1.1). The mixed forest cover and coastal dunes that dominate the site partially obscure the rich archaeological record. Most notably a series of high-status Imperial Roman villas and infrastructure indicating a past shoreline are preserved around 1 km inland from the present coast (Figure 1.2). The coastline has prograded seaward throughout the Holocene as the Estate is located on the southern distal end of the Tiber Delta. The Roman palaeo-shoreline is termed the Laurentine Shore due to the association with *Laurentium* as described by classical sources<sup>2</sup> (Figure 1.3).

---

<sup>1</sup> An extensive bibliography focussed largely upon ecology and conservation is online at <http://www3.corpoforestale.it/flex/cm/pages/ServeAttachment.php/L/IT/D/D.effc92cd7de8309642cb/P/BLOB:ID%3D447> (last accessed 5/08/2009).

<sup>2</sup> Younger Pliny's letters...to Gallus II.17 (description of his Laurentine Villa); to Minutius Fundanus I.9 (attractions of his Laurentine Villa); to Catillus Severus I. 22 (his activities); to Cornelius Tacitus I. 6 (on boar hunting).



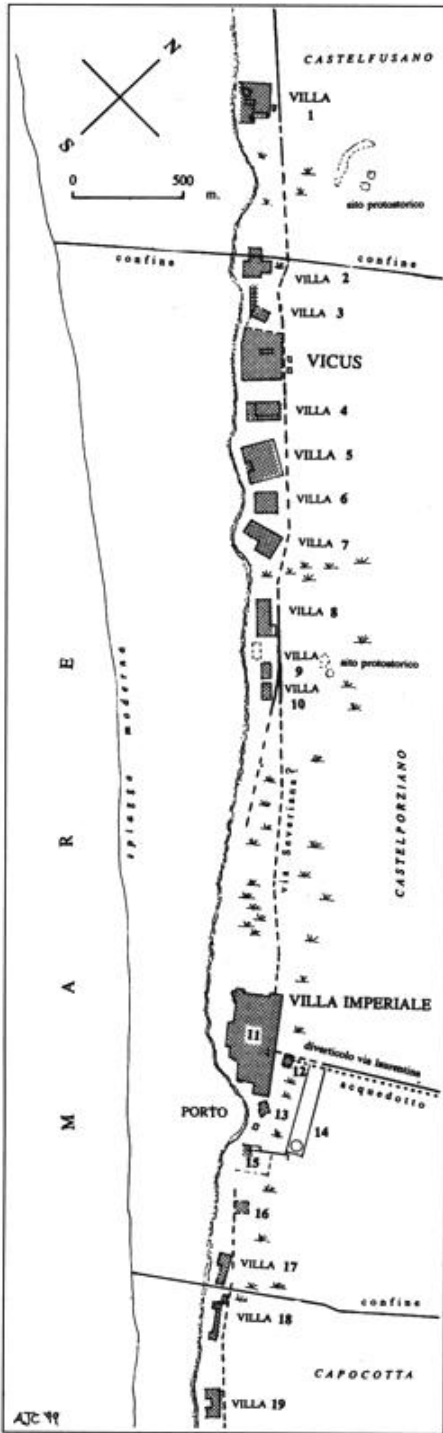


**Figure 1.3:** Distribution of 'Laurentine Shore' villa sites within Castelporziano Estate (A. Claridge, 2000). Villa 1 is described as the Villa del Plinio and lies within Castel Fusano to the NW; the neighbouring Estate, now a public park.

## 1.2. Research at Castelporziano

The Castelporziano Estate's protected status and relatively unexploited nature has also provided a key location for ecological, biological, pedological, atmospheric and coastal management research (Milli & Zarlenga 1991; Manes et al. 1997; Seufert et al. 1997; Arnoldus-Huyzendveld & Gisotti 1999; Busuoli et al. 2001; De Lillis et al. 2004; Francaviglia et al. 2004; Fares et al. 2009). Conservation of the wild mammal fauna and raptors is ongoing, with *Sus scrofa* (wild boar)

(Barbisan et al. 2009) and deer a common sight in the woodland areas. Research focusing on the omnipresent *Formicidae* within the Estate (Mei 1992) is also in progress.

Conservation strategies have been developed in light of this ongoing research programme. Regarding the geoarchaeological records, reforestation of parts of the site, notably in the vicinity of the *Vicus Augustanus* may have implications for the local preservation of the archaeological landscape. Mechanically ploughed furrows are highly visible on aerial photos and magnetometer surveys. The effect on the dune ridge record has been to partly fragment the continuous shore-parallel topography in these areas; however it is still possible to track individual ridges through the site. The development of the modern forest ecology has been investigated as part of the wider Laurentine Shore Project (Brown In preparation).

### **1.2.1. The Laurentine Shore Project**

This thesis is part of a larger research group consisting of collaboration between the Dept of Classics (RHUL) directed by Prof. Amanda Claridge, and the Dept of Geography (Loughborough University) directed by Prof. Helen Rendell. Within this thesis some of the work from the wider research project has been incorporated. This consists of the Digital Elevation Models (DEMs) of the *Vicus Augustanus* and *piscinae* produced by various researchers from RHUL<sup>3</sup>. In addition preliminary research and ongoing expertise in constraining the development of the Tiber Delta at Castelporziano by Prof. Helen Rendell (Rendell et al., 2007) has been incorporated into some of the analysis and interpretation in chapter 5. In addition a palaeoenvironmental perspective of the Late Holocene has been investigated by Brown (in preparation) and has contributed to the overall project. Analysis and interpretation from that thesis (Brown, in preparation) are not integrated into this thesis. All other work presented in this thesis is the work of the author and assistance is acknowledged where appropriate.

Archaeological work at Castelporziano has been undertaken since 1983 under the direction of the Soprintendenza Archeologica di *Ostia* and Professor Amanda Claridge (BSR / RHUL) (Lauro 1985; Lauro 1988; Lauro 1998; Lauro forthcoming). The high levels of preservation of the *Vicus Augustanus* and the high-status villas collectively known as the Laurentine Shore provide a rich archaeological record (figure 1.3). The protected status of the Estate and *relatively* undisturbed dune ridge dominated landscape provide a rare opportunity to investigate an *archaeological landscape*. Unlike many sites now preserved under ploughed fields, the well-preserved geomorphological record at Castelporziano (CP) can be integrated with the archaeological record without some of the deleterious effects that typically affect archaeological sites due to subsequent human alteration of the landscape.

---

<sup>3</sup> Dr Jari Pakkanen, Dr Peter Rose, Dr James Andrews and Time Evans (ADS) have been instrumental in developing the DEMs of the *Vicus Augustanus* and *piscinae*, their substantial work is gratefully acknowledged.

As part of the Laurentine Shore Project<sup>4</sup>, the Rome's Maritime Façade aspect integrates this long-term investigation of the Castelporziano archaeological record with bespoke geomorphological (Hansom 1998; Rendell 1998; Rendell et al. 2007) and palaeoenvironmental studies. The present thesis is primarily the result of the geomorphological study incorporating some palaeo-environmental aspects. The project is funded by AHRC grant APN 18211 and is undertaken in collaboration with the Segretariato Generale della Presidenza della Repubblica Italiana, Soprintendenza per i Beni Archeologici di *Ostia Antica* and the Tenuta di Castelporziano.

Major elements in addition to the archaeological excavation and recording of major buildings and complexes are the development of a Digital Elevation Model (DEM) incorporating the topography around the *Vicus Augustanus* and *Piscinae*<sup>5</sup>. Magnetometry survey has also proved to be an effective means of remotely sensing buried archaeological features within the surveyed area of the DEM.

A preliminary study investigating the archaeological record's relationship to the development of the Tiber delta successfully identified the potential for a further geoarchaeological study linking delta progradation and the relict archaeological shoreline, and the effectiveness of K-feldspar luminescence dating techniques to accurately date the geomorphological record (Rendell et al. 2007).

### **1.3. Aim**

The overall aim of this thesis is to understand how the Laurentine Shore, on the southern, distal end of the Tiber Delta, has developed during the Holocene using a Geoarchaeological approach. Several key objectives have been identified to fulfil this aim.

### **1.4. Objectives**

#### **1.4.1. To examine the processes affecting the coastal development of the site during the Holocene**

The contemporary geomorphology of the Laurentine Shore reflects developments in the Late Pleistocene and Holocene (Bellotti et al. 1994; Bellotti et al. 2007; Bellotti et al. 1995). The lowstand of sea level during the last glacial maximum (LGM) and the associated downcutting of the Tiber river mouth underpins the coastal topography, driving the hydrogeology and geomorphology of the site. The episodic development of the Tiber Delta is highlighted by significant shoreline progradation during the Holocene. It is therefore necessary to understand this history, in order to understand the relationships between formation processes and their geomorphological expression within the Holocene development of the Laurentine Shore.

---

<sup>4</sup> <http://www.rhul.ac.uk/Classics/LaurentineShore/> (last Accessed 5/08/2009).

<sup>5</sup> [http://www.rhul.ac.uk/Classics/LaurentineShore/MaritimeFaçade/MF\\_Reports.html](http://www.rhul.ac.uk/Classics/LaurentineShore/MaritimeFaçade/MF_Reports.html) (last accessed 5/08/2009).

#### **1.4.2. To examine the chronological development of the landscape, principally by dating coastal dune ridges, sand sheets and archaeological sites**

The macro-scale relationship between baseline eustatic sea level changes since the LGM (ca.18 ka BP) has a diachronic relationship to the formation of coastal foredunes linked to delta front progradation. By investigating the timing of formation of preserved dune ridges, other aeolian geomorphic features and archaeological remains, primarily through optical luminescence dating, the chronological development of the southern, distal end of the Tiber Delta and therefore Laurentine Shore can be established.

#### **1.4.3. To examine how the geoarchaeology of the Laurentine Shore is driven by macro-, and meso-scale processes of relative sea level change, delta progradation and key anthropogenic factors**

By examining the site at a range of spatial scales, it should be possible to understand the development of the geomorphological, environmental and archaeological records across a similar range of temporal scales. For example, meso-scale formation or preservation of individual coastal dune ridges is driven by the micro-scale processes of aeolian transport of sand-sized sediment grains with subsequent preservation by the development of a vegetation cover. Over decadal to centennial time-scales these individual dune ridges develop into the coastal dune field observed today and are affected by diagenetic alteration processes and anthropogenic activity. Processes of formation and alteration are mediated by a close relationship to hydrogeology driven by the interaction of the non-marine water-table and relative sea level. Anthropogenic initiatives and responses to environmental change must also be considered.

### **1.5. Research Questions**

To fulfil these objectives and the overall aim a series of research questions was developed.

**1.5.1. How has the coastline of the Laurentine Shore developed during the Holocene?**

**1.5.2. What are the processes of coastal development acting on the Laurentine Shore?**

**1.5.3. What is the chronology of these coastal changes?**

**1.5.4. What are the key interactions between anthropogenic and geomorphological processes?**

**1.5.5. What are the benefits of a multi-scale geoarchaeological approach and the implications for future research?**

### **1.6. Theoretical models**

In order to consider a Geoarchaeological approach, both the underpinning geomorphological and geoarchaeological models and frameworks must be made explicit. In the case of the Laurentine Shore, coastal dunes dominate the geomorphological record and the integration of pertinent theory must be discussed.

### **1.6.1. Geomorphological model**

#### **1.6.1.1. The study of sand dunes**

Bauer and Sherman (1999) discuss two schools of dune studies. *Mechanistic-Reductionist* research focuses upon detailed understanding of underlying physical processes of dune formation and sediment transport and deposition, and the ecology of the entire dune environment. Research is often long-term and models of this kind outline empirical relationships and the limits of the physical processes at work.

*Holistic-Constructivist* models observe the relationships and development of dune systems over varying scales of time and space; with a focus upon the meso-scale interactions of littoral, beach and dune systems (Hesp 2002). Models of this kind are useful for inferring the evolution of systems but are often limited to a particular scale and time. Without the rigour of long-term empirical measurements problems of equifinality are of concern. However, due to the large spatial and temporal scales and anthropogenic co-evolution involved in the development of the site, a holistic-constructivist approach has been taken.

#### **1.6.1.2. Holistic models: beach & foredune sediment budgets**

*“The fundamental concept in coastal geomorphology is that processes of wind, waves, and currents act upon the sediments to produce a set of landforms that are causally related. This relationship is described as a process-response model and it is the conceptual foundation for all geomorphological inquiry”* (Psuty 2008:11). At Castelporziano, understanding the interaction of changing relative sea level, delta progradation, and sediment budget upon inception, formation and preservation of dune ridge morphology underpins key macro- and meso-scale interactions. An integrated understanding of plant succession (Miyanishi & Johnson 2007) interlinked with coastal dune-beach development and sediment budget (Psuty 2008) is also valuable. The coastal foredune is developed and preserved at the back of the beach. Relatively stable, compared to the dimensional and temporal sensitivity of beach and offshore bar morphology to change (Psuty 2008), coastal foredunes and relict forms are the geomorphological focus of this thesis.

Several related sediment budget models have been provided for meso-scale beach – dune interactions (Short & Hesp 1982; Sherman & Bauer 1993; Psuty 1992) (Figure 1.4) and expanded pictorially by Miyanishi and Johnson (2007) (

Figure 1.5). Based on examining the effects of sediment budget variation upon spatial variation of dune and beach morphology, these models attempt to achieve an understanding of the whole system without the direct limitations of empirical models (Sherman & Bauer 1993). Psuty (1992:12) describes the prime conditions for foredune development as a slightly negative beach sediment budget where sand transport potential to the foredune is continuous. In order for foredunes to endure, the sediment deposition on the lee-side must be positive compared to that of erosion at the dune toe and face.

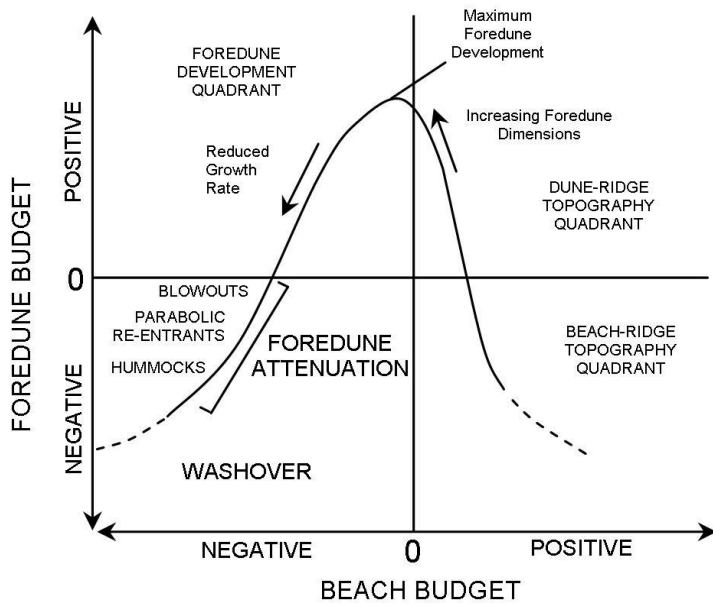


Figure 1.4: Sediment budget model (redrawn from Psuty, 1992).

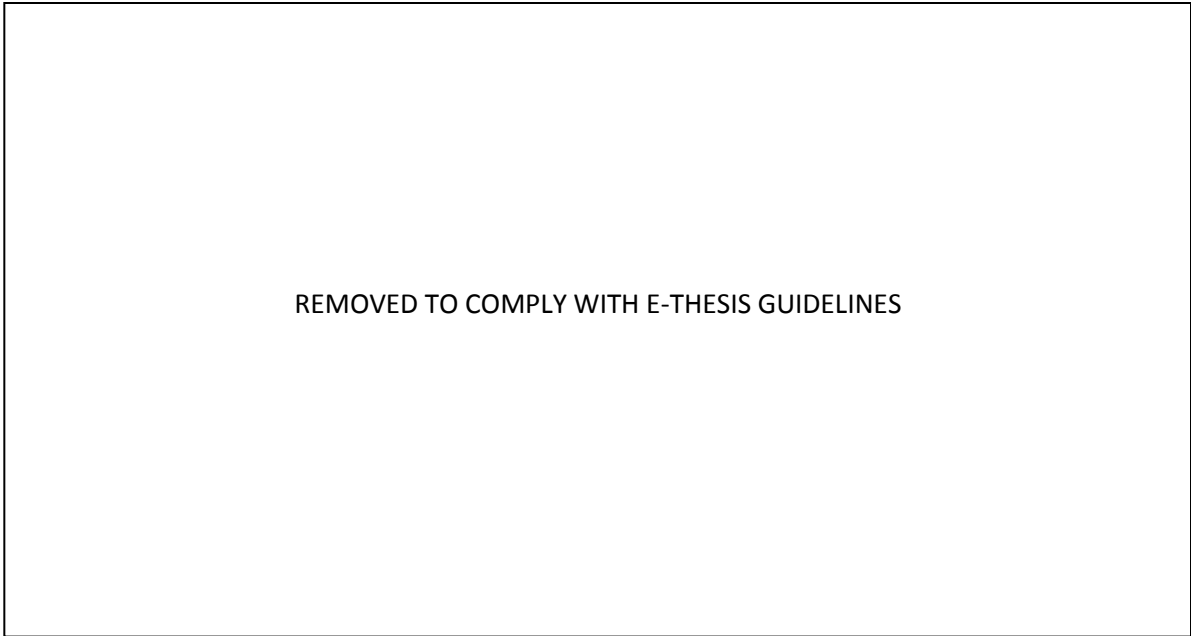
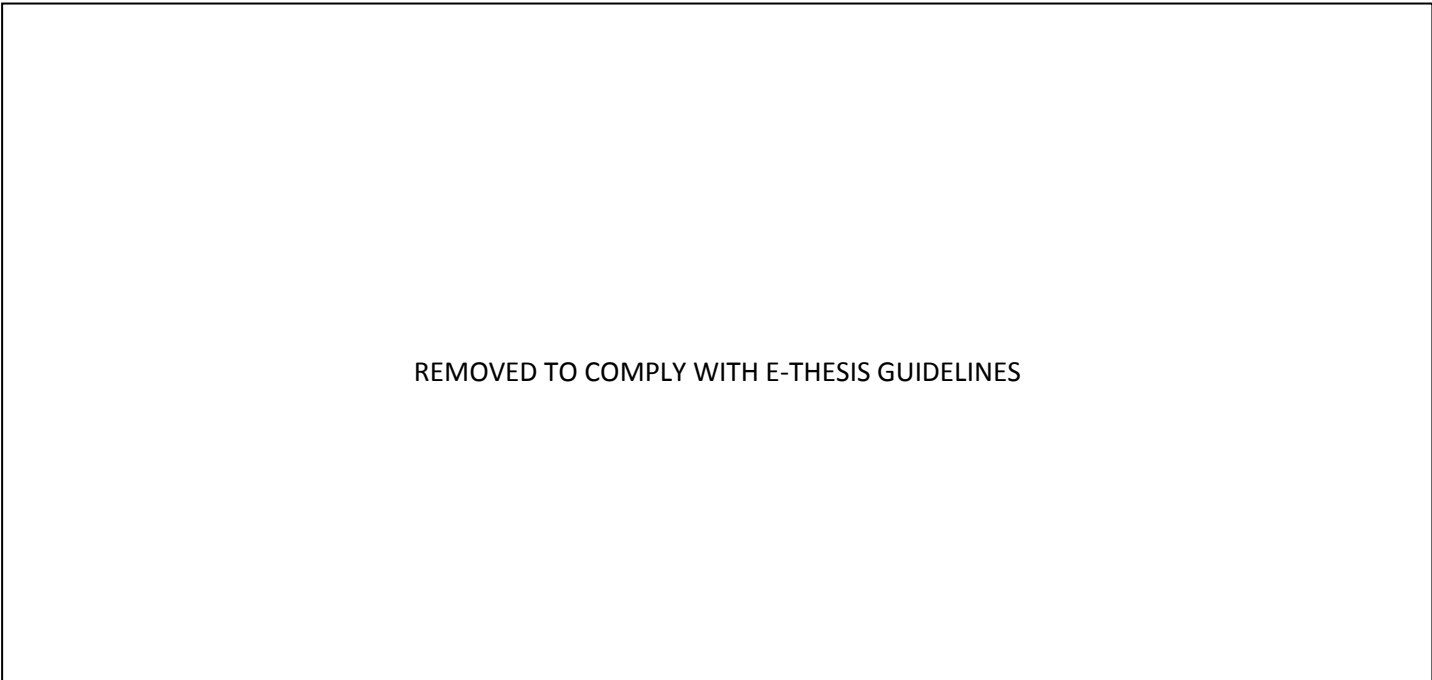


Figure 1.5: Pictorial representation of Psuty sediment budget model (Miyanishi and Johnson, 2007).

Spatial and temporal variations are important too. Alongshore variations in sediment affect the balance of the sediment budget which may change over time. Thus the “waxing and waning mode” of the sediment budget can be seen to continuously dictate the form of the beach-dune interactions (Psuty 1992:12). However, across different timescales comparisons in coastal dune research may be problematic (Sherman 1995). It must be noted that foredune morphology is spatially variable and linked to small-scale disturbance. Therefore changes in beach-dune profiles may not be fully representative of the alongshore extent of coastal foredunes (Figure 1.6). Hesp (2002), based on sediment budget models but with the integration of sea level change, provides a holistic model for describing the evolution of

coastal foredunes and outlines the dynamic equilibrium of several processes acting at different scales. The effect of a progradational coastline upon foredune morphology echoes morphology described by the sediment budget model of Psuty (Figure 1.4). The potentially pronounced impact of storm events is also highlighted (Figure 1.6 box D). Hesp also discusses problems of equifinality, especially in terms of interpreting the impact of sea level change upon coastal foredunes. The dynamic equilibrium of several processes that ultimately defines the morphology of foredunes at any given time can be significantly altered following change in one or more of these processes. Sand supply, wind regime, climate and potentially sea level changes are shown to induce a “relatively wide range of medium to long-term responses [from] a relatively small range of initial established foredune stages” (Hesp 2002: 254). By understanding the key formation processes and Holocene context of coastal development at Castelporziano, narrowing down the dune ridge formation parameters may improve the effectiveness of interpreting the geomorphological record in terms of these conceptual models.



**Figure 1.6:** Long-term morphology developments of coastal foredunes in respect to shoreline progradation (A), increasing levels of shoreline erosion (B) and ultimately (C). Box D highlights the impact of short-term wave erosion following storm events. Evolution of foredune morphology may occur (see stages 1 – 5) and development during accretion or revegetation may relatively improve stability (Hesp 2002). Box A also describes the relative morphological development of coastal foredunes presented in figure 1.5 linked to the sediment budget model (Figure 1.4).

### 1.6.1.3. Notes on coastal dunes at Castelporziano



**Plate (1a):** Looking NE, view of current foredune and strandline. **(1b)** Cleaned foredune section, aeolian sorting of light and heavy sand grains is recorded by dark bands of volcanic minerals. **(1c)** Looking NW, small nebkhas (20-30 cm across) aligned to onshore westerly wind (April 2008, A Bicket).

Field observations suggest that the sediment reaching the CP beach is very well-sorted, with further sorting by density occurring on the beach leading to a heavy mineral dominated beach surface between nourishment phases (plate 1a). Heavy minerals are incorporated into the modern foredune, visible as distinct laminations (plate 1b).

Winds are predominantly onshore, from a westerly direction (plate 1c), producing an oblique angle relative to the NW-SE orientation of the beach. The current coastal foredune displays extensive disturbance as blowouts, which may be partly due to seasonal storm activity rather than vegetation disturbance caused by recreation activity. Blowouts and occasional parabolic dunes are frequently observed as relict features within the inland dune ridge record. The current sediment budget at Castelporziano and all along the modern shoreline is argued to be negative. Fluvial management schemes (particularly damming) along the Tiber River catchment have reduced finer-grained sediment supply into the river (Iadanza & Napolitano 2006), and the effective armouring of the coastal regions by modern construction shifts sediment deposition along the shore (Lamberti et al. 2005; Ranasinghe & Turner 2006). Therefore it is highly likely that sediment supply to Castelporziano has been significantly modified during the 20<sup>th</sup> century. Beach nourishment has also been conducted at *Ostia* to the north since the early 1990s in an effort to preserve the tourist beaches from longshore erosion and counter-act the deposition of black sands for aesthetic reasons (Lamberti et al. 2005; Ranasinghe & Turner 2006). Preservation of the beach area has been attempted at Castelporziano by the plantation of *Ammophila littoralis* to fix at least some areas of the foreshore from erosion (De Lillis et al. 2004). Low hummocky dune forms, <50cm high, have developed with around 50% estimated vegetation coverage on the seeded areas after 10 years. The initial planting of *A. littoralis* has initiated the development of a small ecosystem of pioneer plant species, involving *Sporobolus-Elymetum farcti* and *Salsolo kali-Calkiletum maritimae* associations. The presence of capers (*Capparis* sp.), restharrow (*Ononis variegata*) and sea medick (*Medicago marina*), a species in symbiosis with nitrogen-fixing bacteria (*Sinorhizobium meliloti*), was also noted during fieldwork (pers comm FSJ Brown, 2008). The fact that after 10 years the dune forms have not developed into more imposing dunes is argued to be due to poor dune-building properties of *A. littoralis* (De Lillis et al. 2004), but may also be directly related to a reduced sediment supply. Towards the southern end



of the site, towards Tor Paterno, *tomboleti* dunes are preserved behind the modern foredune (Manes et al. 1997). These hummocky, nebkhas-like dunes, formed during historical times, appear to be post-depositionally modified by aeolian action, but the complex topography may also be related to the compression of dune formations towards the distal end of the Tiber delta as accommodation space decreases.

### 1.6.2. A Geoarchaeological approach for Castelporziano

*“Good research always combines inductive and deductive procedures and creative but rigorous testing”* (Butzer 2008:409).

Geoarchaeology is in essence the application of earth science techniques and concepts to answering archaeological questions (Renfrew 1976; French 2003; Rapp & Hill 2006). A discussion of contemporary Geoarchaeology is developed in chapter 6.

The ability to ask meaningful geoarchaeological questions is fundamentally linked to providing an accurate, data-driven geomorphological and archaeological context. This ability is driven by scale interactions. Understanding of scale is partly a function of sampling strategy and data quality but also of an evolving study of key processes driving the development and preservation of archaeological landscapes (Butzer 2008; Brown 2008).

Palaeo-environmental reconstruction, conditions and processes of geomorphological formation, an accurate chronological framework embedded in taphonomic and diagenetic history are key components of the geoarchaeological approach presented in this thesis. This kind of natural science approach can relatively easily answer questions of **what**, **how** and **when**, (Rapp & Hill 2006) but archaeological questions of **why** are much harder to resolve without subjectivity and speculative deductive inferences. Understanding human responses and initiatives in relation to their environment purely in geological/geomorphological terms is clearly of minimal help. However, in theory, with appropriate multi-proxy datasets and an integrated geo-archaeological approach, some geoarchaeological questions of **why** can be investigated. In reality in complex sites this may be achievable only in an inductive fashion by limiting the possibilities, by removing variables; *Occam’s razor* remains a fundamental tool of interpretation.

Therefore, a Geoarchaeological approach must go beyond a collection of sediment profiles from the vicinity of archaeological sites (Helgren & Brooks 1983); primarily because geoarchaeological questions can only be effectively discussed within a data-driven multi-proxy context considering archaeological and palaeo-environmental evidence equally. A focus upon understanding site formation processes (an enduring element of Geoarchaeological approaches i.e. taphonomy and diagenesis) is also critical for improving confidence in derived interpretations (Renfrew 1976; Butzer 2008). This evidence must also act on appropriate scales (see below); e.g. valley-scale geomorphological processes are unlikely to be sensitive enough to interpret human responses and initiatives in a particular location. Similarly understanding the archaeological development of a particular villa will not provide an understanding of the wider

landscape. Environmental determinism (Grove & Rackham 2001) or anthropocentric phenomenology are discouraged (Fleming 2005; 2006), and further clarification must be made between theory-driven *Landscape Archaeology* (Walsh 2008) and a data-driven Geoarchaeological approach. Recent meetings<sup>6</sup> focusing upon “*Geoarchaeology*” with considerable emphasis on developing a theoretical underpinning have portrayed an emerging discipline founded primarily in earth science and geomorphology<sup>7</sup>.

#### **1.6.2.1. A question of scale**

Issues of scale within geoarchaeology have been argued by Anthony Brown to be process dependent (Brown 2008). This suggests we must consider specific issues of scale for each key process and unravel their interactions. A multi-scale approach may then enable improved interpretative potential. For example, macro-scale research must focus upon macro-scale spatial/temporal interpretations (Wilkinson 2005); they are less able to clarify human responses and initiatives at particular locations and/or times due to this scale focus. Change within this scale is then understood in the context of macro-scale processes e.g. eustatic sea level change, catchment-scale sedimentation, regional climate. Macro-scale investigations are clearly insensitive to smaller scale variability and complexity. Likewise, meso-scale studies are less directly sensitive to macro-scale processes as smaller-scale signals may become dominant over long time-series processes due to spatially focused sampling strategy. It must be noted that in the literature scale is often considered on comparable spatial and temporal scales, i.e. macro-scale spatial with macro-scale temporal etc. Recent and extensive Geoarchaeology-focused special editions of the journal *Geomorphology* (2008, vol. 101, issues 1-2 & 3) have generally focused upon macro-scale spatial and temporal research or synthesis.

#### **1.6.2.2. A multi-scale approach**

The Tiber delta shoreline is considered as macro-scale, both spatially being several kilometres long and temporally, developing on millennial timescales (Bellotti et al. 2007). However, the archaeological development of the Laurentine Shore can be considered on meso-scale time, occurring on decadal to centennial timescales linked to specific phases of Tiber Delta progradation and directly to changing political regimes; the scale being directly related to the processes driving the development and preservation of the site. Geoarchaeological aspects of multi-scale / process inter-relationships are discussed in Bicket et al., (In review). Within a multi-scale context, human responses and initiatives are more sensitively recorded. Short-duration, but perhaps pronounced magnitude events have greater visibility and are therefore more viable as drivers of change within a multi-scale context. An example from Castelporziano would be the burning of large areas of the coastal forest following the Allied landings at the end of the Second World War that also brought in an invasive fungal infection to *Pinus* on the Estate from untreated crates (pers comm. FSJ Brown, 2009).

---

<sup>6</sup> <http://www.shef.ac.uk/scidr/geoarchaeology2009>  
<http://meetingorganizer.copernicus.org/EGU2009/session/652>

<sup>7</sup> See Renfrew (1976) in reference to early geoarchaeology and a desire to more fully integrate geomorphological tools and concepts.

These events, although not likely to be preserved in future regional pollen records, are important for the meso-scale history of the Castelporziano Estate by altering the modern forest ecology and inducing a variety of anthropogenic responses and initiatives linked to conservation. An archaeological example would be the evidence for storm damage destroying a 2<sup>nd</sup> century AD Severian-period sea wall near to the Imperial villa at Tor Paterno. Preservation of high-magnitude but short-lived weather events is likely to be very rare within the archaeological record but perhaps important for understanding human responses and initiatives to environmental variability.

### **1.6.2.3. Asking geoarchaeological questions**

In summary, considering a *Geoarchaeological Approach*, the ability to ask meaningful geoarchaeological questions, is effectively based on data quality and sampling strategy (Bicket et al. In review). Consideration must be made of site-specific human and geomorphological factors driving interactions that may or may not be scalable out-with the confines of the *site* and initial sampling strategy. There is a constant multi-scale dynamic equilibrium between all factors driving the form and preservation of the *site* including regional climate, tectonics and eustatic sea level down to site-specific (and sample-specific) events and processes of taphonomy and diagenesis. Reconstructing the past from palaeo-records requires an understanding of the recovered information within a set of interacting process-driven scales (Brown 2008). These dynamics may develop, or be observable on different spatial and temporal scales and preserve to a greater or lesser extent. Therefore the ability to ask and answer meaningful geoarchaeological questions is a product of these process-scale interactions and an evolving multi-proxy methodology and fundamentally linked to the underlying influence of geomorphological concepts and techniques. The quality and effectiveness of geochronological frameworks must also be vigorously assessed. The ability to accurately assess timing and change within geoarchaeological records is fundamentally underpinned by our ability to effectively constrain and accurately date them.

### **1.7. Thesis outline**

Bearing this approach in mind, Chapter 2 develops the site setting and the context of the overall geoarchaeological approach. Chapter 3 outlines the key methods with results and analysis discussed in Chapter 4. Chapter 5 develops these analyses and attempts to reconstruct the Holocene Development of the southern distal end of the Tiber Delta within the wider context of the Lower Tiber Valley and, regional and global environmental changes where appropriate. Finally, Chapter 6 provides answers to the research questions and proposes future work in methodology, techniques and fieldwork of benefit to research at Castelporziano and its environs. An assessment of a geoarchaeological approach in light of the primary literature and findings of this research and Geoarchaeology in general is also made.

## 2. Setting

The geoarchaeological development of the site can only be understood by examining the multi-scale context as described in chapter 1. The relative importance of long-term processes and short-duration events changes between scales of examination but all have an effect. Appropriate methodology is driven by these processes and events. Although the scales of context for geomorphological and anthropogenic processes and events are not necessarily directly comparable they must be accounted for. This also requires a conceptual view. An assessment of current geoarchaeological approaches within the longer-term context of geoarchaeological concepts is made below which informs the methodology and overall 'geoarchaeological' approach of this thesis.

### 2.1.A Geoarchaeological Approach

The Geoarchaeological approach simply described in chapter 1 is a commonplace description of the discipline found in the introduction of many of the published papers - i.e. *Geoarchaeology is the application of earth science methods to archaeological problems*. This sound-bite definition is generally upheld and is reminiscent of Rapp and Hill (2006). In order to more effectively answer the research questions outlined in chapter 1 a brief (but not exhaustive) review of other key Geoarchaeology reference texts is made below in order to derive a broader account of the Geoarchaeological standpoint. However it must be noted that this is primarily derived from geomorphologically focused Geoarchaeological research so as to provide a comparative context for the approach presented in this thesis and within the context initially set out by Renfrew (1976). English-language publications and European and North American researchers and institutions are also dominant but not exclusive; the scope of the research is, however, generally global. Examining issues of *Geoarchaeology: an international journal* and *Journal of Archaeological Science* confirms this. A recent in-depth review of the *Journal of Archaeological Science*, including the journal's contribution to the overall Geoarchaeological literature, is currently awaiting publication (Marriner In press). International and multi-lingual journals such as *Géomorphologie: relief, processus, environnement* and *Zeitschrift für Geomorphologie* also publish a broad range of Geoarchaeological research. Access to literature is the primary cause of this Western focus but is also representative of the dominant internationally available literature. An assessment of the Geoarchaeological approach attempted within this thesis is then made.

#### 2.1.1. Geoarchaeology: 1976

“...every archaeological problem starts as a problem in geoarchaeology” (Renfrew 1976:2).

In Colin Renfrew's preface to the 1976 volume “Geoarchaeology: Earth Science and the Past” (Davidson & Shackley 1976), whilst coining the term *Geoarchaeology*, he outlines several key objectives for the development of this emerging sub-discipline of Environmental Archaeology. These focal points are summarized here with reference to the terms set

out in this thesis; (1) chronology and stratigraphy, (2) taphonomy and diagenesis (site formation processes), (3) palaeoenvironmental reconstruction. With respect to point 2, Renfrew felt that the concepts and methods of geomorphology were yet to be fully integrated (Renfrew 1976:4). Also still of relevance is the assertion that the full potential of geoarchaeological research,

*“can only be realized...if fieldworkers perceive simultaneously both the archaeological aims and the technical methods appropriate for their realisation. And this perception can be made effective only by close collaboration actually in the field, by specialists who understand each other’s perspectives and language, by a real meeting of disciplines”* (Renfrew 1976: 5).

The practical experience of the individual reader will widely differ in this respect.

### **2.1.2. Geoarchaeology: an archaeological viewpoint**

In addition to providing an explicit scale framework for Geoarchaeology and a wide-ranging survey of Geoarchaeological research, Goldberg and MacPhail (2006) develop Renfrew’s concerns over interdisciplinary communication and provide a practical focus for integrating Geoarchaeology within multi-disciplinary projects and discussing the responsibility for publishing produced data (including the grey literature). Being able to glean and effectively communicate all the pertinent details from both archaeological and geomorphological research to be understood by specialists in both disciplines is not a simple undertaking.

Charles French offers a definition of Geoarchaeology from the viewpoint of Archaeology (2003).

*“Geoarchaeology is the combined study of archaeological and geomorphological records and the recognition of how natural and human-induced processes alter landscapes. The main aim of geoarchaeology is to construct integrated models of human-environmental systems and to interrogate the nature, sequence and causes of human versus natural impacts on the landscape. It is really only one major strand of environmental archaeology, which generally needs the collaborative support of several other sets of data, but a good understanding of it is essential for reading landscapes”* (2003: 3).

Three themes of Geoarchaeology are discussed, (1) recognition and decipherment of landform formation and transformation, (2) Recognising human impacts upon the landscape/environment, (3) Site formation processes (taphonomy and diagenesis). The first deals with prospection and understanding the geomorphological context of the archaeological sites, the second with integrating archaeological and geomorphological records. Scales and magnitudes of change, chronology, and a synthesis of long-term human-environment interaction in the landscape are seen as key outcomes, *“to identify interrelationships between the land, climate and humans”* (French 2003: 8). The third discusses

our ability to investigate these records as we find them which may often be dictated by very specific processes requiring a broad knowledge of methods for examining Geoarchaeological records.

### 2.1.3. Geoarchaeology: the state of the art

A brief synopsis of recent geoarchaeological research with a geomorphological focus is developed below. Of the 143 “Geoarchaeology” articles, meetings and books published in last 5 years included in Web of Knowledge (WoK) (on 7/09/2009), most articles are described under Geology, with just over half also described under Archaeology subject areas. The many more minor headings in part describe the vast array of methods and approaches to Geoarchaeological problem solving that are currently undertaken. This portrayed focus on geology and archaeology is clearly shown by the key subject areas of *Geoarchaeology – an international journal* (John Wiley & Sons). Of the 246 articles published in the last 5 years they are described 100 % by the subject headings Geology and Archaeology in WoK (7/09/2009) (figure 2.1). The recent development of Geoarchaeology as a distinct discipline is suggested by the inclusion of a specific “geoarchaeology” section (Luchsinger 2008) in the 2008 edition of the Encyclopedia of Archaeology (Pearsall 2008) since the 2001 edition (Murray & Credo 2001).

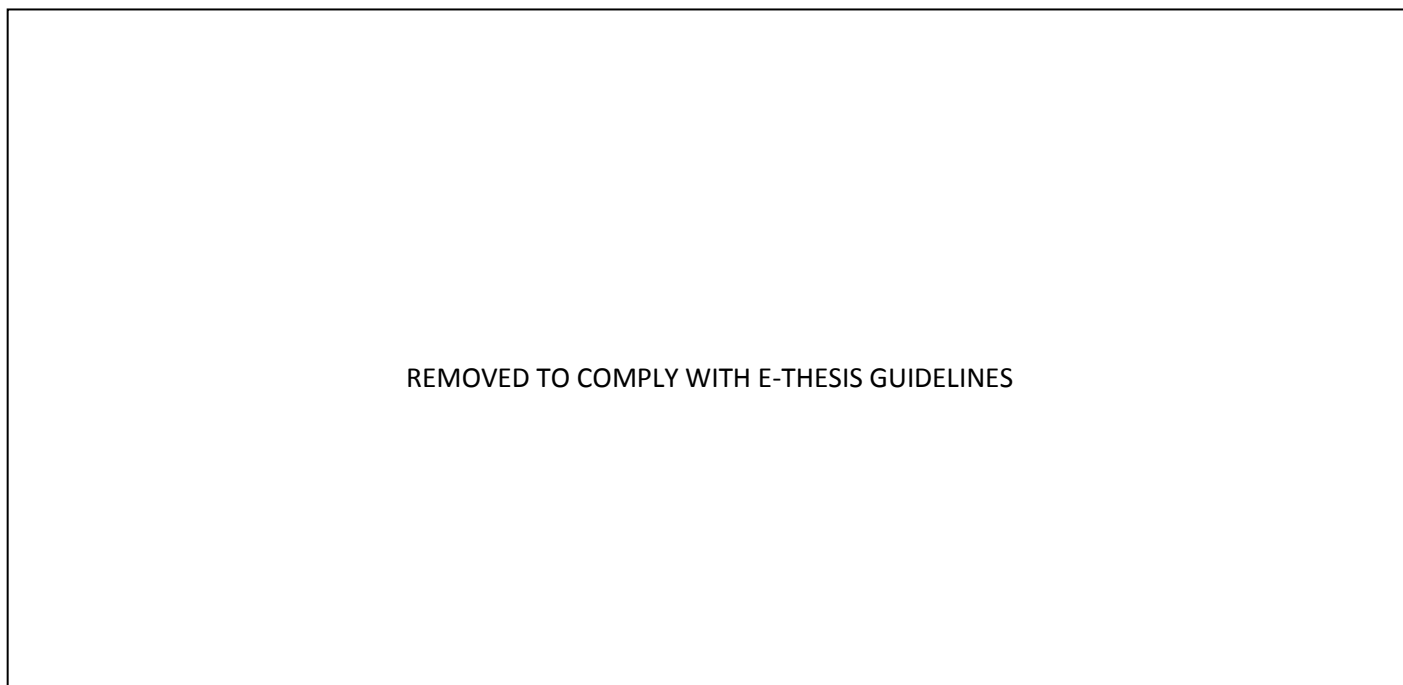


**Figure 2.1:** Subject areas of 143 Geoarchaeology (topic) meetings, books and articles citations featured in ISI Web of Knowledge (Thomson Reuters) within the last 5 years (7/09/2009). (<http://wok.mimas.ac.uk/>).

Key themes can be identified from a survey of the recent geomorphologically focused Geoarchaeology literature. The increasing body of ‘applications’ papers are indeed concerned with site- or region-specific geoarchaeological problems solved with appropriate multi-proxy methods and datasets (e.g. Ghilardi et al. 2008; Parker et al. 2008; Parker & Goudie 2008; Uribelarrea & Benito 2008; Bicket et al. In press). Additionally, specific papers focusing on appropriate and

adequate dating are of primary importance to Geoarchaeologists (e.g. Fuchs & Lang 2009). Conceptual models are being developed (e.g. Brown 2008; Hudson et al. 2008). Furthermore, assessment of taphonomy and diagenesis as precursors for more confident interpretations are extremely valuable (e.g. Bettis et al. 2008; Draut et al. 2008; Fanning et al. 2008; Waters 2008). Integrated methodologies and landscape prospection are also key areas where geoarchaeological approaches can provide valuable archaeological and geoarchaeological data (e.g. Wilkinson 2005; Brown 2009; Ghilardi & Desruelles 2009). The development of a 'Geoarchaeological approach' has been recently discussed at the Sheffield *Geoarchaeology: from landscape to laboratory* meeting with publications forthcoming in 2010. From this author's point-of-view, with recent advances in low-cost and effective GPS technology, rapid large-area surveys of ancient site distributions, infrastructure and palaeo-environmental and geomorphological resources are cheaper and more accurate than ever before. Geoarchaeological landscape prospection in conjunction with the GIS integration of long published datasets, site distributions, remote sensing and aerial photography back-catalogues, new hypotheses and reassessment can effectively be made (e.g. Guccione 2008), especially in areas where modern human activity has fundamentally altered or obscured the archaeological topography. Recent work by the British School at Rome and the Tiber Valley Project exemplifies this point<sup>8</sup>.

The explicit contribution of geomorphology to geoarchaeology, the primary focus of this thesis, is discussed in *Geomorphology* volume 101, issue 3 (Beach et al. 2008). An international and multi-scale discipline is portrayed. The editors argue for geoarchaeology to involve more geomorphic context and understanding of key formation processes; recently published work suggests this is underway (Thorndycraft et al. 2008). Recent research examining sediment budgets and cutting-edge landscape investigations could clearly be integrated with geoarchaeological perspectives in the near future (e.g. Brown et al. 2009).

Beach et al (2008) also discuss how Geoarchaeology could be of prime importance for developing initial surveys in regions of the world not yet well investigated (where resources and access allow). Within the context of this thesis this volume of *Geomorphology* also includes 3 articles investigating (and reassessing) Mediterranean Valley fills across a variety of scales, (Beach & Luzzadder-Beach 2008; Casana 2008; Cordova 2008). The ability to integrate this multi-scale research with regional climate records is also highlighted, improving the impact of the research within contemporary science as a whole and future climate change research. In this vein, the Editor's overall synopsis of Geoarchaeology is both realistic and hopeful, they "*continue to see geoarchaeology as a relatively under-used tool in understanding the long-term human–environment interactions, because research in this field can potentially provide a deeper appreciation for how these coupled dynamics play out over different timescales, and, thus, inform contemporary and even future-*

---

<sup>8</sup> [http://www.bsr.ac.uk/bsr/sub\\_arch/BSR\\_Arch\\_01Tiber.htm](http://www.bsr.ac.uk/bsr/sub_arch/BSR_Arch_01Tiber.htm) (last accessed 7/09/2009).

*oriented studies. This long-term perspective on the interplay of human activities and environmental change will, indeed, become an ever more important tool that guides future environmental planning”* (Beach et al. 2008: 414).

Geoarchaeology as a tool for understanding and contributing to long-term and future climate change is also developed by Butzer (2008). His discussion of the challenges that face Geoarchaeology focuses primarily on understanding taphonomy and diagenesis. However, a call for Geoarchaeology (and Archaeology for that matter) to engage further with historical and urban impacts upon the landscape i.e. conservation and social science, is also sounded to bring Archaeology of all persuasions into a more key role in the university curriculum.

#### **2.1.4. Reassessing Geoarchaeology**

With respect to the initial review of emerging Geoarchaeology (Renfrew 1976), the current literature and recent meetings suggest that Geoarchaeology is increasingly well-served by geomorphological concepts and methods. Effectively integrating the myriad datasets and specialist contributions may however be a huge and problematic undertaking (Wilkinson 2009). What may be more variable and harder to ascertain from the literature is the primary contribution of archaeologists to the research goals and approaches. The ability to understand the meso-scale temporal and spatial development of the landscape using palaeo-environmental reconstructions may not be completely useful to archaeologists trying to understand the micro-scale development of particular structures. For example, the ability of a Geoarchaeological approach to understand, contextualize and integrate the micro-scale archaeological record is increasingly well-served by micromorphological examination of archaeologically important deposits (e.g. Liu et al. 2009; Mallol 2006; Shillito et al. 2009; Tsatskin et al. 2009; Weiss et al. 2008; Vissac 2005) but all geoarchaeological research is fundamentally limited by the accuracy and precision of dating methods and then potentially the scale-sensitivity of coeval sediments in the landscape that would provide a broader landscape synthesis. In effect reconciling rapid but archaeologically (and geomorphologically) important processes and events is an ongoing restriction for Geoarchaeology and its contributing disciplines.

Taphonomic awareness is generally well developed in modern geoarchaeology if relatively rarely the prime focus of publications (e.g. Fanning et al. 2008). Geochemical and sedimentological techniques are now commonplace. Renfrew’s observation that “the methods of the geomorphologist [have] yet to be fully exploited” (4) has been addressed. Ground-truthing of geomorphological and palaeoenvironmental records in the archaeological record is not performed solely by interpreting change in terms of possible human impacts. Being a compound term, the archaeological component is deserving of a more central place in descriptions of “Geoarchaeology”. If Geoarchaeology is the application of Earth Science methods to archaeological problems, without a specific archaeological investigation where do the archaeological problems derive from? Without a specific and direct human element, descriptions of



archaeological remains in purely earth science terms are likely to underplay the significance of human initiatives and responses to their environment. Likewise interpreting environmental change in reference to a non-descript human factor is viable but does not reach the full potential of a Geoarchaeological approach (e.g. Waters et al. 2009; Wilkinson 2005; Wilkinson 2003). This is in part probably a consequence of larger-scale investigation where the integration of generalised datasets is sought to interpret broadly focused sampling strategies. For example trying to understand increased sediment supply in reference to anthropogenic deforestation across a valley may be preserved in alluvial and colluvial deposits but archaeological research has the potential to diachronically reconstruct the economy of sites to ascertain the demand and use for natural resources with which to better explain observed environmental change. Clearly interpretations can be made from either a geomorphological or archaeological point-of-view but integrating both records provides a more robust (Geoarchaeological) outcome, especially with consideration of similarly-scaled regional climate records.

As the term suggests, an integration of archaeological and geomorphological perspectives, in a holistic way may generate interpretations that are greater than the sum of their parts. At Castelporziano although it is clear from literary sources and site surveys that the upstanding archaeological remains had a strong relationship with the coast, they provide few details on the dynamics of the regional climate and macro-scale processes that have led to the progradation of the Tiber Delta which is ultimately linked to their existence and function. Equally a geomorphological approach allows us to understand these processes, but the responses and initiatives of the human communities living on the relict shoreline to environmental change elude this kind of examination. Only with detailed and integrated investigation of both these disciplines can we begin to understand the details as well as the bigger picture.

## **2.2. Multi-scale context**

The multi-scale context of the site is discussed below. Major archaeological, palaeo-environmental and geomorphological features of the site are outlined in general terms. Principal Geoarchaeological case-studies are described, highlighting the importance of their specific multi-scale context for understanding their formation and preservation and also ability to be adequately examined. The geoarchaeological approach is discussed in terms of asking meaningful questions founded in an integrated geomorphological/archaeological framework.

**Table 2.1:** Temporal scale framework of Tzedakis (2009).

	<b>Environmental regimes</b>	<b>Vegetation responses</b>
Mega-scale (10 <sup>6-7</sup> yr)	Tectonic transformation of continental and oceanic palaeogeography, long-term changes in atmospheric and oceanic circulation patterns and changes in atmospheric concentrations of greenhouse gases. Long periodic orbital variations	Evolutionary changes (adaptation, speciation, extinction). Appearance of new biomes
Macro-scale (10 <sup>4-5</sup> yr)	Orbitally driven (Milankovitch) climate variability, ice sheet build-up and decay	Glacial-interglacial vegetation cycles (ecosystem changes, individualistic response, refugia, migration, extirpations, divergence). Population contraction/expansion, replacement
Meso-scale 10 <sup>2-3</sup> yr	Millennial/centennial sub-orbital climate variability	Population contraction/expansion, replacement
Micro-scale 10 <sup>0-1</sup> yr	Interannual climate variability, fire, volcanic eruptions, pathogenic attacks	Disturbance, population collapse

Following the descriptive temporal framework of Tzedakis (2009) (table 2.1), from a physical geography perspective, the ‘scales’ considered in this thesis can be linked to the key processes of formation. In this way, the site-specificity can be linked directly to a wider context enabling comparison between sites and palaeo-records. With a certain level of introspection, the suitability of these geographical scales for assessing geoarchaeological development will be made throughout the thesis as the data allow. One immediate observation is that these geographical scales do not allow for specific human action, the principal focus of archaeology and therefore a critical component of a *geo-archaeological* approach. Within micro- and meso-scales anthropogenic influence may be most pronounced within the archaeological and associated palaeo-environmental records.

Mega-scale investigations are not in the scope of this study, but the key contribution of these processes is the building of the Italian peninsula. The development of relief and ultimately the Tiber valley, and the development of the western Mediterranean basins during the last 30 Ma (Mather 2009), especially the Tyrrhenian, constrain the immediate mega-scale context of the site. The global climate system is a key factor for understanding Holocene trends in climate variability within the Mediterranean, but also for understanding the causes of micro-scale extreme events, particularly those affecting human populations.

### 2.3. Macro-scale context (10<sup>4-5</sup>)

The focus of this project is primarily aimed at understanding the Roman-period palaeo-shoreline within a Holocene context. Therefore the macro-scale constrains the development of the site. Key interactions between eustatic sea level, the development of the Tiber River catchment and delta, regional (and globally-related) climatic forcing and also anthropogenic exploitation of the Tiber valley are important factors on the macro-scale.

#### 2.3.1. Sea level

Within the Holocene context of eustatic sea level, the downwasting of glaciers and the retreat of the polar ice caps following the late Pleistocene LGM drive the sea level within the Mediterranean basin. A limited connection to the Atlantic Ocean is made through the Straits of Gibraltar which sees the influx of cold Atlantic water driving a circuitous thermohaline circulation pattern around the Mediterranean Sea (Rohling et al. 2009). With particular relevance to this thesis important sea level reconstruction work has been undertaken by Lambeck and colleagues (Lambeck et al. 2004a; Lambeck et al. 2004b; Lambeck & Purcell 2005). Rapid sea level rise following deglaciation during the early Holocene was followed by a quasi-stillstand with a relatively slower rise in sea level during the late Holocene. Similar sea level curves have also been recently produced from the central Tiber Delta by Bellotti et al (Bellotti et al. 2007) (Figure 2.2).

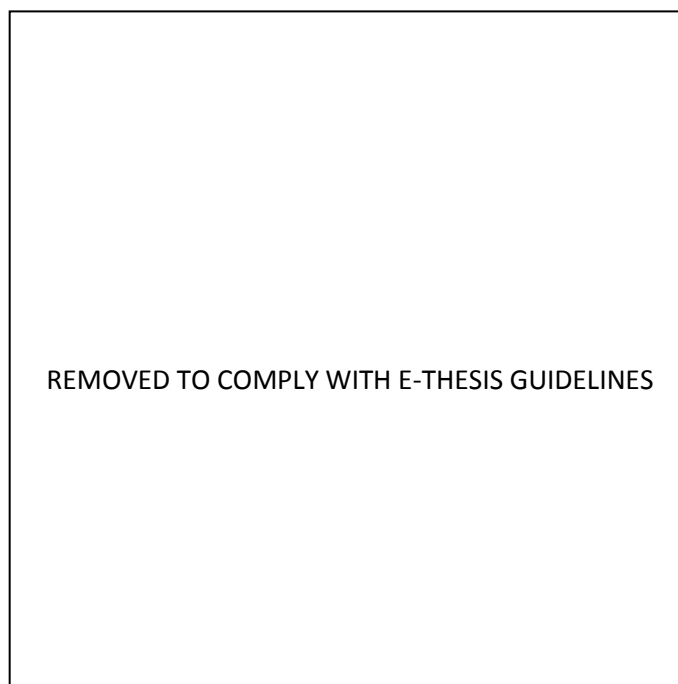


**Figure 2.2:** Sea level curve from central Tiber Delta (Bellotti et al., 2007).

## **2.3.2. Weather systems**

### **2.3.2.1. Exterior systems**

The characteristic seasonal Mediterranean climate of dry summers and wet winters is partly produced by global circulation patterns. The relative position of the polar front and sub-tropical jet-streams demarcates the extent of cooler and warmer air masses, affecting the distribution of surface weather patterns. Superimposed upon this global system is the seasonal position of the westerly wind belt and sub-tropical high pressure zone (Harding et al. 2009). During the summer, the northerly position of the sub-tropical high-pressure zone over the Mediterranean ensures a hot, dry climate. During the winter, a more southern position exposes the Mediterranean (especially the western Mediterranean) to the westerly wind belts bringing cooler and wetter weather.

The more maritime character of the western Mediterranean (including central Italy) is driven by the North Atlantic Oscillation (NAO). A weak NAO drives the track of north Atlantic storms and low-pressure systems into the western Mediterranean, which in turn induces weather systems within the Mediterranean basin (Harding et al. 2009).

### **2.3.2.2. Interior systems**

Climate variability within the Mediterranean basin can be summarised as the Mediterranean Oscillation (MO) calculated from pressure differences between the western and eastern regions. A key influence of the MO is the negative relationship with rainfall in the western Mediterranean (Piervitali et al., 1999 cited in Harding et al., 2009).

### **2.3.3. Cyclones & local winds**

A principle effect of north Atlantic weather systems is the development of cyclones in the Mediterranean; the active Gulf of Genoa cyclone being a key consideration for the western coast of Italy (Harding et al. 2009). Heavy rains occurring across the western Mediterranean, especially during the winter, are associated with 60 cyclones in an average year. During a SE tracking cyclone 26 storms have been recorded affecting Italy in a year (HMSO 1962: cited in Harding et al., 2009).

Depending upon the track of the Genoa system the development of the Bora or Scirocco wind is influenced. Two winds affecting Italy are the *Maestro* and *Gregale* (Harding et al. 2009). The *Maestro* is a NW summer wind associated with light cloud and pleasant weather. The *Gregale* is a cold, NE winter wind producing gale-force winds and rain (Harding et al. 2009: 78). In addition the winter *Libeccio* wind experienced on the western central part of Italy flows through the Straits of Bonifaccio and has been observed to produce a storm gyre in the Tyrrhenian Sea (Zecchetto & Cappa 2001). Storm waves associated with the wind can reach over 5 m above RSL (Zecchetto & Cappa 2001).

#### **2.3.4. The Tiber River**

The Tiber River drains an area of 17, 156 km<sup>2</sup> and is the largest catchment in Italy. Rising at Monte Fumaiolo in the central Apennines some 1,268 m above RSL, the Tiber flows 409 km southwards, and enters the Tyrrhenian Sea at *Ostia*, with a smaller branch entering at Fiumicino. Mean annual discharge has been estimated at 232.49 m<sup>3</sup>/s (Aldrete 2007). However, this masks a pronounced seasonality. Minimum and maximum annual discharges are around 60 – 1500 m<sup>3</sup>/s, respectively (Iadanza & Napolitano 2006). The river is served by 3 major tributaries, the Paglia, Nera and Aniene, of which the Nera and Aniene are the largest. The Aniene is notable as it drains the now dormant Alban Hills volcanic complex inland of Castelporziano. The sediment load measured between 1934 and 1973 was about 290 ton/km<sup>2</sup> (Iadanza & Napolitano 2006). The precipitation regime of the upper catchment is sub-coastal with most rainfall occurring in autumn and spring. The lower catchment is affected by a marine precipitation regime and receives most rainfall in the winter (Iadanza & Napolitano 2006), July being on average the driest month, November the wettest (Aldrete 2007).

#### **2.3.5. Geomorphology of the Tiber basin**

The Tiber basin drains a variety of rock types from carbonaceous to volcanic. The complex suite of rocks ultimately derives from the orogeny developed during the closing of the Tethys Ocean and the collision of several tectonic plates. The catchment is characterised by 4 geomorphological areas; carbonate Apennines, volcanic coastal, Pliocene marine and Pleistocene colluvium/alluvium in the valleys, and fine-grained flysch (Marra et al. 2008) and colluvial sediments in the upper catchment (Iadanza & Napolitano 2006).

### 2.3.5.1. Neotectonics

Bellotti and colleagues (Bellotti et al. 1994; Bellotti et al. 1995) present a series of shore parallel and obliquely orientated faults in relation to the Tiber delta shoreline (figure 2.3). Activity within these faults has not been presented as a major geomorphological process, with several recent studies describing the Tiber delta shoreline and lower Tiber catchment as stable (Lambeck et al. 2004a; Lambeck et al. 2004b). An uplift rate of 0.15 mm/yr has been suggested for the Lower Tiber plain (Lambeck et al. 2004a); since the Roman period an uplift of around 300 mm may have occurred, but the effects upon the Tiber Delta coastline are not well understood.

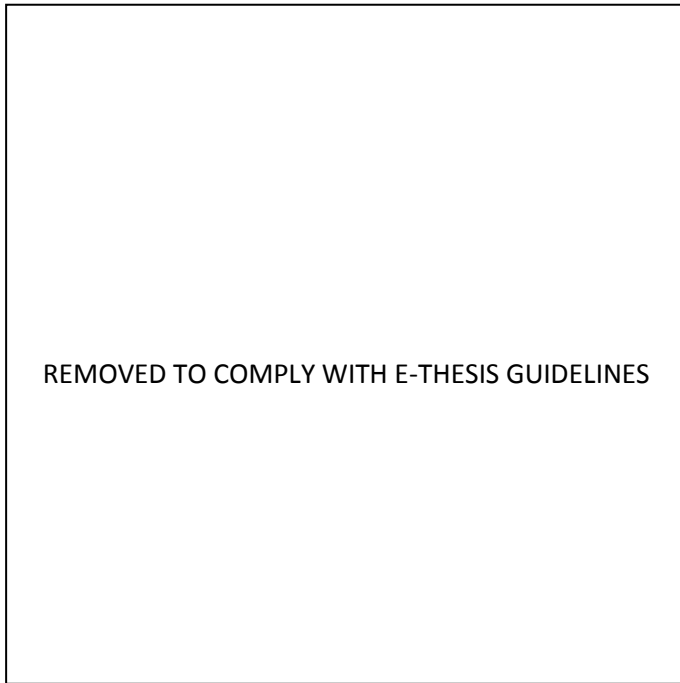


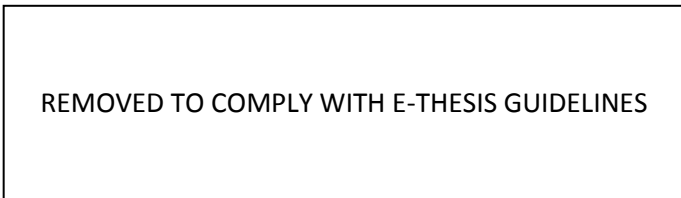
**Figure 2.3:** Geological context of the Tiber Delta (1) recent & present sediments, (2) volcanoclastic deposits, (3) acid vulcanites, (4) Plio-Pleistocene sediments, (5) Meso-Cenozoic sediments, (6) main tectonic lines (Bellotti et al., 1995).

### 2.3.5.2. Sediment supply

Sediment supply to the Tiber delta is predominantly from the Tiber catchment, with some elements of alongshore transport recorded by petrological studies (Garzanti et al. 2002). The sand-sized sediments from the site derive from two major geological sources. A volcanoclastic assemblage dominated by Augite and other ferro-magnesian silicates derives from the magmatic-arc that constitutes the uplands adjacent to the Tyrrhenian coast. Drainage from the Alban Hills volcanic complex into the Aniene tributary is a key pathway to the Tiber delta. The majority of the light silicate minerals, quartz and feldspars derive from the weathering of the back-arc basin exposed in the upper Tiber catchment (Coccioni et al. 2008). This back-arc basin relates to the Alpine Orogeny and provides remobilised detritus from uplifted basement rocks associated with this orogeny. Therefore this is also the only major source of metamorphic minerals into

the Tiber River (Garzanti et al. 2002). The major sediment sources feeding the delta can be characterised by this mixed provenance. 90% of the total sediment load of the Tiber is accounted for by the suspended sediment load (Iadanza & Napolitano 2006). Suspended sediment load discharging through Rome is presented in Table 2.2. Due to damming of the Tiber during the last century, the sediment load reaching the delta has diminished significantly (Aldrete 2007). The delta front is now undergoing erosion due to a negative sediment budget (Bellotti et al. 2007; Giraudi et al. 2009).

**Table 2.2:** Diminishing Tiber River sediment load measured at Rome between 1934 and 1993 (Iadanza and Napolitano, 2006) around 90% is suggested to be suspended sediment load.



### **2.3.6. Tiber Delta sequence stratigraphy**

The work of Bellotti and colleagues (Bellotti et al. 1994; Bellotti et al. 1995; Bellotti et al. 2007) provides a valuable examination of the central Tiber Delta and its Pleistocene and Holocene development (figure 2.4), the Tiber Depositional Sequence (TDS). This work uses a parasequence systems approach (e.g. Mitchum Jr & Van Wagoner 1991) to describe the macro-scale development of the Tiber delta. It is useful to consider an overview in these terms. The sequence stratigraphy sits upon an unconformity representing erosion during the Würmian/Devensian last glacial maximum (19 - 23 ka BP (Tzedakis 2009)) when the lowstand of sea level (ca. -120 m) exposed the sediments on the continental shelf. These deposits were later reworked during sea level rise, exhibiting significant gully erosion, and now sit below the present delta plain (figure 2.3).

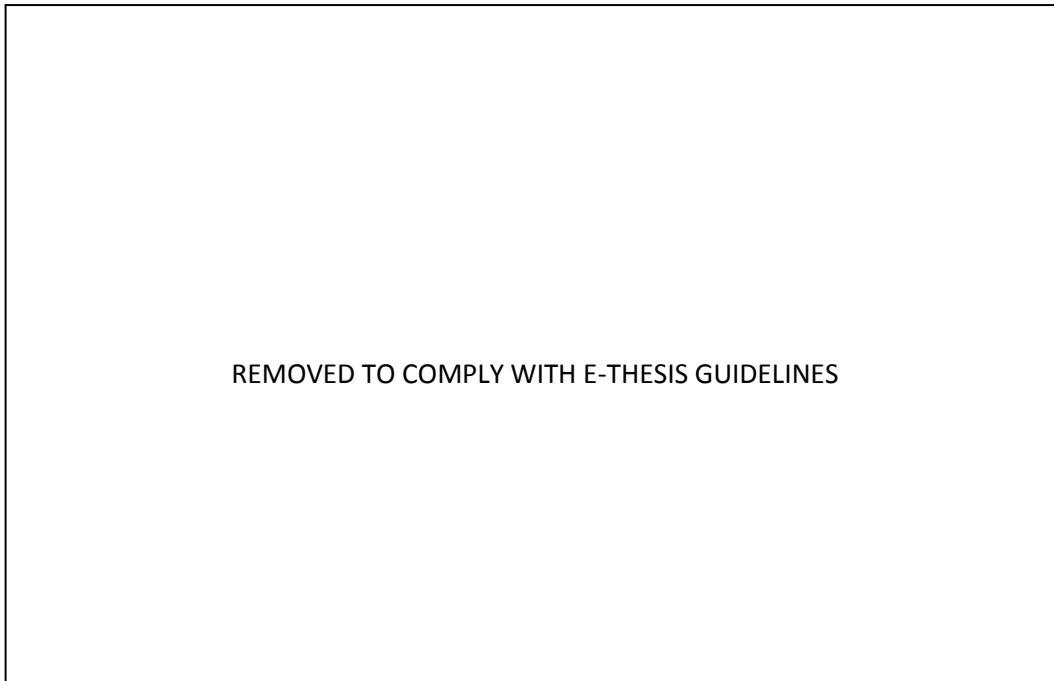


**Figure 2.4:** Central Tiber Delta Holocene parasequence stratigraphy (Amorosi and Milli, 2001).

The Transgressive Systems Tract (TST) sits upon the unconformity; the lack of a lowstand systems tract would appear to be a characteristic of the Tiber delta. The TST is by far the thickest and most laterally widespread set of deposits within the sequence; dimensions that are driven by the post-lowstand morphology of the basin. By 13ka BP sea level rise flooded the incised valley forming a bay. This shifted the river mouth progressively upstream. The river mouth position stabilised by ca. 9.5ka BP. The rate of sea-level rise drove the amount of accommodation space. As rates of accommodation space creation diminished, the deltaic sediments spread out with the Tiber river valley. The sediments retrogradationally stack landward and record three phases of lagoonal deltas dating from the latest Pleistocene to mid-Holocene (see figure 7c,d & e in Bellotti et al, 2007). Bellotti et al (1994, 1995, 2007) describe them as “fluviially-dominated deltas flowing into a lagoon protected by a coastal barrier” (1994:428). The sediment load was deposited mainly on the continental shelf. Peat deposits within the lagoon stratigraphy provided radiocarbon dates for periods of stillstand during sea level rise. These deposits also exhibit a coarsening-upward of facies associated with the rising sea level. The connection to the sea afforded the lagoon its brackish nature, which is reflected in the microfaunal record. From ca. 7 ka BP the Tiber delta becomes increasingly fluviially-dominated, but rising sea level still played a key role recorded by the retrogradational stacking of sediments. During the T<sub>3</sub> delta phase (figure 7e Bellotti et al, 2007) the lagoon began to infill up to the coastal barrier due to coastline retrogradation depositing the sediment load further inland. Thus the continental shelf became starved of sediment. Infilling occurred between ca. 5.2 - 4.7 ka BP.

The Highstand Systems Tract (HST) sits upon the maximum flooding surface of the parasequence stratigraphy (figure 2.4), below modern sea level. Sediment supply greatly outstripped accommodation space, leading to a progradational



delta front. This led to the development of a marshy coastal strip with frequently occurring ponds. By ca. 4ka BP the mouth of the Tiber reached the Tyrrhenian Sea. The delta became wave-dominated and developed into its cusped form. During the Imperial Roman period two harbours were built into the coastline roughly in the Fiumicino channel region of the delta; one built under Claudius in AD 52 the other under Trajan in AD 110. The Via Severiana runs along this old coastline through the Castelporziano estate, outlining the 1.8 ka BP shoreline (Bellotti et al 1995).

Bellotti et al (1994, 1995) argue that progradation was minimal until AD 1400-1500 when sedimentation rapidly increased with one quarter of the entire delta's volume being deposited in the last 500 years, which is also suggested by preliminary work at Castelporziano further to the south (Rendell et al. 2007). Initially the shoreline advanced at around 9 m/yr in the central part of the delta, the rate decreasing until the 1900s. As already mentioned, modern development and fluvial management have greatly reduced sediment supply at the delta front and erosion is intensive (Bellotti et al. 2007).

### **2.3.6.1. Expression of delta progradation at the distal ends of the delta**

Castelporziano lies on the southern, distal end of the Tiber delta. Although the coastline development is strongly tied to the development of the Tiber delta as a whole, the sequence of sediments in the parasequence stratigraphy is markedly different to that of the central delta region studied by Bellotti et al (1994, 1995). The central delta area is founded upon a deep and complex suite of fluvial sediments; the infill of the incised Pleistocene Tiber channel driven by the lowstand of eustatic sea level (Bellotti et al. 2007). Castelporziano lies outside this central zone, abutting a sequence of 'Pleistocene' sands (figure 2.5). The preserved geomorphology, driven by delta sedimentation, is linked to Holocene shoreline progradation but remote from direct fluvial activity. The landscape continued to be dominated by coastal shore-parallel dunes with the development of mixed oak forest with marshy depressions existing across this coastal zone (Hansom 1998). Within this context we must consider human initiatives and responses to the developing coastline. As the harbours at *Ostia* and around the delta area become infilled and sea level and shorelines changed due to sediment deposition and wave action, strategies for management and mitigation may also have changed.

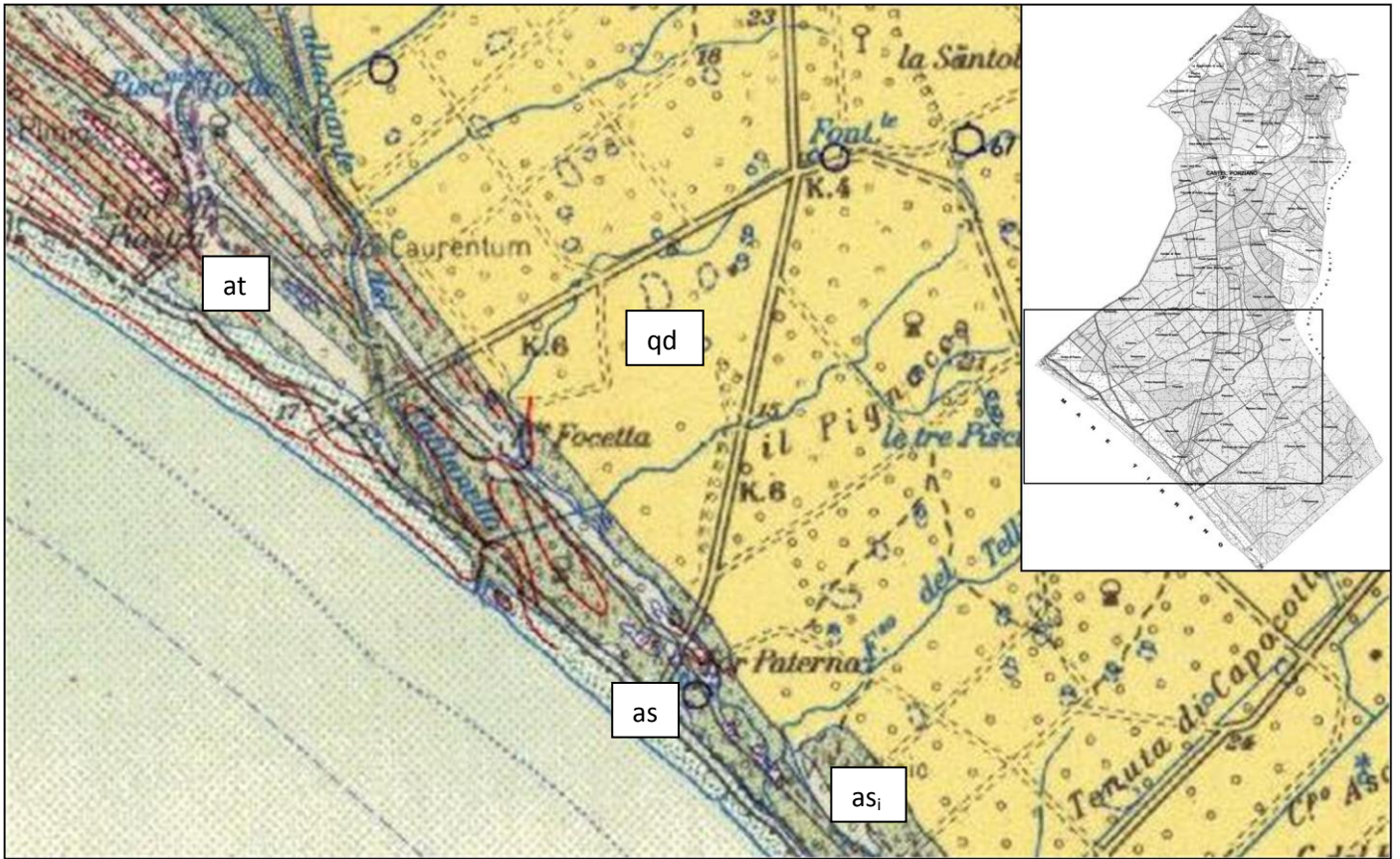


**Figure 2.5:** Detail of Carta Geologica D'Italia Foglio 149 (Cerveteri), focusing upon the Laurentine Shore between Tor Paterno and the *Vicus Augustanus* (Scavi di Laurentum). (**as**) refers to Deltaic littoral dunes and (**as<sub>i</sub>**) interdune deposits. (**at**) refers to ancient deltaic alluvium - filled with lime, yellow clay, peaty layers with malacological remains and palustrine flora. The pale amber inland formations are described as (**qd**), ancient reddened sands with ferric coatings; small interdune depressions (piscine); blanketed by siliceous gravel from streams from the ancient coastal plain ([http://www.apat.gov.it/Media/carta\\_geologica\\_italia/tavoletta.asp?foglio=149](http://www.apat.gov.it/Media/carta_geologica_italia/tavoletta.asp?foglio=149) last accessed 9/09/2009).

### 2.3.6.2. Marine transgression & delta progradation: a complex relationship with Holocene eustatic sea level rise

The early- to mid-Holocene morphology of the wave-dominated Tiber delta is characterised by relative sea level rise and significant marine transgression (Bellotti et al. 1994; Bellotti et al. 1995; Bellotti et al. 2007). In contrast, the late Holocene is characterised by delta progradation as the Tiber delta becomes fluvially-dominated but with relative sea level still rising. Rendell et al (2007) have estimated a five-fold increase in delta sedimentation during the post-Roman abandonment of Castelporziano. The inference is that fluvial sediment transportation has substantially increased whilst creating a complex relationship between coastline progradation and marine transgression. Understanding the geomorphological response to sea level rise is therefore an important research goal. Sea level research along the adjacent Tyrrhenian coast has estimated Roman sea level at  $-1.35 \pm 0.07$  m (Lambeck et al. 2004a). Sea level provides the base-level for coastal dune formation, whilst also driving the surface area for dune and beach sediment supply (Psuty 2008; Psuty 1992). So considering a 1m rise in sea level over the last 2000 years is critical for spatial

understanding of macro-scale processes. These processes are coupled to an increase in delta sedimentation and the underlying conditions for the formation of the coastal dune system which in turn impacts upon anthropogenic activity on the Laurentine Shore. The archaeological record must be placed within a wider temporal and spatial context of Tiber Delta development to fully understand its development during the late Holocene. To that end, preserved coastal dune ridges and sand sheets have been examined.

#### **2.4. Unraveling the climate of Castelporziano**

A relatively more arid Mediterranean-type climate has been argued to have existed for around 5000 years (Grove & Rackham 2001; Magny et al. 2002; Marchetto et al. 2008). With hot, stormy summers and associated drought and milder, wet winters this is an important consideration for examining dune ridge diagenesis which is driven by the hydrologic, geochemical and temperature climates (Pye 1981). It is also important for the preservation of palaeoenvironmental and geomorphological records in general. Unlike NW Europe, the preservation of pollen, diatom and other biological records is more fragmentary and significantly more site specific due to fluctuations in waterlogging and water tables. Castelporziano exhibits an alkaline geochemistry (pers. comm. F, Brown 2008), which does not favour the preservation of pollen. Therefore detailed *in situ* palaeoenvironmental records currently elude analysis within Castelporziano. This is due in part to the terrestrial influence of alkali ions in groundwater and sea spray key drivers of vadose diagenesis, acting along this littoral site, (McLaren 2001; Gustafsson & Franzen 2000; Gustafsson & Franzen 1996). Specific elements of the climate are discussed below with reference to scale.

#### **2.5. Meso-scale context ( $10^{2-3}$ )**

##### **2.5.1. Geoarchaeological scale**

In this case it is useful to define the meso-scale in a geoarchaeological context. The entire Castelporziano Estate, covering an area of a few kilometres square, can be categorised as a meso-scale site as it developed over the Pleistocene and throughout the Holocene. Sediment supply to the site is a meso to macro-scale process but the reworking of beach sand into a foredune is represented temporally and spatially, as a micro-scale process. The instigation, development and fixing of the foredune may take around 30-50 years (Hesp 2002). If we were to examine the archaeology at Castelporziano at this scale, we would catch a glimpse of the lifetime of a building but be ignorant to the larger-scale processes that created the ground beneath the foundations. The development of the entire dune ridge record at Castelporziano driven by delta progradation would be viewed as a meso-scale geomorphological process taking 100-1000+ years to be fully expressed. Archaeologically this would encompass the duration of the entire Roman Empire. Clearly if we wish to derive a more detailed understanding of human initiatives and responses within the environment, the meso-scale must be broken down. In a Braudelian sense, we can view the disparate micro-scale

processes (événements) as building into the meso-scale processes and paradigms that can be examined in relation to the context of the macro-scale *longue-durée* (Braudel 1972). This implies that as we focus on increasingly larger scales we must generalise and homogenise the data. Whilst this may be appropriate with the geomorphological record, the richness of the archaeological record argues for retaining a sense of distinctiveness and a network of individual places (Horden & Purcell 2000). Asking geoarchaeological questions on this scale goes beyond merely applying earth science techniques to archaeological sites (Rapp & Hill 2006). Recent geoarchaeological meetings would suggest that the geomorphological toolkit may have limitations for fully integrating the archaeological record, and sediment profiles are poor proxies for human endeavour. An integrated multi-strand narrative may also be problematic (Wilkinson 2009).

### **2.5.2. Interaction of key processes in the coastal zone**

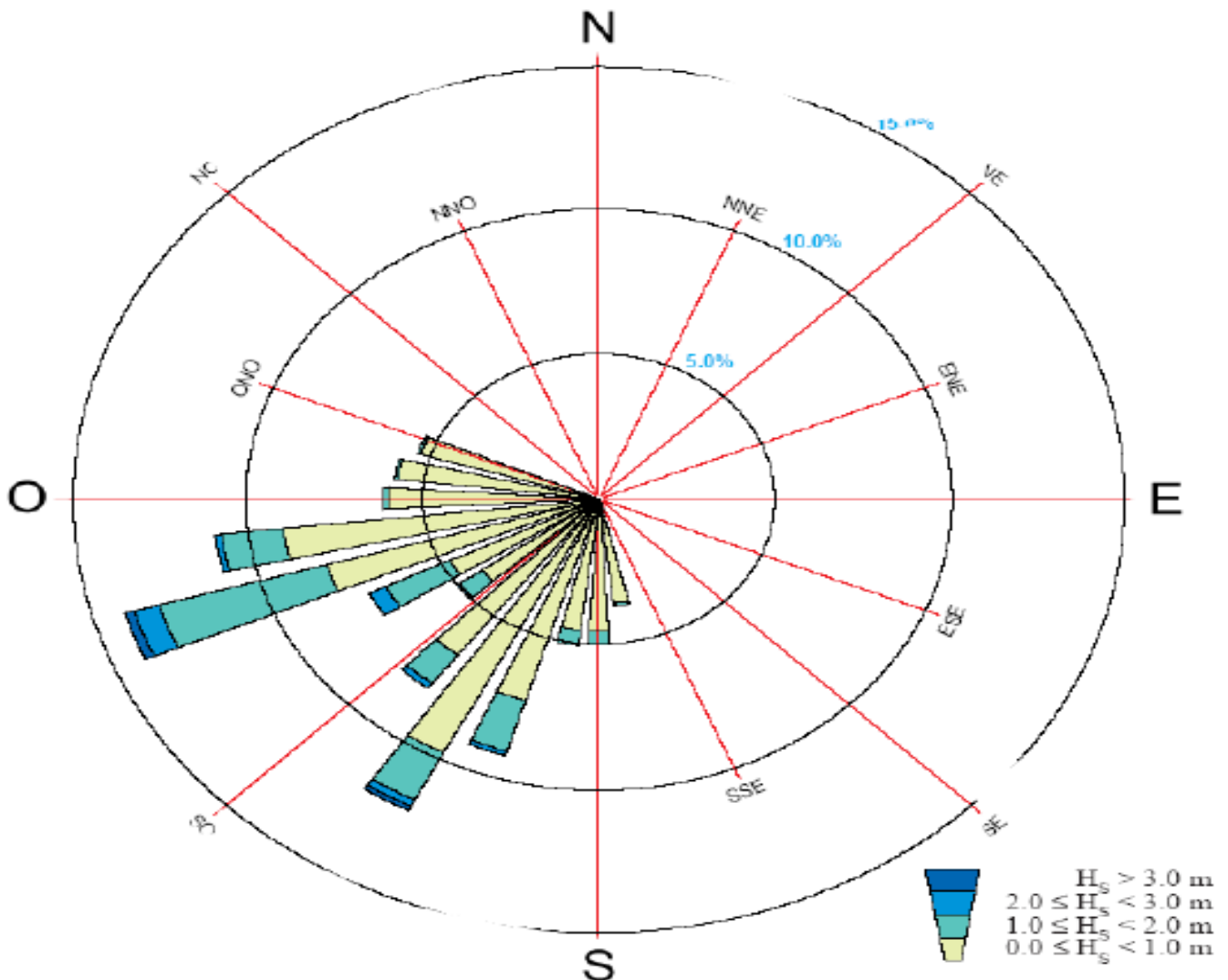
On millennial timescales, the progradation of the Tiber Delta from a bayhead to a cusped wave-dominated delta is the key geomorphological development underpinning the development of the coastline at Castelporziano. The maturation of a particular progradation phase - the formation of a foredune, stabilisation and development of vegetation cover - must be considered as the product of many interacting micro-scale processes. The centennial meso-scale processes that describe the geomorphological context of the Laurentine Shore will therefore be discussed in terms of these micro-scale processes and key features pertaining to the geomorphological record; with specific reference to Castelporziano where studies and data are available. An overall discussion of coastal dune systems is presented, following the holistic approach outlined in chapter 1.

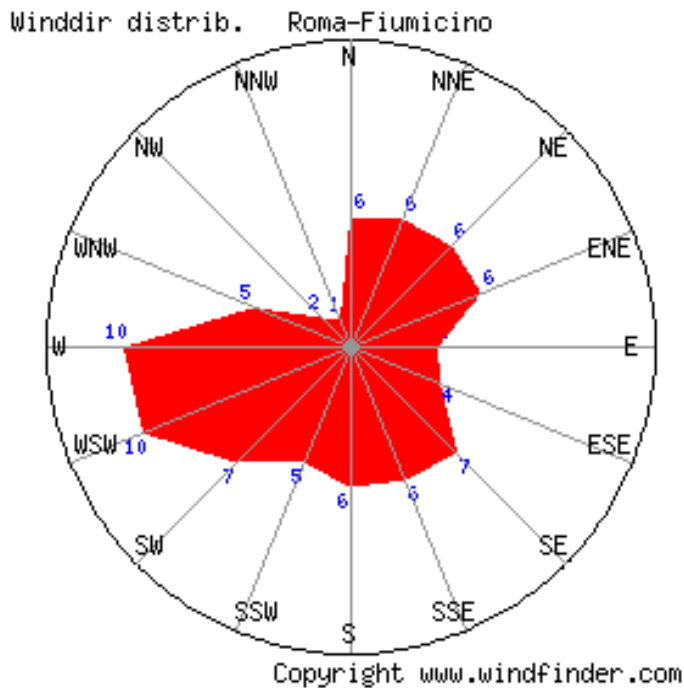
## 2.6. Micro-scale context ( $10^{0-1}$ )

### 2.6.1. The effect of tides, waves and winds on the Castelporziano shoreline

The tidal range of the Mediterranean is classed as micro-tidal (i.e. <2m) (Bourrin et al. 2007). At Fiumicino, central Tiber delta, the tidal range is around 0.4 - 0.6 m (Bellotti et al. 2007). Although the Mediterranean is an enclosed sea, there is still a substantial fetch area for waves to be developed, with storm winds exerting significant energy upon the coasts of relatively small basins like the Tyrrhenian Sea. The onshore wave direction at Lido di *Ostia* is WSW to SSW (figure 2.6) (Colzani et al. 2004) and is linked to the wind regime (figure 2.7). The sediment supplied to the contemporary beach is primarily transported by alongshore processes, by wave and tidal action across the delta front. Waves acting at the apex of the Tiber delta are deflected along the cusped delta front, leading to this alongshore sediment transportation. This alongshore current is at odds with the offshore SE-NW current of the Tyrrhenian Sea along this part of the coastline.

Figure 2.6: Wave magnitude and direction at Fiumicino (Colzani et al. 2004).





REMOVED TO COMPLY WITH E-THESIS GUIDELINES

**Figure 2.7:** (a) Average wind direction at Fiumicino between 10/2000 – 6/2009 daily measurements between 0700-1900 (local time)([www.windfinder.com](http://www.windfinder.com)). (b) Diurnal wind regime at Castelporziano during early summer (adapted from Fares et al., 2009). The dashed outline refers to the wind regime between 0600 – 2100 suggesting that a SW direction is dominant during this time of year.

The dynamic equilibrium exhibited by aeolian dune building is partly linked to beach sediment-supply (Hesp 2002). The current foredune also experiences significant disturbance and the exhibited blowouts in the current foredune are probably a result of aeolian erosion coupled to seasonal human disturbance (see chapter 1). Stability may be gained overtime with revegetation and/or dune accretion (Hesp 2002). There is a well-preserved series of dune ridges surviving at Castelporziano, providing the topography and pedogenic properties upon which much of the Estate’s arboreal plantation is founded (Francaviglia et al. 2004; Fares et al. 2009).

In winter, winds are generally offshore, in summer a strong onshore trend is maintained between April and September at Fiumicino<sup>9</sup>. The NE distribution of winds may be related to the winter *Gregale*, whereas the SE distribution may relate to cyclogenesis in the Gulf of Genoa (see above). However, there appears to be a diurnal wind regime affecting Castelporziano (Fares et al. 2009) (Figure 2.7b) with constructive onshore winds (dashed) prevailing during the day (0600-2100 hours). Summer is when precipitation in the catchment is reduced along with the frequency of flooding and therefore sediment supply (Aldrete 2007). The summer months are therefore likely to be the period of most dune building with favourable onshore daytime winds and a reduced sediment budget to the beach. The cusped morphology

<sup>9</sup> [www.windfinder.com](http://www.windfinder.com) (last accessed 30/07/2009).

of the Tiber delta means that this oblique WSW wind regime generally acts normal to the shoreline orientation (broadly NW-SE) which drives the orientation of coastal dunes at Castelporziano.

Whereas the general character of the onshore winds is constructive in terms of dune building, storm winds can also have a destructive effect, causing blowouts leading to wider instability of the foredune by weakening vegetation cover and the development of parabolic dunes. Greater energy drives waves further up the beach, eroding the nearshore area, leading to a fairly steep gradient on the nearshore beach and an angular berm; behind which a new generation of foredune may form. Onshore winds are responsible for mobilising the sand-sized sediments on the beach (Figure 2.7) driving them towards the foredune whilst sorting occurs due to grain-size, shape and density (and combinations thereof, related to the wind regime). The eroded foredune and deflated beach cross-section observed today suggests that this sediment supply is insufficient and that the sediment budget is currently negative.

### **2.6.2. Coastal Dunes**

The only true coastal dune is the foredune (Carter et al. 1990b; Bauer & Sherman 1999; Klijn 1990; Nordstrom et al. 1990). It is distinct from continental dunes by the interplay between aeolian processes and wave action (Hesp 1984) and other coastal processes such as long-term relative sea-level rise. The key components of foredune formation are sand supply, aeolian regime, rates of aeolian transport and erosion and deposition patterns (Bird 2000); influenced by vegetation communities (Arens 1996; Pluis & De Winder 1990), hydrology (Bakker 1990; Wiggs et al. 2004b) and soil formation (Jungerius 1990).

Themes of scale and variation are important when examining the formation and development of sand dunes. The aeolian mobilisation of single grains of sand and their development into extensive dune fields incorporates small to large-scale processes and provides a number of challenges to the researcher. Most notably are empirical field measurements of surface shear-stress ( $\tau$ ) (Sherman & Hotta 1990; Sherman 1995; Jackson & McCloskey 1997; Wiggs et al. 2004a; Hesp et al. 2005; Livingstone et al. 2007). Coastal dune systems, like other ecological habitats, vary with the yearly seasons and climate change, so the interactions between geomorphological and biological processes are in continuous flux (Bakker 1990; Clemmensen et al. 2006; Bate & Dobkins 1992; Jungerius 1990).

### **2.6.3. Incipient foredune formation**

Sand deposited upon the shoreline, damp and exposed to the drying effects of the wind and sun, becomes available for aeolian transport (Carter et al. 1990b; Bird 2000). Onshore winds drive dry sand grains, preferentially moving the smaller, lighter grain sizes towards the back of the beach. The density sorting can lead to the development of a lag surface due to deflation. Therefore spatial variations in grain-size can be observed. Alongshore sediment transport may add another axis of sorting to the sediments arriving on the beach (Frihy & Komar 1991; Abuodha 2003), a factor that is certainly important at Castelporziano. Vegetation, beach detritus or any other obstacle to the airflow above the sand

surface causes the deposition of aeolian sand by increasing surface roughness and, decreasing the transport capacity of the wind. This is achieved by inducing turbulence and decreasing the wind velocity. Sand grains thus accumulate within the base of vegetation communities (Hesp 1984), over rough shell pavements (Carter & Wilson 1990) and in the lee of beach obstacles. This initial phase of dune building is termed an *incipient foredune* (Hesp 2002). Hesp (2002) argues that incipient dunes may only form seasonally depending on the longevity of the plant species around which they coalesce. Preservation and development of incipient dunes may thus be controlled by plant succession (Mountney & Russell 2006). On some beaches, berm terraces created by tidal reworking of beach sediments to reduce the slope of the beach profile may also help to induce deposition as they form a new strandline for detritus and location for pioneer vegetation at the seaward, berm ridge (Otvos 2000). The implication of this incipient foredune fragility is that they are at the mercy of unseasonably strong or above average tidal action and winds until they can be fixed by vegetation or become established enough to be resistant to complete destruction.

#### **2.6.4. Foredune development**

Vegetation is a primary facilitator of foredune development (Arens 1996; Hesp et al. 2005). Sand transport across the dune surface is controlled by airflow. Airflow is affected by the incipient topography that is founded on, and augmented by, the vegetation cover (Arens 1996). As foredunes become increasingly established, unhindered by wind or tidal erosion they may develop almost continuously as neatly stratified structures or episodically (Carter & Wilson 1990). Erosion by wave and wind action serve to complicate the preserved stratigraphy as erosion features are infilled by new sand (Hesp 1988). Sand blowing across the surface is deposited around the pioneer vegetation, colonising the surface. Deposition also occurs on the dune toe (Arens 1996), and the lee side of the growing crest (Frank & Kocurek 1996). The height and spacing of foredunes depends upon the rate of sand supply, history of cut and fill events and positioning and stability of incipient foredune formation on the beach plain. Positioning is dependent upon the location of berm terraces (Otvos 2000), surface texture and efficiency of the specific plant community to trap aeolian sand (Carter & Wilson 1990). Thus the foredune gains height and width until sand supply is reduced by seaward, incipient foredune formation, restricting sand accretion to the stoss slope and dune crest of the previous foredune (Hesp 1988). Inland sand flux may be as little as 10 – 15 % after the formation of incipient foredunes (Carter & Wilson 1990).

#### **2.6.5. Foredune flora**

Throughout this period of foredune growth, vegetation is subjected to burial by the influx of sand, erosion of the sand surface and inundation and damage by storm waves and winds respectively. Therefore dune plants require suitably rapid growth rates and a hardy nature to continuously colonise the dune surface. However, Carter and Wilson (1990) observe that sand influx, burying plants, is quickly dispersed from the foredunes before it is consolidated but this is less efficient in more sheltered leeside locations making vegetation cover spatially variable across the dune cross-section. Damage can lead to a reduction in stabilising vegetation cover and the potential for erosion and blowout development



increases. Effective stabilising plant species are salt-tolerant, hardy, fast-growing, and may possess rhizomatous or stoloniferous root systems that increase their ground coverage and anchorage. Such are species of *Ammophila*, *Carex* and *Elymus* (Jungerius 1990). Carter and Wilson (1990) showed that vegetation biomass developing on mature foredunes increases significantly during the initial 10 to 15 years before stabilising, whilst producing small but increasing amounts of organic matter content. Moss (Carter & Wilson 1990) and Algal communities also have a significant role in dune stabilisation (Pluis & De Winder 1990). Algal mats growing throughout the dune structure, around the wet margins of dune slacks and on newly exposed areas of eroding dune surface, bind the dune sand with mucus extrusions (McLachlan et al. 1996; Grootjans et al. 1998). It has also been observed that they aid the germination of other dune plants by preserving moisture and nutrients within reach of developing dune-surface flora (Vazquez et al. 1998).

### 2.6.6. Dune soils

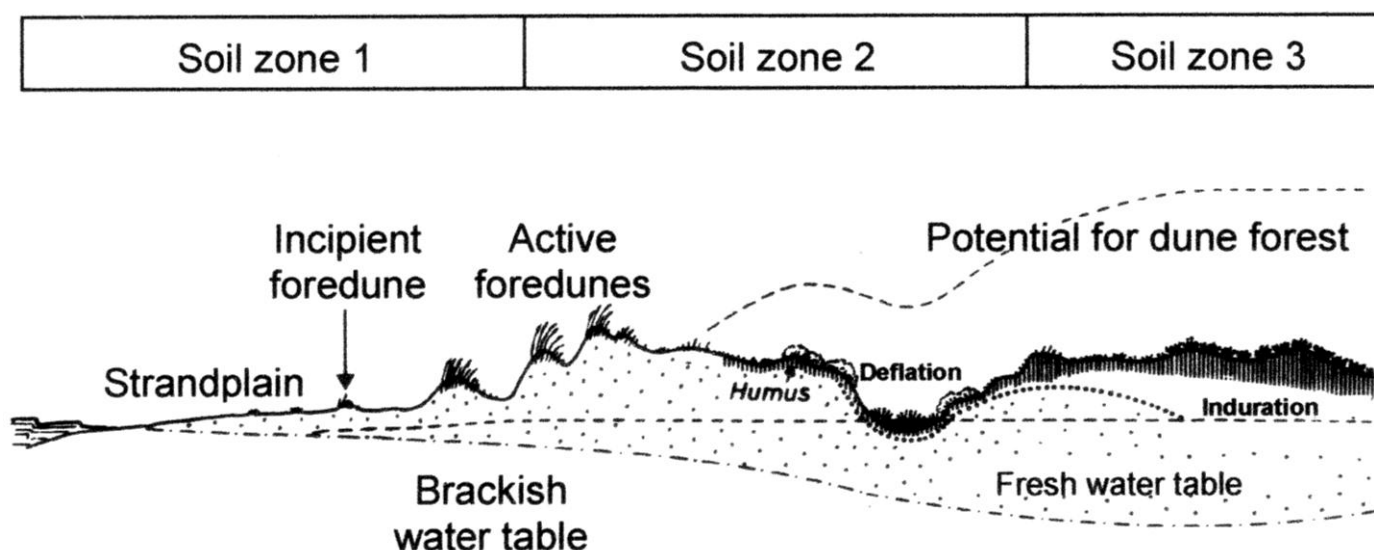


Figure 2.8: Dune soil zone schematic (adapted from Jungerius 1990).

Jungerius and van der Meulen (1988) proposed a model of dune soil formation based on work along the Dutch coast, the general features of which may be applicable to the coastal zone at Castelporziano. The model argues that significant interruptions by aeolian and hydrological processes during pedogenesis, not experienced in other continental soils, form a balanced system of destructive geomorphological and constructive biological processes. The geomorphological processes erode and rework the landscape, driving young and poorly developed soil profiles. The biological processes serve to stabilise and develop dune soils and landforms (Jungerius 1990). Jungerius (1990) outlines three distinct soil zones depending on the balance between the geomorphological and biological processes at work across the coastal dune landscape profile (figure 2.8). Zone 1 at the active foredunes and beach transition is characterised by a lack of organic A-horizons due to the instability caused by aeolian sand movement. Salt from sea spray influx is concentrated in this geomorphologically-active zone (McLaren 2001) and pioneer vegetation is possible but scarce.

Zone 2 is much more variable. Morphology varies over time and space linked directly to the local balance between geomorphological and biological processes. Relict foredunes and slacks are prevalent with highly localised soil profile development depending upon the spatial distribution of vegetation. B-horizons may be well-developed but colluviation causes erosion on slopes greater than 15°. Sediment profiles display alternations between soil horizons and sand burial. General trends in coastal soil formation were observed on foredunes on Magilligan Point, Northern Ireland (Carter & Wilson 1990) (however not within a Mediterranean climate). Soil organic matter content increased non-uniformly over a 20 year period exhibiting some binding of humus and mineral grains forming organic-enriched Ah horizons. Initial enrichment was slow but was seen to accelerate after around 15 years of dune stability. Concurrently, decalcification – reduction of CaCO<sub>3</sub> concentration – occurred, perhaps by leaching and vegetation root action (Stuyfzand 1998). The authors noted that humus accumulation was not dependent upon the initial carbonate content of the dunes and leaching of carbonate thereafter.

The coastal forests that cover much of Castelporziano have developed within a brown forest soil (Francaviglia et al. 2004). B-horizons are observed to be generally diffuse with only relative enrichment in organic content to differentiate ‘soil’ from underlying sand. In conjunction with the transition from the active coastal dunes to the inland relict dune ridges, pedogenesis is linked to gradients in salinity, acidity and organic matter accumulation. These processes drive variation in vegetation cover throughout coastal dune and slack environments (Sykora et al. 2004). Although much of Castelporziano is susceptible to soil acidification, the potential risk is limited to the small areas of reforested *Pinus pinea* and grassland (see section 2.6.10) (Francaviglia et al. 2004).

Zone 3 is dominated by biological processes. Vegetation stabilises the relict dune forms and certainly within the Castelporziano Estate the succession of plant species is well-developed with deciduous forests covering the majority of the littoral areas of the site (Manes et al. 1997). Pedogenesis is uninterrupted and soil profiles become increasingly well-developed. Moving inland, through zones 1-3, we can therefore see increasing stability, away from active aeolian



**Plate 2.1:** Section through mature forest soil; sampling location for CP07/22. Beneath humus-rich A-horizon a mottled carbonate-rich horizon is encountered. This is probably derived from the aeolianite parent material below. Test-pit is 1.2 m deep.

processes (plate 2.1). Zoning of dune soil ecotones has been observed elsewhere (Nishijima & Nakata 2004; Chen et al. 2005). Spatial variation across dune profiles is produced by local geology (Hansom 2001), climate (Clemmensen et al. 2006), hydrology (Bakker 1990) and biology (Goralczyk 1998), making the nature of individual sites unique on micro- and meso-scales but with identifiable larger-scale themes. At Castelporziano the inland reddened sand sheets (Old Dunes) are described as *Albic Luvisols* with rarer *Eutric Planosols* towards the most inland area of the Castelporziano Estate (Arnoldus-Huyzendveld et al. In Press). Their age has been suggested at around 125 ka, developing during the last interglacial the “Tyrrhenian” (Milli & Zarlenga 1991). These soil types are relatively rare within Italy and Europe (more commonly occurring in South America and Australia). The complex interaction between underlying volcanic parent material from the Alban Hills volcanic region, aeolian siliclastic sands and fluvial reworking drives formation, accounting for the relatively rare distribution across the coastal areas of Lazio and Latium (figure 2.9).

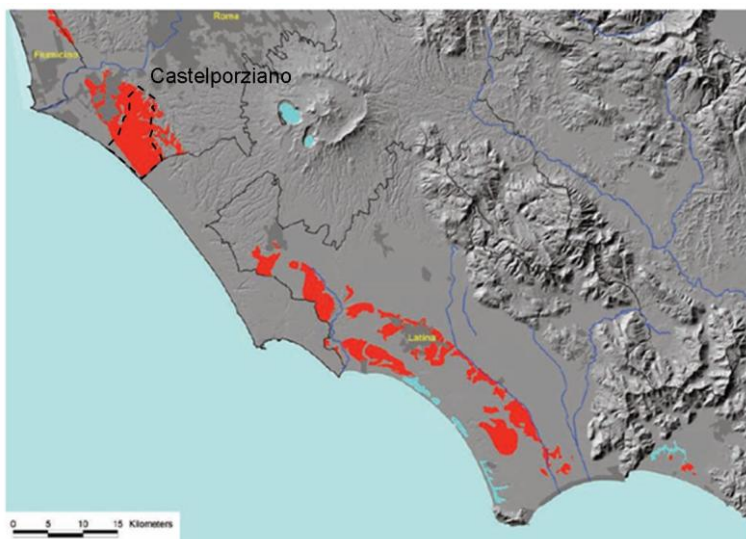


**Figure 2.9:** Distribution of planosols and luvisols in Lazio and Latium (adapted from Arnoldus-Huyzendveld et al., in press). The Tiber Delta and Alban Hills are clearly discernible in the NW of the map. The large extent of these rare soils characterises much of the inland area of the Castelporziano Estate.

Eutric Planosols (plate 2.2a) are not considered as good agricultural soils as they harden during the summer drought and have an acidic character. The peculiar soil properties relate to an elluvial upper horizon overlying an illuviated lower horizon rich in clay. Psuedo-gley and irregular interdigitation between the horizons is characteristic (Arnoldus-Huyzendveld & Gisotti 1999). The seaward portions of the reddened dunes at Castelporziano Estate were sampled during this project and are characterised by *Albic Luvisols* (plate 2.2b). Similar to Eutric Planosols, they are less well-developed, with a more discrete transition between the eluvial and illuvial horizons (Arnoldus-Huyzendveld & Gisotti 1999).

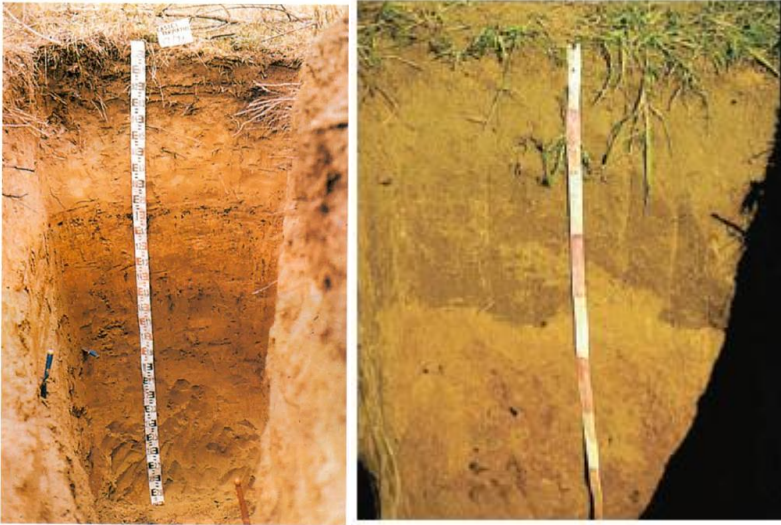


**Plate 2.2** (a) Eutric Planosol section; (b) Albic Luvisol section, both excavated within the Castelporziano Estate (Arnoldus-Huyzendveld et al., in press).

## 2.6.7. Foredune erosion

### 2.6.7.1. Wave truncation

During storm activity, increased magnitude waves can erode the front of the foredune, truncating the dune toe (Carter et al. 1990a). Reworking of the sediments can produce gently sloping pre-foredune terraces – berm terraces (Otvos 2000). On prograding or aggrading beaches with effective sand supply a new incipient foredune may form on the berm terrace, provided there are favourable sand supply and revegetation conditions (Hesp 2002). Infilling of truncated portions occurs at the steep, cliffed dune-toe provided that rapidly-repeating erosive events are not forthcoming (Bird 2000). This serves to preserve the dune cross-section, with the relict structures of aeolian bedding and past erosion events preserved within the body of relict foredunes (Hesp 1988).

### 2.6.7.2. Blowouts

The most characteristic feature of foredune erosion must be the blowout (Hesp 1988; Hesp 2002) (Plate 1a, Figure 2.10). Weakening of the vegetation cover on established foredunes occurs by seasonal or increasing climatic aridity, human activity, animal communities, or simply depletion of soil nutrients by the plant communities themselves (Carter et al. 1990a). Storm winds and tidal action reaching far up the beach bury plants with sand. They can also destroy the root bedding, killing off or exposing more of the plants to other erosion events, unless the plant communities can re-establish themselves (Hesp 2002). Rhizomatous or stoloniferous plants benefit from their extensive ground coverage and increased anchorage into the dune surface, prolonging their resistance to disturbance.

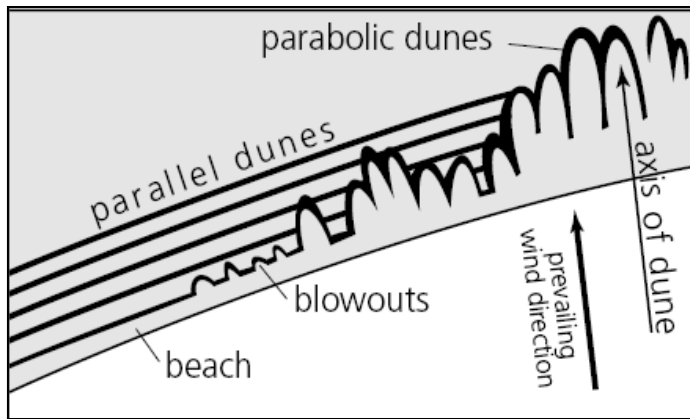


**Figure 2.10:** Schematic sequential development of coastal dune forms, from *foredunes* and *blowouts*, to *parabolic dunes* to detached *transgressive dunes* (adapted from Bird 1972, cited from [www.epa.qld.gov.au/register/p00080aa.pdf](http://www.epa.qld.gov.au/register/p00080aa.pdf) last accessed on 5/08/2009).

On areas of the foredune surface that have had their vegetation cover reduced, foredune sand is reworked by downwind transportation. Prolonged aeolian excavation leads to open breaches in the foredune and a fully expressed blowout. In less severe blowout erosion it has been observed that algal mats can rapidly colonise and stabilise the exposed surface (Pluis & De Winder 1990). The reworked foredune sand collects downwind of the breach either as an undulating sand sheet or developing as a parabolic dune.

### 2.6.7.3. Parabolic dunes

Parabolic dunes can develop from blowouts (Figure 2.10) and vice versa (pers comm. A Goudie, 2009). The apex of the dune forms from onshore aeolian sand transport with the seaward arms of the dune fixed by vegetation, anchoring the dune in place. Sand is transported up the convex stoss slopes of the dune depositing at the crest and lee side of the dune, widening the arc of the dune. If the vegetation is removed the parabolic dune becomes mobile, pushing inland as transgressive dunes to disrupt sequences of relict foredunes (Hesp 1984; Hesp & Thom 1990; Bate & Dobkins 1992; Bird 2000) (depicted in Figure 2.10). The recent dune ridge record at Castelporziano is characterised by several well-developed relict dune ridges but also by the formation of a large parabolic dune immediately inland from the coastal highway (see chapters 3 and 4 for further details).

## 2.6.8. Features behind the active foredune

### 2.6.8.1. Dune ridges

Dune ridges are a specific geomorphological form (Otvos 2000). They are “intertidal-supratidal, narrow, relict landforms” (Otvos 2000:105) and are essentially relict foredunes (Hesp 1984). The term ‘dune ridge’ will be used throughout this thesis and refers only to relict foredunes that no longer interact with the current beach. Furthermore, **primary** dune ridges will be categorised as relating directly to Tiber Delta progradation and foredune formation, whereas **secondary** dune ridges relate to remobilisation and are not directly linked to foredune formation.

The Castelporziano examples are also isolated from aeolian activity by the prograding shoreline. The key criterion for assigning the term 'dune ridge' is that the multiple ridge morphology must be a result of repeated strandline/berm formation. A well-preserved and developed beach ridge is a potential sea level marker, theoretically signified by the boundary of intertidal sediments and an overriding aeolian sand deposit (Otvos 2000), but this is not universally the case or well-proven (Otvos 2005).

#### **2.6.8.2. Deflation hollows**

Interdune areas, directly behind the active foredune undergo erosion/ deflation by turbulent, separated airflow on the lee-side (Frank & Kocurek 1996) This may continue until the susceptible grain sizes have been removed leaving an immobile surface lag deposit e.g. shell fragments (Carter & Wilson 1990). In sheltered areas, soil and vegetation may develop but this potential is increased once a significant new foredune is formed seawards of its predecessor, diminishing the affect of aeolian activity (Jungerius 1990; Otvos 2000). Once a foredune and associated post-dune slack/deflation hollow becomes preserved in this way, erosional and diagenetic processes increasingly homogenise the topography whilst the development of vegetation communities increasingly protects the relict dune system.

#### **2.6.8.3. Erosional processes acting on relict dunes**

Spatial and temporal variation exists within the coastal dune profile (Figures 2.8 and 2.10). Moving inland from the active foredunes, the effectiveness of aeolian sand transport, deposition and erosion diminishes and becomes increasingly marginal. Features of the coastal dune profile developing behind the foredune are now subject to other forms of erosion. Rain-splash and overland flow become more effective agents of erosion on stabilised, relict foredunes due to slope (Jungerius & Dekker 1990). Colluvial transport of sediments into the interdune areas occurs under unconcentrated slope wash conditions but during storm events, rills and alluvial fans can be created. The effect of this water erosion is to increasingly level the topography, filling in hollows and lowering dune crests (Jungerius & Dekker 1990:185). Slope wash erosion has a close relationship to the density of dune vegetation cover as on any other slope, with complete vegetation cover providing the most effective protection. This homogenisation of dune topography is well developed at Castelporziano with dune ridge crests becoming increasingly subtle to discern moving inland. The effect of aeolian redistribution must also be borne in mind as a major erosive process during periods of instability.

### **2.6.9. Hydrogeology of the Castelporziano Estate**

The interaction between fresh, salt and brackish water tables is important in the back dune area (Bakker 1990) especially with regards to the preservation of palaeoenvironmental proxy records linked to the hydrogeology of the Castelporziano Estate. Less dense freshwater floats above the saltier water tables at or near the vadose zone interface with the saturated, phreatic zone; intrusion by salt water into the freshwater table is governed by the balance of fresh water supply from the hinterland. Under dune ridges, the water table is higher than under slacks and may have an acidic, meteoric composition, with alkalinity derived from storage and transport as groundwater. The raised water table under dune crests may be exposed in the adjacent slacks as pools creating further ecotonal variation. Again, these forms are not static and vary temporally. Migrating transgressive dunes (i.e. parabolic dunes) may obliterate wet slacks, transforming adjacent areas into slacks (McLachlan et al. 1996). It has been observed that dune surfaces are highly water repellent during dry weather conditions. Repellence is highly spatially variable with vegetation cover and depth (Dekker et al. 2000). The nature and location of the water table relative to the surface clearly has a direct effect upon the nature and abundance of stabilising vegetation.

The macro-scale borehole survey published in 2007 (Bellotti et al. 2007) discovered the presence of a 40m deep incised tributary valley running parallel to the coast towards Castelporziano from the main Tiber channel. Due to the protected nature of Castelporziano, the borehole data do not extend into the Castelporziano study area. It is reasonable to assume that the catchment of this incised tributary valley (figure 2.11a) does, however, extend into Castelporziano, subsequently infilled by fluvial sediments by the early Holocene, c. 9.5ka, and buried under tens of metres of sediment (Bellotti et al. 2007). By 4ka BP, this incised tributary valley had been inundated due to sea level rise, developing as a marshy strand plain (figure 2.11b). These marshlands flanking the central Tiber channel endured until reclamation began in the 19<sup>th</sup> century (Bellotti et al. 2007).

**Figure 2.11:** (a) Lower Tiber River catchment ca. 20 k BP and, (b) ca. 4 k BP (Bellotti et al., 2007). The extent of the “*Ostia* lagoon” is determined by the Pleistocene catchment of the Tiber tributary draining what is now Castel Fusano and Castelporziano. Contours are in metres relative to modern sea level. The Castelporziano Estate is visible in the SE corner of each reconstruction. The dog-legged scar of the Canale del Pantanello is distinctive.

REMOVED TO COMPLY WITH E-THESIS GUIDELINES

Hydrogeological survey at Castelporziano between 1995 - 2000 describes the Pleistocene substratum of the Estate (figure 2.12). Contour lines of the palaeo-topography are directly comparable between Bellotti et al (2007) and Busuoli et al (2001). Elevated areas in the NE of Capocotta and the central part of the Estate between Infernetto and the Castel Porziano constrain the catchment of the Tiber tributary. The flow of freshwater aquifers highlights a bipartite landward and seaward drainage pattern (figure 2.12a). Flow-lines in the NW boundary of the Estate are intercepted by the position of the now-drained *Ostia* delta lagoon formed in the relict tributary valley (figure 2.12b). The coastal area of Castelporziano is, however, supplied with terrestrial groundwater from inland sources, suggesting the Pleistocene topography does not deleteriously divert supplies from the coastal zone of the Estate.



REMOVED TO COMPLY WITH E-THESIS GUIDELINES

**Figure 2.12:** Hydrogeological analysis of the Castelporziano Estate (adapted from Busuoli et al., 2001). (a) The isopach map is directly comparable to the contours of figure 2.7a, relating to the LGM drainage of the lower Tiber catchment. (b) The Holocene substrate burying this topography now constitutes the water-bearing terrestrial aquifers within the Castelporziano Estate.

**Figure 2.13:** Geochemical analysis of 22 wells across the Castelporziano Estate (locations shown in figure 2.12a) (Busuoli et al., 2001). A marine influence (*mare*) upon terrestrial groundwater is not observed in this modern dataset.

REMOVED TO COMPLY WITH E-THESIS GUIDELINES

Geochemical analysis of 22 groundwater wells shows that the aquifers were entirely supplied by terrestrial sources with no marine intrusion. This includes data from at least 5 wells adjacent to the modern coastline (see figure 2.13) (Busuoli et al. 2001).

### 2.6.10. Vegetation at Castelporziano

REMOVED TO COMPLY WITH E-THESIS GUIDELINES

**Table 2.3:** Vegetation cover in the coastal plain (Fares et al., 2009).

The modern vegetation cover of the coastal dune ridge area is dominated by low trees and shrubs typifying the coastal maquis and garigue ecozones (table 2.3). *Arbutus unedo* (strawberry tree), *Rosmarinum officinalis* (Rosemary) and *Quercus ilex* (Holm Oak) make up over 50 % of the ground cover (Fares et al. 2009). Further inland, deciduous trees and hygrophilous species become dominant where hydrology allows. Deciduous oak and sclerophyllous species characterise the northern central part of the Estate, whereas *Carpinus orientalis* (oriental Hornbeam) and reforested *Pinus pinea* (Italian Stone Pine) are prevalent over much of the eastern parts of Castelporziano and Capocotta (figure 2.14). The most inland areas of the Estate are used for experimental agriculture involving ancient species, grazing for herds of buffalo with some long-unharvested cork oak trees.



**Plate 2.3:** (a) Reafforested Italian stone pine (*Pinus pinea*), typically found along roads but also within plantations. (b) Open grassland dominated by asphodel and bordered by deciduous trees. These landscapes are restricted to the “Old dune” sand sheets. The excavating author provides scale. (c) Grassland and pine plantation – sampling location for CP08 4 & 5. (d) The Roman archaeological remains towards the modern coast are dominated by maquis scrub and dense Holm oak forest. This environment is described by



REMOVED TO COMPLY WITH E-THESIS GUIDELINES

**Figure 2.14:** Vegetation map of the Casteloziano Estate (adapted from Fares et al., 2009).

### **2.6.11. Coastal geochemical sediments at Castelporziano**

Broadly speaking, the Castelporziano Estate can be described by two distinct geochemical sediment types linked to early vadose diagenesis, that underlie the entire area (Manes et al. 1997). The inland sand sheets and two inland dune ridges are heavily cemented by iron oxide, whereas the deltaic dune ridges and interdunes towards the coast become increasingly cemented by calcium carbonate with inland distance from the coast. On this basis the sediments can be described as early vadose ferricrete and aeolianite respectively. The rare soil types associated with these red “Old dunes” have already been discussed (Section 2.6.6)

### **2.7. Aeolianite**

Key research by Sue McLaren and Rita Gardner (Gardner & McLaren 1994; Gardner & McLaren 1999; McLaren 2001) has sought to investigate and constrain the alteration of coastal geochemical sediments during the early stages of diagenesis in order to understand the implications for palaeoenvironmental research (McLaren & Gardner 2004). A variety of cements; temporary halite, high- and low-Mg carbonate, aragonite and silicate, are key vectors of sediment consolidation in the unsaturated (vadose) zone of coastal environments. Early vadose diagenesis in coastal dune environments is driven by complex interactions between multi-scale processes. On the macro-scale, climate is a key factor (Nash 2004; McLaren & Gardner 2004; Nash & McLaren 2003). Hydrology (Brooks & Whitaker 1997) and geochemistry (McLaren 2001) are key meso-scale factors driving the concentration and composition of diagenetic cements. Acting on the micro-scale, vegetation root systems (Klappa 1980) and micro-organisms (Jones & Kwok Choi 1988) are important in carbonate precipitation. Marine, terrestrial groundwater and meteoric water sources interact in coastal dune systems whilst the transition from littoral to continental landscapes can lead to significant variation in geomorphology over short distances. Dune morphology especially, can vary considerably over very short timescales (Sherman 1995; Baas & Sherman 2006).

Preserved cemented, aeolian forms, including internal structures, are termed aeolianites (Bateman et al. 2004). McLaren (2007) argues for a broad description for aeolianites “encompass[ing] all aeolian sands (carbonate and siliclastic) that are partially cemented by calcium carbonate under subaerial conditions” (p144). The initial field observations from Castelporziano suggest that the younger dune ridge record is characterised by carbonate-cemented siliclastic aeolianite. Glaebular cements were frequently encountered during sampling. However, it was not always possible to differentiate groundwater or vegetation as the dominant driver of cementation due to the low altitude and therefore close proximity between marine and terrestrial ecotones. The progradational nature of the shoreline also suggests post-depositional changes in proximity to the terrestrial water table; i.e. as progradation develops vegetation may become the dominant driver of cementation as marine influences become more remote. The influence of groundwater is likely to be highly seasonal, so the extent of the ‘vadose’ zone will fluctuate throughout the Mediterranean winter deluge and summer drought cycle. As the hydrogeological surveys suggest, groundwater may be

a key mechanism for flushing geochemical sources from inland towards the coast (Section 0). A complex and seasonal interaction of phreatic and vadose zones must be considered in this low-lying coastal zone of Castelporziano in addition to formation models of geochemical sediments (McLaren 2007; Widdowson 2007).

This cemented aeolianite can preserve the bedding structures of dunes, and therefore the direction of wind flow. The angle of the bedding also serves to distinguish relict beaches from dunes; aeolian dunes preserving bedding angles of 30-34° (McLaren 2007). Impressions of roots and the roots themselves can also be preserved allowing simple palaeoenvironmental inferences to be made in some cases (Bate & Dobkins 1992). The hardened, more durable surfaces of calcrete provide useful markers for past ground surfaces buried under subsequent sand bodies but more intensive chemical analysis of carbonate cemented sediment has been shown to provide useful palaeoenvironmental proxies for changes in groundwater (Nash 2004; Nash & McLaren 2003). The preservation of durable heavy minerals in relict dunes and aeolianite are also valuable records for sediment provenance studies (Kasper-Zubillaga & Dickinson 2001; Kasper-Zubillaga et al. 2007b).

### **2.7.1. Sources of cement**

Generally, in locations where dissolution of carbonate shells or penetration of meteoric water/sea-spray is occurring, in conjunction with the decomposition of organic matter such as in a dune slack environment, the CO<sub>2</sub> emission from the organic decay increases the solubility of the carbonate (Pettijohn et al. 1972). The CO<sub>2</sub> diffuses upwards through the sediment and is lost into the atmosphere. The corresponding drop in CO<sub>2</sub> partial pressure drives the precipitation of organic carbonate (e.g. shells). The ecology of the dune systems is also important here as CO<sub>2</sub> is produced by the microfaunal populations, enhancing the precipitation of carbonate cement (Pettijohn et al. 1972; McLaren 2001). McLaren (2001) cites 5 main factors for cement precipitation in the vadose zone - supersaturated pore fluid, concentration of pore fluids, pore fluid composition, rate of pore fluid movement, and substrate chemistry. Supersaturation occurs by the loss of CO<sub>2</sub>, temperature increase, evapotranspiration, decreasing salinity (e.g. rising non-marine water table) or increasing salinity (e.g. by evaporation or marine intrusion).

The mineralogical composition of the sand changes during deposition and storage. Heavy minerals are prone to dissolution during storage, with apatite, pyroxenes and amphiboles frequently lost (Morton & Hallsworth 1999). Unstable light minerals such as feldspars eventually dissolve in water-laden sediments such as river bars and coastal dune slack environments interacting with the water table. Soil formation processes, for example, acidic conditions caused by podsolisation, also affect the preservation of heavy mineral species. This affects assemblages of minerals used for provenance studies and is the main reason why more durable species of heavy minerals are focused upon in Heavy Mineral Analysis (HMA).

Sea-spray ejected from breaking waves deposits marine carbonate in the immediate vicinity of the shore and also a significant distance inland (McLaren 2001). Dissolved carbonate from meteoric water and *in situ* chemical weathering of carbonate shells and clasts operates within the coastal dunes and slacks (McLaren & Gardner 2004). Carbonate and other liquid extrusions from the roots of coastal vegetation also have a key role in the stabilisation and development of aeolianite in coastal dune fields (Bate & Dobkins 1992; McLaren 2007).

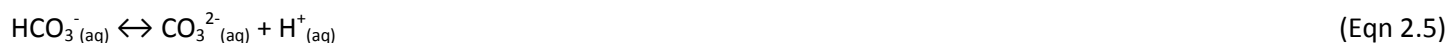
Pettijohn et al (1972:396-397) outline the basic chemical reactions at work in diagenesis. Equation (2.1) is the basic reversible relationship between dissolution and precipitation.



Where, the reaction takes place at 1 atmosphere of pressure and 25°C. A and B are cations, X and Y are anions.

### 2.7.2. Geochemical exchanges and carbonate species

Carbonate cementation of coastal sediments is not a unidirectional process and is subject to equilibrium among several chemical reactions. In reality these reactions typically occur in open-systems (the vadose zone) and would appear to impair accurate measurement of the formation of carbonate geochemical sediments. Equilibrium of carbonate exchanges involving dissolved inorganic carbon (DIC) are described by the following exchanges and are seen to be rapidly occurring relative to dissolution and exchange between gaseous and dissolved CO<sub>2</sub> (exchange 2.2) at the air-water interface of water source (ocean/stream/lake) (Darling et al. 2006):



The equilibrium of these exchanges is controlled by the rates and scale of horizontal transport (advection) and the diffusion of CO<sub>2</sub> at air-water interfaces; CO<sub>2</sub> exchange becomes more efficient during disturbance of this interface i.e. during storms. Equilibrium during exchange (2.3) has been observed to occur within 2—200s, with exchanges (2.4) and (2.5) occurring in a few seconds (Skidmore et al. 2004). The effectiveness of this phreatic relationship is less clear within subaerial vadose contexts.

### 2.7.3. Carbonate hydrolysis & kinetic fractionation of carbonate

In a closed system, DIC carbonate, as mobile ions or in compounds, is in equilibrium (mass balance) (equation 2.6) but in open systems linked to the atmosphere, kinetic effects upset equilibrium.



The precipitation of calcite then involves the consumption/loss of CO<sub>2</sub> and the fractionation of carbon stable isotopes (equations 2.7 and 2.8); solid CaCO<sub>3</sub> being isotopically heavier than dissolved carbonate ions (Darling et al. 2006). Isotopic fractionation between carbon species and CO<sub>2</sub> gas is a function of temperature (Zhang et al. 1995). Zhang et al (1995) found that the equilibrium fractionation of bicarbonate (HCO<sub>3</sub><sup>-</sup>) to CO<sub>2</sub> gas during gas transfer and gas dissolution, was 7.9 to 10.2‰ between 25 and 5°C respectively, the equilibrium fractionation factor of carbonate (CO<sub>3</sub><sup>2-</sup>) being 6.0 and 7.0‰ for the same temperature range.



In an open system, precipitation/dissolution reactions of calcite are augmented in the environment by a reaction with atmospheric CO<sub>2</sub> (Darling et al. 2006). Values for pCO<sub>2</sub> (partial pressure of CO<sub>2</sub> in a theoretical atmosphere where atmosphere and waters are in equilibrium) therefore are often not replicated by DIC measurements due to limitations upon air-water exchange caused by kinetic or physical effects (Skidmore et al. 2004).

Another source of error in DIC measurements is the loss of CO<sub>2</sub> from environmental systems (Darling et al. 2006). McLaren (2001) argued that the loss of CO<sub>2</sub> partial pressure within the vadose zone of coastal sediments improves the rates and levels of early carbonate diagenesis during aeolianite formation. CO<sub>2</sub> produced during the precipitation of calcite, either escaping through sediment pore spaces or CO<sub>2</sub> attributed to microfaunal respiration, leads to this reduction in CO<sub>2</sub> partial pressure, further enhancing the precipitation of carbonate cements. A useful side effect of this reaction, however, is the preservation of δ<sup>18</sup>O records in calcite, reflecting the temperature of the solvent water at time of precipitation and the mean annual air temperature of the climate relative to a local relationship of T-δ<sup>18</sup>O (Clark & Fritz 1997; Zhou & Zheng 2006; Horita & Clayton 2007; Zheng & Zhou 2007).

### 2.8. Early vadose ferricrete: dune reddening geochemistry

Yellow, brown and red colouration on sand grains preserved in dunes have been observed across the humid and arid tropics (Walker 1979; Pye 1981; Gardner & Pye 1981; Widdowson 2007), with reddening occurring more rapidly in the humid tropics due to increased moisture availability. Within the humid tropics, however, hematite formation may be more seasonal; periods of drought and lowered water tables being more favourable conditions. The colouration is caused by iron oxide stains upon clay coatings, or protected from abrasion in pits, on the surface of the sand grains. A



progressive reddening is dependent upon greater accumulation than loss of iron oxide coatings (Gardner & Pye 1981). Pye (1981) argues that dune reddening is a relatively quick diagenetic process occurring within  $10^3$  to  $10^4$  years.

There are several factors contributing to dune sand reddening; (1) a source of iron, (2) availability of moisture, (3) oxidising conditions, (4) sediment stability, and (5) time for development (Gardner & Pye 1981; Walker 1979).

Dune sand reddening occurs concurrently with other mechanisms of dune alteration and weathering (Pye 1983). Reduction in grain size, poorer sorting, reduction in porosity and permeability and increased cementation characterise this early diagenesis. Grain-size reduction and poorer sorting are linked partly to weathering of autochthonous minerals such as feldspars and heavy minerals to clay minerals and also the influx of clay particles as allochthonous dust; a key source of iron. Weathering and cementation leading to reduced porosity and permeability, progressively forms overgrowths of cement material such as calcite, hematite and temporarily in coastal dunes, halite (McLaren 1993). This may present significant difficulties for identifying sand grain transport history from surface textures by microscopy (Moral Cardona et al. 2005).

Rubefaction is a distinctive feature of the older, preserved dunes at Castelporziano; the colouration apparently due to “iron oxides and...clay deriving from the disintegration of adjacent outcrops of pozzuolana and pyroxene-rich lithoid tufa” (Manes et al. 1997:21) found inland towards the Albani caldera.

### **2.8.1. Mineralogy of rubefaction**

The key minerals constituting iron oxide coatings on sand grains are insoluble ferric oxides (oxidised state  $Fe^{3+}$  as opposed to more soluble ferrous, reduced state  $Fe^{2+}$ ). There are a number of hydrated oxides of ferric iron: dimorphous goethite ( $\alpha$ - $FeO.OH$ ) and lepidocrocite ( $\gamma$ - $FeO.OH$ ), and schwertmannite ( $FeO(SO_4)OH.nH_2O$ ) that are products of weathering and give a yellow to brown colour to the sand grains they precipitate on to. The differing mineralogy drives the different colouration, with hematite ( $Fe_2O_3$ ) producing a distinctive blood-red stain. These coatings/stains are typically poorly crystalline except for hematite which can, on older dunes, produce well-developed though small, crystals. Gardner and Pye (1981) suggest that even small amounts of iron-oxide stains (0.4% surface area) can create pronounced colouration. This ferric iron chemistry is a key chemical component of ferricrete development (Widdowson 2007).

### **2.8.2. Goethite ( $\alpha$ - $FeO.OH$ ) and lepidocrocite ( $\gamma$ - $FeO.OH$ )**

The field term *limonite* refers to “hydrated oxides of iron with poorly crystalline characters whose real identity has not been determined” (Deer et al. 1992:582). The amorphous stains are often yellow to brown and consist of cryptocrystalline Goethite or Lepidocrocite. As weathering products, impurities are common. Quartz and hematite are frequently incorporated into deposits whilst isomorphic substitution of manganese ( $Mn^{3+}$ ) and aluminium ( $Al^{3+}$ ) is also common. The substitution of aluminium has been found to stabilise goethite, preventing dissolution and re-

precipitation as hematite (Dominik et al. 2002). As with all ferric oxide coatings, they are frequently derived from iron-bearing minerals. Dissolution of iron-bearing minerals sources is an important *in situ* process for sand dune rubefaction and is discussed below. Goethite and Lepidocrocite are generally formed under oxidising conditions and can be found in marine and meteoric environments, bogs and springs (Deer et al. 1992).

### **2.8.3. Hematite (Fe<sub>2</sub>O<sub>3</sub>)**

Red colouration in sandstones (coatings sometimes acting as a cement), limestones and soil profiles is a product of hematite formation by weathering of iron-bearing minerals within the sediments and reprecipitation. Along with carbonate cementation, rubefaction of sediments is a widespread early diagenetic process at Castelporziano. Hematite has been shown to form from goethite by a sometimes complex dehydration reaction (Fan et al. 2006; Prasad et al. 2006). Transitional stages of hydro-hematite/ferrihydrate formation may or not be observed, whilst the formation of magnetite has also been observed at experimental temperatures over 238°C (Ozdemir & Dunlop 2000). These high temperatures accelerate the dehydration reaction that can take centuries at earth surface temperatures. Ozdemir and Dunlop (2000) argue that this magnetite formation has serious implications for palaeomagnetism studies of goethite-rich sediments, as overprinting with magnetite's strong, saturated-remanent magnetisation ( $M_s$ ) gives an unrepresentative signal.

### **2.8.4. Sources of Iron**

There are a number of possible sources of iron supplying the reddening of sand dunes. (1) the weathering of iron-bearing minerals within the body of the dune, which includes reworking of existing iron oxides (Schwertmann 1991), (2) clay particles transported as aeolian dust (Bullard & White 2005; Bullard et al. 2007), (3) pedogenic processes (Thompson et al. 2007; Carter-Stiglitz et al. 2006), for example leaching during podsolisation, and (4) biogenic precipitation driven by reduction reactions of bacteria (Newman 2001; Cervini-Silva & Sposito 2002; Dominik et al. 2002). The weathering of granular magnetite ( $\alpha$ -Fe<sub>2</sub>O<sub>3</sub>), thermally less stable maghaemite ( $\gamma$ -Fe<sub>2</sub>O<sub>3</sub>) (Liu et al. 1999) and hematite may be locally important sources linked to local geological setting and provenance.

The rate of release of iron is further governed by the mineralogy of iron-bearing minerals. Iron-bearing minerals such as hornblende, olivine, augite and to a lesser extent feldspars do not necessarily weather at the same rate under similar environmental conditions. The temperature, availability of moisture, red/ox potential (Eh) and pore-water acidity (pH) combine to create spatially-variable (and temporally-variable with seasonal changes and meso- and macro-scale climate change) conditions (Gardner & Pye 1981). The rate of the reactions themselves is governed by the reactive surface area (Schwertmann 1991). This rate will clearly change with grain-size; progressive loss of reactive surface area as reactions become more complete and sources become exhausted.

### 2.8.5. Mechanisms of formation

The two most common iron coatings preserved on grains of dune sand are goethite and hematite (Gardner & Pye 1981; Walker 1979). From the hydrolysis of iron to ions in solution, the necessary first step in deriving these coatings, there are several mineral formation pathways that can subsequently occur. Ferrihydrite to goethite or hematite (Cudennec & Lecerf 2006), and, goethite to hematite transformations (Fan et al. 2006) are the most important basic pathways for dune sand reddening. These reactions are dependent upon the combination of local environmental conditions linked to acidity/alkalinity, temperature and moisture availability. Pedogenic (Thompson et al. 2007) and biologically-mediated (Newman 2001; Kaal et al. 2007) processes also have significant effects.

#### 2.8.5.1. Ferrihydrite

“The hydrolysis of  $\text{Fe}^{2+}$  (ferrous) and  $\text{Fe}^{3+}$  (ferric) ions in solutions, gives rise to iron hydroxides, oxyhydroxides or oxides according to the various reacting conditions” (Cudennec & Lecerf 2006:716). Ferrihydrite (the still debated, rough formula  $5\text{Fe}_2\text{O}_3 \cdot 9\text{H}_2\text{O}$ ) generally precipitates first (Cudennec & Lecerf 2006). Crystallisation as goethite or hematite from ferrihydrite then occurs depending upon local environmental conditions

#### 2.8.5.2. Ferrihydrite to goethite or hematite transformation

Ferrihydrite is unstable and crystallises over time to goethite or hematite (Gardner & Pye 1981). The reaction to goethite/lepidocrocite is a dissolution and recrystallisation process (Liu et al. 2007). The reaction to hematite is a topotactic transformation of the crystal lattice (Cudennec & Lecerf 2006). It has been shown that temperature and pH are key factors for which end members will form. Higher temperatures drive hematite formation linked to more rapid dehydration. Therefore in tropical and sub-tropical latitudes hematite may be the dominant form. pH however, plays a more complicated role. Low *and* high pH values (2-5 and 10-14) produce goethite, with neutral pH values of around 7 producing hematite. Both hematite and goethite formation occur simultaneously and compete for dominance with the outcome decided by local reaction conditions. In acidic conditions, Cudennec and Lecerf (2006) argue that the dissolution of divalent iron does not specifically drive goethite crystallisation as discussed by Gardner and Pye (1981) in their early review of dune reddening. Rather, they argue for the presence of hydrated hydroxyl cations,  $\text{Fe}(\text{OH})(\text{H}_2\text{O})_5^{2+}$ ,  $\text{Fe}(\text{OH})(\text{H}_2\text{O})_4^+$  or anions,  $\text{Fe}(\text{OH})_4(\text{H}_2\text{O})_2^-$ ,  $\text{Fe}(\text{OH})_5(\text{H}_2\text{O})^{2-}$ ,  $\text{Fe}(\text{OH})_6^{3-}$ , to drive the reaction towards precipitating goethite. If, however, the iron in dissolution is in the form of hexaaqua ions,  $\text{Fe}(\text{H}_2\text{O})_6^{3+}$  (note the lack of hydroxyl groups), then goethite formation is observed to be prevented and hematite is produced. For high pH values  $>12$ , and therefore high concentrations of hydroxyl groups are present, then only goethite is formed. Recent water chemistry measurements suggest that the Castelporziano terrestrial water table has a pH of ca. 8 (pers. comm. FSJ Brown). The lack of podsoles and strong carbonate geochemistry also suggest a weakly alkaline character providing optimum conditions for hematite formation.

Cudennec and Lecerf (2006) also note that the crystal structures of both ferrihydrite and hematite are related, leading them to develop an argument for a topotactic transformation of the ferrihydrite crystal lattice at low temperatures from wüstite (FeO) to ferrihydrite to hematite, involving a reordering of the crystal matrices. XRD outputs of ferrihydrite show two forms, 2-line and 6-line ferrihydrite. Initially thought to highlight different formation conditions, 6-line ferrihydrite has been shown to be a more-crystalline intermediate ferrihydrite between 2-line, poorly crystalline ferrihydrite and hematite (Majzlan et al. 2004) cited as evidence of hydrated iron oxide crystal reordering.

### **2.8.5.3. Goethite to hematite transformation**

There is controversy over the ageing of ferric oxides being a controlling factor in a conversion of goethite to hematite. A simple dehydration reaction over time is disputed (Fan et al. 2006; Prasad et al. 2006). The thermally-induced dehydration of goethite has been observed to sometimes form hydrated intermediate forms of hematite during thermal treatment, leading to a pathway of goethite > protohematite > hydrohematite > hematite (Prasad et al. 2006). The transformation to hematite occurred at 800°C (Ozdemir & Dunlop 2000). A thermally driven mechanism of diffusion of hydrogen or hydroxyl away from the reaction surface of goethite is argued by Fan et al (2006). The subsequent formation of pores and eventually rinds the surface of the goethite progressively driving internal dehydration, recrystallising as hematite. Smaller particle sizes react much faster due to increased reactive surface area to volume (Prasad et al. 2006).

These studies were carried out at temperatures of over 200°C in order to greatly accelerate the reactions. The reaction rate of the topotactic transformation of goethite to hematite in earth surface conditions is very slow, and progressive reddening is only a rough guide for the age of soil or dune bodies (Walker 1979). It is not a linear process, making absolute or even relative chronologies of soil/sediment reddening inadvisable. The level of reddening is linked to climate but is also site-specific and again palaeoclimatic inferences based on colour are discouraged (Pye 1981; Gardner & Pye 1981).

The presence of impurities has a significant effect upon reaction temperatures. Isomorphic substitution of iron by Cu<sup>3+</sup> ions leads to a drop in the dehydration temperature from 238°C (for pure goethite) to 221°C. As discussed earlier, the replacement by Al (and Cr) leads to an increase in dehydration temperatures (Prasad et al. 2006). Applying this to earth surface conditions (e.g. ~25°C), an increase in transformation temperatures due to micro-scale variations in mineralogy, in conjunction with micro-scale variations in interstitial moisture availability (even morning dew is sufficient) and local temperatures, drives small-scale variability of iron oxide formation and progressive dune reddening. In addition iron oxides may act to concentrate mobile radionuclides (Olley et al. 1996).

At larger scales, regional temperature is important; dehydration takes longer across decreasing temperature gradients and in colder locations it may never happen at all. This perhaps explains the lack of red coatings reported from colder latitudes (Gardner & Pye 1981; Walker 1979).

#### **2.8.5.4. Preservation of hematite**

Goethite is thermodynamically the most stable of the iron oxide species and thus occurs most frequently as an end member in sedimentary contexts (Prasad et al. 2006). “Once formed, the preservation of hematite depends on whether interstitial conditions remain the same. If there is an increase in soil organic matter, a reduction of soil water oxygenation, or an increase in the numbers of iron-reducing bacteria, Eh may fall and pH rise to the point where hematite is reconverted to goethite or even reduced to the ferrous [divalent] form” (Gardner & Pye 1981:520). Therefore the existence of hematite coatings is testament to enduring stability in the micro-, meso- and macro-scale environmental factors that drove their formation in the first instance.

Additionally, chelation, the binding and removal of reaction potential, or transportation of iron by organic molecules produced by plants and bacteria, can be responsible for leaching of iron oxides within oxidising conditions (Schwertmann 1991; Cervini-Silva & Sposito 2002). Gardner and Pye (1981) note that the stability of hematite is increased where the mineral is associated with clay minerals, e.g. as stains upon clay coatings on sand grains. The colouration may be abraded during remobilisation but surface pits preserve some material and grains smaller than 150 µm are thought to be immune from this scouring due to their low mass.

At Castelporziano, the preserved inland sand sheets, attributed to the Pleistocene (Milli & Zarlenga 1991), are characterised by a bright-red coating, indicating, as a rule-of-thumb, that they have been stable for an extended period and suitable conditions for iron oxide formation and hematite preservation are present.

### **2.9. Implications for Castelporziano**

From these reviews of macro-, meso- and micro-scale processes acting upon the geomorphology of the site, a methodology was formulated (chapter 3) to answer the research questions presented in chapter 1. It was decided to focus upon examining the sources of sediment, the transport of sediment to the site, the formation processes underpinning the preserved geomorphology and the diagenetic processes that have altered these landforms during at least the Holocene. In addition, the human impact of development, especially during the last 2000 years, must be considered when examining smaller geoarchaeological scales.

### 3. Methodology

Within the context of the site setting (Chapter 2) and key components of a geoarchaeological approach (Chapter 1) the methodology underpinning this thesis is outlined below. An effective geochronological framework and consideration of taphonomy and diagenesis (site formation processes) are principal elements. Regarding the palaeo-landscape reconstruction required by the research questions, multi-proxy datasets are interrogated where possible. An integrated approach is attempted in order to understand the effects of taphonomy and diagenesis upon the palaeo-environmental records and effectiveness of the geochronological framework primarily using luminescence dating. This technique is fundamentally 'embedded' in the geochemical sediments that characterise the site. Where appropriate preliminary studies are included, although unsuccessful for their initial purpose, they serve to improve methodology in other areas and develop hypotheses for future work.

#### 3.1. The overall approach

Beach sands display clear dynamic gradients in alongshore sediment transport (Frihy & Komar 1991; Li & Komar 1992; Garzanti et al. 2008). The sorting of sediments is driven primarily by grain-size, shape and density (Komar & Wang 1984; Komar et al. 1989) with variations in the primary mechanism down-profile (Li & Komar 1992). Beaches are inherently linked to coastal dune systems (Nordstrom et al. 1990; Aagaard et al. 2004) and further physical sorting of sediments is observed due to aeolian transport. Mineralogical and sedimentological characteristics of the component sand grains are partly preserved from initial erosion, through fluvial and/or alongshore transport, coastal deposition to aeolian redistribution and dune formation phases (Aagaard et al. 2004; Kasper-Zubillaga et al. 2007a). These sedimentary dynamics are particularly suitable for transect-based sampling (Abuodha 2003) and joint sedimentological and petrological investigations (Kasper-Zubillaga & Dickinson 2001; Kasper-Zubillaga et al. 2007a; Kasper-Zubillaga et al. 2007b). In conjunction with luminescence dating and topographic survey, the spatial and temporal development of the site can be investigated within a broader framework. In particular, assessing the geomorphological development of the site in relation to sea level is particularly relevant due to the site's position on the Tiber delta.

In chapter 1, several research questions were outlined, see table 3.1 for brief description of the techniques proposed to answer them.

**Table 3.1:** Techniques applied to answer research questions.

Research Question	Applied techniques / approach
<i>How has the coastline of the Laurentine Shore developed during the Holocene?</i>	<ul style="list-style-type: none"> <li>• D-GPS control points, georeferencing of aerial photography, GIS mapping.</li> <li>• Topographic transect survey of dune ridges.</li> <li>• GPS mapping of archaeologically important dune features.</li> </ul>
<i>What are the processes of coastal development acting on the Laurentine Shore?</i>	<ul style="list-style-type: none"> <li>• Sedimentology of modern beaches and relict beaches and dune ridges.</li> <li>• Petrological analysis of same samples to examine sediment transport dynamics and post-burial development of coastal dune ridges.</li> <li>• Biostratigraphic investigation of archaeologically important palaeo-sea-level to constrain active dune-building context linked to Holocene development of the Tiber delta.</li> </ul>
<i>What is the chronology of these coastal changes?</i>	<ul style="list-style-type: none"> <li>• Luminescence dating of relict dune ridges to determine time since burial / dune ridge formation.</li> <li>• AMS-<sup>14</sup>C dating where appropriate</li> <li>• The construction of age models to examine the stratigraphic progradation of the Tiber delta.</li> </ul>
<i>What are the key interactions between anthropogenic and geomorphological processes?</i>	<ul style="list-style-type: none"> <li>• Integration of data from past and new excavations of archaeological remains linked to the palaeo-shoreline described as the “Laurentine Shore”, ca. 1<sup>st</sup> century AD.</li> <li>• Examination of geomorphological and archaeological data regarding coastal situation of sites and their development over time.</li> </ul>
<i>What are the benefits of a multi-scale geoarchaeological approach and the implications for future research?</i>	<ul style="list-style-type: none"> <li>• Assessment of conceptual models (chapter 1) and their effectiveness for answering preceding research questions and more broadly within recent Geoarchaeological research.</li> </ul>

### 3.2. Site mapping

#### 3.2.1. Geomorphic survey

Due to the dense forest canopy over most of the area of interest, D-GPS survey of the preserved dune ridges was not possible. Raw GPS locations from a handheld Garmin GPS device were taken for all sample locations and dune crests. Access to all dune crests was impossible due to security and the density of vegetation. Mapping of the dune ridges is of key importance for linking the chronological succession of these landforms to the development of the Tiber delta as a whole. To fulfil this requirement, mapping from aerial photography was proposed. Following preliminary surveys and dune ridge dating, it was possible to locate the Roman dune-ridge associated with the coastline ca. 2000 BP. Using a

Garmin GPSmap 60CSx hand-held GPS mapper, with WAAS/EGNOS enabled, it was possible to use the corrected EGNOS GPS signal to derive X & Y positions with < 3m accuracy. By mapping the preserved post-Roman dune ridge, the dune slack directly inland of this ridge and the Roman dune ridge, an estimation of the Roman shoreline could be reconstructed. This estimation assumes that the subsequent phase of foredune formation is linked to delta progradation. This simple approach also assumes that the general width of the beach is recorded by the development of a subsequent phase of foredune development. Assuming that the post-Roman dune ridge has formed on the berm terrace of the preceding beach phase (Otvos 2000), i.e. the Roman period beach, identification of the width of the Roman beach and the relative position of the sea was attempted. Due to the protected status of the Castelporziano Estate it was not possible to excavate sondages to examine the development of successive foredune phases in more detail. On the meso- ( $10^{2-3}$ ) to macro-scale ( $10^{4-5}$ ) the uncertainty of several metres associated with these dune formation assumptions is minimised in the reconstructions. Other features such as pronounced blowouts, parabolic dunes and possible infilled inlets were also mapped. The dune slack features were most easily definable under the dense vegetation cover and was successfully tracked for the majority of the extent within the Castelporziano estate from the Discobolos Villa in the SE (Goalen & Fortenberry 2002), to the Castel Fusano boundary wall in the NW.

### **3.2.2. Dune ridge transects**

Using a Leica total station, recovering detailed inland transects (where access and forest cover allowed) of the dune ridge topography was aimed at providing a context for assessing the distribution of dated dune ridges linked to Tiber delta progradation, and also a context for assessing the archaeological record relative to this.

### **3.2.3. Aerial photography**

Aerial photographs from 1954, 1983 and 2003 were obtained from the Istituto Geografico Militare, Florence. Using ArcGIS 9.2, georeferencing of aerial photos with Ground Control Points (see below) was aimed at digitising the dune ridges and other geomorphological and hydrological features of the Castelporziano Estate and the wider Tiber Delta.

### **3.3. Site georeferencing: Differential-GPS survey**

As a precursor to GIS and site base-mapping, D-GPS survey of key areas was attempted. A Leica SR20 differential-GPS system was used with the post-processing of positions allowing sub-centimetre point quality. Due to the density of the forest canopy over most areas of interest, attaining sufficient satellite signal was problematic over much of the areas of interest. Several key Ground Control Points (GCPs) linked to the high-resolution archaeological (and topographic) Digital Elevation Model (DEM) were identified. Post-processing the raw SR20 data with Leica GeoOffice v5.0 software against the Italian GPS reference network, specifically RINEX files from the INGR-ROMA reference point<sup>10</sup>, high-quality positions could be obtained for all D-GPS measurements. The post-processing of the raw GPS measurements used the EGM-96

---

<sup>10</sup> [http://ring.gm.ingv.it/data\\_month.php?sito=INGR](http://ring.gm.ingv.it/data_month.php?sito=INGR) (last accessed 30/07/2009).



geoid model and a Universal Transverse Mercator projection centred on zone 33n was aimed at also providing meaningful orthometric position heights above sea level.

### **3.3.1. EGM '96 as a modern sea level proxy**

A measurement of contemporary sea level was also made with the D-GPS system. Both antennas were placed on the Castelporziano beach, upon the berm and observed strandline. The antennae were aligned normal to the beach and foredune to incorporate a beach transect and sea-level measured by total-station. The post-processed GPS beach locations recorded a sea level difference of 0.126 m to that of the EGM '96 geoid model as recorded by the D-GPS points from the *Vicus Augustanus* (used to georeference the Archaeological DEM and piscinae coring locations). This variance is within the micro-tidal range of the Mediterranean Sea and therefore argued to provide a useful proxy sea level base level.

### **3.3.2. Biostratigraphic sea level reconstruction: diatom analysis**

In conjunction with the georeferenced coring data from the D6 fishpond (see section 3.6.5) diatom analysis from 0.5m of cored sediment was undertaken. This core records the transition from marshy to more peaty sediment (1.45-1.95m below base of fishpond) (Battarbee 1986). Diatom analysis is a sensitive and precise method for assessing sedimentary sea level records (Gehrels et al. 2001; Lamb et al. 2006). Caution has been urged by some researchers regarding the compression of some Holocene marsh sediments and therefore lower records of sea level. A  $\pm 1$  m error is suggested (Lambeck et al. 2004a). However, for the relatively shallow sediments, detailed examination of palaeo-ecological records may improve confidence in palaeo-sea level inferences (Lamb et al. 2006). Archaeological records of sea level exist from Roman rock-cut *Piscinae* on the west coast of Italy (Lambeck et al. 2004b). Assessment of palaeo-sea level relative to these features is made with the *Piscinae* diatom record from Castelporziano.

### **3.4. Site Transects**

In order to investigate the site, a framework of transects was constructed within which the geomorphological, sedimentological, geochemical, archaeological and chronological data could be understood. This framework consists of four major transects (figure 3.1). An alongshore transect is designed to examine the contemporary coastal dynamics of sediment supply to the site. Linked to delta morphology and coastal processes (primarily onshore winds, wave/tide action etc), the alongshore transect represents processes on a variety of scales, these have been discussed in chapter 2.

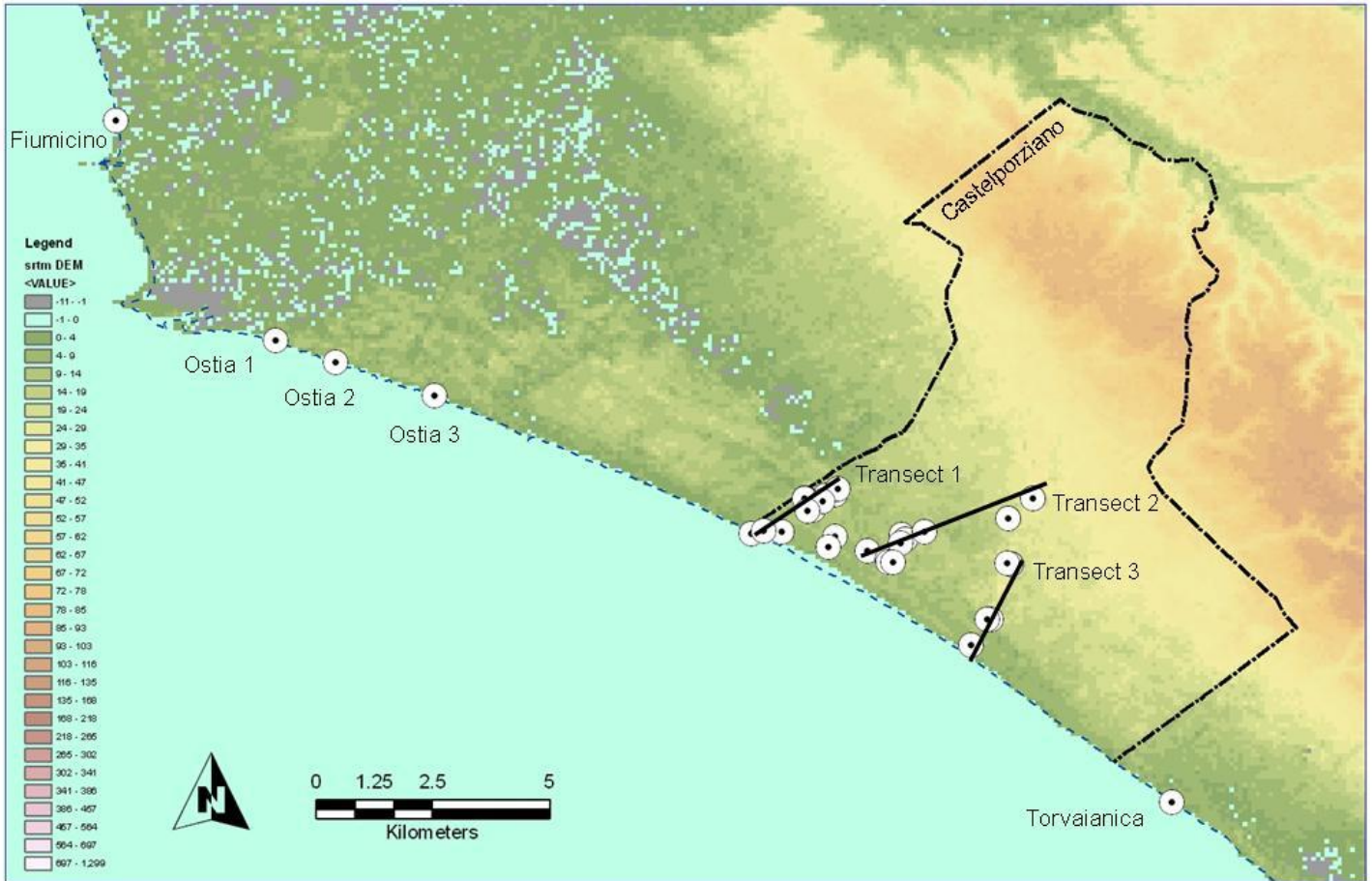


**Figure 3.1:** Location of transect sampling strategy. Location of samples is dictated largely by access and opportunity. The SRTM DEM base map is further discussed in chapter 4. A detailed view is presented in Figure 3.2, values are in metres relative to modern sea level. Ladispoli beach was also sampled, and is located on the northern flank of the Tiber Delta at the farthest distal position. Sampling locations are denoted by  $\Theta$ .

### 3.4.1. Sampling transects

Seven samples from Ladispoli on the northern distal edge of the Tiber Delta, Fiumicino and Lido di *Ostia* (3 samples) at the river mouth, and Castelporziano Beach and Torvaianica on the southern distal end create a contemporary beach transect primarily used for examining contemporary alongshore transportation. The inland transects (figure 3.2) relate to the relict dune topography and are records of the sediment washed onto the beach during the Holocene and Late Pleistocene which is then sorted by tidal and aeolian processes, moving towards the back of the beach and sorted further during foredune formation. Diagenetic processes then become dominant after the dunes become fixed as the series of dune ridges develops over time. Within a sediment provenance methodology this sampling is 3<sup>rd</sup> order (Ingersoll et al. 1993), providing regional information relating to the combined transportation by rivers and coastal processes. Sampled beach locations were sampled in an attempt to retrieve sediment from across the beach cross-section to incorporate size and density sorting occurring after deposition on the beach.

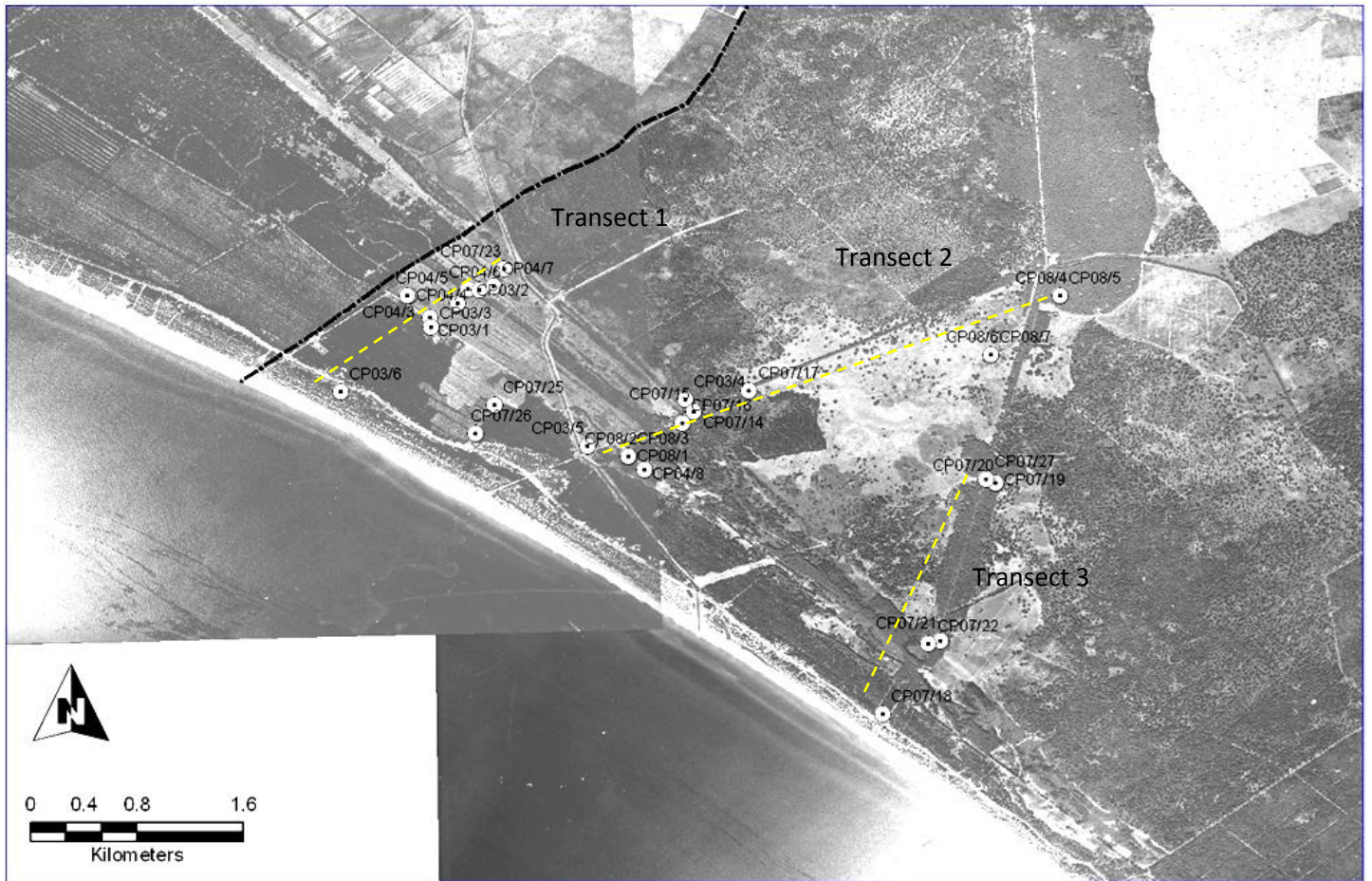


**Figure 3.2:** Detail of sampling locations described in Figure 3.1. NW Castelporziano Estate boundary is shown in black dot-dash over georeferenced aerial photographs taken in 1954. This is discussed in detail in chapter 4. Due to access restrictions, samples CP07/25 and CP07/26 had to be recovered from an area to the south of the other samples included in transect 1.

**3.4.2. Inland transects**

Three inland transects have been constructed to incorporate different aspects of the anthropogenic record within Castelporziano in relation to the stratigraphic development of the Tiber Delta and geomorphological field surveys (figure 3.1 and 3.2). Moving southwards, Transect 1 incorporates the modern beach, foredune and archaeological remains of the *Vicus Augustanus*, the village servicing the Imperial estate on the Laurentine Shore. Transect 2, crosses the remains of the *Piscinae* investigated in 2007/08 set within phases of dune-ridge formation directly linked to delta progradation. Samples along transects 1 and 2 record a mid-to-late Holocene sequence. Transect 3 covers the greatest temporal range, stretching into the late Pleistocene. This is due in part, to the compression of the delta morphology at this farthest, distal point, but also to the relative ease of access for sampling.

With this framework of sampling transects it should be possible to examine archaeological and geomorphological records of the site during the Holocene. By formally assessing site development in terms of spatial and temporal scale a

structured approach is taken to understanding the multi-scale context of the site. By incorporating the contemporary mechanics of the modern delta and dune building, effectively at the meso-scale ( $10^{2-3}$ ) but contextualised by the macro-scale ( $>10^3$ ) site setting and micro-scale ( $\leq 10^1$ ) formation and alteration processes, the reconstruction of key geoarchaeological periods is attempted.

### 3.4.3. Sampling

Sampling was undertaken by digging out sections to depths of ~1.0 - 1.5 m in the dune ridges and also by coring to depths of ~2.0 m using a sand auger. Samples for luminescence dating were collected by hammering lengths of opaque plastic pipe into the sections or by transferring augered samples into opaque plastic bags under cover of a tarpaulin. Additional bulk samples were taken for grain size, petrographic and other analyses.

A summary of beach samples, sampled sections and a core, and undertaken analyses is presented in table 3.2. Core 14 was removed from the base of the *Piscinae* D6 using a 0.5 m Russian peat corer (the sampling site is located with CP04/8 in the centre of figure 3.2, transect 2). Sampling depths (cm) are included in the sample codes for the core 14 samples only (e.g. core14/145 was sampled from 145 cm from the top of the core. Sampling sites are presented in (figure 3.2).

**Table 3.2:** Summary of sampled beach locations, sections and core, and techniques undertaken in this thesis.

Analysis	GSA		LOI		Diatom	Luminescence			Sedimentary		Environmental	Geochemistry	
	LPS	Bulk	Mode & Fines	Dating		SAAD-IRSL	$\alpha$ -TSAC	$\beta$ -TSBC	Petrology	Provenance	Magnetic susceptibility	XRD	CHN
LADISPOLI	X	X	X										
FIUMICINO	X	X	X						X	X		X	
OSTIA 1	X	X	X						X	X		X	
OSTIA 2	X	X	X						X	X		X	
OSTIA 3	X	X	X						X	X		X	
CP BEACH	X	X	X						X	X		X	
CP DUNE	X	X	X						X	X		X	
TORVAIANICA	X	X	X						X	X		X	
CP07/14	X	X	X			X	X	X	X	X		X	
CP07/15	X	X	X			X	X	X	X	X		X	
CP07/16	X	X	X			X	X	X	X			X	
CP07/17	X	X	X			X	X	X	X			X	
CP07/18	X	X	X			X	X	X				X	
CP07/19	X	X	X			X	X	X				X	
CP07/20	X	X	X			X	X	X	X			X	

CP07/21	X	X	X		X	X	X	X			X
CP07/22	X	X	X		X	X	X	X			X
CP07/23	X	X	X		X	X	X	X	X		X
CP07/24	X	X	X		X	X	X	X	X		X
CP07/25	X	X	X		X	X	X		X		X
CP07/26	X	X	X		X	X	X				X
CP07/27	X	X	X		X			X			
CP03/1	X	X			X	X	X				X
CP03/2	X	X			X	X	X		X		X
CP03/3	X	X			X	X	X				X
CP03/4	X	X			X	X	X				
CP03/5	X	X			<b>MODERN</b>						
CP03/6	X	X			X	X	X		X		X
CP08/1	X	X			X	X	X				
CP08/2	X	X			X	X	X				X
CP08/3	X	X			X	X	X				X
CP08/4	X	X	X		X	X	X				X
CP08/5	X	X	X		X	X	X				X
CP08/6	X	X	X		X	X	X				X
CP08/7	X	X	X		X	X	X				X
CP04/1	X	X	X		X	X	X				
CP04/2	X	X	X								
CP04/3	X	X	X								
CP04/4	X	X	X								
CP04/5	X	X	X								
CP04/7	X	X	X		X	X	X	X			
CP04/8	X	X	X					X			
SP5		X	X					X			

**Core 14 - *Piscinae* D6 short core (diatom palaeoenvironmental analysis & sea level reconstruction) sub-sample titles denote sampling depth.**

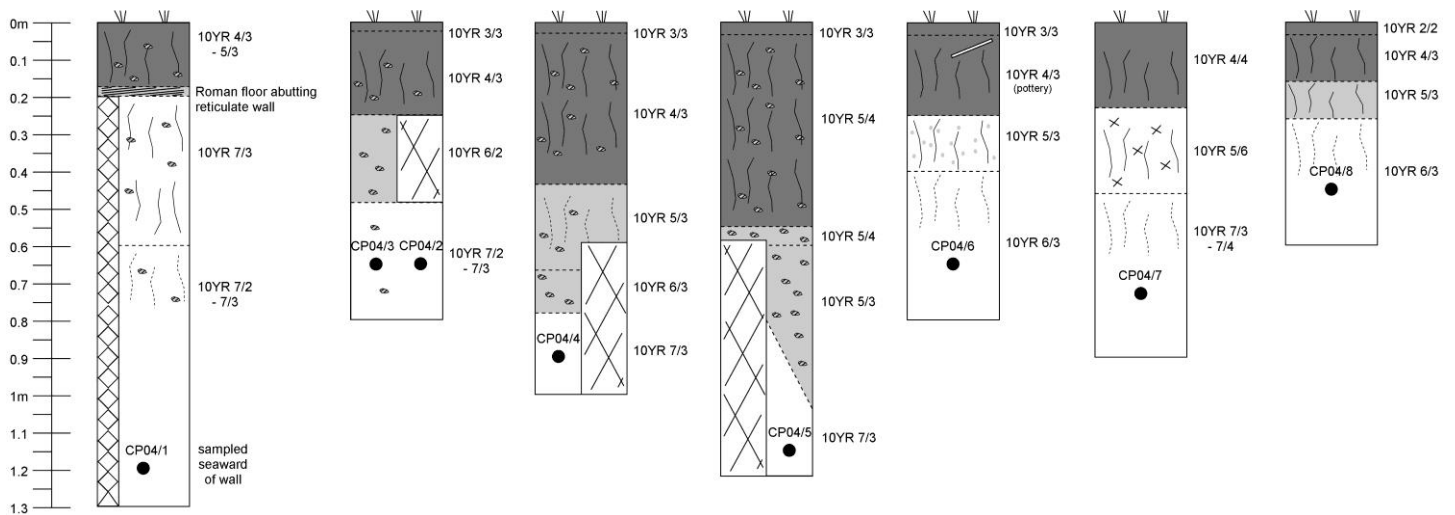
core14/145	X	X		X					X		X
core14/147	X	X		X					X		X
core14/149	X	X		X					X		X
core14/151	X	X		X					X		X
core14/153	X	X		X					X		X
core14/155	X	X		X					X		X
core14/157	X	X		X					X		X
core14/159	X	X		X					X		X
core14/161	X	X		X					X		X
core14/163	X	X		X					X		X
core14/164				X							

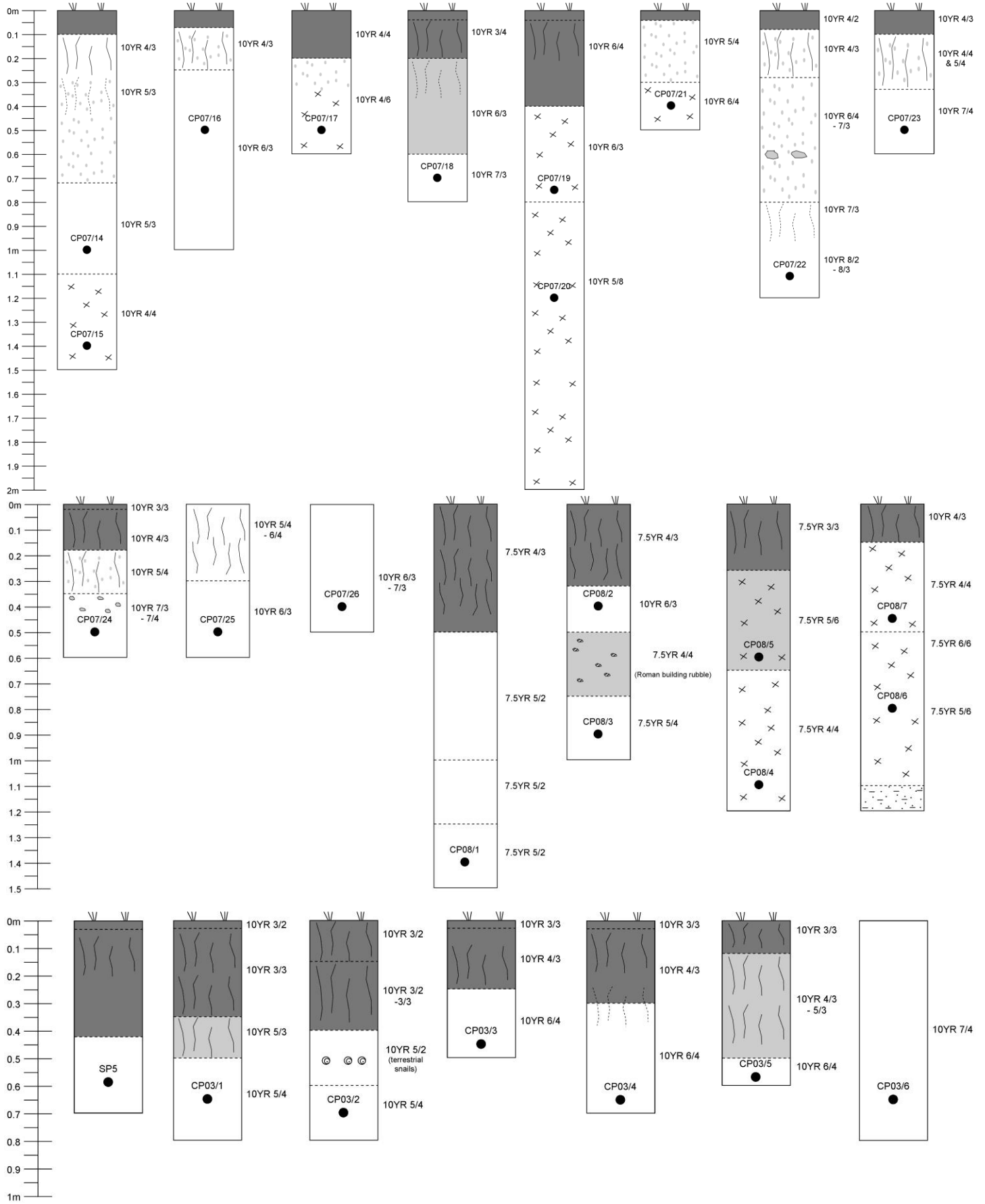
core14/165	X	X	X			X	X
core14/166			X				
core14/167	X	X	X			X	X
core14/168			X				
core14/169	X	X	X			X	X
core14/170			X				
core14/171	X	X	X			X	X
core14/172			X				
core14/173	X	X	X			X	X
core14/174			X				
core14/175	X	X	X			X	X
core14/176			X				
core14/177	X	X	X			X	X
core14/178			X				
core14/179	X	X	X			X	X
core14/180			X				
core14/181	X	X	X			X	X
core14/182			X				
core14/183	X	X	X			X	X
core14/185	X	X	X			X	X
core14/187	X	X	X			X	X
core14/189	X	X	X			X	X
core14/191	X	X	X			X	X

### 3.4.4. Sampled sections

29 sampled sections and 1 sediment core are presented in this thesis (figure 3.3 and 3.4, respectively). These derive mainly from dune ridge crests but with some samples abutting archaeological buildings (CP04/1, 4 & 5). Samples were taken primarily from clean sand where possible to focus analysis on the primary deposition of sediments linked to aeolian or shoreline progradation processes. Munsell colours were recorded from the wet test pit face. A general note of organic content and post-deposition alteration features was also made.

**Figure 3.3:** Schematic diagrams of sampled sections, primarily from dune ridge crests and sand sheets. Samples CP07/24 (dune slack), CP07/22 and CP04/1 – 5 are exceptions (relict beach deposits). The key for figures 3.3 and 3.4 is on page 67.







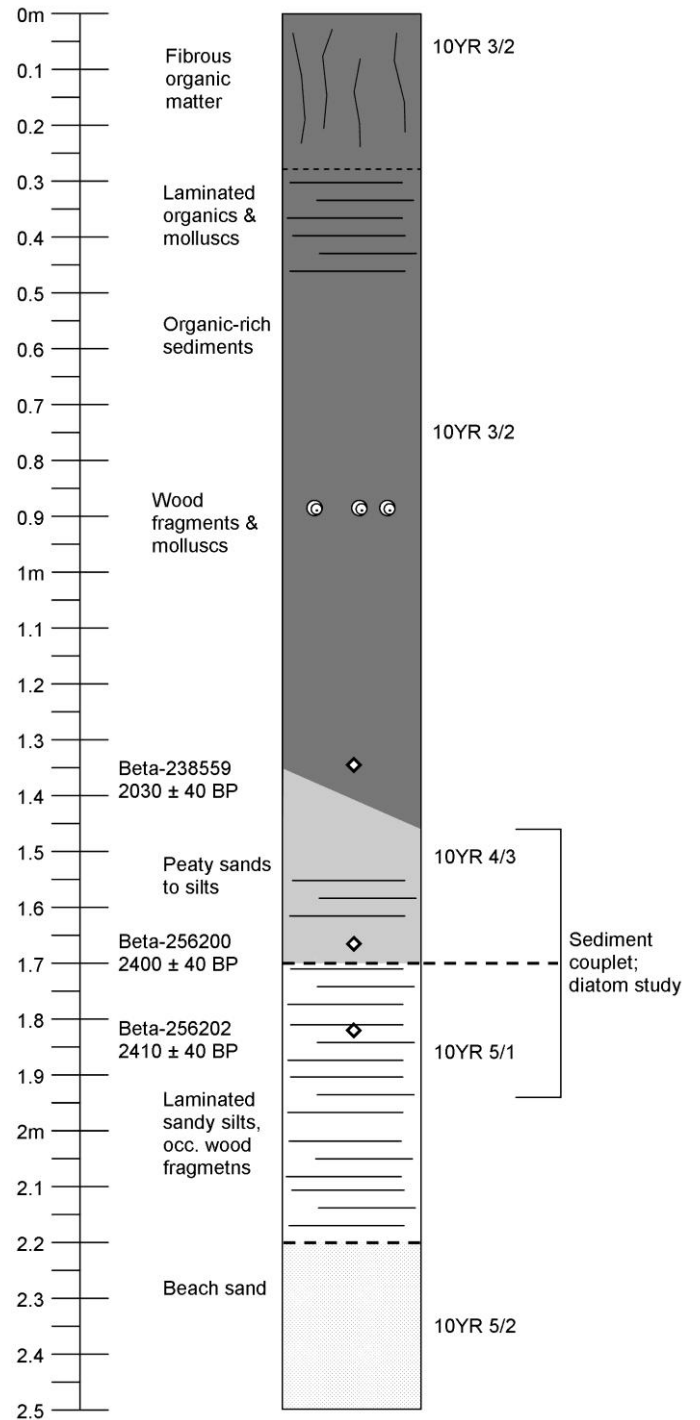
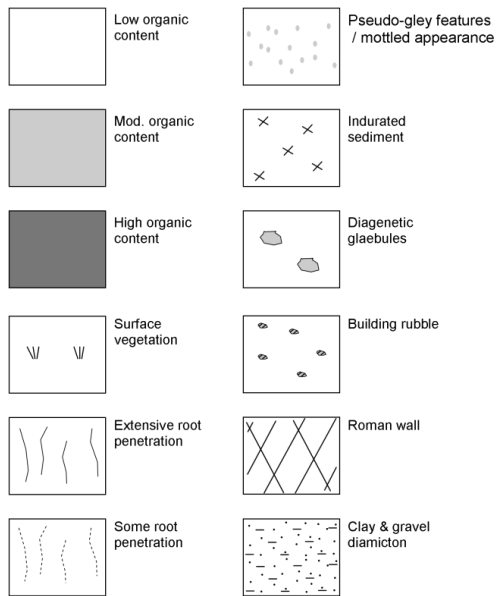


**Figure 3.4:** Core 14A, extracted from the base of *Piscinae* (D6) (see chapter 4, fig 4.6 for the location of core 14). Brief descriptions of the core are given in the diagram. The transition from waterlogged peaty sands to marshy silty sediments at the base was suggestive of inundation. The highlighted subsection across this sedimentary transition was sub-sampled for diatoms and a multi-proxy palaeo-environmental reconstruction was made to ascertain whether this sediment couplet is a meaningful marker of past sea level. A series of AMS-radiocarbon samples from organic sediments provide a stratigraphically consistent age-model for this section of the core, sampling locations are labelled as open diamonds ( $\diamond$ ).

### **3.5. Summary of analytical methods**

#### **3.5.1. Grain-size analysis of sand-sized sediment and grain-coatings**

During sampling it was found that significant amounts of cementation and grain-coatings existed within most of the reddened “Old dunes” samples and some of the carbonate-coated samples. During preliminary sieving much of these coatings were abraded into the sieve pan, making the assessment of the finer grain sizes (<63µm) problematic. The distribution of fine-grained sediments across the inland transects was investigated by laser-particle sizing. The fine-grained sediment may derive from in situ weathering of the dominant sand-sized grains. In addition, an important Saharan dust plume deposits Iron-rich sediment into the Tyrrhenian Sea (Chester et al. 1984; Piccardi et al. 1996), which may ultimately be incorporated into the Castelporziano dune ridges and through weathering and diagenesis preserved as grain-coatings. Due to the well-sorted aeolian nature of the fine sands within the site, most samples passed through a 1.4 mm sieve. This permits accurate laser particle sizing to provide an effective measurement of grain-size distribution. This analysis also elucidates the <63µm grain-size distribution of the sediments. Initial LOI tests upon the CP07 samples showed that across the site organic content was very low, typically less than 1 – 2 % dry weight. It was decided that the organic content would make a negligible contribution to the overall analysis as grain-size distributions appear to derive largely from sand-sized mineral grains and fine-grained diagenetic coatings. Therefore, all samples for laser particle size analysis were untreated prior to measurement.

Two grain-size distributions were measured. Bulk samples and separated grain-coatings were measured in different runs. Bulk samples were split and sub-sampled and washed in a rock tumbler, typically used for polishing pebble and gravel sized aggregates. 20g bulk sediment was placed in the rock tumbler. Using enough deionised water to cover the sample, the sediment was tumbled for 30mins. The resulting suspended sediment contained fine grained material removed from the grain surface without excessive abrasion to the sample providing unrepresentative fine-grained material. The coarser sediments still retained some red colouration. This does not necessarily suggest that the sample preparation process was unsuccessful. A relatively small percentage coating of 5% retained in surface pits is enough to significantly alter the colour of a sand grain (Bullard & White 2002).

The suspended sample and the sand-sized sediment were then separately measured. Potential errors would include aggregation of dust particles by diagenetic cements and meniscus cement flakes with a characteristic bowl-shaped form (as shown by EDX-SEM analysis) having an erroneously large surface area as the analysis assumes a spherical grain.

Using the GRADISTAT v.5 (Blott & Pye 2001) software, mode, mean and median grain-sizes are easily derived by a variety of methods. All sieved and laser particle sized samples were analysed in this way to enable rapid and comparative grain-size measurements across all analyses. Folk & Ward (Folk & Ward 1957; Folk 1966) statistics based on a normally distributed sample were used for all samples. In conjunction with identifying the key grain-size fraction,

sorting (standard deviation), skewness and kurtosis are also calculated by GRADISTAT. For all the other sedimentological methods and also luminescence dating, the mode grain-size was used for each analysis in order to retain some reference to the aeolian deposition of the dune sediments rather than diagenetic finer-grains or in some locations a fluvial character recorded by the presence of gravel sized aggregates (although these fluvial sites are not investigated further within this study).

The cementing effect of vadose carbonate diagenesis has a deleterious effect on a grain-size analysis aimed at understanding the deposited sediment prior to cementation. Occasionally it was necessary to gently disaggregate a sample in a mortar and pestle prior to analysis. In most cases this was sufficient to break up precipitated carbonate or iron oxide nodules but in some cases localised lithification was more pronounced, typically affecting ~1% of the initial bulk weight. These heavily cemented nodules were recorded but the weights removed from the GRADISTAT analysis. Preliminary analysis suggested that a fine-grained clay grain-size was either absent or a very minor component. Therefore inaccuracies due to interstitial water content in clay minerals associated with loss-on-ignition analysis are minimised or not important.

### **3.5.2. Loss-On-Ignition (Organic content, Carbonate equivalent content)**

The organic content and carbonate content of the bulk sediments (and also in some cases the mode and <63 $\mu$ m fraction) was measured by Loss-on-Ignition (LOI). For transect 3 there was enough material to also study the fines fraction (<63 $\mu$ m fraction). As the preserved dunes have undergone significant diagenetic alteration, carbonate cementation and iron oxide cementation, the fines collected during the  $\phi$ -sieving analysis were not representative of fine grained sediments alone, but potentially also included the grain-coatings abraded during the sieving. In order to assess the distribution of organic and carbonate contents within fine-grained diagenetic coatings, LOI analysis was undertaken on both fractions where available samples occurred. In many of the other samples, there was little or no fine-grained content. The geomorphological features are generally well-described by the sand-sized sediment grain-size distribution due to high-levels of sorting by aeolian processes. A key preliminary result from LOI analysis pertinent to the other geochemical and sedimentological and chronological methods discussed below was that organic contents were extremely low ( $\leq 2$  % dry weight) in all examined dune and sand sheet samples. The risk of contamination to fine-grained crystalline / diagenetic material by organic material is therefore assumed to be low, and the use of untreated (H<sub>2</sub>O<sub>2</sub>) bulk sediments is appropriate for minimising disturbance to diagenetic information. Initial tests on the 2007 season samples (see CP07 sample codes) showed that duplicate measurements were closely replicated in all cases. Therefore it was decided to undertake further LOI analysis on single sub-samples of bulk material. Where samples allowed sufficient fine-grained coatings, modes and fines were also measured for CP08 and some samples from earlier seasons (see table 3.2).

### 3.5.3. EDX-SEM chemical analysis of diagenetic grain-coatings

3 inland samples incorporating the change in carbonate to iron-oxide cements were examined with an EDX-SEM (energy-dispersive x-ray/scanning electron microscope) system at the Loughborough University Microscopy Unit. Element maps were produced to qualitatively assess sand-sized grain mineralogy, and the form and distribution of inter-grain diagenetic cements. As a preliminary study for the suitability of C and O stable-isotope analysis, EDX-SEM analysis was also aimed at assessing the presence of Fe-oxides within the carbonate diagenetic environment which would lead to an erroneous O signal due to kinetic fractionation during Fe-oxide formation (chapter 2). Samples CP07/18, CP07/14, and CP07/20 were chosen providing information on a very young carbonate dune, mature carbonate dune and mature reddened dune, respectively (see figure 3.2 for sampling locations). The presence of hydrated Fe-oxides such as *Goethite* (field-termed *Limonite*) is problematic to determine in the field with respect to carbonate cements. The presence of Fe shown by element mapping of bulk sand samples upon Quartz grains, for example, would suggest the presence of Fe atoms in grain-surface diagenetic material.

## 3.6. Provenance & diagenesis analysis

### 3.6.1. Petrological provenance analysis

The provenance of minerogenic sediments washing into the Tyrrhenian basin has been studied in detail by Garzanti et al (2002). The general methodology for the Castelporziano framework and dense mineral provenance study has been based upon this work in order to assess the macro-scale sedimentary transportation processes of the Tyrrhenian basin. A third-order sampling strategy (Ingersoll et al. 1993; Le Pera & Critelli 1997) focussing upon the beaches and downstream fluvial sediments was undertaken at Castelporziano, which allows the regional (macro-scale) provenance of the mineral assemblages (Ingersoll et al. 1993). Although actualistic provenance analysis homogenises some aspects of the Quartz/Feldspar/Lithic (QFL) provenance information that individual mineral species can provide (e.g. grouping nepheline/feldspathoids with feldspars), it is a relatively rapid method for deriving a good general provenance analysis based on simple parameters that are generally easy to identify for the less-experienced worker. Molinaroli et al (1991) show that this method and other similar provenance analyses derive around 85% of the potential information solely from a QFL ternary plot. Recent studies incorporating x-ray diffraction (XRD) analysis and petrological analyses are shown to be effective methods for assessing provenance and diagenesis (Kasper-Zubillaga & Dickinson 2001; Kasper-Zubillaga et al. 2007a; Kasper-Zubillaga et al. 2007b). Within this study 300 grains of both framework and dense minerals were counted, i.e. 600 grains for each sampling location. A sieved half-phi interval containing the modal grain-size was used for the framework grain counts which were mounted in Canada balsam and stained for K-feldspar to allow easy identification of quartz and plagioclase (identifiable by surfaces that are weathered but not stained yellow). The 63-250µm fraction of the bulk sediment sample was used for the dense mineral counts, concentrated by a 2.9g/cm<sup>3</sup>

Sodium polytungstate (SPT) separation. This is primarily due to some mineral species being limited in their crystal size, leading to them being poorly represented by the mode grain-size. However, within the very well-sorted grain-size distribution of a coastal foredune/ridge the under-representation of smaller or larger mineral species may be inherent in this dune system restricting the use of some petrological indices, such as zircon which is usually a small crystal. Thus a simplified set of ratios and parameters were used (Table 3.3). This examination was primarily developed as a training set where the complicating effects of diagenesis should be minimised and identification of the mineral assemblage made simpler.

### 3.6.2. Petrological diagenesis analysis

An examination of the effects of diagenesis upon the sampled sand assemblages was also proposed by petrological analysis. Table 3.3 and 3.4 describe the parameters used for both the *quantitative provenance analysis* and *semi-quantitative diagenesis analysis*. The *quantitative provenance analysis* parameters closely replicate those of Garzanti et al (2002) in which the QFL (framework) counts are based upon the Gazzi-Dickinson point-counting method developed by Ingersoll and colleagues (Ingersoll 1990; Ingersoll et al. 1984; Ingersoll et al. 1993). In the case of the Tyrrhenian basin study by Garzanti et al (2002) regarding the Roma beaches and surroundings that would incorporate the Castelporziano system, the heavy mineral analysis is critical for deriving the local volcanic signature. The QFL framework grains strongly represent uplifted basement-derived detrital grains from the Alpine Orogeny. The provenance analysis clearly requires both light and heavy mineral analysis to provide an adequate reconstruction.

**Table 3.3:** Light and heavy mineral indices used in petrology analysis. Descriptions are provided where necessary. These indices can then be readily transformed into the key indices and ratio parameters utilised by Garzanti et al., 2002 where appropriate minerals exist in the sample assemblages (table 3.4).

Light minerals (LM) < 2.9 g/cm <sup>3</sup>	Description	Heavy minerals (HM) >2.9g/cm <sup>3</sup>	Description	Other
Q	Quartz	CPX	Clinopyroxene	Forams
Qp	Poly-crystalline quartz	OPX	Orthopyroxene	Shell
F	Feldspar (indistinguishable)	Chlorite		Glass
Fp	Poly-crystalline feldspar	Epidote		
K	K-feldspar	Amphibole		
Kp	Poly-crystalline K-feldspar	Hornblende		
P	Plagioclase feldspar	Olivine		
Lc	Carbonate lithics	Melanite		
Lch	Chert lithics	Garnet		
Lv	Volcanic lithics	Hematite		
Lmm	Metamorphic lithics	Opaque		
Muscovite		Spinel		
Biotite				
Apatite				

Calcite  
Dolomite

**Table 3.4:** Indices employed by Garzanti et al., 2002 (supplementary data).

<b>Key Indices - Framework Composition (QFL%)</b>	
<b>Gazzi-Dickinson method</b>	
<b>Q</b>	quartz
<b>F</b>	feldspars and feldspathoids
<b>Lv</b>	aphanitic volcanic and subvolcanic lithic fragments (including diabase)
<b>Lc</b>	carbonate lithic fragments (including marble grains)
<b>Lp</b>	aphanitic terrigenous lithic fragments (shale, siltstone)
<b>Lch</b>	chert lithic fragments (including cherty shale)
<b>Lm</b>	aphanitic metamorphic lithic fragments
<b>Lo</b>	aphanitic serpentine lithic fragments
Ls = Lc + Lp + Lch = total aphanitic sedimentary lithic fragments	
L = Lv + Ls + Lm + Lo = total aphanitic lithic fragments (crystal size < 63 microns)	
Q + F + L = total main extrabasinal framework grains (not including micas and dense minerals)	
<b>Ratio parameters - Framework Composition (%)</b>	
<b>Gazzi-Dickinson method</b>	
<b>P/F</b>	plagioclase (not including chessboard-albite) / total feldspars and feldspathoids
<b>Traditional method</b>	
<b>Qp/Q</b>	polycrystalline quartz (not including chert) / total quartz
<b>Vm/V</b>	microlitic and lathwork to diabase rock fragments / total volcanic rock fragments
<b>Cd/C</b>	dolostone rock fragments / total carbonate rock fragments
<b>Mb/M</b>	metabasite rock fragments / total metamorphic rock fragments
<b>Mp<sub>1</sub>/Mp</b>	slate grains / total metapelite rock fragments
<b>Sc/S</b>	cellular serpentinite grains / total serpentine rock fragments
<b>Key Indices - Dense Mineral Suites (HM%)</b>	
<b>ZTR</b>	ultrastable minerals (zircon, tourmaline, rutile)
<b>T&amp;</b>	titanium minerals (sphene, anatase, brookite) and other minerals
<b>A</b>	amphiboles
<b>CPX</b>	clinopyroxenes
<b>OPX</b>	orthopyroxenes
<b>O</b>	olivine
<b>S</b>	spinel
<b>LgM</b>	low-grade metamorphic minerals (epidotes, chloritoid, prehnite, pumpellyite)
<b>Gt</b>	garnet
<b>HgM</b>	high-grade metamorphic minerals (staurolite, andalusite, kyanite, sillimanite)
PX = CPX + OPX = total pyroxenes	
OS = O + S = olivine and spinel	
MM = LgM+Gt+HgM = total metamorphic minerals	
HM = ZTR + T& + A + PX + OS + MM = total transparent dense minerals (density > 2.9 g/cm <sup>3</sup> )	

### 3.6.3. Diagenesis analysis methodology

During the sampling, it was observed there was a sharp change from the inland reddened iron-oxide cements to white, carbonate cements towards the coast. This is most clearly recorded by the test-pit incorporating samples CP07/14 (white) & 15 (red), (Figure 3.3). This abrupt change effectively bisects the site. Understanding these diagenetic environments is therefore an important factor for understanding the development of the site as a whole. These samples have also been examined by the IRSL dating and SEM geochemical analysis (Table 3.2). Mode grain-size sediment from the alongshore locations and CP07 samples covering the 3 inland transects were mounted untreated under cover-slips. Grain coatings and calcite grains remained in the slides, allowing an examination of the relative development of the dune sediment over time and the ability to identify the minerals constituting the sand-sized fraction. Each sample was distinctive, with weathering, roundness, proportions of light and heavy minerals, lithics and cementation the major variables.

Two methods were employed to examine the sand assemblages. A quantitative analysis of 3<sup>rd</sup> order sampled sediments (Ingersoll et al. 1993) using the Gazzi-Dickinson point counting method (Ingersoll et al. 1984) was undertaken as a training set. The study was aimed as a comparison with the macro-scale study by Garzanti et al (2002) of the detrital sediment provenance within the Tyrrhenian basin. A semi-quantitative analysis was also undertaken upon samples from across the site in order to examine the relative development of the sand assemblage over time linked to vadose diagenesis. This approach aimed to understand the link between the cementation (reducing porosity) and the weathering of specific mineral species over time. The *quantitative provenance analysis* in conjunction with the regional provenance study of Garzanti et al., (2002) would provide the 'contemporary assemblage' used as a reference against which the *semi-quantitative diagenesis analysis* was gauged.

### 3.6.4. Point counting

For both the provenance and diagenesis analysis, a *transect* method similar to that used in diatom analysis was used to navigate around the slides, to avoid recounting grains and avoid any potential density sorting of grains during preparation across the area of the thin section. In addition to the overall methodology of Ingersoll et al., (Ingersoll et al. 1984) when a grain is encountered the entire grain is characterised based on the nature of the whole grain. Ingersoll et al (1984) describe the conflicting categorisation of grains based upon the area of the grain under the cross-hair rather than the whole grain which may have a metasomatic alteration rim on one side of the grain and be volcanic in the rest of the grain. Therefore, 90% of the time the grain would be categorised as Lv (volcanic lithic) and 10% as Lmm (metamorphic lithic). To maximise the process information represented by the whole grain this slightly altered method was deemed useful to this study, and this grain would be categorised as Lmm 100% of the time. An ongoing record of relative percentages was kept, with the percentage of relative mineral components checked after 100, 200 and 300 counts to verify that more counts would not significantly alter the proportions. At least 300 grains were counted on

each slide in keeping with the previously outlined research method of other workers and provenance analysis in general.

The slides generally contained a suite of silicate lighter-density minerals with lithics and carbonates, and a suite of heavy ferromagnesian silicates. Within both suites there were metamorphic and volcanic minerals. Following a preliminary survey, a description of the main mineral suites encountered and their geological context follows here as the rationale for further techniques derives from these initial findings (see section 3.6.5).

### **3.6.5. X-ray Diffraction (XRD) analysis**

As discussed in the loss-on-ignition section, deriving significant volumes of fine-grained diagenetic cements was problematic across a dune ridge transect. Preliminary tests suggested that several kilograms of bulk material would be required in some cases to derive a 10 g inter-grain cement sample for XRD analysis, which was not practically or logistically possible. An alternative approach was taken based on assessment of change within the sand-sized mineralogical *sources* rather than the development of *products* during early vadose diagenesis. Additionally, due to practical restrictions on the scale of sampling (hand-dug test pits and hand augering) access to the full depth of weathering profiles was not possible. Due to the allochthonous nature of the geochemical sediments present on the site, a key geochemical source is the sand grains themselves. Therefore a relatively coarse assessment of post-deposition alteration must presently be made. The relative youth of the geochemical sediments under investigation is characterised by the preservation of easily weathered garnets in the sampled “Old dunes” (Borger, 2000 cited in Widdowson, 2007). It should then be kept in mind that the diagenesis study is restricted to the upper sediment profile in the vadose zone generally out-with observed pedogenic horizons with interactions between percolating meteoric water and potentially seasonal exposure to groundwater, allochthonous chemical sources. In the broadest sense, the sediments sampled at Castelporziano can be preliminarily described as early vadose aeolianites and early vadose ferricretes (following the simple scheme of Widdowson, 2007). In the oldest sand sheet samples, bearing in mind the rare pedogenic environments previously described at Castelporziano (Milli & Zarlenga 1991; Arnoldus-Huyzendveld & Gisotti 1999) a degree of laterisation may also occur from the weathering of lithoid tufas and other volcanically derived parent material that characterise the inland portions of the Castelporziano Estate (Manes et al. 1997). The joint application of petrological analysis and XRD on bulk samples was therefore applied to study the weathering trend in the sand-sized minerals with additional diagenetic information expected to be recorded by the X-ray diffractograms. In particular, the low-angle peaks ( $< 15 2\theta$ ) record specific clay mineralogy data (e.g. Van Olphen & Fripiat 1979; Lanson 1997). A semi-quantitative technique, XRD provides relative abundance information of key mineral phases. In conjunction with the petrological microscopy, this combined methodology allows a multi-proxy approach for both provenance and diagenetic studies (Kasper-Zubillaga et al. 2007b). 30 samples from across the range of diagenetic environments pertaining to the range of dune ridges and sand sheets were chosen for analysis.



### 3.7. Optically Stimulated Luminescence (OSL) chronology from K-feldspar

Optically-stimulated luminescence (OSL) dating is an extension and application of luminescence principles discovered during the development of thermoluminescence (TL) from the 1940s onwards (Garlick & Gibson 1948; Randall & Wilkins 1945b; Randall & Wilkins 1945a; Daniels et al. 1953; Aitken et al. 1968; Wintle & Huntley 1979). Both techniques utilise the production of photons from the recombination of electrons into the atomic structure of phosphorescent minerals after an input of energy (thermal or light dependent on technique) into the crystalline lattice. The intensity of the produced luminescence emission is relative to the dose of ionising radiation that mineral grains have received over time by their surroundings. It is this property that permits the phenomenon to be used as a dating technique (Daniels et al., 1953). A bleaching event such as kiln firing (TL) or exposure of sediment to sunlight (OSL) resets the clock by discharging previously accumulated charge. After which, the build-up begins again in pottery or after reburial in sediment dating.

Feldspars and Quartz are the two most significant mineral dosimeters used in luminescence dating techniques. Although both mineral dosimeters display clear thermoluminescence glow-curves, the distribution of traps and recombination centres (and therefore emission peaks) differs significantly due to the atomic and structural impurities and structure of the minerals themselves. Feldspars commonly display brighter luminescence emissions and possess higher saturation levels and therefore older dating limits (ca. 500 ka BP) (Auclair et al. 2003). Feldspars should theoretically be the preferred dosimeter. Due to long-held concerns of anomalous fading (Wintle 1973), dating applications for feldspars have been relatively limited (see Alexander 2007 and references therein). Recent research suggests that feldspars of different composition fade to a greater or lesser degree with sedimentary K-feldspar performing best (Huntley & Lian 2006)<sup>11</sup>. Fading potential may be strongly related to microstructure linked to geological provenance (Lee et al. 1995; Lee & Parsons 1995; Alexander 2007). However, detailed geological provenance analysis is not undertaken as standard for luminescence dating applications. An additional distinction must be made against signal loss due to thermal instability of shallow traps and 'anomalous fading' (Chen et al. 2000). The ability to remove thermally unstable emissions associated with the ~290nm TL peak is undertaken using long sample preheats ( $\geq$  than 10 minutes (Clarke & Rendell 1997; Alexander 2007). Higher temperature preheats may also be suitable (Murray et al. 2009) but this may be sample specific and weakly fading samples may also not respond to higher preheat temperatures (Wallinga et al. 2000a). Avoiding the use of regenerative dose protocols upon feldspars may also be advisable (Blair et al. 2005) for coarse-grained material (as used in this study). Less intensive, additive dose-protocols are then preferable (see below).

---

<sup>11</sup> The use of museum specimens and very high (several thousand Gy) and geologically instantaneous laboratory doses has been suggested to be a poor proxy for examining 'anomalous' fading in natural samples Alexander, S. A., (2007). The stability of the remnant luminescence emissions of alkali feldspar, in *Department of Geographical & Earth Sciences Glasgow: University of Glasgow*, 334.

### 3.7.1. IRSL dating of sedimentary sample framework

Prior research conducted by Rendell and colleagues has shown the Castelporziano site to be suitable for both thermally and optically stimulated luminescence dating protocols using K-feldspar (Rendell 1998; Rendell et al. 2007). In addition, the dating control provided by the archaeological remains further enhances the chronological framework of the site.

**Table 3.5:** SAAD-IRSL protocol used for all samples.

Step	Procedures
1	<ul style="list-style-type: none"> <li>• Sample aliquot preheated to 220°C for 300 s</li> <li>• IRSL readout, 0.5 s at 50 °C</li> </ul>
2	<ul style="list-style-type: none"> <li>• Beta-irradiation, for n (s)</li> </ul>
3	<ul style="list-style-type: none"> <li>• Sample aliquot preheated to 220°C for 300 s</li> <li>• IRSL readout, 0.5 s at 50 °C</li> </ul>
4	<ul style="list-style-type: none"> <li>• Beta-irradiation, for 2n (s)</li> </ul>
5	<ul style="list-style-type: none"> <li>• Sample aliquot preheated to 220°C for 300 s</li> <li>• IRSL readout, 0.5 s at 50 °C</li> </ul>
6	<ul style="list-style-type: none"> <li>• Beta-irradiation, for 3n (s)</li> </ul>
7	<ul style="list-style-type: none"> <li>• Sample aliquot preheated to 220°C for 300 s</li> <li>• IRSL readout, 0.5 s at 50 °C</li> </ul>
8	<ul style="list-style-type: none"> <li>• Beta-irradiation, for 4n (s)</li> </ul>
9	<ul style="list-style-type: none"> <li>• Sample aliquot preheated to 220°C for 300 s</li> <li>• IRSL readout, 0.5 s at 50 °C</li> </ul>
10	<ul style="list-style-type: none"> <li>• Beta-irradiation, for 5n (s)</li> </ul>
11	<ul style="list-style-type: none"> <li>• Sample aliquot preheated to 220°C for 300 s</li> <li>• IRSL readout, 0.5 s at 50 °C</li> </ul>
12	<ul style="list-style-type: none"> <li>• Beta-irradiation, for 6n (s)</li> </ul>
13	<ul style="list-style-type: none"> <li>• Sample aliquot preheated to 220°C for 300 s</li> <li>• IRSL readout, 0.5 s at 50 °C</li> </ul>
14	<ul style="list-style-type: none"> <li>• Sample aliquot preheated to 220°C for 300 s</li> <li>• IRSL readout, 0.5 s at 50 °C</li> </ul>
15	<ul style="list-style-type: none"> <li>• Sample aliquot preheated to 220°C for 300 s</li> <li>• IRSL readout, 0.5 s at 50 °C</li> </ul>
16	<ul style="list-style-type: none"> <li>• Sample aliquot preheated to 220°C for 300 s</li> <li>• IRSL readout, 0.5 s at 50 °C</li> </ul>

A single aliquot additive dose-infrared stimulated luminescence (SAAD-IRSL) protocol upon K-feldspar separates was applied (Rendell et al. 2007) to all samples (Table 3.5). As discussed K-feldspar is a more sensitive dosimeter, producing

a greater noise-to-signal ratio for younger samples than quartz (McKeever 1985; Aitken 1998). The Single Aliquot Additive Dose-protocol (Duller 1991; Blair et al. 2005) allows estimated dose measurements from each sample aliquot. The repeated heating of the material during analysis may lead to changes in sensitivity (Wallinga et al. 2000a) and an underestimation in Equivalent Dose (DE) and therefore sample age. However, this behaviour may be directly linked to provenance (Preusser 2003)<sup>12</sup>. As a check 6 aliquots, in addition to the 12 dating aliquots, are measured at the preheating and readout temperatures used in the dating run (220°C and 50°C, respectively). Data from this procedure is then used to correct for sensitivity changes during the dating measurements. Following a test-run using 1 aliquot, the additive dose interval was assessed based upon the estimated dose/s calculated from this single aliquot. Additive doses are produced as a function of the source dose-rate over time  $n$  (s). Short-shine readouts of 0.5 s are used for all IRSL readouts.

Steps 13 – 16 are repeated readouts of the same 6n additive dose. During curve-fitting, readouts 14 – 16 should sequentially produce lower readouts as stored charge is removed by each subsequent short-shine measurement. These additional readouts are removed during curve-fitting to derive the growth-curve for each individual aliquot. The x-intercept is then extrapolated from this growth curve to derive the estimated dose (DE). K-feldspar does not respond well to regenerative protocols that are now standard for quartz dosimeters which has been shown to produce sensitivity changes (Wallinga et al. 2000b; Blair et al. 2005). Due to DE extrapolation poor curve-fitting performance will produce less accurate x-intercept values. Age control by high-status archaeological buildings is possible for several samples, and the progradational nature of the dune ridge record suggests stratigraphic order should be fulfilled.

#### **3.7.1.1. Fading experiment**

According to Huntley and Lian (2006) all feldspars display some degree of ‘anomalous’ fading. In order to ascertain the samples’ propensity for signal loss over time, 6 samples from across the age range and diagenetic environments of the site were tested. 4 aliquots of K-feldspar separates from each sample were prepared. The first 2 aliquots were given laboratory doses ( $\beta$ ) of a similar magnitude to the measured DE of each specific sample. The remaining 2 aliquots were given laboratory doses of  $2\beta$ . Short-shine readouts were used (0.5s). Readouts after laboratory dosing and after 14 weeks were made. The ratio of  $\beta/2\beta$  was calculated for aliquots 1 and 3, and 2 and 4 respectively. The ratio between the initial readout and 14 week readout ratio was then calculated. Signal loss would be observed as a ratio of  $< 1$ . A variance of  $< 10\%$  was proposed as suitable data quality following Alexander (2007) and generally accepted precision for luminescence dating applications.

---

<sup>12</sup> Also notable is that the young quartz from Alpine Orogenic sources has been observed to display poor or absent luminescence properties, making it a potentially unsuitable dosimeter for luminescence geochronology (Preusser, 2003). The major source of quartz to Castelporziano has been shown to ultimately derive from Alpine sources (Garzanti et al., 2002).

### **3.7.1.2. Age control**

Age control is provided by radiocarbon dated chronology of dune ridges from the vicinity of *Portus* (Giraudi et al. 2009), which describes the same phases of dune ridge development as that sampled further alongshore at Castelporziano, providing context for the aeolianite deltaic dunes. Currently there is no age control for the ferricrete sand sheets and samples except by stratigraphically pre-dating the aeolianite dune-ridge chronology. In addition, the high-status archaeological remains can often be dated on multi-decadal time-scales due to distinctive building styles or more commonly dated brick stamps. In some cases the age of construction can be known to a single year. This precision is generally better than the standard error in age estimates from luminescence chronology. In some cases AMS-<sup>14</sup>C dates from specific areas of the site also provide a temporal reference for assessing the luminescence chronology such as at the *Piscinae*. It is not thought that contamination by old carbon is a significant problem for radiocarbon dating. Intrusion by marine water is not thought to be significant (Busuoli et al. 2001). Intrusion of DIC in carbonate-rich groundwater is the most likely source of contamination and where possible care has been taken to remove inorganic carbonate using HCl treatments. As a result <sup>14</sup>C dating material used in this thesis is taken exclusively from organic sediments. Roots and plant macrofossils have been avoided due to risk of anomalous stratigraphic locations (root penetration) and post-depositional movement/turbation in the case of plant macrofossils.

### **3.7.1.3. Luminescence dosimetry**

In a Retsch Ball Mill, 60g of dried bulk dosimetry sample were ground at 300rpm for 15minutes. The produced fine-milled sample was used for all thick-source alpha (Aitken 1998) and beta (Sanderson 1988) radiation dosimetry measurements (see McKeever 1985: 274-281).

### **3.7.1.4. Alpha dosimetry protocol**

3g of milled sample was placed in the sample container containing a filter, measured previously for the background alpha radiation level in the lab. Samples were measured for at least 3000 counts in a Daybreak Alpha Counter. The sample container was then unsealed and spacers were placed under the seal to prevent full closure. An unsealed count was made to assess the potential loss of Radon gas driving disequilibrium in dosimetry calculations.

### **3.7.1.5. Beta dosimetry protocol**

Using a SUERC Thick-source Beta counter (TSBC) (Sanderson 1988), 15g of ground sample were measured for their beta-radiation emission. A Shap granite standard and Magnesium oxide (MgO) was measured (4 x 1 hour) prior to and following sample measurement (12 x 1 hour) to calibrate the sample readout against the known radioactivity of the standards.

### **3.8. Application of methods**

Chapter 4 presents and analyses the results of the methodology outlined above. Chapter 5 then attempts to apply this analysis to answering the research questions within a multi-scale Geoarchaeological approach focused primarily, but not exclusively, upon meso- to macro- spatial and temporal scales. These scale relationships are outlined in chapter 2 and interrogated in chapter 5.

## 4. Results & Analysis

The results and analysis are ordered with reference to Chapter 3: Methodology. However, because the integrated approach predominantly affecting the geochronology, and taphonomy and diagenesis aspects often leads to results that relate to disparate portions of the text, links are provided for clarity. The bespoke GIS-based mapping outlined here is then copiously used throughout chapter 5 to illustrate the key geographical relationships between the various strands of the analysis. Statistical analyses are presented for various results, most notably regarding diagenetic petrology and the luminescence-based geochronology.

### 4.1. Topographic Survey

#### 4.1.1. Aerial photography

Aerial photographs (APs) were provided by the Istituto Geografico Militare, Florence. Coverage of the southern flank of the Tiber Delta from 1954, 1983, and 2002 was obtained. Due to a lack of modern building coverage, the 1954 series' APs record substantial geomorphological information on the distribution of dune ridges, palaeo-channels and some unexcavated archaeological remains. Reduced forest cover due to Allied activity during the latter stages of the Second World War was also beneficial for examining the immediate vicinity of the *Vicus Augustanus*. The central Tiber Delta area around *Portus* and *Ostia Antica* is also devoid of the intensive building that characterises the current Tiber river mouth and delta front. In particular, much of the road network within the Castelporziano Estate appears in its current state prior to 1954 providing valuable locations for ground control points (GCPs) useful for all subsequent AP sets. The 1954 AP series provide an effective mapping scale of around 1:30,000. A key feature of the 1954 AP series is the relatively depleted canopy due to a significant forest fire. Large areas in the vicinity of the *Vicus Augustanus* exhibit only sparse vegetation, increasing the visibility of some archaeological remains and of coastal dune topography. The 1983 series' APs are photographed at a lower altitude and provide an effective mapping scale of around 1:20,000, preserving detailed geomorphological information of dune ridges even under the forest canopy and coastal hydrology. More in-depth photogrammetry based on these photosets was, however, constrained by the limited distribution of possible GCPs. Recent canopy growth over several potential GCP locations prevented accurate D-GPS measurements due to poor GPS signal reliability.

For clarity, key archaeological and historical sites are presented by name in figure 4.1; site codes relate to (Lauro & Claridge 1998). Of these D5 and D6 are the Roman *Piscinae* (fish ponds), F2 is the sea wall, and G3 is the Villa del Discobolos. The selected AP photosets are presented and georeferenced below in section 4.2.



**Figure 4.1:** Key archaeological sites mentioned in the text in relation to the contemporary geomorphology and 1954 series aerial photographic record. Site codes refer to Lauro and Claridge (1998) and are described in the text. Modern hydrology and relict dune ridges are also shown, details of this mapping can be found in section 4.2. The pertinent dune ridges associated with the ‘Laurentine Shore’, Roman-period palaeo-shoreline are highlighted in bold. The area of archaeological interest is primarily within the 5 m contour. Also of note is the large parabolic dune aligned with the dominant onshore westerly wind, seaward of D3.

#### 4.1.2. Digital Elevation Models (DEM)

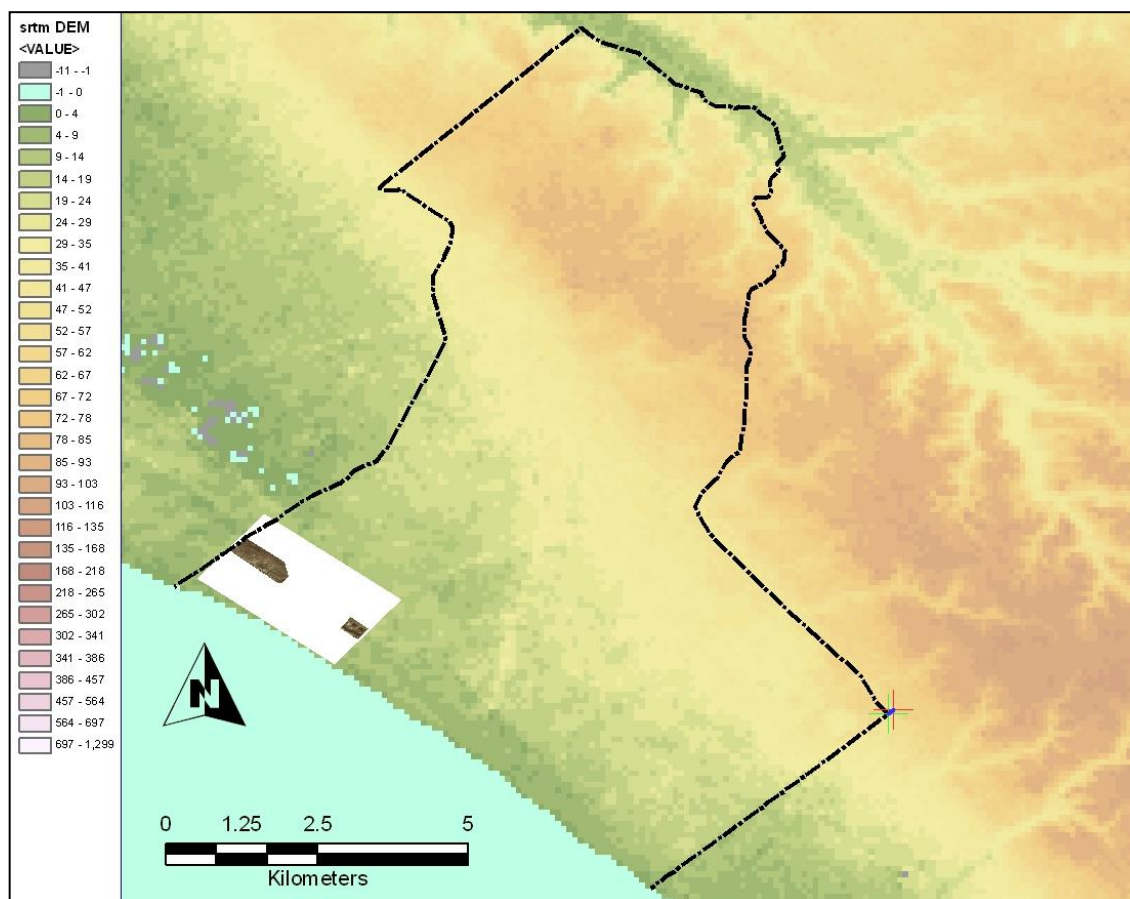


**Figure 4.2:** Location of archaeological DEM within the Castelporziano Estate around the *Vicus Augustanus* (NW) (figure 4.3) and *Piscinae* (SE) (Figure 4.6). Details are presented below. SRTM topographic data, re-coloured in ArcGIS 9.2, provides a regional base map for the southern Tiber valley and immediate Tyrrhenian Sea coast. Legend scale is in metres.

Digital elevation models (DEM) produced from detailed total station measurements (Figure 4.2) encompass the vicinity of the *Vicus Augustanus* (Figure 4.3) and *Piscinae* (Figure 4.6). The survey work was carried out by researchers from RHUL Dept of Classics between 2003 and 2009 on a local coordinate system. These models provide valuable geomorphological information regarding the context of the archaeological remains and the phase of dune ridge formation immediately following the Imperial Roman occupation of the site. D-GPS georeferencing of key points within the total station survey has allowed the DEM to be corrected to both relative sea level (RSL) and estimates of Roman sea level at ca. 2ka BP. The total station survey is also a primary survey record of the archaeological excavations. Therefore, the archaeological structures can also be considered in relation to RSL and estimates of Roman-period sea level, ca. 2000 BP. In addition shuttle radar topographic mission (SRTM)<sup>13</sup> data are readily downloadable from the US Geological

<sup>13</sup> <http://srtm.usgs.gov/> (last accessed 15/09/2009).



Survey (USGS). The 90 m resolution makes it unsuitable for detailed, micro-scale representation as provided by the total station DEM but provides valuable macro-scale georeferenced (WGS84) topographic context.

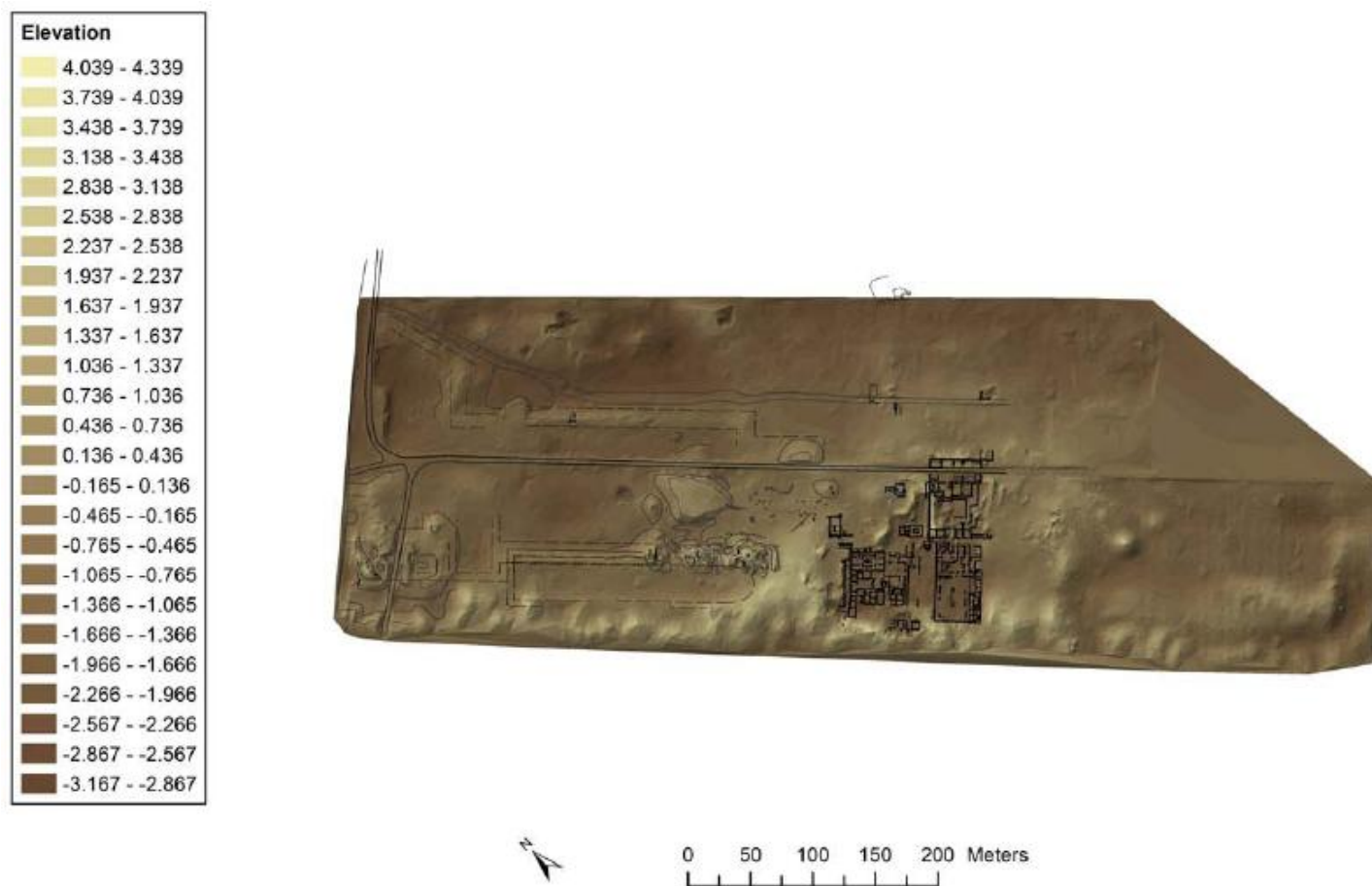


**Figure 4.3:** DEM of *Vicus Augustanus* and environs (RHUL, Dept of Classics). The considerable volumes of aeolian sand that buries much of the archaeological remains can be seen along the base of the image (J. Andrews, 2009).

#### 4.1.3. Dune ridge transects – wavelength, frequency and amplitude

Four inland dune ridge transects were surveyed using a Leica total station with coverage limited to the late Holocene by dense forest cover and security access (Figure 4.4). The Tyrrhenian coast is effectively perpendicular to the orientation of the topographic transects. Associated dune-ridge transects are presented below (Figure 4.5). The hinterland behind the *Vicus Augustanus*, which is relatively free from historical & modern excavation spoil heaps, is presented its westerly portion is incorporated into the *Vicus* DEM (Figure 4.3). The *Piscinae* transect position is also overlain onto the *Piscinae* DEM in Figure 4.6. All dune transects are adjusted relative to a published Roman period sea level estimate of -1 m RSL (Lambeck et al. 2004b) (figure 4.5). The modern coastal topography that is associated with the archaeological remains is typically 2- 3 m above Roman period sea level; the archaeological remains being at or very close to the modern ground surface. The extent of this transect constrains the area occupied by the upstanding archaeological remains of the

'Laurentine Shore' from 350 – 600 m of this surveyed topography. Between 0 – 400 m and around 1000 – 1200 m there is a clear decrease in wavelength and an associated increase in frequency of the dune ridge topography (taking into account the complicating effect of post-formation remobilisation of secondary dune forms). The amplitude of the dune topography is liable to be altered by erosion of the dune topography increasing further inland, linked to age and also with foci of anthropogenic activity. Post-deposition erosion and also smaller ridge-like topography that appears to be superimposed upon the larger dune ridges makes assessment of amplitude change problematic but in general dune crest amplitude appears broadly comparable with this dataset. Pre- and post-Roman dune ridge topography (i.e. dune ridges inland and seaward of the archaeological remains) displays a wavelength of roughly 50 m. In the areas where key Roman remains have been discovered the dune ridge wavelength increases to over 150 m. This trend is also seen between the area occupied by the *Vicus Augustanus* and its inland environs after around 300 m.

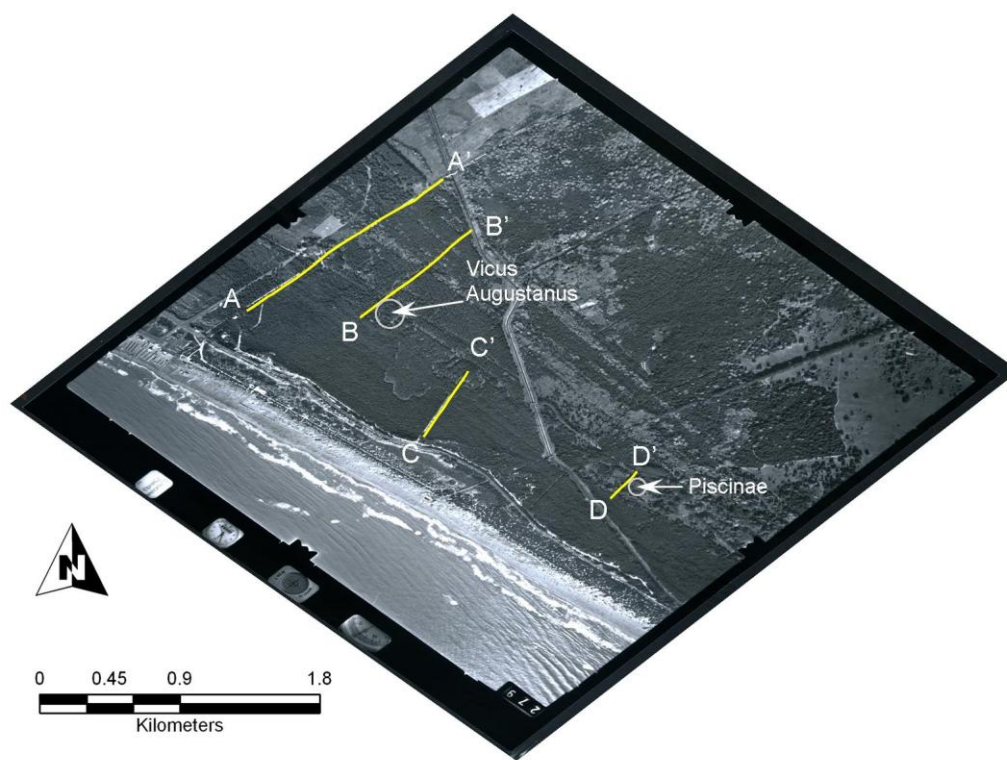


**Figure 4.4:** Extent of dune ridge transects overlain onto 1983 series aerial photograph #279. The general position of key archaeological sites is also shown. Transect **A-A'** bisects the large Villa B1 that continues in the neighbouring Castel Fusano to the NW. Transect **B-B'** covers the *Vicus Augustanus* and its inland environs. Transect **C-C'** records the topography of the Grotte di Piastra (Villa Magna) and the post-Roman dune ridge record. Transect **D-D'** focuses upon the context of the *Piscinae* (figure 4.6).

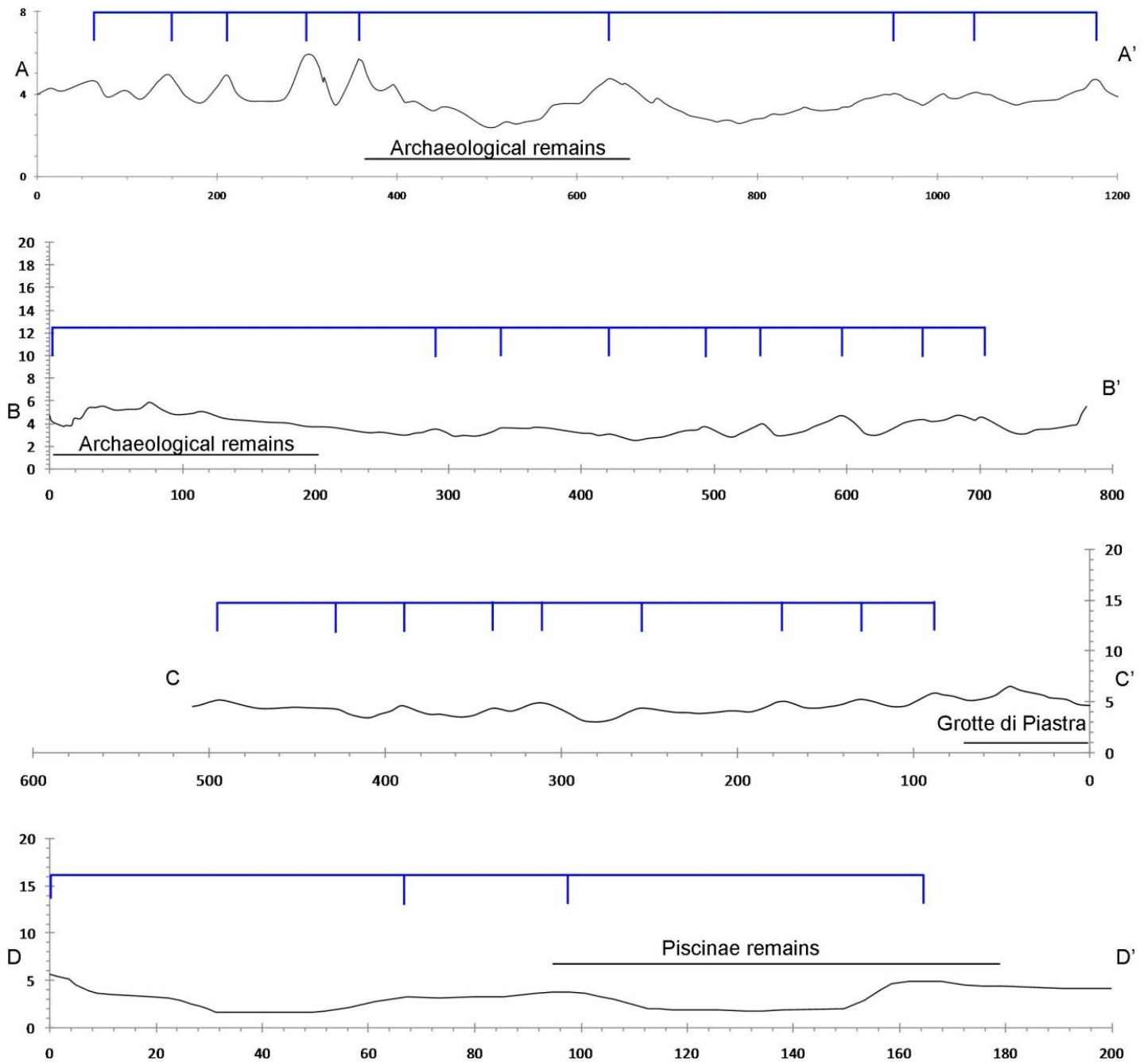


**Figure 4.5:** Dune ridge transects labelled in figure 4.4, dune heights are corrected to Roman period sea level of -1 m RSL. The upstanding archaeological remains are thus consistently around 3 m above their contemporary sea level around 2000 BP. Dune ridge wavelengths of prominent higher-amplitude dune ridges are highlighted above each cross-section. The general horizontal extents of the key Laurentine Shore archaeological sites are also labelled, note that these labels do not represent the depth of the remains. Pre- and post- Laurentine Shore dune ridge frequencies especially clear from transects A and B, respectively are relatively increased. Conceptually, this change may be due to changing progradation rates of the Tiber Delta. The presence of smaller dune ridges that appear superimposed upon a greater amplitude wave form is a common feature of the dune ridge morphology. In addition in the vicinity of archaeological remains old excavation spoil heaps and human disturbance in general complicate the topography.

The dune ridge topography immediately in front of the *Villa Magna (Grotte di Piastra)* likely post-dates the Roman shoreline and is also characterised by a higher frequency, lower wavelength dune ridge topography;  $\lambda \approx 50$  m. Assuming that this dune ridge topography is of a similar 'Prograding Coast' nature to that described in the models of Hesp (Figure 1.6, box A) then the threefold increase in dune crest transect wavelength in the vicinity of the Laurentine Shore remains could be interpreted as the effect of changing progradation rates, with an increased progradation rate linked to increased sediment supply. Due to the many multi-scale variables affecting coastal dune formation Hesp (2002) emphasises problems of equifinality when interpreting dune ridge morphology. Several contrasting sets of conditions can cause similar expressions of dune form. Sea level during the likely period of formation, i.e. during the late Holocene, has continued to rise at a relatively slow rate (see chapter 2). The regional climate is characterised by the summer drought / winter deluge seasonal cycle, whereas on centennial time-scales sub-orbital climate fluctuations driving the relatively warm/dry and cold/wet periods such as the Roman Warm Period and Little Ice Age, respectively may be important for dune formation and sediment supply. Storm effects may be very important but the records presented here are unlikely to preserve a clear record without a dedicated micro-scale sampling strategy. Within the context of the site setting (chapter 2) it is possible to argue that the micro-tidal and slowly rising Mediterranean Sea is unlikely to be a critical factor for interpreting the dune ridge topography during the late Holocene as the magnitude of change is on decametre scales. Certainly sea level lowering is not thought to have occurred (Lambeck et al. 2004a), negating the implications of this change upon coastal fore dune morphology (Hesp 2002). Thus the significant variability observed in dune ridge wavelength and frequency are perhaps more likely driven by climate and / or sediment supply. The sites' deltaic position suggests that sediment supply is likely to be fundamental to any interpretation of the macro-scale context of the Laurentine Shore palaeo-coastline.

In the vicinity of the *Piscinae*, the dune ridge transect suggests a smaller wavelength of 80 m. During excavations, the low-ridge at 100 m was found to be aeolian sand burying a seaward wall of the *Piscinae's* associated buildings. A corresponding wall on the landward side of the ponds at 160 m is also buried by structureless aeolian sand, suggesting both anthropogenic and aeolian processes have partially obscured the initial dune ridge topography, making interpretations solely on cross-section topography less effective in the vicinity of archaeological remains. The relatively smaller wavelength exhibited here is probably primarily due to the alongshore position of this transect and associated narrowing of the Tiber Delta towards the southern distal end. The *Piscinae* transect is also interrupted by the Fossa dei Muraccioli which runs roughly parallel to the modern shoreline predominantly along the lines of the inter dune slacks. This relatively natural drainage network is then intercepted by the Canale del Pantanello just to the NW of the *Piscinae*.

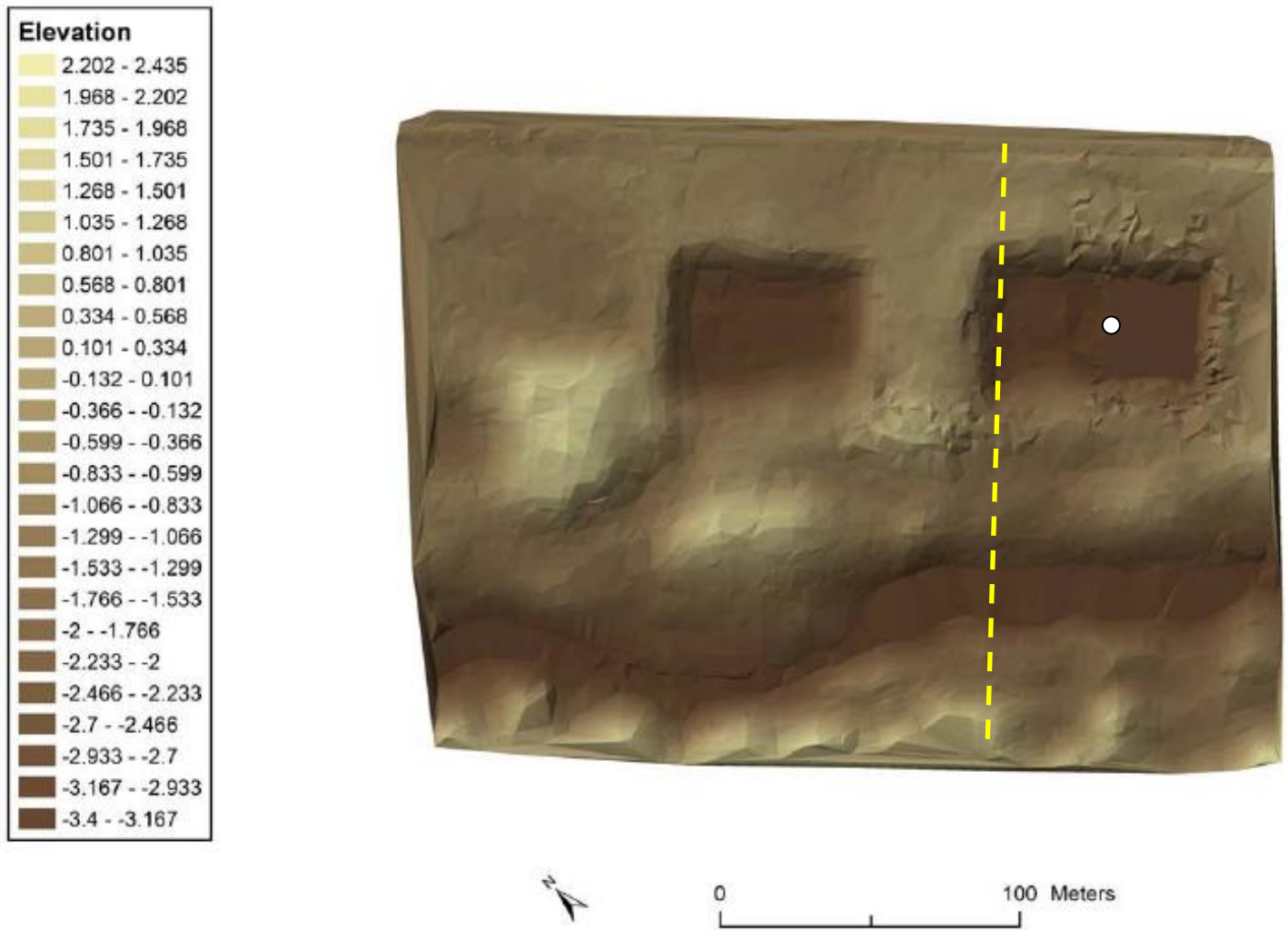


Figure 4.6: *Piscinae* DEM and transect D-D' alignment (adapted from original by J. Andrews, 2009), core 14 coring location is also highlighted (O).

## 4.2.D-GPS georeferencing

### 4.2.1. Summary of system & method

Due to a lack of suitable fixed points within the Castelporziano Estate, a locally georeferenced survey was required in order to relate the various topographic surveys to sea level and global coordinate systems. All survey positions are presented in the WGS84 coordinate system. Two Leica SR20 single-frequency D-GPS receivers with AT501 tripod-mounted antennas were used for all D-GPS measurements. Due to the dense forest canopy, reliable GPS signal reception and therefore measurement locations were severely limited. GCPs from road junctions across the Castelporziano Estate provided 7 high-quality positions (Table 4.1). Further positions were measured on DEM fixpoints in order to georeference the existing total station survey. In this difficult survey environment, in order to obtain <3m GDOP (General Dilution of Precision) in the raw GPS counts, it was necessary to undertake long counts often over 1- 3

hours. This data were then post-processed using RINEX reference files from the INGR-Roma GPS station, ca. 25 km NE of the site. Leica Geo-office v5.0 was used for all post-processing calculations. A Universal Transverse Mercator (UTM) projection, centred on zone 33n and the EGM '96 Geoid model, underpins each position. Geoid separation values were then calculated producing meaningful orthometric heights above current sea level. The EGM '96 geoid model<sup>14</sup> was tested against modern sea level and found to produce effective results (section 3.3.1). Data post-processing typically produced centimetre precision on position altitude. Where multiple measurements of the same positions were able to be made, position accuracy was also typically sub-centimetre on latitude, longitude and, critically, altitude (see below).

**Table 4.1:** Ground control points, positions and point quality.

Code	Latitude	Longitude	Orthometric height (m RSL)	Description
<b>GCP 1</b>	41°42'42.29738" N ± 0.007 m	12°21'46.22818" E ± 0.006 m	5.0577 ± 0.15	ALI 2008 fixpoint. Western boundary wall, canale bridge NE corner
<b>GCP 2</b>	41°42'23.32292" N ± 0.016 m	12°21'18.59436" E ± 0.02 m	3.169 ± 0.028	Junction of Via Telefono & Via Mare adjacent to B1 villa
<b>GCP 3</b>	41°42'30.72773" N ± 0.004 m	12°21'49.59669" E ± 0.005 m	4.8884 ± 0.009	Canale bank, north of <i>Vicus Augustanus</i>
<b>GCP 4</b>	41°41'54.27477" N ± 0.006 m	12°22'2.28717" E ± 0.005	4.5976 ± 0.016	Canale bridge / Via Telefono SW corner
<b>GCP 5</b>	41°41'46.47769" N ± 0.016 m	12°22'14.57217" E ± 0.014 m	3.6471 ± 0.04	Junction of Via Telefono / Presidential Chalet road, SE corner
<b>GCP 6</b>	41°41'17.97489" N ± 0.004 m	12°22'52.43942" E ± 0.003 m	3.1732 ± 0.01	Via Telefono bridge / Fossa del Figurone della Santola, NW corner
<b>GCP 7</b>	41°42'30.19396" N ± 0.004 m	12°24'1.38540" E ± 0.004 m	20.5831 ± 0.013	Fontana, E junction of mid-point spar. Junction of Tor Paterno road / Chalet road / la Santola road
<b>INGR-Roma</b> Post-processing reference	41°49'41.10316" N ± 0 m	12°30'53.28119" E ± 0 m	56.0507 ± 0 m	Rooftop pillar, Istituto Nazionale Di Geofisica E Vulconologia, Roma University. Via Di Vigna Murata 605, 00143 ROME.

<sup>14</sup> <http://cddis.nasa.gov/926/egm96/egm96.html> (14/06/2009).

#### 4.2.2. GCP locations & GIS construction

GCPs are shown in figure 4.7 and figure 4.8. Seven points yielded precise D-GPS positions. The area encompassed by these positions contains the majority of the archaeological remains and relict dune ridges. The seaward portion of the site, containing the post-Roman geomorphology, is relatively devoid of suitable or accessible GCP locations. Tie-points were created based on the modern coastal highway and permanent beach structures such as the Presidential beach chalet. This combined approach permitted the georeferencing (using ArcGIS 9.2) of APs and maps in lieu of GCPs in all areas of interest. Root mean square (RMS) errors from georeferencing were typically small (Table 4.2).

**Table 4.2:** Aerial photo georeferencing. GCPs used for each photo and numbers of tie-points. Transformation type and RMS error of fitting are given.

Aerial Photo ID	GCPs used	Transformation	RMS error
279 (1983)	1, 2, 3, 5	1 <sup>st</sup> order polynomial	0.00002
293 (1983)	5, 6 + 1 tie point	1 <sup>st</sup> order polynomial	0.00000 (requires 4 points)
748 (1954)	1, 4, 5, 6, 7	2 <sup>nd</sup> order polynomial	0.00003
764 (1954)	1, 2, 3, 4, 5, +5 tie points	1 <sup>st</sup> order polynomial	0.00014
765 (1954)	4 tie points	1 <sup>st</sup> order polynomial	0.00021
455 (1954)	5 tie points	1 <sup>st</sup> order polynomial	0.00008
456 (1954)	6 tie points	1 <sup>st</sup> order polynomial	0.00009

The georeferenced aerial photographs (APs) underpin the digitisation of the current delta morphology, dune ridge features and Roman period archaeological remains from within the Castelporziano Estate and also the southern flank of the Tiber delta from Fiumicino to the Capacotta Estate on the southern margin of the Castelporziano Estate. The 1983

APs provide a high quality record of the coastal margin of the Castelporziano Estate incorporating the Laurentine Shore archaeological remains of the *Vicus Augustanus* (Lauro & Claridge 1998) to the *Villa del Discobolos* (Goalen & Fortenberry 2002) (figure 4.1).

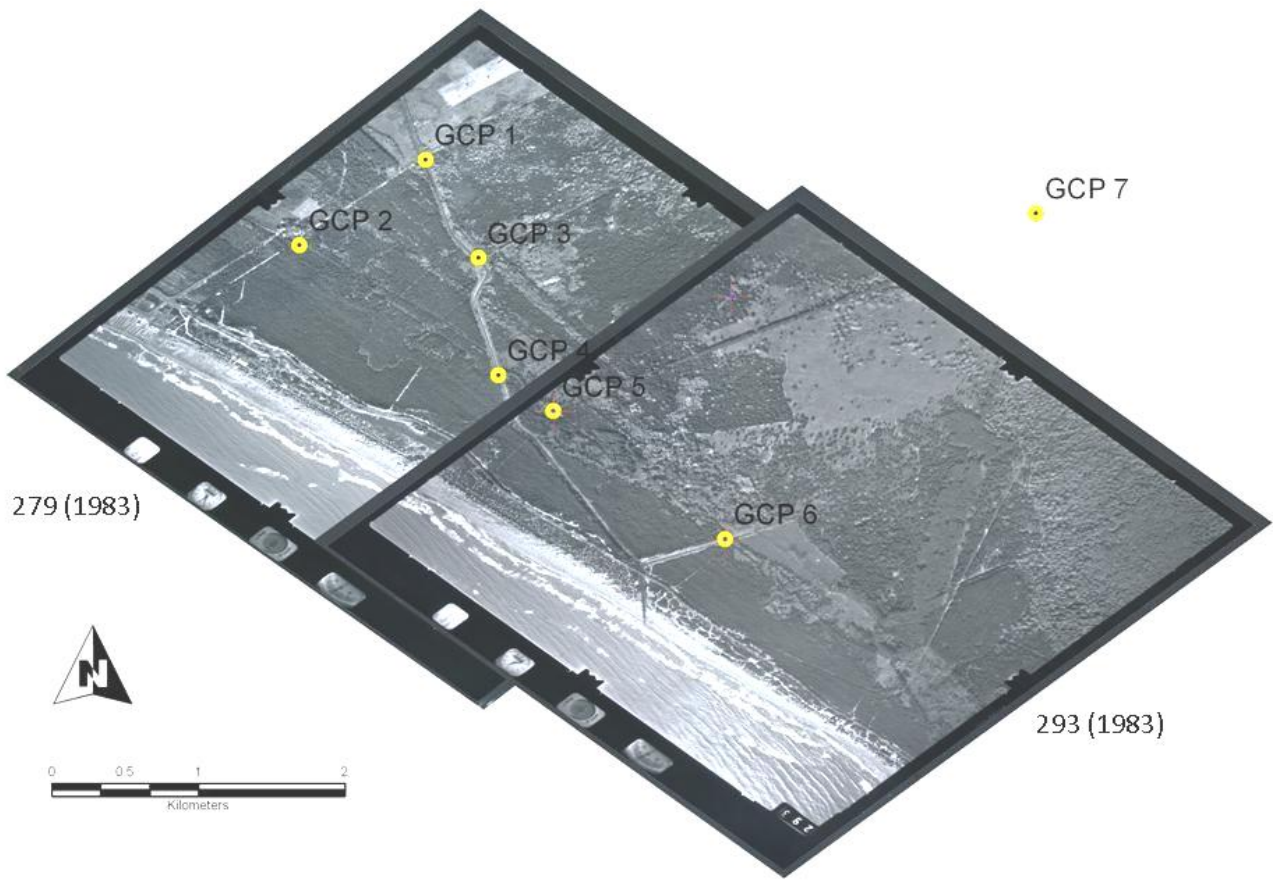


**Figure 4.7:** Georeferenced aerial photographs taken in 1983 (Istituto Geografico Militare) (frame codes are shown with year taken in brackets). The path of the Canale del Pantanello is clearly visible running from NW to SE through the site adjacent to GCPs 1, 3 and 4. The dense forest cover over most of the area of interest severely limits the choice of GCP locations. Security considerations also prevent access to much of the modern coastal zone. However, the excellent site preservation due to an almost complete lack of modern development at the site does allow a fairly unique geomorphological and archaeological record to be investigated.



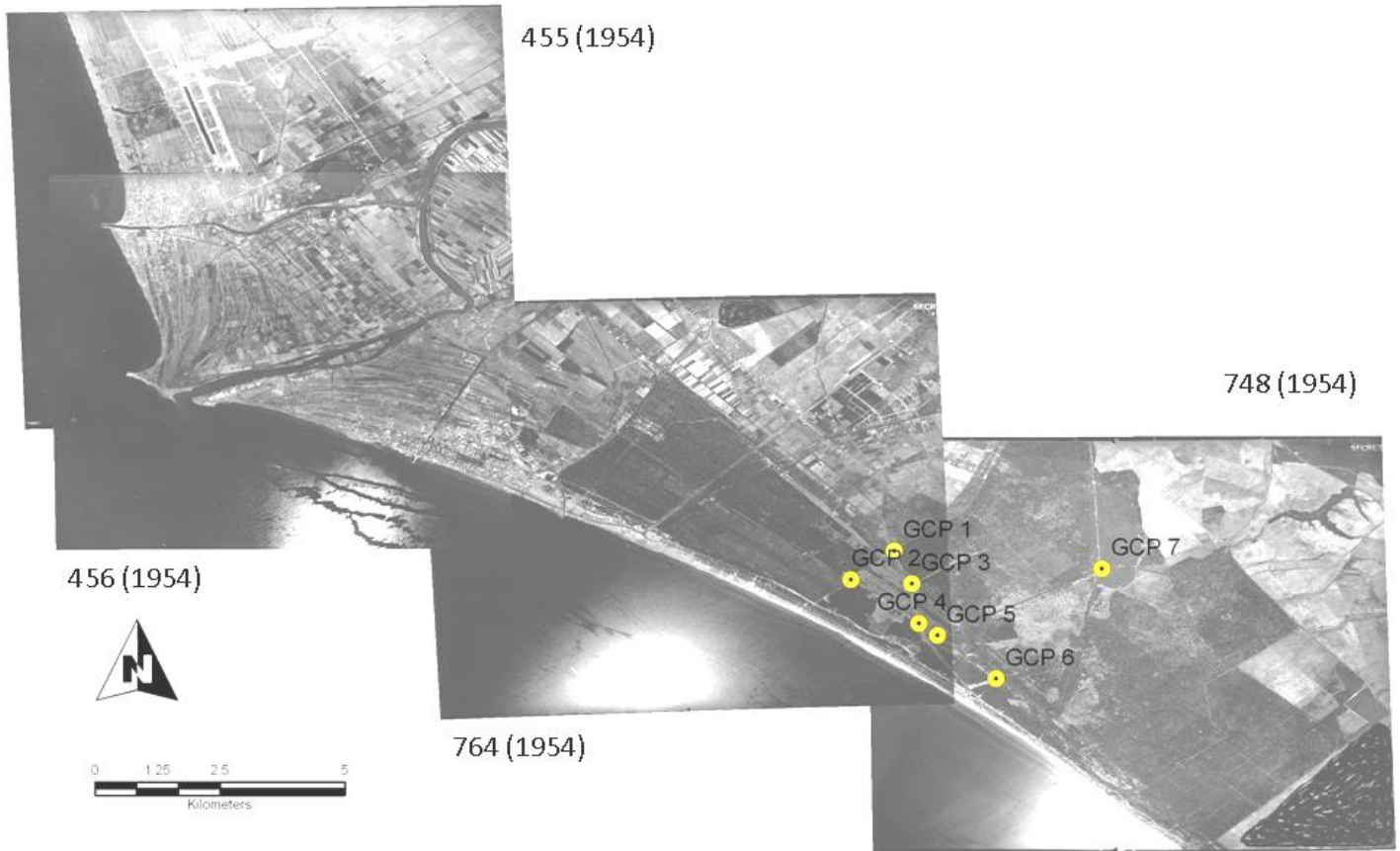


**Figure 4.8:** Georeferenced 1954 aerial photographs (Istituto Geografico Militare). Tie points are used out with the coverage of the Castelporziano GCPs. RMS errors are typically small for all images providing an accurate base-map for GIS mapping. The AP georeferenced coastline also agrees well with georeferenced SRTM topographic data.

GIS reconstruction of the broader geomorphological and archaeological context of the Tiber delta is based on several key datasets and maps (figure 4.9). The reconstruction of the Laurentine Shore within the Castelporziano Estate is borne largely from field measurements and AP interpretation which is described in the following sub-sections. The broader Tiber delta context of the Laurentine Shore is well-presented by the 1954 APs. Due to the relative lack of extensive construction on the Tiber Delta in 1954, dune ridge and delta structure is well-preserved in these images. Georeferencing of this archive provides the modern coastline presented in GIS-reconstruction maps (as the shoreline from 1983 APs showed little difference). The preservation of delta structure and relict dune ridges has also permitted the tracing of the Roman-period palaeo- shoreline characterised within the Castelporziano Estate to be extended towards the remains of *Ostia Antica* (Heinzelmann 1998) and *Portus* (Keay 2005) (figure 4.9). The reconstruction of the 2<sup>nd</sup> century AD shoreline was made in conjunction with these published maps and the dune ridge chronology presented below. Further key geomorphological data were supplied by the macro-scale late Quaternary reconstruction of the Tiber Delta by Bellotti and colleagues (2007) and dune ridge phases around *Portus* by Giraudi et al (2009) (not shown in figure 4.9).

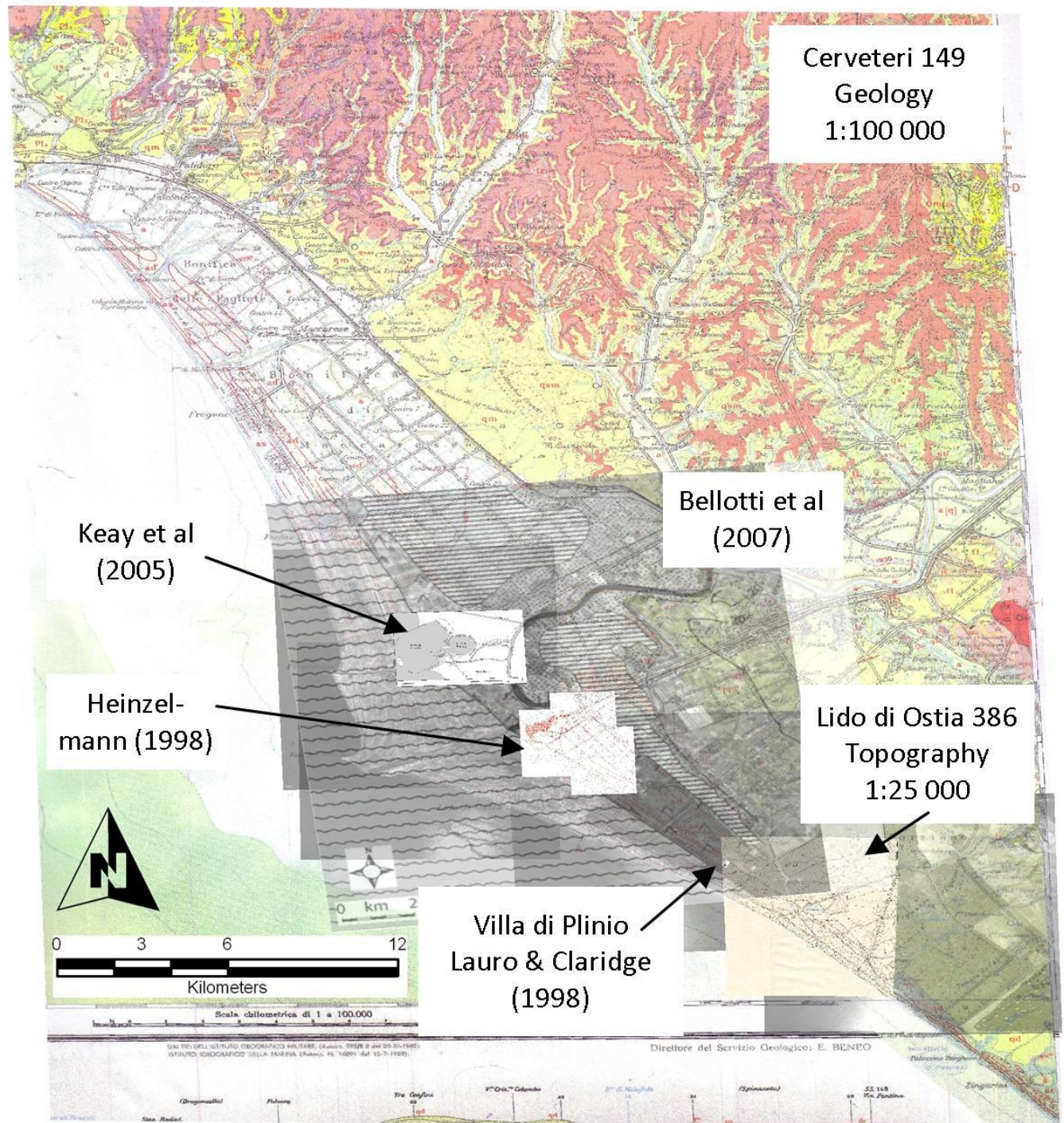


**Figure 4.9:** GIS integration of selected geological and topographic mapping, aerial photography and archaeological mapping datasets

#### 4.2.2.1. Mapping hydrology

Roman hydrological features such as the *Piscinae* can be easily recognised by the change in forest canopy associated with the presence of Ash, rather than Oak. These seasonally flooded areas favour this change in tree cover. This change to a lighter coloured canopy also aids the identification of the location of other wet areas (figure 4.10). The extent of delta lagoons, landward of *Portus* and *Ostia Antica* is digitised from the data of Bellotti et al (2007) and constrained by AP evidence included in Heinzelmann (1998) and also from the 1954 and 1983 (using stereoscopically observed un-georeferenced) APs. The extent of the southern lagoon in particular is described by the presence of ‘tide marks’ preserved as crop marks in arable fields (figure 4.11).

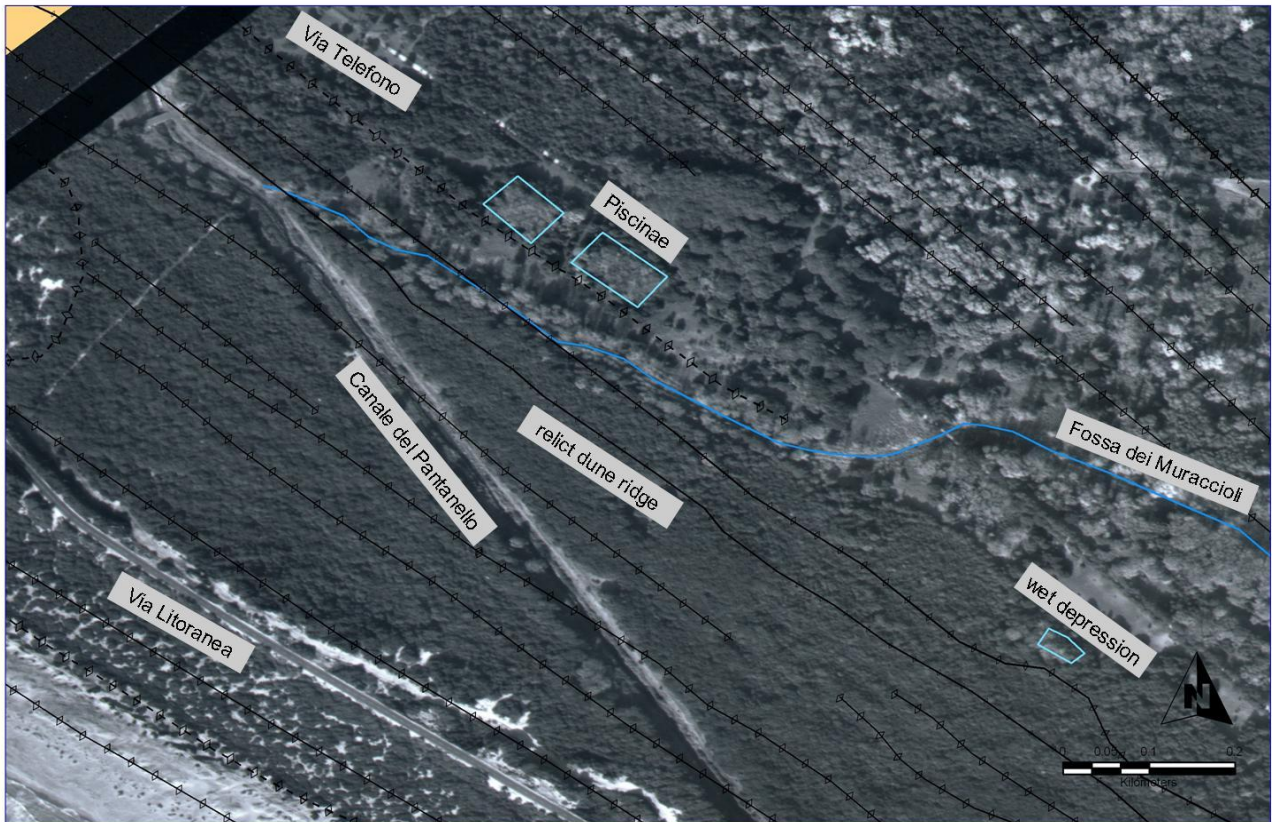


**Figure 4.10:** Digitisation of hydrological features and dune ridge topography. Black linear features superimposed with open diamonds denote relict dune ridges.



**Figure 4.11:** Crop-marks preserving 'tide-marks' of relict delta lagoon adjacent to *Ostia Antica* abutting the NW boundary of the Castelporziano Estate.

#### **4.2.2.2. Mapping dune ridges**

Figure 4.10 also shows the clarity of relict dune ridges in the 2003-series APs. In conjunction with handheld GPS locations it was possible to map the extent of these features even under the dense forest canopy and where dune ridge topography was unclear from the photographs.

### **4.3. Sea-level Reconstructions**

In addition to providing GCPs, the D-GPS system was also used to precisely locate key sea level features; the silt/peat transition preserved in *Piscinae* D6, and tide-cut notch in the sea wall F2. A tidal interpretation is suggested for the notch based on the concave, eroded form, of a similar morphology to other examples studied from the western Italian coast (e.g. Antonioli et al. 2002). Above the notch the bricks comprising the main facing of the structure have well-defined corners and edges and are generally in good condition. Level with, and below the notch the bricks are

destroyed or significantly rounded and eroded due to the action of water. This selective and highly partitioned erosion pattern suggests that aeolian erosion is not the cause.

#### **4.3.1. Core 14 sedimentary transition – *piscinae* D6**

Direct measurement of the D6 core site was not possible due to the broad canopy of several mature ash trees growing within the infilled *Piscinae*. The DEM of the fish ponds did however include several fixpoints within the base of the feature. The altitude of the sediment cores was therefore precisely calculated using the georeferenced DEM and local measurements of the core location and the depth of the stratigraphic change (see section 4.11). The greatest error within this system of calculations is the microtidal range of the Mediterranean Sea. Therefore all sea level measurements, whether contemporary or historical are cited with  $\pm 0.2$  m error. The constituent measurements are, however, much more precise. By this method, the precise altitude of the sharp peat/marsh contact was obtained at  $-1.25 \pm 0.2$  m RSL (see section 4.11 for full details).

#### **4.3.2. Sea wall notch**

Due to the position of the sea wall structure under dense canopy, direct D-GPS measurement of tidal notch positions was also not possible. A suitable clearing adjacent to the sea wall remains permitted repeat measurements of a local control point. Utilising total station survey and also relative levels using a Leica NA720 system ensured a precise measurement of the tide-cut notch preserved in the seaward face of the sea wall F2. Following D-GPS post-processing, the mid-notch height is  $+1.756 \pm 0.2$  m RSL (n.b. the depth upper and lower limits of the notch is 0.4 m).

### **4.4. Sedimentology**

#### **4.4.1. Grain-size analysis**

All grain-size analysis was conducted with a Beckman Coulter LS230 laser particle sizer. Measurements were made in triplicate, the average of which was used for grain-size analysis calculated using GRADISTAT v5 (Blott & Pye 2001). This method of analysis assumes a spherical grain shape. Due to the aeolian and well-travelled nature of the sediments under study roughly spherical grains are the norm; this is confirmed by microscopy. Grain-size measurements are then conceptually simple (Blott & Pye 2008). Sand-sized sediments showed highly stable grain-size distributions during laser particle sizing with minor variation between repeat measurements. Fine-grained silty sediments recovered from the *Piscinae* D6 (see diatom analysis section 4.12.1 for further details) were more problematic to analyse but comparable repeat measurements were possible after 3 – 6 measurement cycles. Folk and Ward statistics (Folk & Ward 1957; Folk 1966) are presented throughout in metric units.

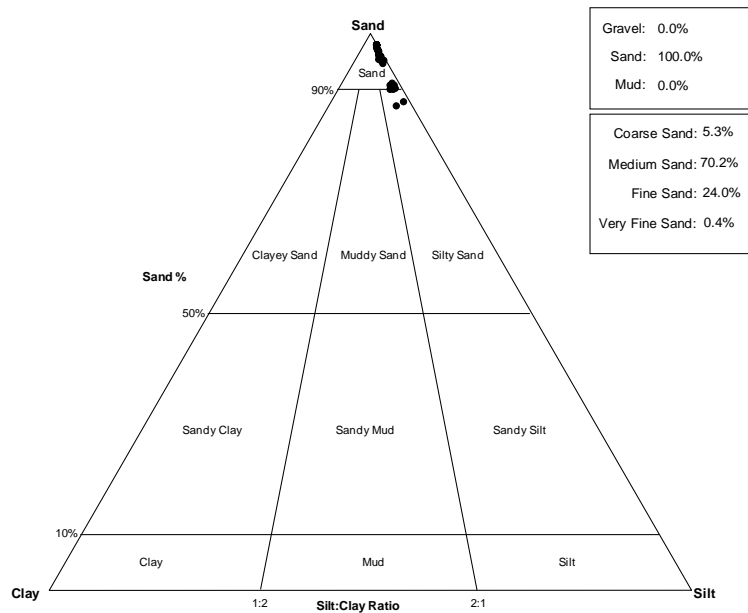


**Figure 4.12:** Grain-size ternary plot (Gradistat v.5) (Blott & Pye 2001). All samples from modern beach and relict dune features are described as medium to fine sands.

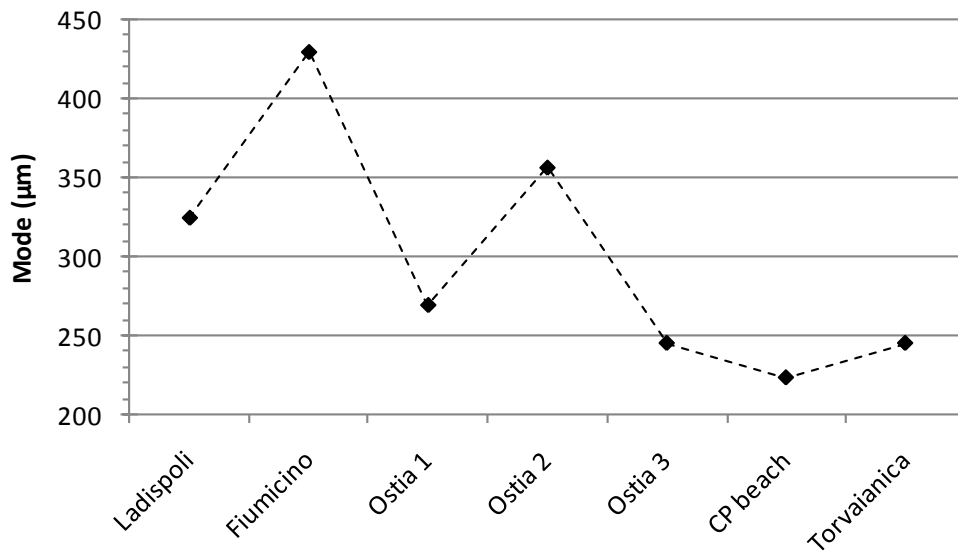


**Figure 4.13:** Modern delta beach samples, modal grain-size.

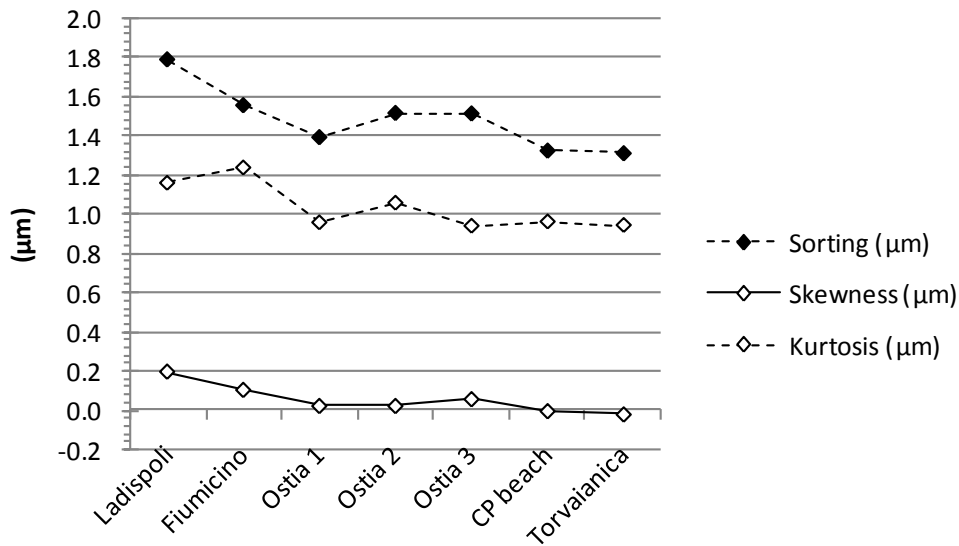


**Figure 4.14:** Modern Tiber beach samples; additional grain-size parameters, sorting ( $\sigma$ ), skewness and kurtosis.

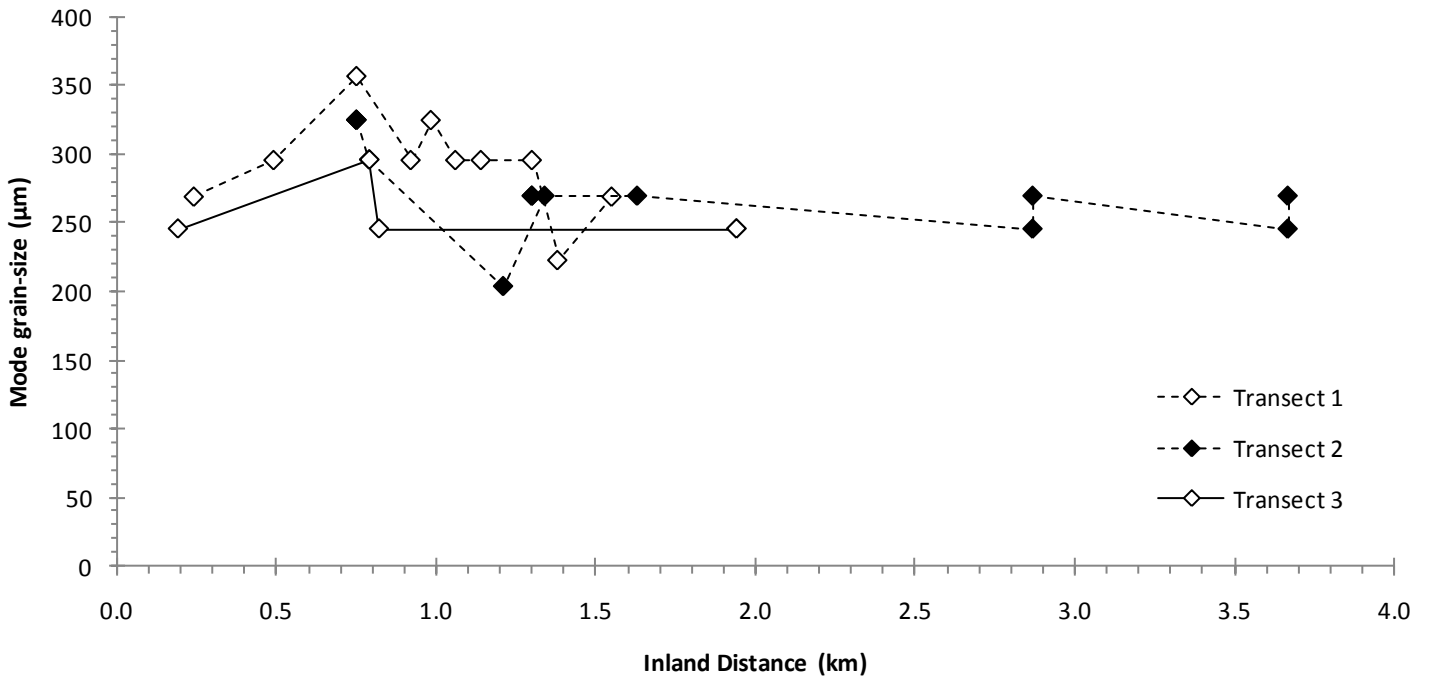


**Figure 4.15:** Inland transects modal grain-size. Grain-size appears to oscillate within the more coastal aeolianite dunes, whereas the inland sandsheet samples after around 2 km inland distance, display a more stable trend in modal grain-size. In cases of bimodal distributions, the dominant mode is presented; being discerned by LPS analysis, this refers to the greater % volume.

Gradistat analysis describes the modern beach, relict dune and sandsheet samples as medium to fine-sands (figure 4.12 and 4.13). Generally samples are moderately well-sorted to well-sorted (e.g. 4.14). Full sample descriptions are presented in appendix A1. Organised into transects (selected samples), the modern beaches alongshore distribution highlights the action of transport equivalence with increasing distance from the Tiber river mouth between Fiumicino and *Ostia* (figure 4.13 and 4.14). The position of a substantial beach nourishment scheme in the vicinity of the *Ostia* 2

sample may explain the fluctuating trend in mode grain-size on this part of the alongshore profile (Lamberti et al. 2005; Ranasinghe & Turner 2006). Although alongshore density sorting is occurring, as shown by samples located after *Ostia* 2, the Tiber sediment source is augmented by the coastal nourishment. These measurements are not fully representative of the main fluvial source of sediments that constitute the relict dune ridges. Similar fluctuating trends are observed for sorting and kurtosis. Alongshore samples at Castelporziano and Torvaianica display increased sorting to that of central delta beach samples at Fiumicino and *Ostia* as one would expect due to transport equivalence. The introduction of a second grain-size distribution from the submerged beach structure in the vicinity of the *Ostia* 2 sample may induce the less well-sorted distributions at *Ostia* 2 and 3; this theme is further discussed in section 4.6.3.3.

Grain-size distributions from transect 2 (figure 4.15) are presented as this transect extends from the carbonate dunes into the reddened “Old dunes” and sand sheets (figure 4.16). The aeolian character of the sand-sized mode is clear from the well-defined and well-sorted grain-size distributions. Both the trend in larger-grain-size bimodal distributions and the development of fine-grained sediments between 1 - 100  $\mu\text{m}$  within the Old red dunes and sand sheets suggest they are linked to inter-grain cementation and weathering of sand-sized grains, respectively. Note that the  $< 63 \mu\text{m}$  sample volumes are around 10 times larger for the carbonate dune samples (CP08/2 – CP07/14), giving some idea of amounts of fine-grained sediment between the early vadose diagenetic (EVD) zones of aeolianite and ferricrete. Figure 4.16 highlights the same transect but incorporates the separated fine-grained coatings. The  $< 63 \mu\text{m}$  grain-size distributions are characterised by several modes. A clay sized peak ( $\leq 2 \mu\text{m}$ ) is discernible across the transect with individual samples displaying a greater clay peak, suggesting sample-specific weathering conditions. A key component across the transect are clear 5  $\mu\text{m}$  and 15  $\mu\text{m}$  medium silt modes. A further coarse silt-sized mode lies between 30 – 40  $\mu\text{m}$ . CP07/15 displays a very distinct grain-size distribution, with discrete clay and fine silt modes,  $\leq 10 \mu\text{m}$ , and sand-sized grains.



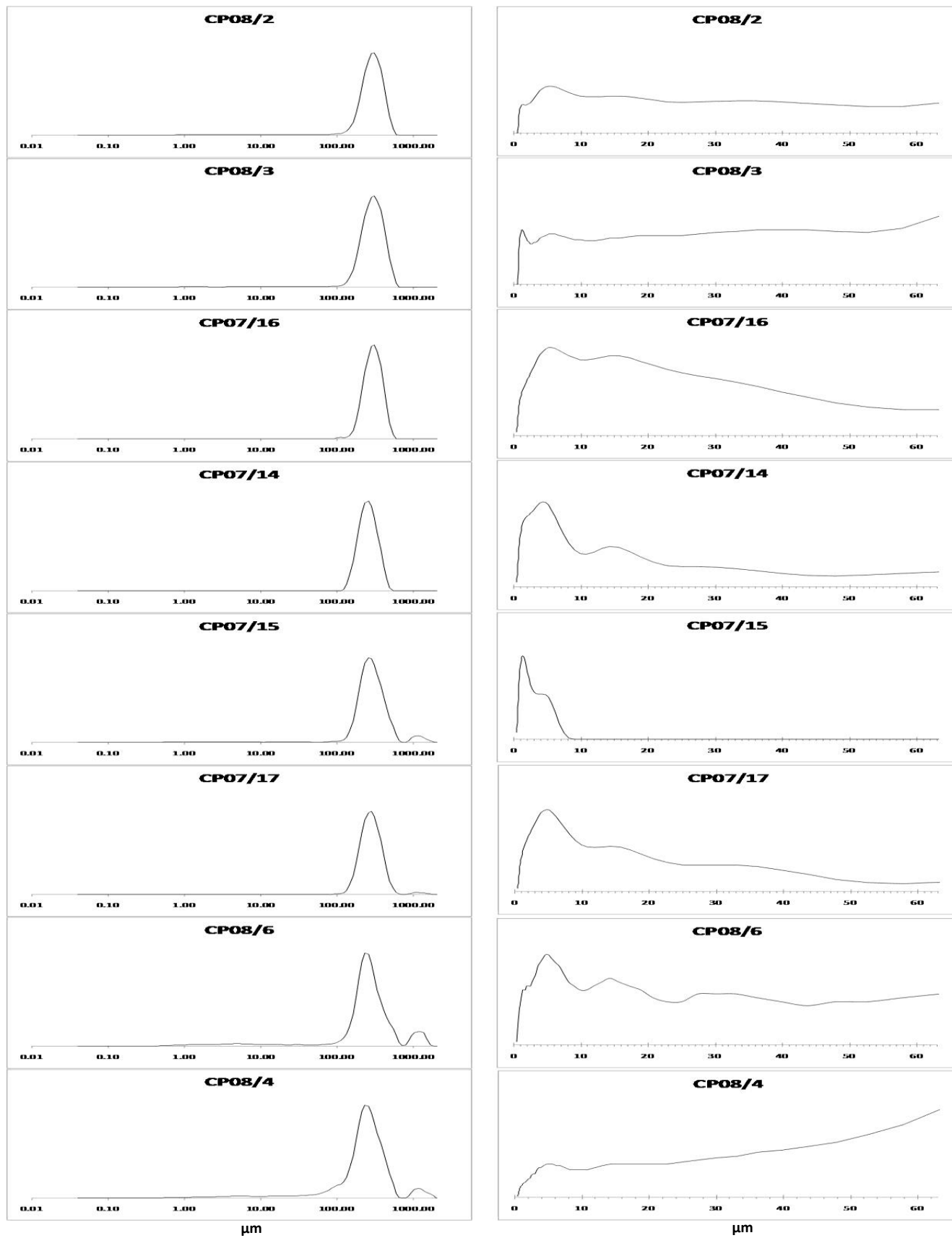


**Figure 4.16:** Sub 1.4 mm grain-size distributions of transect 2 samples (left). Sub 63  $\mu\text{m}$  measurements are shown on the right highlighting the silt-sized particle-size distribution. All scales are displayed in microns ( $\mu\text{m}$ ).

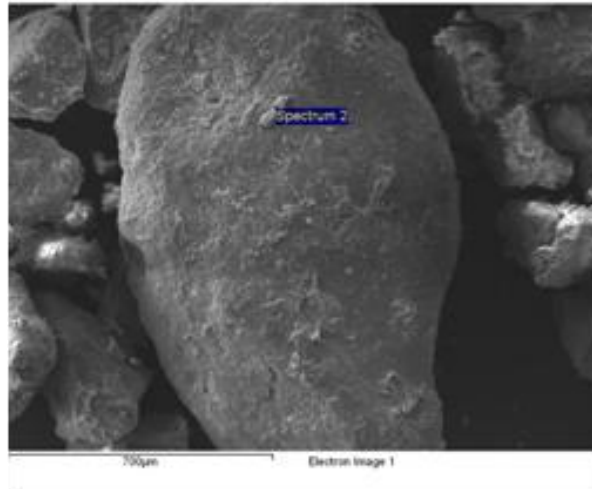


**Figure 4.17:** SEM micrograph of CP07/14. Amorphous carbonate diagenetic coatings are clearly visible on the larger grain's surface. Micrograph scale is 700 µm

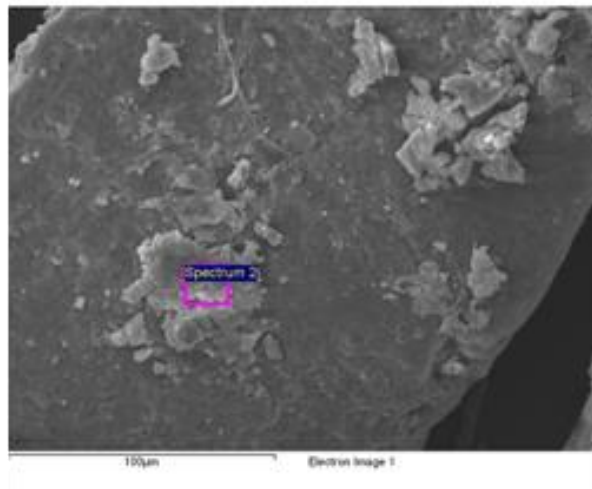


**Figure 4.18:** Micritic carbonate cements and amorphous platy coatings on sand grain surface (CP07/14). Micrograph scale is 100 µm.

SEM imaging suggests these silt-sized fractions may derive exclusively from the micritic and amorphous grain-coatings (Figure 4.17 and Figure 4.18, in this case calcium carbonate cement observed from CP07/14). Clay-sized particles can also be observed adhering to the sand-sized grains. The chemistry of these coatings suggests they are *in situ* products of weathering and diagenesis. Thus the ultimate source of their component mineralogy is more problematic to discern.

#### 4.4.2. Loss-on-ignition (LOI)

Loss-on-ignition dry sediment weight measurements of organic content<sup>15</sup> and carbonate content<sup>16</sup> were made on 24 sub-samples of wet-sediment following the UCL methods. A measurement of % dry weight water content is also made during this analysis but the wide variation between samples is not thought to be representative of naturally occurring (especially seasonally occurring sediment water contents). Preliminary tests typically showed 10 % variability in LOI values between pairs of samples. LOI values are relatively crude compared to other geochemical analyses but trends in organic content and carbonate content are consistent with field observations, petrology, CHN and bulk XRD analysis. EDX-SEM and petrological thin section analyses (see below) have also confirmed that the carbonate content derives largely from calcite and micritic calcium carbonate cements, suggesting loss-on-ignition estimates of calcium carbonate equivalent content are methodologically robust.

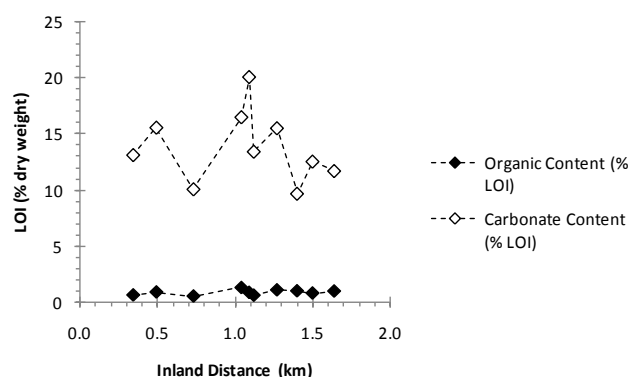


**Figure 4.19:** Transect 1 organic carbon and carbonate equivalent content loss-on-ignition (% dry weight). Throughout the site organic content is typically very low. Carbonate content appears to rise to a maximum then reduce.

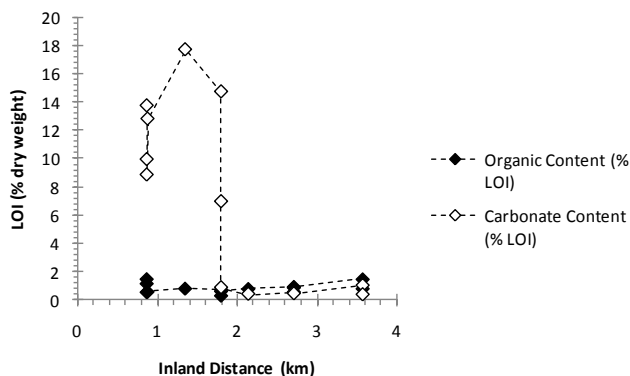


**Figure 4.20:** Transect 2 organic carbon and carbonate equivalent content loss-on-ignition (% dry weight). The change from the aeolianite to ferricrete EVD environments is clearly shown by the almost decalcification trend after around 1.75 km inland distance. A similar oscillating trend in carbonate content to that of transect 1 is also recorded in transect 2, suggesting a ‘maturity’ trend. A similar trend is also seen with the biostratigraphy study in section 4.13.1

<sup>15</sup> <http://www.geog.ucl.ac.uk/about-the-department/support-services/laboratory/laboratory-methods/lake-sediment-analysis/loss-on-ignition> (13/06/2009).

<sup>16</sup> <http://www.geog.ucl.ac.uk/about-the-department/support-services/laboratory/laboratory-methods/lake-sediment-analysis/percentage-carbonate-content> (13/06/2009).

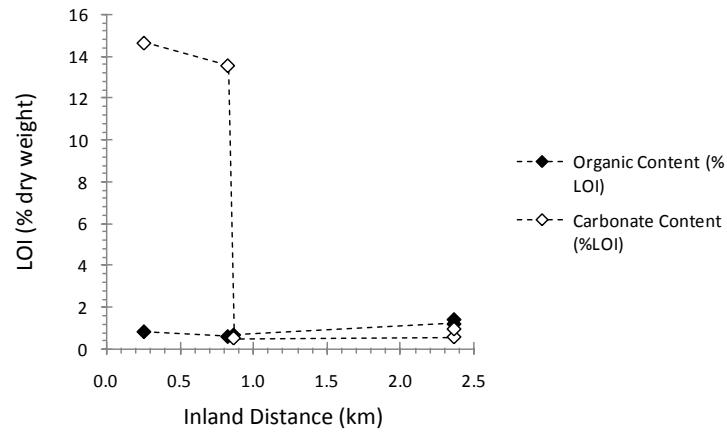


**Figure 4.21:** Transect 3 organic carbon and carbonate equivalent content loss-on-ignition (% dry weight). A similar decalcification trend is observed associated with the inland ferricrete samples.

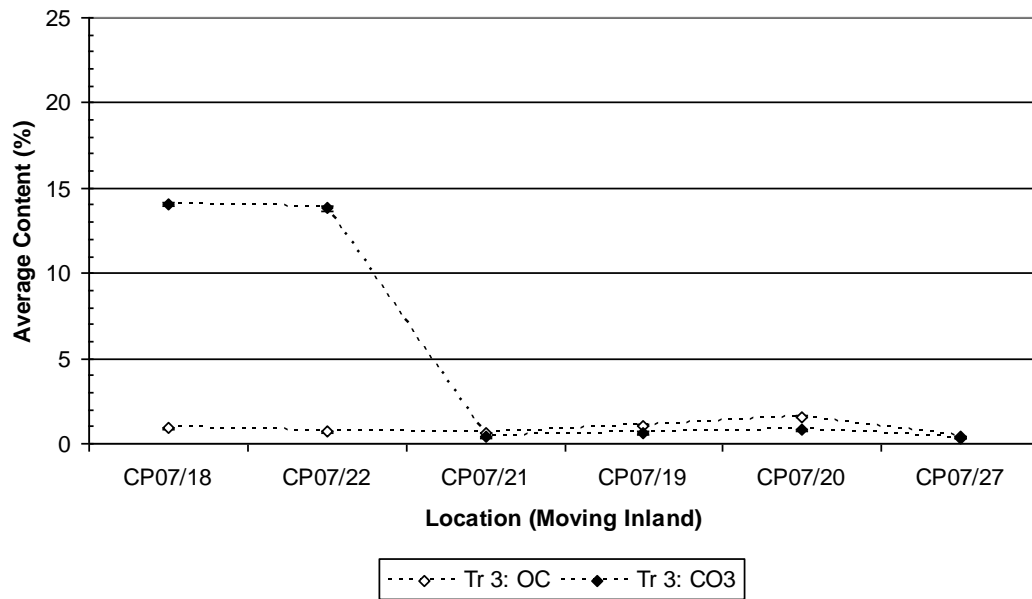


**Figure 4.22:** Transect 3 modal grain size LOI. Carbonate lithics, marine calcite and EVD diatomite probably drives the sand-sized grain carbonate distribution. The modern ephemeral stream (Fossa) sample CP07/27 is devoid of both carbonate and organic content suggested by its likely origin from remobilised inland ferricretised Pleistocene material. Grain coatings are not observed in this sample likely due to mechanical abrasion during fluvial transportation and rehydration.

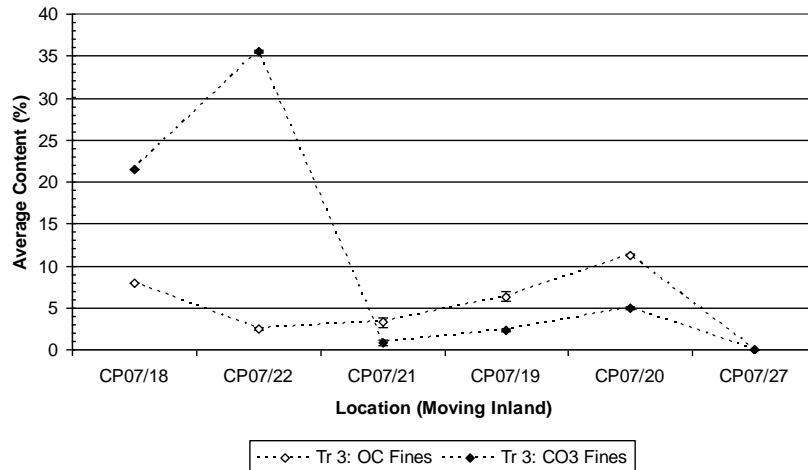


**Figure 4.23:** Fine-grained sediments derived primarily from diagenetic grain coatings display a similar trend to that of Figure 4.22. As would be expected, a greater proportion of the fines are represented by the organic content. A similar decalcification trend is observed in the ferricrete samples (CP07/21 onwards). A relatively higher proportion of the carbonate content appears to be present in the fines, linked directly to early vadose diagenetic coatings in the aeolianite coastal sediments.

LOI values organised into transects are presented in figures 4.19 – 4.21. Organic content is low, as observed during sampling in the field. In transects 2 and 3 the change from carbonate to iron oxide diagenetic environments is clearly shown by the step change to very low carbonate contents ( $\leq 1\%$ ). The absence of carbonate is characteristic of the sampled ferricrete formations.

Across a single transect, deriving at least 1 g of fine-grained coatings for LOI was not always possible without using the entire bulk sample. Transect 3 contained enough fine-grained material in all samples within around 100 g of bulk sediment; LOI was performed on both the mode grain-size and the  $< 63\ \mu\text{m}$  sieved fraction (figure 4.22 and 4.23).

Two trends are observed. (1) Organic material is predominantly fine-grained material, (2) both sand-sized and fine-grained sediment contribute to the carbonate content of the bulk sediment shown by the EDX-SEM pilot study. The overall trend of very low carbonate content in the reddened samples is preserved. Notable is the 15% increase in fines carbonate content between samples CP07/18 and CP07/22 (figure 4.23). The former derives from the *tomboleti* dunes behind the Via Litoranea at Tor Paterno, whereas the latter sample derives from a palaeo-beach within the older carbonate dunes showing that inter-grain cementation becomes more developed over time. CP07/27 was sampled from the dry bed of an ephemeral stream, inland of Tor Paterno. Seasonally active, the Fossa transports sand-sized sediments back towards the coast and is both depleted in carbonate and organic content.

#### 4.5. Preliminary study: C & O stable isotope analysis of diagenetic carbonate grain coatings

##### 4.5.1. Iron oxide contamination for stable isotope analysis

Table 4.3: Sample data for EDX-SEM analysis of diagenetic grain coatings.

Sample	Sample Location	Diagenetic Environment
CP07/18	Young, <i>tomboleti</i> carbonate cemented dunes	Early vadose aeolianite
CP07/14	Oldest carbonate-coated dune, directly above older iron oxide coated dune	Early vadose aeolianite
CP07/20	Exposed Torrente section, weathered sand sheet sediment, Old dunes	Early vadose ferricrete

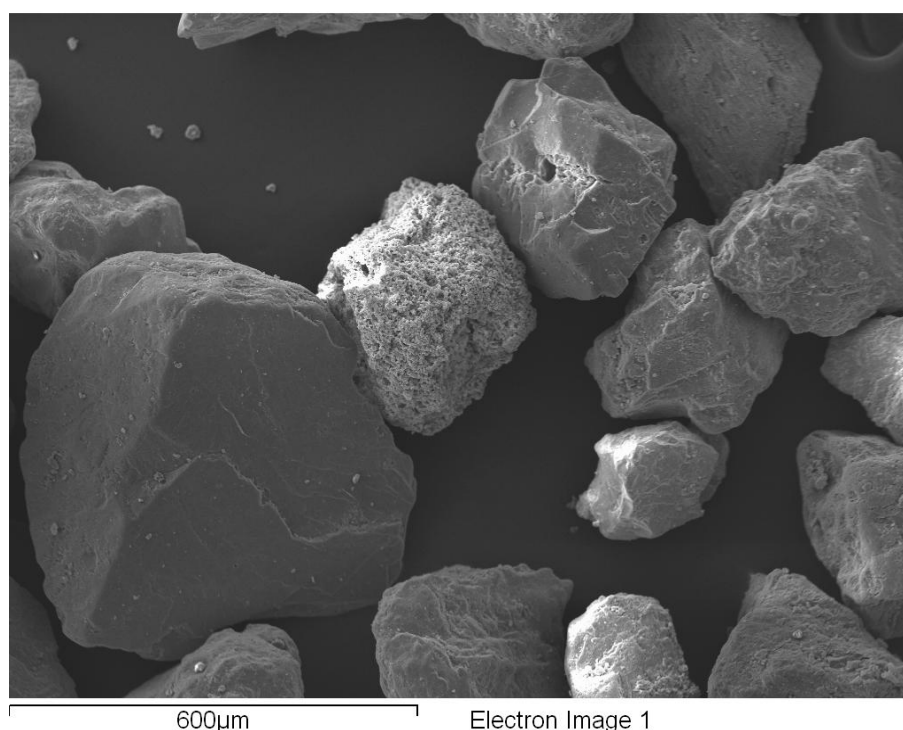
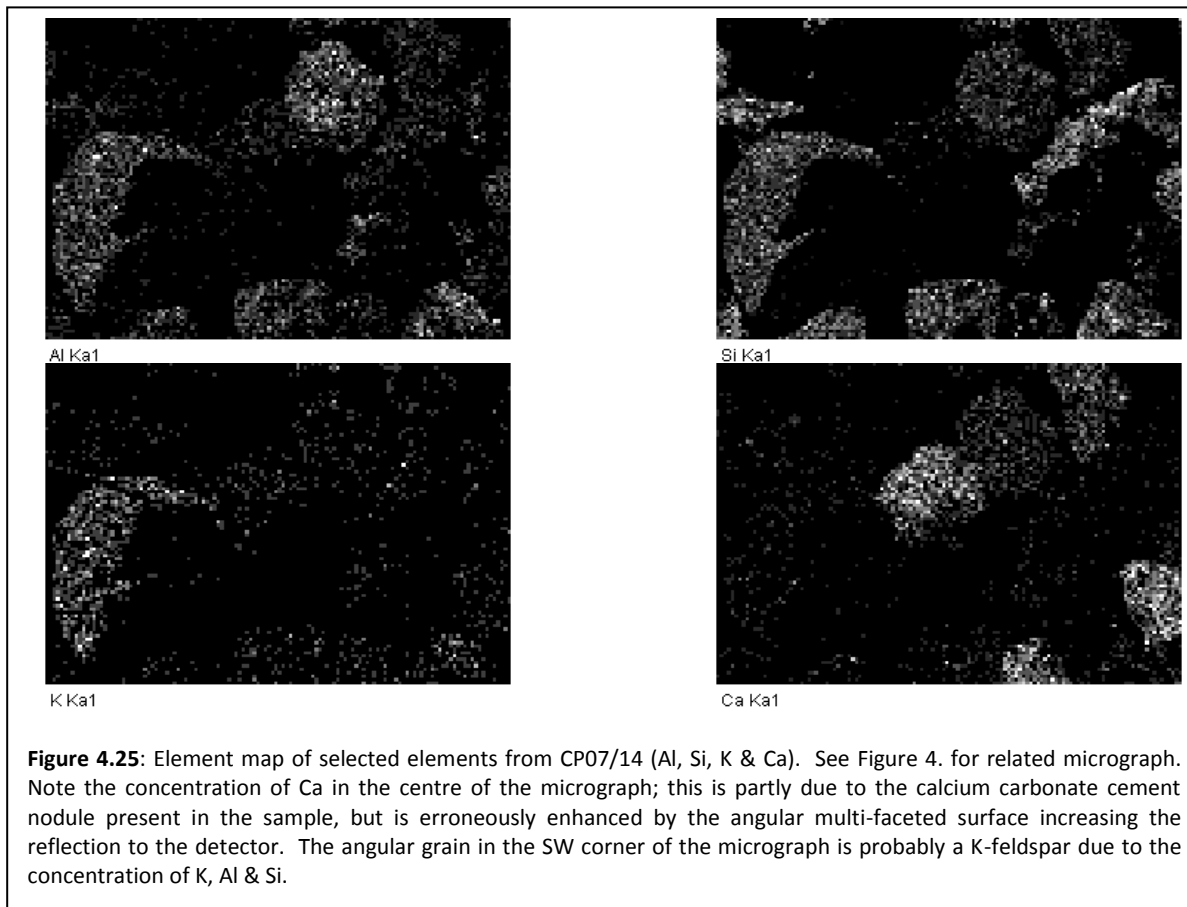


Figure 4.24: SEM micrograph of CP07/14. Element maps are presented for this view in Figure 4.25.

A preliminary examination of 3 samples representing the general diagenetic environments on the site were undertaken at the Loughborough Materials Characterisation Centre, Loughborough University. Table 4.3 outlines the general features of the samples. Bulk samples taken directly from the exposed section and sealed in plastic vials, were mounted on adhesive-coated carbon discs. The mounted samples were adhered to an SEM stub and coated with gold, the sediments being nonconductive materials. 100-200 grains were mounted on each stub.



Spectra from an area of the sample were measured, producing high-quality imagery of sand-sized grains and coatings (figure 4.24). Element maps were recorded, highlighting the concentration of elements from the grain surface only (figure 4.25). Measuring spectra from an area appears to give an overall assessment of grain coatings and general chemistry. Quantitative chemical analysis is not possible with this technique; mineral identifications must be inferred from the elements present. From the detailed characterisation of the mineral assemblage by optical microscopy, this is not necessarily a problem. By examining spectra from small areas and  $1\mu\text{m}$  points of interest, from cements and grain surfaces without cements, it was possible to identify quartz and K-feldspar from their strong Si and O signatures and K, Al, Si and O signatures, respectively. Ferromagnesian grains were also readily identifiable based on the additional presence of Mg and Fe but also by the distinctive crystal habit and cleavage in some examples of amphibole and pyroxene.

From this preliminary analysis, grain-coating characteristics linked to diagenesis could be quickly and easily observed. Spectra from these 3 samples clearly show these distinctions. It is possible to determine the structure of clay/dust particles, microcrystalline cements, grain surface features and crystal habits. The diagenetic environment can also be determined by the presence or absence of Ca. This element appears to be absent from the surface of the red-weathered sample's grains, linked directly to diagenetic alteration (figures 4.26 and 4.27).

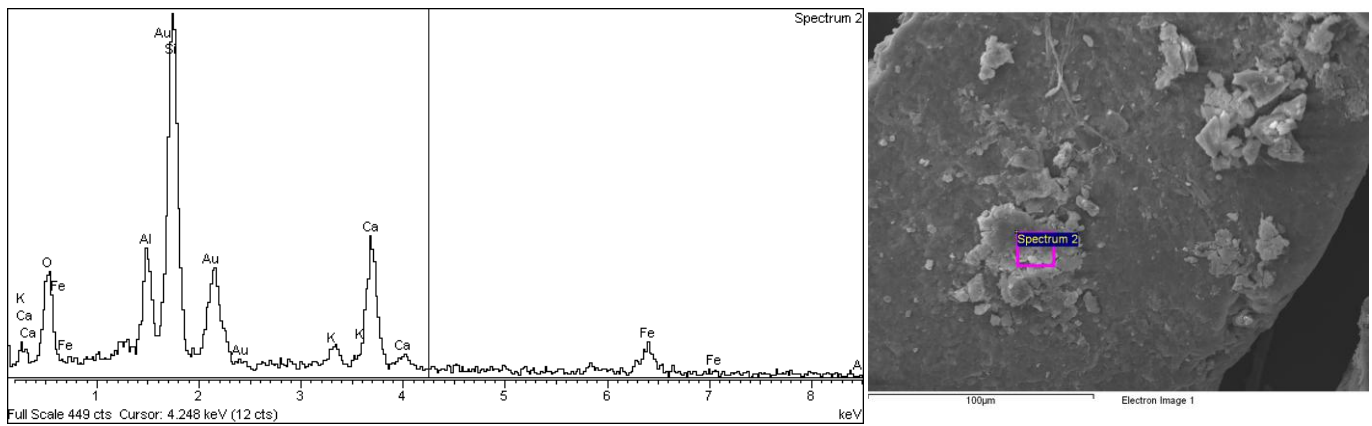


**Figure 4.26:** CP07/14. Clay coating spectra, note the Ca, Al, Si peak. The coatings on this grain appear to be of clay and also of crystalline material (NE microcrystalline cluster – spectra not shown). Fe appears to be present in both types of coating, perhaps derived from both dust and recrystallisation of dissolved ferromagnesian minerals.

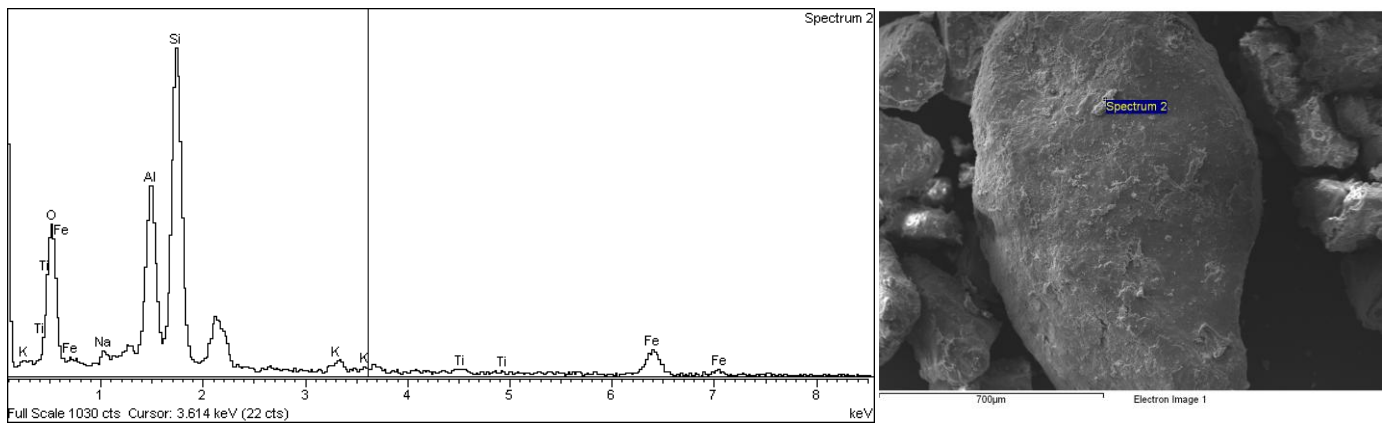


**Figure 4.27:** CP07/20. This spectrum is representative of the general surface of the whole sample. Ca is absent, clay (dust & in situ dissolution derived) and microcrystalline cements are present. Note the presence of Fe peaks in both CP07/14 & 20, carbonate & iron oxide coated dunes respectively. The difference between these two diagenetic environments appears to be characterised by the presence or absence of Ca (linked to calcium carbonate coatings). The lack of carbonate cements, lithics and nodules is also recorded in the optical microscopy study; being a feature of the geochemical alteration experienced during vadose diagenesis.

It does appear that Fe (and assumed oxides – limonite, hematite etc) is prevalent within both diagenetic environments. This is linked to clay/dust coatings and also microcrystalline cements. The existence of both types of coatings is important for assessing the contribution of aeolian dust to the sedimentary and geochemical nature of the site. These factors are important for understanding the meso-scale context of the site on both the macro- and micro-scale.

To conclude, the Fe content of microcrystalline cements is deleterious to reliable inferences made by C and O stable isotope analysis (discussed in detail in section chapter 2). A preliminary study could be undertaken but the reliable isolation of a palaeotemperature proxy signal from  $\delta^{18}\text{O}$  cannot be guaranteed by standard sample preparation and measurement. General palaeo-temperature inferences can be made from the site pollen analysis, the sampling of this



probably covering the last 2000 years. Further work on stable-isotope analysis was abandoned due to this preliminary study.

## **4.6. Petrology**

### **4.6.1. Preliminary results**

#### **4.6.1.1. Light silicate suite**

The majority of the light suite minerals are quartz with plagioclase and K-feldspar. There is also a flux of lithic carbonates and calcite that is dominant in some samples. There is also a flux in phyllosilicate minerals – the micas. Biotite, muscovite/white mica and chlorite are commonly observed. Within the alongshore, contemporary transect the micaceous minerals with an intermediate density between Feldspar and the heavy minerals (~2.5 and 2.9gcm<sup>3</sup>, respectively) appear to be sorted. These lighter mica's are sorted by increased transport equivalence due to their thin, platy crystal fragments. This variation in density is a useful guide to the dynamics of the alongshore coastal processes. Sorting of the bulk sediment is shown to increase with distance alongshore from the river mouth, and within this, there is a further sorting linked to mineral density shown by the bulk, mode assemblage.

There is also a strong metamorphic signal within the lighter mineral suite. Polycrystalline grains are the most easily recognisable under the polarising microscope. The effect of heating and pressure during metamorphic episodes reorders the crystal's boundary. Under PP (plain polarised light) the grain's edge appears intact, and the grain is colourless with low relief as normal. Under XP (crossed polarising light) they appear as many crystals within the interior of a single grain, orientated in different directions giving a patchwork effect as different compartments randomly move through extinction as the stage is rotated (plate 4.1). Polycrystalline grains occur in both quartz and feldspars. In some cases the polycrystalline effect can be attributed to feldspar as the laminar twinning patterns under XP can still be seen, albeit distorted. But, in most cases it is not possible to determine from the optical characteristics whether a polycrystalline grain is quartz or feldspar without staining. The mono-crystalline quartz is also affected by metamorphism, adopting a biaxial interference figure due to pressure alteration (Starkey, 2000, Sastry and Krishna Rao, 1964). There are also very few feldspar grains that display the characteristic twinning and cleavage. Most feldspar is grey and featureless and easily confused with quartz. The only way to distinguish them without staining is by obtaining an interference figure for every grain, which is both time consuming and still inconclusive. Distinguishing between feldspars is impaired by the indistinct interference figures assumed to be due to metamorphic effects.

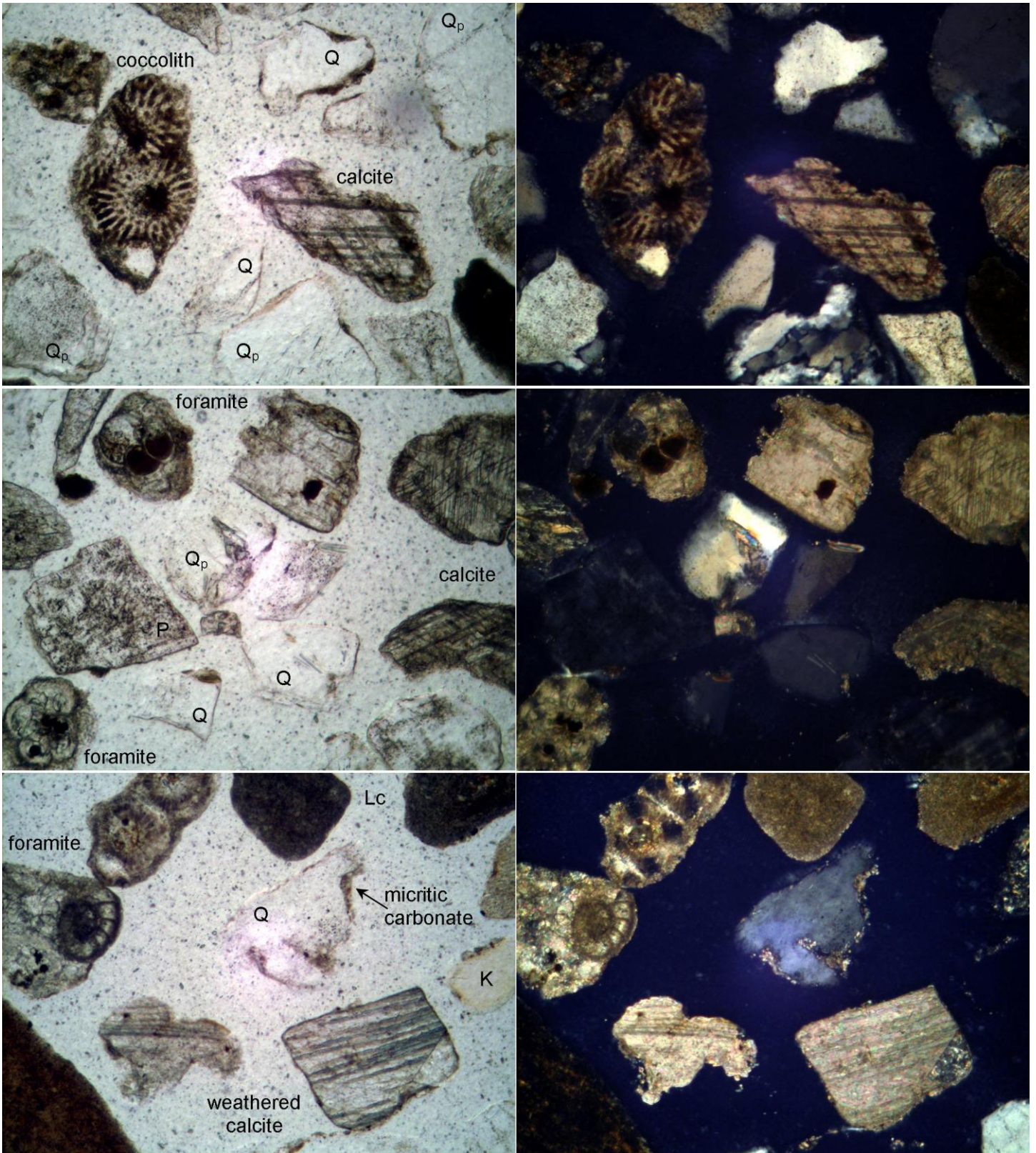


**Plate 4.1:** CP04/7 light mineral suite in PP (left) and XP (right) light (x200). Carbonate diagenetic coatings are prevalent on many grain surfaces. Micritic foramites are also common (coccoliths are rarer) in many samples appearing in cross-section due to thin section polishing. Fine-grained carbonate lithics (Lc) are common. K-feldspar (K) is stained yellow in PP light, whereas plagioclase feldspar (P) appears weathered and unstained.

#### **4.6.1.2. Carbonates and lithics**

The other key features of the framework assemblage (the light minerals and lithics together) are the carbonates and lithics. As one would expect, the coastal sediment assemblage found in the beaches and foredunes incorporates a heavy marine influence seen as calcite/dolomite ( $\text{MgCO}_3$ ) grains. It was observed that these, like the ferromagnesian minerals become less common in the inland samples, and this is assumed to be due to weathering. Further staining would permit the distinction between calcite and dolomite but within the study this is not a key objective. Staining to distinguish quartz and feldspar involves HF treatment. Therefore losing calcites and grain coatings as the grains surfaces are etched (HF etching is also used during quartz preparation for luminescence dating to remove the grains surface and fluorides, in conjunction with HCl treatments to remove carbonates). The extreme birefringence and patternation is characteristic of both calcite (plate 4.1) and dolomite but dolomite is more resistant to weathering, retaining a rhomboid crystal form sometimes observed under the microscope. Both these minerals were grouped under 'Calcite' as weathering was often so pronounced that distinction could not accurately be made in practice.

#### **4.6.1.3. Heavy ferromagnesian silicates suite**

This suite is mostly indicative of volcanic origins but also contains distinct metamorphic elements. The heavy mineral assemblage is dominated by augite (clinopyroxene). The distinctive cleavage, birefringence, inclined extinction (generally  $35^\circ$ , but ranging from  $30$  to  $50^\circ$  in lighter-darker green crystals respectively – linked to variation of Ca, Mg and Fe content) and edge alteration are helpful for identification. Orthopyroxene is also common, determined by straight extinction and distinctive low interference colour (birefringence). A series of amphiboles are also present categorised as either Hornblende in strong-coloured crystals displaying anomalous interference colours and higher range of extinction angles ( $10$ - $30^\circ$ ), or Amphibole (actinolite) in less heavily-coloured examples with lower range of extinction angle ( $10$ - $20^\circ$ ). In both cases the characteristic cleavage angles ( $120^\circ$ ) aid identification from pyroxene. Rarely, other minerals such as epidote, hematite and olivine occur. Each is distinctive and easy to identify. There are also occasionally opaque minerals that do not permit the passage of light through their crystal matrix. Opaque minerals are counted in their own category and no further analysis undertaken.

#### **4.6.1.4. Metamorphism in heavy ferromagnesian silicates suite**

The characteristic metamorphic indicators in the heavy mineral assemblage are garnet and andradite/melanite (a rare deep-brown Ti-garnet variety) as discussed by Garzanti et al (2002:10). Both minerals are isotropic; they are visible under PP but are isotropic under XP light. Andradite/melanite is a rich dark brown colour in PP derived from Ti and Fe impurities in this Ca-garnet. The crystals often exhibit a strong, rhombic crystal outline. Both can exhibit weathering, usually as surface pitting, perhaps linked to preferential weathering at inclusion sites characteristic of garnet. Garnet is clear but can be tinged with a variety of colours depending on impurities such as Fe, Cr and Mn. Within the Castelporziano assemblage, Garnet is usually colourless, easing the distinction with andradite/melanite.

Andradite/melanite originates from alkaline igneous rocks (Deer et al., 1992:45) often associated with skarns (Perkins and Henke, 2004). Skarns are rocks formed by metasomatism (alteration) during contact metamorphism. Alternatively, the paragenesis of andradite/melanite is within alkali igneous rocks associated with nepheline syenites (igneous plutonic) and nephelinite (igneous volcanic) rock. Nepheline is a feldspathoid, similar to feldspar but containing less silica (Deer et al., 1992). In thin section this mineral looks very similar to the quartz and untwinned feldspar, all of which exhibit grey birefringence and lack cleavage and twinning. Nepheline is, however, easy to distinguish by its interference figure (uniaxial negative).

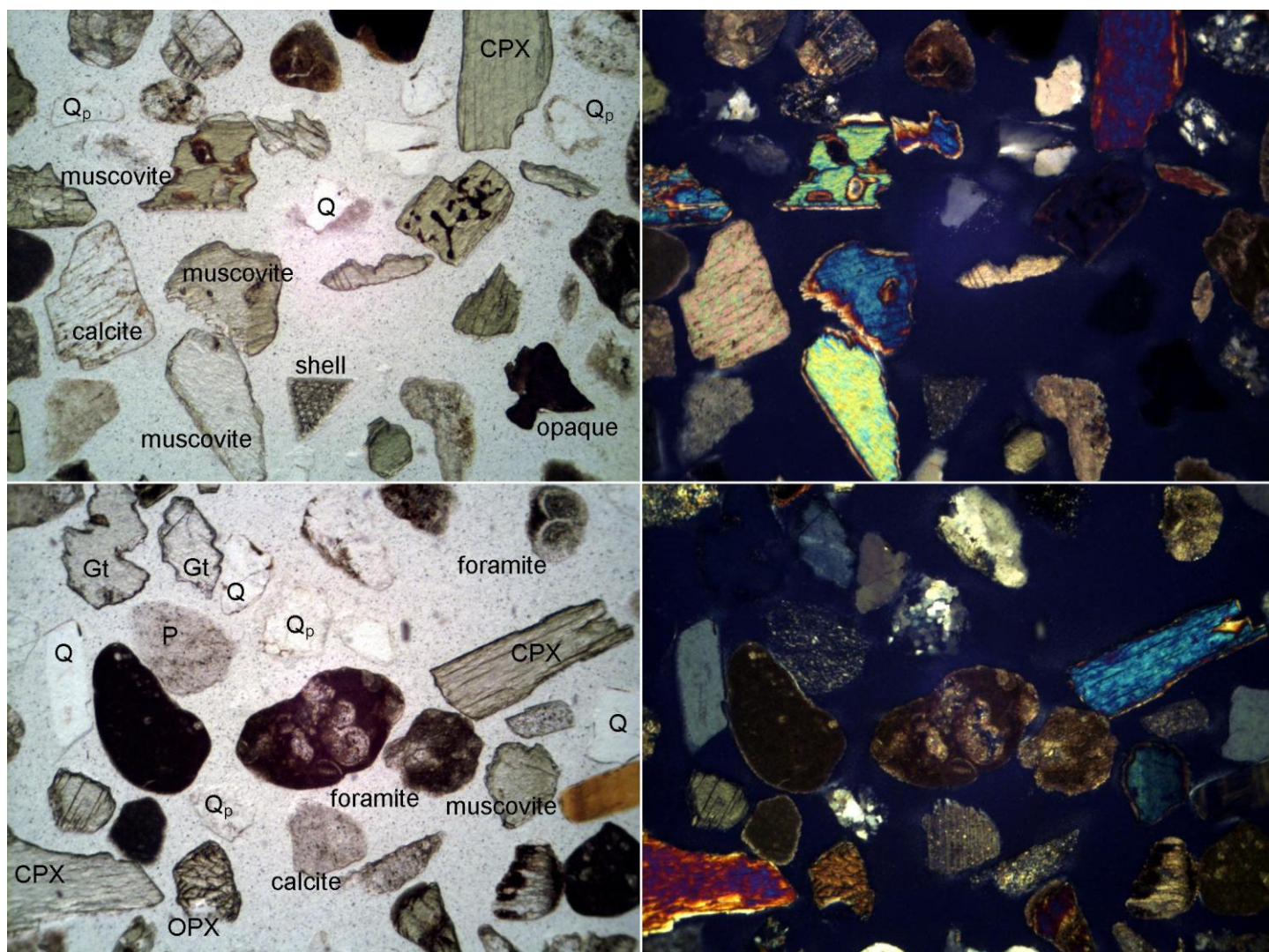


**Plate 4.1:** CP foredune sample (x40) PP (left) XP (right). Light silicates, carbonates, volcanic and metamorphic (Garnet – Gt) suites.

It is possible to stain for nepheline and plagioclase feldspar (Keith, 1939, Shand, 1939). Using the Gazzi-Dickinson method, however, feldspars and feldspathoids (i.e. nepheline) are grouped under 'F' so distinction on a technical level is not necessary except to distinguish from quartz. Therefore an interference figure is necessary to confirm all light, silicate grains not exhibiting cleavage or twinning in the absence of a complex suite of stains that are not undertaken by

every commercial facility. The provenance signal is homogenised by combining feldspars and feldspathoids as the paragenesis for these mineral groups is very broad, but by using framework (QFL) and heavy mineral analysis together, an appropriate provenance analysis can be undertaken (Kasper-Zubillaga and Dickinson, 2001, Molinaroli et al., 1991).

#### 4.6.2. Provenance training set

Bulk samples from 6 modern beach locations from Fiumicino to Torvaianica were recovered. Sampling aimed to derive averaged mineralogical sediments at each location. Sediment was treated with 10% HCl to remove carbonates. Washed and dried sediment was then separated using SPT heavy liquid at 2.9 gcm<sup>-3</sup> to produce light mineral (LM), and heavy mineral (HM) fractions. Light mineral fractions were then HF vapour treated and stained to distinguish K-feldspar. Both heavy and light fractions were mounted in Canada balsam and polished to 0.03 mm and sealed with cover slips.

#### 4.6.3. Results

Averaged LM and HM results from the Tiber beaches sampled in 2007 are presented alongside re-evaluated material from similar locations between Campo di Mare and Ardea, ca. 1975 – 1984 (Garzanti et al. 2002) (tables 4.4 and 4.5). Grain counts are presented in appendix A2. Indices are described in chapter 3.

**Table 4.4:** LM indices of modern Tiber beaches sampled in 2007 and between 1975-1984.

Index	CP Average		Garzanti et al '02		Change
	2007 (n=6)	St. Dev.	1975-84 (n=7)	St. Dev.	
Q	49	7	25	8	24
F	33	8	24	5	9
Lv	3	2	7	4	-4
Lc	13	5	31	9	-19
Lp	0	0	4	3	-4
Lch	1	1	6	5	-4
Lm	3	1	2	1	1
Lo	0	0	1	0	-1

**Table 4.5:** HM indices of modern Tiber beaches sampled in 2007 and between 1975-1984.

Index	CP Average		Garzanti et al '02		Change
	2007 (n=6)	St. Dev.	1975-84 (n=11)	St. Dev.	
ZTR	0	0	0	0	0
T&	2	1	1	1	1
A	7	3	0	0	6
PX	59	15	90	6	-31
OS	1	1	1	1	-1
LgM	7	4	1	1	6
Gt	19	12	7	5	12
HgM	6	2	0	0	6

Quartz (Q) (38-58%) and Feldspar (F) (23-44%) were the dominant LM species. Carbonate lithics (Lc) were also important components in most samples. The sands were dominated by augite clinopyroxene (CPX) with garnet/melanite (Gt) in the HM assemblage. The dominant mineral indices are the same in each dataset. However, the LM assemblage is relatively enriched and the HM assemblage relatively depleted compared to the earlier study. Regarding sediment provenance, there are several diagnostic accessory minerals within the LM and HM assemblages. It is useful here to assess the mineralogy sampled in 2007 in relation to the existing regional survey of Tyrrhenian beach sediments by Garzanti et al (2002). The Tiber beach material has a mixed provenance of reworked foredeep turbidites and volcanoclastic undissected arc sources within the Tiber catchment.

#### 4.6.3.1. LM provenance indicators

Garzanti et al (2002) describe the key minerals relating to a foredeep turbidite source as quartz, feldspar and terrigenous lithic fragments, with limestone and chert lithic fragments deriving from the Umbria pelagic succession (Coccioni et al. 2008). Leucite and sanidine are also cited in the volcanic component of the light minerals, but few K-silicates of any kind with complex twinning were observed during the study. The inherent difficulty of differentiating the LM components is linked to the metamorphic history of the material. The reorganisation of grain boundaries, lack of twinning in K-feldspar and other microstructural properties suggest that the vast majority of the quartz and feldspar have formed under or been affected by metamorphic processes (Vernon 2004). Rarely, twinning was seen in feldspar grains, allowing differentiation between plagioclase and K-feldspar. There is also a constant metamorphic lithic ( $L_m$ ) component throughout the studied material (ca. 3%).  $L_m$  grains generally exhibited complex re-crystallised fine-grained crystals occasionally with observable deformation structures. Volcanic Lithics ( $L_v$ ) were generally defined by microgranitoid-type and fine-grained basaltic structures. In both categories of lithic ( $L_m$  and  $L_v$ ) there may be a small

proportion of grains indistinguishable in detrital form, i.e. a volcanic rhyolitic microstructure appears similar to metamorphic metarhyolitic microstructure with only the small cross-section provided by a 1mm broad sand grain polished to 0.03 mm thickness.

#### 4.6.3.2. HM provenance indicators

Key HM minerals in the Roma province are augite, “with minor garnet and locally melanite [black andraditic garnet] or olivine” (Garzanti et al. 2002:9). Olivine was not found in this study, but garnet and melanite (derived from contact metamorphism between volcanic and carbonate/evaporate rocks (Garzanti et al. 2002; mindat.org 2009)) were prominent isotropic dense minerals. Garnet (Gt including melanite) represents the foredeep turbidites source. The HM assemblage is dominated by clinopyroxene species (CPX). Further speciation of CPX was not undertaken as provenance indices are amalgamated to CPX or PX (pyroxene). The assemblage of CPX with orthopyroxene (OPX) and abundant phyllosilicate micas is indicative of basaltic rocks.

#### 4.6.3.3. Problems of provenance

As has been suggested above, several key minerals reflect a misleading provenance signal. “Abundant **quartz** and **feldspars** in modern Tyrrhenian sands (and mainly **garnet** among dense minerals) are not ultimately derived from the Apennines, which do not involve basement rocks, but from the Alps. Being recycled through several sedimentary cycles from remnant-ocean and foredeep turbidites fed long distances during successive development stages of the Alpine belt since the Late Cretaceous, they represent a spurious provenance signal, typical of high-relief collision orogens and not of low-relief accretionary wedges” (Garzanti et al. 2002:12). This overprinting of an Alpine source, remote in time, accounts for the vast majority of the detrital sands deposited on the modern Tiber beaches sampled, and by association the dune ridge record preserved in Castelporziano. The foredeep turbidite material does, however, have a distinctive detrital signature; notably Q and Lv indices are not similar to the Undissected Arc data (table 4.6 and figure 4.28).

**Table 4.6:** Modern beach samples comparison with mixed provenance of Tiber catchment.

Index	CP		Foredeep		Undissected	
	2007 (n=6)	St.Dev.	Turbidites (n=26)	St.Dev.	Arc (n=4)	St.Dev.
Q	49	7	48	9	4	2
F	33	8	23	6	30	8
Lv	3	2	2	2	56	12
Lc	13	5	11	5	7	6
Lp	0	0	6	5	2	1
Lch	1	1	1	1	0	0
Lm	3	1	8	4	0	0
Lo	0	0	1	1	0	0

**Figure 4.28:** QFL ternary plot of Tyrrhenian basin provenance, erroneous modern Tiber beach signal is plotted (adapted from Garzanti et al., 2002). Beach nourishment with quartose sand has erroneously enhanced the Q and F proportions of modern Tiber beaches. Petrological thin sections show that this material has been quarried from Tiber catchment derived sources highlighted by the metamorphic & biaxial properties of the sand grains.

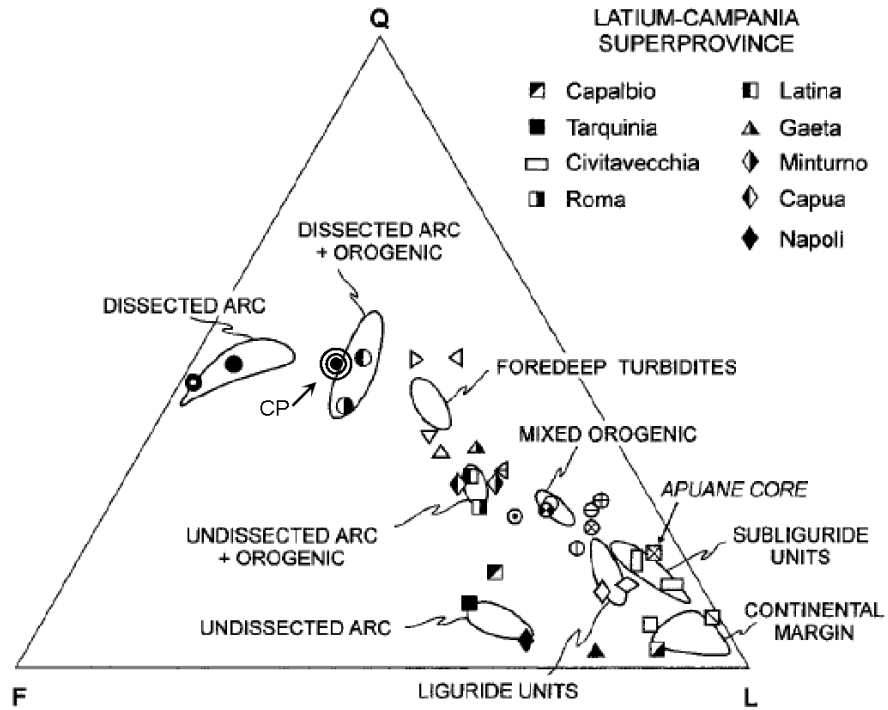


**Table 4.7:** HM provenance indices of 2007 sampling with Garzanti et al., 2002 data.

Index	CP		Garzanti et al '02		
	2007 (n=6)	St.Dev.	1975-84 (n=11)	St.Dev.	Change
ZTR	0	0	0	0	0
T&	2	1	1	1	1
A	7	3	0	0	6
PX	59	15	90	6	-31
OS	1	1	1	1	-1
LgM	7	4	1	1	6
Gt	19	12	7	5	12
HgM	6	2	0	0	6



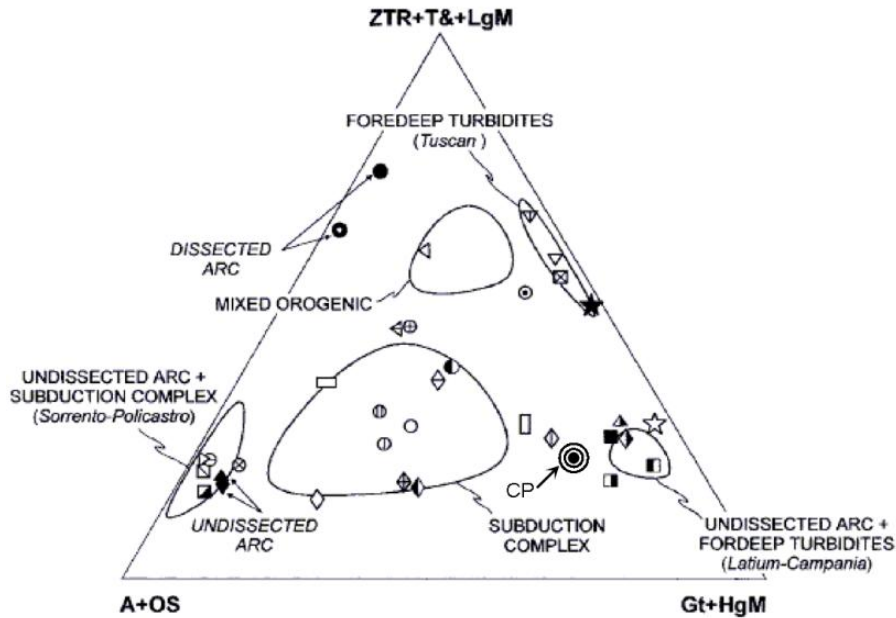


**Figure 4.29:** HM ternary plot of Tyrrhenian Basin provenance. Modern Tiber beaches sampled for this study are included (CP) (see figure 4.28 for symbol codes) (adapted from Garzanti et al., 2002). Beach nourishment activities have affected the proportions of HM thus skewing the provenance signal towards a subduction complex provenance.

Comparison of published data from a similar stretch of Tiber delta beaches published between 1975 - 84 shows comparable dominant LM and HM mineral indices but very different provenance signatures. QFL ternary plots of framework grains (LM) now exhibit a Dissected Arc / Orogenic provenance signature similar to beaches on Elba and Giglio over 100 km offshore to the NW of the Tiber Delta. The proportion of Q and F in these dissected-arc sites is close to an ideal arkosic composition (Garzanti et al. 2002) with dominant quartz. There is clearly a discrepancy in provenance signal, and an enrichment of framework grains. In 1990, 1,300,000 m<sup>3</sup> of beach nourishment was begun along a 2.7 km stretch of coastline between Vittoria Pier and Pescatori Canal at *Ostia* (Lamberti et al. 2005), partly quarried from offshore shelf sources and inland Tiber delta sources. It is unclear whether these quarries ultimately derive from Tiber catchment sources, but similar metamorphic microstructures are present in both diagenetic (unaffected provenance) and modern sands (affected provenance). This suggests some commonality but with misleading proportions of 'soft' sand (Lamberti et al. 2005). The aim was to prevent coastal erosion and protect recreational beaches. An alongshore transport rate of 50,000 m<sup>3</sup>/yr has been recorded eroding from this structure (Ranasinghe & Turner 2006) thus enriching LM compositions, particularly it appears, Q and F indices. Accurate sediment provenance using modern beach sediments on the southern flank of the Tiber delta is not now possible with traditional QFL data. Figure 4.29 incorporates provenance data from selected HM indices. ZTR+T&+LgM, A+OS, Gt+HgM are shown by Garzanti et al., (2002) to effectively describe the mixed Undissected Arc / Foredeep Turbidite provenance of material prior to modern beach nourishment works. The 2007 sampled sediments show an enrichment in A, LgM, HgM (+6%) and Gt (+12%), producing an outlying distribution from the initial Tiber beach material (Garzanti et al. 2002). The *Ostia* beach nourishment works did not use HM-rich material, changing the beach sands from dark to light, for aesthetic

reasons in order to promote recreation (Lamberti et al. 2005). These significant offshore and beach management events are clearly observable using traditional petrology techniques, but make accurate provenance analysis using contemporary beach sands problematic. Arguably, the HM indices derive a closer relationship with the provenance data of Garzanti et al (2002) but the resulting plot is poorly described by any of the provenance groups inferred by the wider study of the Tyrrhenian basin.

#### **4.6.4. Diagenesis analysis**

Loose-grain petrological thin-sections (0.03 mm) were used for diagenetic analysis of samples from dune ridges and inland sand sheets (n=21). Bulk sand was mounted in Canada balsam and polished to 0.03 mm, without acid treatment to preserve diagenetic coatings and carbonates along with the overall minerogenic assemblage of sand. At least 300 grains were counted and classified according to Garzanti *et al* (2002) utilising a modified Gazzi-Dickinson method (Ingersoll *et al.*, 1984). Ratios and standard deviations of heavy mineral (HM) and light mineral (LM) assemblages were derived from at least 4 cumulative counts of at least 600 grains (i.e. ratios calculated at ~200, ~300, ~400 etc were used to calculate standard deviations). Most samples displayed a stable HM:LM ratio through the cumulative counts. Samples that did not, also generally displayed an enriched HM:LM ratio (table 4.8).

#### **4.6.5. Problems of identification**

There are several issues of correct identification incorporating human error, crystal orientation and diagnostic microscopy techniques. There will be some inherent variation between the identification of mineral species between operators. This should, however, be minimised using the Gazzi-Dickinson method (Ingersoll et al. 1984) and a single consistent investigator. A key aim of the Castelporziano provenance study is to examine the findings of Garzanti et al (2002) to be able to place the site within this larger scale system. This is readily achievable qualitatively as metamorphic minerals are sourced only from uplifted basement rocks of the Alpine Orogeny and the adjacent Alban Hills volcanic complex. The Tiber catchment provides the rest of the assemblage as common volcanic pyroxenes, micas and amphiboles.

A semi-quantitative analysis is more challenging due to the metamorphic nature of some of the sand grains. The common silicates that make up the bulk of the Earth's crust and sediments, quartz and the various feldspars, become more problematic to distinguish under the petrologic microscope once subject to metamorphic processes. The characteristic properties used as identification guides become substantially homogenised or fundamentally altered in some cases.

##### **4.6.5.1. Metamorphic alteration of framework silicates**

Undulatory extinction, generally a characteristic of quartz is also imparted onto feldspars by metamorphic compressional stresses. Characteristic twinning, cleavage and interference colours associated with plagioclase and K-

feldspars are less often observed. The fundamental tool for distinguishing similar minerals is the grain's interference figure, examined under high magnification and conoscopic light conditions. Quartz is diagnostically a uniaxial-positive mineral, exhibiting a cross-shaped figure, which does not separate under rotation of the stage. Feldspars are biaxial minerals, and the angle of the isogyres in the NE section of the viewfield is diagnostic between plagioclase and K-feldspars. Due to compressional stress during metamorphic conditions quartz has been observed to produce a biaxial interference figure (Sastry & Krishna Rao 1964; Deer et al. 1992; Starkey 2000) (figure 4.30).

#### 4.6.5.2. Obtaining problematic interference figures

In many cases it is possible to distinguish between the biaxial quartz and feldspar due to the biaxial 'effect' being limited to an isogyre 2V angle of up to 22° (Starkey 2000). This is observed as hairpin isogyres that completely leave the field of view, whereas feldspars have 2V angles of 60 to 90°, observed as a slightly curved isogyre across the field of view. An observation made by this researcher is that the interference figures also become less distinct, perhaps due to the internal rearrangement of the crystals, impairing the distinction between plagioclase and K-feldspar. Plagioclase 2V angles ranges from 60-65°, whilst K-feldspar ranges from 75-90°. In practice, these ranges produce quite subtle differences to the interference figure, and due to the impaired clarity of the interference figures, attributing an otherwise homogenous grain to plagioclase and K-feldspar is not possible. For the sake of completeness it is desirable to separate the two groups of feldspars, but within the provenance analysis amalgamating these categories into a single feldspar category would have little detrimental effect.

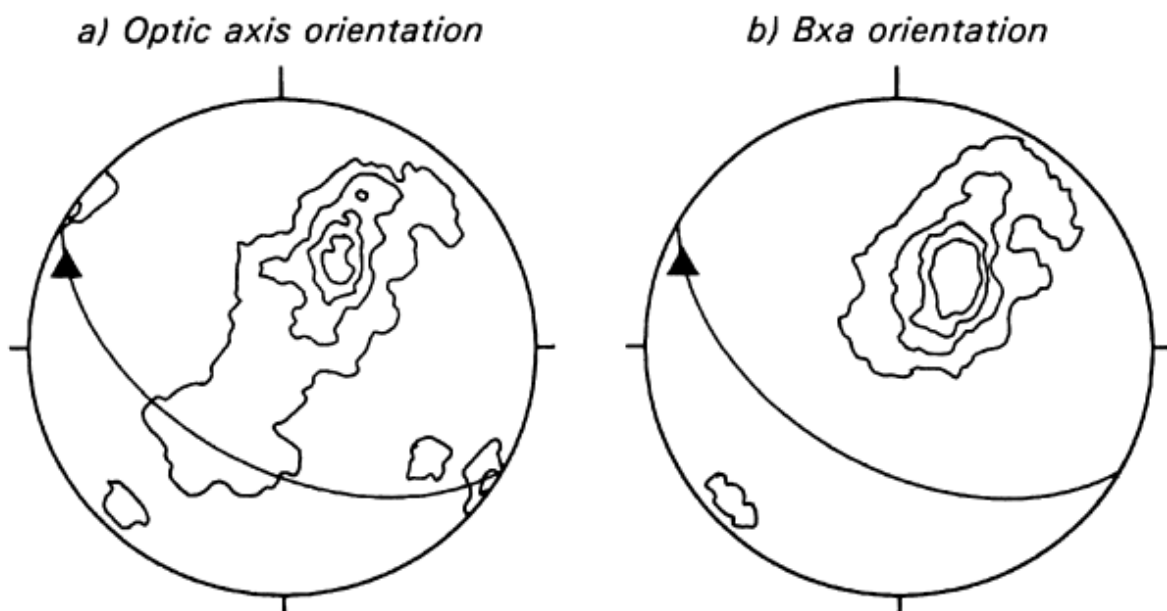


**Figure 4.30:** Stress-induced biaxial interference figures in Quartz (Starkey, 2000) orientated to the optic axis (a) and acute bisectrix (Bxa) (b) up to 22° from the optic axis.

In general there is also a problem with obtaining a useful Bxa/Bxo interference figure for every grain. Bxo figures look similar to other interference figures but do not provide the diagnostic information. When examining a slide of weathered loose grains, the crystal orientation cannot be readily understood from the weathered crystal outline making some grains unsuitable for deriving the 2V interference figures. In most cases of mineral identification it is sufficient to use the physical appearance (relief, grain-shape, colour, cleavage, and characteristic alteration), extinction angle and birefringence to discern a mineral species with the interference data providing the final clarification between similar minerals. For quartz and feldspar where no cleavage is exhibited, twinning is not apparent and the low birefringence produces similar interference colours for each mineral, staining of the slides is necessary to confidently distinguish the plagioclase and K-feldspars and quartz. This is also critical for differentiating polycrystalline quartz from polycrystalline feldspar, where interference figures are unobtainable due to the internal reordering of the crystals. The staining process uses hydrofluoric acid which makes it unsuitable for preserving the calcite, and carbonate coatings linked to the depositional environment of interest in this project. Two slide datasets were therefore required to investigate both diagenetic processes and quantitative provenance analysis.

#### **4.6.6. Results**

Following similar categorisation as the provenance study, grain-counts from the diagenesis study were organised by general provenance (figure 4.31) with key provenance indices utilised by Garzanti et al (2002) presented in figures 4.32 and 4.33. Note that some carbonate lithics derive from the upper Tiber source but the majority occur as micritic nodules related directly to *in situ* early vadose diagenesis. Other forms of carbonate are sand-sized crystals of calcite (typically weathered) which may have a marine source. It is clear that the dominant diagenetic environments contain very specific sand-sized mineralogy. Stark changes are observed suggesting rapidly occurring gradients of change and / or clear partitioning of geochemical environments across the site driven by different processes. Gradients of change are seen to occur *within* diagenetic zones but gradients do not appear to occur *between* diagenetic zones. Outlying samples are caused directly by alongshore position and are related to transport equivalence rather than to diagenesis. Samples displaying enriched HM:LM ratios are also highlighted in figure 4.34. Transport equivalence effects can be seen between plotted transects of HM:LM ratio (table 4.8, figure 4.34). Moving alongshore transect 2 derives lower ratios than transect 1, and transect 3 displaying generally lower ratios than transect 2, following the alongshore depleting trend in the modern beach samples.

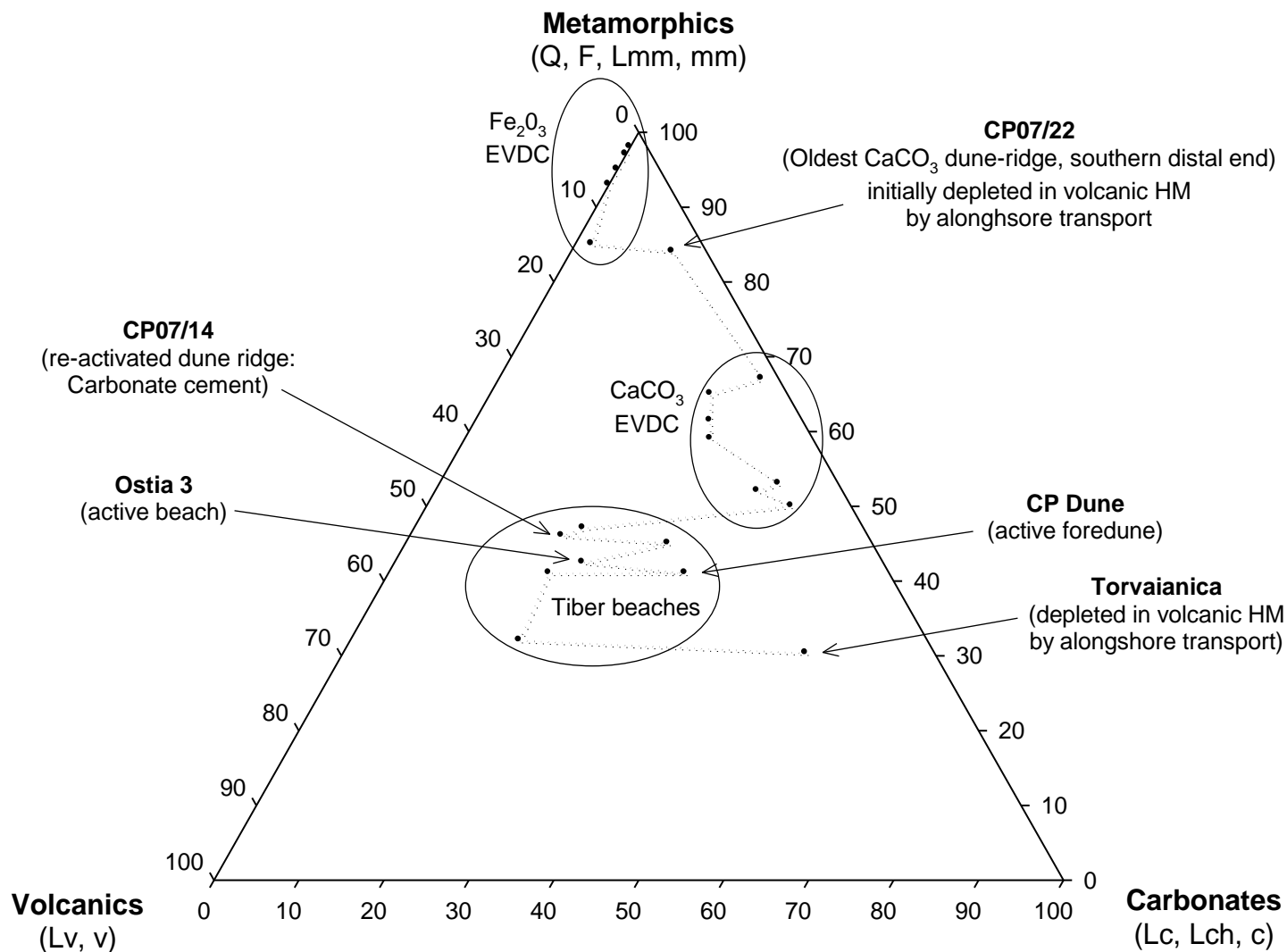


**Figure 4.31:** Diagenesis ternary plot sorted by dominant mineralogy (i.e. metamorphic content). The key sources of sand-sized minerals to Castelporziano are assigned to the axes. Carbonates are a mixed provenance group deriving partially from Lc from the upper Tiber catchment with the metamorphic axis minerals, but also derive from a marine source and in situ diagenetic mechanism producing micritic Lc which are problematic to discern from the Upper catchment Lc. Outlying samples relate to alongshore locations initially depleted in HM contents due to transport equivalence sorting by density. Sample groups are distinct and relate directly to their modern beach, carbonate EVD or iron oxide EVD environment source. Gradients between the groups are not clearly definable suggesting distinct conditions of diagenesis acting on each zone.

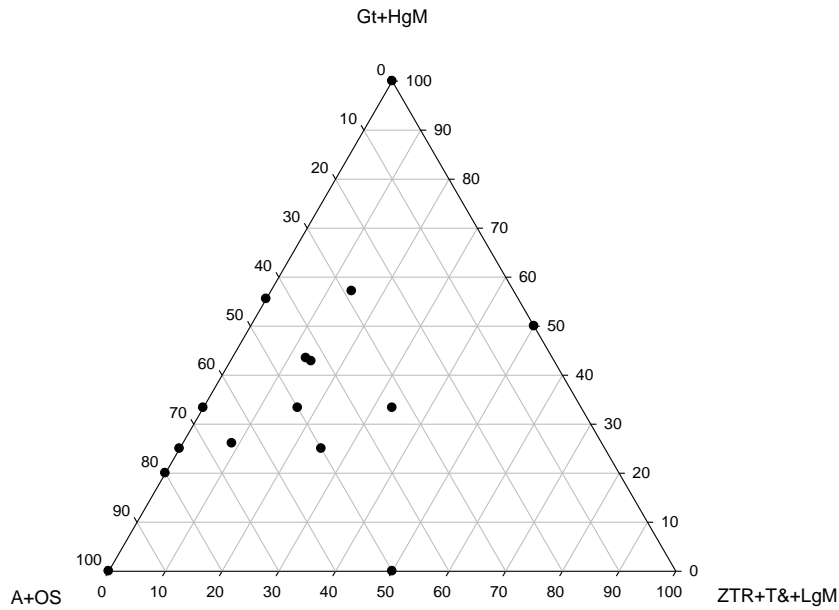


**Figure 4.32:** Key provenance indices used by Garzanti et al (2002) focusing upon extracting metamorphic provenance information. Due to diagenetic alteration, significant spread is induced into the sample distribution. Several samples plot on vertices or at the apex of axes making comparisons problematic. Sample-specific alteration conditions are inferred. Small counts for some of the indices are also problematic for making interpretations.

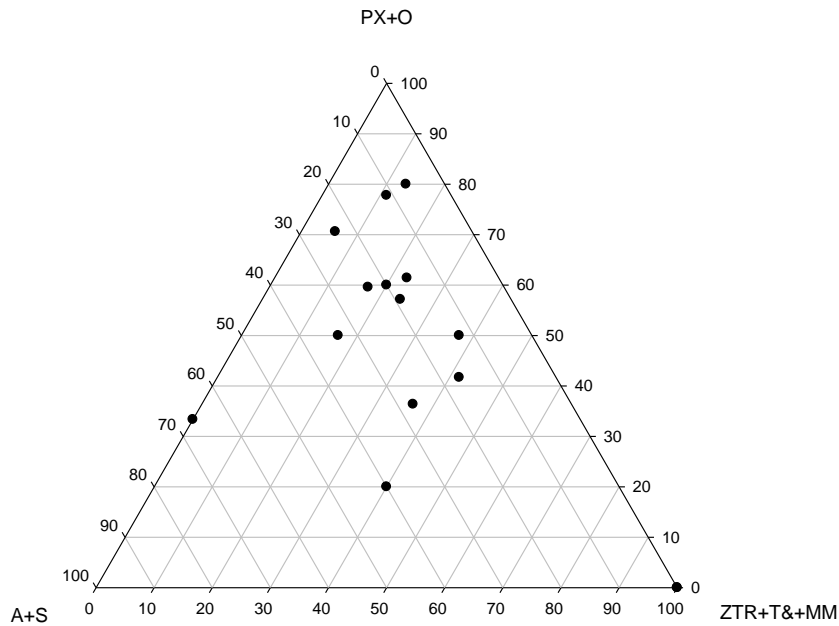


**Figure 4.33:** Key provenance indices used by Garzanti et al (2002) with the effect of differentiating important volcanic sources (PX) and metamorphic sources (MM). The volcanic-rich nature of these samples is suggested by the alignment along the PX+O axis but the reducing trend in HM content (primarily PX) and other volcanic highlighted in Figure 4.31 is repeated here. The effect of diagenesis is clearly to induce noise into the provenance signal. Although general trends can be deduced, sample-specific conditions appear to complicate the interpretation of clear weathering and alteration gradients across the site.

Key indices presented by Garzanti et al (2002) are replicated for the diagenesis counts from the inland samples only . There is a wide spread in distributions from samples derived from the similar petrological sources. This suggests that although general trends in diagenetic environment can be discerned clearly, there is substantial inter-sample noise linked to *in situ* alteration. The alongshore gradients in density and grain-size sorting, in conjunction with the inland trends in HM:LM ratios, suggest this ‘noise’ is partially driven by the initial mineralogical assemblage of each sample.

In any case, the strong diagenetic trend highlighted in figures 4.32 and 4.33 impacts upon a clear provenance assessment. A clear *gradient* in mineralogical alteration is not observed (figure 4.31) more that a distinct *partitioning* of mineralogical assemblages due to the specific diagenetic environments exists with samples within each distinct diagenetic group displaying sample-specific properties. There are effectively 3 distinct petrologic zones; modern beach, younger carbonate early vadose diagenesis (EVD) and older iron oxide EVD. It is not possible to petrologically link the ferricrete “old dunes” to the deltaic aeolianite dunes in a continuous diagenetic gradient. The reddening of the old dunes has been attributed to the underlying volcanic material (Manes et al. 1997) which has produced a rare pedogenetic environment (Arnoldus-Huyzendveld & Gisotti 1999). Although, similar metamorphic light silicates and garnet and melanite heavy minerals are observed in both the aeolianite and ferricrete EVD environments, suggesting that the upper catchment foredeep turbidite source has provided the sediment. In each case reworking of ancient fluvial sources from an earlier Tiber delta phase or uplifted Pliocene basin may be possible.

**Table 4.8:** HM:LM ratios from modern Tiber beaches and inland transect samples.

Transect	Sample	HM:LM	St. Dev.	% var.	Transect	Sample	HM:LM	St. Dev.	% var.
<b>Alongshore</b>	Fiumicino	0.712	0.016	2.253	<b>Transect 2</b>	Soil Pit 2	0.262	0.018	6.797
	<i>Ostia 1</i>	0.914	0.013	1.394		CP04/8	0.222	0.012	5.464
	<i>Ostia 2</i>	0.124	0.001	1.036		CP07/16	0.156	0.012	7.379
	<i>Ostia 3</i>	2.041	0.285	13.984		CP07/14	1.671	0.086	5.122
	CP Beach	0.324	0.018	5.667		CP07/15	0.195	0.015	7.774
	Torvaianica	0.060	0.005	7.552		CP07/17	0.055	0.006	11.631
<b>Transect 1</b>	[cp beach]	0.324	0.018	5.667	<b>Transect 3</b>	CP07/22	0.064	0.001	2.077
	CP DUNE	0.675	0.025	3.724		CP07/21	0.033	0.003	10.398
	SOIL PIT 5	0.136	0.013	9.581		CP07/20	0.019	0.001	6.104
	CP07/24	0.229	0.013	5.473	<b>Fosso del Figurone della Santola<sup>17</sup></b>	CP07/27	0.102	0.002	2.274
	CP04/7	0.048	0.005	10.561					
	CP07/23	0.136	0.011	8.181					

<sup>17</sup> The HM:LM ratio recorded from the Fosso del Figurone della Santola bed sample is reminiscent of samples from the area adjacent to the transition between the “Old dunes” and the carbonate dunes. The Fossa transports sediment from the interior of the Estate to the coast. Although not shown in the diagenesis ternary plot, CP07/27 has a similar mineralogical assemblage to that of CP07/17 suggesting local provenance information may be preserved after reworking.

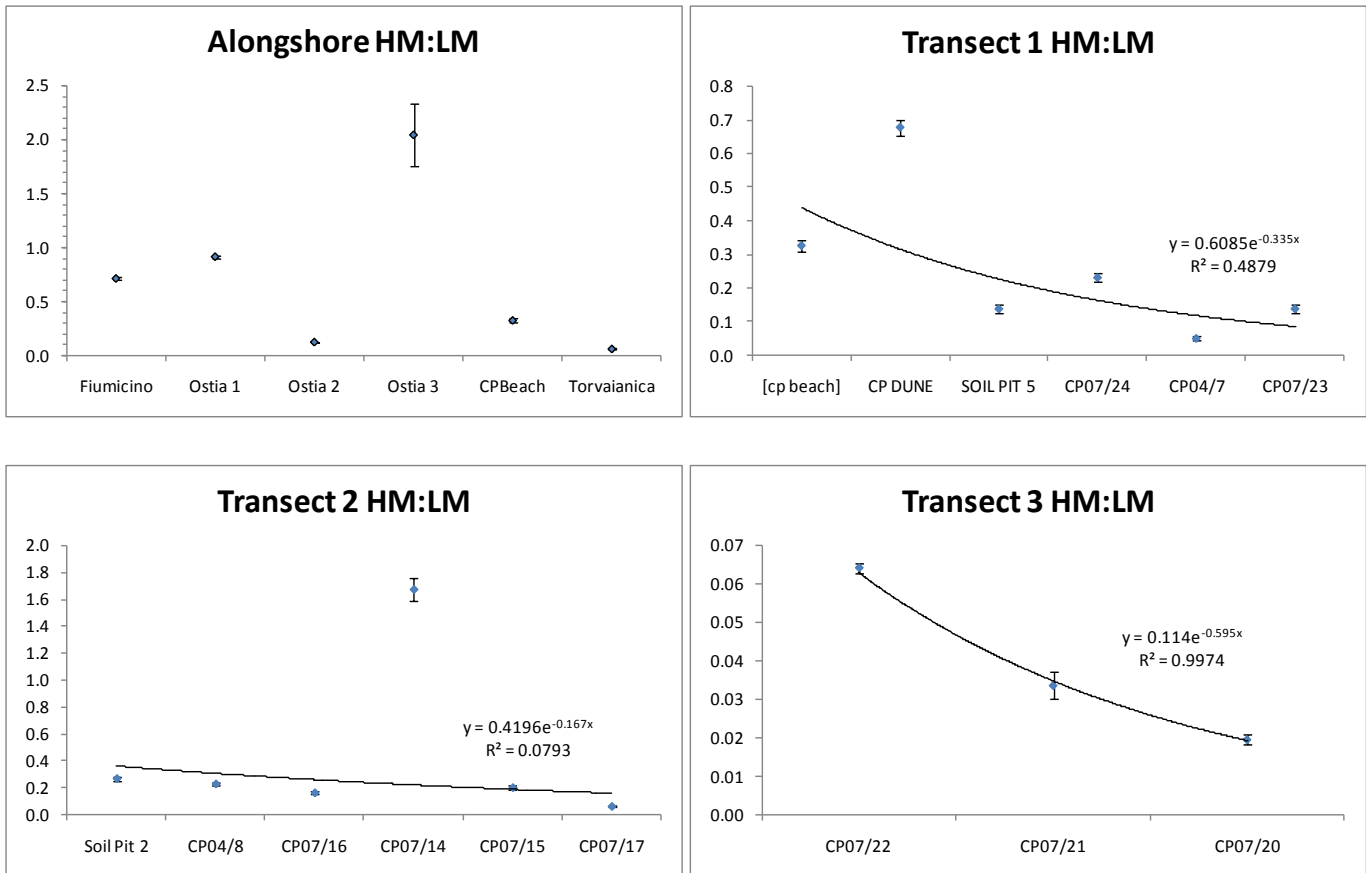


**Figure 4.34:** HM:LM ratios organised by transect moving inland (exponential trend lines shown), increasing age since deposition is inferred by this ordering. The impact of modern beach nourishment is clearly observable in the complex trend exhibited in the alongshore transect. The inland transects (1-3) suggest that a decreasing trend in HM:LM ratio is dominant. Localised processes may account for outliers but specific processes cannot be currently attributed.

#### 4.6.7. X-Ray Diffraction analysis (XRD)

Powder X-ray diffraction (XRD) analysis was undertaken on bulk sands (n=30) using a Philips PW 1710 diffractometer emitting Cu-K $\alpha$  radiation. The analysis was carried out by David Townrow of Analytical Services, School of Applied Sciences, University of Wolverhampton. It was apparent from the XRD results that early vadose diagenesis has a substantial impact on the clarity of XRD diffractogram recognition. Although the major minerals were easily distinguished, only the stoichiometric chemical formulas were interpreted by the comparison software. The effect of early vadose diagenesis upon the chemical composition is clearly complicated. The large range in unidentified chemical compound signatures produced makes interpreting the relative abundance data problematic. Typically quartz and diopside are identified, relating to the two most abundant mineral groups identified during petrographic microscopy. Diopside is a clinopyroxene (CPX) mineral. A range of mineral compositions are identified as CPX during the microscopy. No attempt was made to systematically assign a more detailed CPX species (linked to different Fe, Mg etc components in the mineral grains composition). The signature of 'diagenesis' is not necessarily clear from the XRD mineral



identifications; however the diffractograms themselves provide valuable data for interpreting the diagenetic process. Low angle peaks, below  $15 \theta$ , relating to clay minerals are typically absent or on the detection limit of the XRD system (1-5%). This suggests that clay formation is a minor process in the diagenetic development of these sediments i.e. that the cementation of the sand grains is not achieved primarily by clay minerals. From this analysis it is assumed that the complex iron oxide chemistry within these sampled sands is the key source of inter-grain cements.

In addition to the petrological analysis, further techniques for analysing the diagenetic alteration proved problematic to apply. The young and allochthonous nature of the sediments across the site, especially the carbonate deltaic dune ridges, precludes the rigorous use of bulk x-ray fluorescence (XRF) measurements as in more developed ferricretes and autochthonous laterite profiles (e.g. Schellmann, 1986 cited in Widdowson, 2007), respectively.

Diffractograms have been organised into transects (Table 4.9) and key mineral phases (Table 4.10). This transected data exhibit clear diagenetic trends. Diffractograms can be found in appendix A3. Clear distinction between Na and K-feldspars can be made. However the presence of calcite and Ca-rich ferro-magnesian volcanic minerals likely masks this signature. Transect 1 (A3.1), and contains only samples from the younger, carbonate-cemented features. A similar range of peak spacings is observed across the sample transects, but with variations especially visible within the 4 highest-magnitude peaks that relate to quartz, calcite, feldspars and ferro-magnesian (volcanic) minerals. By contrast, transect 2 (A3.2) displays samples within both carbonate and iron oxide diagenetic environments. The well-developed peak at  $\sim 29 \theta$  associated with the presence of calcite at  $\sim 35 \theta$  associated with volcanic ferro-magnesian minerals is absent or reduced in the reddened dunes. This trend is also observed within transect 3 (A3.3).

**Table 4.9:** XRD samples organised by transect

Transect 1	Transect 2	Transect 3
CP03/6	CP08/2	CP07/18
CP07/26	CP08/3	CP07/22
CP07/25	CP07/16	CP07/21
CP03/3	CP07/14	CP07/20
CP03/1	CP07/15	
CP07/24	CP07/17	
CP03/2	CP08/6	
CP07/23	CP08/4	

**Table 4.10:** Mineral indices highlighted in diffractograms.

Mineral	Description & example composition
Q	Quartz: $\text{SiO}_2$
Or	Orthoclase: $\text{KAlSi}_3\text{O}_8$
Ab	Albite: $\text{NaAlSi}_3\text{O}_8$
C	Calcite: $\text{CaCO}_3$
	Augite: $\text{Ca}(\text{MgFe})\text{Si}_2\text{O}_6$
CPX	Diopside: $\text{Ca}(\text{MgAl})(\text{SiAl})_2\text{O}_6$  : $\text{CaMg}(\text{SiO}_3)_2$

#### **4.6.8. Diagenetic decalcification**

The clearest trend observed from LOI, petrological and XRD analyses is the absence of carbonate within reddened dunes and sand sheets. Although a decalcification trend may also be observed in the most inland carbonate EVD dune ridges (this is further developed in chapter 5), very low numbers of Lc grains are seen in the reddened dune ridges and are absent from the older red sand sheets. Calcite peaks are absent or severely diminished in the XRD diffractograms with bulk LOI measurements highlighting a drop to ~1 %, from substantially higher values within the carbonate-cemented samples. Decalcification is a characteristic of ferricrete development (Widdowson 2007) but as previously discussed, the distinct partitioning of petrological information precludes arguing for a sequential gradient linking the modern beaches and carbonate dunes to the red “Old dunes”. Whereas the modern beaches and carbonate dunes are linked geomorphologically to delta progradation and the wider system, the Old dunes appear to be a separate system. The simplest reasoning is that the Old dunes are a predominantly terrestrial system linked to landward processes and the subsequent lateral expansion of the Tiber Delta to this southerly position on the Tiber coast produces the carbonate and contemporary systems.

#### **4.6.9. Principal components analysis (PCA)**

Clear trends can be observed within the various measurements and parameters of the diagenesis study. To further analyse the relative importance of these parameters Principal Components Analysis (PCA) was undertaken utilising the diagenesis petrology counts, loss-on-ignition and a restricted set of grain-size parameters. A similar approach has recently been applied with some success (Barbera et al. 2009) for understanding the effects of diagenesis upon sedimentary provenance. By compressing the dataset matrix of N samples and n variables (species) into a set of eigenvalues and eigenvectors, PCA analysis identifies the key components that account for the greatest amount of the inter-sample variance (Davis 2002). Thus complex environmental datasets can be reduced and interpreted using a relatively few key components. The 1<sup>st</sup> principal component describes the greatest variance with subsequent components describing a sequentially decreasing amount of variance. Variables will contribute more or less to these principal components, graphically aligning along the axis the variable best describes. Variables partially correlated with other principal components are observed with increasing angle from a primary axis. Additionally variables that plot at 90° angle to each other are either uncorrelated or very weakly correlated to each other, providing an interpretative ability based on environmental proxy information relating to each of the variables.

Each variable is entirely linked to the variation induced in the other variables. Therefore large variations can be induced by variables with a relatively minor importance in the environment; care is therefore required when selecting primary variables. Boyer (1999) found that principal components analysis was constrained by skewness and kurtosis grain-size distribution parameters, limiting the assessment of variability within other parameters of interest. Furthermore, the effect of these parameters, especially kurtosis, upon understanding trends in early vadose diagenesis is unclear. To this

end only mode grain-size and sorting are included as *species* in the PCA, with loss-on-ignition organic content (OC) and carbonate content (CO3), and petrological indices.

**Table 4.11:** Diagenesis petrology counts implemented in PCA analysis.

SPECIES	FIUMICINO	OSTIA 1	OSTIA 2	OSTIA 3	CP BEACH	TORVAIANIC A	CP DUNE	Soil Pit 5	CP07/24	CP04/7	CP07/23	Soil Pit 2	CP04/8	CP07/16	CP07/14	CP07/15	CP07/17	CP07/20	CP07/21	CP07/22
Q	125	40	155	161	174	151	46	73	100	138	125	78	104	75	48	129	155	111	88	85
Qp	69	22	49	30	60	33	15	32	37	22	31	34	26	33	20	31	31	31	67	47
F misc	0	0	0	0	0	0	31	39	76	59	38	50	52	54	16	51	67	82	74	67
Fp	0	0	0	0	0	0	20	27	10	37	25	24	31	29	14	35	29	48	29	35
K-feldspar	2	3	1	1	4	1	7	3	5	6	2	1	0	4	0	2	2	16	10	10
Plag	1	4	2	3	3	3	1	3	1	3	3	1	0	6	2	1	3	4	5	4
Lc	63	40	49	93	56	99	50	65	18	30	25	40	33	55	14	2	1	0	0	33
Lch	17	10	6	6	4	0	13	3	4	3	3	7	14	12	5	1	0	0	0	0
Lv	32	17	16	1	8	11	10	5	0	1	1	2	0	0	0	0	0	0	0	0
Lmm	5	14	23	5	4	2	13	14	8	10	4	9	5	5	3	10	4	26	20	12
Muscovite	34	19	50	43	62	34	22	8	12	3	16	11	9	7	30	14	11	0	3	3
Biotite	14	6	6	22	32	22	26	10	14	3	10	17	27	13	48	19	3	1	3	4
Apatite	0	0	0	0	0	0	2	1	0	0	1	0	0	0	0	1	0	0	0	0
Calcite	30	35	113	30	69	244	82	100	67	73	67	61	102	89	36	4	0	0	0	0
Dolomite	5	3	5	3	6	24	0	0	0	0	0	0	0	0	0	0	0	0	0	0
CPX	128	159	42	114	79	33	22	5	3	0	12	12	4	7	35	4	0	1	1	3
OPX	16	14	2	3	15	6	6	0	0	0	0	0	0	0	0	0	0	0	0	0
Chlorite	45	51	40	48	55	23	24	12	13	3	6	23	7	7	46	12	6	0	3	5
Epidote	1	1	4	1	0	0	0	0	0	0	0	0	1	1	3	1	0	1	0	0
Amphibole	28	30	11	20	15	3	11	2	1	0	1	4	1	1	7	2	0	2	2	2
Hornblende	20	7	3	10	11	1	4	0	2	0	0	0	2	0	1	0	0	0	1	0
Olivine	0	0	0	1	0	0	0	0	0	0	0	0	0	0	0	0	0	0	0	0
Melanite	3	1	3	7	5	3	2	2	1	0	0	3	0	0	4	2	0	1	0	0
Garnet	6	13	3	16	6	5	4	2	0	2	1	2	2	0	6	1	1	0	0	1
Hematite	1	3	5	2	0	8	0	0	2	1	0	0	1	0	0	0	0	0	0	0
Opaque	6	5	10	13	20	4	0	0	0	1	0	0	0	0	1	0	1	0	0	0
Spinel	0	1	0	0	1	0	0	0	0	0	0	0	0	0	2	1	0	0	0	0
Forams	7	9	13	9	6	40	0	9	10	22	9	2	19	2	8	0	0	0	0	4
Shell	2	4	1	4	2	3	0	0	0	0	1	0	0	0	0	0	0	0	0	0
Glass	0	1	4	1	0	0	0	0	0	0	0	0	0	0	0	0	0	0	0	0

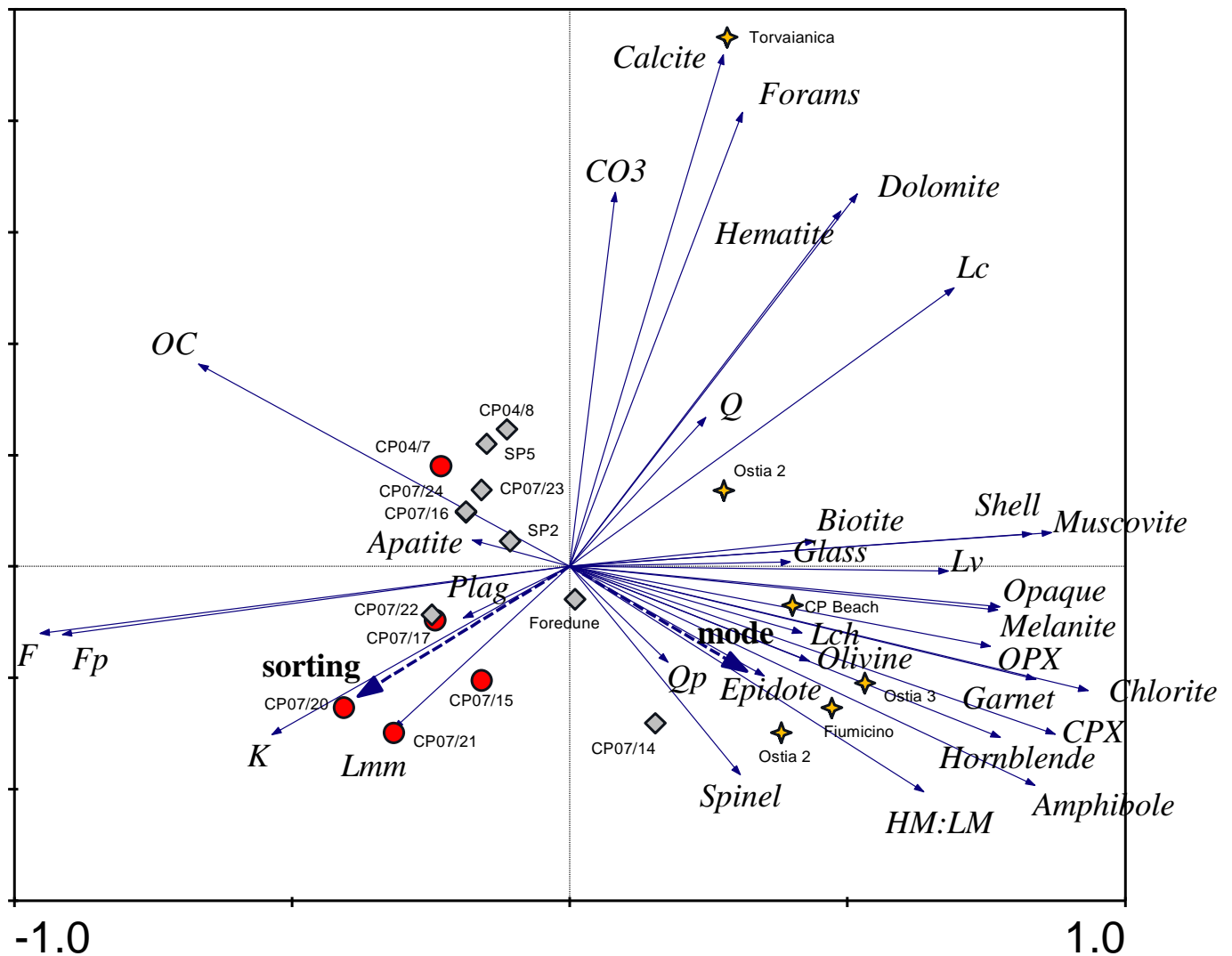
**Table 4.12:** Supplementary sedimentology parameters used in PCA analysis.

<b>SAMPLE</b>	<b>HM:LM</b>	<b>OC (%)</b>	<b>CO3 (%)</b>	<b>Mode (<math>\mu\text{m}</math>)</b>	<b>Sorting (st. dev)</b>
<b>FIUMICINO</b>	0.712	0.453	10.740	429.650	1.558
<b>OSTIA1</b>	0.914	0.451	6.070	269.450	1.398
<b>OSTIA2</b>	0.124	0.678	10.860	356.450	1.519
<b>OSTIA3</b>	2.041	0.299	6.308	245.450	1.517
<b>CPBEACH</b>	0.324	0.649	10.439	223.650	1.330
<b>TORVAIANICA</b>	0.060	0.811	18.011	245.450	1.317
<b>CP DUNE</b>	0.675	0.746	15.682	356.450	1.341
<b>Soil Pit 5</b>	0.136	1.225	21.703	302.500	1.362
<b>CP07/24</b>	0.229	1.116	15.482	295.850	2.233
<b>CP04/7</b>	0.048	0.822	12.526	223.650	1.742
<b>CP07/23</b>	0.136	1.008	11.688	269.450	1.315
<b>Soil Pit 2</b>	0.262	0.953	12.648	215.000	1.325
<b>CP04/8</b>	0.222	0.945	14.674	215.000	1.305
<b>CP07/16</b>	0.156	0.833	17.783	203.700	1.589
<b>CP07/14</b>	1.671	0.321	6.989	269.450	1.327
<b>CP07/15</b>	0.195	0.644	0.876	269.450	1.486
<b>CP07/17</b>	0.055	0.807	0.412	269.450	1.419
<b>CP07/20</b>	0.019	1.411	0.924	245.450	1.992
<b>CP07/21</b>	0.033	0.667	0.489	245.450	2.131
<b>CP07/22</b>	0.064	0.594	13.593	295.850	1.314

Using Canoco for Windows 4.5 (ter Braak & Smilauer 2002) 20 samples and 30 species were analysed (table 4.11). An initial linear Detrended Correspondence Analysis (DCA) was undertaken to assess the variance within the dataset. The total variance (inertia) of the dataset is 0.40586 (the sum of eigenvalues), showing that around 40.6 % of the sample variability is explained by the species data. Due to the palaeoenvironmental nature of this dataset it is not currently possible to derive further environmental parameters to explain the remaining variance as records of palaeo-groundwater conditions, for example, do not exist. Well dated local palaeo-environmental records are sporadic. Future work in this area may then be beneficial for developing further a comparable and more comprehensive set of palaeoenvironmental parameters to understand early vadose diagenesis. In effect, PCA on this dataset is restricted to understanding variance caused by weathering of mineral species and the development of carbonaceous sources and

diagenetic products. Diagenetic trends are also suggested by variability in mode grain-size, but this is also driven by aeolian formation processes. Sorting in this context is more suitable for inferring the development of weathering products. Due to the difference in measurement units, species are centred and standardised (0-1). Although relatively increasing and decreasing small and large variance respectively (Davis 2002), it is necessary when incorporating diagenetically pertinent information.

**Figure 4.35:** PCA bi-plot of diagenetic petrology data. Modern beach samples (gold stars), aeolianite (grey diamonds) and ferricrete samples (red circles). Sedimentological characteristics of mode grain-size and sorting are supplementary variables in the analysis and are plotted with their relationship to the principal components describing the variance in the sample mineralogy across the site. The first principal component describing most variance (horizontal axis) is strongly positively correlated with many of the heavy minerals primarily from metamorphic (garnet, melanite) or volcanic sources (mostly CPX). The second principal component is described by carbonate species and carbonate geochemistry in general.



Following PCA, 54.3 % of the variance induced by this restricted set of parameters (species) is accounted for by the 1<sup>st</sup> and 2<sup>nd</sup> principal components (Figure 4.35). Samples are coded by sampling environment (see legend). The 1<sup>st</sup> principal component is best described by phyllo-silicates and ferro-magnesian silicates such as muscovite, melanite, garnet and

CPX in order of decreasing effect. The clustering of predominantly HM-rich modern beach samples and CP07/14, which has a very high HM:LM ratio, shows that the 1<sup>st</sup> principal component is positively correlated with the diagenetically young and relatively-enriched samples. There is a strong negative gradient in feldspar species. Remembering that due to lack of microstructure feldspars are less reliably distinguished by petrological microscopy, therefore K-feldspar and Plagioclase feldspar are underestimates based solely on the preservation of microstructure – the primary index of feldspar within this dataset is therefore F and Fp (polycrystalline feldspar). With a positive correlation to HM species, there is a strong negative correlation with feldspar species. The sequential clustering of relict dune ridge samples on this side of the diagram highlights a key diagenetic trend, that of the weathering of feldspar species.

The 2<sup>nd</sup> principal component axis is driven by variance in predominantly carbonate-rich species. Torvaianica at the most southern point of sampling, remote from the mouth of the Tiber river, can be seen to be uncorrelated with HM species and consisting almost entirely of carbonate materials. Thus the 1<sup>st</sup> and 2<sup>nd</sup> principal components clearly describe the initial mineralogy of the samples rather than diagenetic weathering. Further gradients can be seen to describe early vadose diagenesis, especially in the distribution of the samples. Although mode grain-size is shown to be a relatively poor descriptor of variance, a stronger gradient in sorting (standard deviation) is observed; samples with high values of sorting predominantly derive from the “Old dunes”. Complexity within the carbonate-cemented samples is induced by the carbonate content and organic content, but generally the carbonate EVD samples cluster associated with the carbonatic 2<sup>nd</sup> principal component. Within a diagenetic context, the relatively poor positive correlation in Q is probably linked to its stability and little-varying abundance throughout all the samples. The very poor correlation of HM and carbonate vectors (i.e. perpendicular to each other) can also be interpreted to derive from the petrological and geomorphological partition that has been shown to exist between the ferricrete “Old dunes” and carbonate-cemented aeolianite dune ridges linked to the envelopment of the Tiber Delta HST during the mid-Holocene.

In addition to traditional petrological ternary plots, PCA is sensitive to early vadose diagenetic trends, but provides additional graphical information on the relative importance of petrological, geochemical and grain-size parameters for change within the system. The ternary plots describe how the modern beach samples are rich in HMs, which is also suggested by the distribution of the modern samples to the right of the diagram (Figure 4.31). Aeolianite samples are aligned generally along the axis of the 2<sup>nd</sup> principal component (but also with a relationship along an axis characterised by strongly negative relationship between OC and HM:LM) as would be expected and generally display a weak negative correlation to the 1<sup>st</sup> principal component related to HM content. The relative enrichment of HM content described by HM:LM ratios is also shown here by the weak positive correlation in the modern foredune sample and CP07/14, retrieved from the most inland aeolianite dune.

The ferricrete samples are more problematic to interpret, partly due to the relatively small sample size, but they display a moderate negative correlation to HM contents; again initially highlighted by the ternary plot of similar data (figure

4.31). These samples appear to align with trends in feldspar content, shared by variance in sorting of grain-size distributions. This could be interpreted as relating to diagenesis and weathering.

#### **4.7. Summary of sedimentology and diagenesis**

Grain-size distribution, loss-on-ignition, petrological microscopy and XRD analyses describe the site as a discrete set of diagenetic environments. The modern and carbonate-EVD zone are connected geomorphologically as they share a common deposition mechanism linked to alongshore sediment supply and the development of the Tiber Delta. However, due to rapid early vadose carbonate diagenesis the provenance signature of the contemporary sediment supply is altered. Gradients between the distinct aeolianite and ferricrete EVD environments are not seen. The inland ferricretised sand sheets are characterised by an order of magnitude greater volume of fine-grained sediment and carbonates are effectively absent. Preliminary SEM imaging from 3 samples across the EVD environments suggests that the < 63  $\mu\text{m}$  grain-size distribution may be derived largely from diagenetic grain coatings. The trend of decreasing heavy mineral components shown by petrological microscopy suggests that a key source of ions for diagenetic cements is the *in situ* weathering of sand-sized HM crystals. Allochthonous sources may also be important, including dust (Chester et al. 1984; Piccardi et al. 1996) and groundwater, but this cannot be confirmed by the current analysis.

#### **4.8. Chronology**

##### **4.8.1. Sampling**

Sampling was undertaken by digging out sections to depths of ~1.0 - 1.5 m in the dune ridges and also by coring to depths of ~2.0 m using a sand auger. Samples for luminescence dating were collected by hammering lengths of opaque plastic pipe into the sections or by transferring augered samples into opaque plastic bags under cover of a tarpaulin. Additional bulk samples were taken for grain size, petrographic and other analyses.

##### **4.8.2. SAAD-IRSL protocol**

Dune ridge and sandsheet sediments were dated by the single-aliquot additive dose (SAAD) IRSL method (Duller, 1991). Initial research has shown the suitability of this protocol on Holocene sediments from this site (Rendell *et al.*, 2007). Grain-size fractions approximating the mode were used for each dating sample, typically 180-250  $\mu\text{m}$  or 250-300  $\mu\text{m}$ . This was aimed at ensuring that analysed grains were representative of the aeolian sorting recorded by the sampled geomorphological features. Samples were treated with 10 % HCl to remove carbonates. K-feldspar was isolated using sodium polytungstate (SPT) heavy liquid at densities of 2.62  $\text{gcm}^2$  and 2.58  $\text{gcm}^2$ , to remove quartz and heavy minerals, and plagioclase feldspars, respectively. Small sample aliquots were used, with approximately 5 mg on each disc mounted with silicon oil.



An automated Risø TL/OSL DA 12 reader with  $^{90}\text{Sr}/^{90}\text{Y}$  beta source was used for all luminescence measurements. Optical stimulation was by 31 TEMT484 infrared diodes producing  $40 \text{ mWcm}^2$  with peak emission wavelength of  $880 \pm 80 \text{ nm}$ . The detection system was an EMI9635QA photomultiplier tube with Schott BG-39 and Corning 7-59 colour glass filters, creating a detection window of 320-480 nm. This avoids detection of potentially unstable UV emissions from alkali feldspars (Clarke and Rendell, 1997). All Estimated Dose (DE – the equivalent radiation dose stored as charge in the mineral dosimeter) determinations were made using 12 small-aliquots containing approximately 5 mg of sample. The Single-Aliquot Additive Dose (SAAD) protocol was used for each sample. Aliquots were measured using 0.5 s IR stimulation at  $50 \text{ }^\circ\text{C}$ , and using preheats of  $220 \text{ }^\circ\text{C}$  for 600 s to remove unstable luminescence signal components (Clarke and Rendell, 1997). 6 aliquots were used to correct for signal loss due to repeated heating and measurement during the SAAD protocol.

#### **4.8.3. DE determination**

##### **4.8.3.1. Curve-fitting**

Using a jack-knifing statistical approach, growth curves were fitted using an exponential function. Due to the young (Holocene) age of the sediments under examination, exponential curve fitting is appropriate (Fleming 1971; Zimmerman 1971).

##### **4.8.3.2. Radial plots**

The homogeneity of 12 aliquot stored dose estimates was ascertained using radial plots (Galbraith et al. 1999). Aliquots plotting out-with  $2\sigma$  of the mean were removed from the DE calculation. Very few samples required ‘trimming’. Typically 0, 1 or 2 poorly performing aliquots were removed. DE overdispersion (OD) values following trimming and numbers of aliquots used in DE determinations are presented in table 4.13. OD is calculated as the standard deviation as a percentage of the mean DE.

**Table 4.13:** Percent overdispersion (OD) of Estimated Dose (DE) estimates for all SAAD-IRSL samples.

Sample	OD (%)	n (12)	Sample	OD (%)	n (12)	Sample	OD (%)	n (12)
CP03/1	6.487	12	CP07/16	9.784	11	CP07/26	9.797	10
CP03/2	4.258	12	CP07/17	8.470	11	CP08/1	7.345	11
CP03/3	8.366	12	CP07/18	7.930	10	CP08/2	8.992	9
CP03/4	8.529	9	CP07/19	11.656	10	CP08/3	4.587	12
CP03/5	21.245	12	CP07/20	8.753	10	CP08/4	21.144	11
CP03/6	22.261	11	CP07/21	10.048	9	CP08/5	7.163	10
CP04/1	7.837	12	CP07/22	3.872	12	CP08/6	9.429	8
CP04/7	8.276	11	CP07/23	7.087	12	CP08/7	16.345	11
CP07/14	9.482	10	CP07/24	7.452	12	CP09/1	6.876	11
CP07/15	7.691	10	CP07/25	8.034	12			

Samples displaying OD > 10 % are not considered of high quality. Ages calculated from them must be considered as rough estimates. The increased OD observed in these samples is probably due to incomplete bleaching or involving mixing of partially bleached sediments. Although unsuitable for high-quality luminescence dating, the geomorphological inferences provide valuable additional taphonomic information and a general chronological context. In addition, the very young sample from the modern foredune (CP03/6) may have performed poorly due to low signal to noise ratio. Generally, DE determinations from across the site are of a high quality. The standard error was calculated from the remaining aliquots DE values and used as the error estimate during the age calculations.

#### 4.8.4. Environmental dosimetry

Dosimetry was provided by thick source alpha counting (TSAC) (Aitken, 1998) and thick source beta counting (TSBC) (Sanderson, 1988) methods to identify external U, Th and K dose rates. An internal  $\alpha$ -efficiency value of  $0.2 \pm 0.1$  and internal K component of  $0.8 \pm 0.2$  % were used for each sample (Rendell *et al.*, 2007). Attenuated alpha, beta and gamma dose-rates were calculated for varying estimates of water content. Values of  $5 \pm 3$ ,  $10 \pm 5$ , and  $15 \pm 5$  % water content were used to investigate changes in dose-rate attenuation due to different estimates of hydrological conditions. Cosmic ray dose-rate contributions were calculated from sampling depths following Prescott and Hutton (1988). During TSAC measurements, no loss of radon was observed between sealed and unsealed counts. U and Th ppm were

calculated from TSAC results, with K % calculated from TSBC results. The K component appears to dominate the beta-dose rate received by the samples (see table 4.14) suggested in samples that display comparable U and Th components.

#### **4.8.4.1. Water content**

Laboratory measurements of water content from all IRSL dated samples are very low, typically less than 5% except where samples were taken immediately following periods of rainfall or contain a greater clay component. Due to the Mediterranean climate experienced by the sampling site, sediment water content is likely to be highly variable, both seasonally and over longer timescales. Sampling was undertaken during April and September i.e. flanking the summer drought. More importantly due to changes in relative sea level throughout the burial history of all samples and therefore also the interaction between marine and non-marine water tables, the post-depositional flux in water content is likely to be complex. Laboratory estimates of water content are likely to underestimate the contribution of these variable hydrogeological conditions. Water content will also vary as increasing diagenetic cementation decreases porosity. Post-depositional factors are likely to have a pronounced influence. Laboratory estimates of water content based on oven drying are therefore unlikely to produce representative values. The effect of different water contents upon age determinations was assessed using water content values of  $5 \pm 3$ ,  $10 \pm 5$  and  $15 \pm 5$  %, respectively. Richardson (2001) has previously noted the problems with assessing water content in young coastal sediments. The key consideration is that the effect of dose-rate attenuation due to water content may be more deleterious for accurate dating than variability in DE determinations due to poor bleaching and other elements contributing to age calculations. Water content estimates of  $5 \pm 3$  % are probably too low for this dynamic coastal setting. No samples exhibited water contents as high as  $15 \pm 5$  % water content even following recent precipitation events. The high position of the dune crests above estimates of late Holocene sea level (ca. 3 m+) shown by precisely georeferenced dune ridge transects suggests the intermediate value of  $10 \pm 5$  % may be a more representative water content value with the available data. Accurate water content estimates are likely to continue to be an issue for all luminescence dating applications where hydrology is complex.

#### **4.8.5. Age calculation**

Three age calculations were made for each sample considering dose-rate attenuation due to the 3 estimates of water content outlined above. Trimmed DE determinations were used in all calculations. Calculated ages are high-quality, typically displaying <10 % error. Luminescence age data are presented in table 4.14. All luminescence dates are in the form BP relative to AD 2000.

**Table 4.14:** SAAD-IRSL age estimates, OD, dosimetry for 10 % water content for all samples. \*Samples with archaeological age control

Sample	OD (%)	DE (Gy)	St. Error (Gy)	n (12)	Doserate (Gy/ka)	U (ppm)	Th (ppm)	U/Th	K (%)	Age BP (10% water cont.)	Error (Years)
CP03/1	6.487	3.735	0.070	12	2.716	1.83	6.2	0.295	1.12	1374	100
CP03/2	4.258	5.845	0.072	12	2.819	1.97	6.08	0.324	1.22	2073	144
CP03/3	8.366	4.774	0.115	12	3.207	1.46	6.13	0.238	1.8	1488	100
CP03/4	8.529	6.085	0.173	9	2.676	1.44	5.21	0.276	1.32	2273	164
CP03/6	22.261	0.152	0.010	11	2.887	1.61	7.24	0.222	1.27	52	4
CP04/1*	7.837	5.945	0.140	12	2.923	2.065	7.145	0.289	1.24	2034	146
CP04/7	8.276	6.478	0.162	11	3.386	1.765	6.13	0.288	2.03	1913	119
CP07/14	9.482	13.373	0.423	10	3.145	3.075	9.82	0.313	1.01	4252	316
CP07/15	7.691	18.406	0.448	10	3.662	2.805	8.385	0.335	1.8	5055	331
CP07/16	9.784	8.321	0.245	11	2.191	1.11	3.89	0.285	1.1	3768	268
CP07/17	8.470	20.373	0.520	11	3.756	2.285	7.175	0.318	2.16	5424	343
CP07/18	7.930	1.613	0.039	10	2.774	1.455	6.315	0.230	1.37	581	39
CP07/19	11.656	15.522	0.572	10	4.742	1.8	9.19	0.196	3.28	3273	213
CP07/20	8.753	36.063	0.998	10	4.375	2.845	10.855	0.262	2.43	8243	528
CP07/21	10.048	23.173	0.776	9	3.979	1.15	8.11	0.142	2.67	5823	374
CP07/22	3.872	9.397	0.105	12	2.850	1.3	4.235	0.307	1.62	3297	222
CP07/23	7.087	8.414	0.172	12	2.609	1.0235	4.22	0.243	1.44	3224	224
CP07/24	7.452	5.587	0.120	12	2.509	1.22	5.835	0.209	1.08	2226	168
CP07/25	8.034	4.505	0.104	12	2.758	1.935	8.145	0.238	0.96	1633	123
CP07/26	9.797	2.045	0.063	10	2.832	1.32	5.44	0.243	1.46	722	53
CP08/1	7.345	5.098	0.130	11	3.883	3.45	16	0.216	1.2	1312	93
CP08/2	8.992	5.025	0.151	9	3.156	2.62	7.83	0.335	1.26	1592	116
CP08/3	4.587	6.016	0.080	12	3.475	2.015	7.03	0.287	1.89	1731	109
CP08/4	21.144	47.841	3.050	11	4.549	3.805	13.5	0.282	2.12	10516	923
CP08/5	7.163	26.653	0.604	10	4.532	2.44	8.315	0.293	2.91	5881	347
CP08/6	9.429	43.082	1.436	8	4.082	2.465	7.685	0.321	2.47	10554	687
CP08/7	16.345	19.661	0.969	11	4.167	2.35	8.42	0.279	2.5	4717	352
CP09/1	6.386	6.510	0.131	11	2.891	1.645	5.465	0.301	1.460	2251	156

#### 4.8.6. Fading experiment

After 14 weeks of storage, systematic signal loss was not observed (table 4.15). A very young sample taken from the recent dune ridge less than 100 years old displayed very poor response, which appears to be due to the low radiation dose applied during the test. One sample appears to show an increase in signal over time i.e. recuperation which is linked to trapped charge moving to IRSL traps from other trap locations. Similar behaviour was also observed in a single sample by Alexander (2007). The remaining 4 samples display no observable fading after 14 weeks of storage. Excellent comparisons with archaeological age control were possible across the site, also suggests that signal loss is not an inherent problem with the K-feldspar material presented in this study.

**Table 4.15:** Signal storage ratio after 14 weeks. Systematic signal loss is not observed. Samples derive from across the sampling framework. Column 1 samples are foredune and carbonate EVD environment. Column 2 is red dunes and sand sheet samples.

Sample	DE/s	14 weeks	Sample	DE/s	14 weeks
CP03/6	16	0.684	CP07/15	1980	1.326
	16	0.996		1980	1.126
CP08/2	300	0.979	CP07/20	2150	0.978
	300	1.044		2150	1.018
CP07/14	1440	1.038	CP08/4	5010	1.034
	1440	1.092		5010	1.067

#### 4.8.7. Mineralogical control on stored signal loss

During petrological microscopy, it was observed that very few grains of feldspar or possible feldspathoids displayed any form of twinning. In addition microstructures of any kind were rarely observed. Polymineral grains containing some or all of K-feldspar, plagioclase feldspar and quartz were quite common but again displayed little evidence of small-scale micro-structures. An index of poly-crystalline K-feldspar as a percentage of total K-feldspar ( $K_p/K$ ) has been derived from the stained LM provenance thin sections (table 4.16). The  $K_p/K$  index incorporates both small-scale microstructures and polymineral grains, but is dominated by polymineral grains. Due to the variations in density polymineral grains are much less likely to be measured during luminescence measurements, being removed during the two phase heavy liquid density separation. Studies using similar detrital material that use a single  $2.58 \text{ g/cm}^3$  density separation stage to quickly obtain the K-feldspar fraction, will be more prone to poly-mineral grain contamination. The  $K_p/K$  index presented here is therefore likely to be a significant overestimate. The modern nourishment of the *Ostia* beach and alongshore erosion of this material suggests that quarries are derived from similar geological sources of metamorphic detritus to that of the inland dunes at Castelporziano. What is clear is that the K-feldspar fraction used for luminescence chronology is dominated by grains without complex microstructure (plate 4.3); material that has been shown to not exhibit systematic loss of stored signal (*anomalous fading*).

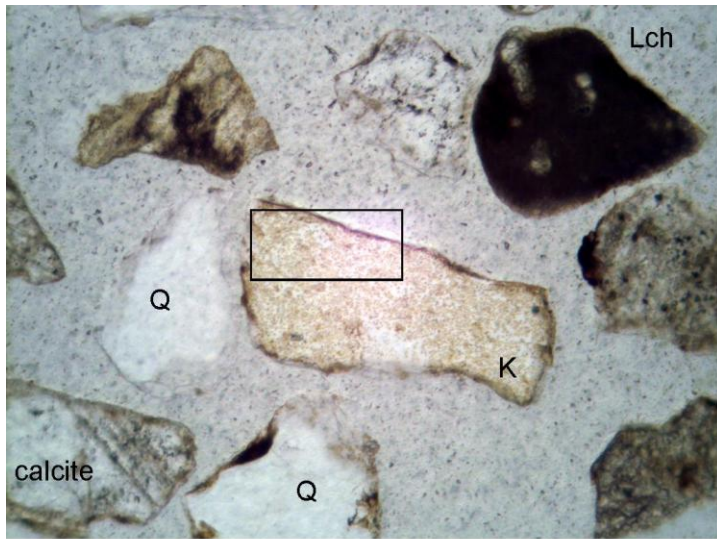
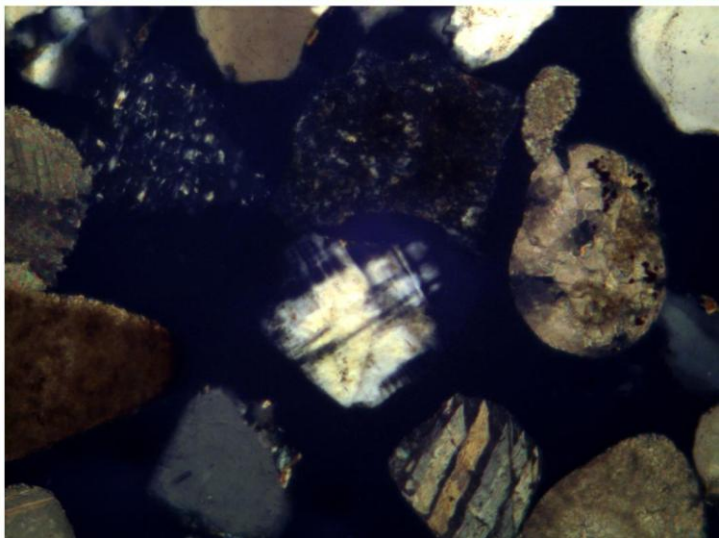
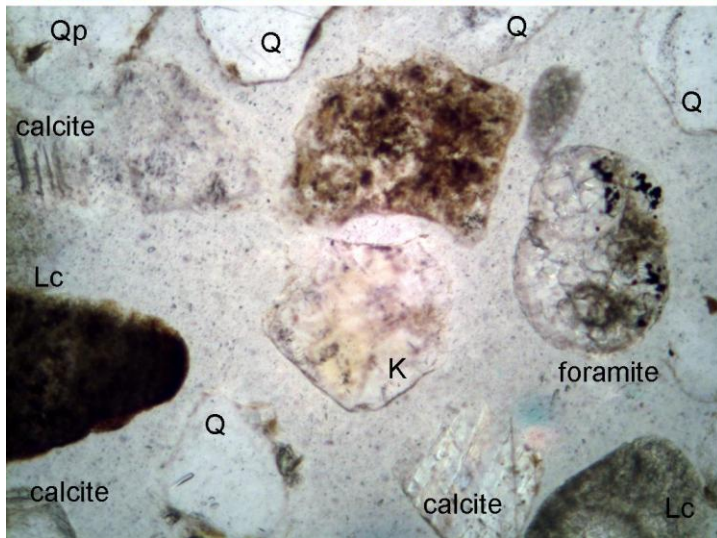
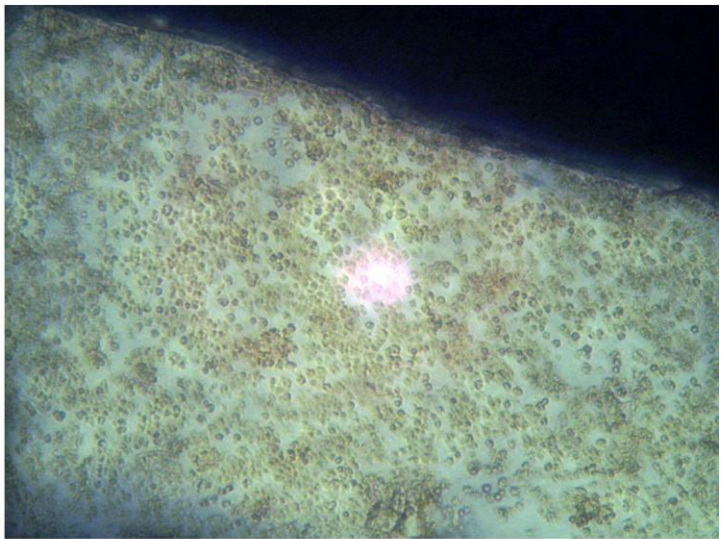
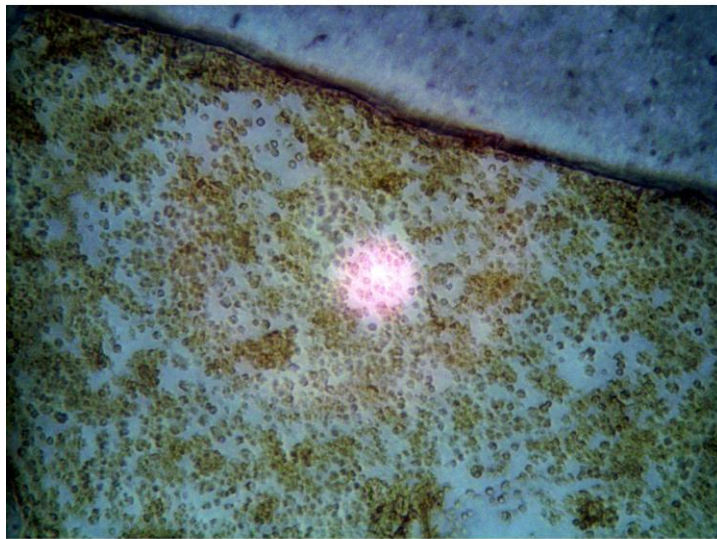


**Plate 4.3.:** K-feldspar (stained yellow) exhibiting a lack of twinning and complex small-scale microstructure in general microstructure (CP03/2) PP light x 100 (top left). Detail PP x 1000 (middle left), XP (middle right). Stained microcline (K) grain exhibiting characteristic twinning (PP light x 100) (CP07/25) (bottom left); XP light x 100 (bottom right).



Small-scale microstructures have been recently argued to harbour high-energy boundaries that may be preferred sites for electron tunnelling and therefore stored signal loss (Alexander 2007). However, these high-energy boundaries may also be preferential sites of weathering (Lee & Parsons 1995; Lee et al. 1995) which may be a key variable in removing the potential for *anomalous fading*. Microscopy has shown that the reworked and complex transportation history of light silicate grains (primarily the key luminescence dosimetry minerals quartz and feldspar) from the upper Tiber catchment has supplied well-rounded sand-sized material. The metamorphic origins of this sediment lacks small-scale microstructure (Vernon 2004), further removing the potential for stored signal loss borne out by the fading test. The hypothesis that geological provenance and post-erosional weathering remove the potential for stored signal loss due to tunnelling at high-energy sites is put forward in conjunction with recent research (Alexander 2007). Detailed sediment provenance and grain texture analysis is not a standard feature of the luminescence dating literature based primarily on quartz or feldspar. Future work incorporating mineral provenance or at least detailed microscopy of grain textures and sample mineralogy may then develop an empirical rationale for understanding fading potential within feldspars to underpin the existing theoretical models of quantum tunnelling (Spooner 1994; Huntley & Lian 2006; Huntley et al. 2007).

**Table 4.16:** Proportion (%) of detrital K- feldspar exhibiting complex microstructures and therefore potential sites for tunneling of stored electrons from traps ( $K_p/K$ ). Luminescence dates derived from this kind of metamorphically derived material is therefore dominated by K- feldspar grains without complex microstructures.

<b><math>K_p/K</math>: Alongshore Samples</b>					
<b>Fiumicino</b>	<b>Ostia 1</b>	<b>Ostia 2</b>	<b>Ostia 3</b>	<b>CP Beach</b>	<b>Torvaianic a</b>
36.92	23.96	17.82	18.18	23.21	18.75

<b><math>K_p/K</math>: Inland Samples</b>							
<b>CP Foredune</b>	<b>CP03/2</b>	<b>CP03/6</b>	<b>CP07/14</b>	<b>CP07/15</b>	<b>CP07/23</b>	<b>CP07/24</b>	<b>CP07/25</b>
15.25	24.44	7.5	24.14	15.28	21.74	14.29	21.21

#### **4.8.8. Archaeological age control**

Archaeological age control is provided for CP04/1 (Table 4.14). Sampling associated with archaeological building remains has been shown to provide excellent agreement with central SAAD-IRSL ages from Castelporziano (Rendell et al. 2007).

#### **4.8.9. IRSL ages**

The SAAD-IRSL samples show increasing age with distance inland of the current shoreline as expected (see section 4.9). The age determinations suggest that some dune ridges and sand sheet features are remobilised material - a fact not immediately suggested by field observations. The reddened dunes and inland sand sheet samples suggest deposition since at least the late Pleistocene until ca. 5 k BP. The carbonate dune ridges show deposition from ca. 5 k BP until the last 50 years as denoted by the modern foredune sample CP03/6 ( $52 \pm 4$  BP).

##### **4.8.9.1. Dose-rate trends**

The general observed trend is that dose-rate increases with distance inland and therefore also the age of the sample and the development of the early vadose diagenetic environment. In particular, iron oxide coated sediments exhibit greater environmental dose-rates to that of the carbonate cemented sediments. Figure 4.36 highlights the increase in dose-rate with distance from the current shoreline (relative to the dune ridges position along transect 1). Some samples from within the carbonate EVD environment also display an enriched dose-rate compared to adjacent samples. Field evidence shows low-level weathering, increased clay or organic content are associated with these samples. There is a clear clustering of dose-rate values within many of the carbonate EVD environment samples, whereas dose-rates in the reddened sediments and weathered carbonate sediments display enrichment and/or a broad spread in dose-rate value. Provenance analysis suggests that the source of sediment (i.e. the Tiber river catchment) has remained dominant during the period of deposition and formation. However, the method of deposition has changed from remobilised coastal shelf sands during Pleistocene lowstand sea level to sands deposited during Holocene delta progradation following the lateral expansion of the Tiber Delta reaching Castelporziano during the last 5000 years (Bellotti et al. 2007).



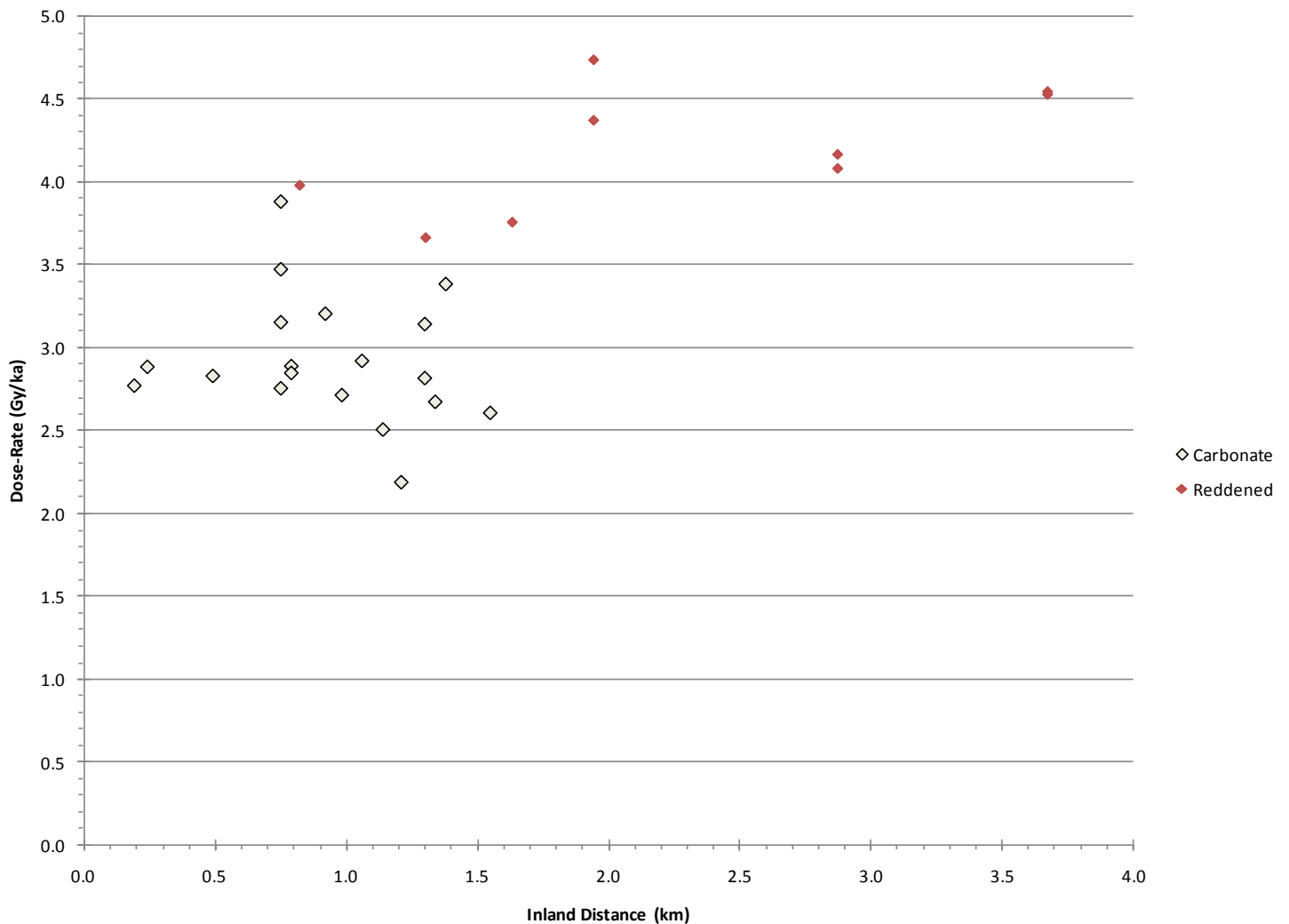


**Figure 4.36:** Distribution of environmental dose-rate with inland distance relative to dune ridges along transect 1. Carbonate aeolianite and reddened ferricretes are distinguished.

Weathering linked to iron oxide diagenetic environments has been shown to prevent accurate luminescence dating (Zhang et al. 2008). Generally in luminescence dating methodology it is assumed that the dose-rate remains unchanged during the burial lifetime of the sample. Dose-rate measurements are based on bulk sediment samples from the vicinity of the dating sample. If all products of weathering are retained in vicinity of the sample then conceptually changes in dose-rates and also the consequent increase in the rate of trapped charge storage (i.e. DE) would balance and laboratory measurements of dose-rate and DE would produce a representative age estimate for the sample. The relative mobility of U to the stability of Th is sensitive to weathering effects. Decreasing trends in U/Th ratios are driven by weathering of mineral sources of these elements with removal from the system. Figures 4.37 and 4.38 highlight the trends in the 3 main components of a luminescence dose-rate calculation, U, Th (both ppm) and K %. Petrology results show clear trends in depletion of heavy minerals with respect to quartz content which is partitioned within diagenetic environments. Because luminescence dating environmental dosimetry values are based upon bulk ground samples,

differentiating weathered dosimetry components and clastic components is not generally made. In a closed system where weathering products are completely stored without loss or mobility, one would expect a clear linear trend in U/Th across the sample range. There is a very weak positive relationship observed in U/Th ratios from all samples (figure 4.37 and 4.38). Figure 4.37 shows an exponential increase in K % content ( $r^2 = 0.9731$ ) used in the dose-rate calculations between the samples with the lowest and highest K % contents. All samples plotting above the average are reddened ferricrete EVD sands except CP03/3, CP04/7 and CP08/3 which have the same or greater K % as CP07/15, the most seaward reddened dune ridge. This pronounced dosimetry gradient suggests the storage and accumulation of K, increases exponentially with diagenesis. Petrological data show that feldspar minerals, key sources of K, are less abundant within the reddened sands. It must be noted that the order of samples in figure 4.37, 4.38 and 4.39 is not ordered by age or distance inland, suggesting that post-depositional alteration is sample specific but generally similar within the specific EVD environments. Weathering may be partly due to biogenic and / or pedogenic processes, however the depth of sampling in clean sand away from observed pedogenic horizons suggests pedogenesis is not a dominant factor. The effect of seasonal groundwater-derived allochthonous geochemistry must also be considered (McLaren & Nash 2007). The early vadose diagenetic weathering and mobilisation of clastic K sources is argued to be the key variable for observed enrichments in environmental dose-rate. The mobilisation of metal cations from the surface of multi-oxide silicates such as albite and pyroxenes has been shown experimentally (Oelkers et al. 2009).

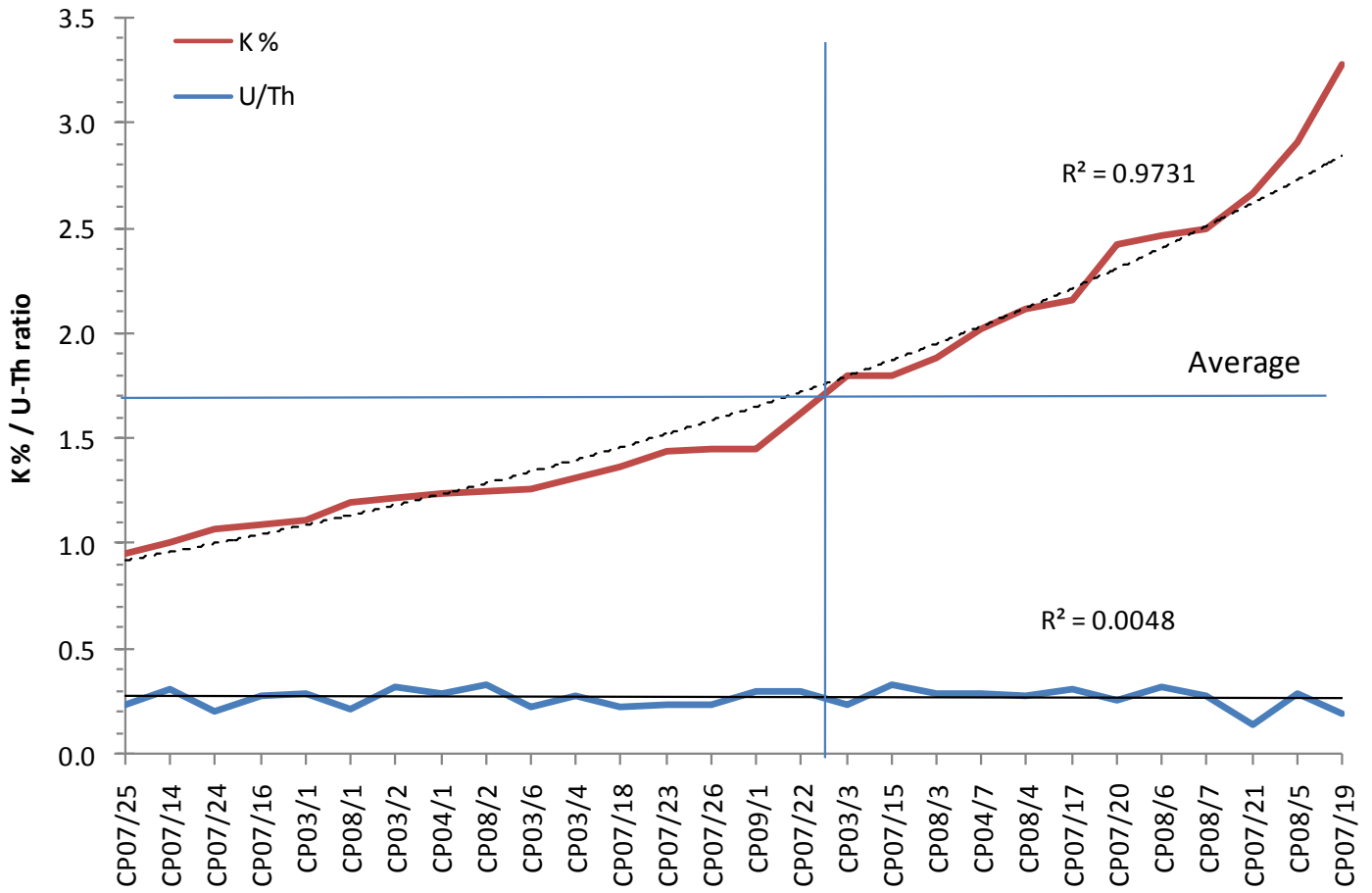


**Figure 4.37:** Principal dose-rate components. Samples are ordered by K % content plotted with exponential trend line. U/Th ratio is plotted with a linear trend line. Samples plotting above the average with the exception of CP03/3 are reddened dune ridge or sand sheet samples. A clear trend in accumulation and storage of K is observed probably due to *in situ* weathering during early vadose diagenesis. U/Th ratio should be stable if loss from the system has not occurred. The poor performance of a linear trend line and a decreasing trend in U with respect to Th from CP08/7 – CP07/19 suggest that not all dose-rate components are stored and accumulated. Therefore the measured dose-rate cannot be assumed to be accurate for the lifetime of the sample or directly related to the measures  $D_E$ .

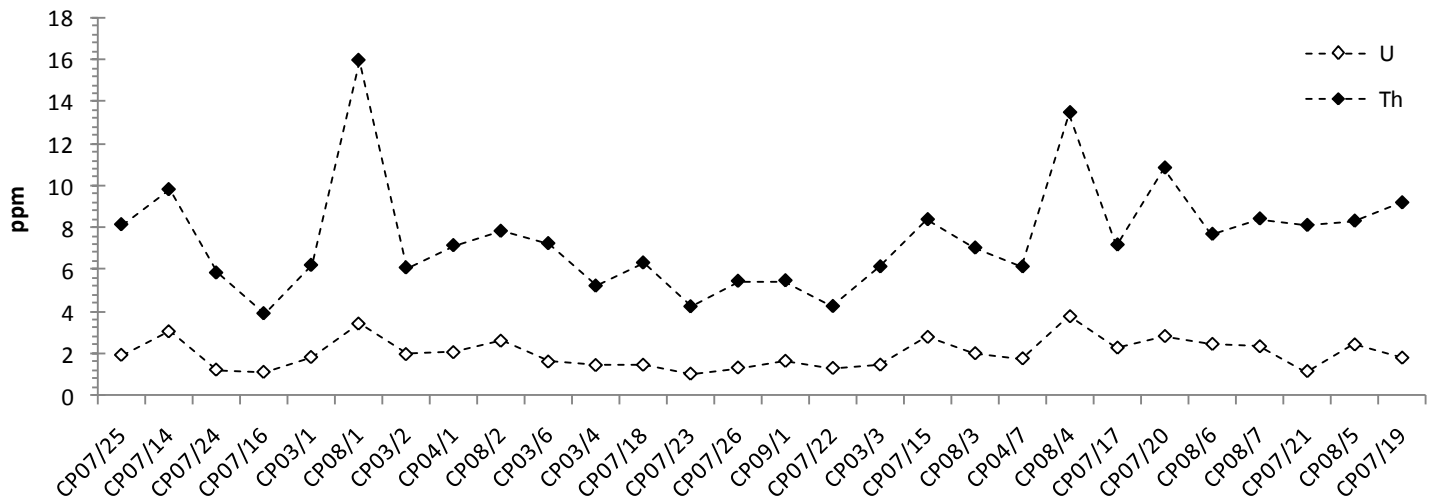


**Figure 4.38:** Trend in U and Th (ppm), following sorting by increasing K % (figure 4.37). Generally it is observed that trends in U are similar to corresponding trends in Th. However, the samples to the extreme right of the graph show some evidence for a decreasing trend in U with an increasing trend in Th.

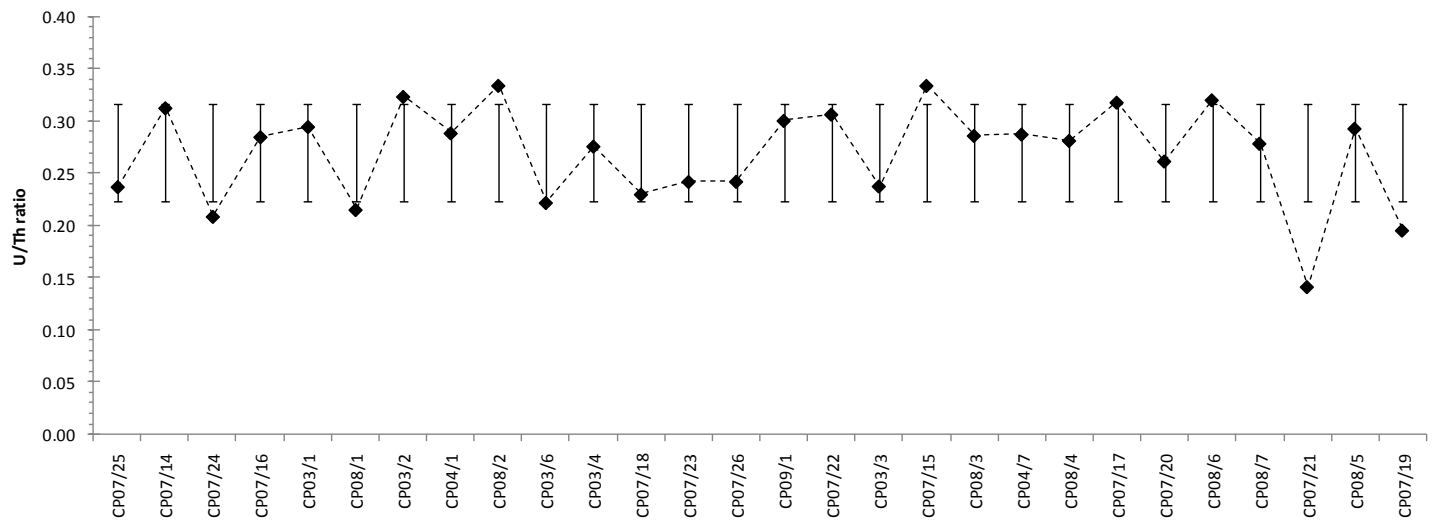


**Figure 4.39:** U/Th ratio with standard deviation bars. Sample order is relative to increasing K %. Most samples display a homogeneous U/Th ratio however spread is likely due to sample-specific diagenetic conditions making assessment of trends in dose-rate components problematic to interpret.

The weathering of K ions and therefore their mobilisation and potential loss suggests a mechanism for storage and accumulation. The most obvious mechanism would be storage within early vadose diagenetic cements. Within the ‘white’ dunes the accumulation medium may be the micritic and amorphous cements recorded by EDX-SEM analysis. The widespread presence of Fe atoms was also noted by element mapping during EDX-SEM analysis, suggesting Goethite or other hydrated iron oxides are also present as early vadose diagenetic coatings. Similar analysis of the reddened dunes and WRD and loss-on-ignition (LOI) analysis show that carbonates are largely absent with an order of

magnitude decrease in carbonate (% dry weight) values recorded by high-temperature LOI between the carbonate and reddened dunes respectively. As a working hypothesis, with regards to radioactive elements in particular, it is proposed that early vadose diagenetic coatings act as a medium for the storage and accumulation of radioactive elements that are incorporated into the primary dose-rate evaluation for luminescence dating. Therefore, as diagenesis continues over time, the specific conditions experienced at each sampling location will produce a sample-specific dose-rate but also a cumulative enrichment of dose-rate throughout the time of burial due to the accumulation of weathered radioactive elements within diagenetic inter-grain cements.

However, it must not be assumed that the sampled dose-rate is representative of that experienced by the luminescence sample (Zhang et al. 2008). It is clear that K has been stored and accumulated during diagenesis, but the various data also suggest that dose-rate components and weathering are sample specific, so interpreting these trends may not adequately identify samples where bulk dose-rate measurements are not representative of the cumulative stored dose. A further consideration must also be that if sample specific weathering and diagenesis are occurring, it is not possible to interpret the stability of U or Th from perceived trends across the site. Although Th is generally assumed to be immobile compared to U, recent research suggests this may not be the case (Yang et al. 2007; Olley et al. 1996). The fairly large flux in Th ppm across the site may also suggest that EVD environments are relatively dynamic. The decreasing trend in HMs due to diagenesis, especially in the older red dunes, suggests that weathering and dissolution is a key process and chemical products are likely to possess a certain level of mobility, especially in an environment where groundwater table flux and meteoric precipitation are seasonally pronounced. Significant research goals still remain within luminescence dosimetry. Although the existing literature of luminescence applications on ferricretes and red-weathering is small and focused on older sediments than observed at Castelporziano (e.g. Zhang et al. 2008), the ferricrete samples have been treated cautiously.

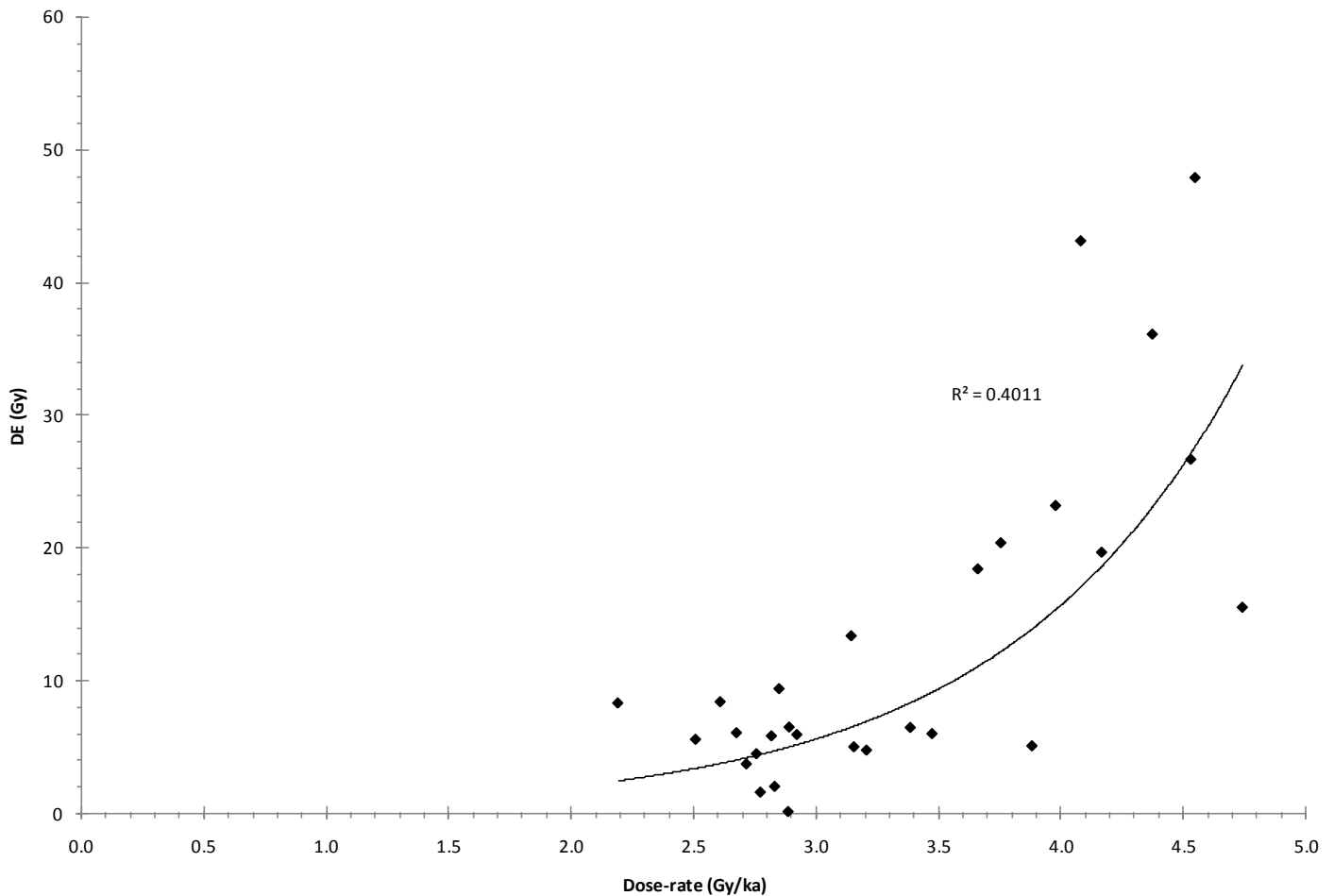


**Figure 4.40:** DE vs dose-rate. DE can be seen to exponentially increase with the exponential increase of K content in particular (see figure 4.37). However the spread in the data may again highlight sample-specific burial conditions that combine to derive the luminescence age.

One would expect to see a clear linear relationship between dose-rate and  $D_E$  if strong gradients existed in the dosimetry variables contributing to the DE. The significant spread in is likely due to sample specific conditions experienced during burial. As with K % an exponential relationship exists but is less well described by the data (figure 4.40). Based on interpreting simple trends in the graphed data, it is problematic to investigate the sample-specific relationship between DE and the mean dose-rate calculated from laboratory measurements. For effective luminescence dating it is generally assumed that measured dose-rates and recovered DE are equivalent. However, the effects of weathering and diagenesis upon dosimetry are not well understood. Age estimates based primarily on the reddened geomorphic features (but also some weathered carbonate-cemented samples) are therefore treated with caution due to post-burial dose-rate variation and uncertainty about the equivalence of recovered DE. Affected samples must then be considered as minimum age estimates.

#### 4.8.9.2. Intra-dune age estimate variability

A chronological framework, by its nature suggests chronological control in at least 2 dimensions. Age estimates are thought to be meaningful across inland transects. The effectiveness of alongshore chronology, within coeval formation phases is developed below. Gradients in alongshore transport equivalence exist and are clearly recorded in the sedimentary records at Castelporziano. These gradients provide valuable information on the variability of sediment dynamics and mineralogy across the site, but as a consequence, limit the cross-site comparison of other key techniques, importantly assessing the variation in dosimetry components within similar phase dune ridges. Where the opportunity exists to sample the same phases of relict dune ridge or palaeo-shoreline such as the youngest reddened dune ridge (CP07/15 & CP07/21) or pronounced carbonate dune ridge and palaeo-beach samples (CP07/23, CP07/16 and CP07/22, respectively) complexity rather than simplicity is observed (table 4.17). Data in Table 4.17 are organised by increasing alongshore distance from river mouth.

**Table 4.17:** Age estimate, LOI and grain-size data for samples from similar dune-ridge formations organised by iron oxide early vadose diagenesis (EVD) and carbonate environments.

Iron oxide EVD													
Sample	HM:LM	st dev	Age (BP)	error	D <sub>E</sub> (Gy)	error	Dose-rate (Gy/ka)	U (ppm)	Th (ppm)	K (%)	OC (%)	CO3 (%)	Mode GS (µm)
CP07/15	0.195	0.015	5055	331	18.406	0.448	3.662	2.805	8.385	1.800	0.644	0.876	269
CP07/21	0.033	0.003	5823	374	23.173	0.776	3.979	1.150	8.110	2.670	0.667	0.489	245

Carbonate EVD													
Sample	HM:LM	st dev	Age (BP)	error	D <sub>E</sub> (Gy)	error	Dose-rate (Gy/ka)	U (ppm)	Th (ppm)	K (%)	OC (%)	CO3 (%)	Mode GS (µm)
CP07/23	0.136	0.011	3224	224	8.414	0.172	2.609	1.024	4.220	1.440	1.008	11.688	269
CP07/16	0.156	0.012	3768	268	8.321	0.245	2.191	1.110	3.890	1.100	0.833	17.783	204
CP07/22	0.064	0.001	3297	222	9.397	0.105	2.850	1.300	4.235	1.620	0.594	13.593	296

Although differences in alongshore mineralogy will ensure different dose-rates along the coast, coeval formation should derive the same age estimate from the material if dose-rates are stable during burial. The sample-specific effect of post-depositional dose-rate change is suggested by the discrepancy between luminescence age estimates for samples CP07/15 and CP07/21.

HM:LM ratios decrease (within error ranges) as expected with increased distance from the river mouth source. However all samples here have experienced early vadose diagenesis, whether reddening or carbonate-cementation and

dissolution of heavy ferro-magnesian minerals and/or feldspars, respectively will have occurred. The two sample sets are believed to derive from similar but separate phases of dune ridge formation, respectively. In the broadest possible terms the dunes can be attributed to millennial phases of formation due to inter-sample variability, at ca. 5-6 ka BP (red dune ) and 3-4 ka BP (carbonate dune). Ideally we would like to constrain them more effectively. DE determinations are broadly internally consistent within the carbonate dune ridge samples. However, the previously discussed dose-rate enrichment due to dune reddening appears to have caused significant enrichment in DE between samples CP07/15 and CP07/21. Rather than observing a lower dose-rate linked to a reduced HM component, the opposite is seen. It could be argued that this lower HM:LM ratio and increased DE and dose-rate indicate that the weathered ions (reducing the HM:LM ratio) are preserved locally in diagenetic products but alongshore transport equivalence must be taken into account making interpretation problematic. The dosimetry data suggests that K is stored and accumulated in the reddened "Old dunes". Due to the sample-specific nature of the post-depositional weathering and diagenesis interpreting U with respect to Th, perhaps linked to the solubility of U and therefore increased mobility away from the site of weathering, is more problematic. In particular, an increased dose-rate appears to occur with an increase in the K dose-rate component, which I argue to be due to weathering of light silicates, particularly K-feldspar. Assuming that Th is stable and not likely to be removed during burial, Table 4.17 suggests that Th between the two similar dune phase samples (CP07/15 and CP07/21) is similar and that the difference in dose-rate is derived from relatively increased K content with CP07/21 also showing a reduced U content. Even though U is apparently lost, the increased mean dose-rate is achieved primarily by K related beta dose-rate (see table 4.14), leading to the discrepancy in age of what is thought to be a coeval dune ridge. Relying upon Th series beta-radiation emissions to constitute the vast majority of the beta dose-rate may not be viable. Therefore caution over the ferricrete age estimates may currently be justified *in lieu* of further dedicated studies from this site but also in the luminescence dosimetry literature as a whole. Further detailed and dedicated study on the variability of dosimetry throughout ferricretised dune forms would be a valuable next step for increasing confidence in these environments and out with the scope of this thesis.

Field survey and GIS mapping shows that samples CP07/23 ( $3224 \pm 224$  BP) and CP07/16 ( $3768 \pm 268$  BP) derive from the same relict dune ridge. DE determinations are similar,  $8.414 \pm 0.172$  Gy and  $8.321 \pm 0.245$  Gy, respectively. Owing to a significantly lower dose-rate than any other dated sample, CP07/16 is estimated at around 500 years older than CP07/23. Dose-rate enrichment by *in situ* weathering is not observed in K-dose-rate values. For the sake of argument, by applying the dose-rate correction methodology described above, the mean age for CP07/16 quoted with the standard deviation of the maximum (3768) and minimum (2979) age estimates is  $3374 \pm 558$  BP, placing the three samples from the same dune ridge in good agreement. The mode grain-size of CP07/16 is noticeably smaller than the other samples and the carbonate content higher. It may be that the effective dose-rate is not representative of the dose-rate received by the luminescent minerals due to an increased proportion of inter-grain cements to grain-surface



area (Nathan & Mauz 2008). Thus the local diagenetic conditions experienced by individual samples may introduce further noise into the chronological framework of the site.

#### **4.8.10. Multivariate analysis of DE and environmental variables**

PCA was also proposed using the environmental dosimetry data for 28 luminescence dating samples (table 4.18). Utilising standard measurements and dose-rate components, 14 variables were incorporated into the initial analysis. However, DCA shows that around 3.3 % of the sample variance is related to species (dosimetry) variance making the data unsuitable for PCA (table 4.19). At first glance this may appear a disappointing result. However, strong 'independence' is desirable between the key factors underpinning the luminescence age estimates, otherwise a change in one component would affect many of the others, rendering accurate age estimates impossible.

A simple modelling analysis was undertaken to assess the effectiveness of Estimated Dose (DE) determinations in relation to the key dosimetry values used to calculate a luminescence date. The scope of this thesis is to ask meaningful geoarchaeological questions of the Laurentine Shore rather than solely focusing upon luminescence dating methodology. Therefore this multi-variate analysis is limited to a preliminary study.

In theory variance in the DE should correlate 100 % with the variance in the dosimetry variables used in the age calculations. In this way an assessment of the effectiveness of luminescence dating within this study could conceptually be made. By setting DE as the sole species with the remaining variables as environmental variables the relationship between DE and the 5 key dosimetry variables (alpha, beta, gamma, cosmic ray and internal beta dose rates) was assessed. A multiple regression analysis was undertaken using the RDA settings in CANOCO 4.5. Automatic forward selection was used and 499 permutations a partial Monte Carlo analysis was performed. The performance of key environmental dosimetry variables are presented in Table 4.20. Incorporating only the key dosimetry components used in the age calculations 88.8 % the sample DE correlates with these environmental variables (Table 4.21) with 78.9 % of the variance described. P-values suggest the dosimetry variables are highly significant as one would hope.

**Table 4.18:** Luminescence, dosimetry and environmental variables used in dosimetry multivariate analysis.

Sample	U (ppm)	Th (ppm)	K (%)	int. beta (μGy/a)	Alpha (μGy/a)	Beta (μGy/a)	Gamma (μGy/a)	U/Th	Th/OC	Cosmic (μGy/a)	OC (% dry)	Mode (μm)	CO3 (% dry)	DE (Gy)
CP03/1	1.83	6.2	1.12	669.7	119.72	1028.6	712.38	0.295	7.003	186	2.269513	325	2.511883	0.885
CP03/2	1.97	6.08	1.22	660.77	123.48	1107.11	742.51	0.324	5.908	185	2.267172	296	2.471292	1.029
CP03/3	1.46	6.13	1.8	660.77	107.75	1426.9	818.57	0.238	4.595	193	2.285557	296	2.471292	1.334
CP03/4	1.44	5.21	1.32	602.38	106.26	1110.8	670.51	0.276	6.796	186	2.269513	270	2.431364	0.767
CP03/6	1.61	7.24	1.27	669.7	114.6	1046.32	722.47	0.222	11.217	201	2.303196	356	2.55145	0.645
CP04/1	2.065	7.145	1.24	660.77	137.15	1150.21	805.59	0.289	11.539	169	2.227887	296	2.471292	0.619
CP04/7**	1.765	6.13	2.03	497.66	150.54	1654.91	898.91	0.288	7.454	184	2.264818	224	2.350248	0.822
CP07/14	3.075	9.82	1.01	602.38	212.72	1173.18	981.29	0.313	30.573	175	2.243038	270	2.431364	0.321
CP07/15*	2.805	8.385	1.8	602.38	187.82	1629.28	1058.23	0.335	13.018	184	2.264818	270	2.431364	0.644
CP07/16	1.11	3.89	1.1	451.55	103.4	932.47	528.82	0.285	4.673	175	2.243038	204	2.30963	0.833
CP07/17*	2.285	7.175	2.16	602.38	156.75	1784	1027.62	0.318	8.888	185	2.267172	270	2.431364	0.807
CP07/18	1.455	6.315	1.37	547.98	128.97	1177.75	733.85	0.230	7.645	185	2.267172	246	2.390935	0.826
CP07/19*	1.8	9.19	3.28	547.98	175.86	2521.97	1313.47	0.196	7.670	183	2.262451	246	2.390935	1.198
CP07/20*	2.845	10.855	2.43	547.98	234.57	2110.78	1312.28	0.262	7.695	169	2.227887	246	2.390935	1.411
CP07/21*	1.15	8.11	2.67	547.98	138.82	2031.18	1066.51	0.142	12.153	195	2.290035	246	2.390935	0.667
CP07/22	1.3	4.235	1.62	660.77	83.71	1258.38	676.08	0.307	7.132	171	2.232996	296	2.471292	0.594
CP07/23	1.0235	4.22	1.44	602.38	81.16	1125.14	608.76	0.243	4.187	192	2.283301	270	2.431364	1.008
CP07/24	1.22	5.835	1.08	660.77	97.16	933.4	625.44	0.209	5.228	192	2.283301	296	2.471292	1.116
CP07/25	1.935	8.145	0.96	669.7	143.65	973.88	778.29	0.238	15.002	192	2.283301	357	2.552668	0.543
CP07/26	1.32	5.44	1.46	660.77	96.39	1180.58	699.25	0.243	5.910	195	2.290035	296	2.471292	0.920
CP08/1	3.45	16	1.2	669.7	268.61	1436.19	1345.55	0.216	10.549	163	2.212188	325	2.511883	1.517
CP08/2	2.62	7.83	1.26	669.7	160.99	1232.46	897.46	0.335	6.562	195	2.290035	325	2.511883	1.193
CP08/3**	2.015	7.03	1.89	669.7	133.85	1557.76	935.47	0.287	12.226	178	2.25042	325	2.511883	0.575
CP08/4*	3.805	13.5	2.12	547.98	301.65	2063.18	1464.29	0.282	8.983	172	2.235528	246	2.390935	1.503
CP08/5*	2.44	8.315	2.91	602.38	174.48	2309.2	1257.69	0.293	10.050	188	2.274158	270	2.431364	0.827
CP08/6*	2.465	7.685	2.47	547.98	182.88	2033.97	1136.18	0.321	8.020	181	2.257679	246	2.390935	0.958
CP08/7*	2.35	8.42	2.5	602.38	172.51	2035.57	1165.03	0.279	9.323	192	2.283301	270	2.431364	0.903
CP09/1	1.645	5.465	1.46	660.77	106.99	1215.34	733.14	0.301	9.054	175	2.243038	296	2.471292	0.604

\*\*Old dunes" ferricretes

\*\*aeolianite EVD samples affected by red weathered sediments

**Table 4.19:** DCA summary data for luminescence dosimetry and environmental variables shown in table 4.18.

<b>Axes</b>	<b>1</b>	<b>2</b>	<b>3</b>	<b>4</b>	<b>Total inertia (variance)</b>
Eigenvalues:	0.024	0.003	0.001	0	0.033
Lengths of gradient:	0.416	0.231	0.267	0.24	
Cumulative percentage variance of species data:	74.8	84.8	87.1	88.3	
Sum of all eigenvalues:					0.033

**Table 4.20:** Multiple regression (RDA) summary output, all samples.

<b>N</b>	<b>name</b>	<b>(weighted) mean</b>	<b>stand. dev.</b>	<b>inflation factor</b>
1	SPEC AX1	0	1.126	
2	SPEC AX2	0	1	
3	SPEC AX3	0	0	
4	SPEC AX4	0	0	
5	ENVI AX1	0	1	
6	ENVI AX2	0	0	
7	ENVI AX3	0	0	
8	ENVI AX4	0	0	
4	int.beta	610.6193	59.9491	5.1874
5	alpha	150.0871	53.1274	66.5344
6	beta	1472.875	455.029	64.1796
7	gamma	918.4157	253.3823	182.3772
10	Cosmic	183.6071	9.4579	1.4094

**Table 4.21:** Multiple-regression summary data, model effectiveness.

<b>Axes</b>	<b>1</b>	<b>2</b>	<b>Total variance</b>
Eigenvalues:	0.789	0.211	1
Species-environment correlations:	0.888		
Cumulative percentage variance of species data:	78.9	100	
of species-environment relation:	100		
Sum of all eigenvalues			1
Sum of all canonical eigenvalues			0.789

**Table 4.22:** Forward selection for Monte Carlo tests. Marginal effects highlights the variance described by each individual environmental variable ( $\Lambda-1$ ) in order of variance explained. “Conditional effects” highlights the additional variance of the individual environmental variables when added to the model. The significance of each variable during Monte Carlo tests is shown by the P-value.

Marginal Effects			Conditional Effects				
Variable	Var.N	$\Lambda-1$	Variable	Var.N	$\Lambda-A$	P	F
beta	6	0.57	beta	6	0.57	0.002	33.88
gamma	7	0.54	alpha	5	0.07	0.032	5.42
alpha	5	0.43	gamma	7	0.1	0.008	9.58
int.beta	4	0.23	int.beta	4	0.05	0.06	4.73
Cosmic	10	0.07	Cosmic	10	0	0.89	0.03

High variance inflation factors for alpha, beta and gamma suggest that they are poorly performing variables against the other variables in the analysis (table 4.20). Noting the poor correlation between variables (table 4.21) this may account for this trend in these three most important variables considered in the luminescence age calculation. Table.4.22 outlines the marginal effects; the variance described by individual environmental variables. The importance of alpha, beta and gamma dose-rate components with additional internal and cosmic dose rate components upon DE is clear (Aitken 1998). Other variables must be responsible for the outstanding variance. The effects of diagenesis have been shown to be critical factors for understanding the site; therefore an expanded set of 10 environmental variables was developed (table 4.23).

**Table 4. 23:** Rationale for additional environmental variables.

Variable	Description	Rationale / hypothesised impact	Literature
<b>U/Th</b>	Ratio of U to Th (ppm) calculated from TSAC and TSBC dosimetry.	<ul style="list-style-type: none"> <li>Sample-specific variations in U and Th content and observed trends in decreasing U with respect to increasing Th in some of the “Old dunes” samples may suggest a loss of key dosimetry variables.</li> </ul>	
<b>Th/OC</b>	Ratio of Th (ppm) to organic content (% dry weight loss-on-ignition)	<ul style="list-style-type: none"> <li>Increases in OC may contribute to concentrating Th contents.</li> </ul>	(Sanderson & Murphy In Press)
<b>OC</b>	Organic content (% dry weight loss-on-ignition)	<ul style="list-style-type: none"> <li>Sampling was aimed at retrieving material from clean sand devoid of organic contents. Therefore localised increases in organic content may have a more pronounced effect upon the efficiency of environmental radiation to the luminescence dosimeters under study.</li> </ul>	
<b>CO3</b>	Carbonate equivalent content (% dry weight loss-on-ignition)	<ul style="list-style-type: none"> <li>Carbonate cementation has been shown to attenuate the environmental dose-rate experienced by luminescence dosimeters.</li> <li>The bipartite diagenetic environments on the site with respect to decalcification in the ferricretes and mature aeolianite samples may be important.</li> </ul>	(Nathan & Mauz 2008)
<b>mode</b>	Mode grain-size ( $\mu\text{m}$ ) calculated from Folk and Ward statistics by GRADISTAT v5	<ul style="list-style-type: none"> <li>Diagenetic weathering of grain surfaces may reduce to mode grain-size during burial.</li> <li>The diameter of the luminescence dosimeter also relates to the efficiency with which it is dosed by ionising environmental radiation.</li> </ul>	(Aitken 1998)

**Table 4.24:** Multiple regression summary data, all samples using expanded environmental factors.

Axes	1	2	Total variance
Eigenvalues:	0.857	0.143	1
Species-environment correlations:	0.926		
Cumulative percentage variance of species data:	85.7	100	
of species-environment relation:	100		
Sum of all eigenvalues			1
Sum of all canonical eigenvalues			0.857

**Table 4.25:** Forward selection summary data, all samples using expanded environmental variables.

Marginal Effects			Conditional Effects				
Variable	Var.N	$\Lambda-1$	Variable	Var.N	$\Lambda-A$	P	F
CO3	15	0.63	CO3	15	0.63	0.002	44.310
beta	6	0.57	OC	14	0.06	0.040	4.950
gamma	7	0.54	mode	12	0.05	0.046	4.340
alpha	5	0.43	Cosmic	10	0.03	0.112	2.730
mode	12	0.26	U/Th	8	0	0.378	0.750
int.beta	4	0.23	int.beta	4	0.01	0.524	0.450
OC	14	0.1	alpha	5	0	0.722	0.120
Cosmic	10	0.07	Th/OC	9	0	0.550	0.370
U/Th	8	0.02	gamma	7	0.01	0.450	0.620
Th/OC	9	0.01	beta	6	0.07	0.020	7.850

Multiple regression analysis of all samples across all diagenetic environments shows that the DE correlate 92.6 % with the environmental variables and 85.7 % of the observed variance is described (Table 4.24, with forward selection data in table 4.25). Graphically this is described by the positive angle on the DE vector away from the 1<sup>st</sup> axis (Figure 4.41). As would be expected, alpha, beta and gamma dose-rate variables are strongly positively correlated with DE. Internal beta dose-rate and mode grain-size are moderately negatively correlated to DE again relating to the sand-sized K-dosimeters rather than the environmental radiation received by these dosimeters. Notable is the strong negative correlation between carbonate content and DE (also highlighted by the variance  $\Lambda-1$  in Table 4.25). This may be related to the effect of carbonate concretions attenuating the dose-rate experienced by the luminescence dosimeters (e.g. Nathan & Mauz 2008). However within the context of this site, the negative correlation is probably significantly skewed by the samples with the highest DE having almost no carbonate content due to decalcification during ferricrete diagenesis.

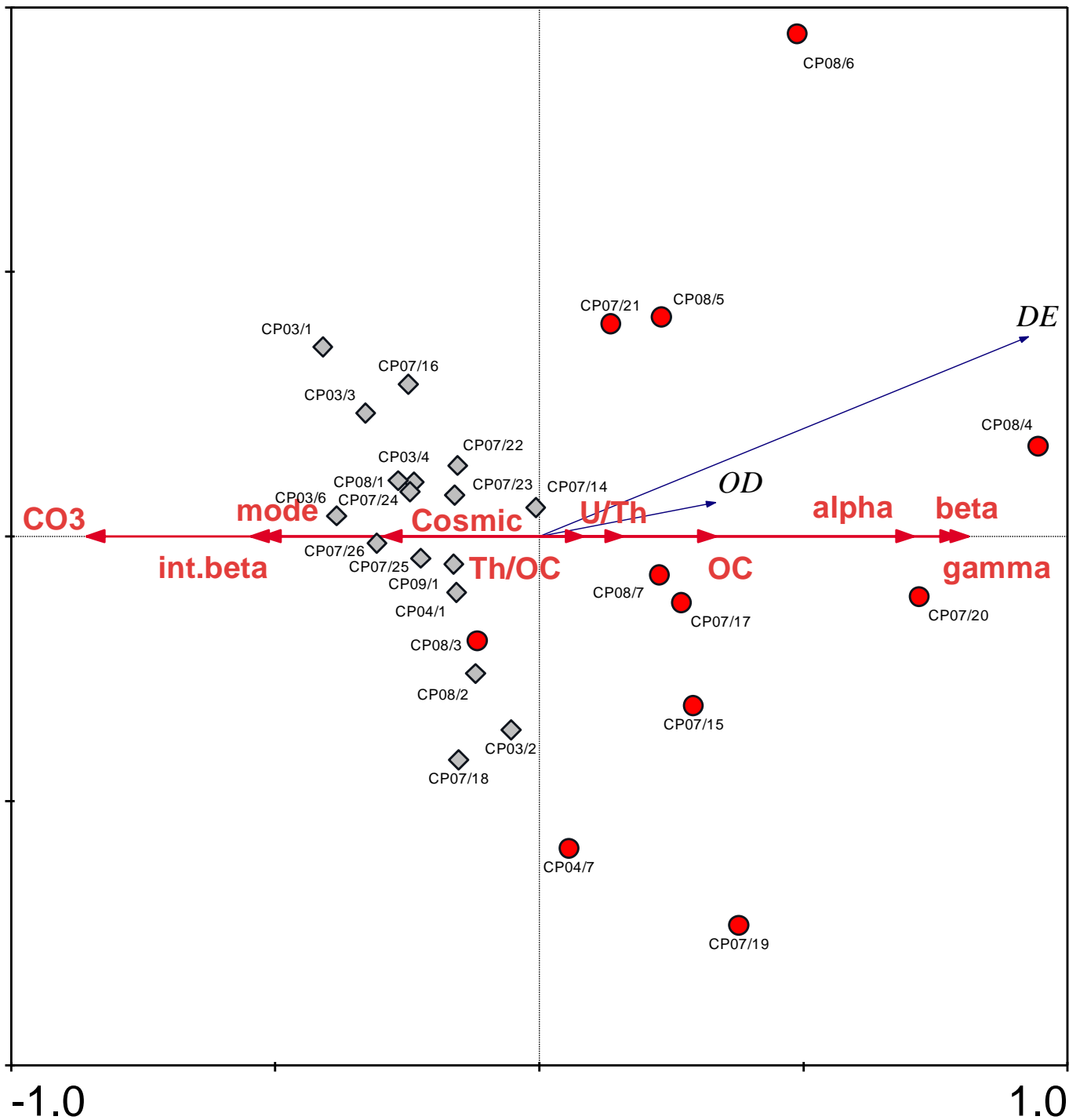


**Figure 4.41:** Multiple regression bi-plot plus environmental data. As would be expected the aeolianite samples (grey diamonds) plot towards the left of the DE vector appropriate to their relatively young age compared to the ferricrete samples (red circles). The ferricrete samples display an increased level of spread, interpreted to be caused by EVD processes. CP08/3 and CP04/7 are also loosely described as ‘ferricretes’ as during sampling they are associated with reddened sediments.

Although the variation in DE (Figure 4.41) is highly correlated (92.6 %) to the environmental variables, 85.7 % of the variance is accounted for. The remaining proportion unaccounted for is conceptually deleterious for accurate age estimation and is likely to be partly a function of measurement noise (however the discrepancy is larger than typically accepted 10% precision). From this initial analysis an additional hypothesis was developed. This relatively low level of discrepancy may be accounted for by observed decreases in U with respect to increases in Th only occurring in some of the “Old dunes” samples. It has been shown that the carbonate and iron oxide EVD environments are petrologically discrete. Therefore further multiple regression analysis restricted to samples within each EVD environment was undertaken to examine this hypothesis.

**Table 4.26:** Forward selection summary data, **aeolianite** EVD samples only.

Marginal Effects			Conditional Effects				
Variable	Var.N	$\Lambda-1$	Variable	Var.N	$\Lambda-A$	P	F
Cosmic	10	0.27	Cosmic	10	0.27	0.024	6.4
U/Th	8	0.25	U/Th	8	0.14	0.06	3.59
Th/OC	9	0.19	Th/OC	9	0.07	0.164	2.09
mode	12	0.17	mode	12	0.11	0.088	3.86
CO3	15	0.15	int.beta	4	0.04	0.284	1.24
OC	14	0.09	CO3	15	0.02	0.41	0.75
int.beta	4	0.07	gamma	7	0.02	0.358	0.87
alpha	5	0.03	OC	14	0.09	0.078	3.68
beta	6	0.01	beta	6	0.09	0.036	5.68
gamma	7	0	alpha	5	0.01	0.66	0.23

**Table 4.27:** Multiple-regression summary data, **aeolianite** EVD samples only.

Axes	1	2	Total variance
Eigenvalues:	0.859	0.141	1
Species-environment correlations:	0.927		
Cumulative percentage variance of species data:	85.9	100	
of species-environment relation:	100		
Sum of all eigenvalues			1
Sum of all canonical eigenvalues			0.859

Diagenetically related variables such as U/Th and Th/OC are key variables within the aeolianite EVD, explaining 25 % and 19 % of the variance, respectively (Table 4.26). The cosmic ray dose-rate explains most of the variance but other dose-rate factors are relatively unimportant, although they explain more of the variance once added to the model

(conditional effects). This suggests that the additional environmental variables add a significant amount of variance but also effectively account for it. 85.9 % of the variance is accounted for by the analysis, with the DE correlating 92.7 % with the extended environmental variables (Table 4.27). P-values for U/Th suggest that this variable is significant to 94 % and not likely to be randomly encountered (Table 4.26). However interpreting this result is problematic. U/Th is not statistically significant and explains very little of the variance observed in the ferricrete samples. It was observed earlier that decreasing trends in U may occur with increasing trends in Th within some of the “Old dunes” ferricretes. If we assume that this trend is responsible for these U/Th effects in the multi-variate analysis then we may interpret low P-values (significance) as relating to constructive effects upon the DE. The model is based on several variables and is not sensitive to contextual knowledge. Therefore overly ambitious interpretations at this early stage of modelling should be discouraged.

**Table 4.28:** Forward selection summary data, **ferricrete** EVD samples only.

Marginal Effects			Conditional Effects				
Variable	Var.N	$\Lambda-1$	Variable	Var.N	$\Lambda-A$	P	F
alpha	5	0.65	alpha	5	0.65	0.014	14.68
mode	12	0.48	int.beta	4	0.07	0.216	1.95
int.beta	4	0.48	U/Th	8	0.09	0.136	2.68
gamma	7	0.48	CO3	15	0.01	0.568	0.4
OC	14	0.46	Cosmic	10	0.04	0.336	1.16
CO3	15	0.25	Th/OC	9	0.01	0.834	0.05
beta	6	0.16	OC	14	0.07	0.278	2.25
Cosmic	10	0.14	gamma	7	0	0.892	0.03
Th/OC	9	0.07	beta	6	0	1	0
U/Th	8	0.01	<i>Mode not used as fit cannot be improved.</i>				

**Table 4.29:** Multiple-regression summary data, **ferricrete** EVD samples only.

Axes	1	2	Total variance
Eigenvalues:	0.943	0.057	1
Species-environment correlations:	0.971	0	
Cumulative percentage variance			
of species data:	94.3	100	
of species-environment relation:	100	0	
Sum of all eigenvalues			1
Sum of all canonical eigenvalues			0.943



The ferricrete EVD samples perform better with the available environmental variables (table 4.28), with 97.1 % of the variance in DE correlating with the environmental variables as opposed to 92.7 % in the aeolianite EVD environment. The total variance explained by this analysis is 94.3 % and 85.9 % in the ferricrete (table 4.29) and aeolianite environments, respectively. Therefore it is not currently possible to solely assign the Ferricrete EVD environment as deleterious to DE determination. Although U and Th values perform poorly under linear regression, it is possible to account for much of the variance in DE with an extended set of environmental variables; variables that partially incorporate diagenetic effects as well as the key dose-rate components. As discussed above, water content for this dataset is set at a uniform 10 % due to the unrepresentative nature of laboratory measurements within the Mediterranean climate regime. Although not currently possible to confirm, it is hypothesised that the remaining DE discrepancy may be partly due to poorly measurable water content estimates. Further development of variables may also produce different results. The variables presented here are developed from standard methods and from data generated during the course of standard luminescence dating methodology and so as a first step are highly relevant to the analysis presented here.

Furthermore, this analysis although potentially useful for assessing the effectiveness of the laboratory measurements that contribute to the luminescence age estimates, is still not sensitive to post-burial changes. It is this sample-specific un-measurable factor that may be primarily responsible for the outstanding unaccounted for variance. Of course the varying precision and accuracy of the myriad measurements and calculations that are integrated to produce a luminescence date will inevitably contribute.

In summary, early vadose diagenesis has been observed to introduce noise into many of the laboratory measurements made as standard for luminescence dating. Although multi-variate analysis of the entire luminescence dataset has shown that diagenetic effects partially account for variance in DE determinations, reconstructing the sample specific diagenetic conditions experienced throughout the burial lifetime is not possible. This will likely be an ongoing issue for luminescence dating work. Recent research from southern China highlights this problem further within a similar geochemical setting (Zhang et al. 2008). Although U and Th down-profile trends appear relatively stable, similar to the variability shown by the data from this study, stratigraphically anomalous age estimates were returned from red-weathered sediments. The episodically prograding nature of the Tiber delta dune ridge record may mask this effect preventing sample ages from completely overlapping; feasibly only causing a younger skewing of age estimates. Samples displaying post-deposition weathering effects in their dosimetry data must be treated with caution to avoid erroneous age estimates based on the assumption that dose-rate and DE enrichments cancel each other out. More critically, if we are to ask geoarchaeological questions the accuracy of the chronological framework must be optimised.

#### 4.8.11. Dose-rate correction

Many of the carbonate EVD environment sediments do not show a relative enrichment in dose-rate due to weathering or aeolian remobilisation (section 4.8.9.1). On this basis it is argued that due to the provenance of sediments being similar during the period of formation (section 4.6.2) a dose-rate correction could be derived from the younger carbonate dune ridges that display no remobilisation and post-depositional reddening. Nine samples were chosen based on these criteria. Their average dose-rate is  $2.793 \pm 0.09$  Gy/ka (table 4.30). Utilising this as a ‘corrected dose-rate’ unaffected by post-depositional diagenetic enrichment, age estimates for reddened, weathered and remobilised samples were recalculated. Dose-rate vs DE is presented in figure (4.42) highlighting that DE is independent of dose-rate within the samples used in the dose-rate correction.

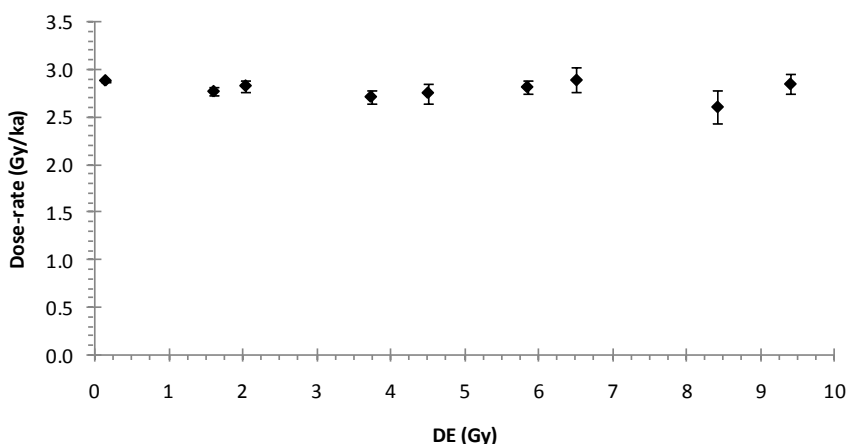


**Figure 4.42:** Dose-rate plateau of selected carbonate EVD environment samples showing that in these samples DE are independent of dose rate and *vice versa*.

**Table 4.30:** Samples displaying a homogenous dose-rate (Gy/ka). All samples derive from the carbonate EVD environment and display similar K, U and Th components.

Sample	Dose-rate (Gy/ka)	DE (Gy)
CP03/6	2.887	0.152
CP07/18	2.774	1.613
CP07/26	2.832	2.045
CP03/1	2.716	3.735
CP07/25	2.758	4.505
CP03/2	2.819	5.845
CP09/1	2.891	6.510
CP07/23	2.609	8.414
CP07/22	2.850	9.397
<b>Average</b>	<b>2.793</b>	<b>4.691</b>
<b>St. Dev.</b>	<b>0.090</b>	<b>3.136</b>

Diagenesis petrology data also provides key context. It is clear that the older reddened sediments are strongly depleted in heavy minerals and carbonates due to early vadose diagenesis. The key mineral species are consistent with the mixed Tiber catchment sources shown for modern beach sediments (Garzanti et al. 2002). Diagenesis petrology, LOI geochemistry and environmental dose-rate data do not show a clear gradient in post-depositional alteration; sharp step changes occur within these datasets. The conditions for deposition are also different between the deltaic, carbonate-cemented samples and the early Holocene / late Pleistocene reddened sands; direct alongshore deposition not necessarily occurring in the mid-Pleistocene bayhead Tiber delta morphology in evidence during deposition of the now ferricretised samples. The sources are likely the same. However, the relative proportions of volcanoclastic heavy minerals to siliclastic light minerals and therefore estimated *unweathered* dose-rate are less clear. Due to lower sea levels and an increased exposure of coastal shelf sediments, transport equivalence by density may have been a much more pronounced mechanism of sorting. Late Pleistocene coastal dune ridges are not preserved, so aeolian winnowing of light minerals may have occurred much further inland (than that of a back-beach dune-ridge). There is a real possibility that relative depletion in heavy minerals but also allochthonous geochemical sources not investigated, such as aeolian dust, prevents dose-rate correction on these reddened sediments. Using the unweathered mineralogical component of deltaic sands is likely to be unrepresentative of the late Pleistocene and early Holocene sands that were transported and deposited by different mechanisms. Dose-rate correction of weathered and LM depleted features is then geomorphologically restricted to the deltaic aeolianite dune-ridges.

#### **4.8.12. Age correction**

Whereas key trends in diagenesis can be discussed in the context of stratigraphically-ordered (horizontally rather than vertically) dune ridge development linked to delta progradation, the vertical weathering profile cannot be fully constrained for each sample making direct inter-sample comparisons more problematic. Sampling was aimed at retrieving sediment from the preserved core of the foredune crests, so a good degree of comparability is assumed which is borne out in the generally cohesive results.

Stratigraphically anomalous K (%) content derived from bulk laboratory dosimetry measurements is observed for the transected aeolianite IRSL samples, at levels similar to that found in the ferricrete samples. A threshold value of 1.8 K % is observed, shown between the partitioning of aeolianite and ferricrete samples in Figure 4.37 with samples selected in table 4.31.

**Table 4.31:** Transected IRSL dosimetry data, moving inland. Ferricrete “old dunes” samples are partitioned by the thick border. Aeolianite samples displaying a stratigraphically anomalous K % and post-depositional weathering noted in field assessment is highlighted. These samples are proposed for dose-rate correction due to diagenetic weathering.

Transect 1	U	Th	K	Transect 2	U	Th	K	Transect 3	U	Th	K
	(ppm)	(ppm)	(%)		(ppm)	(ppm)	(%)		(ppm)	(ppm)	(%)
CP03/6	1.610	7.240	1.270	CP08/1	3.450	16.000	1.200	CP07/18	1.455	6.315	1.370
CP07/26	1.320	5.440	1.460	CP08/2	2.620	7.830	1.260	CP07/22	1.300	4.235	1.620
CP07/25	1.935	8.145	0.960	<b>CP08/3</b>	2.015	7.030	<b>1.890</b>	<b>CP07/21</b>	1.150	8.110	<b>2.670</b>
<b>CP03/3</b>	1.460	6.130	<b>1.800</b>	CP09/1	1.645	5.465	1.460	<b>CP07/19</b>	1.800	9.190	<b>3.280</b>
CP03/1	1.830	6.200	1.120	CP07/16	1.110	3.890	1.100	<b>CP07/20</b>	2.845	10.855	<b>2.430</b>
CP04/1	2.065	7.145	1.240	CP03/4	1.44	5.21	1.32				
CP07/24	1.220	5.835	1.080	CP07/14	3.075	9.820	1.010				
CP03/2	1.970	6.080	1.220	<b>CP07/15</b>	2.805	8.385	<b>1.800</b>				
<b>CP04/7</b>	1.765	6.130	<b>2.030</b>	<b>CP07/17</b>	2.285	7.175	<b>2.160</b>				
CP07/23	1.024	4.220	1.440	<b>CP08/6</b>	2.465	7.685	<b>2.470</b>				
				<b>CP08/7</b>	2.350	8.420	<b>2.500</b>				
				<b>CP08/4</b>	3.805	13.500	<b>2.120</b>				
				<b>CP08/5</b>	2.440	8.315	<b>2.910</b>				

Post-deposition weathering as denoted by increased K component can theoretically be corrected for using the assumed *unweathered* samples dose-rate discussed above. All dune-ridge samples are proposed as suitable for age correction as their assumed back-beach formation is similar to that of the younger carbonate dune ridges. Palaeo-delta morphology from ca. 7ka BP to the present also appears to provide an alongshore sediment supply to the region now occupied by the Castelporziano Estate (Bellotti et al. 2007). The uncorrected age estimates are calculated using both an enriched dose-rate that may not equal the actual mean dose-rate over the lifetime of burial and also *increased* DE. Therefore uncorrected ages of suspect samples must be regarded as a **minimum age estimate**. If dose-rate correction is undertaken then the derived age must be regarded as a **maximum age estimate**, as the partially enriched DE accounts for some of the dose-rate enrichment effect. Therefore, based on measured data, it is possible to advocate the **mean age** between these two extremes as *corrected* dates. Following this procedure, potential underestimation of central ages is between 7 – 11 % for the qualifying samples (table 4.32).

Corrected samples are cited with the standard deviation as percentage error and denoted by ~, e.g. ~4520 ± 379 BP and 2251 ± 156 BP for corrected and uncorrected dates, respectively. The ability to accurately date the ferricrete samples by luminescence methods is conceptually constrained by diagenesis and by key differences in depositional environment and transport conditions. The ferricrete samples are uncorrected and cited with > denoting the underestimation of age due to difficulties in assessing the equivalence of post-depositional dose-rate and DE measurements.

**Table 4.32:** Carbonate EVD samples exhibiting potential post-deposition weathering enrichment of K % content. Corrected ages are presented linked to the method outlined in section 4.8.12.

Sample	Min. Age* BP	Error	Max. Age† BP	Error	Mean Age BP	Error	Rationale	Percent underestimate (rel. to mean estimate)
CP03/3	1488	100	1709	171	1599	156	Post-deposition weathering; increased K-dose rate	7
CP04/7	1913	119	2319	232	2116	287	Post-deposition weathering; increased K-dose rate	10
CP08/3	1731	109	2154	215	1943	299	Post-deposition weathering; increased K-dose rate	11

\*Uncorrected age estimate based on standard methodology

†Dose-rate corrected

#### 4.8.13. Geomorphological consideration of corrected age estimates

Owing to the possibility that age correction is theoretically possible for the deltaic carbonate-cemented sediments, a geomorphological consideration should be made based on the derived reconstructions. It appears that age correction is possible for the young carbonate dunes, where dose-rate enrichment is primarily due to the *in situ* weathering of K-feldspar leading to an enriched K dose-rate component. However, only 3 of the carbonate-cemented luminescence samples qualify on the grounds of primary deposition, and post-depositional weathering; being CP03/3, CP04/7 and CP08/3. Dating accuracy is limited for the reddened dune ridges and sand sheets due to sample-specific diagenesis and difficulties assessing whether individual samples DE and dose-rate estimates are fully equivalent. Minimum age estimates must currently suffice *in lieu* of data regarding un-weathered mineralogical composition for these aeolian features. In effect, the progradation of the Tiber delta and associated alteration to sediment delivery to the Castelporziano region of the palaeo-shoreline prevents the extension of possible age correction as these diagenetic environments have been shown to be petrologically discrete. Although the sources of the sediment are the same, the relative mineralogical proportions are subsequently skewed by diagenesis.

For the sake of argument, because of the possible severity of age underestimation due to diagenetic dose-rate enrichment, age correction was calculated for the reddened dune ridge and inland sand sheet samples. Based on the ‘minimum’ age estimates provided by the standard age calculation, the unweathered, non-reddened dose-rate of 2.793

Gy/ka to provide an estimated ‘maximum’ age, then using the mean as an estimate of an un-enriched DE value, ‘corrected’ mean ages and percent age underestimation relative to the mean age estimate are presented (Table 4.33). Age under-estimates using the standard methodology may theoretically be 13 – 26 % too young due to the effects of post-depositional weathering and dune reddening. Increased age discrepancy is not clearly related to the ‘older’ samples, with remobilised coversands such as CP07/19, CP08/5 and CP08/7 displaying a substantially larger discrepancy than their age may suggest (see chapter 3 for sampling logs). Hypothetically speaking, these remobilised coversands may be derived from already reddened sediments, accounting for their enhanced dosimetry behaviour and potential age underestimation. The sample specific, non-linear nature of these multiple effects is not suitable for simple corrections.

**Table 4.33:** Potential age under-estimation based on raw ‘uncorrected’ and mean ‘corrected’ age estimates for ferricrete samples. Samples are sorted by percent age underestimate

Sample	Min. Age* BP	Error	Max. Age† BP	Error	Mean Age BP	Error	Percent underestimate (rel. to mean estimate)
CP07/15	5055	331	6590	659	5808	1106	13
CP07/17	5424	343	7295	729	6359	1322	15
CP07/21	5823	374	8297	830	7060	1749	18
CP08/6	10554	687	15426	1543	12990	3445	19
CP08/7	4717	352	7040	704	5879	1642	20
CP07/20	8243	528	12913	1291	10578	3301	22
CP08/4	10516	923	17130	1713	13823	4676	24
CP08/5	5881	347	9543	954	7712	2589	24
CP07/19	3273	213	5558	556	4415	1615	26

\*Uncorrected age estimate based on standard methodology

†Dose-rate corrected

#### 4.9. Early vadose diagenesis: development of geochemical sediments & geochronological influences

In light of the multi-proxy datasets and reconstruction of key phases of the Tiber Delta’s development during the Holocene, a reassessment of the two geochemical sediments developing and preserved at Castelporziano follows below. These geochemical, early vadose diagenetic environments are effectively discrete - a clear and sequential developmental gradient of formation between them is not observed by this study. The expansion of the Tiber Delta HST to this southerly position of the Lazio coast after about 5000 BP appears to be the key factor in the development of the early vadose aeolianite dune ridge record.

#### 4.9.1. Aeolianite

Geochemically, the aeolianites are characterised by moderate calcium carbonate content. This is present partly as marine calcite crystals, carbonate lithics and sand-sized glaebules. Fine-grained micritic calcium carbonate also develops as inter-grain cements; loss-on-ignition suggests that similar proportions of the mode and fine grain-sizes are present as calcium carbonate material. Petrological microscopy also suggests that an additional source of cements may be the weathering of marine foraminifera. In some samples cemented forams are fairly common, suggesting the micritisation mechanism outlined by Reid and Macintyre (1998) may also be occurring within these sediments. Diagenetic effects are often sample-specific with trends in calcium carbonate LOI unclear. A fluctuating trend where values increase to a maximum and fall back may be suggested by the transect 1 and 2 values (section 4.4.2). However this phenomenon is most clearly shown by the D6 *Piscinae* short-core. Within each distinct zone shown by discrete trends in diatom flora, geochemistry and grain-size parameters, there is a clearly oscillating but overall decreasing trend in calcium carbonate content (% dry weight LOI) suggesting some kind of maturity signal. This may also be the case but on a much larger temporal and spatial scale within the Tiber delta dune ridges. Dosimetrically, the aeolianites display an accumulation of K and a fairly stable U/Th ratio suggesting that dose-rates derived from this material are diagenetically enriched but that storage of the weathering products is held locally. This is an important process for assessing the reliability of luminescence age estimates from this material. Although dose-rates become enriched post-deposition, loss from the system of key dose-rate components is not clearly observed, suggesting that both dose-rate and DE are coeval. Petrological investigations suggest that weathering is at an early stage with garnets still present and showing only moderate surface weathering, (typically pits). Increased K dose-rate is therefore likely to be a product of early stage surface weathering of the most susceptible crystals such as feldspars. The dosimetry results then suggest that ions are relatively immobile during weathering; that the dune ridges are a relatively stable and low-energy diagenetic system. The effects of meteoric or groundwater flushing of weathering products may be of concern in other parts of the weathering profile but this is not observed with the samples presented here. However, prior to the development of the generally thick forest soil cover over much of these dune ridges, marine aerosols may be the most important source of ions for early vadose diagenetic cements (Bate & Dobkins 1992; McLaren 2001).

In the only sample from the carbonate dune ridge sequence to be associated with a reddened horizon, CP04/7 highlights a key decalcification trend associated with the development of early vadose ferricrete. A decreasing gradient in the more inland carbonate dune ridges may be suggested by LOI. A stronger micro-scale oscillating maturity trend is observed with carbonate content within the *piscinae* core. Carbonate content is seen to oscillate to a maximum and decrease to a minimum within each palaeo-environmental phase of this relict dune slack. Overprinted to this rapid oscillating trend is an overall trend of decreasing carbonate content. Further geochemical analysis could be used to examine the development of iron oxides within this micro-scale dune slack environment as on the macro-scale there appears to be a transition phase where surface concentrations of Fe develop during decalcification. During the EDX-

SEM preliminary examination the presence of Fe across the surface of all grains during element mapping suggested that in the mature calcium carbonate sample hydrated iron oxides (e.g. Goethite) may be present in addition to the calcium carbonate cements. Visually, both appear similar in the field. The 'maturity signal' in calcium carbonate content may then be driven by the later development of iron oxides. Petrological analysis suggests that the two main early vadose diagenetic environments are effectively separate systems and the reddened dune ridges are not just a more advanced form of the carbonate dune ridges. This decalcification trend observed in the delta HST carbonate dune ridges is therefore argued to be driven by *in situ* weathering of allochthonous sediments not linked to underlying volcanic parent material as in the reddened dune ridges. The development of iron sesquioxides may be primarily derived from more advanced surface weathering of the abundant ferro-magnesian sand-sized minerals circuitously derived from the lower Tiber catchment via the Tiber Delta.

Within the carbonate EVD dune ridges a 3 phase model can be derived (figure 4.43). (1), foredune formation on the active beach is rapidly cemented by calcium carbonate, becoming petrologically distinct on decadal time-scales. (2), on millennial time-scales a maximum carbonate cements content is reached, occurring at Castelporziano after ca. 2000 years. (3), Carbonate contents decrease relative to the increasing development of iron sesquioxides linked to diagenesis. From ternary plots, it is clear that the ferricretised "Old dunes" are in an advanced stage of phase 3 of this simple model with little to no carbonate content observed. The ferricretised dunes are petrologically distinct from the carbonate dune ridges, perhaps arguing for an additional 4<sup>th</sup> phase of this model.

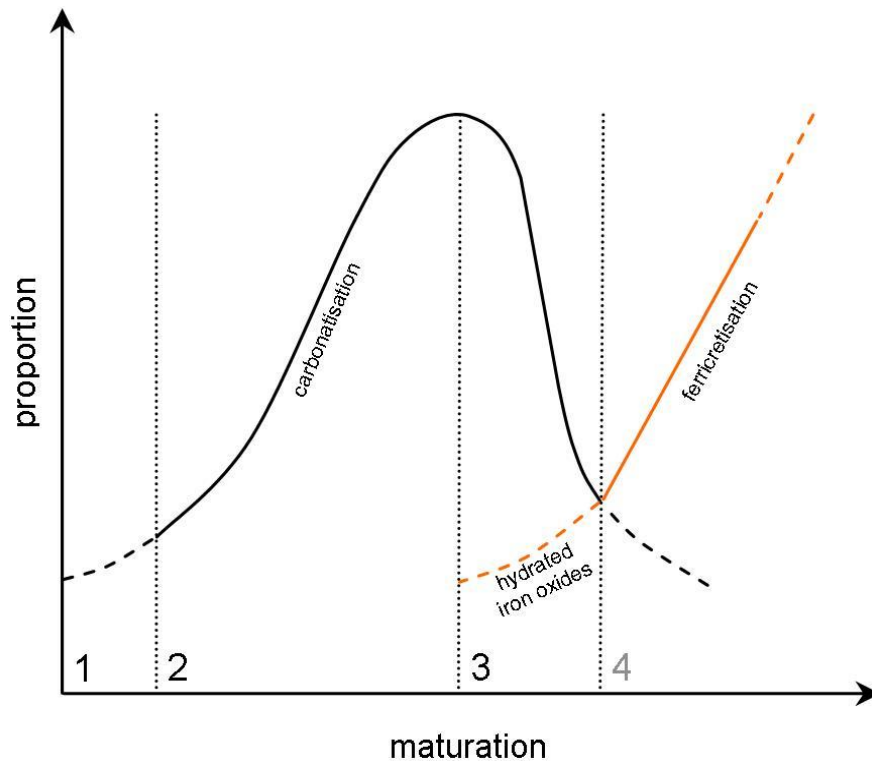


Figure 4.43; Preliminary diagenesis model of Castelporziano geochemical sediments.



#### 4.9.2. Early vadose laterised ferricrete

Other than colour, the early vadose ferricretes preserved as two ferricrete dune ridges and extensive and remobilised sand sheets are distinguished by very low calcium carbonate content (shown by LOI and suggested by XRD analysis). Petrology shows that this is mainly preserved as carbonate lithics in the reddened dune ridges. Calcium carbonate glaeboles and grain-surface cements are not observed. These sediments are geologically dissimilar to the deltaic carbonate dunes, being more closely related to underlying volcanic parent material. In this respect it is more accurate to describe these sediments as *early vadose* examples of *laterised ferricretes* (Widdowson 2007) thus accounting for the allochthonous mineralogy that derives partially from the metamorphic uplifted Alpine Orogenic sources in the upper Tiber catchment (quartz, feldspar and garnet in particular). Dosimetrically, there is some evidence to suggest these sediments are less able to effectively store and accumulate U with respect to Th. U can be seen to decrease with observed increases in Th values, suggesting greater mobility of soluble U within this more advanced diagenetic environment. However, the storage and accumulation of weathered K is pronounced within this environment compared to the aeolianite EVD environment. Iron oxides have been shown to be related to an accumulation of radionuclides (Olley et al. 1996; Olley 1994). This mobility of radionuclides and concerns that the ferricrete diagenetic environments examined here are not 'closed' systems means that luminescence age estimates cannot be *assumed* to be reliable as sample DE may not be directly comparable to laboratory dose-rate measurements. Multi-variate statistical analysis suggests that derived DE (the cumulative stored dose of all radioactivity experienced by the K-feldspar dosimeters) is not fully accounted for by laboratory dosimetry measurements on bulk sediments. Percolating meteoric water and / or fluctuating groundwater tables may be important factors for radionuclide mobility. Accumulation and storage of K is a key process for understanding the increase in  $\beta$ -dose rate in particular, and Th may be relatively stable. However, the statistical analysis of the variance in dosimetry components typically used for age calculations do not fully account for the variance in sample DE, suggesting a loss from the system. I.e. the post-depositional environment is an open system. There is not a clear trend with age, or inland distance, suggesting the importance of small-scale sample specific processes. Micro-dosimetry effects linked to porosity and sedimentary context may induce significant variation in the effectiveness of particular components of the luminescence dosimetry (e.g. Murray & Roberts 1997). The primary focus of this thesis is answering Geoarchaeological questions. Therefore, a dedicated dosimetry study was not possible or within the scope of the current research. Micro-dosimetry studies in a variety of geochemical sediments and depositional environments are likely to be valuable endeavours, especially at a time where luminescence measurement protocols, models and analysis are in an advanced state.

#### 4.10. Geochronological framework

The geochronological framework centred upon age models for each sampling transect is developed below. This framework incorporates the implications of diagenesis discussed above. By organising aeolian features into primary and remobilised /eroded based upon sedimentary petrology, dose-rate, DE and horizontal stratigraphic context it is possible to understand the chronological development of the site with more clarity. The meso-scale inter-sample interpretation is discussed along with pertinent macro-scale context.

##### 4.10.1. Transect 1

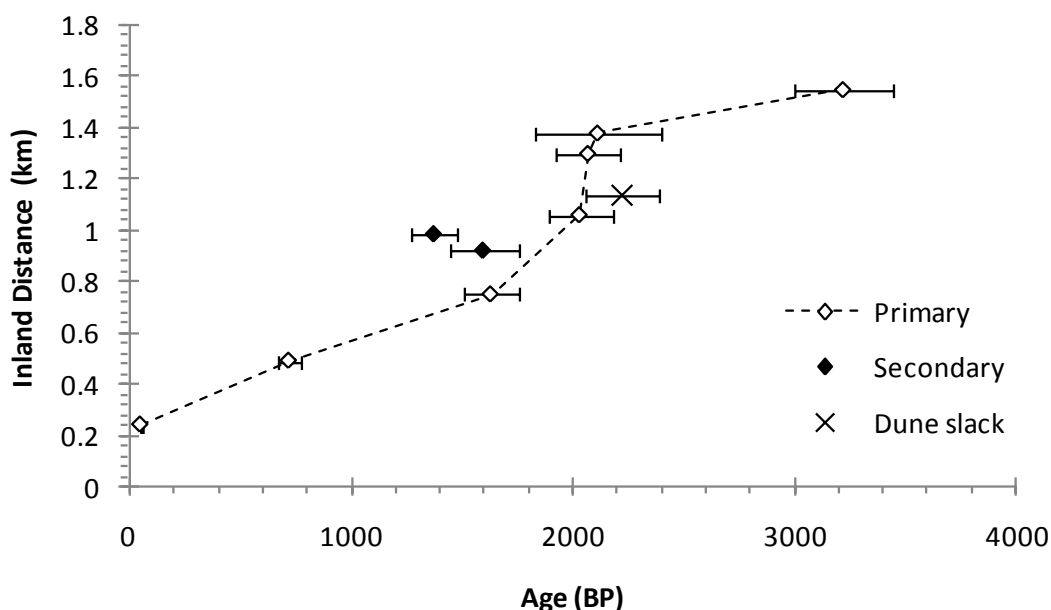


**Figure 4.44:** Transect 1 age model. Remobilised, secondary dune forms and a dune slack sample are also presented. The sharp inflection around 2000 BP highlights a relatively rapid increase in shoreline progradation at this time.

Transect 1 is characterised by aeolianite sediments. Only 2 samples displayed dose-rate enrichment due to *in situ* weathering of mineralogical K sources, with only CP04/7 contributing to the age model. The extent of this transect covers the modern foredune, post-Roman dune ridges, remobilised post-Roman parabolic dunes, Roman *Vicus* settlement and pre-Roman dune-ridges. This spans a period of ca. 3500 years BP and a spatial extent of ca. 1.7 km inland from the modern shoreline. This transect also contains a dated pre-Roman dune slack (CP07/24, 2226 ± 168 BP). The slightly increased age of this feature compared to the surrounding dune ridge dates is probably due to increased dose-rate attenuation in the more saturated water content of the dune slack.

##### 4.10.1.1. Shoreline progradation rates

Transect 1 is focused upon the Tiber Delta progradation, permitting estimates of shoreline progradation during the late Holocene, (i.e. during the last 3500 years). Age estimate ranges of primary aeolian features (i.e. not remobilised or

diagenetically affected) and inter-sample distance normal to the modern coastline (based on GIS dune ridge mapping) were used to estimate average progradation rates (table 4.34, figure 4.45). Integration of data from different transects is not possible due to the narrowing of the delta towards the southern distal end (transect 3).

**Table 4.34:** Progradation rates derived age ranges from transect 1 dune ridge age model.

Date Range (BP)	Range (yr)	Progradation (m)	Rate (m/yr)
3448-1929	1519	250	0.165
2217-1510	707	380	0.537
1756-669	1087	170	0.156
775-48	727	250	0.344

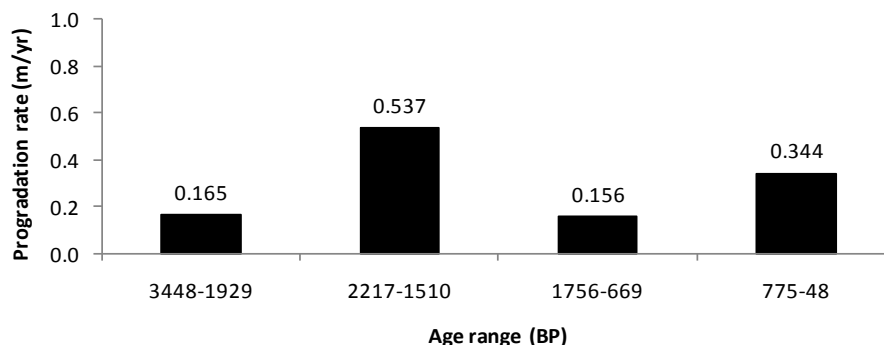


**Figure 4.45:** Progradation phases and rates derived from age ranges of transect 1 age model.

A distinct period of increased delta (and therefore Castelporziano shoreline) progradation is clearly defined during the Roman-period occupation of the Laurentine Shore (between ca. 2100 – 1600 BP). A more subtle increase in mean progradation rate is observed during the last 700 years denoted by the formation of a dune ridge (CP07/26 transect 1) and the *tomboleti* dunes (CP07/18) near Tor Paterno ca. 580 BP (transect 3).

#### 4.10.1.2. Pre-Roman development

A major dune ridge that appears to be preserved across much of the lateral extent of the Castelporziano Estate was formed ca. 3224 ± 224 BP (CP07/23). This date is replicated in the most distal end of the samples site, in transect 3 (CP07/22, 3297 ± 222 BP) by the associated palaeo-beach. The feature is denoted by the 5 m contour. This formation event is interpreted as the development of the Tiber Delta attaining a lateral extent similar to modern times. Previously the delta area was constrained to an area adjacent to the main river channel (Bellotti et al. 2007) and partially envelops the ‘Castelporziano’ coast around 4.2 ka BP (CP07/14). This process appears to have occurred during a period of relatively low delta progradation rate between 3448 – 1929 BP. An increase in delta progradation is observed between

ca.2217-1510 BP, beginning prior to the establishment of the *Vicus Augustanus* in the 1<sup>st</sup> century AD. Dune ridge development associated with the progradation of the Tiber delta continued until 2073 ± 144 BP. The formation of the dune ridge CP03/2 (2073 ± 144 BP) denotes the cessation of the preceding phase of delta progradation (figure 4.46). The test-pit profile incorporating sample CP04/1 (2034 ± 146) and also an under-drain sample from the *Vicus Augustanus* (CP895, 2050 ± 240 BP) (Rendell et al. 2007) clearly show that the foundations of the Roman settlement at this point on the Shoreline were built directly onto sediments dating from this phase of delta progradation. It must be noted that these sampling locations are towards the landward extent of the site and are relatively insensitive to an intervening phase of dune formation on the seaward extent of the *Vicus Augustanus* that is preserved outside this zone of intensive anthropogenic activity.

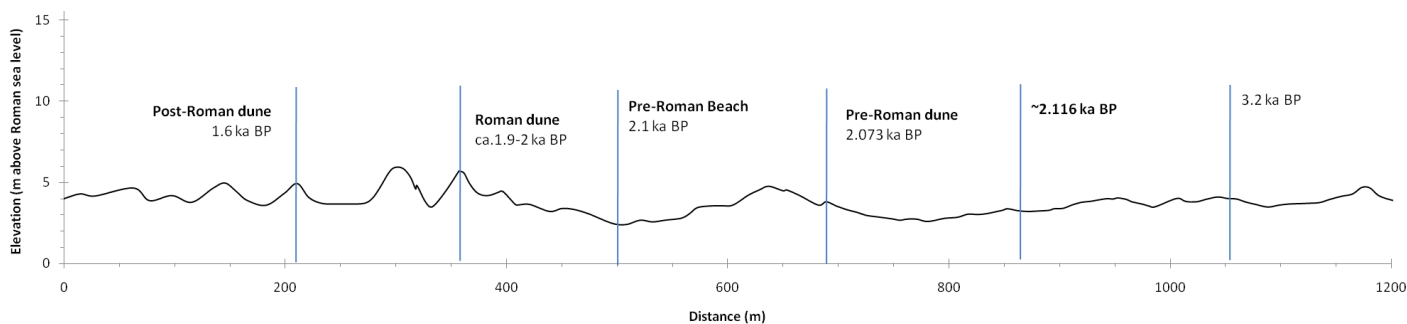


**Figure 4.46:** Boundary wall dune ridge transect relative to Roman period sea level (-1 m RSL). GIS mapping of comparable dune crests and age estimates from transect 1 age model are highlighted (Vertical exaggeration = x 40).

#### 4.10.1.3. Roman settlement

The initial construction of the *Vicus Augustanus* complex is dated to the early 1<sup>st</sup> century AD and expanded during the 2<sup>nd</sup> and early 3<sup>rd</sup> centuries AD. This is in good agreement with the age of the preceding dune ridge (CP03/2, 2073 ± 144 BP) and beach sediments exposed beneath the walls of the Roman period structures (CP04/1, 2034 ± 146 BP). The *Vicus Augustanus* covers an area of ca. 6 ha in a broadly rectangular grid-square plan (Lauro & Claridge 1998). The initial Roman settlement can be seen to occur during a phase of shoreline progradation (figure 4.45). The estimated average progradation rate bordering the initial Roman settlement is ca. 0.165 m/yr, increasing to an estimated average rate of 0.537 m/yr during the period of Roman occupation of the site. That is to say increased progradation rates are not linked directly to the occupation of the Laurentine Shore but shoreline progradation was experienced at an increased rate during the occupation of this palaeo-shoreline.

A dune ridge associated with the foundations of many archaeological features of the site was intermittently preserved across much of the site. The sea wall (F2), *Grotto di Piastra* villa, and B1 villa are located immediately on or built into the sea ward face of this dune ridge in the case of the sea wall. It was noted that this ridge was not preserved around the *Vicus Augustanus*. This is partly due to the complexity of the site, but probably also to later phases of secondary

dune formation and extensive archaeological excavation during the recent centuries. The delineation of the following Roman period settlement is clearly shown by the formation of the post-Roman dune ridge. The preservation of an intermediate progradation phase and / or dune ridge existing prior to the founding of the *Vicus Augustanus* is not currently known. The spatial extent of the archaeological remains and the dated dune ridge and beach sediment suggest the *Vicus Augustanus* was constructed on a coeval coastal area ca. 400 m wide. The height of the archaeological remains preserved within the dune ridges above Roman sea level (figure 4.46, figure 4.47, figure 4.48) suggests that building onto the dune ridge topography provides a suitable building site above sea level, minimising the risk of flooding.

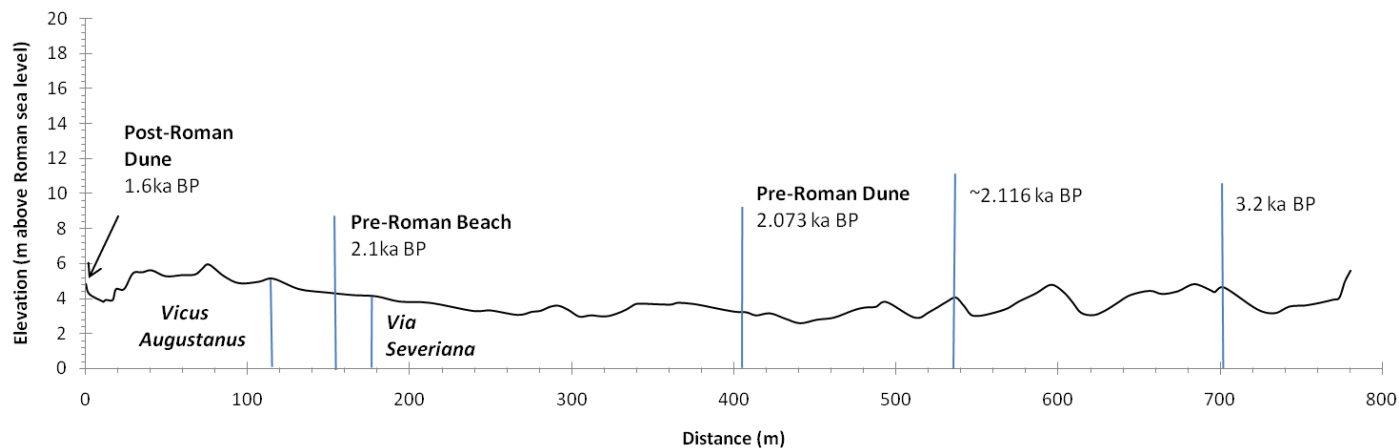


**Figure 4.47:** Dated dune ridge transect from *Vicus Augustanus* inland to the *Canale del Pantanello* relative to Roman period sea level (vertical exaggeration = x 40).

#### 4.10.1.4. Post-Roman Abandonment

The post-Roman dune ridge at this point on the shoreline is dated to  $\sim 1599 \pm 156$  BP (CP03/3). This feature can be traced the entire length of the palaeo-shoreline and denotes the phase of dune ridge formation and associated delta progradation that defines the Laurentine Shore.

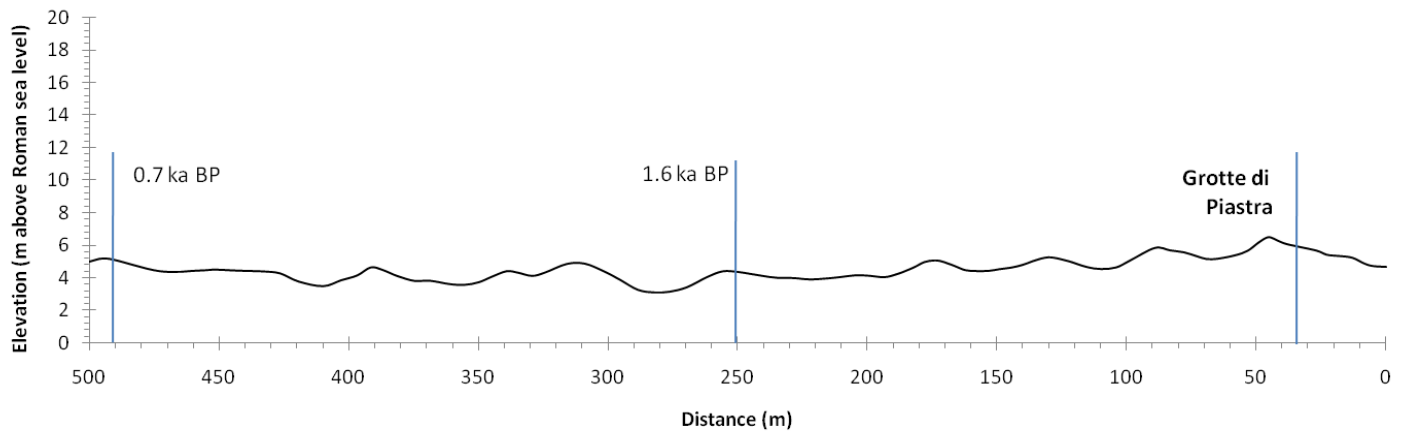


**Figure 4.48:** Dated Grotte di Piastra early Imperial Roman villa dune ridge transect relative to Roman period sea level (vertical exaggeration = x 40).

A sampled parabolic dune formed over the seaward side of buildings on the seaward extent of the *Vicus Augustanus* suggests inundation by these dune features from at least  $1374 \pm 100$  BP (CP03/1). This suggests aeolian remobilisation and / or landscape instability around the early 7<sup>th</sup> century AD, ca. AD 626. Dated dune ridges occur at  $1633 \pm 123$  BP and  $722 \pm 53$  BP, with the modern foredune dated to the mid- to late- 20<sup>th</sup> Century.

#### 4.10.2. Transect 2

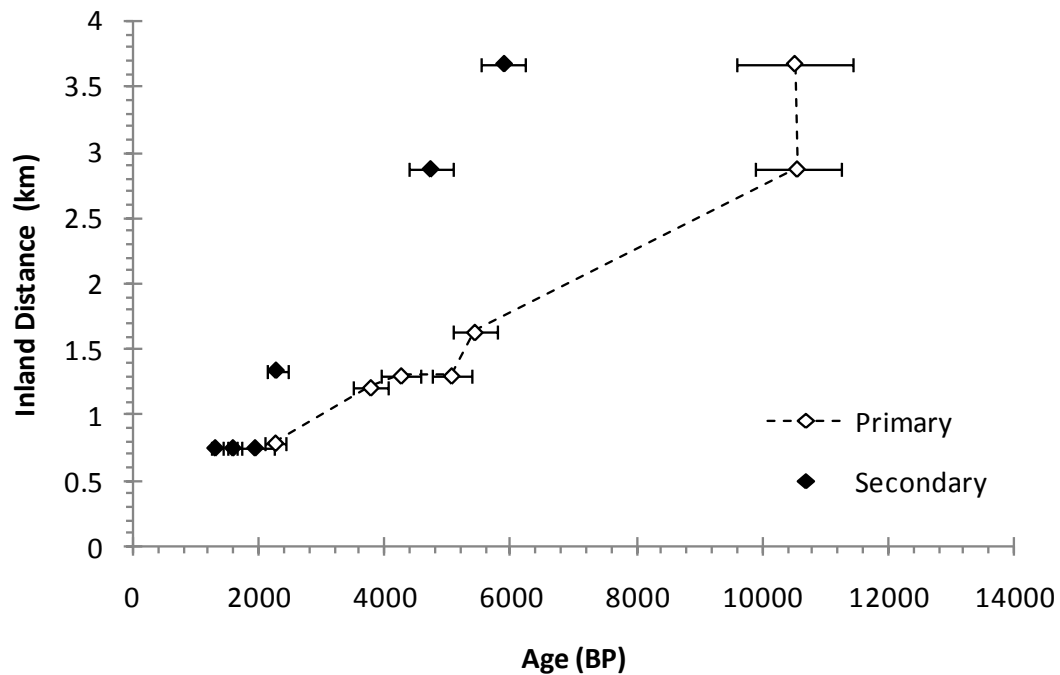


**Figure 4.49:** Transect 2 age model with remobilised, secondary dune form ages. Prior to the step inflection observed in transect 1 (figure 4.44) a relatively stable rate of development is observed; the linear fit for the Primary dune ridge formation being  $R^2 = 0.9375$ . The transect 2 age model ceases at the point of Roman occupation of the *Piscinae*, and does not cover the period of increased delta progradation rate recorded in transect 1. The oldest two samples although

ferricretised sand sheet sediments and potentially unreliable may suggest that sand sheet development occurred across large areas at a roughly a similar time.

Transect 2 is characterised by varied geomorphology and contrasting diagenetic environments. The samples record the transition between late Pleistocene reddened sandsheets, early to mid-Holocene reddened dune ridges and late Holocene carbonate-cemented dune ridges. Critically, the earliest Roman construction on the site, that of the *Piscinae*, and their subsequent abandonment is also incorporated into transect 2. The *Piscinae* are key features as they preserve a valuable palaeoenvironmental record and possible sea level marker. The transect extends between 0.87 – 3.57 km inland of the modern shoreline. Being more distally positioned compared to transect 1, there is a relatively narrowed profile.

#### **4.10.2.1. Late Pleistocene and early Holocene aeolian features**

The oldest sampled features from the study are reddened sand sheets inland of the dune ridge sequence. The sand sheets are indurated and heavily cemented by iron oxide. A suitable initial description would be *early vadose ferricretes* as allochthonous drivers of alteration from groundwater and meteoric hydrology may be seasonally important and / or allochthonous dust inputs may also occur. Typically the upper metre or so of the ferricrete appears to be remobilised material. Reddening of this remobilised material also appears to be rapid, within a few thousand years of deposition. Only minor changes in colour were observed, darkening down-profile; the remobilisation being highlighted by a relict ground-surface. The ability to luminescence date these features is potentially limited by post-depositional dose-rate changes but the sand sheet deposits were formed from at least  $>10.5 \pm 0.9$  ka BP (CP08/4 & CP08/6,  $>10.5 \pm 0.7$  ka BP). The continuation of these sandsheets beneath the mid-Holocene dune ridge record was not possible to be sampled. Geological mapping<sup>18</sup> suggests that reddened Pleistocene material probably underlies the mid-Holocene reddened dune ridges. The seaward spatial extent of these reddened aeolian sediments constitutes the coastline prior to late Holocene delta progradation. This must be understood in the context of post-Glacial rising eustatic sea level, with sand supply from a greater exposure of the coastal shelf. Maximum age estimates for phases of remobilisation date to  $>5.9 \pm 0.35$  ka BP (CP08/5) and  $>4.7 \pm 0.35$  ka BP (CP08/7), suggesting periodic landscape instability. Dune ridge formation occurred by  $\sim 6.36 \pm 1.3$  ka BP (CP07/17) and  $\sim 5.8 \pm 1.1$  ka BP (CP07/15). These dunes are now reddened, cemented and depleted in carbonate. The flattened trend in the transect also suggest that this period, ca. 6-7 k BP, exhibits an increased rate of accumulation, and also a phase of remobilisation in the inland sand sheets. Sea level at this time was around 5 m below modern RSL (Lambeck et al. 2004a).

#### **4.10.2.2. Mid-Holocene aeolian remobilisation**

A further remobilisation event is observed at  $2.27 \pm 0.16$  ka BP (CP03/4), expressed as a secondary dune ridge depleted in heavy minerals due to density sorting by aeolian winnowing. Remobilisation by aeolian winnowing is distinguished by

---

<sup>18</sup> [http://www.apat.gov.it/Media/carta\\_geologica\\_italia/tavoletta.asp?foglio=149](http://www.apat.gov.it/Media/carta_geologica_italia/tavoletta.asp?foglio=149) (last accessed 8/10/2009).

lower dose-rates, and low HM:LM ratio. Post-depositional early vadose weathering is not thought to be an issue due to low K-dosimetry values. These events have been preserved by carbonate cementation. Due to this aeolian sorting of light and dense minerals assessment of post-depositional dose-rate changes is more complex. Petrological data show that CP07/14 is strongly enriched in heavy minerals, suggesting a winnowing of light minerals. However, the age and macro-scale geomorphological context suggest this sample represents the lateral extension of the Tiber delta ca. 7-4 ka BP (Bellotti et al. 2007). Therefore CP07/14 is more likely to be a placer deposit, rich in HMs due to density sorting on the beach of that time.

#### 4.10.2.3. *Piscinae* construction

The formation of the *Piscinae*, focussing upon the feature D6, is constrained by two dune ridges with the pond between them (figure 4.50). Artificial banks appear to have been constructed perpendicular to the shoreline orientation, effectively forming two orthogonal ponds from the inter-dune ridge slack. The landward dune ridge formed by 2251 ± 156 BP (CP09/1). Architectural evidence suggests a 1<sup>st</sup> century BC date for the start of construction. The heavily damaged remains of a boundary wall sit atop the seaward ridge. Subsequently this feature has been buried by up to 3 phases of aeolian sand alternating with a weathered layer of sand. The sequence is sealed by a thick layer of organic rich sand which constitutes early pedogenesis. The burial of this wall occurred ~1943 ± 299 BP (CP08/3), with further inundation phases at 1592 ± 116 BP and 1312 ± 93 BP on the lee side of the wall (interior of the infilled *Piscinae*). Abandonment, or at least the cessation of maintenance of this seaward wall, therefore occurred in the early 5<sup>th</sup> Century AD (ca. AD 408 ± 116) (CP08/2). This date is in good agreement with the final abandonment of the *Vicus Augustanus* after AD 420, based on coin evidence (pers. comm. Prof. Amanda Claridge, 2007). It is likely, in consideration with the lack of industry at the *Piscinae*, that they were abandoned prior to this date.

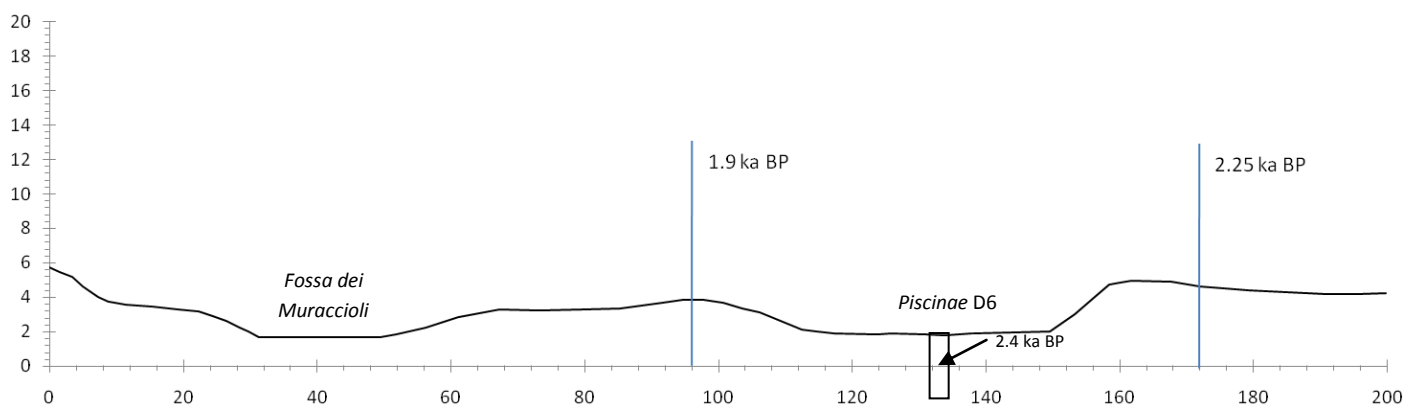


**Figure 4.50:** Dated *Piscinae* transect relative to Roman period sea level. Position of core 14 sea level marker is highlighted (vertical exaggeration = x 20).



The post-Roman dune-ridge dated in transect 1 (CP03/3,  $\sim 1599 \pm 156$  BP) is preserved seaward of the *Piscinae* sequence separated by the course of the *Fossa dei Muraccioli*. It can be inferred from this dating and field survey that the Fossa has downcut and laterally bisected the Roman-period beach parallel to the coast. The initial working hypothesis was that the *Piscinae* developed in the lee of the contemporary foredune. The timing of burial by aeolian sand of the seaward D6 bank ( $\sim 1943 \pm 299$  BP) is a *terminus ante quem* date for the construction of the *Piscinae*, constrained by the *terminus post quem* under-wall date from the northern bank ( $2251 \pm 156$  BP). This suggests agreement with the age of the Roman period shoreline ( $2073 \pm 144$  BP,  $2034 \pm 146$  BP) recorded in transect 1, associating the position of the *Piscinae* with this phase of shoreline development.

#### 4.10.3. Transect 3

Transect 3 is the most distally located from the mouth of the Tiber river. There is a significant compression of the trans-delta profile relative to the modern shoreline and only two dune ridges are clearly preserved. Like transect 2, the samples here are taken from reddened sandsheets, a reddened dune ridge, a carbonate-cemented palaeo-beach and heavily-eroded coastal *tomboleti* dunes. Sampling occurred between 0.26 – 2.37 km inland of the modern shoreline (figure 4.51).

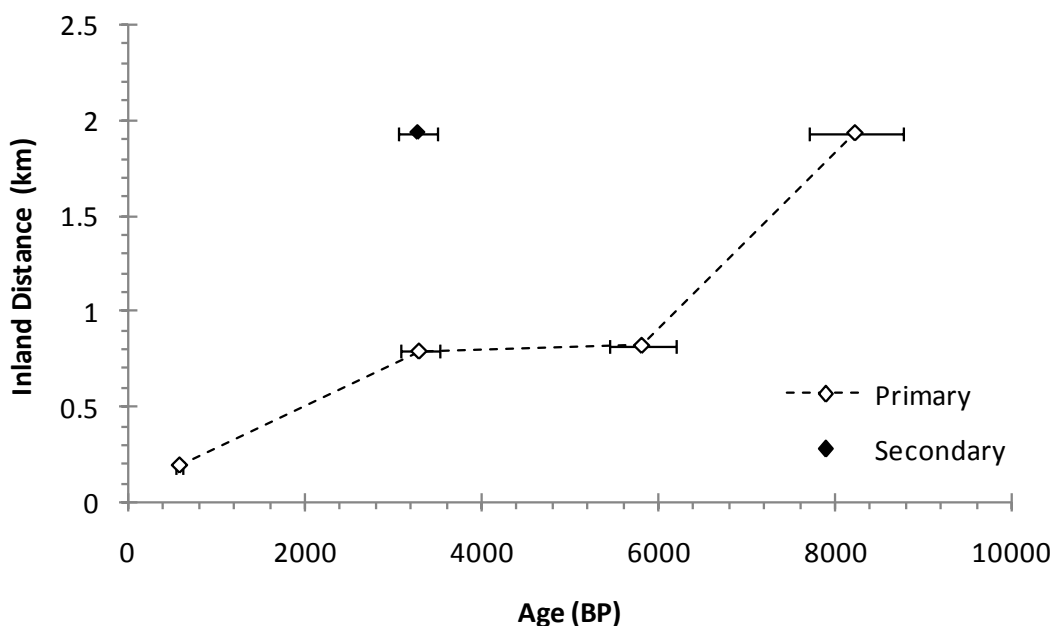


**Figure 4.51:** Transect 3 age model with remobilised, secondary formations. Due to a lack of features to sample the resolution of this age model is lower than the preceding models and is not sensitive to changes in Delta progradation rate. However the plateau between ca. 6000 – 3000 BP is likely due to the lateral extension of the Tiber delta to this distal position on the coastline around 4.25 ka BP (see transect 2).

#### 4.10.3.1. Early Holocene aeolian development

Again the older, reddened sand sheets display mid-, to late-Holocene remobilisation of sand-sized sediments that are significantly affected by early vadose ferricretisation. This occurred at  $>8.2 \pm 0.5$  ka BP (CP07/20) and  $>3.27 \pm 0.2$  ka BP (CP07/19), respectively. Early Holocene dune ridge formation occurred by  $>5.8 \pm 0.4$  ka BP (CP07/21) and is now reddened. The steep inflection between 6000-3000 BP is also suggested in the early region of the transect 1 age model. Due to the compression of the delta morphology at this southern distal end and lack of definable preserved dune ridges to sample the record is less sensitive than more centrally located transect 1 to late Holocene delta progradation.

#### 4.10.3.2. Late Holocene and Historic development

A palaeo-beach, distinguished by marine shells, was sampled from the interdune area landward of the Tor Paterno archaeological remains. Dating suggests it is coeval with the landward dune ridge of transect 1, developing at  $3297 \pm 222$  BP (CP07/22). The dating sample has been accurately located at +2.35 m RSL, with the surface of the inferred palaeo-beach at this point being +2.67 m RSL. Considering lowstand sea level ca. 3000 BP, on the western coast of Italy estimated at -1 m RSL (Lambeck et al. 2004a), and the central Tiber delta at -4 m RSL (Bellotti et al. 2007) (although the dating for this latter curve is potentially systematically under-estimated), this position on the palaeo-beach surface is inferred to be around +3 – 4 m above contemporary still-stand sea level of the time. This suggests a back-beach location for the sampling.

The *tomboleti* coastal dunes are heavily eroded relict dunes. Local erosion and redistribution of sand has led to a complex disorganised hummocky topography. Sampling from a substantial *tomboleti* feature was aimed at dating the initial phase of formation and mixing of poorly bleached sediments. *Tomboleti* formation developed  $581 \pm 39$  BP. A mean progradation rate during this period is 0.21 m/yr, comparable with the underlying rates of progradation recorded in transect 1. The *tomboleti* sampling location is 260 m from the current shoreline at this distal position of the Tiber delta, suggesting a rough progradation rate during the last 500 years of 0.45 m/yr. This rate is an overestimation due to distal narrowing of the beach.

#### 4.11. Holocene timeline of geomorphological activity

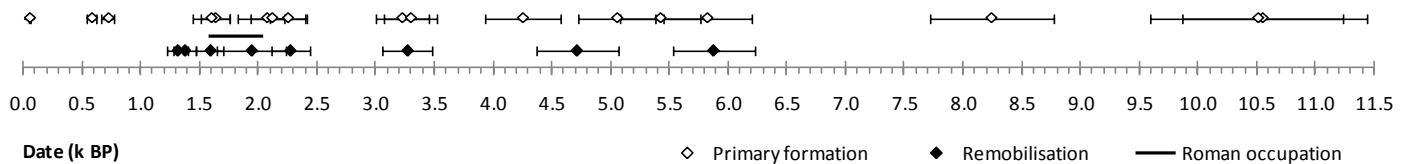


Figure 4.52: Timeline of primary aeolian formations, remobilised features and Roman period occupation of Castelporziano.

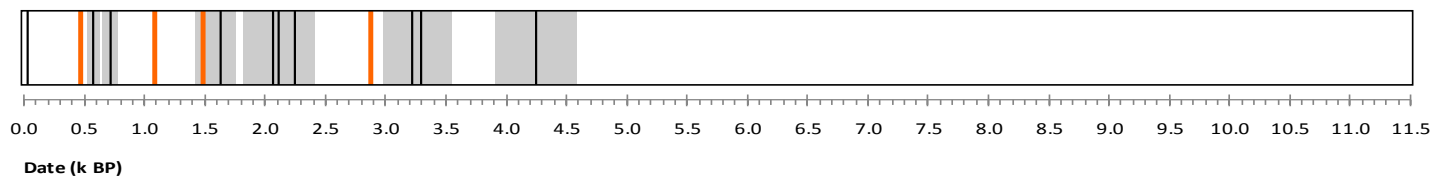
Figure 4.52 depicts the primary and secondary (remobilisation) formation of dune and sand sheet features within the Castelporziano Estate area. The period of Roman activity within the site is also highlighted. From ca. 6 - 1ka BP remobilisation phases are generally associated with dune ridge formation phases. Secondary phases of formation due to this remobilisation of material occur within the sand sheets on the interior of the site, but are often observed as secondary dune ridges superimposed upon the primary dune ridge record. The profile of site dune ridge transects appear to show this diachronic dune ridge formation. This record is further discussed within chapter 5.

Based on the transect 1 age model, estimated ages of unsampled primary dune ridges were calculated. These dunes are recorded as large, well-formed dune features in the dune-ridge topographic cross-sections. Central age estimates of dated dune ridges (denoted as *reference*) incorporated into the progradation rate estimates were used (Table 4.35). Only age estimates considered unaffected by dose-rate alteration are included. Therefore a more complete record of primary dune ridge formation during the last 4.5 kyr is presented in Figure 4.53. Grey areas represent SAAD-IRSL age ranges with the central age highlighted in black. Modelled dune ridge ages are shown in orange.

**Table 4.35:** Modelled dune ridge ages for unsampled primary dune ridges. Data are based on transect 1 age model and boundary wall dune ridge transect.

Inland Distance (m)	Reference Distance (m)	Distance range (m)	Reference Age (yr)	Rate (yr/m)	Estimated Age (yr)
1477	1550	73	3224	4.604	<b>2888</b>
710	750	40	1633	3.504	<b>1493</b>
600	750	150	1633	3.504	<b>1107</b>
400	490	90	722	2.68	<b>481</b>

**Figure 4.53:** Timeline of primary dune ridge formation at Castelporziano. The dates are recovered only from Deltaic, aeolianite dune ridges. Central ages are highlighted in black, with error estimates in grey. Modelled dune ridge ages are shown in orange.



#### 4.12. *Piscinae* D6 Palaeoenvironmental Reconstruction

As outlined in section 4.3.1, a biostratigraphic study of past sea level was undertaken on a sharp peat/marsh contact preserved within the basal sediment of the D6 *Piscinae*. Due to the very different nature of the sediments the particular methodology of all methods applied to this short core are outlined below for clarity. 24 samples taken at alternating

centimetre resolution were measured for grain-size, organic content, carbonate content loss-on-ignition, and magnetic susceptibility. Sub-samples prepared for diatom analysis.

#### 4.12.1. Diatom analysis

A 50 cm length of cored sediment from the base of *Piscinae* D6 was sub-sampled for diatom analysis and also a variety of sedimentological analyses. Initially 24 samples were taken at alternating centimetre intervals, followed by a further 16 samples at 0.5 cm resolution constraining the silt / peat transition at the centre of the core section. The 40 sub-samples were prepared using the UCL water bath method<sup>19</sup>. 0.1 g of wet sediment was treated with 30 % hydrogen peroxide to remove organic material. The material was measured to 4 decimal places, allowing diatom concentrations to be calculated<sup>20</sup>. Refined sediment cleaned of mineral and fine-grained organic material was mounted in naphrax with cover slips<sup>21</sup>. At least 300 valves were counted on each slide using phase-contrast microscopy. For slides displaying very high valve to microsphere ratios, valves were counted until at least 50 microspheres were encountered.

Stratigraphic diagrams were produced using C2 software<sup>22</sup>. Species data are organised by weighted averages and presented as percentages permitting comparison of relative abundance between each sample.

#### 4.12.2. Sedimentology

1 g of wet sediment was treated with 70 % hydrogen peroxide to remove organic material. Dried sediments were measured using a Beckman-Coulter LS230 Laser Particle Sizer. Data were analysed using GRADISTAT v5.0. Mode and standard deviation measurements (using Folk & Ward methods) are presented in micrometres.

#### 4.12.3. Geochemical analysis

LOI was undertaken using already stated methods. CHN analysis was undertaken by A. Daley, Loughborough University, Dept of Chemistry. An Exeter Analytical CE-440 was used for all analysis. Wet sediment samples were treated with 10 % HCl to remove carbonates. Around 2 µg of dried sediment was used in the analysis and mounted in tin capsules. Samples were combusted at 940°C in pure oxygen catalysed by the tin capsule housing the sample. The CHN analysis therefore measured organic carbon, total hydrogen, total nitrogen, and minerogenic residue. <sup>organic</sup>C/<sup>total</sup>N ratios were derived from the measurements.

---

<sup>19</sup> <http://www.geog.ucl.ac.uk/about-the-department/support-services/laboratory/laboratory-methods/lake-sediment-analysis/diatom-preparation> (13/06/2009).

<sup>20</sup> <http://www.geog.ucl.ac.uk/about-the-department/support-services/laboratory/laboratory-methods/lake-sediment-analysis/use-of-microspheres-in-the-determination-of-diatom-concentration> (13/06/2009).

<sup>21</sup> <http://www.geog.ucl.ac.uk/about-the-department/support-services/laboratory/laboratory-methods/lake-sediment-analysis/diatom-slide-preparation> (13/06/2009).

<sup>22</sup> <http://www.ncl.ac.uk/gps/research/publication/33510> (last accessed 4/09/2009).

#### 4.12.4. Magnetic Susceptibility

Prior to sub-sampling, the core section was measured for ( $R_k$ ) magnetic susceptibility using a calibrated Bartington Instruments MS2E core sensor. Measurements were made at 2 cm intervals corresponding to later sub-sampling locations

#### 4.12.5. Chronology

3 AMS- $^{14}\text{C}$  dates were produced from sediments within the diatom core with a further 2 from cored material above this portion of the core and also from a correlated duplicate core. AMS-RCD results are presented in table 4.36. An age/depth model was constructed using these data (figure 4.54). The 50 cm studied sedimentary record was deposited between ca. 2219 – 2417  $\pm$  40 BP. In order for comparison with the luminescence geochronology, further reference to these calibrated dates has been made with a correction to AD 2000 as BP reference date rather than AD 1950. BP will be used as the dating format.

**Table 4.36:** Calibrated radiocarbon dates used in *Piscinae* core 14 age/depth model.

Sample	Depth (cm)	Calibrated Age (BP)	Max. Age (BP) ( $1\sigma$ )	Min. Age (BP) ( $1\sigma$ )	Sedimentation Rate (cm/yr)	yr/cm
Beta-238559	134	2030	2050	1980	0.109	9.211
Beta-256200	167	2400	2410	2390	1.5	0.667
Beta-256202	182	2410	2510	2400		

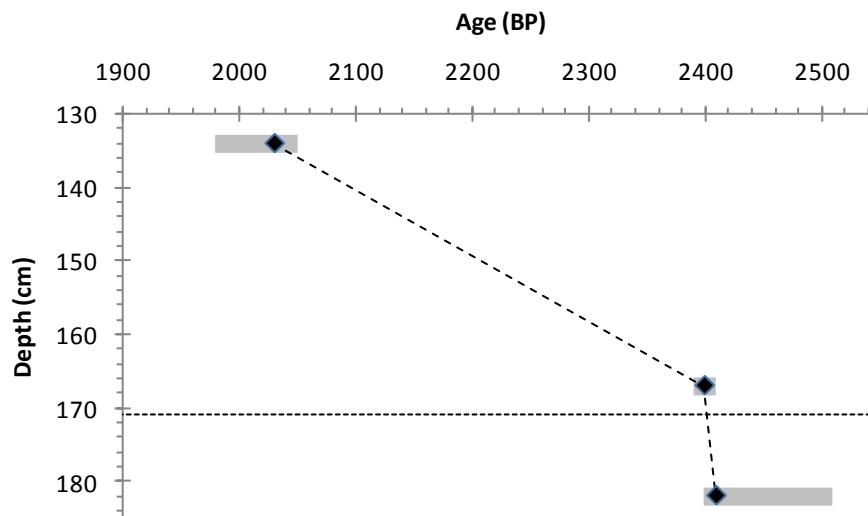


**Figure 4.54:** Age/depth model for core 14 diatom record. Calibrated ( $1\sigma$ ) age intercepts (black diamonds) with age ranges shown in grey are presented. The sedimentary transition at 171 cm from upper peats to lower marshy sediments is highlighted with corresponding change to more rapid sedimentation rate in the older, basal sediments.

#### 4.12.6. Zone Interpretation

A simple age model was developed from the AMS dating of core 14 (figure 4.54). Interpreting the stratigraphic diagram of diatom and sedimentology record (figure 4.55), four zones can be identified (table 4.37, figure 4.55). The hypothesised sea level marker (silt/peat couplet) at 171cm therefore dates to 2403 ± 40 BP.

**Table 4.37:** Zone interpretation and dating of diatom record.

Zone	Interpreted environment	Trophic conditions	Date (BP)
1	Non-marine marsh / lagoon	Mesotrophic	>2417-2409
2	Progradation	Oligotrophic (except eutrophic at 173cm)	2409-2403
3	Dune slack	Meso-oligotrophic	2403-2326
4	Mature dune slack	Increasingly eutrophic	2326-<2216

The interpretation of zone 2 displays rapid oscillation from mesotrophic – oligotrophic – eutrophic – oligotrophic represented by the two *C. microcephala* peaks at 175cm and 171cm, bracketing the distinct peak in *S. hantzschii fo. tenuis* at 173cm. The associated peak in *N. palea* at 173cm is indicative of high nutrient concentrations and heavy organic pollution, which may be linked to anthropogenic activity (pers comm. K. Mills, 2009). These zones are discussed in detail in section 4.13.5. A summary of the dominant taxa is discussed here.

The dominant diatom species are all freshwater to weakly brackish species. At the base, the community shows little diversity, being dominated by *Pseudostaurosira brevistriata*, *Staurosira elliptica* and *Staurosirella pinnata var pinnata*. Diatom concentrations are an order of magnitude higher at the base than the peaty sediments, the vast majority being *P. brevistriata* (Round et al. 1990). These species bloom in a wide variety of environments, and may be related here to nutrients associated with the palaeo-marsh suggested by the sediments. As a result of these wide tolerances, there is limited palaeoenvironmental information to be suggested by zone 4 in the diatom diagram. The transfer functions attempted upon this data (EDDI pH, conductivity and an alkalinity model; and MOLTEN salinity), were not well constrained in zones 3 and 4 and appeared to contradict the basic ecological inferences that the assemblage would suggest (pers comm. D. Ryves 2009). The pH and conductivity reconstructions also appear to be similar, suggesting that they are not the most important variables driving the sampled diatom assemblages. These transfer functions have not been used further and are not included in the analysis. The ecology of zones 2 and 3 suggests they are transitory between zones 1 and 4 which contain completely different taxa.

The zone 1 assemblage is dominated by alkaliphilous and carbonate tolerant species, suggesting similar groundwater environments to that of the modern surface of the fish ponds and other wet areas on the site. There is also the presence of *Achnanthes hungarica*, an epiphyte, suggestive of littoral and pond vegetation. The *Aulocaseira* species in

this zone are non-marine species, and the presence of *Caloneis bacillum*, which is found in standing alkaline waters<sup>23</sup> (Patrick & Reimer 1966-1975), also suggests that terrestrial groundwater is more dominant. I infer a post-abandonment pond environment, reminiscent of a mature dune slack. The slump in organic carbon (OC) during this zone may also be suggestive of a mature dune slack-type environment (pers comm. FSJ Brown, 2009). There appears to be a suggestion of a weakly brackish environment in zone 1 and 2 by the strong and continuous presence of *Amphora veneta* and the minor occurrence of *Navicula halophila*<sup>24</sup>

Zone 3 between 169-175cm downcore depth, exhibits peaks in *Stephanodiscus hantzii fo tenuis*, *Nitzschia palea*, and the decline of *S. elliptica*, *S. pinnata*, and notably *P. brevistriata*. This major change in microflora at 171cm is interpreted as the response to flooding.

#### **4.13. D6 *Piscinae* Discussion of Results**

##### **4.13.1. LOI Geochemistry**

Generally, there is a clearly decreasing, but fluctuating trend in percent carbonate content. The peaks may relate to the maturity of the particular environments and the transition to the next. The overall decreasing levels of carbonate could neatly suggest this concept of decreasing maritime influence as progradation occurs but this must be understood in the context of early vadose carbonate diagenesis which is prevalent across the late Holocene dune ridge sequence. Due to the alkaline and hard, carbonate groundwater experienced at Castelporziano, there is still a strong carbonate signal throughout the late Holocene dune ridge sequence. Effectively differentiating alkaline sea water with considerable marine carbonate (calcite/dolomite) from early vadose diagenetic (calcium) carbonate is not achieved by bulk measurements such as LOI or XRD, but the sedimentary petrology microscopy study suggests both sources contribute sand-sized material. It does appear that biogenic calcite is far less stable in diagenetic environments, suggesting that the carbonate grains recorded in the petrology study may be largely inorganic in origin (Tribble et al. 1995). The early diagenetic recrystallisation of calcite in the shallow, coastal waters is observed to be an important process within the calcium carbonate grains (Reid & Macintyre 1998). There appears to be an alteration gradient from well-formed calcite (some maybe dolomite but weathering is problematic for identification), with micritic structures increasingly important as the weathering of grains continues. This process is probably a key element in the development of inter-grain cementation. There are also many instances of foraminifera and other carbonaceous microfossils being incorporated into carbonate grains.

---

<sup>23</sup> C. Bacillum, according to Patrick & Reimer (REF) is also found in “soft, hard or slightly brackish waters; lakes, rivers and bogs” (587). The presence of *Aulocaseira* sp. suggests it is the alkaline water affinity that is represented.

<sup>24</sup> N. Halophila, as the name suggests has a brackish affinity but also responds to high mineral content (Patrick & Reimer, REF). The strong calcium carbonate diagenetic environment and the alkali groundwater may then mask the brackish signal. The low abundance of this species may suggest that it is the mineral content and alkalinity rather than salinity that is driving the zone 1 diatom assemblage.

As carbonate decreases with time, organic content increases significantly, with the upper peaty sediments exhibiting the high OC levels at the top of the core, one would expect.

#### **4.13.2. Grain-size analysis**

Mode and sorting (standard deviation) grain-size parameters are presented. Silt-sized sediments are recorded from the base of the core until around 183 cm downcore depth. The sediments are well sorted. There is a peak in grain-size at the boundary of zone 1 and 2 associated with a change to fine sand sized-sediments. There is a sharp decrease in grain-size at the base of zone 2 to well-sorted silts which develops an increasing trend to fine-sand, again peaking at the zone boundary at 171 cm. This increase in grain-size is coeval with a sharp oscillation to poorer sediment sorting between ca. 177 – 171 cm. These peaks in grain-size coinciding with diatom zone boundaries may reflect lag surfaces indicative of erosion; the inference being an exposed ground surface and/or periods of stability between phases of environmental change. Zone 3 displays an oscillating trend in mode grain-size that peaks at 165 cm recording medium sand. Between 165 – 145 cm in zone 3 and 4, the mode grain-size displays a fluctuating but decreasing trend to fine sand sized sediments. Sorting also peaks at 165 cm suggesting poorer sorting with the increase in mode during this period.

#### **4.13.3. Core interpretation**

The diatom record examined consists almost entirely of alkaliphilous (pH >7), fresh to weakly brackish preferring species. It appears that nutrient concentration may be the dominant factor in the development of the sampled record. A direct marine influence (generally slightly alkaline but with a clear salinity response) is not clearly observable, due to the alkaline nature of the terrestrial groundwater and highly carbonate-rich mineralogy of the sample location.

#### **4.13.4. Sediment Properties**

There is a strong and oscillating trend in negative magnetic susceptibility ( $R_k$ ) values, suggesting the dominance of diamagnetic material. Diamagnetic properties are derived from non-iron bearing materials such as quartz, feldspar, calcium carbonate, organic material and water. Dearing argues that “[n]ormally, the diamagnetic component is very weak relative to the sum of all the other [magnetic properties] and can be ignored. Exceptions to this are where the sample is almost all water, quartz, calcium carbonate or organic matter” (Dearing 1999:36). The zones 2-4, are characterised by a relatively stable, weak magnetic susceptibility signal from canted antiferromagnetic minerals such as the volcanic heavy mineral assemblage observed at Castelporziano and paramagnetic hydrated iron oxide and hematite, (Dearing 1999). This suggests that zone 1 is devoid of iron-bearing minerals, perhaps surprising for a coastal salt marsh sediment (Berry & Plater 1998; Kostka & Luther III 1994). One explanation is that volcanic mineralogy is not present in these sediments due to tidal sorting. I.e. inadequate transportation of heavy minerals to this location linked to elevation (Allen 1990); “the rate of minerogenic sedimentation being a decreasing function of saltmarsh elevation” (Berry & Plater 1998:467). Due to the blooms in relatively palaeoenvironmental insensitive diatom taxa preserved within these marsh sediments it is not currently possible to distinguish marine or non-marine conditions. Alternatively,



or coevally, *in situ* dissolution of iron-bearing minerals, and early vadose diagenetic Fe-reduction may also be key processes (Kostka & Luther III 1994; Haese et al. 1997; Audry et al. 2006).

### 4.13.5. Diatom assemblage interpretation

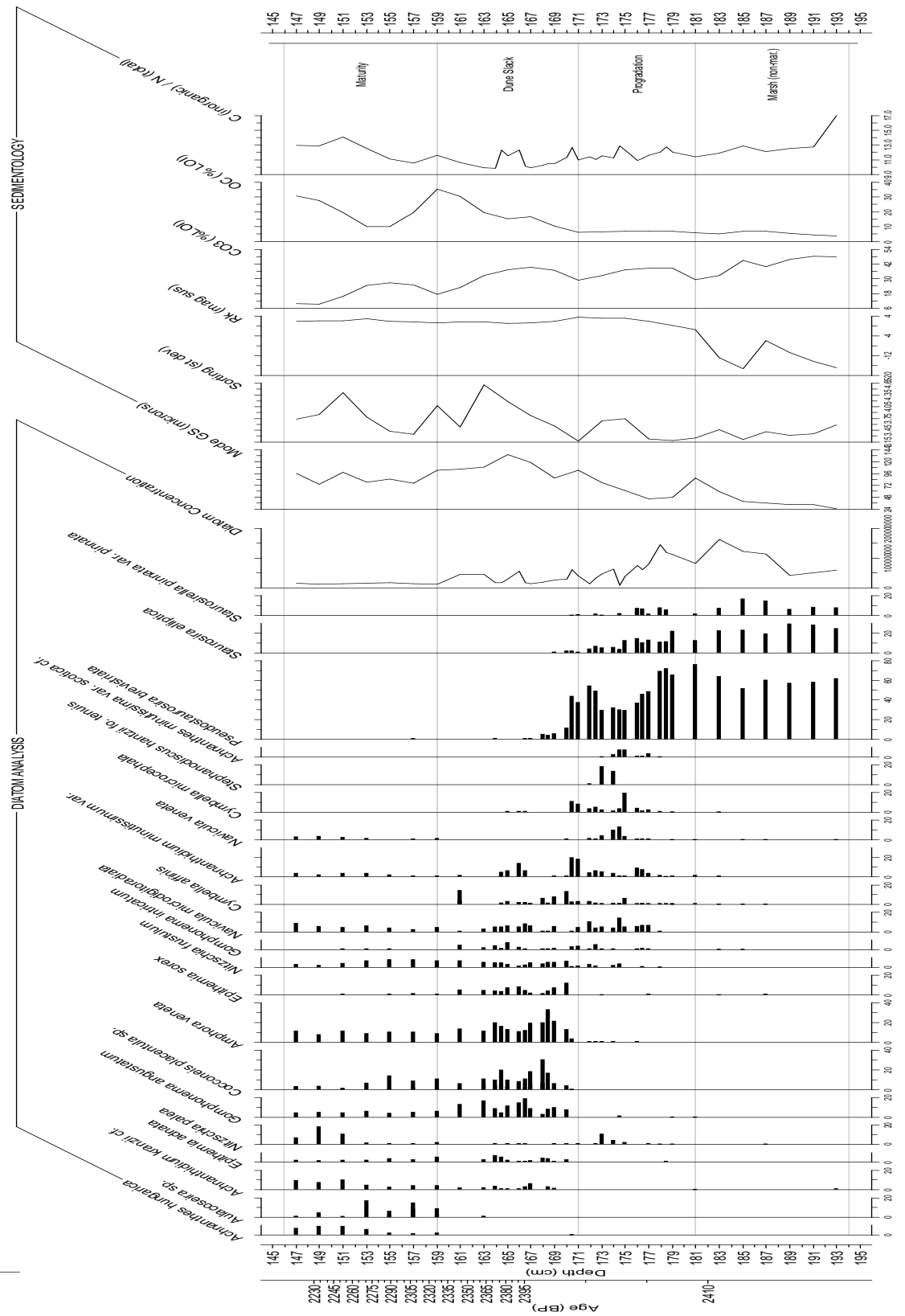


Figure 4.55: Diatom analysis of core 14a sedimentary sea level couplet. Geochemistry, magnetic susceptibility and mode and sorting grain-size parameters are presented.

#### 4.13.5.1. Zone 1

At the base of the cored material (zone 1), the assemblage is completely dominated by *Pseudostaurosira brevistriata*, with *Staurosira elliptica* and *Staurosirella pinnata var. pinnata*. These species are epipsammic and alkaliphilous. The presence in strong numbers of both *S. pinnata var. pinnata* and *S. elliptica* suggests mesotrophic conditions<sup>25</sup>. The order of magnitude higher numbers of *P. brevistriata* suggest optimum conditions for this species; this zone is therefore interpreted as recording moderate to high nutrient concentrations. The minority presence of *Amphora copulata* ( $\leq 1.57\%$  in base of core) is potentially indicative of eutrophic conditions (Parsons et al. 2006) due to increased nutrient concentrations (Anderson et al. 2002). *A. Copulata* is generally found in low numbers, in the riverine epilithon but also in the substrate around the edges of ponds (craticula.ncl.ac.uk, 2009). Constraining the existence or development of the eutrophic condition of the inferred salt marsh sediment prior to the Roman construction and occupation of the *Piscinae* is not possible with this dataset. It may be that high nutrient levels (N and P) are linked to the Tiber catchment, and the considerable anthropogenic activity linked to Rome. Further palaeoenvironmental work in this area would be valuable for investigating the development of the Tiber delta in more detail.

#### 4.13.5.2. Zone 2

Zone 2 is characterised by a declining trend in *P. brevistriata*, and *S. elliptica* with the effective disappearance of *S. pinnata var. pinnata*. Organic content is stable through this period at around 7%. Carbonate content is still relatively high between around 30 – 40%. The  $R_k$  values increase to their maximum and stable values by the end of this zone, 3.55 cgs. Corresponding with the peak in carbonate contents at 177cm (ca. 2407  $\pm$  40 BP), more oligotrophic species appear. *Cymbella affinis* and *Cymbella microcephala* prefer low nutrient conditions, explaining the drop in the dominant eutrophic species in zone 1. The appearance of *Navicula microdigitoradiata*, and minority *N. halophila* is notable. *N. microdigitoradiata* is a fresh brackish species but also has a preference for hard water (Patrick and Reimer, 1966:516). According to Patrick and Reimer (1966), *N. halophila* is found in “water of high mineral content, or brackish water” (467). This species constitutes <3% of each sample assemblage but is usually present from 175-145cm. The palaeoenvironmental inference in conjunction with the dominant species in the upper section of the core is that beginning from 175cm the alkali groundwater and carbonate-rich mineralogy of the core site becomes increasingly dominant.

*C. Microcephala* (20% of assemblage) shows a marked peak, suggesting a stronger oligotrophic signal. Then, at 173cm there is a similarly strong peak in *Stephanodiscus hantzschii fo. tenuis*. *S. hantzschii* has been used as an indicator of lake eutrophication (Wessels et al. 1999). The minority occurrence of *Navicula tripunctata* (4.88%) and *Stephanodiscus parvus* (0.24%) in the same sample is also indicative of higher nutrient concentrations. It has been suggested that the

---

<sup>25</sup> *S. pinnata var. pinnata* being meso/eutrophic (craticula.ncl.ac.uk, 2009) and *S. elliptica* being oligo/mesotrophic. *P. brevistriata* is tolerant of a wide range of environmental conditions such as allochthonous inputs, is polytrophic and tolerant of a wide range of salinity. This may go some way to explain the species complete dominance of this diatom record (up to 77% at 181cm).

*tenuis* form of *S. hantzschii* occurs under silicon limited conditions (Kling 1992). The observed valves are indeed poorly silicified (as are all centric diatoms counted). At first glance, it seems difficult to imagine silicon limitation being an issue in a quartz-rich dune slack. If silicon limitation is indeed the case, it appears that the condition is related to the sinking of silicate through the water column; with uptake by benthic species, out of reach by pelagic species. *S. hantzschii* being pelagic also suggests that the water level in the dune slack was higher than previously (as does the presence of the other pelagic, centric diatoms in this zone). *Nitzschia palea* also peaks at 173cm. Krammer and Lange-Bertalot (1991; [2/2]:86) describe *N. palea* as cosmopolitan, with a preference for decaying organic material, and thriving in raw and industrial waste-rich waters, but also peatland drainage ditches. Oligotrophic preferences appear contrary to the eutrophic signal of *S. hantzschii*, but recent work suggests *N. palea* is indicative of anthropogenic disturbance of the catchment (pers comm, K. Mills, 2009).

Increasingly oligotrophic conditions are suggested by the increase in *Achnanthisidium minutissimum* through zone 2. The *A. minutissimum* peak, constituting 18.3% of the assemblage at 171cm, corresponds to the change to peaty sediments. Important changes occur from 175cm upwards in zone 2. This relatively rapid fluctuation between enduring mesotrophic to briefly oligotrophic conditions at 173cm, then to eutrophic at 171cm suggests some significant but short-lived processes are recorded by the diatom record.

#### **4.13.5.3. Zone 3**

Zone 3 is characterised by the absence of the dominant epipsammic diatoms. Diatom concentrations are significantly lower. Highly organic-rich peaty sediments with less but still significant carbonate content are recorded. There is a strong increase in organic content during this zone, likely related to the onset of coastal peat formation. Magnetic susceptibility is effectively stable, as is the anion concentration, linked to alkalinity, which is at a higher level than previously. Most of the minority diatom species present within the rest of the recorded stratigraphy are absent from this zone. The centric diatoms characterising the palaeoenvironmental change in zone 2 are also absent. There is a clear partitioning of several species above this horizon. *Gomphonema parvulum*, *G. Angustatum*, *Cocconeis placentula* sp (incl. *lineata*), *Amphora veneta*, and *Nitzschia frustulum* dominate. *Epithemia sorex*, and small *Achnanthisidium minutissimum* forms (Round & Bukhtiyarova 1996) reminiscent of *Achnanthes minutissima* var. *saprophila*/*A. kranzii* (Krammer & Lange-Bertalot 1991:T74, 13-19 & 25-33, respectively), are more minor but clearly partitioned species in zone 3. *Cocconeis placentula* sp., cosmopolitan, circumneutral/alkaliphilous with a fresh/fresh brackish preference, is an epiphytic and epilithic pioneer species. Both *G. parvulum* and *G. angustatum*<sup>26</sup> have a more

---

<sup>26</sup> There is considerable variability within *G. angustatum* valves (McBride and Edgar, 1998). Within the observed Castelporziano assemblage, the fine-striae form is dominant (McBride and Edgar, 1998: Fig.1 right image). Coarse-striae *Gomphonema* in the assemblage is assigned to *G. intricatum*, exhibiting a shorter transapical axis, short striae and lower striae density with a very coarse raphe. *G. Parvulum*, and *G. Angustatum* are similar in shape and striae density but have been separated based on the coarseness of central striae; *G. Parvulum* exhibiting consistent striae thickness across the valve, *G. Angustatum* exhibiting coarse central striae.

mesotrophic/macrotrophic preference, but similar pH and salinity preferences. *G. parvulum* has been argued to precipitate micritic calcite (Plenkovic-Moraj et al. 2002). *Amphora veneta* is aerophilous and found widely in hard waters (Patrick and Reimer, 1966:73). However, *A. veneta* is tolerant of organic pollution, with a poly/hypertrophic preference, and is notably alkalibiontic (only pH >7) (craticula.ncl.ac.uk, 2009).

#### 4.13.5.4. Zone 4

Zone 4 is characterised by the dominance of *Aulocaseira* sp., and then increasingly, *Achnanthes hungarica* a classic epiphyte (pers comm NJ Anderson, 2008). The oscillating trend from high to low to high levels of organic content suggests this zone can be interpreted as a mature dune slack. Low levels of organic content are indicative. The wholly fresh and alkaliphilous *Aulocaseira* species<sup>27</sup> and the endurance of similarly favouring species from lower zones suggests a terrestrial dune slack, with little direct influence from marine conditions should be inferred. This suggests that post-abandonment, the D6 *Piscinae* effectively reverted back to a 'natural' environment, in a relatively short space of time. This seems to have occurred whilst the Laurentine Shore was still occupied by the Imperial Roman culture.

#### 4.13.6. Assessment of sea level marker

Due to the complete dominance of *P. brevistriata* within the marsh sediments at the base of the studied core effectively determining whether the sediment couplet refers to a change from salt marsh to terrestrial peat or from fresh-water marsh is not currently possible with this dataset. The georeferenced altitude of the silt/peat transition is  $-1.25 \pm 0.2$  m RSL dated to  $2403 \pm 40$  BP (figure 4.56). This value is in general agreement with published sea level markers from the western coast of central Italy (Lambeck et al. 2004a; Lambeck et al. 2004b; Bellotti et al. 2007) although considerable variation exists in these records in both chronological control and altitudinal accuracy partially linked to tectonic activity (figure 4.57). Field GPS survey and the dune ridge chronological framework show the position of the D6 slack. Tectonic uplift is not thought to be a major cause of inaccuracy on this stable region of coastline (Lambeck et al. 2004b) and no field evidence has been discovered to suggest uplift is an issue. Assuming a steady rate of sea level rise from this data a rate of 0.52 mm/yr is derived. Therefore a comparison with the other Italian west coast *Piscinae* can be made. An early date is thought for the construction of the *Piscinae* at Castelporziano; by 50 BC (353 year's difference) it is estimated that sea level had risen by around 18.36 cm to  $-1.066 \pm 0.2$  m RSL. The sedimentary transition from silt to peat preserved in the basal sediments of the D6 *Piscinae* is therefore presented here as a meaningful record of past sea level; a sea level marker that underpins important geoarchaeological questions of human initiatives and responses to their coastal situation. The corollary of this is that during the Roman period reorganisation of the dune ridge and inter-dune slack morphology, removal of this sedimentary record did not occur. Further palaeo-environmental work on the upper

---

<sup>27</sup> Three species of *Aulocaseira* were categorised during counting, *A. islandica*, *A. italica*, and *A. crenulata*. It became clear that accurately differentiating *A. italica* and *A. crenulata* was not necessarily possible due to observed poor preservation of punctae alignments and densities. For the purposes of discussing the general palaeoenvironmental conditions represented by these species, it seemed prudent to group these species under one heading.

*Piscinae* sediments show little conclusive evidence that these features were completed or used for any period of time (pers. comm. FSJ Brown) although considerable construction of high-status architecture was completed prior to inundation by aeolian sand by  $1592 \pm 116$  BP (ca. AD 408). The dated dune ridge record suggests the landward dune ridge was formed between 2407 – 2095 BP (CP09/1). The diatom core age model shows the formation of the D6 dune-slack phase to occur between  $2425 \pm 40$  and  $2335 \pm 40$  BP, suggesting the landward dune-ridge formed towards the older end of the age range.

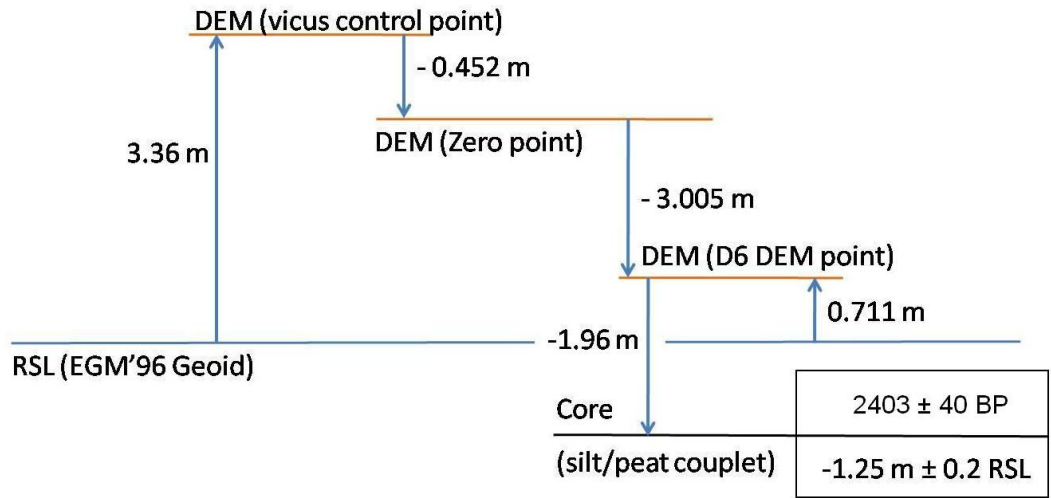


**Figure 4.56:** Georeferencing of sediment couplet recovered from *Piscina* D6. Orthometric heights above sea level are calculated from the EGM '96 geoid separation. Utilising a D-GPS position incorporated into the DEM, it was possible to georeferenced the DEM zero point (datum). This was a necessary step as the datum point is under dense canopy. Using this georeferenced datum it is then possible to relate any DEM survey point to modern sea level thereby allowing precise georeferencing of the *Piscina* core location to modern sea level as this location is also under dense canopy preventing direct D-GPS measurement.

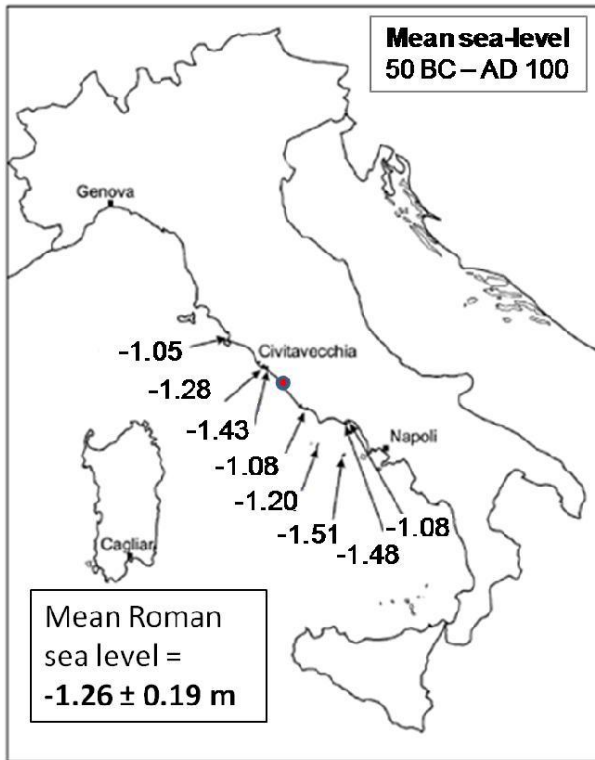


**Figure 4.57:** *Piscinae*-derived sea level comparison. Adapted from Lambeck et al.,(2004b). Mid-point marker heights are shown, variability is typically 0.2 m. All values are given relative to modern sea level. Castelporziano is highlighted, with an estimated sea level of  $-1.066 \pm 0.2$  m RSL by 50 BC.

#### 4.14. Summary of results & analysis

Following extensive assessment of the luminescence data in light of primary investigation of the mineralogy, petrological provenance and post-deposition weathering and diagenesis, increased confidence in the accuracy of the geochronological framework is achieved. The age models and examination of the dune ridge development and accurate topographic survey permit further analysis and palaeoenvironmental reconstruction.

Armed with these results, particularly the effective geochronological framework and late Holocene sea level context, chapter 5 develops a reconstruction of the macro-scale context of

the site in relation to regional (and global) climate. The palaeoenvironmental sensitivity of the dune ridge record is ascertained, allowing comparison with key regional datasets. Further reconstructions of key archaeological periods are also developed focusing upon the Late Bronze Age/Early Iron Age, Late Republic/Imperial Roman period (The Laurentine Shore) and post-abandonment dune activity. Critically the relationship between the ‘Laurentine Shore’ and the wider Imperial Roman coastline is discussed in relation to key sites such as *Ostia* and *Portus*. A preliminary reconstruction of road links between archaeologically/historically important locations is also begun. Historical activity is discussed where data exist. Where possible the interaction of anthropogenic and geomorphological activity is investigated. The effectiveness of this geoarchaeological approach is then discussed in chapter 6 in light of the primary literature and recent state-of-the-art geoarchaeological work.

## 5. Holocene Reconstruction

The results and analyses developed in chapter 4 are used to reconstruct key periods in the archaeological record at Castelporziano. Pre-Roman palaeo-shoreline reconstructions from the mid-Holocene, Late Bronze Age / Early Iron Age (LBA/EIA) are suggested based on field measurements and the multi-proxy datasets presented above. These reconstructions are primarily temporally and spatially meso-scale. The efficacies of the analyses are first discussed to assess the scale-sensitivity of the overall approach for asking meaningful Geoarchaeological questions and for usefully answering them. The integration of the conceptual models outlined in chapter 1 as means of understanding these scale-process relationships is also developed.

### 5.1. Scale-process sensitivity & Holocene context

#### 5.1.1. Dune ridge scale-sensitivity

Although unsuitable for discussing the construction phase of a single Roman coastal villa for example, the primary dune ridge records are sensitive to change on centennial timescales. This provides an appropriate context for examining the relationship of the multi-phase Roman occupation of the site between the 1<sup>st</sup> century BC and 5<sup>th</sup> century AD with the collapse of the Roman Empire. Thus it is possible to develop a clearer definition of *geoarchaeological scale*, which has been conceptually drawn along the lines of the key processes acting upon the site's formation and diagenesis (Brown 2008). The meso-scale at Castelporziano is therefore defined by centennial-scale ( $10^2$ ) temporal and spatial units; describing phases of progradation and anthropogenic activity. The macro-scale is defined as millennial-scale ( $10^3$ ) and greater, temporal and spatial units. This adequately describes the context of the Laurentine Shore (and other expressions of the palaeo-shoreline) in terms of the development of the Tiber delta as a whole and the wider context of eustatic sea level change, tectonics and regional climate change.

#### 5.1.2. Progradation and foredune-building sediment budgets

The Psuty sediment budget model (Psuty, 2008) describes progradation phases as driven by a **positive beach sediment budget**, i.e. during periods of increased sediment supply to the beach. Foredune building and overwash are described by phases of **negative beach sediment budget**. Progradation rates show that sediment supplies have fluctuated over time, and the spatial area of the delta has grown relative to this macro-scale sediment supply. The sediment budget model suggests that foredunes can only develop during periods where sediment budgets on the beach are negative; the deflation of the beach supplying the growth of the foredune. At an even simpler level a positive beach sediment budget drives seaward development of the beach/foredune system and a negative beach sediment budget drives an aggrading or transgressing dune system. When considering the effect of sediment supply to Castelporziano and the impact upon



the coastal settlements this is an important factor. A well-developed relict foredune is therefore a record of a reduced beach sediment budget linked to supply, and therefore is indicative of the end of a progradation phase.

### 5.1.3. Sediment supply: the Tiber flood record at Rome

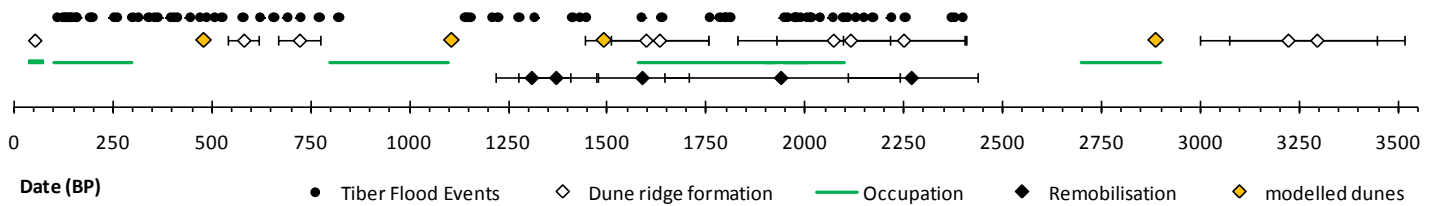


**Figure 5.1:** Late Holocene timeline of major Tiber floods (data from Bersani and Bencivenga, 2001), primary and secondary dune ridge formation at Castelporziano and periods of known human occupation on the site.

A semi-quantified record of major Tiber flood events in Rome (generally > 14 m above modern sea level) has been compiled by Bersani and Bencivenga (2001) with similar data presented by Aldrete (2007) and Stewart and Morhange (2009:404). The record consists of classical texts and historical records (such as tombstone inscriptions of flood victims) ranging from 411 BC – AD 2000. Large magnitude floods between 2411 – 108 BP are presented in a timeline (Figure 5.1). Phases of occupation on the Castelporziano Estate and phases of primary (and modelled) and secondary dune ridge formation are also included during the last 3.5 kyr, linked directly to the progradation of the Tiber delta. Of the presented floods, water heights range between + 13.84 – 19.56 m. “Most sedimentation in deltas occurs during relatively rare river flood events” (Giosan & Bhattacharya 2005:4), therefore understanding the wider context of this flood record is important as a record of sedimentation events feeding delta progradation. The first point to note is that high-magnitude flooding of the Tiber in Rome is not a rare event within the last 2.5 ka or so. Flooding is episodic with several phases of ‘stability’ observed at 2.4 – 2.25, 1.9 – 1.8, 1.76 – 1.64, 1.59 – 1.45, 1.41 – 1.3 ka BP. There is a long cessation of recorded flood events between 1.15 – 0.8 ka BP (AD 860 – 1180) partly due to unreliable or unpreserved historical records (Bersani & Bencivenga 2001). A bimodal distribution of high-frequency flood events is noted; at ca. 2.25 – 1.9 ka BP and during the last 800 years (Figure 5.2). Recorded flooding also progressively increases in frequency with the highest water levels (+ 19.56 m RSL) recorded in 402 BP (AD 1598). The end of the record may be related to the major construction efforts that saw the building of the *Canale di Pantanello* through the Castelporziano Estate, in order to relieve Rome of flooding by 1925 (Bersani & Bencivenga 2001). A frequency plot organised by century AD, further highlights the bimodal distribution of flooding (Figure 5.2).

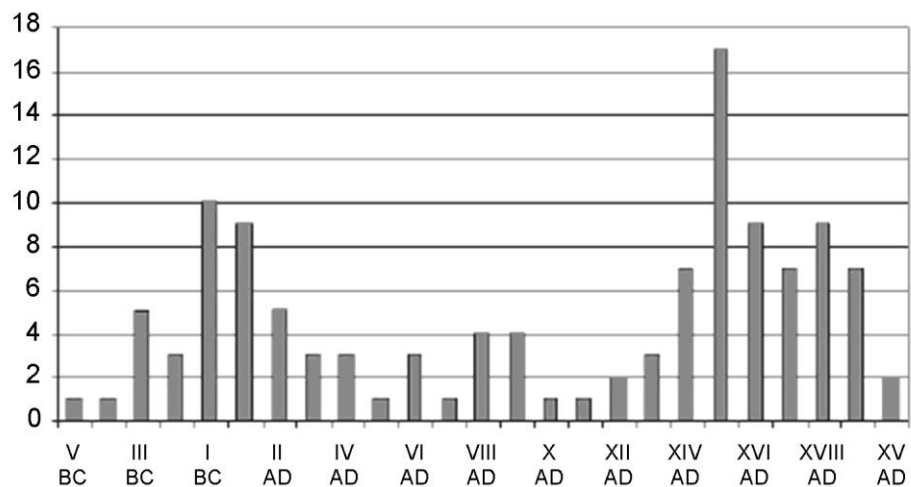


Figure 5.2: Historical record of Tiber flooding frequency at Rome (Bersani & Bencivenga 2001).

Progradation rates based on inter-dune ridge distance highlight similarly timed phases of increased progradation rate to peaks in the flooding record, suggesting that sediment supply and flooding are indeed closely linked. However, this record is driven by historical accounts. The oscillating trend in flood frequency also correlates well with the population of Rome (see Aldrete 2007), advising caution when directly interpreting these records; reduced reports of flooding may simply be a function of reduced population and / or preservation of records. A more reliable but less temporally sensitive record of sediment supply is the trend in progradation rates obtained between dune ridges. At Castelporziano maxima occur during the Roman development of the Laurentine Shore after ca. 2.1 ka BP (*Piscinae* construction) and a marked increase in delta area during the last 500 years (Rendell et al. 2007). The overall pattern from these records is that macro-scale pulsed sediment supply and deltaic construction processes (2<sup>nd</sup>-order) are dominant over 1<sup>st</sup>-order processes such as a flux in dune-building wind regime. Seasonality within the Tiber catchment may also be a factor masked by the larger-scale processes. The Mediterranean climate produces the majority of rainfall during the autumn at Rome (Thornes et al. 2009), with flooding in the winter and spring (Aldrete 2007). Processes on these smaller-scales may be ultimately superimposed upon 3<sup>rd</sup> and 4<sup>th</sup> order regional climate processes. The scheme outlined by Tzedakis (2009) provides a useful descriptive scale framework.

#### 5.1.4. Fore-dune development

Progradation phases can be well described by increased sediment supply linked to flooding (sedimentation) events. The development of fore-dune development however, driven by multi-scale coeval processes, is more problematic. With the sediment budget relationship in mind (section 5.1.2), centennial-scale grouping of periods of reduced flooding frequency in the Tiber catchment should relate to the formation of a fore-dune linked to reduced sediment supply to the delta and reduced sediment budgets. Lower-frequencies are observed around 2.5, 1.5, 1.3, 1-0.9 ka BP, and in the last century BP (figure 5.1). The chronostratigraphy highlights the identified phases of primary fore-dune formation at

Castelporziano. The results are mixed (see section 5.1.5). Direct correlation between reduced flooding/sediment supply and foredune formation is not clearly seen. There is no primary foredune observed at 2.5 ka and following 1 ka BP. Foredunes *are* observed at 1.5 ka BP and the current foredune is very young, around 50 years old.

At the macro-mega-scale linked to eustatic sea level rise, correlated delta sequences of global sea level highstands, constrain intervening progradation then aggradation phases during the last 8000 years (Somoza et al. 1998), (see section 5.4). Aggradation phases and therefore foredune building phases (linked to the sediment budget model, chapter 1) occurring after progradation phases occur prior to the dated sequence of highstand events. In theory, foredune building events should occur just prior to these events. The dating of this sequence is reliant on highstand peat formation so the age model is poorly constrained for determining the transition between aggradational and progradational sequences. The lag time between maximum age estimates of foredune phases and the next highstand phase is between 200-500 years. More accurate correlation is prevented by the centennial uncertainty in age estimates. The developing picture is that the inception of a foredune is not clearly attributable to second-order and greater scale processes. The micro-scale events may be critical in this regard (e.g. Figure 1.6, Box D).

A more complex relationship underpins the inception of foredune development, rather than simply macro-scale and greater, processes of sediment supply, and eustatic sea level change. The frequency with which the sampling strategy recovered sediments from stratigraphically, petrologically and dosimetrically anomalous secondary (remobilised) dune ridges is perhaps the clearest evidence that sediment budgets during the mid-to late-Holocene have frequently been strongly negative, producing significant inland movement of aeolian sand. Suitable conditions for the growth of foredunes are a relatively rare event, Psuty's own description of "*slightly negative*" for the prime foredune building conditions is perhaps vague for a reason (Psuty 2008).

Giraudi et al (2009) describe 8 phases of dune ridge formation flanking the remains of *Portus*. The oldest phase (I) is not apparently recorded on the southern side of the delta. Radiocarbon dating chronology converted to, years BP (AD 2000) is presented in Table 5.1. Correlations with age ranges of luminescence dated dune ridge formations at Castelporziano are made where appropriate. The dune ridge record from the central Tiber delta is in good general agreement with the dune ridge record from the southern distal end of the delta, suggesting that the former, radiocarbon chronology provides effective age control for assessing the validity of the luminescence chronology presented in this thesis. The prograding Roman period shoreline is represented between VI-a and VI-b, again in agreement with the Castelporziano reconstructions (discussed below). However, 2 key dune ridge phases of dune ridge formation are not presented in the findings from Giraudi et al (2009), between phases IV – V, and VI-b – VII of their scheme. These phases are labelled CP IV and CP VIII, respectively within the less disturbed Castelporziano record. Notable is the good agreement of the simply modelled dune ridge ages calculated from the luminescence age models within the wider context of the Tiber delta. The 2 outstanding dune ridge phases may simply be due to sampling

opportunities within the heavily modified central delta area. Alternatively variations in sediment supply distribution may not have produced dune ridges at this central position on the delta shoreline. All 8 phases of the Giraudi et al (2009) chronology have a well-correlated phase of dune building at the southern end of the delta. Due to the decreased confidence in the age estimates of the reddened dunes it is not currently possible to confirm a more robust correlation between phases I – III. If coeval, then periods of dune building in the delta sediments *and* the hard coast to the south (prior to delta envelopment of the coast) are linked by other processes; the regional climate being a key consideration during the mid-Holocene (section 5.1).

The 4 periods of delta retreat described by Giraudi et al (2009) and recorded in the delta parasequences (Bellotti et al. 1994; Bellotti et al. 1995) between phases I and II, V and VI-a, VI-a and VI-b, and VI-b and VII are not preserved by the dune ridge records at Castelporziano (table 5.1, figure 5.3). This geomorphological record is only sensitive to progradational or aggradational phases which are already episodic. Detecting a hiatus within this record is extremely difficult.

Although sediment budgets can be shown to provide a useful framework for associating macro-scale sediment supply flux to phases of increased delta progradation, the specific condition facilitating the delineating foredune formations are more problematic to discern. What is driving the formation of a series of substantial relict foredunes under very specific sediment budget conditions? A clear relationship with macro- and mega-scale climate episodes is not observed. The pollen-based aridity record for the western Mediterranean appears to conform most closely, to progradation phases correlating well with intervening cooler/wetter climate phases. A reduction in moisture during warmer/drier periods would conceptually be beneficial for dune building.

**Table 5.1:** Comparison of dune ridge phases between Giraudi et al (2009) and at Castelporziano (this study).

Giraudi <i>et al.</i> , 2009		Castelporziano		
Dune phase	Age (BP)	Dune sample	Age (BP)	Dune Phase
I	5700 – 6000	“Old dune” ridges	> 5000	CP I
II & III	5275 – 4930	CP07/15	>5386 - 4724	CP II
IV	4140 – 3920	CP07/14	4568 – 3936	CP III
-----	-----	CP07/23	3448 – 3000	CP IV
V	2910 – 2800	<i>Modeled</i>	2888	CP V
VI-a	2400 – 1800	CP04/7 CP03/2	~2404 – 1829 2217 – 1929	CP VI
--- The Laurentine Shore ca. 2100 BP ---				
VI-b	1700 – 1100	CP07/25 <i>Modeled</i> <i>Modeled</i>	1756 – 1510 1493 1107	CP VII
-----	-----	CP07/26	775 – 669	CP VIII
VII – VIII	600 – 200	CP07/18 <i>Modeled</i>	620 – 542 481	CP IX

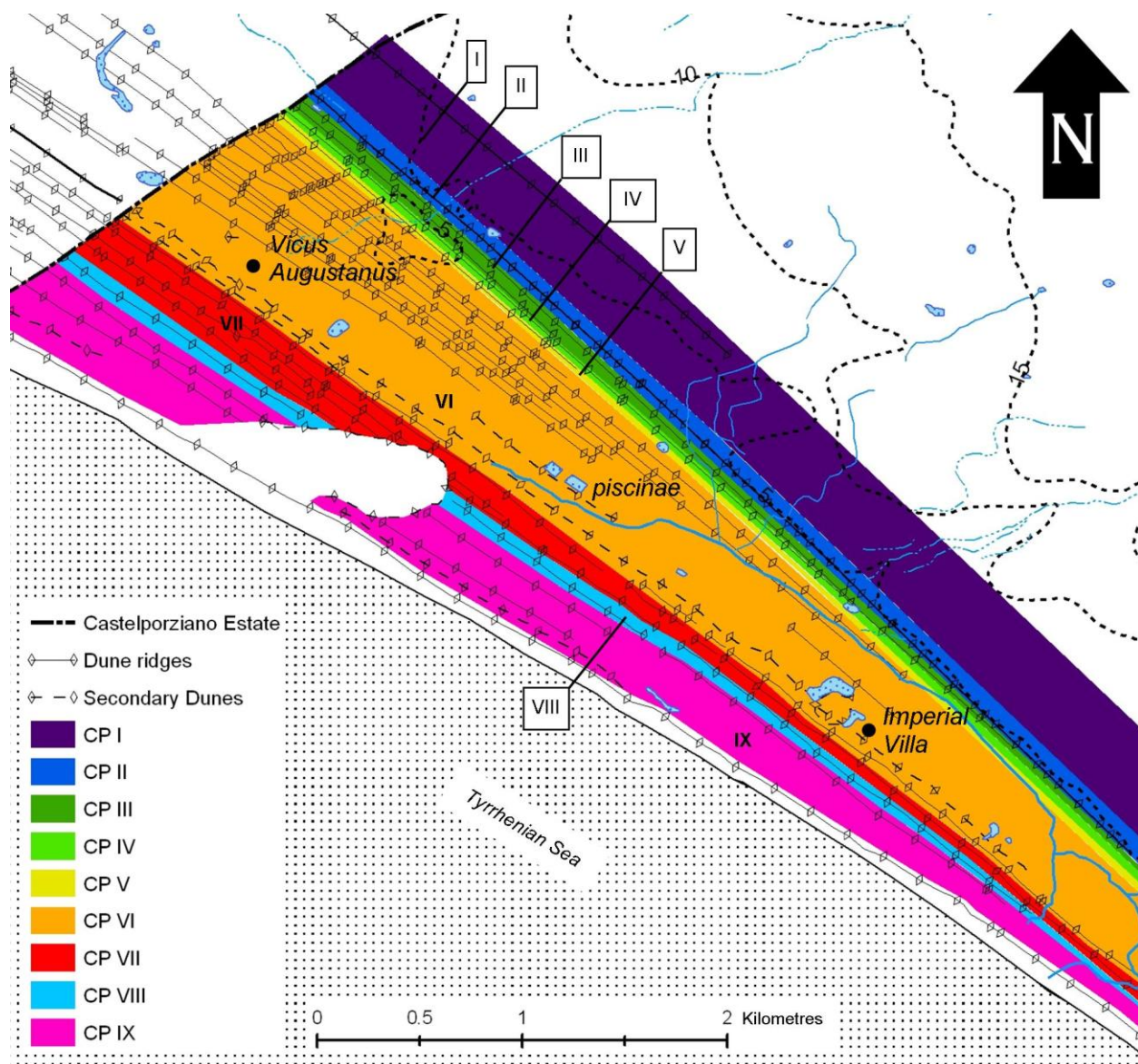


Figure 5.3: Dune phases at Castelporziano based on table 5.1.

One possibility suggested by the close-proximity and overlapping waveforms of the Roman and directly post-Roman dune ridges (see boundary wall transect in particular, figure 4.45) at Castelporziano is that seaward truncation of the foredune profile due to storm wave erosion may instigate foredune formation on a newly created berm terrace (Hesp 2002). In this way foredune formation due to increased sediment supply from the Tiber catchment is facilitated by localised events acting directly upon the shoreline. The higher frequency and overlapping waveforms recorded in the dune ridge transects (figure 4.45) may be suggestive of wave scarping and subsequent foredune formation within a prograding coastline context (Figure 1.6). Due to the short-term nature of storm-events, this signal is not likely to be observed without high-resolution examination through the dune ridge section (Hesp 1988). During sampling, the preservation of dune ridge bedding was not observed across the site. What is inevitable is that multi-scale temporal and spatial processes interact to drive the timing and morphology of shoreline changes. These changes can only be

discussed in a holistic way without several high-resolution records that are similarly scale-sensitive, and across meso-to macro-scales. As discussed previously, sea level change is not likely to be a critical factor during late Holocene dune formation in comparison to the flux in sediment supply emanating from the mouth of the Tiber River. In addition to centennial-scale climatic oscillations critically, anthropogenic factors associated with driving increases in catchment sedimentation rates and thus fluvial sediment load, are argued to be more likely within the macro-scale context of the Tiber delta system. The effects of sediment supply upon beach sediment budgets and thus foredune and dune ridge morphology may then stem from these multi-scale processes.

#### **5.1.5. Holocene chronostratigraphy**

Following assessment of the scale-process sensitivity of the dated dune-ridge record, a chronostratigraphy incorporating multi-scale records relating to the local, regional and hemisphere-scale climate trends during the Holocene has been constructed in order to assess the macro-scale formation of the Castelporziano dune-ridge record (figure 5.4).

Cacho et al (2001) describe a sequence of short sea-surface temperature (SST) cooling events during the Holocene. The magnitude of cooling is greater within the Tyrrhenian basin linked to the amplification of winter winds. During weakened phases of the Atlantic thermohaline circulation, cold Atlantic water penetrated the Straits of Gibraltar leading to a cooling of the western Mediterranean basins. However, the poor correlation and reduced frequency may suggest that the Tyrrhenian Sea is relatively insulated from the direct influence of the colder Atlantic water, perhaps due to the enclosed bathymetry of the basin and the Gulf of Lions gyre to the NW preventing effective circulation of colder deep water. Cooler/wetter periods are also seen within the Lago Albani algal records at 8.2, 6.4 and 3.8 ka BP (Ariztegui et al. 2001). Within the Castelporziano primary dune ridge record, foredune formation shows some relationship with periods of aridity recorded by Holocene pollen ratios with effects observed across Europe (Jalut et al. 2000). Wanner et al (2008) summarise the global climate changes during the mid- to late-Holocene and highlight within decadal to multi-centennial timescales the complexity of understanding 1500-year (Bond) cycles suggested by some northern hemisphere palaeo-environmental proxy records. In addition, culturally important climate phases, especially the LIA, may be limited to the northern hemisphere but linked to the coincidence of several global forcing factors such as “unusually low solar activity and a high number of major volcanic events” (Wanner et al. 2008: 1819).

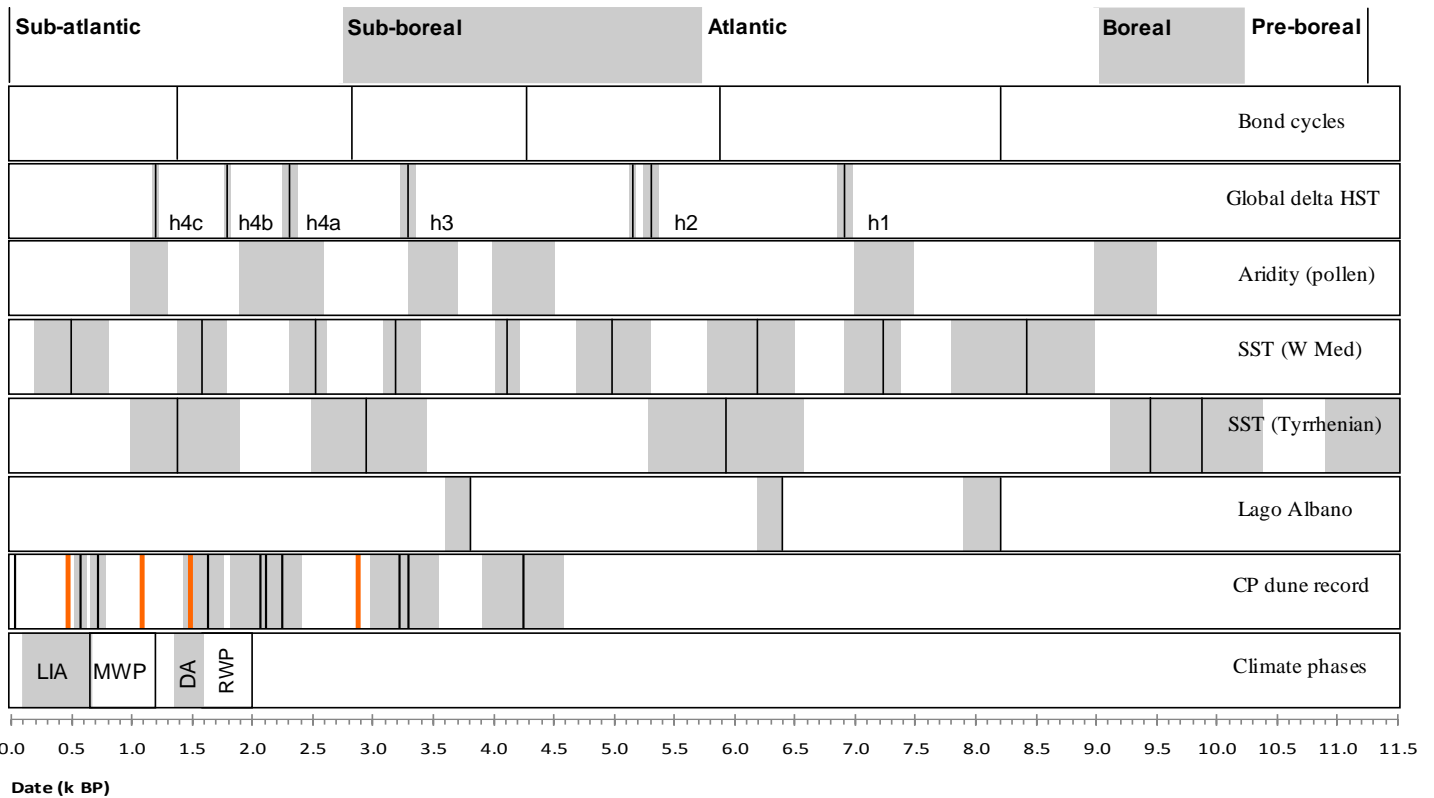


**Figure 5.4:** Holocene chronostratigraphy of major climatic events, in order of scale. Grey areas denote age uncertainty. Blytt and Sernander climatic phases follow the reassessed Italian stratigraphy by Ravazzi (2003). 1500-year Bond cycles (2001) are included for reference as there is some support for their existence within the northern hemisphere (Wanner et al. 2008), but the driving factors behind them are currently unclear and complex (Debret et al. 2007; Dima & Lohmann 2009). Global delta HST development is based on data from Somoza et al., (1998). Aridity based on European pollen ratios is taken from Jalut et al., (2000). Sea surface temperature abrupt cold events for the Western Mediterranean and Tyrrhenian Sea are provided by Cacho et al., (2001) and Frigola et al., (2007). Cold events recorded in the Lago Albano algal record is taken from Ariztegui et al., (2001). The timing of archaeologically important climate phases is taken from Rohling et al., (2009) (LIA & MWP). Dates for a dark ages cold period are sparse but climatic deterioration following the RWP is suggested by Giraudi et al., (2009). Central ages and age estimate ranges for diagenetically reliable Castelporziano (CP) primary dune ridges record is presented for the last 5000 years BP. Modelled dune ridge ages are shown in orange. Arid phases and cold/wet phases alternately, with CP dune building phases occurring generally during arid phases. However this trend may be mediated by reduced sediment supply flux (linked to the sediment budget model) rather than directly driven by the climate. Anthropogenic activity especially during the RWP may be responsible for preventing dune building due to increased sediment supply driven progradation rather than foredune aggradation.

Following the aridisation of the Mediterranean around 5 ka (Magny et al. 2002)<sup>28</sup>, an oscillating series of arid – cooler/wetter – arid periods develops. There is however some debate as to whether these arid phases, in particular the Roman warm period (RWP) were actually warmer than subsequent or preceding periods (see Taricco et al. 2009 and references therein). Recent Holocene pollen records from the central Tiber delta area show that between 7 - 4 ka BP,

<sup>28</sup> The Global perspective of Wanner et al (2008) suggests that during the last 6000 years, the ITCZ has shifted south due to the effect of orbital forcing increasing insolation to the southern hemisphere, leading to a weakened NAO. The effect of a weakened NAO is to increase the seasonal wetness of the western Mediterranean by increased storm activity predominantly in winter which at first glance would seem at odds to an overall aridisation of the Mediterranean during the same period. However due to the global scale of the research the dataset used does not contain comprehensive Mediterranean proxy datasets but does highlight a ‘much drier’ central Italian lake level record (their figure 3). Understanding the impacts of these macro- to mega-scale trends upon human responses and initiatives and therefore geoarchaeological records is not likely to be forthcoming at these larger scales of examination. Meso-scale relationships within a macro-scale context are argued to be far more sensitive for the purposes of this thesis.

NAP (non-arboreal pollen) had increased to around 20% of the assemblage with a consequent decrease in the representation of AP. There is also an increase in olive and wheat linked to significant human settlements in the region (Bellotti et al. 2007). Around 4500 BP the Maccarese Lake (northern Tiber delta pond) nearly dried up completely apparently due to the erosion of the coastal dune ridges (Giraudi 2004, cited in Bellotti 2007). The direct influence of dune ridge erosion upon lake level lowering is not however obvious. The coastal location and confluence of marine and terrestrial watertables suggests water supply would be a problem during arid phases. Both the coastal lake lowering and reduction in tree pollen may be more effectively linked to the relative aridisation of the climate during this period.

#### **5.1.6. Summary**

Dune ridge records from Castelporziano are representative of the whole Tiber delta and perhaps preserve two additional phases of dune ridge formation not recorded adjacent to the Tiber channel (Giraudi et al. 2009). A tentative correlation based on local, regional and global scale records suggests dune ridge formation at Castelporziano during the last 5000 years is best described during periods of aridity. However, the warmer/ drier climatic conditions may not be the key factor inducing foredune formation. There is a general agreement between progradation during cooler/wetter periods and dune ridge formation during intervening warm/dry phases. Cooler/wetter conditions are partly responsible for increased sediment supply into the Tiber River and thence the delta beaches. This positive sediment budget facilitates progradation of the coastal plain. This is partly at odds with the sediment supply record inferred from periods of increased flooding frequency of the Tiber River and high-altitude lake levels within the Tiber catchment (see section 5.4.3). Increased progradation rates and flooding frequency can be seen to occur during both the cooler/wetter LIA, but also during the warmer/drier RWP suggesting that the climate is not the dominant driver of sedimentation into the Tiber River during the RWP, (or perhaps more accurately the Roman Cultural Period (Taricco et al. 2009)). Anthropogenic exploitation of the Tiber catchment may be partly responsible for increased sediment supply during the last 2 centuries BC. Fore-dune development can be seen to occur during periods of reduced beach sediment budget, superimposed onto the regional climate signal. The development of a foredune can be conceptually seen to demarcate the cessation of a delta progradation phase. Therefore the relict foredune ridges are effective temporal markers of progradation linked to sediment budget flux but the drivers of foredune formation are more problematic to discern from these centennial-scale records. Smaller-scale storm events may be more important for eroding the beach/dune profile facilitating the development of a foredune during periods of suitable sediment budget. However they are effectively invisible to meso-scale sampling strategies and centennial-scale palaeo-environmental records.



## 5.2. Holocene cross-section of Castelporziano

Bearing this context of Holocene and multi-scale processes inducing the form of the shoreline, the reconstruction of key geoarchaeological phases will be developed below, with further discussion of macro-scale processes linked to regional climate and anthropogenic activity. Figure 5.5 describes a schematic cross-section of the Castelporziano coastal area and inland hinterland.

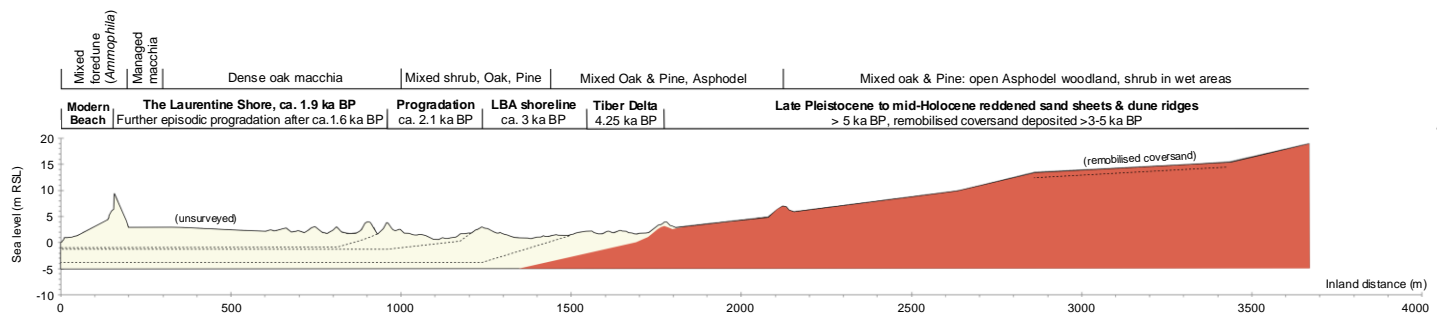


**Figure 5.5:** Schematic cross-section of the Tiber delta dune ridge sequence and "Old dunes" ferricretes. The diagram is constructed from the integration of topographic survey transects, D-GPS control points and sea level reconstruction both from this study and published sources. The diagram is orientated relative to modern sea level as described by the EGM '96 Geoid model. Dune ridge positions and heights are also accurate based on the extension of GIS mapped dune ridges to the route of transect 1. The altitude of the pre-delta (ca. 5 ka BP) and LBA shorelines are cited from reconstructions by Bellotti et al (2007) and Lambeck et al (2004a). The D6 sea level reconstruction and derived mean rate of sea level increase underpins the other presented sea levels. The beach slopes are simple estimates based on the convergence of sea level and the position of the adjacent seaward primary dune ridge and similar to the slope of the modern beach. The area of remobilisation in the reddened sand sheets is also displayed; this may extend further landward and seaward but is not constrained by other sampling locations. A generalised vegetation scheme describes the dominant vegetation moving inland from the modern beach.

## 5.3. Late Pleistocene – Mid Holocene coastal sandsheets and dune ridge formation

The extent of the coastline can be estimated from the extent of the reddened late Pleistocene to mid-Holocene sand sheets and later dune ridges partly extracted from the regional geology map (figure 5.6). The shoreline is characterised by these reddened aeolian features. Luminescence dating suggests these sand sheets have been sequentially deposited and later reworked during several phases during the mid- to late-Holocene. Reddening can be seen to occur due to *in situ* weathering of ferro-magnesian minerals within the sand-sized clasts of the aeolian sediment. A contribution from groundwater cannot be discounted as a possible allochthonous source of ions derived from pre-existing reddened sediments. However the mobility of groundwater upwards through the profile may be questioned. The relatively high altitude of the coversands to observed streambeds and water tables could suggest important meteoric geochemical sources. These old dunes may have been partly deposited during the last interglacial (Milli & Zarlenga 1991) but they have clearly continued to develop during the Holocene linked to a mid-Holocene dune building phase recorded in the central Tiber Delta (Giraudi et al. 2009).

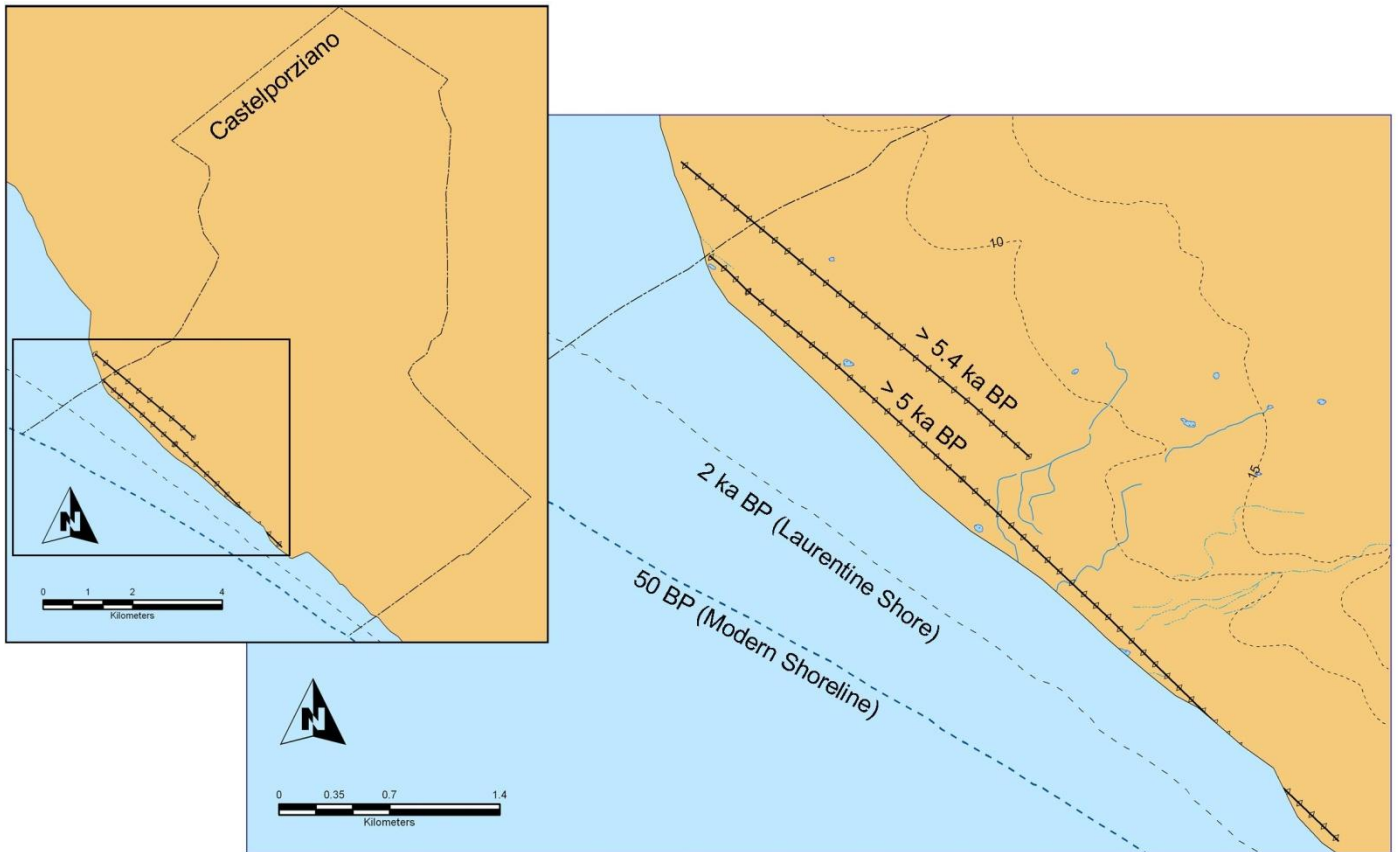


**Figure 5.6:** Reconstruction of mid-Holocene ferricrete dune-ridges and sandsheets, ca. 5000 BP.

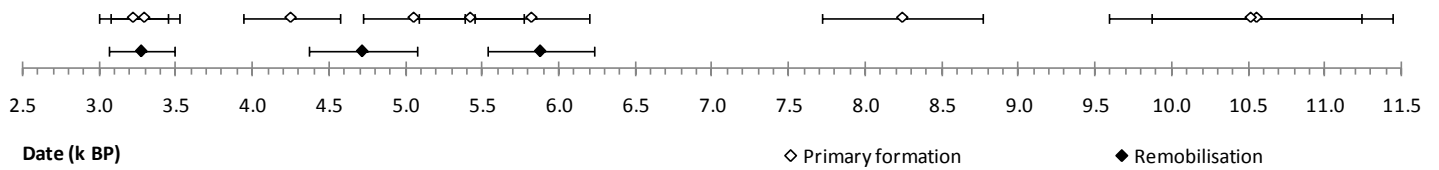


**Figure 5.7:** Timeline of pre-settlement dune ridge formation. The earliest evidence of human occupation of the coastal area of the site is ca. 2700-2900 BP.

A timeline of primary and secondary (remobilisation) phases is presented in Figure 5.7. The problematic effect of diagenetic dose-rate flux is clear, with increasingly poorly constrained age estimates over time. Two reddened dune ridges can be observed at the site today dating to ca.  $>5055 \pm 331$  BP and  $>5424 \pm 343$  BP. The younger ridge is buried by later phases of aeolian sand at ca.  $\sim 4.3 \pm 0.3$  ka BP (and again at  $\sim 2.3 \pm 0.16$  ka BP). Unpreserved dune ridge features may have existed and been post-depositionally eroded by an aeolian or another mechanism. Aeolian remobilisation of reddened sediments is suggested by the upper horizons of all sampled early vadose ferricretes. These remobilisation phases date to at least the mid- and late Holocene, with overlapping age ranges to a phase of dune ridge formation occurring after ca. 5.5 ka BP.

The sediment supply is estimated to have been substantial and prolonged as the region characterised by Pleistocene red dunes by the Geographical Institute of the Italian Army (IGM: Cerveteri 149, 1:100,000) (collated by ISPRA<sup>29</sup>) is the “most common and extensive stratigraphic formation from Acilia to the Fosso di Malafede valley [northern portion of the Castelporziano Estate]” (Manes et al. 1997:21). However the description of dune reddening by Manes et al (1997) as being caused by the weathering of outcropped pozzuolana and pyroxene lithoid tufa, is not applicable to the young and seaward dune ridge sediments that are likely derived from littoral sediments. Furthermore, considering the sequentially older chronology of primary reddened sand sheet features moving inland, sand sheet sediments are more likely to have been deposited sequentially from a seaward rather than landward direction (i.e. from an indirect fluvial-marine-beach source rather than a direct volcanic source) followed by *in situ* weathering. This seaward origin is further suggested by the sequential depletion of HM moving inland as shown by diagenetic petrology data (figure 4.31).

#### **5.4. Mid-Holocene progradation of Italian & western Mediterranean deltas**

The estimated mid-Holocene shoreline at Castelporziano is presented in figure 5.6. Sea level was lower and a quasi-stillstand existed at ca. – 4-6 m RSL between 7 – 4 ka BP (Lambeck et al. 2004a; Bellotti et al. 2007). These sea level conditions would suggest an expanded beach fetch due to increased exposure of the coastal shelf but at this position of the coastline a detailed profile of the shelf prior to delta progradation is lacking (reconstructions exist for the incised LGM Tiber channel at the core of the delta, Bellotti et al., 1995, 2007). Therefore the coastline position estimated in figure 5.6 is likely a slight overestimation of inland position constrained by the dated reddened dune ridges. The Ombrone delta began to prograde following 6 ka BP with subsequent progradation events during Etruscan and Roman phases (Bellotti et al. 2004). Comparisons of the Tiber, Po and global deltas (Amorosi & Milli 2001) argue that progradation phases (i.e. the development of highstand systems tract (HST) parasequences) begin around 6-5 ka BP driven by the eustatic sea level baseline stillstand. The development of the HST within the Arno coastal plain suggests development soon after ca. 7820 ± 130 cal. yr BP but with a poorly constrained age model (Amorosi et al. 2009). Somoza et al (1998) show that the Ebro delta (NE coast of Spain) developed a maximum flooding surface and overlying HST parasequences from around 6.9 ka BP (figure 5.8). The authors compared the Mississippi delta and dated highstand deposits from around the Spanish coast, showing a good correlation between progradation and aggradation phases during the last 8000 years; aggradation phases being important for driving the formation of coastal peats providing a means to effectively date the successions.

---

<sup>29</sup> Istituto Superiore per la Protezione e la Ricerca Ambientale  
<http://www.isprambiente.it/site/en-GB/default.html> (9/07/2009)

REMOVED TO COMPLY WITH E-THESIS GUIDELINES

**Figure 5.8:** Holocene development of the Ebro Delta (Somoza et al. 1998).

#### 5.4.1. Delta Progradation at Castelporziano

REMOVED TO COMPLY WITH E-THESIS GUIDELINES

**Figure 5.9:** Reconstruction of the central Tiber Delta area at ca. 7000 (a) and 4000 BP (b) (Bellotti et al. 2007). The development of the coastal strand-plain is the key development during this period, creating the familiar cusped delta morphology from the preceding bayhead delta morphology. The Castelporziano Estate is just visible in the bottom right corner of each reconstruction. The distinctive route of the Canale di Pantanello and heavily-vegetated boundary is clearly visible.

Due to the constraining effect of the incised lowstand late-Pleistocene Tiber valley, the expansion of the HST alongshore to Castelporziano occurs around 1000 years later by  $4252 \pm 316$  BP. These developments represent an alteration to the sediment supply system to Castelporziano, previously by alongshore transport to the 'hard coast' from a bayhead delta upstream of the current position (Figure 5.9). There is then a centennial to millennial lag between the development of the HST in the main Tiber channel to its expression at Castelporziano. Although sensitivity to change is relatively poor during this phase of shoreline development, once the Tiber delta attained a cusped morphology by 4 ka BP, the position of the river mouth at the coast and continuous shoreline suggests that sediment supply to the Castelporziano area is then subsequently more direct and more sensitive to macro-scale changes in delta front progradation.

Between ca. 4-5 ka BP, following several alternating phases of sequential sand sheet / dune ridge formation and remobilisation (figure 5.7), a second phase of remobilisation is observed. This oscillating trend in landscape instability/stability during the mid-Holocene could be related to several processes. Sediment supply is ultimately linked to the mid-Holocene stillstand sea level, the filling of accommodation space and the progradational development of the Tiber delta. Phases of remobilisation are more problematic to interpret and may be due to a combination of more

locally expressed processes such as vegetation disturbance linked to changes in sediment budget, climatic, hydrological or wind regimes, and anthropogenic activity. Specifying a single cause is not possible with this dataset but can be described within the context of the sediment budget model. Phases of sand remobilisation and overwash (ca. 5.9 ka BP and 4.7 ka BP) occur during dune negative/beach strongly negative sediment budgets, whilst progradation (ca. 5-5.5 ka BP) and dune ridge formation occur under dune positive/ beach positive and dune positive/beach equilibrium or slightly negative conditions (Miyanishi & Johnson 2007; Psuty 2008). Within the macro-scale context of the Tiber delta, negative dune and strongly negative beach sediment budgets are not suggested by the enduring eustatic sea level conditions and global development of HST delta parasequences. Smaller-scale processes are thus more likely causes of instability. What also must be considered are high magnitude, short-duration storm events; events that will not be recorded by macro-scale records. Furthermore, dune ridge sampling strategy fundamentally drives the records presented here. As discussed in chapter 4, every dune ridge preserved on the site cannot be directly measured, so sampling must be prescriptive. However, the integration of the various datasets retrieved does allow a consideration of primary and secondary (remobilisation) dune ridges and therefore consideration of sediment budgets at specific points in time.

#### **5.4.2. Regional climate and mid-Holocene delta progradation**

Understanding the macro-scale Holocene and late Pleistocene climate history of the Mediterranean is complex. Discriminating between scale/process-sensitivity of palaeo-environmental indicators and seasonal precipitation must be developed from multiple proxy records (Tzedakis 2007:2060), often with variable sampling resolution and chronological control. Macro-scale trends have been identified from Holocene proxy records across the Mediterranean. A *bipartite* Holocene has been discussed by Magny et al (2002). Due to the northward displacement of the ITCZ (intertropical convergence zone) and STA (subtropical anticyclone) during the early Holocene winter and summer temperatures were lower by around 2 °C, leading to an increase in moisture. Following a wetter period between 6.5 – 5 ka BP recorded in terrestrial valley sedimentation (Eppes et al. 2008), a period of aridity is then seen to occur across the Mediterranean from around 5 ka BP, observed in lake level lowering and palaeoecological proxy records (see Magny et al. 2002 and references therein). After around 5.5 ka BP a southerly shift in the ITCZ due to increased solar irradiance to the southern hemisphere (due to orbital forcing) (Wanner et al. 2008), the associated change to a more negative NAO impacts upon the Mediterranean regional climate leading to more arid conditions in the late Holocene. However on finer, centennial timescales, correlating palaeoecological and palaeoenvironmental proxy records is problematic and displays significant noise to signal.

It has been argued that the current 'rhythm' of the Mediterranean climate, the summer drought and winter deluge, was developed by 5 ka BP following an increase in aridity of the climate (Wunsam et al. 1999; Grove & Rackham 2001). Stable isotope and pollen data from the Lake Golhisar, SW Turkey suggest an oscillating trend between arid and humid

conditions (8800 – 5100 cal. yr BP), with the onset of aridisation after ca. 5100 cal. yr BP (Eastwood et al. 2007). Global climatic drivers of increased Tiber delta sedimentation have recently been reiterated by Giraudi et al (2009). Alluviation during the LIA and so-called Dark Ages cold period, are attributed directly to Bond cycles in the North Atlantic. A link between colder western Mediterranean SST, induced by the penetration of cold NA water and Tiber delta progradation during these cold periods, is again described.

### 5.4.3. The changing course of the Tiber

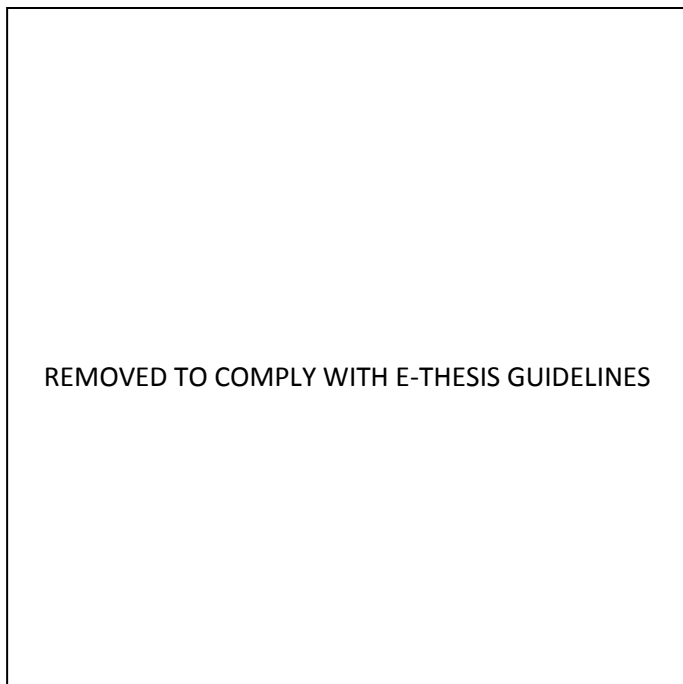


**Figure 5.10:** Geoarchaeological reconstruction of the relict course of the Tiber River at *Portus* (Trajan Basin) (Giraudi et al. 2009).

It has been argued for a considerable period that the Tiber River previously flowed straight out into the Tyrrhenian Sea at a position immediately SW of the Claudian and Trajanic harbours (see Giraudi et al. 2009 and references therein). A second smaller branch ran to the north of this position but is poorly preserved (Giraudi et al. 2009) (figure 5.10). This also led to an anomalously seaward position of a foredune between the two branches of the river. The harbours are constructed into alluvium from this older course of the Tiber River. They argue that the modern Fiumicino channel occupies the position of the relict primary channel of this previous course. This route changed after ca. 2400 BP, with the founding of *Ostia* occurring on the new river mouth during the 4<sup>th</sup> century BC (Meiggs 1973). However the date of this change is stratigraphically inferred from charcoal fragments from preceding alluvial deposits and therefore not well-constrained. With regards to delta progradation vs. dune building, the 4<sup>th</sup> century BC saw the cessation of a long but lower-level progradation phase. Average rates between ca. 3.5 – 1.9 ka BP were around 0.165 m/yr. Giraudi et al (2009) argue for a phase of delta retreat between dune ridge phase V and VI-a (800 – 400 BC). A dune ridge formed between 2217 - 1929 BP confirms this relatively stable position of the shoreline linked to a reduced sediment budget on the beach. There is a transition from periods of colder SST within the western Mediterranean (Cacho et al. 2001), to a

period of increased aridity (Jalut et al. 2000). Geomorphological developments linked to the southward shift in the river mouth are then occurring during a period of transition between several interlinked multi-scale climatic and geomorphological processes.

What may be a significant factor for channel avulsion is a change in base-level linked to relative sea level position. At Castelporziano, the sea level at  $2403 \pm 40$  BP is recorded at  $-1.25 \pm 0.2$  m RSL. Conceptually linked to the end of a progradation phase, is the filling of the available accommodation space. Without more specific palaeo-climatic data, a pulse in flooding frequency is recorded during the 3<sup>rd</sup> century BC (Figure 5.2) (Bersani & Bencivenga 2001; Aldrete 2007; Stewart & Morhange 2009). Without accommodation space in the nearshore delta plain, increased alluviation during this period is liable to back-up in the lower catchment of the river, altering the gradient of the river. A flattening of the gradient may underlie this change in the Tiber's course. Channel avulsion during periods of climatic and sedimentation flux linked to a lack of accommodation space has been observed elsewhere (e.g. Fielding et al. 2006). However, accommodation space is one of several coincident factors. The increase in flooding and sediment supply during this period has been attributed to an increase in precipitation during the 2<sup>nd</sup> centuries BC to AD, which is also recorded in the Tiber flood record (Giraudi 2005). This conclusion is based on an increased level of Lake Fucino on the NE edge of the Tiber catchment in the central Apennines. However the presented chronostratigraphy by Giraudi (2005) does not accurately show a high lake level during the 2<sup>nd</sup> century BC (figure 5.11). A recorded low lake level occurs prior to the increased flooding frequency in Rome during the 2<sup>nd</sup> century BC. Based on this lake level evidence, it is not possible to attribute a climatically driven change to flood frequency and sediment supply in the lower Tiber catchment. The increased exploitation of the Roman hinterland in the Tiber valley between Lake Fucino and the Tiber Delta (Aldrete 2007) is more likely; anthropogenic activity thereby laying the foundations of the Imperial Roman shoreline several centuries in advance of the actual construction.



REMOVED TO COMPLY WITH E-THESIS GUIDELINES

**Figure 5.11:** Late Holocene chronostratigraphy of fluvial, alluvial and lacustrine events linked to climatically driven glacier expansion in the central Apennines (Giraudi 2005).

Increased precipitation linked to a high level Lake Fucino during the later Roman period upon an exploited and deforested Tiber valley can then be seen with the data from Giraudi (2005) (figure 5.11). During the mid-Holocene, the Tiber delta has gone through 3 phases of bayhead delta morphology with an associated anastomosing fluvial morphology (Bellotti et al. 1994; Bellotti et al. 1995). Within this context of complex transition, an improved chronology of changes to the delta and river mouth morphology in periods prior to a significant human presence in the catchment would be beneficial for isolating the impact of natural and anthropogenic forcing upon fluvial and delta morphology. In any case a high-resolution integrated and multi-proxy palaeoenvironmental study within the Tiber delta is required. High-resolution grain-size analysis of fine-grained sediment records for example in the *Portus* harbours or offshore shelf may recover a hyperpycnite record of flooding (Mulder et al. 2003) that can be related more accurately to flooding frequency and fluvial sediment supply. On the Holocene scale, Bellotti et al (2007) have shown the preservation of pollen to be generally sound. In addition to pollen, and the significant accumulated knowledge of sedimentological sequences of the delta, an integrated diatom study and vastly improved age model would be sensitive to developments within the terrestrial and fluvial/marine systems.

#### **5.4.4. Mid-Holocene aeolian sand remobilisation**

With the widespread significance of aeolian remobilisation in dune ridges and sand sheet locations during the mid-Holocene, a key question must be “where was the stabilising vegetation cover?” The form of the mid-Holocene remobilised material occurs as metre thick coversands lying unconformably over the early Holocene ( $>8.2 \pm 0.53$ ) and

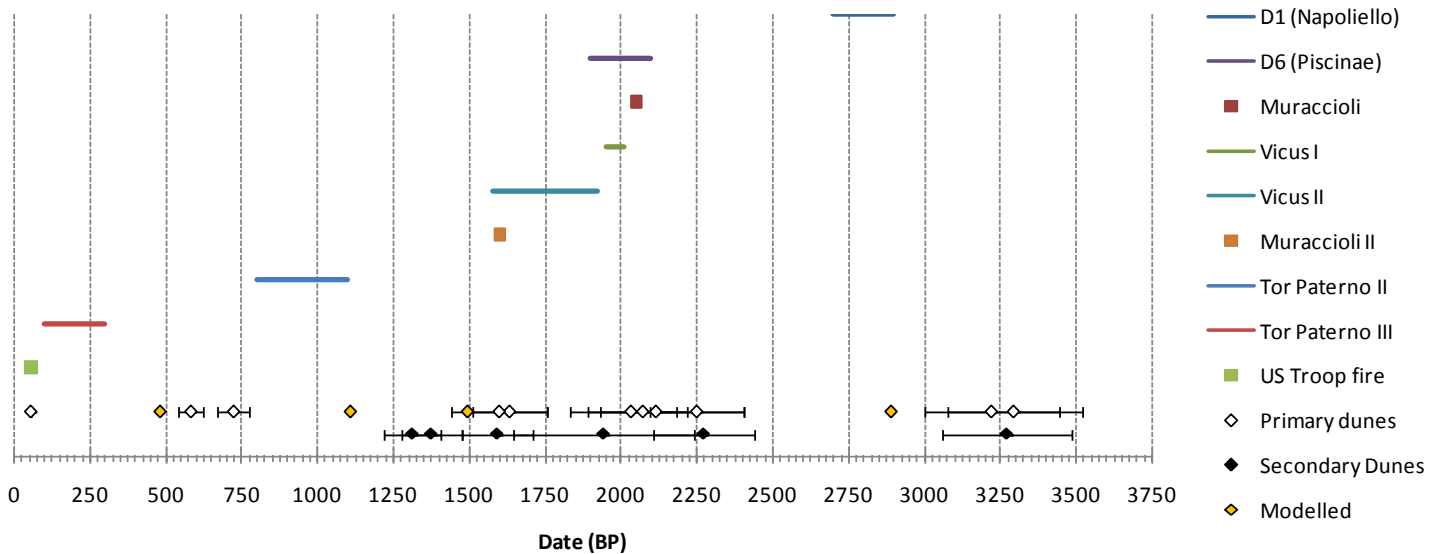
late Pleistocene ( $>10.5 \pm 0.7$  &  $>10.5 \pm 0.9$  ka BP) sand sheets. The sampling locations are 1.5 – 2 km inland from similarly aged dune ridge forms suggesting a lack of impediment between source areas and deposition at least  $>5.9 \pm 0.4$  ka BP,  $>4.7 \pm 0.35$  ka BP and ca.  $>3.3 \pm 0.2$  ka BP. Within the Castelporziano, impediment to inland aeolian movement is provided either by archaeological buildings, relict dune ridges, or the dense vegetation cover. During the mid-Holocene, the presence of substantial architecture can be ruled out as the first known period of anthropogenic activity occurs ca. 2.9 – 2.7 ka BP (Lauro & Claridge 1998) and is restricted to localised pottery scatters. Primary dune ridges are preserved at  $>5.8$  ka BP,  $> 5.4$  ka BP,  $>5$  ka BP and  $4.25 \pm 0.3$  ka BP. Due to diagenesis within both the dune ridges and remobilised coversands the ability to link possibly related phases of sand movement is prevented due to likely significantly underestimated formation dates in the reddened sediments. What can be argued is that inland sediment supply after the formation of the CP07/14 dune ridge ( $4252 \pm 316$  BP) is likely to have decreased significantly except following disturbance in the active dune ridge during periods of negative sediment budget in both the beach and active foredune. Therefore, the sediment flux linked to the nature of the vegetation cover of the time is the meso-scale key factor for ascertaining the stability of the developing coastal dunes to sand remobilisation. However, both sediment budget and vegetation cover are linked to the hydrological conditions of the time. The remobilised sediments lie close to the 15 m contour line, whereas the coastal dune ridges of this period are adjacent to the 5 m contour line. Sea level was at a quasi-stillstand, up to 10 m below the position of the (now-reddened) coastal foredunes. This relatively high altitude position above the confluence of marine and terrestrial water tables may explain why the sparse contemporary vegetation cover over much of the reddened inland sand sheets is limited to *asphodel* and large, mature, reforested *Pinus pinea* with hygrophilous vegetation adjacent to ephemeral, seasonal *Fossa* streams and a sparse distribution of small ponds.

Within the reliably dated younger dune ridges  $< 5$  ka BP, it appears that secondary dune ridge features are coeval with primary dune ridge formation on the site. This suggests that sediment budgets within the primary foredunes were negative and that inland transportation of aeolian sand frequently occurred in significant volumes. Dune ridge transects suggest that these smaller, secondary features form in the lee of a primary foredune, but also on the stoss slope. It may be the case that the density of vegetation around inter-dune slacks and the wavelength of dune ridge crests may preferentially deposit remobilised aeolian sediments at these seaward positions on the relict dune ridges. Increased sediment budgets inundating coastal vegetation and/or localised foredune erosion linked to storm activity are possible causes of remobilisation. These processes cause sufficiently small-scale and locally-expressed effects to require a higher-resolution sampling strategy for validation. Certainly relict blowouts and parabolic dunes have been observed associated with relict dune ridges of various ages. These disturbance features are clearly recorded by the DEM.

## 5.5. Mid-Late Holocene

The first, known phase of human activity within the Castelporziano Estate, between 2900 – 2700 BP (figure 5.12), is represented by Late Bronze Age (LBA) to Early Iron Age (EIA) ceramics found in low mounds adjacent to the marshy area known as *Pozzo Napoliello* (Lauro & Claridge 1998). This area lies towards the centre of the Estate within transect 2. Although direct sampling of this area was not undertaken, the extent of the coastline can be reconstructed using the transect age models and GIS dune ridge mapping in conjunction with the known ages of key periods in the archaeological record (figure 5.13). The Tiber delta had developed into a cusped form, and episodic drying of the northern, Maccarese coastal lake is recorded at 3 ka BP and 2 ka BP (Bellotti et al. 2007). The southern extent of the *Ostia* coastal lake abuts the northern boundary of the Castelporziano Estate, recorded by tide marks preserved in the aerial photographic records (chapter 4). By this time a relatively thin veneer of deltaic sediments had enveloped the Castelporziano shoreline region, and at least 3 phases of dune ridge formation had occurred since ca. 5 ka BP. A more accurate assessment of the relict dune ridge record between these periods is hampered by the widespread construction disturbance along the course of the *Canale di Pantanello* beginning in the late 19<sup>th</sup> century. Giraudi et al (2009) describe how the western side of the northern jetty of *Portus* was constructed onto the dune ridges dated to ca. 2800 – 2900 BP. The GIS shoreline reconstructions are partly based on the dated sequence of dune ridge phases recorded around *Portus* and *Ostia Antica* (Giraudi et al. 2009: figure 1).

**Figure 5.12:** Late Holocene timeline of human occupation (pers. comm. A. Claridge 2009) and dune ridge formation. D1, refers to the LBA/EIA sites (section 5.5) in the vicinity of Pozzo Napoliello (Lauro & Claridge 1998).



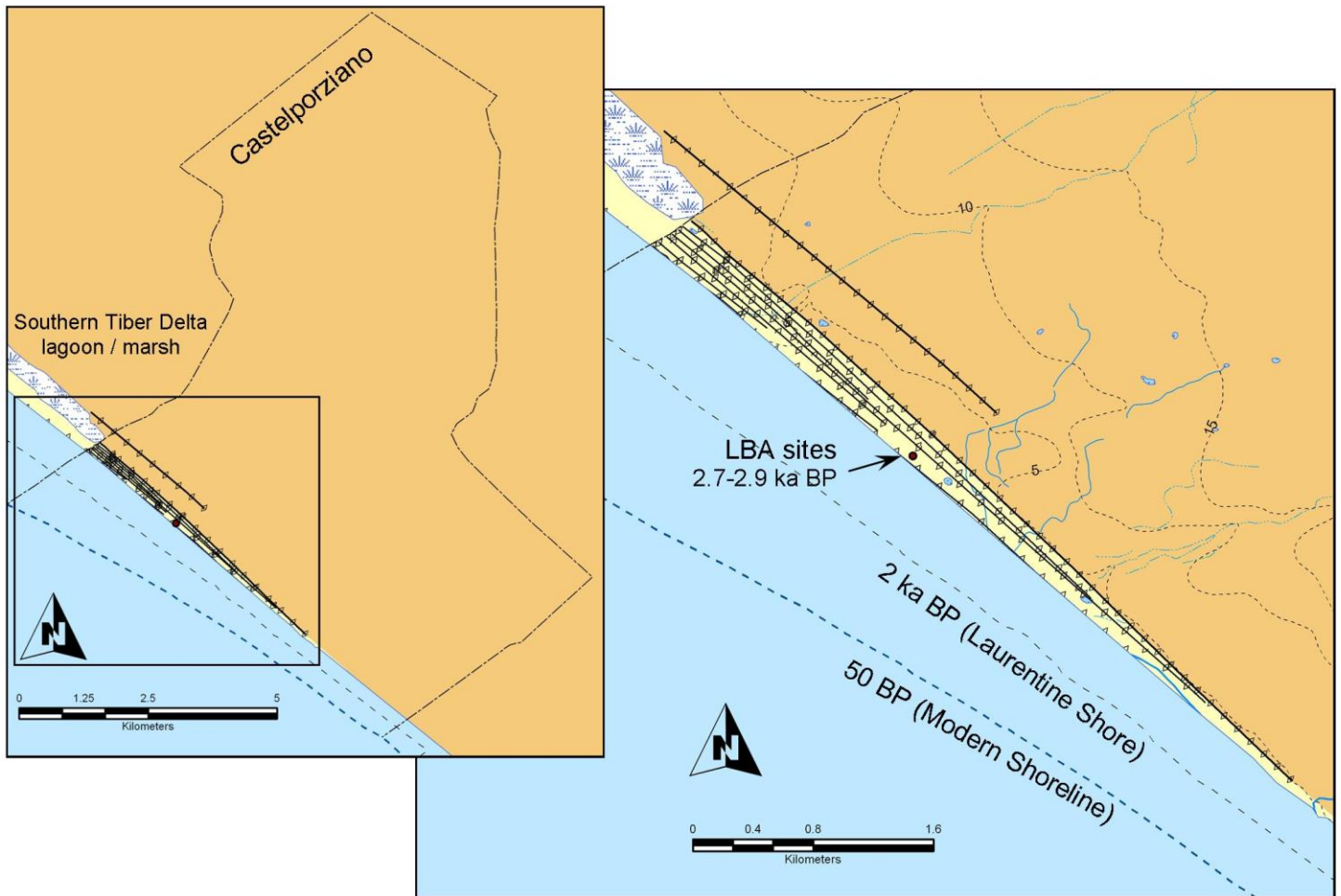


**Figure 5.13:** Reconstruction of Tiber Delta shoreline at Castelporziano during Late Bronze Age (LBA) based on transect age models and archaeological survey. The archaeological remains dated by pottery evidence to ca. 2700-2900 BP are marked. The transect 1 age model suggests the position of the shoreline at this time is around 1.5 km inland of present, this distance decreasing due to the compression of the delta morphology towards transect 3 in the southern portion of the site.

Average progradation rates between 3448 – 1929 BP suggest the shoreline was relatively stable during the LBA/EIA period of occupation. An age-modelled dune ridge (~2888 BP) and dune ridge phase V recorded by Giraudi et al (2009) confirms the cessation of progradation and suggests the LBA / EIA sites at Castelporziano were in close proximity to the palaeo-shoreline of ca. 3 ka. Considering the alongshore position of the artefactual evidence from transect 1 (the data used to calculate progradation rates), the experienced rate of progradation may have been less, due to alongshore depletion compression of the delta morphology. Sea level is estimated to be around -5m RSL (Lambeck et al. 2004a; Bellotti et al. 2007).

## 5.6. The Laurentine Shore

### 5.6.1. Macro-scale context of the Laurentine Shore

The wider Imperial Roman context of the Laurentine Shore during the 1<sup>st</sup> and 2<sup>nd</sup> centuries AD is dominated by two key sites, *Portus* and *Ostia Antica* (figure 5.14). A string of coastal villas and supporting infrastructure constitutes the shoreline between the *Vicus Augustanus* and *Ostia*. Keay et al (2005) describe a paucity of contemporary sites in the northern flank of the delta, perhaps linked to the extensive area of the Maccarese marsh during the late Holocene.

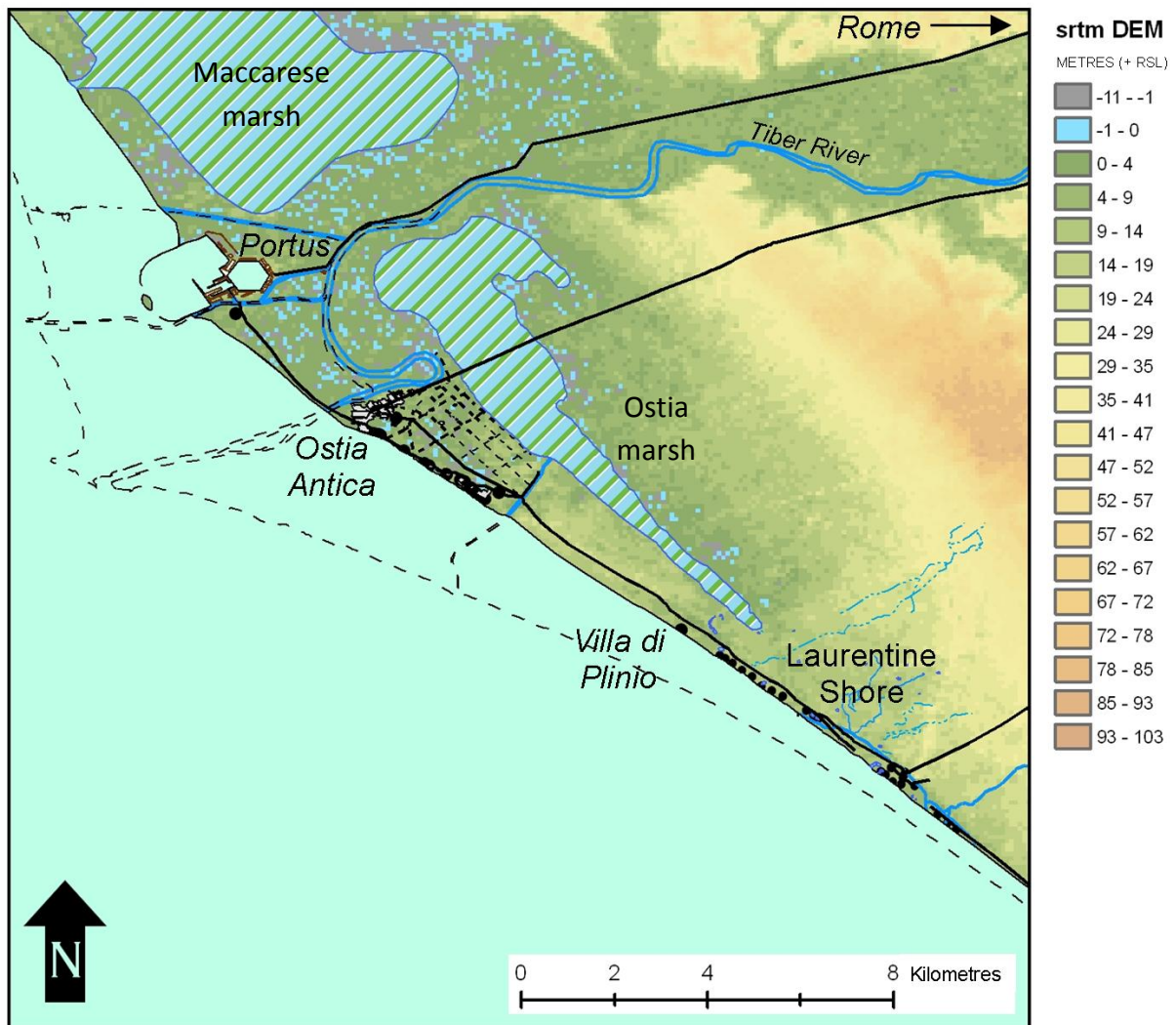


**Figure 5.14:** Reconstruction of the wider Laurentine Shore, Tiber Delta context. *Portus* and *Ostia Antica* provide critical gateways between Rome and the wider Empire. This is the core of Rome's maritime façade. The Via Severiana links the Laurentine shore to *Ostia* thence to *Portus*. The Via Laurentina in the SE, and the Via Ostiensis once navigated across the *Ostia* marsh connects the Laurentine Shore directly to Rome. The route of these roadways is mapped from available data (see the Laurentine Shore Project website for CP maps) and aerial photography evidence. The extent of *Ostia* and surrounding hinterland is digitised with permission from Heinzelmann (1998). The form of *Portus* is digitised from Keay and colleagues (2005).

### 5.6.2. Local geomorphological context

The Roman-period occupation of the site (2050 – 1580 BP), occurs between two phases of dune ridge formation (figure 5.15). There is a transition between the Late Republic and Imperial Roman periods during the late first century BC around 27 BC (2027 BP), which is recorded in changing architectural styles across the site. The end of the Roman settlement at the Laurentine Shore is of course constrained by the end of the Roman Empire in the 5<sup>th</sup> century AD.

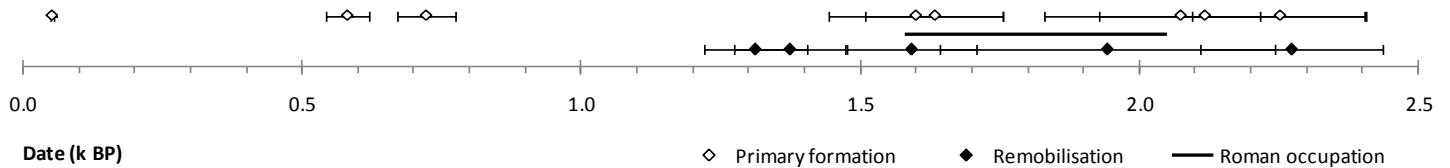


**Figure 5.15:** Timeline of dune ridge formation and Roman period of occupation of the Laurentine Shore archaeological record.

Remobilisation phases are associated temporally with a pre-settlement phase of dune ridge formation at ca. 2.25 ka BP, the early settlement of the Laurentine Shore at ca. 1.9 ka BP and both anthropogenic activity and dune ridge formation (linked to shoreline progradation) at ca. 1.6 ka BP. The Tiber flood record and progradation rates suggest that the initial Roman settlement of the shoreline around 2100 BP occurred around the transition from a phase of lower to higher progradation rates. The progradation rate linked to the increased flooding frequency of the Tiber River displays a threefold increase during this period from 0.165 to 0.537 m/yr. What can be seen is that the Roman coastal structures are built onto a coeval coastal plain about 350 m wide suggesting significant sediment supply during the preceding centuries. Minimum age estimates for the inception of this increased progradation phase are from 2217 BP (CP03/2). The deforestation of the Tiber catchment from the 3<sup>rd</sup> century BC onwards has been cited as a key process for increased Roman-period flooding (see Aldrete 2007 and references therein). An anthropogenic cause seems likely; the timing of this progradation phase should be interpreted in conjunction with the expansion of the Rome hinterland.

Therefore, the Laurentine Shore was not a 'stable' iteration of the coastline. The Roman period settlement of the delta coastline occurred midway through a significant and rapid phase of delta progradation linked to pronounced anthropogenic activity within the catchment. On the other hand, the Roman culture directly created the coastal area that was later inhabited (figure 5.16).

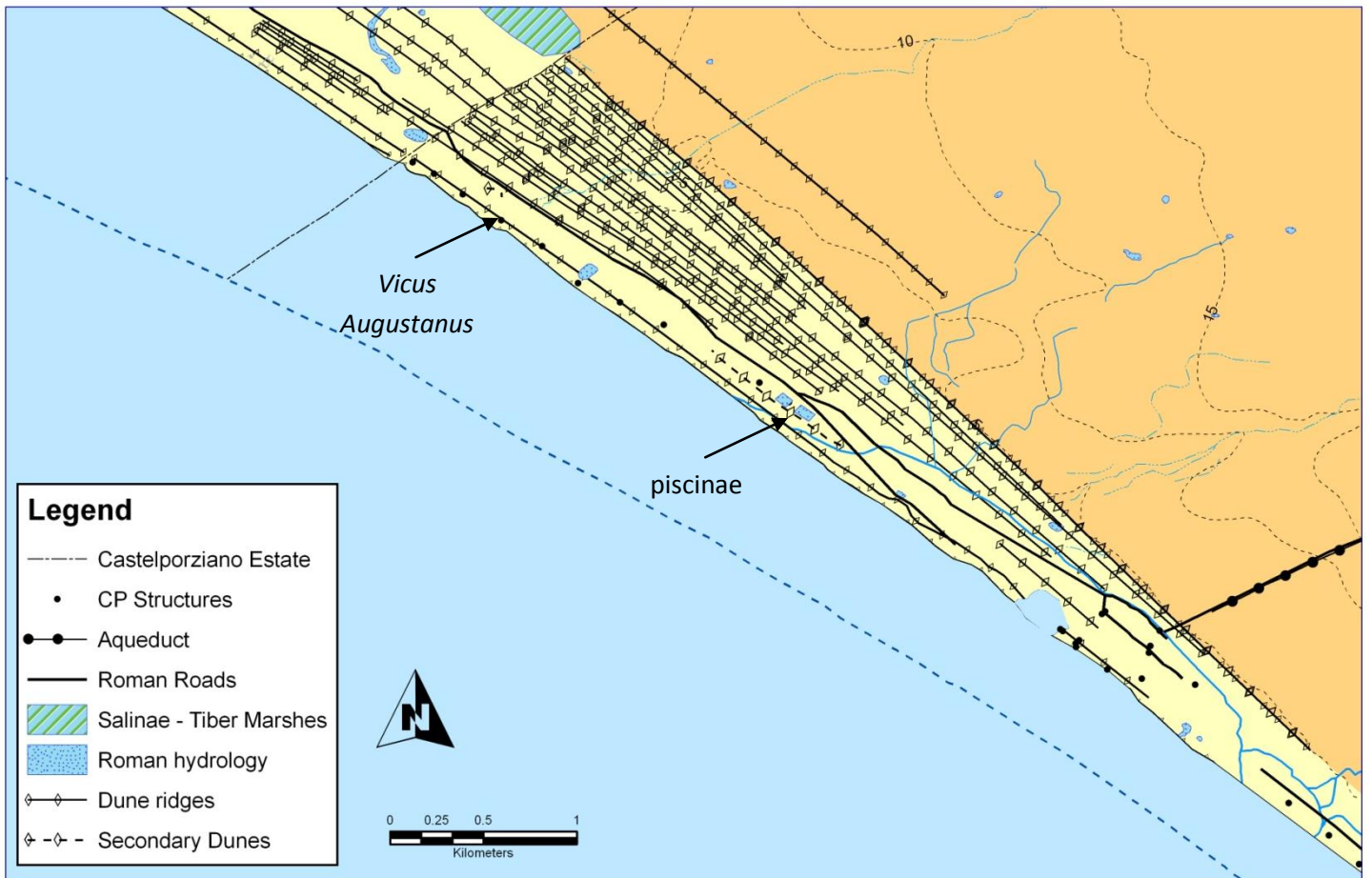


**Figure 5.16:** Geomorphological map of the Laurentine Shore. Reconstructions of Roman hydrological features from seasonally wet depressions are included.

### 5.6.3. Sea level context

The *Piscinae* sedimentary sea level marker at  $-1.25 \pm 0.2$  m RSL at  $2403 \pm 40$  BP suggests an average rate of sea level rise of 0.52 mm/yr. By the beginning of construction on the Laurentine Shore, of the *Piscinae* around 2050 BP, sea level is estimated to be ca. -1.066 m RSL. This level defines the baseline for coastal dune formation, terrestrial erosion, hydrogeological interactions between marine and terrestrial water tables and accommodation space available for sedimentary infilling during delta progradation phases.

### 5.6.4. A question of Roman dune management

A further complicating factor is that in the vicinity of major archaeological remains along the palaeo-shoreline, Roman-period relict dune forms are not clearly preserved, whereas in intervening areas the terrain is far more undulating. This may be suggested by comparing the Boundary wall and Vicus dune ridge transects; the boundary wall transect being associated with the inland area of a villa (B1) compared to the more intensively occupied Vicus. With hindsight, due to problems in identifying primary foredunes and secondary remobilised dune ridges in the field, a 'natural' cross-section

of the Roman dune ridge has not necessarily been recovered. This is clearly shown by the DEM of the *Vicus* and its environs. Interpreting this as being directly related to anthropogenic activity is more problematic in relation to the macro-scale sediment budget model which suggests that in periods when sediment supply and progradation are positive then foredunes are likely to be more poorly developed. Field evidence does not record a Roman-period foredune *per se* but rather the Roman period occupied shoreline is delineated by the slack of the following phase of dune ridge formation, which has developed on the Roman period beach. Conceptually on the macro-scale it could be argued that during the long-term progradation phase within which the Laurentine Shore was occupied a foredune was not well-developed due to the enduring, positive beach sediment budget associated with increased sediment supply during delta progradation. Local, small-scale variations may be important here but are not effectively constrained by the meso-scale sampling strategy. The relative flattening/increase in dune crest wavelength (compared to inland and post-abandonment topography) in the inland dunes may in theory then be partly due to Roman occupation and reworking. This must remain as a hypothesis as in the vicinity of the *Vicus Augustanus* a pine plantation in the mid-20<sup>th</sup> century may have also disturbed the landscape. Significant amounts of aeolian sand partially bury the Roman structures making assessment of Roman-period dune topography directly associated with structures logistically impossible. Further survey and substantial excavation could investigate this relationship further.

The Roman building sites are several metres above the contemporary sea level of the time lessening the risk of flooding due to seasonally fluctuating water tables interacting adjacent to sea level. However, the impact of coastal storms and increased wave heights cannot be as easily avoided. The foredune (or perhaps in hindsight better described as – back-beach) location of many of the villas and building complexes along the shoreline suggests they were exposed during high-magnitude storms. Pliny the Younger’s exclamation that the sea came through his dining room window may well be the case, as the Villa complex (as are most Villas along this palaeo-shoreline) described in his name is closely associated with the Roman-period shoreline (figure 5.14). These coastal locations would have afforded excellent views of the seascape but along with storm events, the mobilisation of beach sand inland was likely a problem, especially if dune management and/or recreational erosion of the coastline had occurred. The primary dune ridge of similar age to the abandonment of settlement at the *Vicus Augustanus* (5<sup>th</sup> century AD) is around 70 m seaward of the limit of construction with coeval phases of remobilisation burying part of the western end of the *Vicus* and also the seaward boundary wall of the D6 *Piscinae* (see below).

#### **5.6.5. *Piscinae* (2100 – 1900 BP)**

The earliest Roman structures currently found on the site are the *Piscinae*. Developed in the late first century BC, the ponds themselves are around 80 x 30 m, with the long axis parallel to the coast. In relation to the Roman period shoreline, field dune ridge mapping has continuously traced the post-Roman dune ridge from the vicinity of *Tor Paterno* to the Estate boundary wall with *Castel Fusano*, for a distance of around 7 km (all Roman period structures are



preserved associated with the inland relative to this one) (figure 5.16). The *Fossa dei Muraccioli* now flows through an incised channel following the contours of the Roman-period beach (section 4.9.2.3). The *Piscinae* therefore must lie in the slack inland of the Roman period beach. This sequence is constrained by the previous foredune phase preserved under the *D6 piscina* northern boundary wall (see below). Excavations by this project during April 2008 discovered the remains of high-status architecture around and between the ponded areas. Three seaward facing vaults were discovered on the northern interior edge of D6, the easternmost pond. A colonnade was excavated on the bank between the two ponds, running parallel to the coast. Possible breeding tanks were uncovered on the northern portion of the inter-pond bank and a series of parallel walls running around the exterior of the ponds were also discovered<sup>30</sup>. Luminescence dating associated with these perimeter walls is further discussed in section 4.9.2.3. The *piscinae* DEM suggests significant alterations to the natural dune and slack topography during the construction of these features, with at least 3 areas of infilling required to form the outline of the ponds (figure 4.6). The modification of a natural dune slack is proposed based on the ponds' position in the progradational history of the dune ridge sequence and contextualised by the diatom palaeoenvironmental record. Conditions similar to a mature dune slack develop in the pre-*Piscinae* slack between 2335 – 2208 ± 40 BP. The northern boundary wall is constructed on a dune ridge formed ca. 2.25 ± 0.16 ka BP, with a similarly timed remobilisation phase (2.27 ± 0.16 ka BP) recorded from the lee side of the youngest red dune / delta sediment dune (CP07/15 & 14, respectively) some 550 m inland of the *Piscinae*. The seaward dune ridge – which is problematic to date due to a complex series of remobilised aeolian phases burying highly disturbed Roman wall rubble – dates to at least 1.9 ± 0.3 ka BP. Burial of this seaward wall occurred in at least 3 phases, but notable is the phase dating to 1.6 ± 0.12 ka BP, which is coeval with a major phase of inundation over a large portion of the *Vicus Augustanus* (see below). The DEM shows several mounds of sand on the western seaward corners which are probably partly remobilised and/or spoil heap deposits. If these mounds are remobilised sand from the predominantly westerly winds then a mechanism for their deposition on the seaward side of the ponds must exist, such as obstacles or structures to stabilise around. An alternative explanation is that they are *in situ* remnants of the contemporary foredune. Unless stabilised by sufficient vegetation their rapid erosion would however seem likely.

The preservation of earlier silts and peaty material, dating from 2403 ± 40 BP cored from the base of the *D6 Piscinae* (- 1.25 ± 0.2 m RSL) suggests that excavation of these ponds was not undertaken to this depth. The age model and sediments from this sequence do not show any clear evidence of a hiatus or 'occupation' layers. Diatom analysis from this cored material provides an age-modelled sea level during the early phases of construction at Castelporziano of - 1.066 ± 0.2 m RSL comparable to other nearby estimates from Roman *Piscinae* (Lambeck et al. 2004b). This provides a quandary. As the sediments at the base of the *piscinae* were not removed and are around 300 years older than the beginning of construction on the site, the baseline water depth in the pond was at least 15 cm. The diatom record for

---

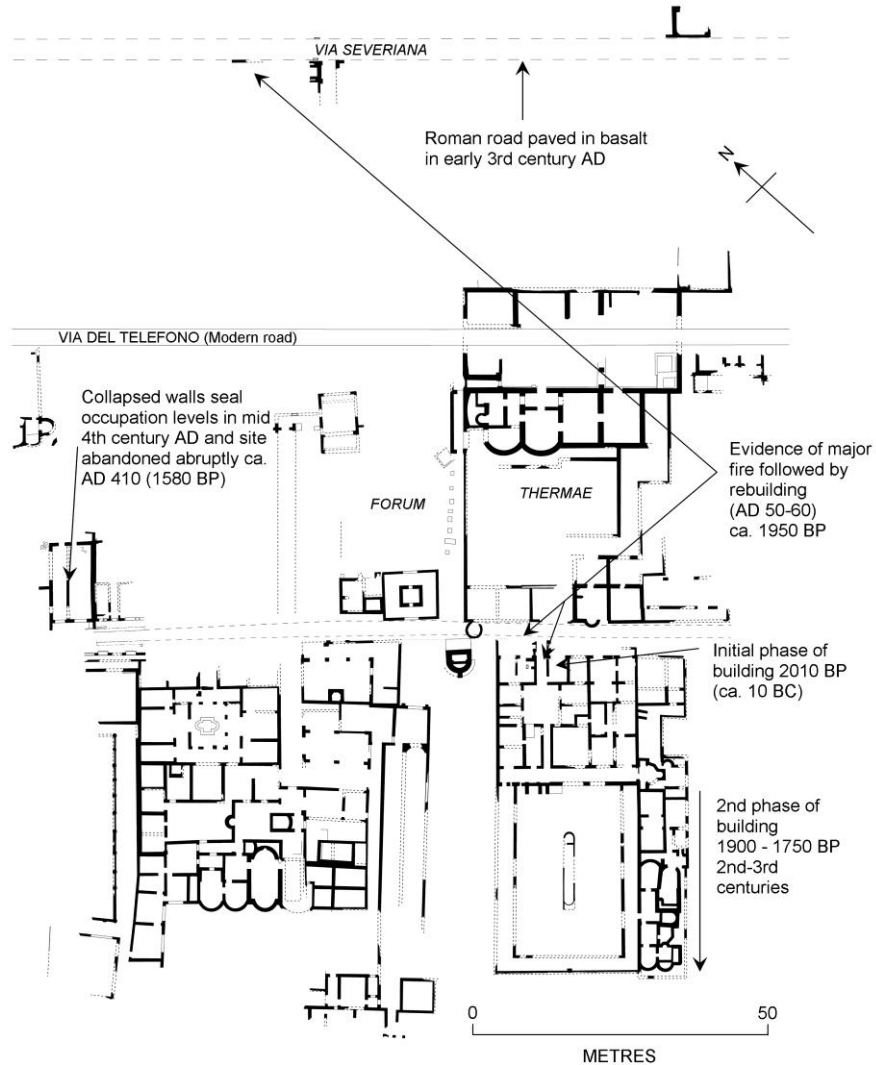
<sup>30</sup> <http://www.rhul.ac.uk/Classics/LaurentineShore/ASSETS/PDF-files/Tim%20Evans%20Castel%20geophys%20report%20April%2008.pdf> Magnetometry field report (last accessed 15/09/2009).

the basal sediments above the sea level are all fresh to weakly-brackish species characterised by planktonic diatoms indicative of a water column. This is also logical with the position of the ponds in the dune slack adjacent to the Roman beach. The water-logged organic-rich sediments, geochemistry and diatom taxa indicating a mature dune slack environment developed by 2208 BP suggest that water levels were at least 25 cm above Roman sea level prior to construction. However this water depth is filled by peaty sandy sediments. Columella in his instructions for building inland *Piscinae* just above the level of the sea suggests excavating to a depth of 2.65 m with connective channels to the sea 59 cm from the top, ensuring that the pond's water level is around 1.18 m below the top of the pond (Higginbotham 1997). A water depth of around 1.5 m is inferred. During the excavations of the D6 *Piscinae*, a lead pipe was discovered in the tumbled remnants of an interior wall built around the wet area of the pond. The installation of systems for allowing the periodic draining and cleaning of the pond's was also a key feature (Higginbotham 1997). A truncation of sediment accumulation is not clearly observed at Castelporziano which suggests that a palaeoenvironmental record of their use could exist in the sediments. Planned management of the ponds hydrology with freshwater also seems likely. However, the ponds do not appear to have been commissioned prior to their abandonment. The archaeological evidence suggest they were abandoned by around 1900 BP which is in agreement with phases of remobilised aeolian sand around the seaward perimeter wall from ca. 1943 ± 299 BP.

#### **5.6.6. *Vicus Augustanus* (2010 – 1580 BP)**

The *Vicus Augustanus* displays 2 phases of construction beginning around 2010 – 1950 (figure 5.17). It has been suggested that following a major fire at the *Vicus Augustanus* between 1950-1925 BP (AD 50-75) a rebuilding effort was undertaken at a higher level and closer to the sea (pers. comm. Prof. A. Claridge). The second building phase, on the seaward side of the initial complex, is recorded between 1750 – 1900 BP (Rendell et al. 2007) (figure 5.17). Underlying sand from beneath the first phase of the *Vicus* is dated to 2050 ± 240 (Rendell et al. 2007) around 950 m inland of the current shoreline. This date is in good agreement with another abutting-wall sample (CP04/1, 2034 ± 146 BP) and inland primary dune ridge (CP03/2, 2073 ± 144 BP) that describe a coeval coastal plain at least 350m wide. Elevated building sites are provided by the dune ridge topography of at least 2-3 m above the contemporary Roman period sea level. As discussed above the *Vicus Augustanus* and observed at other major sites within the Estate the extent of the buildings plots is far larger than the usual 50 m dune crest width out-with the intervening dune slacks.

**Figure 5.17:** Plan of the *Vicus Augustanus* (adapted from Rendell et al. 2007). The shoreline is at the base of the map.



Significant progradation is clear prior to the Roman occupation. This date, within errors, is also in agreement with the transect 1 age model for samples from this position inland (figure 4.43). The dating of dune ridge formation after this period until 1.6 ka BP is hampered by several phases of remobilised dunes and aeolian deposits obscuring primary dune formations. In the vicinity of the Vicus, remobilised material from ca. 1.6, 1.37 (this study), and likely at 1.15 ka BP is recorded (Rendell et al. 2007); the lesson is that primary dune ridge formation is not easy to discern in the field. A key constraining factor is that archaeological remains are not found further seaward of this recorded series of buildings.

This relationship dates the minimum shoreline position at 830 m inland to 1750 BP, which again is in good agreement with the transect 1 age model.

Whether or not a shift in shoreline was directly *experienced* by the Roman population is dependent on the timing of episodic delta progradation; data not recorded by the inter-dune long-term average progradation rates. Relative sea level rise during the settlement of the *Vicus* was on the scale of centimetres so an increase in accommodation space is unlikely to be a mitigating factor for shoreline advance on the decametre-scale. As has been previously discussed, sediment supply to the site is driven by the sediment load of the Tiber River. During the 1<sup>st</sup> centuries BC and AD (2100-1900 BP) it has been shown that high-magnitude floods within the lower Tiber catchment at Rome increased significantly (Figure 5.2). An increased sediment supply during flooding of the Tiber River ca. 2000 BP is argued to drive a positive sediment budget on the delta beaches, leading to progradational beach topography.

Within this geomorphological context integrating the archaeological data is useful for assessing possible impacts upon the coastal settlements and their occupants. Based on the 70 m distance between age estimate of the first phase of the *Vicus* (2010 BP, which is in good agreement with luminescence date CP895 from sediment lying stratigraphically below (Rendell et al. 2007)), and the minimum age estimate for the dune ridge coeval with abandonment of the *Vicus* in the 5<sup>th</sup> century, i.e. 1510 BP (CP07/25), an average progradation rate of 0.14 m/yr is derived for the period during the occupation of the *Vicus Augustanus*. Assuming that progradation was a low-level, and relatively constant process, this suggests that shoreline advance was not of concern on yearly timescales but is observable on decadal to multi-decadal time-scales; at least during the lifetime of an individual witness.

During the occupation of the first phase of the *Vicus* (2010-1950 BP), an estimated progradation of 8 m occurred. During the longer second phase (1925-1580 BP) an estimated 48 m of progradation occurred. This progradation records the long-term sediment budget flux to the shoreline. The expression of dune progradation is dependent upon positive sediment budgets in both the beach and foredune (Miyanishi & Johnson 2007) (see section 5.1.2). The presence of the relict dune ridge betrays a reduced sediment supply and transition to negative beach and positive dune budgets driving either foredune aggradation or inland overwash; the latter being more problematic for Roman coastal settlements. What is certain is that the dune ridge coeval with the abandonment of the archaeological sites along the Laurentine Shore at Castelporziano (and also the collapse of the Roman Empire) formed upon a beach that was around 70 m seaward of the initial Roman coastal settlement (5.18). The discrepancy between building plots from the first phase of the *Vicus* settlement and the second is also around 70 m (pers. comm. A. Claridge, 2009) suggesting a human response to shoreline progradation can be inferred.

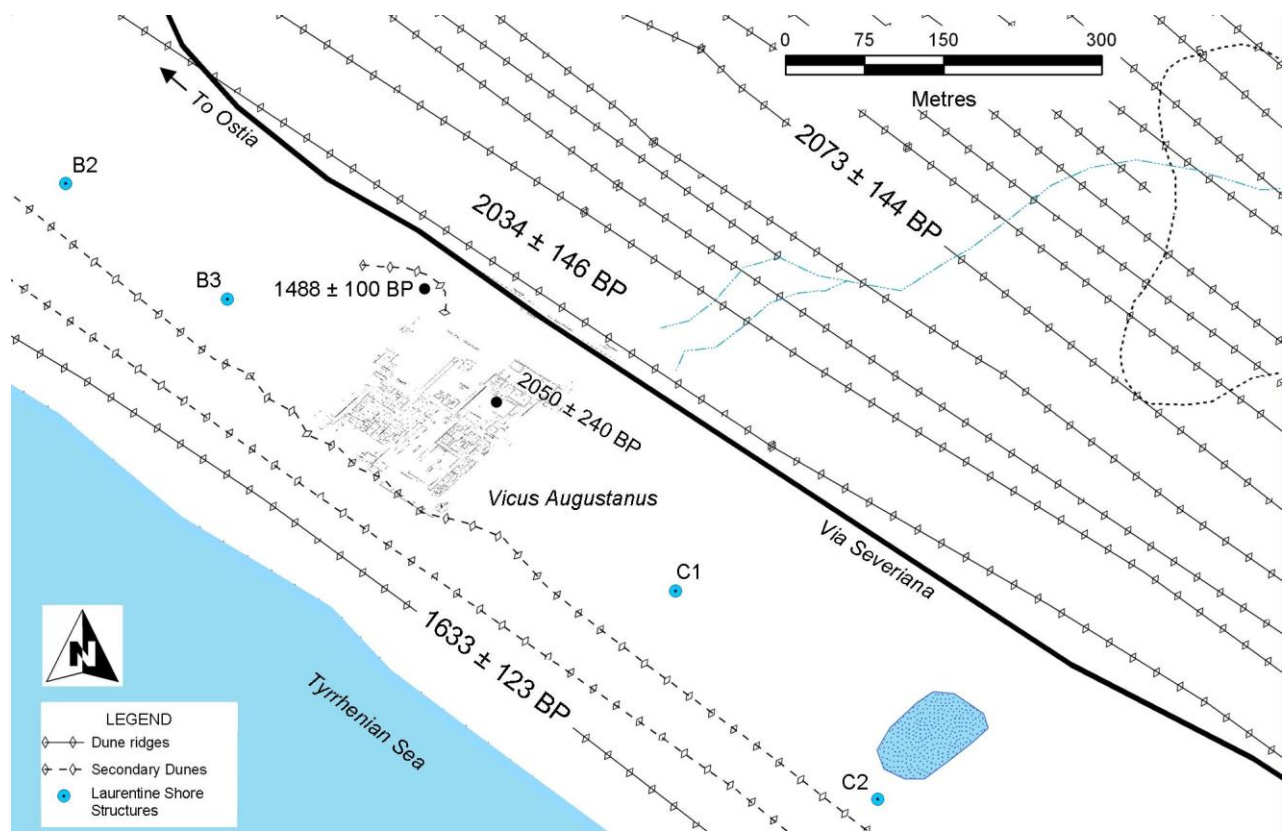


**Figure 5.18:** Post-abandonment reconstruction of the *Vicus Augustanus* ca. 1600 BP.

Further high-resolution work could be targeted on understanding the impact of decadal-scale progradation during the Roman occupation of the shoreline. Whether or not the ground beneath the second phase of the Vicus existed whilst the first phase was occupied is a key question, but requires a specific sampling strategy. The ability of luminescence chronology to precisely date (within accepted centennial error bars) such rapid and spatially defined processes is also a key consideration.

### 5.6.7. The Severian-period sea wall and storms

The key archaeological marker of sea level on the Laurentine Shore is the well-preserved remains of a sea wall (F2) (figures 5.19, 5.20 and 5.21). The archaeological context and building style suggest construction during the 2<sup>nd</sup> century AD. The structure is around 3 m high above modern sea level, confirmed by repeat D-GPS measurements. The face of the wall displays severe wave damage and a tidal notch running along the preserved length. The exterior moles are badly damaged and are preserved as tumbled stumps of masonry. The overall construction is a concrete and rubble core faced in brick. Erosion of the brick edges suggests a strong directionality of tidal force, predominantly from the west. The bricks in the central slipway display light to no wear on the edges of the bricks, whereas this becomes much more pronounced towards the NW mole. Substantial force has been concentrated in the NW interior corner, causing massive damage to the structure. It is hypothesised that this is due to wave refraction around the NW mole (breakwater) focusing the westerly wave energy at this point on the wall (Plate 5.1 and figures 5.20 and 5.21).

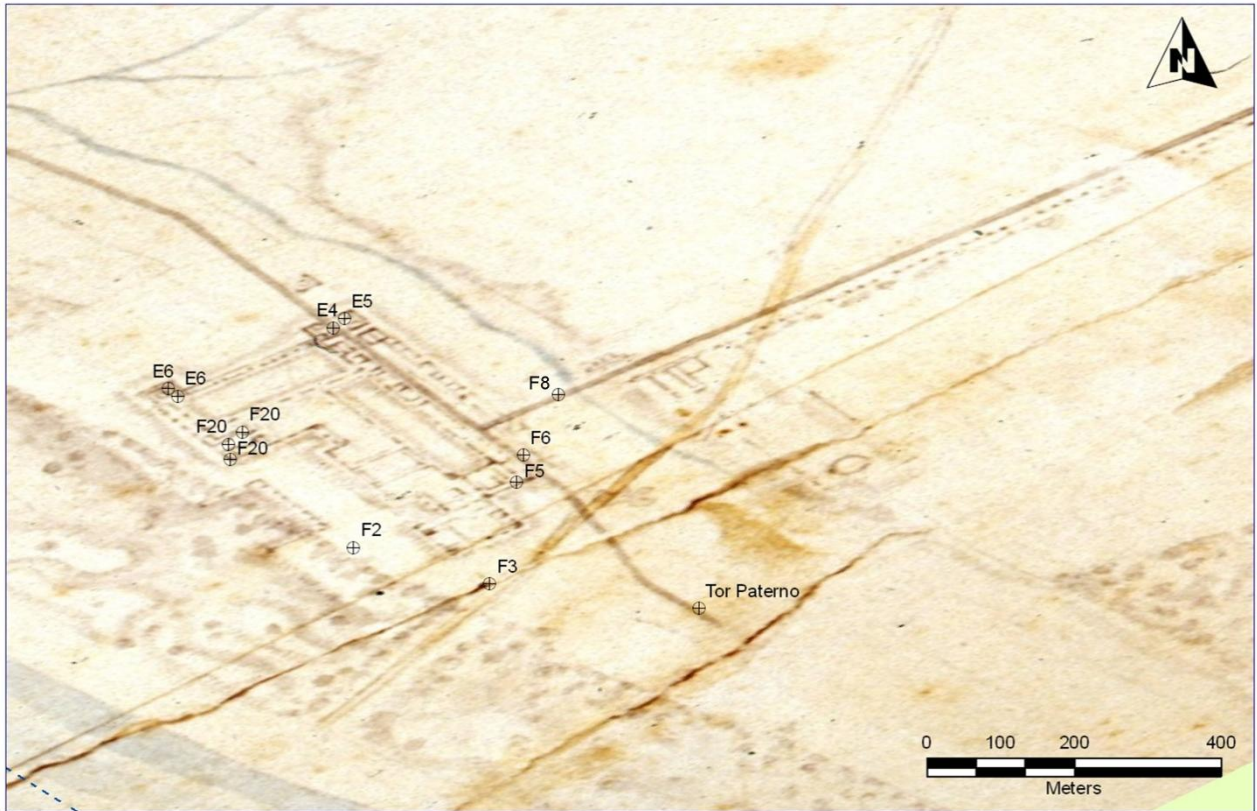


**Figure 5.19:** Georeferenced detail of 1903 archaeological map by Pietro Rosa<sup>31</sup>. The GPS location of the sea wall (F2) is further SE than mapped here a century ago. The trident form of the sea wall is recorded between structures F2 and F20. However the general proportions of the Imperial Villa (here shown with GPS positions of external structures) is relatively accurate. Similarly the villas connection with the *Via Laurentina* (F8) leading directly to the NW and linking to *Lavinium* and *Ardea* in the East is roughly accurate.

<sup>31</sup> [http://www.rhul.ac.uk/Classics/LaurentineShore/MaritimeFacade/MF\\_Maps.html](http://www.rhul.ac.uk/Classics/LaurentineShore/MaritimeFacade/MF_Maps.html) (last accessed 15/09/2009).

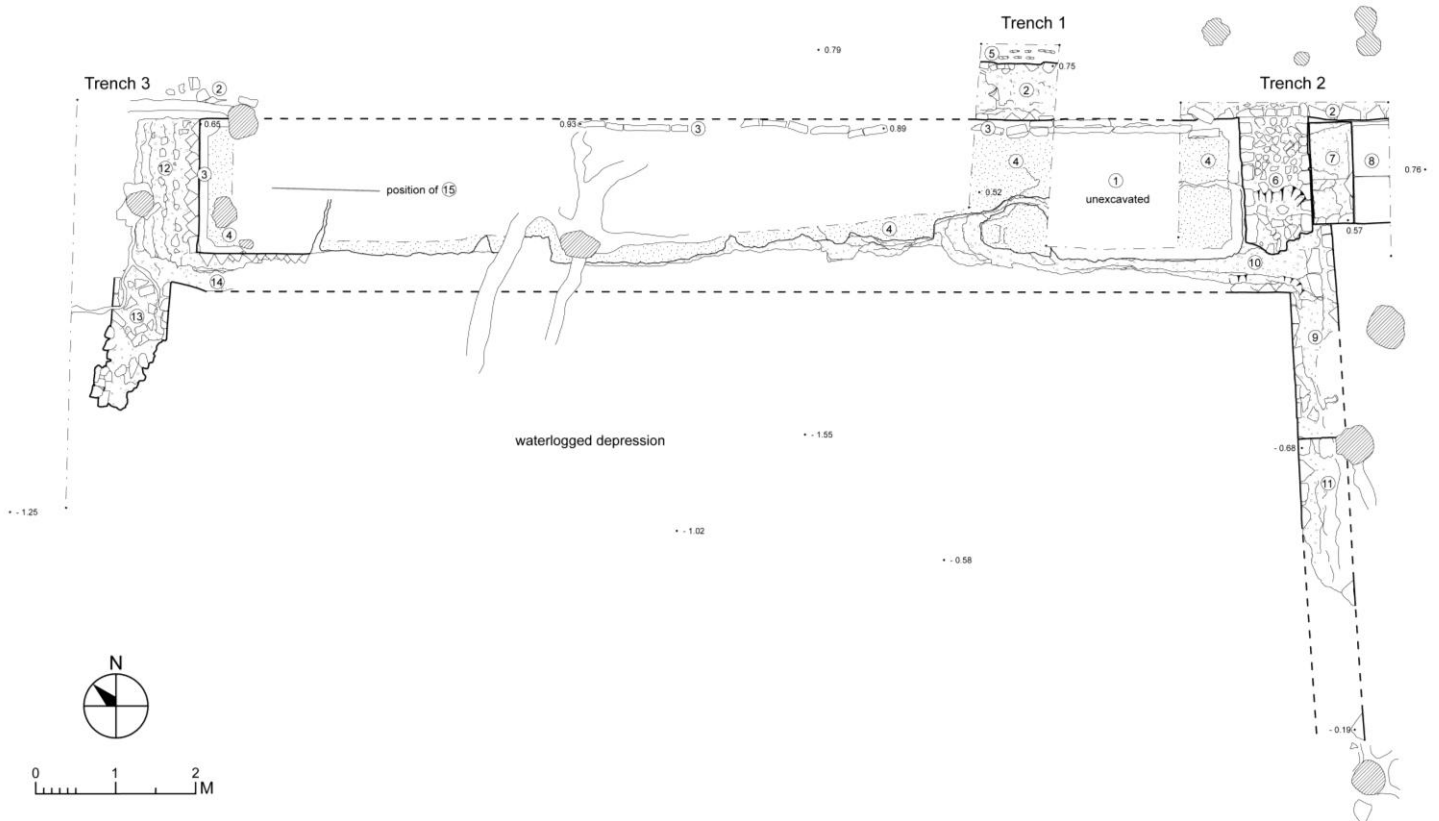


**Figure 5.20:** Plan of investigated area of sea wall (F2), northwest portion, the sea is to the base of the image. The remains of moles (breakwaters) are preserved at the distal ends of the structure with a much larger mole or perhaps slipway in the centre (on the right of this image). This layout is repeated in mirror-image with the axis of symmetry on the right-edge of this plan, forming a trident structure. The central part is obscured by a later blowout developed from the subsequent dune ridge. The waterlogged depression which is now the slack of the subsequent dune ridge phase is seasonally flooded. It is inferred that due to the position of this structure and the wave damage visible in section (Plate 5.1), that this structure was open to the sea during the period of use. The wall is capped by a rectangular water-proof *Opus signinum* tank potentially for use as an ornamental pond for fish or plants. The wall shows reconstruction on several occasions; the re-facing of the seaward aspect being a significant repair phase (Illustration by J. Andrews, 2009).

**Plate 5.1:** Sea wall looking north. Wave energy is concentrated heavily on the NW interior corner. The waterlogged depression in front of the wall is partially filled with aeolian sand and rubble. A small wave-eroded pillar is the only thing preventing the mid-portion of the wall from collapsing under the weight of the mature Holm oaks now growing out of the ornamental pond. The badly damaged NW mole (breakwater) is visible on the extreme left of the image as a low tumble of masonry delineated on the exterior face by extensive tree-roots.



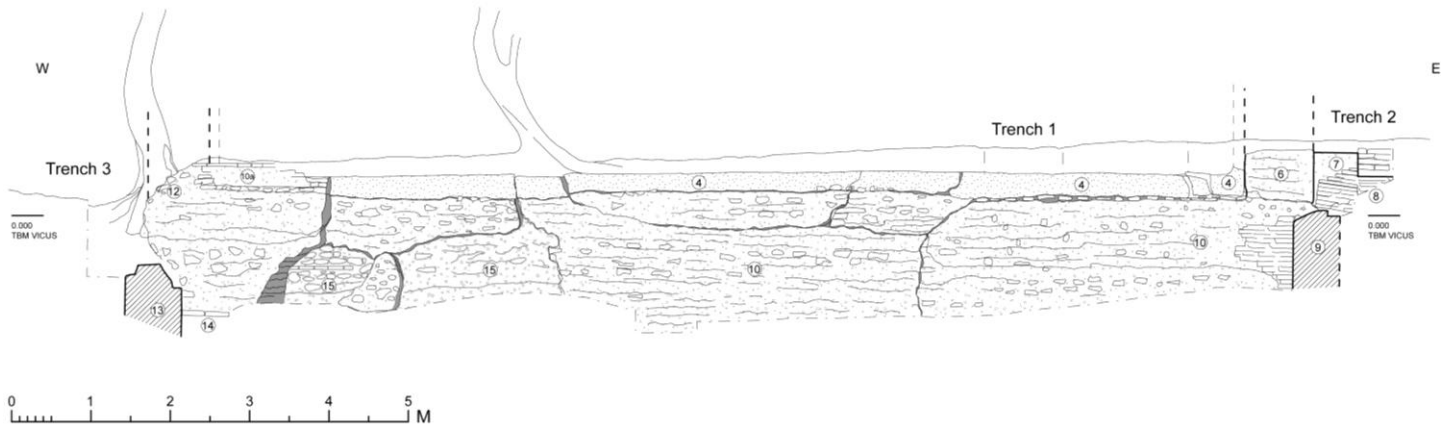


**Figure 5.21:** Western portion of sea wall, elevation looking NE. Lower limit of drawing is defined by upper limit tidal damage. The remnants of the northern and central moles can be seen in cross-section (9 & 13). At least 3 phases of construction are represented. Substantial damage focussed in the NW internal has exposed the earliest phase (15) which is refaced by (10). The ornamental tank (4) is well-preserved capping both these phases of construction. Further reconstruction or later building phases is suggested on top of the central mole (Illustration by James Andrews, 2009).

Following repeat D-GPS measurements (n=4) in a clearing adjacent to the structure both levels and total-station points were orientated against this base-point. The sea wall GPS base-point is measured at  $2.024 \pm 0.02$  m RSL. Levels taken from this basepoint record an average notch height of  $+1.795 \pm 0.25$  m RSL (n=3). Using the biostratigraphic sea level marker derived from the *Piscinae* diatom record ( $-1.25 \pm 0.2$  m RSL at  $2425 \pm 40$  BP) and an estimated linear rate of sea level rise of 0.5 mm/yr, a local estimate of sea level during the 2nd century AD (1900 BP) is ca. - 0.98 m RSL. Thus the tidal notch lies around 2.8 m *above* the Roman period sea level. Clearly this erosion is not caused by the average tidal conditions and is anomalously high even for modern tidal ranges of the Mediterranean. It is hypothesised that this tidal damage may be caused by more extreme events.

Short duration high-magnitude events are not likely to be preserved explicitly in palaeoenvironmental records. Although significant “above modern sea level” variation is displayed in sea level markers partially derived from the Italian coastline (Lambeck et al. 2004a), these records are typically poorly dated coastal peats and their direct relationship to sea level cannot be confirmed (Figure 5.22).

The substantial height of the notch above the micro-tidal range of the Mediterranean Sea (~ 40 cm) suggests a significant wave height and also a significant exposure time to this erosive energy. Storms in the Tyrrhenian Sea have been shown to reach high wind speeds in the vicinity of Castelporziano (Zecchetto & Cappa 2001). One measured example is a south-westerly *Libeccio* wind storm funnelled through the Strait of Bonifacio on the 30<sup>th</sup> December 1994 (Figure 5.23). The creation of a gyre off western central Italy produced wind speeds of up to  $14 \text{ ms}^{-1}$  adjacent to the site. Other extreme events have been noted by Speranza et al (2004), suggesting that wave heights during storm events of a similar height to the sea wall tidal notch can be experienced for at least 24 hours (Figure 5.24). Within this contemporary context this mechanism of erosion linked to extreme storm events is tentatively proposed.



**Figure 5.22:** Holocene sea level markers from global and Italian records (Lambeck et al. 2004a). Terrestrial markers are typically peat deposits formed in coastal water-logged environments. Marine data is derived from biostratigraphic records such as biologically encrusted speleothems and tidal notches. Transitional markers are for examples beach rock formations, *Piscinae* and sedimentary couplets such as investigated within this study.

REMOVED TO COMPLY WITH E-THESIS GUIDELINES

REMOVED TO COMPLY WITH E-THESIS GUIDELINES

**Figure 5.23:** The spatial structure of a Libeccio storm wind during the 30<sup>th</sup> December 1994 recorded by the ESR-1 scatterometer (Zecchetto & Cappa 2001). The resultant gyre formed by the funnelling of the wind through the Strait of Boniface between Sardinia and Corsica produces wind speeds of around 14 ms<sup>-1</sup> in the vicinity of Castelporziano. As a proxy for high-energy storm conditions affecting the Castelporziano coastline, these kind of extreme events are tentatively proposed. Castelporziano is highlighted.

REMOVED TO COMPLY WITH E-THESIS GUIDELINES

**Figure 5.24:** Wave data from the Ponza buoy tethered offshore to the SW of Gaeta (Speranza et al 2004). Sea wave heights of similar magnitude to the tidal notch carved into the Castelporziano Roman sea wall (ca. +2.795 m Roman SL) are observed for around 30 hours during this prolonged storm. The effects of this storm at the coast however are unknown. The extreme wave heights within a Tyrrhenian Sea context suggest that tidal notch preserved at Castelporziano has at least some contemporary context.

Localised tectonic uplift is not thought to be a likely mechanism for this discrepancy. Suggested uplift rates for the Tiber Basin of 0.15 mm/yr (Lambeck et al. 2004b), would only account for around 28.5 cm of vertical displacement. Furthermore, metres of significant localised uplift are not visible on the site confirmed by the independent high-quality GPS measurements underpinning the reconstruction. Referencing of the archaeological survey datum located within the *Vicus Augustanus* during the sea level calculations for the *Piscinae* sedimentary marker show that this datum conforms to the top of the sea wall suggesting stability between the *Vicus*, *Piscinae* and sea wall.

#### **5.6.8. Villae & coastal infrastructure**

Foredune mapping has clearly shown the preservation of a post-Roman phase dune ridge from Tor Paterno to Castel Fusano. All major archaeological sites are associated with a position either on or inland of the Roman-period occupied position which can be traced intermittently along the palaeo-shoreline delineated by the succeeding preserved dune slack. There are a wide variety of structures ranging from several bath houses, large villa complexes, a possible wharf associated with the sea wall and the remains of a shorefront *porticus*. In addition to the second, seaward phase of construction of the *Vicus Augustanus*, it has been postulated from excavated remains that a second phase of foundations for the *porticus* on the northern side of the *Vicus*, was reconstructed around 1 m seaward of the original foundations. The *porticus* is a recreational building providing a covered walkway. Within the progradational history of the Roman period, this reconstruction of a significant building purely for recreational purposes can be understood and suggests that human responses to shoreline change involve considerable effort. Parallels between expensive modern beach management for aesthetic value and tourists could be made.

#### **5.6.9. Possible inlets and harbour**

A harbour is discussed on the site in historical and archaeological sources, in the vicinity of *Tor Paterno*. Digitisation of the Italian topographic map has provided the locations of a number of ponded areas preserved in the modern topography; however they may be a legacy from the first edition maps from the late 19 century. The shoreline in figure 5.25 is based on GPS field mapping of relict dune ridges. One such pond area has a compelling relationship with the Laurentine Shore coastline of ca. 100 AD and the Imperial Villa complex and Tor Paterno. Partly due to the modern road construction linking Tor Paterno with the Via Litoranea boundary fence, this wet area was not obviously preserved

during field survey. The disordered *tomboleti* dunes that characterise this area of the coastline also present difficulties in the field for discerning the sequence of the geomorphology.

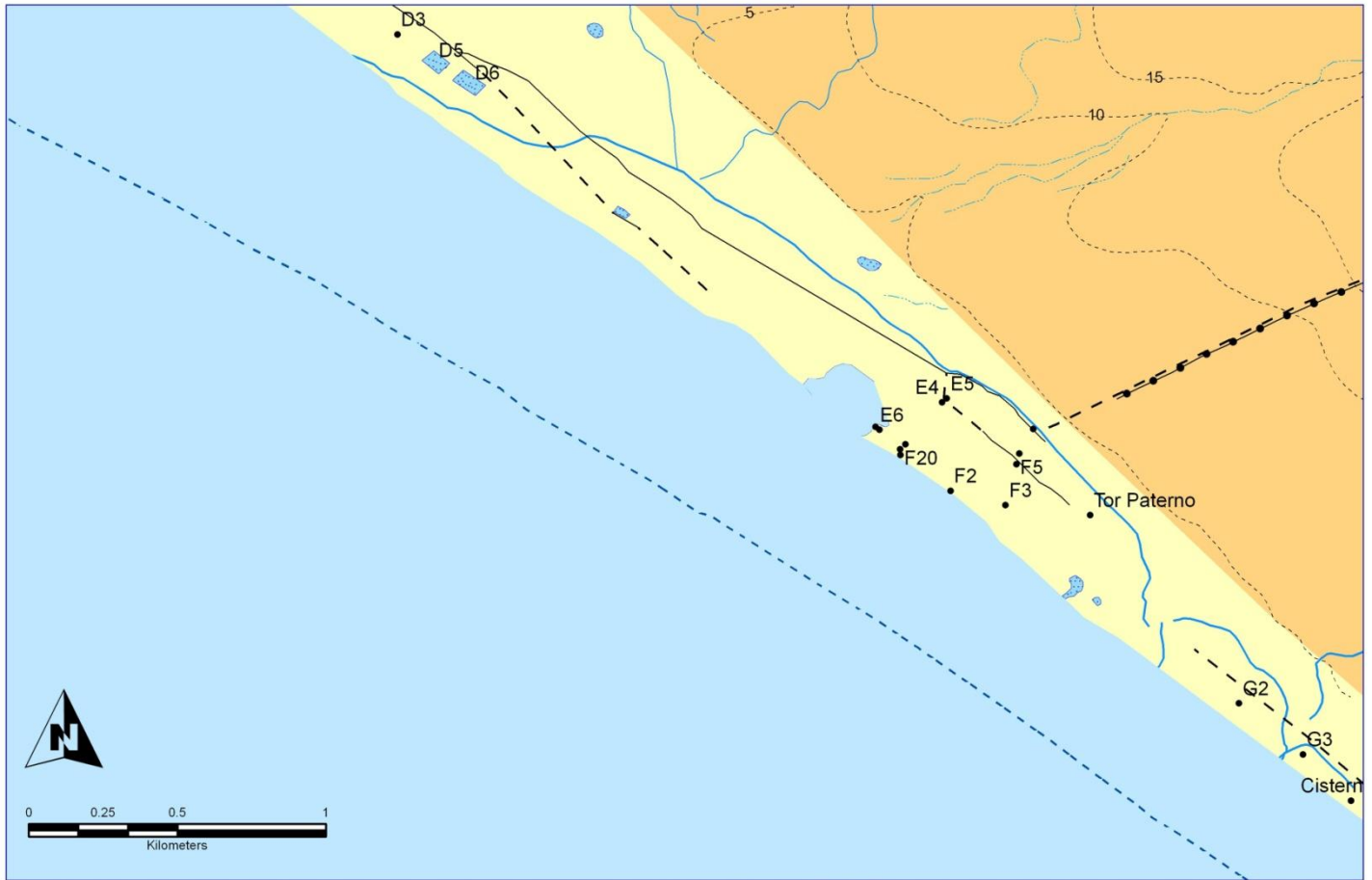


**Figure 5.25:** Detail of key Roman period hydrological features. Site codes refer to Lauro and Claridge (1998). The largest of these features lies towards Tor Paterno in the south of the site. E6 and F20 are bath houses constructed behind the contemporary beach associated with the Imperial Villa shown in Figure 5.19. This large wet depressed feature abuts this Roman period beach front. Further intensive sampling of this location may confirm the GIS-led hypothesis that this relict depressed area may have been an inlet during the Roman period. The inflection of the contour lines inland of this position may betray the position of an earlier drainage pattern, perhaps down-cut during the late Pleistocene. This possible inlet may be a relict form of the now ephemeral drainage pattern. F2 is the Roman period sea wall exhibiting extensive wave damage, strongly suggesting this shoreline reconstruction is accurate.

Due to the progradational nature of the shoreline, the complete infilling of coastal inlets and harbours is highly likely. However, the site transect, (Figure 5.25) shows the close proximity of the late Holocene topography to modern sea level. The *Piscinae* and the slack directly in front of the Roman sea wall are seasonally flooded low-lying slack areas, preserving *in situ* evidence of their proximity to the palaeo-shoreline. The dune ridge and slack morphology is dominant, so any deviation from this repeated geomorphic pattern may be significant. During field-survey of the site, several low-lying areas were identified associated with the Roman-period dune-ridge position. The height of these wet

areas is noticeably lower than the elevation of the slack subsequently formed over the Roman period beach. Detailed topographic survey was not possible, but the areas of interest were recorded by GPS and are visible in the multi-period AP record. Again the difference in forest canopy species and height is reminiscent of other hydrological features on the site (section 4.2.2.1). As a working hypothesis, other similarly low-lying and wet areas with an association to the Roman palaeo-shoreline may have existed during that time. A large sand hill, 10-15 metres higher than the surrounding topography, now obscures the central part of this area. A future research aim would be a detailed examination of these features and associated Roman-period structures to identify the relationship with the Laurentine Shore. D-GPS georeferenced topographic survey and diatom analysis of dated short-cores would provide an accurate assessment of past hydrological conditions and relationship to Roman-period sea level. Diatom analysis in particular would clearly determine an open connection with marine water. Sedimentological analysis of 'harbour' parasequences may also be diagnostic (Marriner & Morhange 2006). A similar approach may also be productive in front of the sea wall (see Plate 5.1).

During the excavation of the southern boundary wall of the *Piscinae*, an indurated surface containing frequent ceramic fragments, concrete nodules and other detritus was uncovered. The sloping surface abuts the boundary wall. The close proximity to the Roman-period coastline led to the suggestion that this feature could represent a makeshift slipway. Around 200 m alongshore of the possible inlet discussed above a more substantial construction lies unexcavated in the centre of the 3-pronged sea wall structure towards Tor Paterno. A wharf (or possible ramp) several metres wide extends into the Roman-period Tyrrhenian sea for at least 5 metres from the centre of the sea wall. This structure is only suitable for harbouring small, inshore boats, perhaps for fishing or unloading larger vessels. An additional hypothesis is that *this* is the 'harbour' at Tor Paterno referred to in historical documents.

#### **5.6.10. Roman-period hydrology and water supply**

A major water supply to the southern Laurentine Shore was established by the completion in the 1<sup>st</sup> to 2<sup>nd</sup> century AD of an aqueduct running adjacent to the *Via Laurentina* between *La Santola* and *Tor Paterno*. Partly subterranean and partly raised, this structure currently represents the most obvious engineering solution for fresh water supply to the Laurentine Shore (Lauro & Claridge 1998). A network of buried pipes distributing water along the coastline has been hypothesised as remains have not yet been discovered. Certainly a substantial water supply is required to support the many bath houses and high-status villas on the Laurentine coast as well as potentially regulating the hydrological conditions within the constructed *Piscinae*. Lanciani<sup>32</sup> discusses the Roman's predilection for bathing in sea water, not on the open coast, but heated in bath-houses. At least 3 bath-houses are described within the *Vicus Augustanus*, two marble-clad *thermae* lie adjacent to the Roman shoreline (E6) and (F20) (and have been located within the geomorphological survey conducted for this thesis) with a further bath house near to the *Villa del Discobolos*; also

---

<sup>32</sup> <http://www.rhul.ac.uk/Classics/LaurentineShore/ASSETS/PDF-files/WANDERINGS%20IN%20THE%20ROMAN%20CAMPAGNA.pdf>

individual Villas likely had their own private bathing facilities. With the reconstruction of the Roman period shoreline presented here, it is clear that the open sea was a few tens of metres from any of the coastal buildings. The proximity of plentiful groundwater in the coastal zone is obvious today as are ephemeral stream channels, but flow is seasonally variable. The younger Pliny in his letter to Gallus describes plentiful fresh groundwater. “*Nothing is wanting to make the Laurentinum perfect but spring water, although one is always sure to find drinkable water a few inches below the level of the sands, fresh enough in spite of the proximity of the sea*”<sup>33</sup>. Shallow wells are also a notable feature of the archaeological record around *Portus* to the north (Keay 2005). Ponds and wet slacks are a key component of the geomorphological record preserved within the Castelporziano Estate. It is argued that a natural water supply was not lacking for the substantial bathing infrastructure, but may have been seasonally unpredictable. Management may have been required to avoid use outstripping availability during the drier months. The current groundwater is around pH 8 and is high in calcium carbonate and other minerals due to early vadose diagenesis. An alternative interpretation is that the natural water supply was simply not to taste as the younger Pliny implies.

#### 5.6.11. Connections to the wider Roman Empire

The most notable remains of connectivity within Castelporziano are the remains of the *Via Severiana* and *Via Laurentina*. These roadways link the southern Laurentine Shore to *Ostia Antica* and *Portus* in the north, *Lavinium* and the south, and more directly to Rome via ancient routes past *Malafede* and *La Santola* inland of *Tor Paterno*. Lanciani describes 4 roads linking Pliny’s villa to the wider Roman world although the villa that bears Pliny’s name now situated in Castel Fusano could be applied to the *Grotte di Piastre* to the south of the *Vicus Augustanus*, as Pliny’s description states his modest villa is separated from the *Vicus* by only one villa. In any case, the *Vicus Augustanus* lying on the *Via Severiana* is linked to Rome by the *Via Ostiensis*, *Via Laurentina*, *Via Laviniatis* and “a cross lane through the *Ager Solonius* (Castelporziano)”<sup>34</sup>. The latter 3 and their relationship with the shore parallel *Via Severiana* are sketched on Lanciani’s map from 1903. Aerial photography and field survey have detected partial routes for *Via Severiana*, *Via Laurentina* and *Via Laviniatis* which is obscured by the inland boundary of the Capacotta Estate and modern road. The route running between the label *Eundus procilianus* running from *Tor Paterno* (a major hub for these ancient routes) towards Rome follows closely the route of the modern estate road connecting *Tor Paterno* and the *Castel Porziano* and is the cross lane described by Lanciani (figures 5.26 and 5.27). A partial reconstruction based on the currently available evidence is presented in (Figure 5.28).

---

<sup>33</sup> Translation by Lanciani, p324; Wanderings in the Roman Campagna. Online at <http://www.rhul.ac.uk/Classics/LaurentineShore/ASSETS/PDF-files/WANDERINGS%20IN%20THE%20ROMAN%20CAMPAGNA.pdf> last accessed, 14/08/2009.

<sup>34</sup> Lanciani p307.

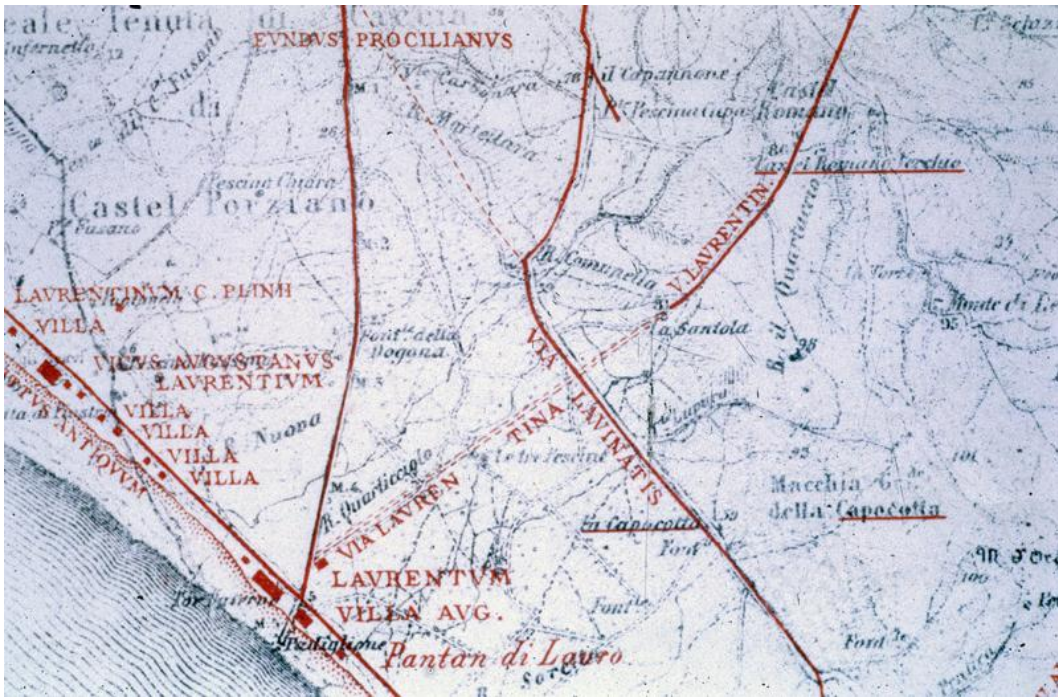


Figure 5.26: Reconstruction of the Laurentine Shore by Rodolfo Lanciani (1903) focusing on Tor Paterno in the SE of the Castelporziano Estate.



Figure 5.27: Detail of Laurentine Shore between Tor Paterno and Castel Fusano (Lanciani, 1903). An additional route connecting the Vicus Augustanus to the Via Laurentina is suggested running inland, however archaeological confirmation is forthcoming.

Evidence for a linking road suggested by Lanciani (1903 – see footnote 35) to the Via Laurentina (Figure 5.26 and 5.27) is sparse on the ground. Modern access tracks into the forest criss-cross the site making detection of ancient routes problematic. Faint traces in the 1954 aerial photography define what appears to be an ephemeral stream track within the sparsely vegetated coastal area following an earlier forest fire rather than a road. However, the path of this feature is meandering and braided, suggesting a fluvial origin. Further survey and remote sensing could potentially resolve the existence of such connections.

Better preserved connections exist between Castelporziano, Castel Fusano and *Ostia* thence to *Portus*. The route of the Via Severiana extends along the coast towards these key locations that are important hubs linking Rome to the rest of the Empire. *Ostia* was founded following the shift in the Tiber's course around the 4<sup>th</sup> century BC (Meiggs 1973; Giraudi et al. 2009) and was Rome's key river port. *Portus*, developed during the reigns of Claudius and Trajan during the 1<sup>st</sup> and 2<sup>nd</sup> centuries AD, and was the largest harbour in the Roman world directly linking Rome to the Mediterranean Sea (Keay 2005) by the *Via Ostiensis* and *Via Portuensis*. Huge amounts of goods passed through these hubs every day and the impact of sedimentation infilling upon economic activity cannot be underestimated. Dredging was undertaken certainly in the 4<sup>th</sup> century AD (*Ostia-antica.org*<sup>35</sup>).

---

<sup>35</sup> <http://www.Ostia-antica.org/Portus/c001.htm> see references therein (last accessed 14/08/2009).

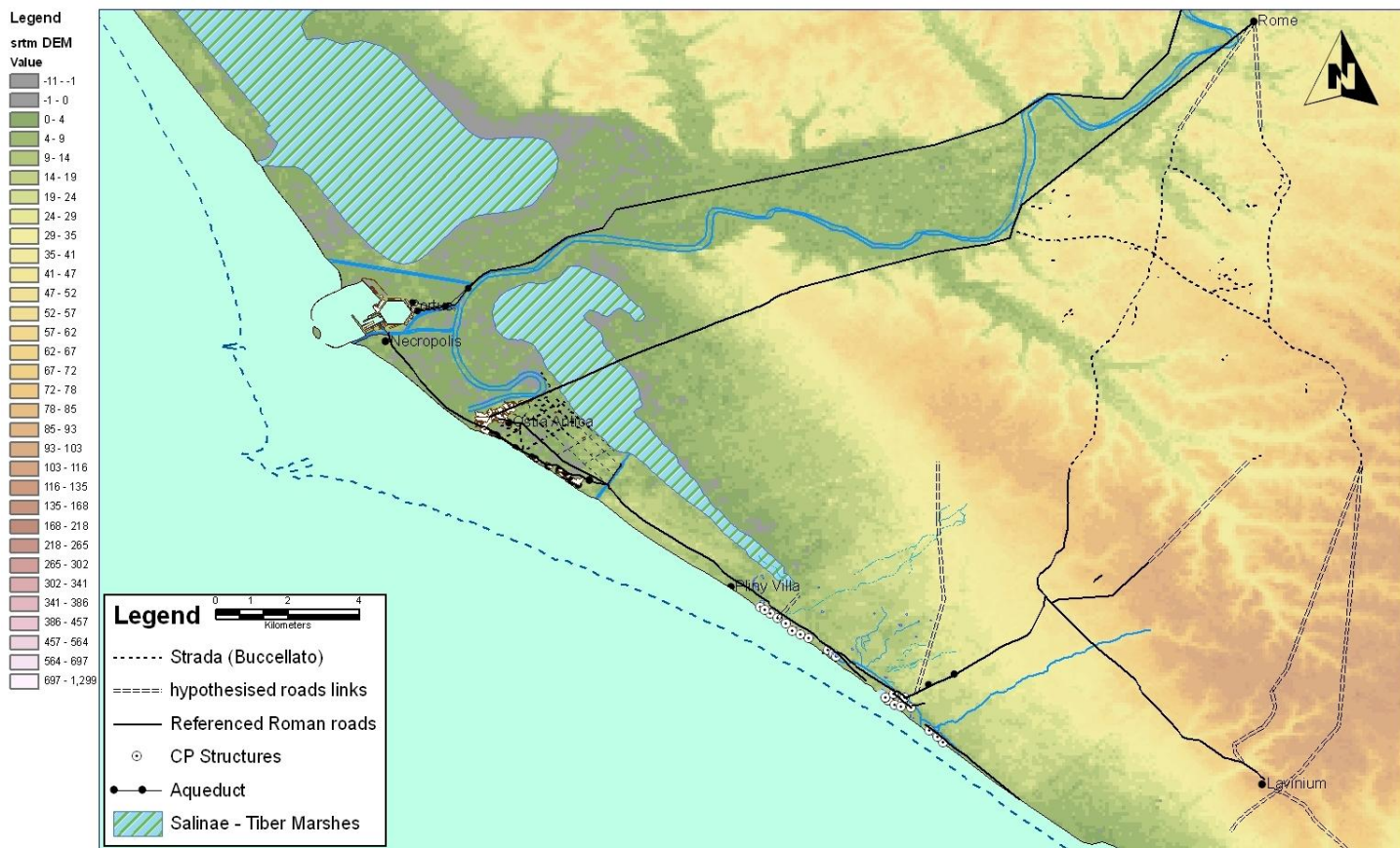


Figure 5.28: Preliminary reconstruction of major road network from available sources around 2000 BP.

### 5.7. The decline and fall of the Laurentine Shore

Excavation evidence from the *Vicus Augustanus* suggests that during the latter period of occupation there was a steady decline in the quality of construction and repair work within the structure of the buildings from the 3<sup>rd</sup> century AD onwards (1800 BP)<sup>36</sup>. The evidence for occupation ceases abruptly around AD 420 (1580 BP) signified by a coin find. Although the minting of the coin is suggested by the date, the final abandonment of the site may be later reflecting the coin's period of circulation and use. During the 4<sup>th</sup> century, a period of increased activity at the *Vicus* and reorganisation of property sizes, there is evidence that building materials were in limited supply as were the skills needed to utilise them. A certain level of recycling appears to have occurred and lime mortar seems to have been in short supply. Maintenance of the *Vicus* street system was undertaken using loose building debris and sand, whilst walls were built with reused tufa blocks and tiles. The lack of lime mortar is shown by a reliance on clay as a bonding agent. Even the mosaics were of recycled material laid in compacted earth<sup>36</sup>. Within the wider Roman Empire, the 5<sup>th</sup> century AD sees

<sup>36</sup> <http://www.rhul.ac.uk/Classics/LaurentineShore/ASSETS/PDF-files/CPIV%20interim%20excavation%20report%20X%20%20SA.pdf> Imperial Vicus excavation report 1995-1998 (A, Claridge).



the widespread collapse of the western Empire. Coeval aeolian burial of the *Vicus Augustanus* and *Piscinae* is recorded by luminescence dating of remobilised sands at around 1600 BP ( $\pm 10\%$ ). This theme is developed below.

### 5.7.1. Aeolian inundation of archaeological buildings

Throughout this chapter the flux in sediment budgets linked to the Tiber sediment supply has been discussed. By the end of the Roman period occupation of the *Vicus Augustanus* in the early 5<sup>th</sup> century AD, the shoreline had prograded around 70 m seaward. A cessation in sediment supply induced a negative sediment budget on the beach and a phase of foredune building had occurred by around  $1633 \pm 123$  BP, delineating the shoreline's position just seaward of this relict dune ridge (figure 5.18). At several key sites on the Laurentine Shore, a coeval phase of remobilised aeolian sand is recorded. A large mound or relict parabolic dune buries the western portion of the *Vicus* ( $\sim 1599 \pm 156$  BP, CP03/3), but also is one of several phases of aeolian inundation recorded on the southern wall of the *Piscina* D6 ( $1592 \pm 116$  BP, CP08/2). These abandonment deposits effectively constrain the Roman period occupation of these sites, in line with coin evidence from the *Vicus* (pers. comm. Prof. A. Claridge).

A further phase of aeolian inundation is recorded at the *Vicus* and *Piscina* D6, at  $1374 \pm 100$  (CP03/1) and  $1312 \pm 93$  (CP08/1), respectively. These locations are 1.5 km apart. Age models suggest the shoreline during 1300-1400 BP at the *Vicus* was around 650 m inland of the current position. Therefore, at least 200 m seaward of the archaeological remains that are buried by the remobilised sand. The dense forest cover observed today suggests that remobilisation in this way is highly unlikely. The modern dense canopy is very effective at inhibiting wind flow. A different vegetation cover may have existed, facilitating inland movements. This assumes that the source of remobilised sand is from the contemporary phase of aeolian activity. If we hypothesise that the sources are from any position on the site (remembering that remobilisation will reset the dating clock of the mineral dosimeters) then we must infer that vegetation cover was not completely suitable for preventing erosion and remobilisation of sand-sized sediment. A reduction in sand-trapping vegetation cover is the simplest explanation. However, this may be linked to a wide variety of natural and anthropogenic activity. The archaeological record on the site suggests that local anthropogenic activity was not substantial; settlements are not recorded during these periods. Sediment supply to the site is relatively reduced until around 700 BP, with the associated reduction in progradation rates indicating a relatively *stable* shoreline position. The form of the dune ridge topography also suggests that sand movement inland of the active foredune is relatively minor. The repeated occurrence of aeolian remobilisation throughout the late Holocene is then a significant event driven by energetic processes that overcome the ability of topography and vegetation cover to prevent the inland movement of sediment. Movements of over a kilometre in substantial volumes are preserved at Castelporziano.

### 5.7.2. Regional climate and aeolian remobilisation

On the macro- to mega-scale, remobilisation during these periods occurs during a lower Tyrrhenian SST phase (Cacho et al. 2001), indicating cooler/wetter terrestrial air conditions (Silva et al. 2006), during the so-called Dark Ages Cold

Period. Aeolian activity is not generally associated with these trends, and increasing stability would be inferred. However some authors have discussed a more complex relationship between late Holocene periods of climate change and aeolian activity (Graham et al. 2007). Clarke and Rendell (2009) argued that during the LIA and similar cooler/wetter periods dune activity in coastal areas occurred due to increased storm activity. Aagaard et al (2007) have shown that during the LIA, sources of sand for dune building were provided by the onshore migration of offshore bars during increased storm surge activity. As discussed, the LIA record of dune activity at Castelporziano is degraded by the construction of the coastal highway, but the post-RWP record of dune remobilisation may be due to similar climatic turbulence. Increased flooding frequency is observed during the 7<sup>th</sup> century AD at Rome (Bersani & Bencivenga 2001) which may be linked to a cooler/wetter and more turbulent climate. Instability and disturbance to the coastal zone occurring during periods of more intense storm activity leading to remobilisation of sand to inland areas is inferred.

## **5.8. Post-Roman Development**

Although not necessarily the key focus of the Geoarchaeological aim of the project, during the research information regarding several features of the post-Roman landscape developed. For the purposes of a relatively complete chronology a brief summary of additional findings is presented here in sections 5.8 and 5.9.

### **5.8.1. Secondary dune formation (aeolian remobilisation)**

Although remobilisation phases are not shown in the timeline after around 1.2 ka BP, this is partly a function of sampling, as access to the coastal strip on the Estate is hampered by dense vegetation cover, security restrictions around Presidential properties and the modern coastal highway, the *Via Litoranea*. It is clear from aerial photography that a large parabolic dune had developed prior to 1954 which now interrupts the preserved coastal dune ridge record (figure 5.3). This feature extends alongshore for 630 m and inland for 370 m. The parabolic dune's axis is aligned to the westerly onshore wind, at an oblique angle to the NW-SE trending shoreline. The inland position would suggest that this parabolic dune formed by the erosion of foredunes ca. 500 years old. However, more likely is that the construction of the coastal highway during the 20<sup>th</sup> century caused this widespread disturbance to the relict dune ridge topography developing into a parabolic dune. The construction of the road also appears to have induced the formation of a secondary dune ridge to the south of the parabolic dune extending along the margins of the road cut.

### **5.8.2. Post-Roman flooding**

The Medieval Warm Period, occurring between AD 800-1200 (1200 – 800 BP) (Grove & Rackham 2001), is in good agreement with the reduction of flood events in Rome (Bersani & Bencivenga 2001). However, the authors note that records during this part of the Medieval period are scarce, and at least two flood events probably occurred but little comparative evidence was found to justify their inclusion (Bersani & Bencivenga 2001). Thus the environmental history

for this period is less reliable, suggesting caution should be encouraged for detailed comparisons of historical records and environmental records.

## **5.9. Modern shoreline management**

During the last 3 centuries substantial modification to the Tiber catchment has occurred. Flood mitigation strategies have been implemented around Rome and the sediment supply to the Tiber Delta has diminished. Two key impacts are summarised below with specific impact upon the modern Castelporziano shoreline; dune ridge seeding and beach nourishment.

### **5.9.1. Dune ridge seeding**

The lack of sediment supply to the modern coastline has prompted the seeding of sand trapping vegetation to instigate the preservation of the beach profile at Castelporziano. These dunes have developed during the last decades but remain as small nebkhas seaward of the current foredune. Thus the relationship between the beach and dune sediment budgets may be satisfied that a strongly negative beach sediment budget does not create a foredune. A further distinction between sand trapping and dune building vegetation may also be made (Carter & Wilson 1990).

### **5.9.2. Beach nourishment**

The major concern of the authorities is that sediment supply reduction to the Tiber delta causes erosion of key tourist beaches. The construction of an offshore mitigation structure at *Ostia* was nourished with petrologically-similar sands to the Tiber Delta *sensu strictu* (chapter 4). For mainly aesthetic reasons the darker volcanic sands dominated by lower Tiber catchment magmatic-arc sediment supply are regarded as unsuitable for recreational activity<sup>37</sup>. Substantial alongshore reworking of nourishment sands has led to an overall 'whitening' of the beaches at *Ostia*, but dark beach sands have been observed out of season on the Castelporziano beach. Due to the seasonal nature of fluvial discharge in the Tiber catchment, the relative proportions of volcanoclastic to quartzose sand is likely to vary the appearance of beaches on the Tiber delta throughout the year; beaches darken following the autumn and winter precipitation events due to increased flushing of sediments from the Alban Hills relative to offshore nourished sands.

## **5.10. Summary of micro-scale themes**

Throughout this thesis micro-scale effects due to secondary (remobilised) dune-ridge formation and/or storminess have acted to complicate the extraction of information from the preserved geomorphological and archaeological records. A summary of these themes and their impacts is developed here.

---

<sup>37</sup> [http://www.delos.unibo.it/Docs/Deliverables/D5/secure/questionnaire/detailed/upc\\_es\\_det\\_002.pdf](http://www.delos.unibo.it/Docs/Deliverables/D5/secure/questionnaire/detailed/upc_es_det_002.pdf) Socio-economic questionnaire on the effect of the DELOS project coastal offshore structures (last accessed 12/10/2009)

### **5.10.1. Dune stability & remobilisation**

During the Late Holocene at Castelporziano, primary and secondary dune ridge formation is generally coeval but is spatially varied across the site. Remobilisation events are preserved inland of similarly aged primary dune features. As has been mentioned over the course of this and the preceding chapter, the location of remobilised dune ridges and sand deposits, is stratigraphically and topographically anomalous. Remobilised features are often found substantial distances inland of coeval primary foredunes. Their form is often as small ridges perched on the flank of a large, preserved relict foredune. These relationships are not however clear in the field, and significant laboratory time and post-excavation data analysis in the context of samples from across the entire site is required to identify these remobilised phases. Emerging technologies may inform future sample strategies (Sanderson & Murphy In Press).

During the Roman occupation of the site, the macro-scale shoreline context relating to progradation of the Tiber Delta is well-constrained, and periods of dune building have been linked to inter-progradation phase reductions in sediment supply. Partly due to sampling strategy, but also the observed lack of features to sample, dune activity during the Roman occupation of the Laurentine Shore at Castelporziano has not yet been observed. Within an actively occupied coastline, the development of dunes is surely an undesirable process and a certain level of maintenance seems likely. A more focused sampling of remobilised dune features around key areas of activity may develop a greater understanding of anthropogenically induced remobilisation.

### **5.10.2. Storminess & climate instability: multi-scale effects**

A recurring theme regarding the inception of foredunes and phases of remobilisation is the impact of meso- to micro-scale storminess acting directly upon the coastal zone. The sensitivity of the dune ridge record is on centennial time-scales and therefore less sensitive to these smaller-scale events. However, similarly scale-sensitive regional climatic records of abrupt shifts to cooler/wetter conditions are comparable to similar increases in storminess recorded during the LIA, when detailed historical records exist. Damage to the sea wall and the position of overlapping dune wavelengths may indeed suggest significant erosion by high-magnitude storm waves has occurred on the site. As discussed, remobilisation is generally coeval with a phase of foredune formation. It has been assumed that on the macro-scale foredune building phases are linked to sediment supply from the Tiber River. However on the meso-scale, the flux in flooding frequency is fundamentally linked to climate. The Tiber flooding record is also a record of climate instability, which explains the relationship between the timing of primary foredune development (decreased macro-scale sediment supply) and the timing of remobilisation (increased storminess expressed on the meso- and micro-scales) linked to instability in the regional (macro-scale) climate. The relatively short duration of storms and the expression of their effects upon geomorphology are micro- and meso- scale respectively. There is some evidence from more northerly latitudes that aeolian activity linked to increased storminess is directly linked to climatic fluctuations such as the LIA suggesting that increased humidity rather than aridity is linked to sand mobilisation (de Jong et al. 2007). Future

research investigating similar micro-scale sensitive proxy measures from Mediterranean sediment cores may then be a valuable approach for reassessing the formation of coastal dunes with regards to storminess and the meso- to micro-scale inter-relationships with human responses and initiatives.

#### **5.11. Assessment of a Geoarchaeological approach and conclusions**

Following on from the analysis of results in chapter 4 and their application to reconstructing a multi-scale examination of the sites development during the Holocene above, chapter 6 seeks to assess the Geoarchaeological approach undertaken so far in light of the recent literature and some key Geoarchaeology texts since 1976 (as discussed in chapter 2). The effectiveness of the approach for answering the research questions and addressing the overall aim and objectives of the project are then presented. Future work on both methods and the wider context of the Tiber valley is also discussed.

## 6. Conclusions & future work

### 6.1. Addressing the aim & objectives

In chapter 1 a series of research questions was proposed in order to answer the aim and objectives of this research. The aim was to understand how the Laurentine Shore has developed during the Holocene using a Geoarchaeological approach. A geomorphologically-based multi-scale Geoarchaeological approach was then conceptually developed underpinning the methodology (chapter 3) and analysis (chapter 4) focusing on the objectives of investigating contributing processes, chronology and multi-scale inter-relationships between geomorphological and anthropogenic records. Within this framework a series of archaeologically-important time periods were reconstructed in chapter 5 focusing on key points in the development of the Geoarchaeological records preserved within the Castelporziano Estate. These reconstructions were placed within the wider regional and global context where data allowed. The primary focus has been on meso- and macro- spatial and temporal scales reflected in the overall approach and sampling strategy. In addition, throughout this thesis the importance of micro-scale processes as key drivers of change has also been discussed where appropriate. The Geoarchaeological approach undertaken here is assessed within the context of recent geomorphologically-based Geoarchaeology and the initial tenets of the disciplines inception (Renfrew 1976). In this chapter the research questions are answered, summarising what has gone before. Future avenues of research are also proposed.

### 6.2. Research questions

#### 6.2.1. What are the processes of coastal development acting on the Laurentine Shore?

- **Macro-scale context** ( $10^3+$ )

The southern distal end of the Tiber Delta must be considered within the macro-scale context of mid- to late-Holocene sea level change, in particular the development of the Tiber Delta highstand systems tract (HST) within this accommodation space. HST expansion is recorded in other western Mediterranean and global deltas from around 5000 BP. Changes in the regional climate at this time, notably a relative aridisation compared to the early Holocene are recorded. At key periods increasing anthropogenic activity, especially during the Roman period and more recent centuries, catchment-scale exploitation of natural resources and settlement of the Tiber valley, and resultant or coeval increased sediment supply to the Tiber delta are important factors.

- **Meso-scale context** ( $10^2$ )

Superimposed onto this macro-scale context, culturally important centennial scale climatic fluctuations may also drive sedimentation rates such as during the Little Ice Age (LIA). Therefore, a more complex multi-scale climate interaction with anthropogenic activity exists. The impact of this is to drive the flux sediment supply into the Tiber River and thence the Delta. Alongshore sediment transport and associated transport equivalence allocates this sediment supply across the Delta front driving beach and foredune sediment budgets. Sediment budget flux then induces the form of the active coastal zone, producing a flux between a prograding and aggrading shoreline which is driven on the macro-scale. The sequence of primary dune ridges (those directly linked to delta progradation rather than later remobilisation or coeval inland formation of ridge like structures) can conceptually be linked to this multi-scale interaction with distinct foredunes more likely to develop at the end of a progradation phase once beach sediment budgets have declined from a more positive state to become 'slightly negative'. There may also be a critical relationship with micro-scale processes leading to the inception of foredunes (see below).

- **Micro-scale context** ( $10^{0-1}$ )

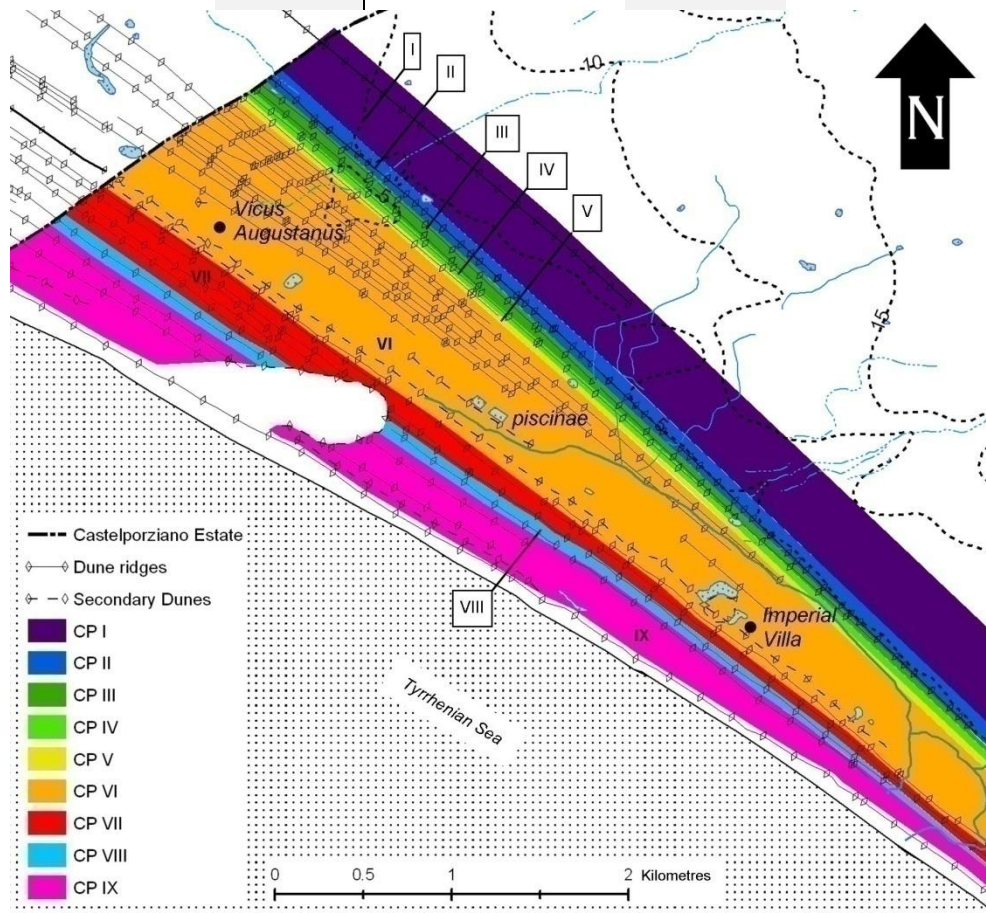
Although not the focus of this thesis, throughout the research micro-scale processes especially storminess may be the most likely to explain variation across the site. Inception of foredune formation perhaps linked to storm wave scarping of the foredune toe may be important within the larger-scale context of sediment budget models and their driving processes described above. There is likely an impact upon archaeological buildings and human occupants, but understanding impact of anthropogenic activity and construction upon the geomorphology is harder to discern due to removal of evidence. During periods of primary dune formation there is also generally a coeval phase of remobilisation or secondary dune ridge formation recorded somewhere on the site, often significantly inland suggesting larger-scale dune formation conditions exist but dune formation is facilitated by specific local conditions.

### **6.2.2. What is the chronology of these coastal changes?**

- The ferricrete dune ridges and inland sand sheets date to at least the mid-Holocene from  $5055 \pm 331$  BP (CP07/15).
- The deltaic aeolianite dune ridges date from  $4252 \pm 316$  BP (CP07/14) which represents the lateral extension of the Tiber Delta Highstand Systems Tract.
- Episodic shoreline progradation linked to increased sediment supply in the Tiber catchment is delineated by the primary dune ridge record. 9 periods of dune ridge formation (CP I – IX) have been identified using luminescence dating age models and with good agreement with existing studies based on radiocarbon dating (Giraudi et al. 2009).

(Table 5.1 and figure 5.3 are repeated here for clarity).

Giraudi <i>et al.</i> , 2009		Castelporziano		
Dune phase	Age (BP)	Dune sample	Age (BP)	Dune Phase
I	5700 – 6000	“Old dune” ridges	> 5000	CP I
II & III	5275 – 4930	CP07/15	>5386 - 4724	CP II
IV	4140 – 3920	CP07/14	4568 – 3936	CP III
-----	-----	CP07/23	3448 – 3000	CP IV
V	2910 – 2800	<i>Modeled</i>	2888	CP V
VI-a	2400 – 1800	CP04/7	~2404 – 1829	CP VI
		CP03/2	2217 – 1929	
--- The Laurentine Shore ca. 2100 BP ---				
VI-b	1700 – 1100	CP07/25	1756 – 1510	CP VII
		<i>Modeled</i>	1493	
		<i>Modeled</i>	1107	
-----	-----	CP07/26	775 – 669	CP VIII
VII – VIII	600 – 200	CP07/18	620 – 542	CP IX
		<i>Modeled</i>	481	





## 6.2.3. How has the coastline of the Laurentine Shore developed during the Holocene?

### 6.2.3.1. Macro-scale context (10<sup>3</sup>+)

On the larger scale, episodic shoreline progradation linked to the Holocene development of the Tiber Delta. Phases of progradation are effectively delineated by the development of coastal dune ridge topography. The site can be regarded as two geochemical sediment systems partitioned by contrasting early vadose diagenetic (EVD) environments, the inland *early vadose laterised ferricrete* dune ridges and sand sheets represent the Pleistocene to mid-Holocene. The expansion of the Tiber Delta's Highstand systems tract (HST) during the mid-Holocene envelops the earlier form of the coastline with sand-sized sediments.

Early vadose diagenesis is then characteristic of these coastal sediments; aeolianite prevalent in the HST deltaic sediments and laterised ferricrete on the 'hard coast'. The ferricretes are described as laterised due to the underlying volcanic parent material derived from the magmatic arc volcanic centres along the western coast of Italy, in this case, predominantly from the Alban Hills complex to the east of the Castelporziano Estate. Petrology has shown that the light silicates and garnets (garnet and melanite) that are produced from weathering of metamorphic mineral-rich turbidites in the upper Tiber catchment are present in the coastal laterised ferricretes suggesting that alongshore transport from the earlier forms of the Tiber Delta and river have been an important allochthonous sediment source for this stretch of coastline at least during the Holocene and likely during the late Pleistocene. Due to this sediment provenance, parent material and complex coastal interactions rare European soil types, *Albic luvisols* and *Eutric planosols*, have developed within the laterised ferricrete geochemical sediments.

The aeolianite EVD environment is partitioned within the deltaic HST sediments, which are dominated by the coastal dune ridge topography. Likely primary sources of calcium carbonate that produce the micritic and amorphous inter-grain cements are marine aerosols, foraminifera, marine calcite, carbonate lithics from the upper Tiber catchment, and seasonally the flux in carbonate-rich groundwater may also be important. The *in situ* weathering of calcium-rich volcanic minerals such as the dominant forms of clino-pyroxene (suggested by XRD analysis) and Ca-feldspar may also be important. Petrology has shown that in general, heavy volcanic minerals are preferentially weathered within both diagenetic environments, but is more pronounced within the laterised ferricretes. The relative youth of the aeolianites diagenesis may be a factor. Substantial aeolianite cementation occurs at least on centennial timescales. But locally may be more rapid.

Anthropogenic impacts upon the Tiber catchment during Roman times and certainly in recent centuries have likely increased sediment supply to the Delta shoreline. During the Roman period and within the last 500 ± 200 years, increases in progradation rates are recorded by the sequential seaward formation of the relict coastal dune ridges. Within the context of Roman settlement on the Laurentine Shore, occupation takes place within the most rapid

recorded progradation phase. By the time of the first buildings, the *Piscinae* around 2050 BP, progradation had created a substantial coeval coastal plain of around 350 m from around 2100 BP. Roman settlement occurs *within* this progradation phase, so by the time of abandonment across the Laurentine Shore in the 5<sup>th</sup> century AD (1580 BP), the contemporary shoreline was around 70 m seaward of the roman coastal structures at the *Vicus Augustanus*, this distance reducing towards the southern distal end of the delta due to the cusped morphology.

Interpretations based on conceptual sediment budget models suggest that on the macro-scale, during phases of progradation foredune ridges are less likely to occur as beach sediment budgets are more positive due to increased sediment supply and alongshore transportation of this sediment across the delta front. This is reflected in the changing frequency and wavelength of the dune ridge shore-normal cross-section during periods of increased progradation rate.

#### **6.2.3.2. Meso-scale context (10<sup>2</sup>)**

Dune ridge age models and dune ridge mapping have shown that human occupation of the immediate shoreline occurs during late Bronze Age / Early Iron Age (LBA/EIA) ca. 2.7 – 2.9 ka BP, and the substantial occupation of late Republic/Imperial Roman period palaeo-shoreline, the *Laurentine Shore* proper.

Interpreting human alteration of the landscape adjacent to the coastal sites (especially the *Vicus Augustanus*) is problematic. On the macro-scale the relative flattening of the dune ridge topography immediately landward of sites can be explained by delta progradation and sediment budget models however some smaller-scale local maintenance is likely as the floor plan of the bigger villas and the village complex far exceeds the wavelength of the typical dune ridge / slack topography even during increased periods of progradation. Historical ploughing and tree plantation makes investigating such issues more difficult. Further dedicated, micro-scale research may be illuminating here. The corollary is that without the macro-scale context of the site investigation focused upon the meso- micro scale context of the site may not be sensitive to the wider progradational context and biased interpretations based *only* on anthropogenic alteration of their landscape may have emerged.

During the lifetime of sites there is an anthropogenically noticeable relationship with shoreline progradation and potentially aeolian remobilization and secondary dune inundation of archaeological features. Rates of progradation, highest during the Roman period, suggest that over the course of decades a single observer would be aware of the seaward movement of the shoreline. Issues of sedimentation against coastal structures may have been an issue long before then but the meso-macro scale sampling strategy focused on in this thesis is not sensitive on micro-scales. There is some archaeological evidence that suggests a seaward relocation of some coastal structures and building plots during the lifetime of the *Vicus Augustanus*.

Inundation of coastal structures is simultaneously reported at the *Vicus Augustanus* and *Piscinae* around 1600 BP. With the collapse of the Roman Empire around this time it is not possible to attribute a causal link between the aeolian and

anthropogenic activity. It may simply be that with the abandonment of the coastal sites maintenance / removal of aeolian sand was not carried out after this point.

### **6.2.3.3. Micro-scale context ( $10^{0-1}$ )**

Short-term anthropogenic impacts during the construction of buildings and development of settlement environs may be important but clear evidence is elusive without a dedicated micro-scale investigation.

Rapid and pronounced micro-scale events, such as storms may be important for shaping the geomorphic record at a scale important to individual communities. Sea wall destruction suggests geologically instantaneous but high-magnitude storms have impacted this coastline. The overlapping wavelengths of well-preserved dune ridges may also suggest storm activity. These events are likely to have more immediate significance to the human occupants of the coastline than larger-scale processes of shoreline progradation although both may have induced responses and initiatives to mitigate their effects.

### **6.2.4. What are the key interactions between the anthropogenic and geomorphological records?**

Within the archaeological record, key phases of human coastal occupation occur during the LBA/EIA (ca. 2.7-2.9 ka BP) and the Late Republic - Imperial Roman period (ca. 2050 – 1580 BP). On the macro-scale, Tiber Delta progradation rates during the Roman period of occupation have been shown to increase threefold and a number of sources relate this to increased flooding frequency of the Tiber River, which provides an increased sediment supply to the coast. This may be directly related to anthropogenic exploitation of the Tiber catchment from ca. 2300 BP. The deforestation of the Rome hinterland is a key factor for consideration.

On the meso-scale, progradation of the Roman occupied shoreline is estimated at around 0.14 m/yr (mean estimated rate). This rate is perhaps noticeable to an individual witness on decadal to multi-decadal timescales. During the shorter first phase of the *Vicus Augustanus* (2010 – 1950 BP), it is estimated that the shoreline prograded by around 8 m. During the longer second phase (1925 – 1580 BP), it is estimated that the shoreline prograded around 48 m. The coeval primary dune ridge associated with the abandonment of the Roman sites at Castelporziano is around 70 m sea ward of the archaeological remains, which agrees with an observed seaward shift in building plots between the phases of occupation at the *Vicus Augustanus* (pers. comm. A, Claridge). This data suggests some anthropogenic response and initiative was taken in regards to shoreline progradation.

Coeval phases of aeolian inundation are recorded at the *Vicus Augustanus* and *Piscinae* at ca. 1600 BP (5<sup>th</sup> century AD). However it is not possible to attribute a link between aeolian activity and human abandonment due to the overall collapse of the Roman Empire at this time.

On the micro-scale, although not specifically the focus of the sampling strategy and thus less well constrained, evidence for the importance of short-duration, high-magnitude events specifically that of storms upon the coastal architecture and dune ridge record have been encountered throughout this study. The anomalously high 'tidal' notch and storm wave damage preserved in the seaward face of the Severian-period sea wall associated with the Imperial Villa near Tor Paterno is recorded at 2.8 m above *Roman* period sea level (ca. 1800 BP). A rationale for understanding the magnitude and duration of modern storm activity within the Tyrrhenian Sea suggests sea levels during storms can easily reach this magnitude. The overlapping dune ridge profiles associated with the Roman period shoreline may also suggest storm induced wave-scarping and the inception of new foredune ridges within the storm-damage profile.

#### **6.2.5. What are the implications for multi-scale geoarchaeological research?**

The integration of conceptual sediment budget models has provided an interpretative framework for understanding the macro-scale context of sediment supply and coastal dune ridge development. This also provides a context for interpreting anthropogenic impacts. The inland areas directly landward of the Laurentine Shore structures are noticeably lacking in the strongly undulating dune ridge topography for around 350 m linked to a significant progradation phase between 2217-1510 BP (delineated by dune-ridges). This coastal plain is dated by luminescence dates (across an inland transect) that describe the relict foredune and palaeo-beach and highlight a single coeval phase of development. The typical height above sea level due to dune formation is typically around 2 – 3 m above the contemporary sea level. This shoreline area is then suitable if not desirable for settlement and development; requiring minimal alteration of the topography to accommodate buildings than would be required in the higher-frequency dune ridge topography too narrow to accommodate the larger building complexes and villas. Whilst it is tempting to interpret changes in dune ridge wavelength and frequency within the environs of the Roman archaeological remains in terms of human alteration of the landscape, within a macro-scale context of changing progradation rates, sediment budget flux and reduced likelihood of dune ridge formation during pronounced progradation phases the meso-scale impact of human alteration of the landscape is problematic to isolate. Whilst human alteration of the landscape is inevitable and a lack of dune ridges could be a result of this, landward of the Laurentine Shore structures, the coeval development shown by the luminescence dated age model makes this interpretation less valid. Without the macro-scale context of understanding the development of the whole delta dune ridge record, micro- and meso-scale sampling strategies may have provided less well constrained data, focusing only on the immediate vicinity of the archaeological remains. Whilst beneficial for examining the impact of storms for example, interpretations may have been biased towards an anthropogenic cause for geomorphological changes. The detailed investigation of archaeological sites also provides an improved interpretative context rather than merely sampling from the vicinity of archaeological sites, interpretations incorporating an anthropogenic aspect can be embedded in actual data – the skills of archaeological excavation being highly specialised and not necessarily found within a geomorphological toolkit. A multi-scale Geoarchaeological approach is then highly beneficial for establishing the relative importance of various site formation

processes and broader interpretative abilities incorporating a greater range of geomorphological and archaeological context.

#### **6.2.6. The Geoarchaeological approach on the Laurentine Shore**

*“...one really needs to be a jack of all disciplines to be a geoarchaeologist...- you must be digger, surveyor, geographer, historian, archaeologist and palaeoenvironmentalist all rolled into one”* (French 2003: 251).

The above quotation effectively sums up the experience of undertaking research for this thesis and the disparate areas contributing to answering the research questions. As French also notes, the practical and logistical aspects of research in the field will inevitably impinge on what is initially desired; the outcome is that Geoarchaeological research is really rather a fluid undertaking and relies on recognising and developing opportunities as they arise. Effectively there is no set way in which to undertake Geoarchaeological research but site-specific qualities and logistics dictate what can be achieved. Within the thematic context of the recent Geoarchaeological literature (outlined in chapter 2), significant attention has been paid to the majority of aspects.

- Applied multi-proxy methods
- Geochronology
- Conceptual models
- Taphonomy and diagenesis (site formation processes)
- Landscape prospection
- Data compilation and reassessment

Sampling within a transect-based strategy and multi-proxy examination of sedimentology, geochemistry and with focused biostratigraphic studies of palaeo-sea level – with associated geochronological framework and high-quality regional literature – has facilitated a quasi-4 dimensional reconstruction of key late-Holocene phases of the palaeo-shoreline of particular importance to the archaeological record in the form of several snapshots of key time periods. The research has focused upon meso- to macro-scale processes and human responses and initiatives related to environmental change. These scales are of key importance for examining the sites fundamental relationship with the Tiber Delta in turn linked to regional (and global) climate and anthropogenic factors within the Tiber catchment. However during the course of the research micro-scale factors have been identified that may be highly significant for interpreting the examined geomorphological and archaeological records; particularly short-duration high-magnitude storm events for interpreting an anomalous sea level record and potential drivers of dune ridge formation that are effectively invisible to larger-scale sampling strategies and dating precision.

The integration of petrological provenance and diagenesis analysis for assessing the effectiveness of the primarily luminescence-based geochronology provides added confidence for interpreting the macro-scale geomorphological development of the site, i.e. site formation processes. The produced age models are also improved by establishing a geomorphological context for aeolian remobilisation and secondary formation of dune ridge topography. Improvements to sampling strategy would usefully be made by onsite prospection of dune ridge relative stratigraphy (Sanderson & Murphy In Press). Age control provided by radiocarbon chronology of the same dune ridge sequences in the central Tiber Delta (Giraudi et al. 2009) has shown excellent agreement with the luminescence age models from Castelporziano. In fact the relative preservation of the dune ridge topography is probably responsible for identifying two additional phases of Tiber Delta dune ridge formation during the last 5000 years not preserved in the central Delta morphology (chapter 5).

Conceptual models have been applied (e.g. Psuty sediment budget model). A holistic relationship between macro-scale foredune building potential and relative change in sediment budgets primarily acting upon the beach have allowed an assessment of dune topography linked to the mid- to late-Holocene progradation of the Tiber Delta. As a result an alternative macro-scale interpretation of a relatively flattened topography associated with the Roman archaeological remains can be suggested. Local anthropogenic reworking is of course likely to be fundamental for inducing the modern form of the preserved landscape. Throughout this thesis issues of scale sensitivity of preserved records have been developed. The ability of a Geoarchaeological approach (and constituent disciplines) to understand complex multi-scaled processes is partly determined by sampling strategy and scale sensitivity of the available records driven by the precision of geochronological frameworks.

Landscape prospection incorporating GPS survey of archaeological sites and key geomorphological features has provided valuable data for GIS compilation of published datasets and aerial photography records. The main strength of this initial (and hopefully ongoing) GIS resource is for identifying locations of potential Geoarchaeological significance for further ground-truthing. Potential locations of inlets and harbours within the Roman palaeo-shoreline have already been hypothesised. Compilation of various contemporary and historic accounts of Roman infrastructure has provided preliminary data for reconstructing Roman road links and site distributions. Again ground-truthing and hypothesis testing can be developed from these emerging datasets. Interpreting these links within the context of data-led palaeo-environmental and palaeo-landscape reconstructions (specifically the likely location of the shoreline) is invaluable for developing future Geoarchaeological hypotheses.

In summary, the Geoarchaeological approach employed within this thesis is directly comparable to the contemporary geomorphologically-focused literature. Several aspects particularly the GIS compilation of datasets and palaeo-landscape reconstruction show good potential for developing future research questions and goals. From a survey of the

contemporary and historic literature the full potential of Geoarchaeology lies within effective inter-disciplinary research and effective exploitation of available resources.

### **6.3. Future work**

#### **6.3.1. Luminescence chronology**

Dedicated studies into the mobility of principal dosimetry components (K, U, Th) and the effectiveness of bulk dosimetry measurements to replicate the dose-rate exhibited by cumulative Equivalent Dose ( $D_E$ ) measurements within early vadose diagenetic environments particularly within ferricrete geochemical sediments would be beneficial. There is a relative paucity of dosimetry literature specifically within the context of luminescence dating applications and diagenesis, the specific literature that does exist suggests the ferricretes may be problematic for accurate dosimetry (e.g. Zhang et al. 2008). Greater confidence in assessing levels of local storage and accumulation of weathered dosimetry elements potentially stored within diagenetic cements may lead to more robust age estimates overall. Issues of sample-specific diagenetic conditions make assessment of trends in dosimetry characteristics problematic to interpret (if not conceptually impossible). The development of statistical tools would also be beneficial for rapidly making these assessments.

Petrological analysis of key luminescence dosimeters quartz and K-feldspars within the context of earlier research (Alexander 2007; Lee & Parsons 1995; Lee et al. 1995) suggesting that small-scale microstructures (so-called high energy locations) may be linked to the propensity for feldspar to lose stored charge over time (i.e. to fade) due to quantum tunneling, highlights the almost complete lack of twinning and other microstructure in these luminescence minerals due to their metamorphic origins. Furthermore, this preceding research suggests that weathering may be preferentially focused upon these high-energy locations removing them over time. HF weathering of mineral thin sections used during K-feldspar staining also appears to highlight these specific locations in the grains typically shown by electron microscopy. Fading experiments upon K-feldspar from samples across the site does not display systematic signal loss as suggested by some recent literature (e.g. Huntley & Lian 2006). It is tentatively proposed here that geological provenance may be strongly linked to the useful luminescence characteristics observed during this research. Further studies specifically examining relationships between geological provenance, micro-structure and the fading potential of stored charge may provide a geological rationale and petrologically based tools for assessing suitable applications of K-feldspars. A joint SEM analysis of grain surface properties and the particular benefits of a thin-section petrological microscopy analysis are rapid assessment of geological formation conditions and overall microstructure. In addition, a single, stained petrological thin section of K-feldspar separates could contain sufficient individual grains (ca. 1000 coarse grains) to be comparative with a typical small-aliquot load on a single Risø reader run. The cost of each slide is low, around £30 – 40 and assessment is rapid (on the scale of minutes to hours depending on the experience of the

operator) using a standard petrological, polarizing microscope which occupy small amounts of precious laboratory space. Using simple ratios of  $K/Kp$  (the proportion of poly-crystalline grains incorporating K-feldspar) and the dominance of complex twinning and small-scale microstructure in general could be developed into a rapid assessment tool.

### **6.3.2. Geoarchaeology**

In general, a multi-scale approach to this site has provided a useful interpretative framework linked to conceptual models of sediment budget. Clearly the specifics of different sites will require bespoke approaches in each case dependent on the research outcomes under scrutiny. Within a coastal setting and the broader context of Holocene climate change and sea level rise, examining the geomorphological development and human initiatives and responses on the macro- and meso-scales to change has provided valuable information for assessing the impact of climate change on coastal communities. Further micro-scale studies building upon this broader context can now be developed to ask even more specific Geoarchaeological questions. Storminess and the micro-scale relationships of coastal settlement and aeolian geomorphological development are important factors on the Laurentine Shore. Holocene palaeo-ecological records extracted from sediment cores in conjunction with an examination of simultaneous aeolian activity such found in the approach of de Jong et al (2007) may be productive at Castelporziano.

During the fieldwork and following GIS examination of AP, GPS and topographic survey several possible inlets and potential harbour sites have been identified associated with the Laurentine Shore geomorphological context. Targeted archaeological survey and excavation, micro-scale palaeo-environmental (especially diatom analysis) and sedimentological examination of sediment cores from these wet depressions may provide clarification for a connection to the sea during the Roman period (Marriner & Morhange 2006). The development of DEM's at Castelporziano is currently limited to hand-crafted measurements using total station survey partly due to security concerns and the dense forest cover. Further integrating elevation models and palaeoenvironmental analyses produces an effective Geoarchaeological approach (Ghilardi & Desruelles 2009) and could provide valuable information regarding the seascape of the archaeological remains and wider links to the Roman world.

Developing this theme, preliminary work has been undertaken in compiling archaeological and topographic data and aerial photography records to reconstruct road links and unexamined archaeological remains. Published archaeological surveys have also been sought and included were currently available. GIS compilation of road links and key settlements such as *Lavinium* and *Ardea* in the east, Rome to the NW and *Portus* and *Ostia* in the west in conjunction with future field surveys and effective GPS surveys is rapidly leading to a GIS that provides a hypothesis generating potential.

Whilst these individual aspects could be developed as stand-alone research programs, they could feasibly be integrated into a larger multi-scale coastal Geoarchaeological project incorporating archaeological research questions as



appropriate. Such questions may be investigating the wider economy of the site, examining the sources of building materials with analytical elemental analyses, petrology and field survey of natural sources of materials like clay, tufa and basalt.

### **6.3.3. Castelporziano and a wider Geoarchaeological context**

Much of the Geoarchaeological results focusing upon the Laurentine Shore may be of interest to the wider archaeological research currently being undertaken in the Tiber valley, research with a prime focus on investigating the archaeological palaeo-landscape. Larger projects are currently underway by the British School at Rome and collaboration with several UK and other European universities<sup>38</sup>, with several Tiber valley projects housed at the McDonald Institute of Archaeology, Cambridge University<sup>39</sup>. The focus of much of this research is the middle and lower Tiber valley, the Laurentine Shore Project therefore occupies a key Geoarchaeological niche in the south eastern Tiber valley and delta. Mapping using a variety of methods and GIS approaches is recurrent throughout this work. Less explicitly discussed is the application of palaeo-environmental tools, key studies have been cited during this thesis. Future expansion of a Geoarchaeological approach may be beneficial for future endeavours.

---

<sup>38</sup> [http://www.bsr.ac.uk/BSR/sub\\_arch/BSR\\_Arch\\_01Tiber.htm](http://www.bsr.ac.uk/BSR/sub_arch/BSR_Arch_01Tiber.htm) Tiber Valley Project  
[http://www.bsr.ac.uk/BSR/sub\\_arch/extra/BSR\\_Tiber\\_SESR01.htm](http://www.bsr.ac.uk/BSR/sub_arch/extra/BSR_Tiber_SESR01.htm) South Etruria Survey reassessment  
[http://www.bsr.ac.uk/BSR/sub\\_arch/extra/BSR\\_Tiber\\_Roman01.htm](http://www.bsr.ac.uk/BSR/sub_arch/extra/BSR_Tiber_Roman01.htm) Roman towns project  
[http://www.bsr.ac.uk/BSR/sub\\_arch/BSR\\_Arch\\_05Roman.htm](http://www.bsr.ac.uk/BSR/sub_arch/BSR_Arch_05Roman.htm) Roman ports project  
(Last accessed 18/09/2009).

<sup>39</sup> <http://www.mcdonald.cam.ac.uk/research/> in addition to the above links, see the Tiber catchment and Tyrrhenian Italy projects  
(last accessed 18/09/2009).

**Appendix A1 – Sediment descriptions**

GRADISTAT V5.0 ANALYSIS	CP03/1	CP03/2	CP03/3	CP03/4	CP03/6	
<b>(Blott &amp; Pye 2001)</b>	<b>ANALYST:</b> ARB,	ARB,	ARB,	ARB,	ARB,	
	<b>SIEVING ERROR:</b>	Unimodal, Well Sorted	Unimodal, Well Sorted	Unimodal, Well Sorted	Unimodal, Well Sorted	
	<b>SAMPLE TYPE:</b>	Unimodal, Well Sorted	Unimodal, Well Sorted	Unimodal, Well Sorted	Unimodal, Well Sorted	
	<b>TEXTURAL GROUP:</b>	Sand Well Sorted	Sand Well Sorted	Sand Well Sorted	Sand Well Sorted	
	<b>SEDIMENT NAME:</b>	Medium Sand	Medium Sand	Medium Sand	Medium Sand	
<b>FOLK AND WARD METHOD</b>	<b>MEAN</b>	308.265	279.970	298.355	253.549	325.461
<b>(µm)</b>	<b>SORTING</b>	1.366	1.376	1.396	1.382	1.352
	<b>SKEWNESS</b>	-0.066	-0.089	-0.062	-0.104	-0.095
	<b>KURTOSIS</b>	0.962	0.999	0.988	1.051	0.987
<b>FOLK AND WARD METHOD</b>	<b>MEAN:</b>	Medium Sand	Medium Sand	Medium Sand	Medium Sand	Medium Sand
<b>(Description)</b>	<b>SORTING:</b>	Well Sorted	Well Sorted	Well Sorted	Well Sorted	Well Sorted
	<b>SKEWNESS:</b>	Symmetrical	Symmetrical	Symmetrical	Fine Skewed	Symmetrical
	<b>KURTOSIS:</b>	Mesokurtic	Mesokurtic	Mesokurtic	Mesokurtic	Mesokurtic
	<b>MODE 1 (µm):</b>	324.7	295.85	295.85	269.45	356.45

	CP04/1	CP04/2	CP04/3	CP04/4	CP04/5	CP04/7
<b>ANALYST:</b>	FS,	FS,	FS,	FS,	FS,	FS,
<b>SIEVING ERROR:</b>						
<b>SAMPLE TYPE:</b>	Unimodal, Well Sorted	Unimodal, Well Sorted	Unimodal, Moderately Well Sorted	Unimodal, Well Sorted	Unimodal, Well Sorted	Unimodal, Moderately Sorted
<b>TEXTURAL GROUP:</b>	Sand Well Sorted	Sand Well Sorted	Sand	Sand	Sand	Sand
<b>SEDIMENT NAME:</b>	Medium Sand	Medium Sand	Moderately Well Sorted Medium Sand	Well Sorted Medium Sand	Well Sorted Medium Sand	Moderately Sorted Fine Sand
<b>MEAN</b>	294.129	256.582	280.067	273.776	268.010	204.743
<b>SORTING</b>	1.376	1.400	1.422	1.391	1.382	1.742
<b>SKEWNESS</b>	-0.038	-0.077	-0.090	-0.054	-0.027	-0.370
<b>KURTOSIS</b>	0.970	1.028	1.047	0.995	0.976	2.460
<b>MEAN:</b>	Medium Sand	Medium Sand	Medium Sand	Medium Sand	Medium Sand	Fine Sand
<b>SORTING:</b>	Well Sorted	Well Sorted	Moderately Well Sorted	Well Sorted	Well Sorted	Moderately Sorted
<b>SKEWNESS:</b>	Symmetrical	Symmetrical	Symmetrical	Symmetrical	Symmetrical	Very Fine Skewed
<b>KURTOSIS:</b>	Mesokurtic	Mesokurtic	Mesokurtic	Mesokurtic	Mesokurtic	Very Leptokurtic
<b>MODE 1 (µm):</b>	295.85	269.45	295.85	295.85	269.45	223.65

	CP07/14	CP07/15	CP07/16	CP07/17	CP07/18	CP07/19
<b>ANALYST:</b>	ARB,	ARB,	ARB,	ARB,	ARB,	ARB,
<b>SIEVING ERROR:</b>						
<b>SAMPLE TYPE:</b>	Unimodal, Well Sorted	Unimodal, Moderately Well Sorted	Unimodal, Moderately Well Sorted	Bimodal, Moderately Well Sorted	Unimodal, Well Sorted	Unimodal, Poorly Sorted
<b>TEXTURAL GROUP:</b>	Sand	Sand	Sand	Sand Moderately Well Sorted	Sand	Muddy Sand
<b>SEDIMENT NAME:</b>	Well Sorted Medium Sand	Moderately Well Sorted Medium Sand	Moderately Well Sorted Fine Sand	Well Sorted Medium Sand	Well Sorted Medium Sand	Fine Silty Fine Sand
<b>MEAN</b>	265.011	297.362	174.965	268.258	258.436	214.256
<b>SORTING</b>	1.327	1.486	1.589	1.419	1.326	2.493
<b>SKEWNESS</b>	0.000	0.077	-0.633	0.044	-0.012	-0.448
<b>KURTOSIS</b>	0.942	1.113	4.626	0.978	0.939	3.316
<b>MEAN:</b>	Medium Sand	Medium Sand Moderately Well Sorted	Fine Sand Moderately Well Sorted	Medium Sand Moderately Well Sorted	Medium Sand	Fine Sand
<b>SORTING:</b>	Well Sorted	Sorted	Sorted	Well Sorted	Well Sorted	Poorly Sorted
<b>SKEWNESS:</b>	Symmetrical	Symmetrical	Very Fine Skewed Extremely Leptokurtic	Symmetrical	Symmetrical	Very Fine Skewed Extremely Leptokurtic
<b>KURTOSIS:</b>	Mesokurtic	Leptokurtic	Leptokurtic	Mesokurtic	Mesokurtic	Leptokurtic
<b>MODE 1 (µm):</b>	269.45	269.45	203.7	269.45	245.45	245.45

	CP07/20	CP07/21	CP07/22	CP07/23	CP07/24	CP07/25
<b>ANALYST:</b>	ARB,	ARB,	ARB,	ARB,	ARB,	ARB,
<b>SIEVING ERROR:</b>						
<b>SAMPLE TYPE:</b>	Unimodal, Moderately Sorted	Unimodal, Poorly Sorted	Unimodal, Well Sorted	Unimodal, Well Sorted	Unimodal, Poorly Sorted	Unimodal, Well Sorted
<b>TEXTURAL GROUP:</b>	Muddy Sand Very Coarse	Sand Poorly Sorted	Sand Well Sorted	Sand Well Sorted	Sand Poorly Sorted	Sand Well Sorted
<b>SEDIMENT NAME:</b>	Silty Fine Sand	Medium Sand	Medium Sand	Medium Sand	Medium Sand	Medium Sand
<b>MEAN</b>	197.601	257.068	288.209	273.396	287.445	332.375
<b>SORTING</b>	1.992	2.131	1.314	1.315	2.233	1.337
<b>SKEWNESS</b>	-0.446	-0.334	-0.026	-0.027	-0.177	-0.050
<b>KURTOSIS</b>	1.855	2.930	0.955	0.952	3.260	0.961
<b>MEAN:</b>	Fine Sand Moderately Sorted	Medium Sand	Medium Sand	Medium Sand	Medium Sand	Medium Sand
<b>SORTING:</b>	Very Fine Skewed	Poorly Sorted	Well Sorted	Well Sorted	Poorly Sorted	Well Sorted
<b>SKEWNESS:</b>	Very Leptokurtic	Very Fine Skewed	Symmetrical	Symmetrical	Fine Skewed Extremely Leptokurtic	Symmetrical
<b>KURTOSIS:</b>	Leptokurtic	Very Leptokurtic	Mesokurtic	Mesokurtic	Leptokurtic	Mesokurtic
<b>MODE 1 (µm):</b>	245.45	245.45	295.85	269.45	295.85	356.45

	CP07/26	CP07/27	CP08/1	CP08/2	CP08/3	CP08/4
<b>ANALYST:</b>	ARB,	ARB,	FS,	FS,	FS,	FS,
<b>SIEVING ERROR:</b>						
<b>SAMPLE TYPE:</b>	Unimodal, Well Sorted	Unimodal, Moderately Well Sorted	Unimodal, Poorly Sorted	Unimodal, Well Sorted	Unimodal, Well Sorted	Unimodal, Poorly Sorted
<b>TEXTURAL GROUP:</b>	Sand Well Sorted	Sand Moderately Well Sorted	Sand Poorly Sorted	Sand Well Sorted	Sand Well Sorted	Sand Poorly Sorted
<b>SEDIMENT NAME:</b>	Medium Sand	Sorted Medium Sand	Medium Sand	Medium Sand	Medium Sand	Medium Sand
<b>MEAN</b>	292.018	361.947	297.953	297.440	304.022	245.477
<b>SORTING</b>	1.329	1.582	2.368	1.413	1.402	2.115
<b>SKEWNESS</b>	-0.027	0.181	-0.413	-0.156	-0.082	-0.258
<b>KURTOSIS</b>	0.946	1.318	3.248	1.142	0.992	2.036
<b>MEAN:</b>	Medium Sand	Medium Sand Moderately Well Sorted	Medium Sand	Medium Sand	Medium Sand	Fine Sand
<b>SORTING:</b>	Well Sorted	Sorted	Poorly Sorted	Well Sorted	Well Sorted	Poorly Sorted
<b>SKEWNESS:</b>	Symmetrical	Coarse Skewed	Very Fine Skewed Extremely	Fine Skewed	Symmetrical	Fine Skewed
<b>KURTOSIS:</b>	Mesokurtic	Leptokurtic	Leptokurtic	Leptokurtic	Mesokurtic	Very Leptokurtic
<b>MODE 1 (µm):</b>	295.85	356.45	324.7	324.7	324.7	245.45

	CP08/5	CP08/6	CP08/7	CP beach	CP dune	Fiumicino
<b>ANALYST:</b>	FS,	FS,	ARB,	FS,	FS,	FS,
<b>SIEVING ERROR:</b>						
<b>SAMPLE TYPE:</b>	Unimodal, Well Sorted	Bimodal, Poorly Sorted	Unimodal, Moderately Well Sorted	Unimodal, Well Sorted	Unimodal, Well Sorted	Unimodal, Moderately Well Sorted
<b>TEXTURAL GROUP:</b>	Sand Well Sorted	Sand Poorly Sorted	Sand Moderately Well Sorted	Sand Well Sorted	Sand Well Sorted	Sand Moderately Well Sorted
<b>SEDIMENT NAME:</b>	Medium Sand	Medium Sand	Sorted Medium Sand	Fine Sand	Medium Sand	Sorted Medium Sand
<b>MEAN</b>	274.322	277.248	278.813	220.309	346.791	445.719
<b>SORTING</b>	1.350	2.551	1.443	1.330	1.341	1.558
<b>SKEWNESS</b>	0.006	-0.133	-0.017	-0.005	-0.074	0.101
<b>KURTOSIS</b>	0.972	3.200	1.063	0.963	0.974	1.244
<b>MEAN:</b>	Medium Sand	Medium Sand	Medium Sand Moderately Well Sorted	Fine Sand	Medium Sand	Medium Sand Moderately Well Sorted
<b>SORTING:</b>	Well Sorted	Poorly Sorted	Sorted	Well Sorted	Well Sorted	Sorted
<b>SKEWNESS:</b>	Symmetrical	Fine Skewed Extremely	Symmetrical	Symmetrical	Symmetrical	Coarse Skewed
<b>KURTOSIS:</b>	Mesokurtic	Leptokurtic	Mesokurtic	Mesokurtic	Mesokurtic	Leptokurtic
<b>MODE 1 (µm):</b>	269.45	245.45	269.45	223.65	356.45	429.65

	Ostia 1	Ostia 2	Ostia 3	Torvaianica	Ladispoli	CP09/1
<b>ANALYST:</b>	FS,	FS,	FS,	FS,	FS,	FS,
<b>SIEVING ERROR:</b>						
<b>SAMPLE TYPE:</b>	Unimodal, Well Sorted	Unimodal, Moderately Well Sorted	Unimodal, Moderately Well Sorted	Unimodal, Well Sorted	Bimodal, Moderately Sorted	Unimodal, Well Sorted
<b>TEXTURAL GROUP:</b>	Sand	Sand Moderately Well Sorted	Sand	Sand	Sand Moderately Sorted	Sand
<b>SEDIMENT NAME:</b>	Well Sorted Medium Sand	Sorted Medium Sand	Moderately Well Sorted Fine Sand	Well Sorted Medium Sand	Sorted Medium Sand	Well Sorted Medium Sand
<b>MEAN</b>	272.190	359.893	255.056	251.825	369.321	311.298
<b>SORTING</b>	1.398	1.519	1.517	1.317	1.788	1.363
<b>SKEWNESS</b>	0.021	0.021	0.055	-0.022	0.192	-0.039
<b>KURTOSIS</b>	0.959	1.061	0.941	0.945	1.164	0.960
<b>MEAN:</b>	Medium Sand	Medium Sand Moderately Well Sorted	Medium Sand Moderately Well Sorted	Medium Sand	Medium Sand Moderately Sorted	Medium Sand
<b>SORTING:</b>	Well Sorted	Sorted	Sorted	Well Sorted	Coarse Skewed	Well Sorted
<b>SKEWNESS:</b>	Symmetrical	Symmetrical	Symmetrical	Symmetrical	Skewed	Symmetrical
<b>KURTOSIS:</b>	Mesokurtic	Mesokurtic	Mesokurtic	Mesokurtic	Leptokurtic	Mesokurtic
<b>MODE 1 (µm):</b>	269.45	356.45	245.45	245.45	324.7	324.7

## Appendix A2 – Petrology counts

### Diagenesis counts

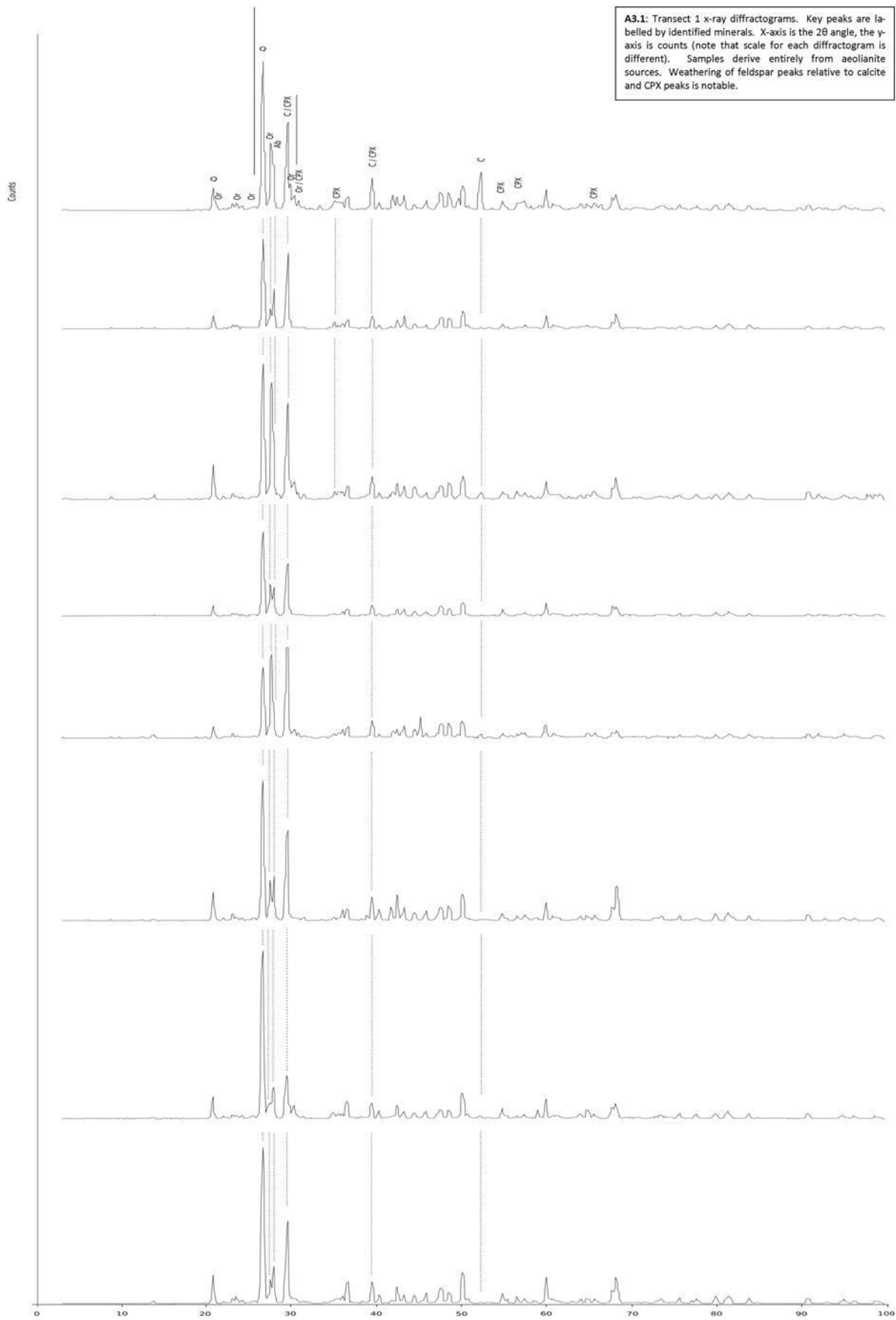
SPECIES	FIUMICINO	OSTIA 1	OSTIA 2	OSTIA 3	CP BEACH	TORVAIANICA	CP DUNE	Soil Pit 5	CP07/24	CP04/7	CP07/23	Soil Pit 2	CP04/8	CP07/16	CP07/14	CP07/15	CP07/17	CP07/20	CP07/21	CP07/22	CP07/27
Q	125	40	155	161	174	151	46	73	100	138	125	78	104	75	48	129	155	111	88	85	106
Qp	69	22	49	30	60	33	15	32	37	22	31	34	26	33	20	31	31	31	67	47	35
Fmisc	0	0	0	0	0	0	31	39	76	59	38	50	52	54	16	51	67	82	74	67	78
Fp	0	0	0	0	0	0	20	27	10	37	25	24	31	29	14	35	29	48	29	35	36
K	2	3	1	1	4	1	7	3	5	6	2	1	0	4	0	2	2	16	10	10	11
P	1	4	2	3	3	3	1	3	1	3	3	1	0	6	2	1	3	4	5	4	2
Lc	63	40	49	93	56	99	50	65	18	30	25	40	33	55	14	2	1	0	0	33	0
Lch	17	10	6	6	4	0	13	3	4	3	3	7	14	12	5	1	0	0	0	0	0
Lv	32	17	16	1	8	11	10	5	0	1	1	2	0	0	0	0	0	0	0	0	0
Lmm	5	14	23	5	4	2	13	14	8	10	4	9	5	5	3	10	4	26	20	12	25
Muscovite	34	19	50	43	62	34	22	8	12	3	16	11	9	7	30	14	11	0	3	3	0
Biotite	14	6	6	22	32	22	26	10	14	3	10	17	27	13	48	19	3	1	3	4	5
Apatite	0	0	0	0	0	0	2	1	0	0	1	0	0	0	0	0	1	0	0	0	0
Calcite	30	35	113	30	69	244	82	100	67	73	67	61	102	89	36	4	0	0	0	0	0
Dolomite	5	3	5	3	6	24	0	0	0	0	0	0	0	0	0	0	0	0	0	0	0
CPX	128	159	42	114	79	33	22	5	3	0	12	12	4	7	35	4	0	1	1	3	12
OPX	16	14	2	3	15	6	6	0	0	0	0	0	0	0	0	0	0	0	0	0	0
Chlorite	45	51	40	48	55	23	24	12	13	3	6	23	7	7	46	12	6	0	3	5	5
Epidote	1	1	4	1	0	0	0	0	0	0	0	0	1	1	3	1	0	1	0	0	0
Amphibole	28	30	11	20	15	3	11	2	1	0	1	4	1	1	7	2	0	2	2	2	4
Hornblende	20	7	3	10	11	1	4	0	2	0	0	0	2	0	1	0	0	0	1	0	0
Olivine	0	0	0	1	0	0	0	0	0	0	0	0	0	0	0	0	0	0	0	0	0
Melanite	3	1	3	7	5	3	2	2	1	0	0	3	0	0	4	2	0	1	0	0	0
Garnet	6	13	3	16	6	5	4	2	0	2	1	2	2	0	6	1	1	0	0	1	1
Hematite	1	3	5	2	0	8	0	0	2	1	0	0	1	0	0	0	0	0	0	0	1
Opaque	6	5	10	13	20	4	0	0	0	1	0	0	0	0	1	0	1	0	0	0	0
Spinel	0	1	0	0	1	0	0	0	0	0	0	0	0	0	2	1	0	0	0	0	0
Forams	7	9	13	9	6	40	0	9	10	22	9	2	19	2	8	0	0	0	0	4	0
Shell	2	4	1	4	2	3	0	0	0	0	1	0	0	0	0	0	0	0	0	0	0
Glass	0	1	4	1	0	0	0	0	0	0	0	0	0	0	0	0	0	0	0	0	0

Heavy mineral counts (>2.9 gcm<sup>-3</sup>)

SPECIES	FIUMICINO	OSTIA 1	OSTIA 2	OSTIA 3	CP BEACH	TORVAIANICA	CP FOREDUNE
Amphibole	12	7	9	7	15	20	18
Analcime	0	1	0	0	0	0	0
Apatite	0	0	0	0	0	0	0
CPX	111	142	119	53	127	114	166
Chloritoid	0	15	12	11	25	28	23
Chlorite	55	32	52	44	40	38	33
Epidote	0	0	0	0	0	0	0
Garnet	11	28	30	59	24	37	16
Hematite	4	0	5	4	1	7	2
Hornblende	2	2	0	0	7	6	5
Kyanite	6	14	13	13	12	24	26
Melanite	8	4	2	12	4	9	5
Olivine	1	0	0	0	0	0	0
Opaque (Blk)	109	78	99	105	53	21	10
Opaque (Blue)	0	0	0	5	0	0	0
Opaque (pyrrhotite)	0	0	0	0	0	1	0
Opaque (R)	16	11	9	28	7	7	4
OPX	21	17	6	4	24	23	27
Spinel	2	0	0	2	2	2	1
Titanite	5	0	2	6	2	7	2
Zircon	1	1	0	2	0	0	0

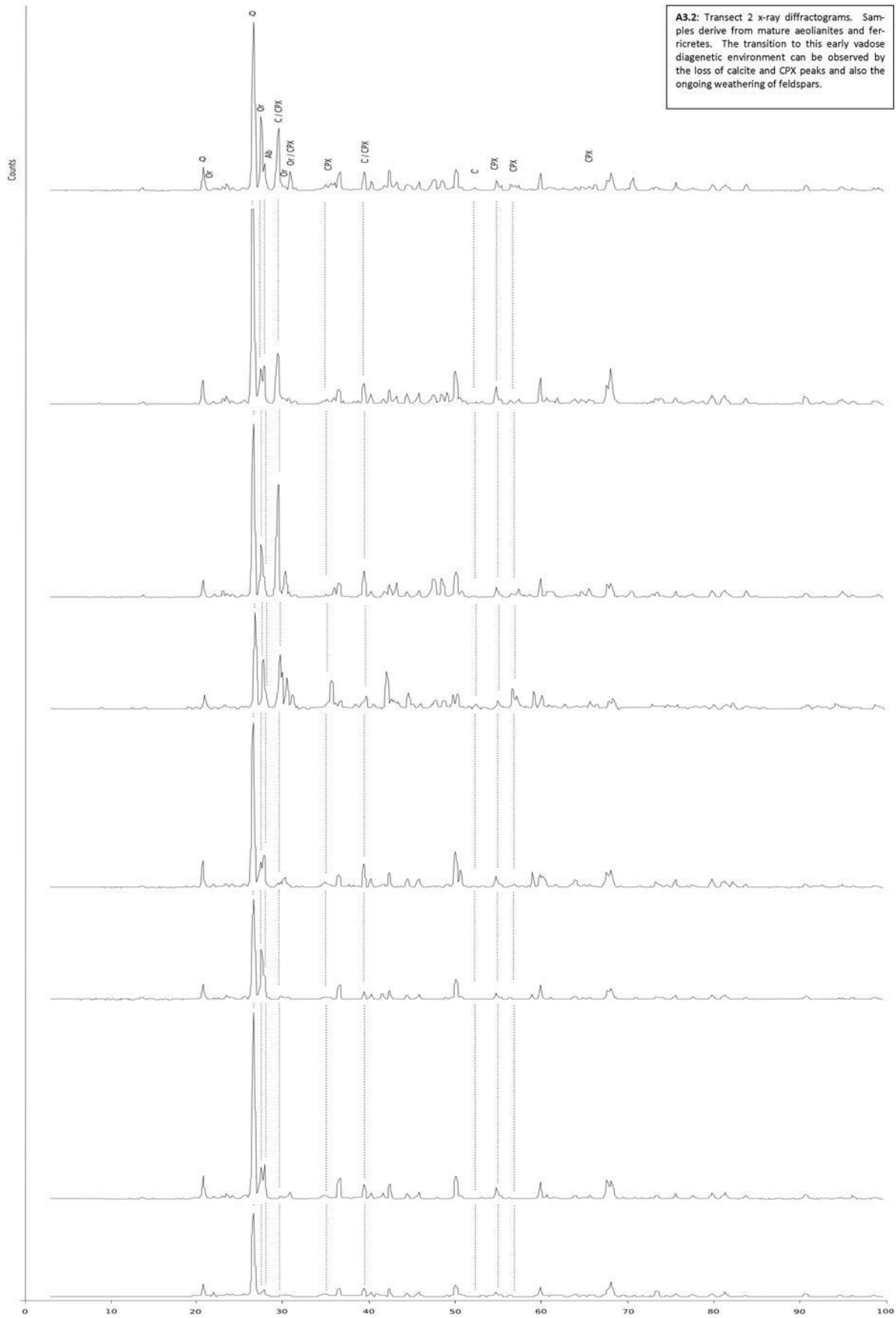
Light mineral counts (<2.9 gcm<sup>-3</sup>)

SPECIES	Fiumicino	Ostia 1	Ostia 2	Ostia 3	CP Beach	Torvaianica	CP Dune	CP03/2	CP03/6	CP07/14	CP07/15	CP07/23	CP07/24	CP07/25
Q	102	116	85	138	140	136	109	124	126	151	125	137	133	141
Qp	69	52	50	60	62	71	66	79	76	77	72	89	83	81
K	41	73	83	27	43	26	50	34	37	22	61	18	36	26
Kp	24	23	18	6	13	6	9	11	3	7	11	5	6	7
Plag	26	23	29	44	28	28	25	22	31	26	30	28	29	27
Plagp	31	28	28	29	23	28	14	10	15	9	9	16	10	13
Lc	0	0	0	0	0	0	0	5	0	0	0	0	0	0
Lch	0	0	0	0	0	0	0	1	0	0	0	0	0	0
Lp	1	1	2	0	0	0	0	0	0	0	0	0	0	0
Lv	0	1	0	0	0	0	0	0	0	0	0	0	0	0
Lmm	13	12	18	11	5	16	32	22	23	19	11	19	13	12

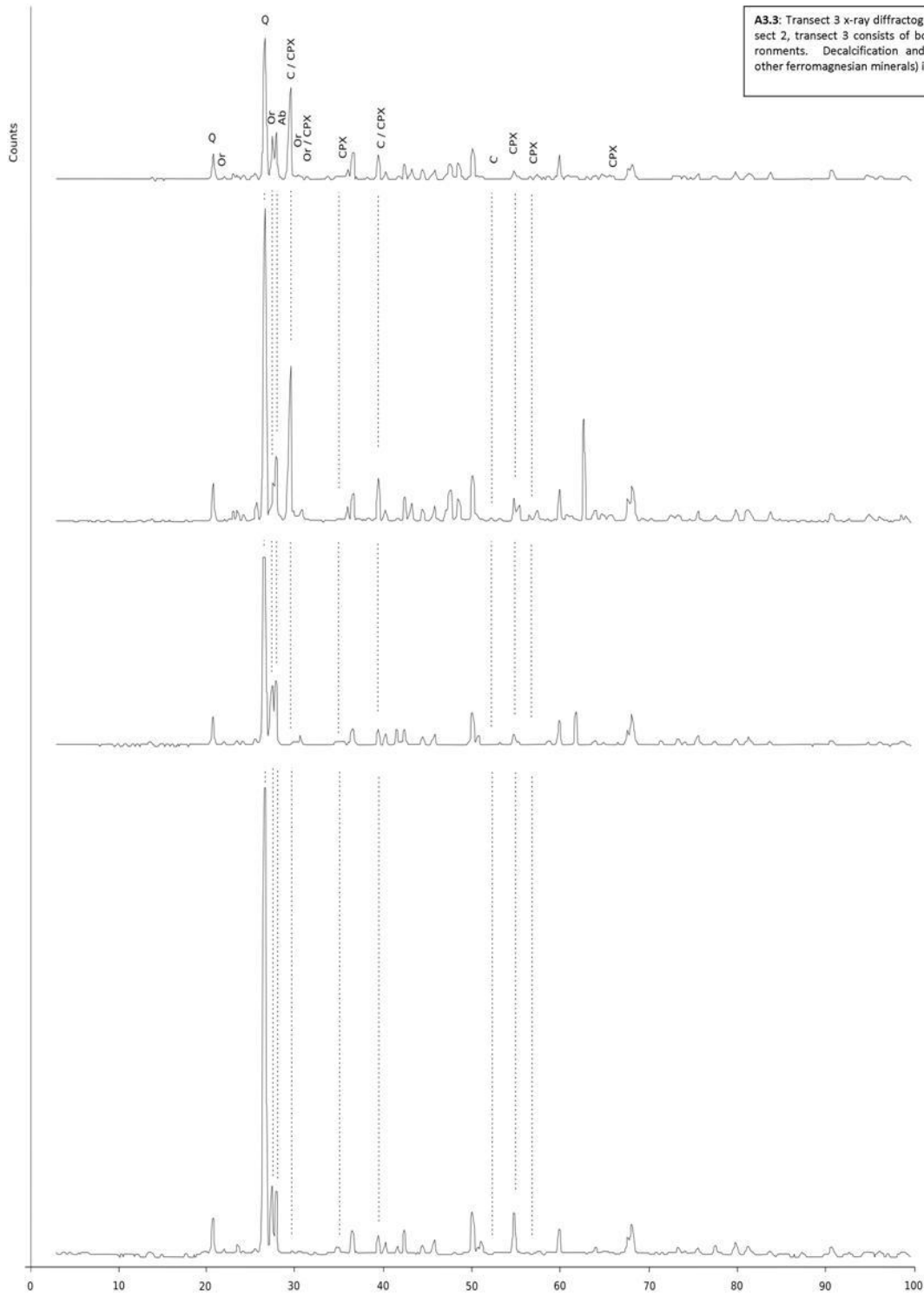


**A3.1:** Transect 1 x-ray diffractograms. Key peaks are labelled by identified minerals. X-axis is the 2θ angle, the y-axis is counts (note that scale for each diffractogram is different). Samples derive entirely from aeolianite sources. Weathering of feldspar peaks relative to calcite and CPX peaks is notable.





**A3.2:** Transect 2 x-ray diffractograms. Samples derive from mature aeolianites and ferricretes. The transition to this early vadose diagenetic environment can be observed by the loss of calcite and CPX peaks and also the ongoing weathering of feldspars.



**A3.3:** Transect 3 x-ray diffractograms. As with transect 2, transect 3 consists of both diagenetic environments. Decalcification and loss of CPX (and other ferromagnesian minerals) is a key process.

## References

- Aagaard, T., R. Davidson-Arnott, B. Greenwood & J. Nielsen, 2004. Sediment supply from shoreface to dunes: linking sediment transport measurements and long-term morphological evolution. *Geomorphology*, 60(1-2), 205-24.
- Aagaard, T., J. Orford & A. S. Murray, 2007. Environmental controls on coastal dune formation; Skallingen Spit, Denmark. *Geomorphology*, 83(1-2), 29-47.
- Abuodha, J. O. Z., 2003. Grain size distribution and composition of modern dune and beach sediments, Malindi Bay coast, Kenya. *Journal of African Earth Sciences*, 36(1-2), 41-54.
- Aitken, M. J., 1998. *An Introduction to Optical Dating: The dating of Quaternary sediments by the use of photon-stimulated luminescence*, Oxford: Oxford University Press.
- Aitken, M. J., D. W. Zimmerman & S. J. Fleming, 1968. Thermoluminescent Dating of Ancient Pottery. *Nature*, 219(5153), 442-5.
- Aldrete, G. S., 2007. *Floods of the Tiber in ancient Rome*, Baltimore: Johns Hopkins University Press.
- Alexander, S. A., (2007). The stability of the remnant luminescence emissions of alkali feldspar, in *Department of Geographical & Earth Sciences Glasgow: University of Glasgow*, 334.
- Allen, J. R. L., 1990. Salt-marsh growth and stratification: A numerical model with special reference to the Severn Estuary, southwest Britain. *Marine Geology*, 95(2), 77-96.
- Amorosi, A. & S. Milli, 2001. Late Quaternary depositional architecture of Po and Tevere river deltas (Italy) and worldwide comparison with coeval deltaic successions. *Sedimentary Geology*, 144(3-4), 357-75.
- Amorosi, A., M. Ricci Lucchi, V. Rossi & G. Sarti, 2009. Climate change signature of small-scale parasequences from Lateglacial-Holocene transgressive deposits of the Arno valley fill. *Palaeogeography, Palaeoclimatology, Palaeoecology*, 273(1-2), 142-52.
- Anderson, D., P. Glibert & J. Burkholder, 2002. Harmful algal blooms and eutrophication: Nutrient sources, composition, and consequences. *Estuaries and Coasts*, 25(4), 704-26.
- Antonioli, F., G. Cremona, F. Immordino, C. Puglisi, C. Romagnoli, S. Silenzi, E. Valpreda & V. Verrubbi, 2002. New data on the Holocene sea-level rise in NW Sicily (Central Mediterranean Sea). *Global and Planetary Change*, 34(1-2), 121-40.
- Arens, S. M., 1996. Patterns of sand transport on vegetated foredunes. *Geomorphology*, 17(4), 339-50.
- Ariztegui, D., C. Chondrogianni, A. Lami, P. Guilizzoni & E. Lafargue, 2001. Lacustrine organic matter and the Holocene paleoenvironmental record of Lake Albano (central Italy). *Journal of Paleolimnology*, 26(3), 283-92.
- Arnoldus-Huyzendveld, A. & G. Gisotti, (1999). The planosol of the "Old dunes" of Castel Porziano (Rome): a rare soil type for Italy and for Europe, in *Memorie Descrittive Della Carta Geologica D'Italia* Istituto Poligrafico E Zecca Dello Stato, 193-7.
- Arnoldus-Huyzendveld, A., C. Perotto & P. Sarandrea, In Press. *I soulo della provincia di Latina Carta, database e applicazioni: a cura della Princia di Latina*, Roma: Gangemi Editore spa.
- Auclair, M., M. Lamothe & S. Huot, 2003. Measurement of anomalous fading for feldspar IRSL using SAR. *Radiation Measurements*, 37(4-5), 487-92.
- Audry, S., G. Blanc, J. Schäfer, G. Chaillou & S. Robert, 2006. Early diagenesis of trace metals (Cd, Cu, Co, Ni, U, Mo, and V) in the freshwater reaches of a macrotidal estuary. *Geochimica et Cosmochimica Acta*, 70(9), 2264-82.
- Baas, A. C. W. & D. J. Sherman, 2006. Spatiotemporal variability of aeolian sand transport in a coastal dune environment. *Journal of Coastal Research*, 22(5), 1198-205.
- Bakker, T. W., (1990). The geohydrology of coastal dunes, in *Dunes of the European Coasts: Geomorphology, hydrology, soils*. CATENA Supplement 18, eds. T. W. Bakker, P. D. Jungerius & J. A. Klijn Cremlingen, Germany: CATENA-VERLAG, 109-19.
- Barbera, G., A. Lo Giudice, P. Mazzoleni & A. Pappalardo, 2009. Combined statistical and petrological analysis of provenance and diagenetic history of mudrocks: Application to Alpine Tethydes shales (Sicily, Italy). *Sedimentary Geology*, 213(1-2), 27-40.
- Barbisan, F., C. Savio, G. Bertorelle, T. Patarnello & L. Congiu, 2009. Duplication polymorphism at MHC class II DRB1 locus in the wild boar ( *Sus scrofa* ). *Immunogenetics*, 61(2), 145-51.

- Bate, G. C. & G. S. Dobkins, (1992). The interactions between sand, aeolianite and vegetation in a large coastal transgressive dune sheet, in *Coastal Dunes: Geomorphology, ecology and management for conservation*, ed. R. W. G. Carter, Curtis, T. G. F., Sheehy-Skeffington, M. J. Rotterdam: Balkema, 139-52.
- Bateman, M. D., P. J. Holmes, A. S. Carr, B. P. Horton & M. K. M. K. Jaiswal, 2004. Aeolianite and barrier dune construction spanning the last two glacial-interglacial cycles from the southern Cape coast, South Africa. *Quaternary Science Reviews*, 23(14-15), 1681-98.
- Battarbee, R. W., (1986). Diatom Analysis, in *Handbook of Holocene Palaeoecology and Palaeohydrology*, ed. B. E. Berglund Chichester: John Wiley & Sons Ltd., 527-70.
- Bauer, B. D. & D. J. Sherman, (1999). Coastal Dune Dynamics: Problems and prospects, in *Aeolian Environments, sediments & landforms*, eds. A. S. Goudie, I. Livingstone & S. Stokes Chichester: Wiley, 71-104.
- Beach, T., N. Dunning & M. Doyle, 2008. Geoarchaeology and geomorphology: Soils, sediments, and societies: A special issue of geomorphology. *Geomorphology*, 101(3), 413-5.
- Beach, T. P. & S. Luzzadder-Beach, 2008. Geoarchaeology and aggradation around Kinet Höyük, an archaeological mound in the Eastern Mediterranean, Turkey. *Geomorphology*, 101(3), 416-28.
- Bellotti, P., G. Calderoni, M. G. Carboni, L. Di Bella, P. Tortora, P. Valeri & V. Zernitskaya, 2007. Late Quaternary landscape evolution of the Tiber River delta plain (Central Italy): new evidence from pollen data, biostratigraphy and 14C dating. *Zeitschrift für Geomorphologie*, 51, 505-34.
- Bellotti, P., C. Caputo, L. Davoli, S. Evangelista, E. Garzanti, F. Pugliese & P. Valeri, 2004. Morpho-sedimentary characteristics and Holocene evolution of the emergent part of the Ombrone River delta (southern Tuscany). *Geomorphology*, 61(1-2), 71-90.
- Bellotti, P., F. L. Chiocci, S. Milli, P. Tortora & P. Valeri, 1994. Sequence Stratigraphy and Depositional Setting of the Tiber Delta - Integration of High-Resolution Seismics, Well Logs, and Archaeological Data. *Journal of Sedimentary Research Section B-Stratigraphy and Global Studies*, 64(3), 416-32.
- Bellotti, P., S. Milli, P. Tortora & P. Valeri, 1995. Physical stratigraphy and sedimentology of the Late Pleistocene-Holocene Tiber Delta depositional sequence. *Sedimentology*, 42(4), 617-34.
- Berry, A. & A. J. Plater, 1998. Rates of Tidal Sedimentation from Records of Industrial Pollution and Environmental Magnetism: The Tees Estuary, North-East England. *Water, Air, & Soil Pollution*, 106(3), 463-79.
- Bersani, P. & M. Bencivenga, (2001). Le Piene del Tevere a Roma: Dal V secolo a.C. all'anno 2000, ed. s. i. e. m. n. Dipartimento per i servizi tecnici nazionali Presidenza del Consiglio dei Ministri.
- Bettis, E. A., D. W. Benn & E. R. Hajic, 2008. Landscape evolution, alluvial architecture, environmental history, and the archaeological record of the Upper Mississippi River Valley. *Geomorphology*, 101(1-2), 362-77.
- Bicket, A. R., H. M. Rendell, A. J. Claridge, P. Rose, J. Andrews & F. S. J. Brown, In review. Multiscale geoarchaeological approaches from the Laurentine Shore, Castelporziano, Lazio, Italy. *Géomorphologie: relief, environnement et processus*.
- Bicket, A. R., D. C. W. Sanderson & L. Whitelaw, (In press). Geoarchaeological Investigation of the Vagnari Landscape, in *Excavations of the Vagnari Site: Volume 1*, ed. A. M. S. Small.
- Bird, E., 2000. *Coastal Geomorphology: an introduction*, Chichester: Wiley.
- Blair, M. W., E. G. Yukihara & S. W. S. McKeever, 2005. Experiences with single-aliquot OSL procedures using coarse-grain feldspars. *Radiation Measurements*, 39(4), 361-74.
- Blott, S. J. & K. Pye, 2001. GRADISTAT: A grain size distribution and statistics package for the analysis of unconsolidated sediments. *Earth Surface Processes and Landforms*, 26(11), 1237-48.
- Blott, S. J. & K. Pye, 2008. Particle shape: a review and new methods of characterization and classification. *Sedimentology*, 55(1), 31-63.
- Bond, G., B. Kromer, J. Beer, R. Muscheler, M. N. Evans, W. Showers, S. Hoffmann, R. Lotti-Bond, I. Hajdas & G. Bonani, 2001. Persistent solar influence on north Atlantic climate during the Holocene. *Science*, 294(5549), 2130-6.
- Bourrin, F., A. Monaco, J.-C. Aloïsi, J.-A. Sanchez-Cabeza, J. Lofi, S. Heussner, X. Durrieu de Madron, G. Jeanty, R. Buscaïl & G. Saragoni, 2007. Last millennia sedimentary record on a micro-tidal, low-accumulation prodelta (Têt NW Mediterranean). *Marine Geology*, 243(1-4), 77-96.

- Boyer, P., (1999). A Geoarchaeological Approach to the Late Quaternary Environmental Change in South Central Turkey, in *Department of Geography Loughborough: Loughborough University*, 306.
- Braudel, F., 1972. *The Mediterranean and the Mediterranean World in the age of Philip II*, Berkeley, California: University of California Press.
- Brooks, S. M. & F. F. Whitaker, 1997. Geochemical and Physical Controls on Vadose Zone Hydrology of Holocene Carbonate Sands, Grand Bahama Island. *Earth Surface Processes and Landforms*, 22(1), 45-58.
- Brown, A. G., 2008. Geoarchaeology, the four dimensional (4D) fluvial matrix and climatic causality. *Geomorphology*, 101(1-2), 278-97.
- Brown, A. G., 2009. Colluvial and alluvial response to land use change in Midland England: An integrated geoarchaeological approach. *Geomorphology*, 108(1-2), 92-106.
- Brown, A. G., C. Carey, G. Erkens, M. Fuchs, T. Hoffmann, J.-J. Macaire, K.-M. Moldenhauer & D. E. Walling, 2009. From sedimentary records to sediment budgets: Multiple approaches to catchment sediment flux. *Geomorphology*, 108(1-2), 35-47.
- Brown, F. S. J., (In preparation). Late Holocene Environmental Change at Castelporziano, in *Geography Loughborough: Loughborough University*.
- Bullard, J. E., G. H. McTainsh & C. Pudmenzky, 2007. Factors affecting the nature and rate of dust production from natural dune sands. *Sedimentology*, 54(1), 169-82.
- Bullard, J. E. & K. White, 2002. Quantifying iron oxide coatings on dune sands using spectrometric measurements: An example from the Simpson-Strzelecki Desert, Australia. *Journal of Geophysical Research-Solid Earth*, 107(B6).
- Bullard, J. E. & K. White, 2005. Dust production and the release of iron oxides resulting from the aeolian abrasion of natural dune sands. *Earth Surface Processes and Landforms*, 30(1), 95-106.
- Busuoli, G., M. Bucci & M. Grillini, (2001). Studi geologici, geomorfologici ed idrogeologici sulla Tenuta Presidenziale di Castelporziano, in *Il sistema ambinetale della Tenuta Presidenziale di Castelporziano. Ricerche sulla complessità di un ecosistema forestale costiero mediterraneo* Accademia Nazionale delle Scienze detta dei XL, 123-55.
- Butzer, K. W., 2008. Challenges for a cross-disciplinary geoarchaeology: The intersection between environmental history and geomorphology. *Geomorphology*, 101(1-2), 402-11.
- Cacho, I., J. O. Grimalt, M. Canals, L. Saffi, N. J. Shackleton, J. Schonfeld & R. Zahn, 2001. Variability of the western Mediterranean Sea surface temperature during the last 25,000 years and its connection with the Northern Hemisphere climatic changes. *Paleoceanography*, 16(1), 40-52.
- Carter-Stiglitz, B., S. K. Banerjee, A. Gourlan & E. Oches, 2006. A multi-proxy study of Argentina loess: Marine oxygen isotope stage 4 and 5 environmental record from pedogenic hematite. *Palaeogeography, Palaeoclimatology, Palaeoecology*, 239(1-2), 45-62.
- Carter, R. W. G., P. A. Hesp & K. F. Nordstrom, (1990a). Erosional landforms in coastal dunes, in *Coastal Dunes: form and process*, ed. K. F. Nordstrom, Psuty, N., Carter, B. Chichester: Wiley, 217-50.
- Carter, R. W. G., K. F. Nordstrom & N. P. Psuty, (1990b). The Study of Coastal Dunes, in *Coastal Dunes: form and process*, ed. K. F. Nordstrom, Psuty, N., Carter, B. Chichester: Wiley, 1-14.
- Carter, R. W. G. & P. Wilson, (1990). The geomorphological, ecological and pedological development of coastal foredunes at Magilligan Point, Northern Ireland, in *Coastal Dunes: Forms and process*, eds. K. F. Nordstrom, N. Psuty & B. Carter Chichester: Wiley, 129-57.
- Casana, J., 2008. Mediterranean valleys revisited: Linking soil erosion, land use and climate variability in the Northern Levant. *Geomorphology*, 101(3), 429-42.
- Cervini-Silva, J. & G. Sposito, 2002. Steady-State Dissolution Kinetics of Aluminum-Goethite in the Presence of Desferrioxamine-B and Oxalate Ligands. *Environ. Sci. Technol.*, 36(3), 337-42.
- Chen, R., P. L. Leung & M. J. Stokes, 2000. Apparent anomalous fading of thermoluminescence associated with competition with radiationless transitions. *Radiation Measurements*, 32(5-6), 505-11.
- Chen, T.-H., C.-Y. Chiu & G. Tian, 2005. Seasonal dynamics of soil microbial biomass in coastal sand dune forest. *Pedobiologia*, 49(6), 645-53.
- Chester, R., E. J. Sharples, G. S. Sanders & A. C. Saydam, 1984. Saharan Dust Incursion over the Tyrrhenian Sea. *Atmospheric Environment*, 18(5), 929-35.

- Clark, I. D. & P. Fritz, 1997. *Environmental Isotopes in Hydrogeology*, Boca Raton: Lewis Publishers.
- Clarke, M. L. & H. M. Rendell, 1997. Infra-red stimulated luminescence spectra of alkali feldspars. *Radiation Measurements*, 27(2), 221-36.
- Clarke, M. L. & H. M. Rendell, 2009. The impact of North Atlantic storminess on western European coasts: A review. *Quaternary International*, 195(1-2), 31-41.
- Clemmensen, L. B., K. Pedersen, A. Murray & J. Heinemeier, 2006. A 7000-year record of coastal evolution, vejjers, SW jutland, Denmark. *Bulletin of the Geological Society of Denmark*, 53, 1-22.
- Coccioni, R., A. Marsili, A. Montanari, A. Bellanca, R. Neri, D. M. Bice, H. Brinkhuis, N. Church, A. Macalady, A. McDaniel, A. Deino, F. Lirer, M. Sprovieri, P. Maiorano, S. Monechi, C. Nini, M. Nocchi, J. Pross, P. Rochette, L. Sagnotti, F. Tateo, Y. Touchard, S. Van Simaëys & G. L. Williams, 2008. Integrated stratigraphy of the Oligocene pelagic sequence in the Umbria-Marche basin (northeastern Apennines, Italy): A potential Global Stratotype Section and Point (GSSP) for the Rupelian/Chattian boundary. *Geological Society of America Bulletin*, 120(3-4), 487-511.
- Colzani, R., P. G. Albano, F. Focaccia, G. Giovannini, A. Mulazzani & A. Pazzi, 2004. *Rapporto sullo Stato dell'Ambiente dell'Area Marina Protetta "Secche di Tor Paterno"*, Roma: RomaNatura.
- Cordova, C. E., 2008. Floodplain degradation and settlement history in Wadi al-Wala and Wadi ash-Shallah, Jordan. *Geomorphology*, 101(3), 443-57.
- Cudennec, Y. & A. Lecerf, 2006. The transformation of ferrihydrite into goethite or hematite, revisited. *Journal of Solid State Chemistry*, 179(3), 716-22.
- Daniels, F., C. A. Boyd & D. F. Saunders, 1953. Thermoluminescence as a Research Tool. *Science*, 117(3040), 343-9.
- Darling, W. G., A. H. Bath, J. J. Gibson & K. Rozanski, (2006). Isotopes in Water, in *Isotopes in Palaeoenvironmental Research*, ed. M. J. Leng Dordrecht: Springer, 1-66.
- Davidson, D. A. & M. Shackley, 1976. *Geoarchaeology: earth science and the past*, London: Duckworth.
- Davis, J. C., 2002. *Statistics and Data Analysis in Geology*, New York: John Wiley and Sons.
- de Jong, R., K. Schoning & S. Björck, 2007. Increased aeolian activity during humidity shifts as recorded in a raised bog in south-west Sweden during the past 1700 years. *Clim. Past*, 3(3), 411-22.
- De Lillis, M., L. Costanzo, P. M. Bianco, A. Tinelli & W. Ritchie, 2004. Sustainability of sand dune restoration along the coast of the Tyrrhenian sea. *Journal of Coastal Conservation*, 10(1), 93-100.
- Dearing, J., (1999). Magnetic Susceptibility, in *Environmental Magnetism: a practical guide. Technical Guide, No. 6*, eds. J. Walden, F. Oldfield & J. P. Smith London: Quaternary Research Association.
- Debret, M., V. Bout-Roumazelles, F. Grousset, M. Desmet, J. F. McManus, N. Massei, D. Sebag, J. R. Petit, Y. Copard & A. Trentesaux, 2007. The origin of the 1500-year climate cycles in Holocene North-Atlantic records. *Clim. Past*, 3(4), 569-75.
- Deer, W. A., R. A. Howie & J. Zussman, 1992. *An Introduction to the Rock-Forming Minerals*, Harlow, England: Pearson Prentice-Hall.
- Dekker, L. W., C. J. Ritsema & K. Oostindie, 2000. Extent and significance of water repellency in dunes along the Dutch coast. *Journal of Hydrology*, 231-232, 112-25.
- Dima, M. & G. Lohmann, 2009. Conceptual model for millennial climate variability: a possible combined solar-thermohaline circulation origin for the ~1,500-year cycle. *Climate Dynamics*, 32(2), 301-11.
- Dominik, P., H. N. Pohl, N. Bousserhine, J. Berthelin & M. Kaupenjohann, 2002. Limitations to the reductive dissolution of Al-substituted goethites by *Clostridium butyricum*. *Soil Biology and Biochemistry*, 34(8), 1147-55.
- Draut, A. E., D. M. Rubin, J. L. Dierker, H. C. Fairley, R. E. Griffiths, J. E. Hazel, R. E. Hunter, K. Kohl, L. M. Leap, F. L. Nials, D. J. Topping & M. Yeatts, 2008. Application of sedimentary-structure interpretation to geoarchaeological investigations in the Colorado River Corridor, Grand Canyon, Arizona, USA. *Geomorphology*, 101(3), 497-509.
- Duller, G. A. T., 1991. Equivalent dose determination using single aliquots. *International Journal of Radiation Applications and Instrumentation. Part D. Nuclear Tracks and Radiation Measurements*, 18(4), 371-8.
- Eastwood, W. J., M. J. Leng, N. Roberts & B. Davis, 2007. Holocene climate change in the eastern Mediterranean region: a comparison of stable isotope and pollen data from Lake Golhisar, southwest Turkey. *Journal of Quaternary Science*, 22(4), 327-41.

- Eppes, M. C., R. Bierma, D. Vinson & F. Pazzaglia, 2008. A soil chronosequence study of the Reno valley, Italy: Insights into the relative role of climate versus anthropogenic forcing on hillslope processes during the mid-Holocene. *Geoderma*, 147(3-4), 97-107.
- Fan, H., B. Song & Q. Li, 2006. Thermal behavior of goethite during transformation to hematite. *Materials Chemistry and Physics*, 98(1), 148-53.
- Fanning, P. C., S. J. Holdaway & E. J. Rhodes, 2008. A new geoarchaeology of Aboriginal artefact deposits in western NSW, Australia: establishing spatial and temporal geomorphic controls on the surface archaeological record. *Geomorphology*, 101(3), 524-32.
- Fares, S., S. Mereu, G. Scarascia Mugnozza, M. Vitale, F. Manes, M. Frattoni, P. Ciccioli, G. Gerosa & F. Loreto, 2009. The ACCENT-VOCBAS field campaign on biosphere-atmosphere interactions in a Mediterranean ecosystem of Castelporziano (Rome): site characteristics, climatic and meteorological conditions, and eco-physiology of vegetation. *Biogeosciences*, 6(6), 1043-58.
- Fielding, C. R., J. D. Trueman & J. Alexander, 2006. Holocene Depositional History of the Burdekin River Delta of Northeastern Australia: A Model for a Low-Accommodation, Highstand Delta. *Journal of Sedimentary Research*, 76(3), 411-28.
- Fleming, A., 2005. Megaliths and post-modernism: the case of Wales. *Antiquity*, 79, 921-32.
- Fleming, A., 2006. Post-processual Landscape Archaeology: a Critique. *Cambridge Archaeological Journal*, 16(3), 267-80.
- Fleming, S. J., 1971. Thermoluminescent Dating Principles and Application. *Naturwissenschaften*, 58(7), 333-8.
- Folk, R. L., 1966. A REVIEW OF GRAIN-SIZE PARAMETERS. *Sedimentology*, 6(2), 73-93.
- Folk, R. L. & W. C. Ward, 1957. Brazos River bar [Texas]; a study in the significance of grain size parameters. *Journal of Sedimentary Research*, 27(1), 3-26.
- Francaviglia, R., L. Gataleta, M. Marchionni, A. Trinchera, R. Aromolo, A. Benedetti, L. Nisini, L. Morselli, B. Brusori, P. Olivieri & E. Bernardi, 2004. Soil quality and vulnerability in a Mediterranean natural ecosystem of Central Italy. *Chemosphere*, 55(3), 455-66.
- Frank, A. J. & G. Kocurek, 1996. Toward a model for airflow on the lee side of aeolian dunes. *Sedimentology*, 43(3), 451-8.
- French, C., 2003. *Geoarchaeology in Action: studies in soil micromorphology and landscape evolution*, New York: Routledge.
- Frihy, O. E. & P. D. Komar, 1991. Patterns of beach-scand sorting and shoreline erosion on the Nile Delta. *Journal of Sedimentary Petrology*, 61(4), 544-50.
- Fuchs, M. & A. Lang, 2009. Luminescence dating of hillslope deposits-A review. *Geomorphology*, 109(1-2), 17-26.
- Galbraith, R. F., R. G. Roberts, G. M. Laslett, H. Yoshida & J. M. Olley, 1999. Optical dating of single and multiple grains of quartz from jinnium rock shelter, Northern Australia: Part I, experimental design and statistical models. *Archaeometry*, 42, 339-64.
- Gardner, R. & S. McLaren, 1999. Infiltration and moisture movement in coastal sand dunes, Studland, Dorset, UK: Preliminary results. *Journal of Coastal Research*, 15(4), 936-49.
- Gardner, R. & K. Pye, 1981. Nature, Origin and Paleoenvironmental Significance of Red Coastal and Desert Dune Sands. *Progress in Physical Geography*, 5(4), 514-34.
- Gardner, R. A. M. & S. J. McLaren, 1994. Variability in early vadose carbonate diagenesis in sandstones. *Earth-Science Reviews*, 36(1-2), 27-45.
- Garlick, G. F. J. & A. F. Gibson, 1948. The Electron Trap Mechanism of Luminescence in Sulphide and Silicate Phosphors. *Proceedings of the Physical Society of London*, 60(342), 574-90.
- Garzanti, E., S. Ando & G. Vezzoli, 2008. Settling equivalence of detrital minerals and grain-size dependence of sediment composition. *Earth and Planetary Science Letters*, 273(1-2), 138-51.
- Garzanti, E., S. Canclini, F. M. Foggia & N. Petrella, 2002. Unraveling Magmatic and Orogenic Provenance in Modern Sand: The Back-Arc Side of the Apennine Thrust Belt, Italy. *Journal of Sedimentary Research*, 72(1), 2-17.
- Gehrels, W. R., H. M. Roe & D. J. Charman, 2001. Foraminifera, testate amoebae and diatoms as sea-level indicators in UK saltmarshes: a quantitative multiproxy approach. *Journal of Quaternary Science*, 16(3), 201-20.

- Ghilardi, M. & S. Desruelles, 2009. Geoarchaeology: where human, social and earth sciences meet with technology. *S.A.P.I.E.N.S.*, 2.2.
- Ghilardi, M., S. Kunesch, M. Styllas & E. Fouache, 2008. Reconstruction of Mid-Holocene sedimentary environments in the central part of the Thessaloniki Plain (Greece), based on microfaunal identification, magnetic susceptibility and grain-size analyses. *Geomorphology*, 97(3-4), 617-30.
- Giosan, L. & J. P. Bhattacharya, (2005). New Directions in Deltaic Studies, in *River Deltas - Concepts, Models and Examples*, eds. L. Giosan & J. P. Bhattacharya Tulsa: SEPM (Society for Sedimentary Geology, 3-10.
- Giraudi, C., 2005. Late-Holocene alluvial events in the Central Apennines, Italy. *The Holocene*, 15(5), 768-73.
- Giraudi, C., C. Tata & L. Paroli, 2009. Late Holocene evolution of Tiber river delta and geoarchaeology of Claudius and Trajan Harbor, Rome. *Geoarchaeology*, 24(3), 371-82.
- Goalen, M. & D. Fortenberry, 2002. The Villa del Discobolo at Castelporziano on the Tyrrhenian coast of Central Italy. *Antiquity*, 76(291), 29-30.
- Goldberg, P. & R. I. MacPhail, 2006. *Practical and theoretical geoarchaeology*, Oxford: Blackwell Science.
- Goralczyk, K., 1998. Nematodes in a coastal dune succession: Indicators of soil properties? *Applied Soil Ecology*, 9(1-3), 465-9.
- Graham, N., M. Hughes, C. Ammann, K. Cobb, M. Hoerling, D. Kennett, J. Kennett, B. Rein, L. Stott, P. Wigand & T. Xu, 2007. Tropical Pacific – mid-latitude teleconnections in medieval times. *Climatic Change*, 83(1), 241-85.
- Grootjans, A. P., W. H. O. Ernst & P. J. Stuyfzand, 1998. European dune slacks: strong interactions of biology, pedogenesis and hydrology. *Tree*, 13, 96-100.
- Grove, A. T. & O. Rackham, 2001. *The Nature of Mediterranean Europe: An ecological history*, New Haven: Yale University Press.
- Guccione, M. J., 2008. Impact of the alluvial style on the geoarchaeology of stream valleys. *Geomorphology*, 101(1-2), 378-401.
- Gustafsson, M. E. R. & L. G. Franzen, 1996. Dry deposition and concentration of marine aerosols in a coastal area, SW Sweden. *Atmospheric Environment*, 30(6), 977-89.
- Gustafsson, M. E. R. & L. G. Franzen, 2000. Inland transport of marine aerosols in southern Sweden. *Atmospheric Environment*, 34(2), 313-25.
- Haese, R. R., K. Wallmann, A. Dahmke, U. Kretzmann, P. J. Müller & H. D. Schulz, 1997. Iron species determination to investigate early diagenetic reactivity in marine sediments. *Geochimica et Cosmochimica Acta*, 61(1), 63-72.
- Hansom, J., (1998). Insediamenti costieri di età romana ed evoluzione della linea di costa a Castelporziano. Rapporto preliminare, in *Castelporziano III: Campagne di scavo e restauro 1987 - 1991*, ed. M. G. Lauro Roma: Soprintendenza Archaeologica di Ostia, 157-60.
- Hansom, J. D., 2001. Coastal sensitivity to environmental change: a view from the beach. *CATENA*, 42(2-4), 291-305.
- Harding, A. E., J. Palutikof & T. Holt, (2009). The climate system, in *The Physical Geography of the Mediterranean*, ed. J. C. Woodward Oxford: Oxford University Press, 69-88.
- Heinzelmann, M., 1998. Beobachtungen zur suburbanen Topographie Ostias, ein orthogonales Strassensystem im Bereich der Pianabella. *Römische Mitteilungen*, 105, 175-225.
- Helgren, D. M. & A. S. Brooks, 1983. Geoarchaeology at Gi, a middle stone age and later stone age site in the Northwest Kalahari. *Journal of Archaeological Science*, 10(2), 181-97.
- Hesp, P., 1984. The Formation of Sand Beach Ridges and Foredunes. *Search*, 15(9-10), 289-91.
- Hesp, P., 1988. Morphology, dynamics and internal stratification of some established foredunes in southeast Australia. *Sedimentary Geology*, 55(1-2), 17-41.
- Hesp, P., 2002. Foredunes and blowouts: initiation, geomorphology and dynamics. *Geomorphology*, 48(1-3), 245-68.
- Hesp, P. & B. G. Thom, (1990). Geomorphology and evolution of active transgressive dunefields, in *Coastal Dunes: Form and process*, eds. K. F. Nordstrom, N. Psuty & B. Carter Chichester: Wiley, 253-88.
- Hesp, P. A., R. Davidson-Arnott, I. J. Walker & J. Ollerhead, 2005. Flow dynamics over a foredune at Prince Edward Island, Canada. *Geomorphology*, 65(1-2), 71-84.
- Higginbotham, J. A., 1997. *Piscinae: artificial fishponds in Roman Italy*, Chapel Hill: University of North Carolina Press.
- HMSO, M. o., 1962. *Weather in the Mediterranean, i, General Meteorology*, London: HMSO.



- Horden, P. & N. Purcell, 2000. *The Corrupting Sea: A study of Mediterranean History*, Oxford: Blackwell.
- Horita, J. & R. N. Clayton, 2007. Comment on the studies of oxygen isotope fractionation between calcium carbonates and water at low temperatures by Zhou and Zheng (2003; 2005). *Geochimica et Cosmochimica Acta*, 71(12), 3131-5.
- Hudson, P. F., H. Middelkoop & E. Stouthamer, 2008. Flood management along the Lower Mississippi and Rhine Rivers (The Netherlands) and the continuum of geomorphic adjustment. *Geomorphology*, 101(1-2), 209-36.
- Huntley, D. J., M. R. Baril & S. Haidar, 2007. Tunneling in plagioclase feldspars. *Journal of Physics D: Applied Physics.*, 40.
- Huntley, D. J. & O. B. Lian, 2006. Some observations on tunnelling of trapped electrons in feldspars and their implications for optical dating. *Quaternary Science Reviews*, 25(19-20), 2503-12.
- Iadanza, C. & F. Napolitano, 2006. Sediment transport time series in the Tiber River. *Physics and Chemistry of the Earth, Parts A/B/C*, 31(18), 1212-27.
- Ingersoll, R. V., 1990. Actualistic Sandstone Petrofacies - Discriminating Modern and Ancient Source Rocks. *Geology*, 18(8), 733-6.
- Ingersoll, R. V., T. F. Bullard, R. L. Ford, J. P. Grimm, J. D. Pickle & S. W. Sares, 1984. The Effect of Grain-Size on Detrital Modes - a Test of the Gazzi-Dickinson Point-Counting Method. *Journal of Sedimentary Petrology*, 54(1), 103-16.
- Ingersoll, R. V., A. G. Kretchmer & P. K. Valles, 1993. The Effect of Sampling Scale on Actualistic Sandstone Petrofacies. *Sedimentology*, 40(5), 937-53.
- Jackson, D., W. T. & J. McCloskey, 1997. Preliminary results from a field investigation of aeolian sand transport using high resolution wind and transport measurements. *Geophysical Research Letter*, 24(2), 163-6.
- Jalut, G., A. Esteban Amat, L. Bonnet, T. Gauquelin & M. Fontugne, 2000. Holocene climatic changes in the Western Mediterranean, from south-east France to south-east Spain. *Palaeogeography, Palaeoclimatology, Palaeoecology*, 160(3-4), 255-90.
- Jones, B. & N. Kwok Choi, 1988. The structure and diagenesis of rhizoliths from Cayman Brac, British West Indies. *Journal of Sedimentary Petrology*, 58, 457-67.
- Jungerius, P. D., (1990). The characteristics of dune soils, in *Dunes of the European Coasts: Geomorphology, hydrology, soils*. CATENA Supplement 18, eds. T. W. Bakker, P. D. Jungerius & J. A. Klijn Cremlingen, Germany: CATENA-VERLAG, 155-62.
- Jungerius, P. D. & L. W. Dekker, (1990). Water erosion in the dunes, in *Dunes of the European Coasts: Geomorphology, hydrology, soils*. CATENA Supplement 18, eds. T. W. Bakker, P. D. Jungerius & J. A. Klijn Cremlingen, Germany: CATENA-VERLAG, 185-93.
- Jungerius, P. D. & F. van der Meulen, 1988. Erosion processes in a dune landscape along the Dutch coast. *CATENA*, 15(3-4), 217-28.
- Kaal, J., K. G. J. Nierop & J. M. Verstraten, 2007. Interactions between tannins and goethite- or ferrihydrite-coated quartz sand: Influence of pH and evaporation. *Geoderma*, 139(3-4), 379-87.
- Kasper-Zubillaga, J. J. & W. W. Dickinson, 2001. Discriminating depositional environments of sands from modern source terranes using modal analysis. *Sedimentary Geology*, 143(1-2), 149-67.
- Kasper-Zubillaga, J. J., G. Ortiz-Zamora, W. W. Dickinson, J. Urrutia-Fucugauchi & A. M. Soler-Arechalde, 2007a. Textural and compositional controls on modern beach and dune sands, New Zealand. *Earth Surface Processes and Landforms*, 32(3), 366-89.
- Kasper-Zubillaga, J. J., H. Zolezzi-Ruiz, A. Carranza-Edwards, P. Giron-Garcia, G. Ortiz-Zamora & M. Palma, 2007b. Sedimentological, modal analysis and geochemical studies of desert and coastal dunes, Altar Desert, NW Mexico. *Earth Surface Processes and Landforms*, 32(4), 489-508.
- Keay, S. J., 2005. *Portus: an archaeological survey of the port of Imperial Roman*, London: British School at Rome: Ministero per i beni e le attività culturali, Soprintendenza per i beni archeologici di Ostia.
- Klappa, C. F., 1980. Rhizoliths in terrestrial carbonates: classification, recognition, genesis and significance. *Sedimentology*, 27, 613-29.
- Klijn, J. A., (1990). Dune forming factors in a geographical context, in *Dunes of the European Coasts: Geomorphology, Hydrology, Soils*. CATENA Supplement 18, eds. T. W. Bakker, P. D. Jungerius & J. A. Klijn Cremlingen, Germany: CATENA-VERLAG, 1-13.

- Kling, H. J., 1992. Valve Development in *Stephanodiscus Hantzschii* Grunow (Bacillariophyceae) and its Implications on Species Identification. *Diatom Research*, 7(2), 241-57.
- Komar, P. D., K. E. Clemens, Z. Li & S.-m. Shih, 1989. The effects of selective sorting on factor analyses of heavy-mineral assemblages. *Journal of Sedimentary Research*, 59(4), 590-6.
- Komar, P. D. & C. Wang, 1984. Processes of Selective Grain Transport and the Formation of Placers on Beaches. *Journal of Geology*, 92(6), 637-55.
- Kostka, J. E. & G. W. Luther III, 1994. Partitioning and speciation of solid phase iron in saltmarsh sediments. *Geochimica et Cosmochimica Acta*, 58(7), 1701-10.
- Krammer, K. & H. Lange-Bertalot, 1991. *Bacillariophyceae*. In: *Süßwasserflora von Mitteleuropa*. 2/4 *Achnantheaceae*, Stuttgart: G. Fischer Verlag.
- Lamb, A. L., G. P. Wilson & M. J. Leng, 2006. A review of coastal palaeoclimate and relative sea-level reconstructions using  $\delta^{13}C$  and C/N ratios in organic material. *Earth-Science Reviews*, 75(1-4), 29-57.
- Lambeck, K., F. Antonioli, A. Purcell & S. Silenzi, 2004a. Sea-level change along the Italian coast for the past 10,000 yr. *Quaternary Science Reviews*, 23(14-15), 1567-98.
- Lambeck, K., M. Anzidei, F. Antonioli, A. Benini & A. Esposito, 2004b. Sea level in Roman time in the Central Mediterranean and implications for recent change. *Earth and Planetary Science Letters*, 224(3-4), 563-75.
- Lambeck, K. & A. Purcell, 2005. Sea-level change in the Mediterranean Sea since the LGM: model predictions for tectonically stable areas. *Quaternary Science Reviews*, 24(18-19), 1969-88.
- Lamberti, A., R. Archetti, M. Kramer, D. Paphitis, C. Mosso & M. Di Risio, 2005. European experience of low crested structures for coastal management. *Coastal Engineering*, 52(10-11), 841-66.
- Lanson, B., 1997. Decomposition of experimental x-ray diffraction patterns (profile fitting): a convenient way to study clay minerals. *Clay and clay minerals*, 45(2), 132-46.
- Lauro, M. G. (ed.) (1985). *Castelporziano I: Campagna di scavo e restauro 1984*, Rome: Viella.
- Lauro, M. G. (ed.) (1988). *Castelporziano II: Campagna di scavo e restauro 1985-1986*, Rome: Viella.
- Lauro, M. G. (ed.) (1998). *Castelporziano III: Campagna di scavo e restauro 1987-1991*, Rome: Viella.
- Lauro, M. G. (ed.) (forthcoming). *Castelporziano IV*.
- Lauro, M. G. & A. J. Claridge, (1998). Litus Laurentium: carta archeologica della zona litoranea a Castelporziano, in *Castelporziano III: Campagne di scavo e restauro 1987-1991*, ed. M. G. Lauro Roma: Soprintendenza Archeologica di Ostia - Viella s.r.l., 39-62.
- Le Pera, E. & S. Critelli, 1997. Sourceland controls on the composition of beach and fluvial sand of the northern Tyrrhenian coast of Calabria, Italy: implications for actualistic petrofacies. *Sedimentary Geology*, 110(1-2), 81-97.
- Lee, M. R. & I. Parsons, 1995. Microtextural Controls of Weathering of Perthitic Alkali Feldspars. *Geochimica et Cosmochimica Acta*, 59(21), 4465-88.
- Lee, M. R., K. A. Waldron & I. Parsons, 1995. Exsolution and Alteration Microtextures in Alkali Feldspar Phenocrysts from the Shap Granite. *Mineralogical Magazine*, 59(394), 63-78.
- Li, M. Z. & P. D. Komar, 1992. Longshore grain sorting and beach placer formation adjacent to the Columbia River. *Journal of Sedimentary Research*, 62(3), 429-41.
- Liu, H., P. Li, M. Zhu, Y. Wei & Y. Sun, 2007. Fe(II)-induced transformation from ferrihydrite to lepidocrocite and goethite. *Journal of Solid State Chemistry*, 180(7), 2121-8.
- Liu, W., X. Z. Wu, Y. Y. Li, C. L. Deng, X. J. Wu & S. W. Pei, 2009. Evidence of fire use of late Pleistocene humans from the Huanglong Cave, Hubei Province, China. *Chinese Science Bulletin*, 54(2), 256-64.
- Liu, X. M., P. Hesse & T. Rolph, 1999. Origin of maghaemite in Chinese loess deposits: aeolian or pedogenic? *Physics of The Earth and Planetary Interiors*, 112(3-4), 191-201.
- Livingstone, I., G. F. S. Wiggs & C. M. Weaver, 2007. Geomorphology of desert sand dunes: A review of recent progress. *Earth-Science Reviews*, 80(3-4), 239-57.
- Luchsinger, H., (2008). GEOARCHAEOLOGY, in *Encyclopedia of Archaeology* New York: Academic Press, 1409-14.
- Magny, M., C. Miramont & O. Sivan, 2002. Assessment of the impact of climate and anthropogenic factors on Holocene Mediterranean vegetation in Europe on the basis of palaeohydrological records. *Palaeogeography, Palaeoclimatology, Palaeoecology*, 186(1-2), 47-59.

- Majzlan, J., A. Navrotsky & U. Schwertmann, 2004. Thermodynamics of iron oxides: Part III. Enthalpies of formation and stability of ferrihydrite ( $\sim\text{Fe}(\text{OH})_3$ ), schwertmannite ( $\sim\text{FeO}(\text{OH})_{3/4}(\text{SO}_4)_{1/8}$ ), and  $[\text{var } \epsilon]\text{-Fe}_2\text{O}_3$ . *Geochimica et Cosmochimica Acta*, 68(5), 1049-59.
- Mallol, C., 2006. What's in a beach? Soil micromorphology of sediments from the Lower Paleolithic site of 'Ubeidiya, Israel. *Journal of Human Evolution*, 51(2), 185-206.
- Manes, F., A. Grignetti, A. Tinelli, R. Lenz & P. Ciccioli, 1997. General features of the Castelporziano test site. *Atmospheric Environment*, 31(Supplement 1), 19-25.
- Marchetto, A., D. Colombaroli & W. Tinner, 2008. Diatom response to mid-Holocene climate change in Lago di Massaciuccoli (Tuscany, Italy). *Journal of Paleolimnology*, 40(1), 235-45.
- Marra, F., F. Florindo & E. Boschi, 2008. History of glacial terminations from the Tiber River, Rome: Insights into glacial forcing mechanisms. *Paleoceanography*, 23.
- Marriner, N., In press. Currents and trends in the archaeological sciences. *Journal of Archaeological Science*, In Press, Accepted Manuscript.
- Marriner, N. & C. Morhange, 2006. The 'Ancient Harbour Parasequence': Anthropogenic forcing of the stratigraphic highstand record. *Sedimentary Geology*, 186(1-2), 13-7.
- Mather, A. E., (2009). Tectonic setting and landscape development, in *The Physical Geography of the Mediterranean*, ed. J. C. Woodward Oxford: Oxford University Press, 5-32.
- McKeever, S. W. S., 1985. *Thermoluminescence of solids*, Cambridge: Cambridge University Press.
- McLachlan, A., G. Kerley & C. Rickard, 1996. Ecology and energetics of slacks in the Alexandria coastal dunefield. *Landscape and Urban Planning*, 34, 267-76.
- McLaren, S., (2007). Aeolianite, in *Geochemical Sediments & Landscapes*, eds. D. J. Nash & S. McLaren Oxford: Blackwell Publishing.
- McLaren, S. J., (1993). Use of cement types in the palaeoenvironmental interpretation of coastal aeolianite sequences, in *The Dynamics and Environmental Context of Aeolian Sedimentary Systems*, ed. K. Pye London: Geological Society, 235-44.
- McLaren, S. J., 2001. Effects of sea spray on vadose diagenesis of late Quaternary Aeolianites, Bermuda. *Journal of Coastal Research*, 17(1), 228-40.
- McLaren, S. J. & R. Gardner, 2004. Late Quaternary vadose carbonate diagenesis in coastal and desert dune and beach sands: is there a palaeoclimatic signal? *Earth Surface Processes and Landforms*, 29(12), 1441-58.
- McLaren, S. J. & D. J. Nash, (2007). Geochemical Sediments and Landscapes: General Summary, in *Geochemical Sediments & Landscapes*, eds. D. J. Nash & S. J. McLaren Oxford: Blackwell Publishing, 443-6.
- Mei, M., 1992. A survey of the socially parasitic ant genera *Epimyrma* Emery, 1915 and *Chalepoxenus* Menozzi, 1922 in Italy (Hymenoptera, Formicidae, Myrmicinae). *Insectes Sociaux*, 39(2), 145-56.
- Meiggs, R., 1973. *Roman Ostia*, Oxford: Clarendon Press.
- Milli, S. & E. Zarlenga, 1991. Analisi di fcies dei depositi tirreniani (Duna Rossa) affioranti nell'area di Castel Porziano Pomezia (Roma). Una revisione ambintale. *Il Quaternario*, 4, 233-48.
- mindat.org, (2009). <http://www.mindat.org/min-223.html>.
- Mitchum Jr, R. M. & J. C. Van Wagoner, 1991. High-frequency sequences and their stacking patterns: sequence-stratigraphic evidence of high-frequency eustatic cycles. *Sedimentary Geology*, 70(2-4), 131-47, 53-60.
- Miyaniishi, K. & E. A. Johnson, (2007). Coastal Dune Succession and the Reality of Dune Processes, in *Plant Disturbance Ecology: the process and the response*, eds. E. A. Johnson & K. Miyaniishi Academic Press, 249-82.
- Molinaroli, E., M. Blom & A. Basu, 1991. Methods of Provenance Determination Tested with Discriminant Function-Analysis. *Journal of Sedimentary Petrology*, 61(6), 900-8.
- Moral Cardona, J. P., J. M. Gutierrez Mas, A. Sanchez Bellon, S. Dominguez-Bella & J. Martinez Lopez, 2005. Surface textures of heavy-mineral grains: a new contribution to provenance studies. *Sedimentary Geology*, 174(3-4), 223-35.
- Morton, A. C. & C. R. Hallsworth, 1999. Processes controlling the composition of heavy mineral assemblages in sandstones. *Sedimentary Geology*, 124(1-4), 3-29.

- Mountney, N. P. & A. J. Russell, 2006. Coastal aeolian dune development, Solheimasandur, southern Iceland. *Sedimentary Geology*, 192(3-4), 167-81.
- Mulder, T., J. P. M. Syvitski, S. Migeon, J.-C. Faugères & B. Savoye, 2003. Marine hyperpycnal flows: initiation, behavior and related deposits. A review. *Marine and Petroleum Geology*, 20(6-8), 861-82.
- Murray, A. S., J. P. Buylaert, K. J. Thomsen & M. Jain, 2009. The effect of preheating on the IRSL signal from feldspar. *Radiation Measurements*, 44(5-6), 554-9.
- Murray, A. S. & R. G. Roberts, 1997. Determining the burial time of single grains of quartz using optically stimulated luminescence. *Earth and Planetary Science Letters*, 152(1-4), 163-80.
- Murray, T. & R. Credo, 2001. *Encyclopedia of archaeology [Electronic book] : history and discoveries*, Santa Barbara, Calif.: ABC-CLIO.
- Nash, D. J. & S. J. McLaren, 2003. Kalahari valley calcretes: their nature, origins, and environmental significance. *Quaternary International*, 111(1), 3-22.
- Nash, D. J., McLaren, S.J., Webb, J.A., 2004. Petrology, geochemistry and environmental significance of silcrete-calcrete intergrade duricrusts at Kang Pan and Tswane, central Kalahari, Botswana. *Earth Surface Processes and Landforms*, 29(12), 1559-86.
- Nathan, R. P. & B. Mauz, 2008. On the dose-rate estimate of carbonate-rich sediments for trapped charge dating. *Radiation Measurements*, 43(1), 14-25.
- Newman, D. K., 2001. Microbiology - How bacteria respire minerals. *Science*, 292(5520), 1312-3.
- Nishijima, H. & M. Nakata, 2004. Relationship between plant cover type and soil properties on Syunkunitai coastal sand dune in eastern Hokkaido. *Ecological Research*, 19(6), 581-91.
- Nordstrom, K. F., N. Psuty & B. Carter, 1990. *Coastal Dunes: forms and process*, Chichester: Wiley.
- Oelkers, E. H., S. V. Golubev, C. Chairat, O. S. Pokrovsky & J. Schott, 2009. The surface chemistry of multi-oxide silicates. *Geochimica et Cosmochimica Acta*, 73(16), 4617-34.
- Olley, J. M., (1994). The use of 238-U and 232-Th decay series radionuclides in sediment tracing, University of New South Wales.
- Olley, J. M., A. Murray & R. G. Roberts, 1996. The effects of disequilibria in the uranium and thorium decay chains on burial dose rates in fluvial sediments. *Quaternary Science Reviews*, 15(7), 751-60.
- Otvos, E. G., 2000. Beach ridges -- definitions and significance. *Geomorphology*, 32(1-2), 83-108.
- Otvos, E. G., 2005. Validity of sea-level indicators: A comment on "A new depositional model for the buried 4000 yr BP New Orleans barrier: implications for sea-level fluctuations and onshore transport from a nearshore shelf source" by F.W. Stapor and G.W. Stone [Marine Geology 204 (2004) 215-234]. *Marine Geology*, 217(1-2), 177-87.
- Ozdemir, O. & D. J. Dunlop, 2000. Intermediate magnetite formation during dehydration of goethite. *Earth and Planetary Science Letters*, 177(1-2), 59-67.
- Parker, A. G. & A. S. Goudie, 2008. Geomorphological and palaeoenvironmental investigations in the southeastern Arabian Gulf region and the implication for the archaeology of the region. *Geomorphology*, 101(3), 458-70.
- Parker, A. G., A. S. Lucas, J. Walden, A. S. Goudie, M. A. Robinson & T. G. Allen, 2008. Late Holocene geoarchaeological investigation of the Middle Thames floodplain at Dorney, Buckinghamshire, UK: An evaluation of the Bronze Age, Iron Age, Roman and Saxon landscapes. *Geomorphology*, 101(3), 471-83.
- Parsons, M. L., Q. Dortch, R. E. Turner & N. R. Rabalais, 2006. Reconstructing the development of eutrophication in Louisiana salt marshes. *Limnology and Oceanography*, 51(1), 534-44.
- Patrick, R. & C. W. Reimer, 1966-1975. *The diatoms of the United States*.
- Pearsall, D. M. (ed.) (2008). *Encyclopedia of Archaeology*, New York: Academic Press.
- Pettijohn, F. J., P. E. Potter & R. Siever, 1972. *Sand and Sandstone*, Berlin: Springer-Verlag.
- Piccardi, G., D. Uncini & R. Udisti, (1996). Relationships among some components of marine aerosol sampled at Leghorn, Tyrrhenian Sea (Italy), in *Impact of Desert Dust across the Mediterranean*, eds. S. Guerzoni & R. Chester, 375-80.
- Plenkovic-Moraj, A., N. Horvatincic & B. Primc-Habdija, 2002. Periphyton and its role in tufa deposition in karstic waters (Plitvice Lakes, Croatia). *Biologia*, 57(4), 423-31.

- Pluis, J. L. A. & B. De Winder, (1990). Natural Stabilisation, in *Dunes of the European Coasts: Geomorphology, hydrology, soils. CATENA Supplement 18*, eds. T. W. Bakker, P. D. Jungerius & J. A. Klijn Cremlingen, Germany: CATENA-VERLAG, 195-208.
- Prasad, P. S. R., K. Shiva Prasad, V. Krishna Chaitanya, E. V. S. S. K. Babu, B. Sreedhar & S. Ramana Murthy, 2006. In situ FTIR study on the dehydration of natural goethite. *Journal of Asian Earth Sciences*, 27(4), 503-11.
- Prescott, J. R. & J. T. Hutton, 1988. Cosmic-Ray and Gamma-Ray Dosimetry for TL and Electron-Spin-Resonance. *Nuclear Tracks and Radiation Measurements*, 14(1-2), 223-7.
- Preusser, F., 2003. IRSL dating of K-rich feldspars using the SAR protocol: Comparison with independent age control. *Ancient TL*, 21(1), 17.
- Psuty, N., (2008). The Coastal Fore-dune: A Morphological Basis for Regional Coastal Dune Development, in *Coastal Dunes*, 11-27.
- Psuty, N. P., (1992). Spatial variations in coastal fore-dune development, in *Coastal Dunes: Geomorphology, ecology and management for conservation*, ed. R. W. G. Carter, Curtis, T. G. F., Sheehy-Skeffington, M. J. Rotterdam: Balkema, 3-14.
- Pye, K., 1981. Rate of dune reddening in a humid tropical climate. *Nature*, 290(5807), 582-4.
- Pye, K., (1983). Early Post-Depositional Modification of Aeolian Dune Sands, in *Aeolian Sediments & Processes*, eds. M. E. Brookfield & T. S. Ahlbrandt Amsterdam: Elsevier, 197-221.
- Ranasinghe, R. & I. L. Turner, 2006. Shoreline response to submerged structures: A review. *Coastal Engineering*, 53(1), 65-79.
- Randall, J. T. & M. H. F. Wilkins, 1945a. Phosphorescence and Electron Traps .1. the Study of Trap Distributions. *Proceedings of the Royal Society of London Series a-Mathematical and Physical Sciences*, 184(999), 366-89.
- Randall, J. T. & M. H. F. Wilkins, 1945b. Phosphorescence and Electron Traps .2. the Interpretation of Long-Period Phosphorescence. *Proceedings of the Royal Society of London Series a-Mathematical and Physical Sciences*, 184(999), 390-407.
- Rapp, G. & C. L. Hill, 2006. *Geoarchaeology: the earth-science approach to archaeological interpretation*, New Haven: Yale university Press.
- Ravazzi, C., 2003. An overview of the Quaternary continental stratigraphic units based on biological and climatic events in Italy. *Il Quaternario - volume speciale INQUA*, 16(1(Bis)), 11-8.
- Reid, R. P. & I. G. Macintyre, 1998. Carbonate recrystallization in shallow marine environments: a widespread diagenetic process forming micritized grains. *Journal of Sedimentary Research*, 68(5), 928-46.
- Rendell, H. M., (1998). Datazione con la termoluminescenza della sequenza sabbiosa di Castelporziano: risultati preliminari, in *Castelporziano III: Campagne di scavo e restauro 1987-1991*, ed. M. G. Lauro Roma: Soprintendenza Archeologica di Ostia - Viella s.r.l., 161-3.
- Rendell, H. M., A. J. Claridge & M. L. Clarke, 2007. Late Holocene Mediterranean coastal change along the Tiber Delta and Roman occupation of the Laurentine shore, central Italy. *Quaternary Geochronology*, 2(1-4), 83-8.
- Renfrew, C., (1976). Preface, in *Geoarchaeology: Earth Science and the Past*, eds. D. A. Davidson & M. Shackley London: Duckworth, 1-5.
- Richardson, C. A., 2001. Residual luminescence signals in modern coastal sediments. *Quaternary Science Reviews*, 20(5-9), 887-92.
- Rohling, E. J., R. H. Abu-Zied, J. S. L. Casford, A. Hayes & B. A. A. Hoogakker, (2009). The marine environment: present and past, in *The Physical Geography of the Mediterranean*, ed. J. C. Woodward Oxford: Oxford University Press, 33-67.
- Round, F. E. & L. Bukhtiyarova, 1996. Four New Genera Based on *Achnanthes* (*Achnantheidium*) Together with a Re-definition of *Achnantheidium*. *Diatom Research*, 11(2), 345-61.
- Round, F. E., R. M. Crawford & D. G. Mann, 1990. *The Diatoms: Biology, morphology of the Genera*, Cambridge: Cambridge University Press.
- Sanderson, D. C. W., 1988. Thick Source Beta-Counting (TSBC) - a Rapid Method for Measuring Beta-Dose-Rates. *Nuclear Tracks and Radiation Measurements*, 14(1-2), 203-7.

- Sanderson, D. C. W. & S. Murphy, In Press. Using simple portable OSL measurements and laboratory characterisation to help understand complex and heterogeneous sediment sequences for luminescence dating. *Quaternary Geochronology*, In Press, Corrected Proof.
- Sastry, A. V. R. & J. S. R. Krishna Rao, 1964. On The Significance of the Anomalous Biaxial Quartz and Scapolite in Granulites from Koduru, Andhra Pradesh. *Current Science*, 21, 650-1.
- Schwertmann, U., 1991. Solubility and dissolution of iron oxides. *Plant and Soil*, 130(1), 1-25.
- Seufert, G., J. Bartzis, T. Bombol, P. Ciccioli, S. Cieslik, R. Dlugi, P. Foster, C. N. Hewitt, J. Kesselmeier, D. Kotzias, R. Lenz, F. Manes, R. Perez Pastor, R. Steinbrecher, L. Torres, R. Valentini & B. Versino, 1997. An overview of the Castelporziano Experiments. *Atmospheric Environment*, 31, 5-17.
- Sherman, D. J., 1995. Problems of scale in the modeling and interpretation of coastal dunes. *Marine Geology*, 124(1-4), 339-49.
- Sherman, D. J. & B. O. Bauer, 1993. Dynamics of Beach-Dune Systems. *Progress in Physical Geography*, 17(4), 413-47.
- Sherman, D. J. & S. Hotta, (1990). Aeolian sediment transport: theory and measurement, in *Coastal Dunes: form and process*, ed. K. F. Nordstrom, Psuty, N., Carter, B. Chichester: Wiley, 15-38.
- Shillito, L. M., M. J. Almond, J. Nicholson, M. Pantos & W. Matthews, 2009. Rapid characterisation of archaeological midden components using FT-IR spectroscopy, SEM-EDX and micro-XRD. *Spectrochimica Acta Part a-Molecular and Biomolecular Spectroscopy*, 73(1), 133-9.
- Short, A. D. & P. A. Hesp, 1982. Wave, beach and dune interactions in southeastern Australia. *Marine Geology*, 48(3-4), 259-84.
- Silva, V. d. P. R., F. d. A. S. Sousa, E. P. Cavalcanti, E. P. Souza & B. B. da Silva, 2006. Teleconnections between sea-surface temperature anomalies and air temperature in northeast Brazil. *Journal of Atmospheric and Solar-Terrestrial Physics*, 68(7), 781-92.
- Skidmore, M., M. Sharp & M. Tranter, 2004. Kinetic isotopic fractionation during carbonate dissolution in laboratory experiments: Implications for detection of microbial CO<sub>2</sub> signatures using [ $\delta$ ]<sup>13</sup>C-DIC. *Geochimica et Cosmochimica Acta*, 68(21), 4309-17.
- Somoza, L., A. Barnolas, A. Arasa, A. Maestro, J. G. Rees & F. J. Hernandez-Molina, 1998. Architectural stacking patterns of the Ebro delta controlled by Holocene high-frequency eustatic fluctuations, delta-lobe switching and subsidence processes. *Sedimentary Geology*, 117(1-2), 11-32.
- Speranza, A., C. Accadia, M. Casaioli, S. Mariani, G. Monacelli, R. Inghilesi, N. Tartaglione, P. M. Ruti, A. Carillo, A. Baragagli, G. Pisacane, F. Valentinotti & A. Lavagnini, 2004. POSIEDON: An integrated system for analysis and forecast of hydrological, meteorological and surface marine fields in the Mediterranean area. *Il Nuovo Cimento*, 27(4), 329-45.
- Spooner, N. A., 1994. The anomalous fading of infrared-stimulated luminescence from feldspars. *Radiation Measurements*, 23(2-3), 625-32.
- Starkey, J., 2000. Bi-axial quartz as a stress indicator. *Journal of Structural Geology*, 22(3), 383-90.
- Stewart, I. S. & C. Morhange, (2009). Coastal Geomorphology and sea-level change, in *The Physical Geography of the Mediterranean*, ed. J. C. Woodward Oxford: Oxford University Press, 385-413.
- Stuyfzand, P. J., (1998). Decalcification and acidification of coastal dune sands in the Netherlands, in *Water-Rock Interaction*, eds. G. B. Arehart & J. R. Hulston, 79-82.
- Sykora, K. V., J. van den Bogert & F. Berendse, 2004. Changes in soil and vegetation during dune slack succession. *Journal of Vegetation Science*, 15(2), 209-18.
- Taricco, C., M. Ghil, S. Alessio & G. Vivaldo, 2009. Two millennia of climate variability in the Central Mediterranean. *Clim. Past*, 5(2), 171-81.
- ter Braak, C. J. F. & P. Smilauer, 2002. *CANOCO Reference Manual and CanoDraw for Windows User's Guide: software for Canonical Community Ordination (version 4.5)*, Ithaca, NY: Microcomputer Power.
- Thompson, A., J. Ruiz, O. A. Chadwick, M. Titus & J. Chorover, 2007. Rayleigh fractionation of iron isotopes during pedogenesis along a climate sequence of Hawaiian basalt. *Chemical Geology*, 238(1-2), 72-83.
- Thorndycraft, V. R., G. Benito & K. J. Gregory, 2008. Fluvial geomorphology: A perspective on current status and methods. *Geomorphology*, 98(1-2), 2-12.

- Thornes, J. B., F. López-Bermúdez & J. C. Woodward, (2009). Hydrology, river regimes, and sediment yield, in *The Physical Geography of the Mediterranean*, ed. J. C. Woodward Oxford: Oxford University Press, 229-53.
- Tribble, J. S., R. S. Arvidson, M. Lane & F. T. Mackenzie, 1995. Crystal chemistry, and thermodynamic and kinetic properties of calcite, dolomite, apatite, and biogenic silica: applications to petrologic problems. *Sedimentary Geology*, 95(1-2), 11-37.
- Tsatskin, A., T. S. Gendler, F. Heller, I. Dekman & G. L. Frey, 2009. Towards understanding paleosols in Southern Levantine eolianites: Integration of micromorphology, environmental magnetism and mineralogy. *Journal of Mountain Science*, 6(2), 113-24.
- Tzedakis, P. C., 2007. Seven ambiguities in the Mediterranean palaeoenvironmental narrative. *Quaternary Science Reviews*, 26(17-18), 2042-66.
- Tzedakis, P. C., (2009). Cenozoic climate and vegetation change, in *The Physical Geography of the Mediterranean*, ed. J. C. Woodward Oxford: Oxford University Press, 89-137.
- Uribelarra, D. & G. Benito, 2008. Fluvial changes of the Guadalquivir river during the Holocene in Cordoba (Southern Spain). *Geomorphology*, 100(1-2), 14-31.
- Van Olphen, H. & J. J. Fripiat (eds.), (1979). *Data handbook for clay minerals and other non-metallic minerals*, Oxford: Pergamon.
- Vazquez, G., P. Moreno-Casanola & O. Barrera, 1998. Interactions between algae and seed germination in tropical dune slack species: a facilitation process. *Aquatic Botany*, 60, 409-16.
- Vernon, R. H., 2004. *A practical guide to rock microstructure*, Cambridge: Cambridge University Press.
- Vissac, C., 2005. Study of a historical garden soil at the Grand-Pressigny site (Indre-et-Loire, France): Evidence of landscape management. *Journal of Cultural Heritage*, 6(1), 61-7.
- Walker, T. R., (1979). Red Colour In Dune Sand, in *A Study of Global Sand Seas*, ed. E. D. McKee Washington: US Govt. Print. Off., 61-81.
- Wallinga, J., A. Murray & G. Duller, 2000a. Underestimation of equivalent dose in single-aliquot optical dating of feldspars caused by preheating. *Radiation Measurements*, 32(5-6), 691-5.
- Wallinga, J., A. Murray & A. Wintle, 2000b. The single-aliquot regenerative-dose (SAR) protocol applied to coarse-grain feldspar. *Radiation Measurements*, 32(5-6), 529-33.
- Walsh, K., 2008. Mediterranean Landscape Archaeology: Marginality and the Culture-Nature "Divide". *Landscape Research*, 33(5), 547 - 64.
- Wanner, H., J. Beer, J. Bütikofer, T. J. Crowley, U. Cubasch, J. Flückiger, H. Goosse, M. Grosjean, F. Joos, J. O. Kaplan, M. Küttel, S. A. Müller, I. C. Prentice, O. Solomina, T. F. Stocker, P. Tarasov, M. Wagner & M. Widmann, 2008. Mid-to Late Holocene climate change: an overview. *Quaternary Science Reviews*, 27(19-20), 1791-828.
- Waters, M. R., 2008. Alluvial chronologies and archaeology of the Gila River drainage basin, Arizona. *Geomorphology*, 101(1-2), 332-41.
- Waters, M. R., S. L. Forman, T. W. Stafford Jr & J. Foss, 2009. Geoarchaeological investigations at the Topper and Big Pine Tree sites, Allendale County, South Carolina. *Journal of Archaeological Science*, 36(7), 1300-11.
- Weiss, E., M. E. Kislev, O. Simchoni, D. Nadel & H. Tschauner, 2008. Plant-food preparation area on an Upper Paleolithic brush hut floor at Ohalo II, Israel. *Journal of Archaeological Science*, 35(8), 2400-14.
- Wessels, M., K. Mohaupt, R. Kümmerlin & A. Lenhard, 1999. Reconstructing past eutrophication trends from diatoms and biogenic silica in the sediment and the pelagic zone of Lake Constance, Germany. *Journal of Paleolimnology*, 21(2), 171-92.
- Widdowson, M., (2007). Laterite and Ferricrete, in *Geochemical Sediments & Landscapes*, eds. D. J. Nash & S. McLaren, J. Oxford: Blackwell Publishing.
- Wiggs, G. f. S., R. J. Atherton & A. J. Baird, 2004a. Thresholds of aeolian sand transport: establishing suitable values. *Sedimentology*, 51(1), 95-108.
- Wiggs, G. F. S., A. J. Baird & R. J. Atherton, 2004b. The dynamic effects of moisture on the entrainment and transport of sand by wind. *Geomorphology*, 59(1-4), 13-30.
- Wilkinson, T. J., 2003. *Archaeological Landscapes of the Near East*, Tucson, Arizona: University of Arizona Press.

- Wilkinson, T. J., 2005. Soil erosion and valley fills in the Yemen highlands and southern Turkey: Integrating settlement, geoarchaeology, and climate change. *Geoarchaeology*, 20(2), 169-92.
- Wilkinson, T. J., 2009. P. Degryse and M. Waelkens, Editors, Sagalassos VI. Geo- and Bio-archaeology at Sagalassos and in its Territory, Leuven University Press, Leuven (2008) 328 pp + viii, ISBN: 978 90 5867 661 005/2008, ppbk, Euros 75. *Journal of Archaeological Science*, 36(9), 2055-6.
- Wintle, A. G., 1973. Anomalous Fading of Thermo-luminescence in Mineral Samples. *Nature*, 245(5421), 143-4.
- Wintle, A. G. & D. J. Huntley, 1979. Thermoluminescence Dating of a Deep-Sea Sediment Core. *Nature*, 279(5715), 710-2.
- Wunsam, S., R. Schmidt & J. Muller, 1999. Holocene lake development of two Dalmatian lagoons (Malo and Veliko Jezero, Isle of Mljet) in respect to changes in Adriatic sea level and climate. *Palaeogeography Palaeoclimatology Palaeoecology*, 146(1-4), 251-81.
- Yang, X., B. Zhu & P. D. White, 2007. Provenance of aeolian sediment in the Taklamakan Desert of western China, inferred from REE and major-elemental data. *Quaternary International*, 175(1), 71-85.
- Zecchetto, S. & C. Cappa, 2001. The spatial structure of the Mediterranean Sea winds revealed by ERS-1 scatterometer. *International Journal of Remote Sensing*, 22(1), 45 - 70.
- Zhang, J., P. D. Quay & D. O. Wilbur, 1995. Carbon isotope fractionation during gas-water exchange and dissolution of CO<sub>2</sub>. *Geochimica et Cosmochimica Acta*, 59(1), 107-14.
- Zhang, J. F., B. Y. Yuan & L. P. Zhou, 2008. Luminescence chronology of "Old Red Sand" in jinjiang and its implications for optical dating of sediments in South China. *Chinese Science Bulletin*, 53(4), 591-601.
- Zheng, Y.-F. & G.-T. Zhou, 2007. Response to the Comment by J. Horita and R.N. Clayton on "The studies of oxygen isotope fractionation between calcium carbonates and water at low temperatures". *Geochimica et Cosmochimica Acta*, 71(12), 3136-43.
- Zhou, G.-T. & Y.-F. Zheng, 2006. On the Direction and Magnitude of Oxygen Isotope Fractionation Between Calcite and Aragonite at Thermodynamic Equilibrium. *Aquatic Geochemistry*, 12(3), 239-68.
- Zimmerman, D. W., 1971. Thermoluminescent Dating Using Fine Grains from Pottery. *Archaeometry*, 13(FEB), 29-52.